

NISTIR 8271 DRAFT SUPPLEMENT

Face Recognition Vendor Test (FRVT) Part 2: Identification

Patrick Grother
Mei Ngan
Kayee Hanaoka
*Information Access Division
Information Technology Laboratory*

This document is a draft supplement of [NIST Interagency Report 8271](#)

2023/03/14



NISTIR 8271 DRAFT SUPPLEMENT

Face Recognition Vendor Test (FRVT) Part 2: Identification

Patrick Grother
Mei Ngan
Kayee Hanaoka
*Information Access Division
Information Technology Laboratory*

This document is a draft supplement of [NIST Interagency Report 8271](#)

November 2022



U.S. Department of Commerce
Gina M. Raimondo, Secretary

National Institute of Standards and Technology
Laurie E. Locascio, NIST Director and Undersecretary of Commerce for Standards and Technology

RELEASE NOTES

2023-03-14: The 1:N track of the FRVT remains open.

- ▷ This document is the twenty first draft update to [NIST Interagency Report 8271](#). It contains results for no first-time participants.
- ▷ The document also includes results for algorithms from nine returning developers: Cloudwalk - Moon-time Smart Technology, Line Corporation, Intema-LGL Group Neurotechnology, NEC, Paravision, Samsung S1, Veridas Digital Authentication Solutions, and Thales Group

2023-02-06: The 1:N track of the FRVT remains open.

- ▷ This document is the twenty first draft update to [NIST Interagency Report 8271](#). It contains results for no first-time participants.
- ▷ The document also includes results for algorithms from seven returning developers: Dermalog, DiluSense Technology, Hangzhuo Allu Network Information Technology, Idemia, Innovatrics, Rank One Computing, and Sensetime Group.

2022-12-15: The 1:N track of the FRVT remains open.

- ▷ This document is the twentieth draft update to [NIST Interagency Report 8271](#). It contains results for one first-time participant: First Credit Bureau Kazakhstan.
- ▷ The document also includes results for algorithms from five returning developers: Gorilla Technology, Pangiam, Qnap Security, SQLsoft, Vixvizon (formerly known as Imagus).

2022-11-09: The 1:N track of the FRVT remains open.

- ▷ This document is the nineteenth draft update to [NIST Interagency Report 8271](#). It contains results for four first-time participant: Mukh, Turing Technology VIP, Verijelas and Verihubs Inteligensia
- ▷ The document also includes results for algorithms from two returning developers: Maxvision and Samsung S1.

2022-09-23: The 1:N track of the FRVT remains open.

- ▷ This document is the eighteenth draft update to [NIST Interagency Report 8271](#). It contains results for two first-time participants: Intema-LGL Group and T4iSB.
- ▷ The document also includes results for algorithms from two returning developers: Cloudwalk - Moon-time Smart Technology, Dermalog, Griaule, Hangzhuo Allu Network Information Technology, Intelivision, Line Corporation, NEC, Sensetime Group, Realnetworks Inc and Vietnam Posts and Telecommunications Group.

2022-07-28: The 1:N track of the FRVT remains open.

- ▷ This document is the seventeenth draft update to [NIST Interagency Report 8271](#). It contains results for one first-time participant: Maxvision.
- ▷ The document also includes results for algorithms from two returning developers: Rank One Computing, and Viettel Group.
- ▷ We have replaced the probe set used in the visa-border benchmark. It was previously comprised of 80 000 images; it now has size 1 212 892 - see amended entries in Table 1. False negative identification rates have increased.
- ▷ We have added images to the probe set used in the visa-kiosk benchmark. It was previously comprised of 21 016 mates and the same number of non-mates; it now has 31 579 mates and 45 460 non-mates - see amended and entries in Table 1. False negative identification rates are improved (reduced) slightly.

2022-06-08: The 1:N track of the FRVT remains open.

- ▷ This document is the seventeenth draft update to [NIST Interagency Report 8271](#). It includes results for algorithms submitted by three first-time participants: Digidata, DiluSense Technology, and Vietnam Posts and Telecommunications Group.
- ▷ The document also includes results for algorithms from five returning developers: Canon Inc, Imagus Technology, Neurotechnology, Thales, and Samsung S1.

2022-04-28: The 1:N track of the FRVT remains open.

- ▷ This document is the sixteenth draft update to [NIST Interagency Report 8271](#). It includes results for algorithms submitted by one first-time participants: Hangzhou Allu Network Information Technology.
- ▷ The document also includes results for algorithms from three returning developers: HyperVerge Inc, Qnap Security, and Realnetworks Inc.
- ▷ The [1:N results page](#) has been updated.

2022-03-30: The 1:N track of the FRVT remains open.

- ▷ This document is the sixteenth draft update to [NIST Interagency Report 8271](#). It includes results for algorithms submitted by two first-time participants: Intellivision, and Pangiam.
- ▷ The document also includes results for algorithms from three returning developers: Fujitsu Research and Development Center, Idemia, and Gorilla Technology.
- ▷ The [1:N results page](#) has been updated.

2022-02-23: The 1:N track of the FRVT remains open.

- ▷ This document is the fifteenth draft update to [NIST Interagency Report 8271](#). It includes results for algorithms submitted by four first-time participants: Cloudwalk - Moontime Smart Technology, Decatur Industries Inc, NotionTag Technologies Private Limited, and Reveal Media Ltd.
- ▷ The document also includes results for algorithms from three returning developers: Cognitec Systems GmbH, Sensetime Group, and Viettel Group
- ▷ The [1:N results page](#) has been updated.

2022-01-20: The 1:N track of the FRVT remains open.

- ▷ This document is the fourteenth draft update to [NIST Interagency Report 8271](#). It includes results for algorithms recently submitted by two first-time participants: Daon and SQISoft.
- ▷ The document also includes results for algorithms from five returning developers: Cyberlink Corp, NEC, Neurotechnology, Paravision, and Rank One Computing.
- ▷ The [1:N results page](#) has been updated.

2021-12-16: The 1:N track of the FRVT remains open.

- ▷ This document is the thirteenth draft update to [NIST Interagency Report 8271](#). It includes results for algorithms from six returning developers: Dahua Technology, Imagus Technology, Line Corporation, N-Tech Lab, Qnap Security, and Realnetworks Inc.
- ▷ The [1:N results page](#) has been updated.

2021-11-22: The 1:N track of the FRVT remains open.

- ▷ This document is the twelfth draft update to [NIST Interagency Report 8271](#). It includes results for algorithms recently submitted by three first-time participants Clearview AI, Griaule, and Mantra Softech India.

- ▷ This document and the [1:N results page](#) also include results for algorithms from six returning developers: Acer Incorporated, Canon, Dermalog, Samsung S1, VisionLabs, and Veridas Digital Authentication.

2021-10-28: The 1:N track of the FRVT remains open.

- ▷ This document is the eleventh draft update to [NIST Interagency Report 8271](#). It includes results for algorithms recently submitted by three first-time participants (20Face, Fujitsu Research and Development Center, and Vision-Box), and five returning participants (Alchera, Gorilla Technology, Tevian, Thales-Cogent, and Visidon). Visidon
- ▷ Both the main [1:N results page](#) and the small-gallery [paperless travel page](#) have been updated.

2021-09-21: The 1:N track of the FRVT remains open. Three news items:

- ▷ This document is the tenth draft update to [NIST Interagency Report 8271](#). It includes results for algorithms recently submitted by six first-time developers: Cubox, Fincore, HyperVerge, Qnap Security, Staqu Technologies, and Tripleize (Aize, 3-ize).
- ▷ It includes results also for four returning developers: Cognitec Systems, Incode Technologies, Innovatrics, Neurotechnology, and Rank One Computing.

2021-08-02: The 1:N track of the FRVT remains open. Three news items:

- ▷ This document is the ninth draft update to [NIST Interagency Report 8271](#). It includes results for algorithms recently submitted by eight participants: Cyberlink Corp, NEC Corp, N-Tech Lab, Realnetworks Inc., Sensetime Group, Veridas Digital, Viettel Group, and Vigilant Solutions.
- ▷ Algorithms submitted since July 24 will be included in the next update scheduled for September 9, 2021.
- ▷ A new report, NIST Interagency Report 8381 - FRVT Part 7: Identification for Paperless Travel and Immigration, has been released [[PDF](#), [webpage](#)]. It documents the use of FRVT 1:N algorithms in positive access control and immigration status update travel applications where the enrolled population size is as low as 420 people for aircraft boarding, and 42 000 for an airport security line. These population sizes are much smaller than those used in the main [1:N evaluation](#). Going forward, we will update the report and webpage with results for new algorithms.

2021-07-07: The 1:N track of the FRVT remains open. One update:

- ▷ This document is the eighth draft update to [NIST Interagency Report 8271](#). It include results for an algorithm from one participant: Kakao Enterprises.

2021-06-22: The 1:N track of the FRVT remains open. Three updates:

- ▷ This is the seventh draft of the update to [NIST Interagency Report 8271](#). It includes results for algorithms from three new participants: Line Corporation, Rendip, and Samsung S1 Corp.
- ▷ We have also added results for algorithms from five returning developers: Imagus Technology, Kneron, Tevian, Visidon, and Xforward AI Technology.
- ▷ The algorithm-specific report cards (examples: [1](#), [2](#), and [3](#)) now include figures showing how low threshold values can be used to reduce candidate list lengths for human review, while (usually) elevating miss rates (FNIR) only modestly. The reports also feature some minor additions and clarifications.

2021-03-26: The 1:N track of the FRVT remains open. Three updates:

- ▷ This is the sixth draft of the update to [NIST Interagency Report 8271](#). It includes results for algorithms from three returning developers: Neurotechnology, Guangzhou Pixel Solutions, and Tech5 SA.

- ▷ We have added results on the webpage and in the report for a new ageing dataset in which border crossing photos are searched against a gallery of border crossing photos collected between 10 and 15 years prior to the mated search photos. See section 2 for a description of the images. Table 1 has a new entry describing the experiment.
- ▷ We will mostly discontinue running the mugshot ageing test, reserving it for algorithms that show high accuracy on the new border-crossing set.

2021-03-26: Regarding the fifth draft of the update to [NIST Interagency Report 8271](#):

- ▷ In addition have added results for first algorithms from two new participants: Viettel Group and Veridas Digital Authentication Solutions.
- ▷ We have added results for algorithms from two returning developers: Idemia and Cognitec Systems.
- ▷ In addition to the report, the [results page](#) and its hyperlinked [report cards](#) have been updated.

2021-02-08: Regarding the fourth draft of the update to [NIST Interagency Report 8271](#):

- ▷ We have added results for eight algorithms submitted by eight developers: Cyberlink, Dermalog, Imagus, Paravision, Sensetime, Trueface, Vigilant Solutions, and X-Forward AI. With the exception of Trueface, all of these developers have participated previously.
- ▷ We anticipate updating this report again in the first week of March 2021.
- ▷ The main [results page](#) has been revised with tabs for the investigative and lights-out identification tables, and a new tab dedicated to speed and resource consumption.
- ▷ The report cards (example [here](#)) hyperlinked from the [results page](#) have been revised to improve content and format.

2020-12-14: Regarding third draft of the update to [NIST Interagency Report 8271](#):

- ▷ We have added results for fifteen algorithms submitted by thirteen developers. The four first-time participants are: Acer, Akurat Satu Indonesia, Canon, and Xforward AI Technology. The ten returning developers are: AllGoVision, Cyberlink Corp, Dahua Technology, Deepglint, Guangzhou Pixel Solutions, IIT Vision, Innovatrics, Rank One Computing, Scanovate, Sensetime Group, Synesis, and VisionLabs.
- ▷ We have added two new datasets to the evaluation: First a set of “visa-border” photos, representing search of an airport immigration lane photo against a database of closely ISO standard portraits; second a “visa-kiosk” set representing search of a photo collected in a registered traveller kiosk against the same ISO portrait gallery. The images are described in section 2.1.
- ▷ As in previous reports, we include results for searching mugshots against a mugshot gallery containing a single image of each of 12 million people. However we have suspending running searches against a gallery in which multiple lifetime photos per person are present, because this is computationally expensive. We retain a N = 3 million search test dedicated to ageing in which mugshots taken up to 18 years after the first photograph are searched - see Table 8.
- ▷ Tables containing computational resource information, Table 2 . . . , now include duration of the finalization step, in which search algorithms can, at their option, build fast-search data structures.
- ▷ We have linked revised per-algorithm PDF report cards from the main [results page](#).
- ▷ We have regenerated all figures and tables to drop algorithms submitted before June 2018. Results for prior algorithms appear in [archived editions](#) of this report.
- ▷ Going forward, we anticipate producing more frequent updates to this report. Developers may submit one algorithm to this evaluation every four calendar months.

2020-03-24: Regarding the second draft of the update to [NIST Interagency Report 8271](#):

- ▷ Adds results for three algorithms from three developers, Dermalog, Innovatrics, and Synesis.
- ▷ Adds Table 8 on ageing showing the increase in false negative rates with time elapsed between two photos. Some of the results were contained in graphs in prior editions of this report, but the table adds results for some newly submitted algorithms.
- ▷ Adjusts frontal mugshot results (for recent and lifetime consolidated galleries) to include the effect of removing some images that should not have been included in image test sets. These images were mostly profile views, images of tattoos containing faces, images of faces on tee shirts, and images of photographs on walls behind the intended subject. This affects many tables and reduces false negative identification rates for all algorithms. The reduction is larger for “recent” enrollments than for “lifetime consolidated” ones with the consequence that accuracy on recent images is now superior.

2020-02-26: Regarding the first draft of the update to [NIST Interagency Report 8271](#):

- ▷ Adds results for 38 algorithms from 31 different developers, eleven of whom are entirely new to the 1:N track of FRVT. These are Allgovision, Cyberlink, Deepsea Tencent, Farbar F8, Imperial College London, Intsys MSU, Kedacom, Kneron, Pixelall, and Scanovate.

DISCLAIMER

Specific hardware and software products identified in this report were used in order to perform the evaluations described in this document. In no case does identification of any commercial product, trade name, or vendor, imply recommendation or endorsement by the National Institute of Standards and Technology, nor does it imply that the products and equipment identified are necessarily the best available for the purpose.

INSTITUTIONAL REVIEW BOARD

The National Institute of Standards and Technology's Research Protections Office reviewed the protocol for this project and determined it is not human subjects research as defined in Department of Commerce Regulations, 15 CFR 27, also known as the Common Rule for the Protection of Human Subjects (45 CFR 46, Subpart A).

ACKNOWLEDGMENTS

The authors are grateful for the support and collaboration of the the Department of Homeland Security's Science & Technology Directorate (S&T), Office of Biometric Identity Management (OBIM), and Customs and Border Protection (CBP).

Additionally, the authors are grateful to staff in the NIST Biometrics Research Laboratory for infrastructure supporting rapid evaluation of algorithms.

Executive Summary

This document is a draft revision of the September 2019 report [NIST Interagency Report 8271](#). That report gave extensive documentation of face recognition applied to mugshots. This report extends that by adding more two more challenging datasets containing images with serious departures from canonical frontal image standards. The report also adds results for algorithms submitted to NIST since in 2019 and 2020. The algorithms, which implement one-to-many identification of faces appearing in two-dimensional images, are prototypes from the research and development laboratories of mostly commercial suppliers, and are submitted to NIST as compiled black-box libraries implementing a NIST-specified C++ test interface. The report therefore does not describe how algorithms operate. The report lists accuracy results alongside developer names and will therefore be useful for comparison of face recognition algorithms and assessment of absolute capability. The report is accompanied by a [webpage](#) with sortable results.

The evaluation uses six datasets: frontal mugshots, profile view mugshots, desktop webcam photos, visa-like immigration application photos, immigration lane photos, and registered traveler kiosk photos. These datasets are sequestered at NIST, meaning that developers do not have access to them for training or testing. This aspect is important because face recognition algorithms are very often deployed without the developer having access to the customers image data. A possible exception to this would be in a cloud-based application where the operational image data is uploaded to a cloud operated by a face recognition developer.

The major result in NIST IR 8271 was that massive gains in accuracy have been achieved in the years 2013 to 2018 and these far exceed improvements made in the prior period, 2010 to 2013. While the industry gains were broad - at least 30 developers' algorithms outperformed the most accurate algorithm from late 2013, there remains a wide range of capability. While this report shows accuracy gains only over the period 2018-2020, the most accurate algorithm reported here is substantially more accurate than anything reported in NIST IR 8271. This is evidence that face recognition development continues apace, and that FRVT reports are but a snapshot of contemporary capability.

From discussion with developers, the accuracy gains stem from the adoption of deep convolutional neural networks. As such, face recognition has undergone an industrial revolution, with algorithms increasingly tolerant of poorly illuminated and other low quality images, and poorly posed subjects. One related result is that a few algorithms correctly match side-view photographs to galleries of frontal photos, with search accuracy approaching that of the best c. 2010 algorithms operating on purely frontal images. The capability to recognize under a 90-degree change in viewpoint - pose invariance - has been a long-sought milestone in face recognition research.

With good quality portrait photos, the most accurate algorithms will find matching entries, when present, in galleries containing 12 million individuals, with rank one miss rates of approaching 0.1%. The remaining errors are in large part attributable to long-run ageing, facial injury and poor image quality. Given this impressive achievement - close to perfect recognition - an advocate might claim that cooperative face recognition is a solved problem, a statement that can be refuted with the following context and caveats:

- ▷ **Mugshots vs. less constrained captures:** The low error rates reported here are attained using mostly excellent cooperative live-capture mugshot images collected with an attendant present. Recognition in other circumstances, particularly those without a dedicated photographic environment and human or automated quality control checks, will lead to declines in accuracy. This is documented here for side-view images, poorer quality webcam images, and, particularly, for newly introduced ATM-style kiosk photos that were not originally intended for automated face recognition. In this case, recognition error rates are much higher, often in excess of 20% even with the more accurate algorithms which variously remain intolerant of face cropping (at image edge) and of large downward head pitch.
- ▷ **Algorithm accuracy spectrum:** Recognition accuracy is very strongly dependent on the algorithm and, more

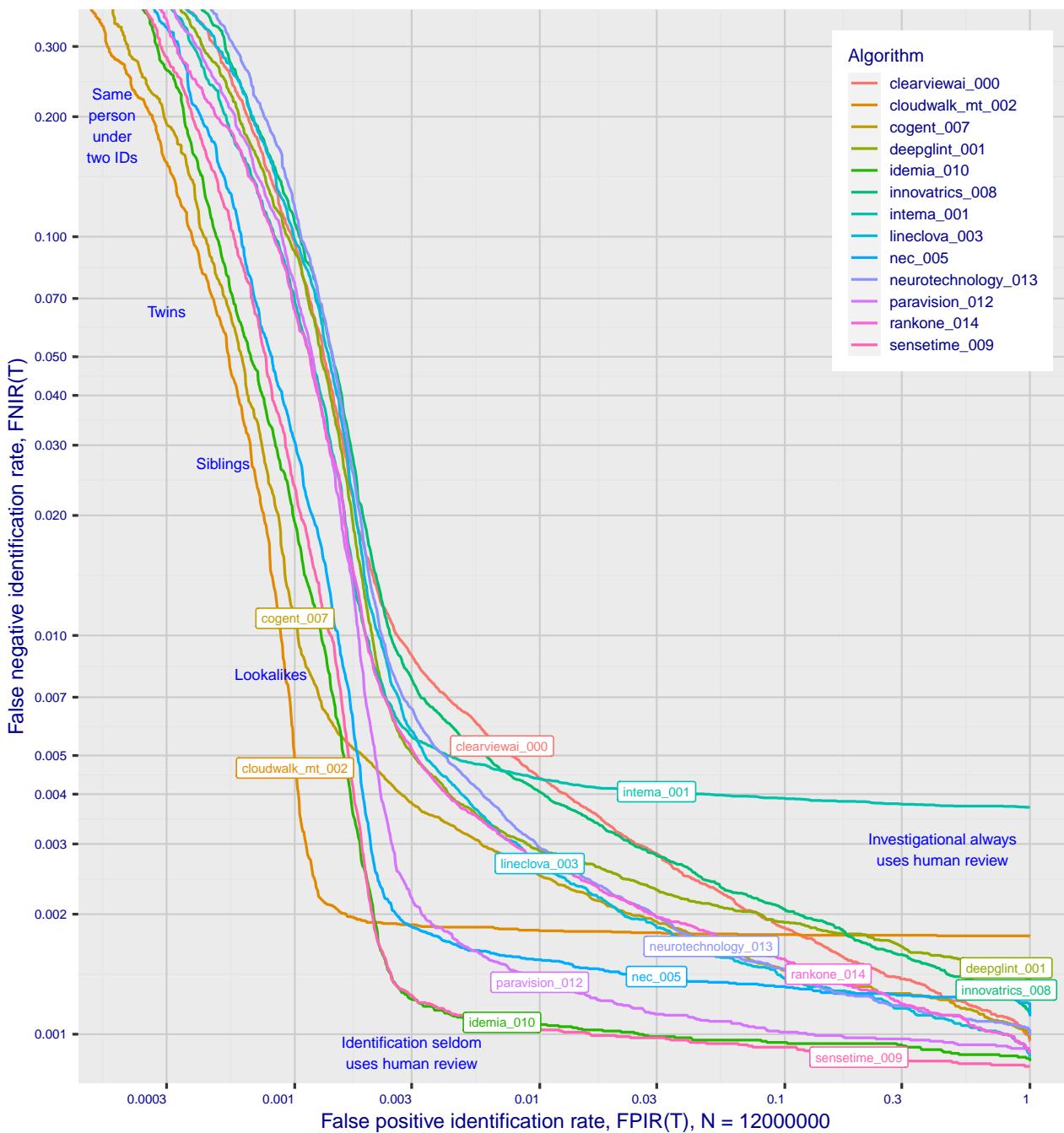


Figure 1: Identification miss rates across the false positive range. N = 12 million individuals are enrolled with one recent image.

generally, on the developer of the algorithm. False negative error rates in a particular scenario range from a few tenths of one percent to beyond fifty percent. This is tabulated exhaustively later: For example Table 12 shows accuracy across datasets. Figure 1 here compares algorithms on mugshot searches in a consolidated gallery of 12 million subjects and 12 million photos. Many algorithms do not achieve the low error rates noted above, and while many of those may still be useful and valuable to end-users, only the most accurate excel on poor quality images and those collected long after the initial enrollment sample.

▷ **Versioning:** While results for up to ten algorithms from each developer are reported here, the intra-provider

accuracy variations are usually smaller than the inter-provider variations. That said different versions give an order of magnitude fewer misses. Some developers demonstrate speed-accuracy tradeoffs¹. See Figs. 18, 19.

- ▷ **Low similarity scores:** In thousands of mugshot cases the correct gallery image is returned at rank 1 but its similarity score is nevertheless low, below some operationally required score threshold. This is not so important when face recognition is used for “lead generation” in investigational applications because human reviewers are specifically required to review potentially long candidate lists and the threshold is effectively 0. In applications where search volumes are higher and labor is not available to review the results from searches, a higher threshold must be applied. This reduces the length of candidate lists and false positive identification rates at the expense of increased false negative miss rates. The tradeoff between the two error rates is reported extensively later.
- ▷ **Population size:** As the number of enrolled subjects grows, some mates are displaced from rank one, decreasing accuracy. As tabulated later for N up to 12 million, false negative rates generally rise slowly with population size. This enables use of face recognition in very large populations. However in most positive and negative identification applications², a score threshold is set to limit the rate at which non-mate searches produce false positives. This has the consequence that some mated searches will report the mate below threshold, i.e. a miss, even if it is at rank 1. The utility of this is that many non-mated searches will return no candidate identities at all. As the error-tradeoff characteristic shows, investigational miss rates on the right side are very low but then rise steadily (in the center region) as threshold is increased to support “lights-out” applications, and ultimately rise quickly (left side) as discussed below. Thus, if we demand that just one in one thousand non-mate searches produce any false positives, the most accurate algorithms there (Sensetime-004 and NEC-3) would fail on between 3 and 5% of mated searches. Even though the graph shows results for the most accurate algorithms, all but two would fail to find the mate in more than 8% of mated searches. While the two most accurate algorithms produce a relatively flat error tradeoff until the threshold is raised to limit false positives to about 1 in 400 non-mated searches³.

Thereafter, as the threshold is raised to further reduce false positives, miss rates rise rapidly. This means that low false positive identification rates are inaccessible with these algorithms, a result that does not apply for ten-finger identification algorithms. The rapid rise occurs because the lower mate scores are mixed with very high non-mate scores, the low scores from poor image quality and ageing, the high non-mates from the presence of lookalikes persons (doppelgangers), twins (discussed next) and, ultimately, the presence of a few unconsolidated subjects i.e. persons present under multiple IDs.

- ▷ **False negatives from ageing:** A large source of error in long-run applications where subjects are not re-enrolled on a set schedule is ageing. Changes in facial appearance increase with the time elapsed between photographs. These will depress similarity scores and eventually cause false negatives. All faces age and while this usually proceeds in a graceful and progressive manner, drug use can accelerate this [28]. Elective surgery may be effective in delaying it although this has not been formally quantified with face recognition. As ageing is essentially unavoidable, it can only be mitigated by scheduled re-capture, as in passport re-issuance. To quantify ageing effects, we used the more accurate algorithms to enroll the earliest image of 3.1 million adults and then search

¹For example, NEC-0 prepares templates much faster than NEC-2 but gives twenty times more misses. Dermalog-5 executes a template search much more quickly than Dermalog-6 but is also much less accurate.

²In a positive identification application such as a registered traveler system, a user is making an implicit claim to be enrolled in the system - most users will be. In a negative application, such as with deportees, the implicit claim is that the subject is not enrolled - most will not be.

³The gallery size here is 12 million people, one image per person. Given 331 201 non-mated searches, an exhaustive implementation of one-too-many search would execute almost 4 trillion comparisons. At a false positive identification rate of 0.0025 the number of false positives is, to first order, 828 corresponding to single-comparison false match rate of $828 / 4 \text{ trillion} = 2.1 \times 10^{-10}$ i.e. about 1 in 5 billion. Strictly this FMR computation is meaningful only for algorithms that implement 1:N search using N 1:1 comparisons, which is not always the case.

with 10.3 million newer photos taken up to 18 years after the the initial enrollment photo. Figure 2 puts ageing into context by contrasting it with the increase in false negatives that occurs when the number of individuals in an enrollment database becomes larger and the chance of a false positive increases such that higher thresholds may become necessary⁴.

The Figure shows, from top to bottom, increases in false negative identification rates (FNIR) with the algorithm being tested. This applies to increases due to N on the left side, and increases due to ageing on the right side. The relative spacing of the dots shows that for all algorithms the dependency of FNIR on N (up to 12 million) is considerably less than on ΔT (up to 18 years). The figure additionally shows the most accurate nine algorithms for each year in which they were submitted, limiting to only one per developer.

In the inset table, accuracy is seen to degrade progressively with time, as mate scores decline and non-mates displace mates from rank 1 position. More accurate algorithms tend to be less sensitive to ageing. The more accurate algorithms give fewer errors after 18 years of ageing than middle tier algorithms give after four. Note also we do not quantify an ageing rate - more formal methods [2] borrowed from the longitudinal analysis literature have been published for doing so (given suitable repeated measures data).

See Figures 60, 91 and 106.

⁴Some algorithms implement strategies to automatically adjust scores to account for increased population size. This relieves the system owner of having to increase thresholds as N increases.

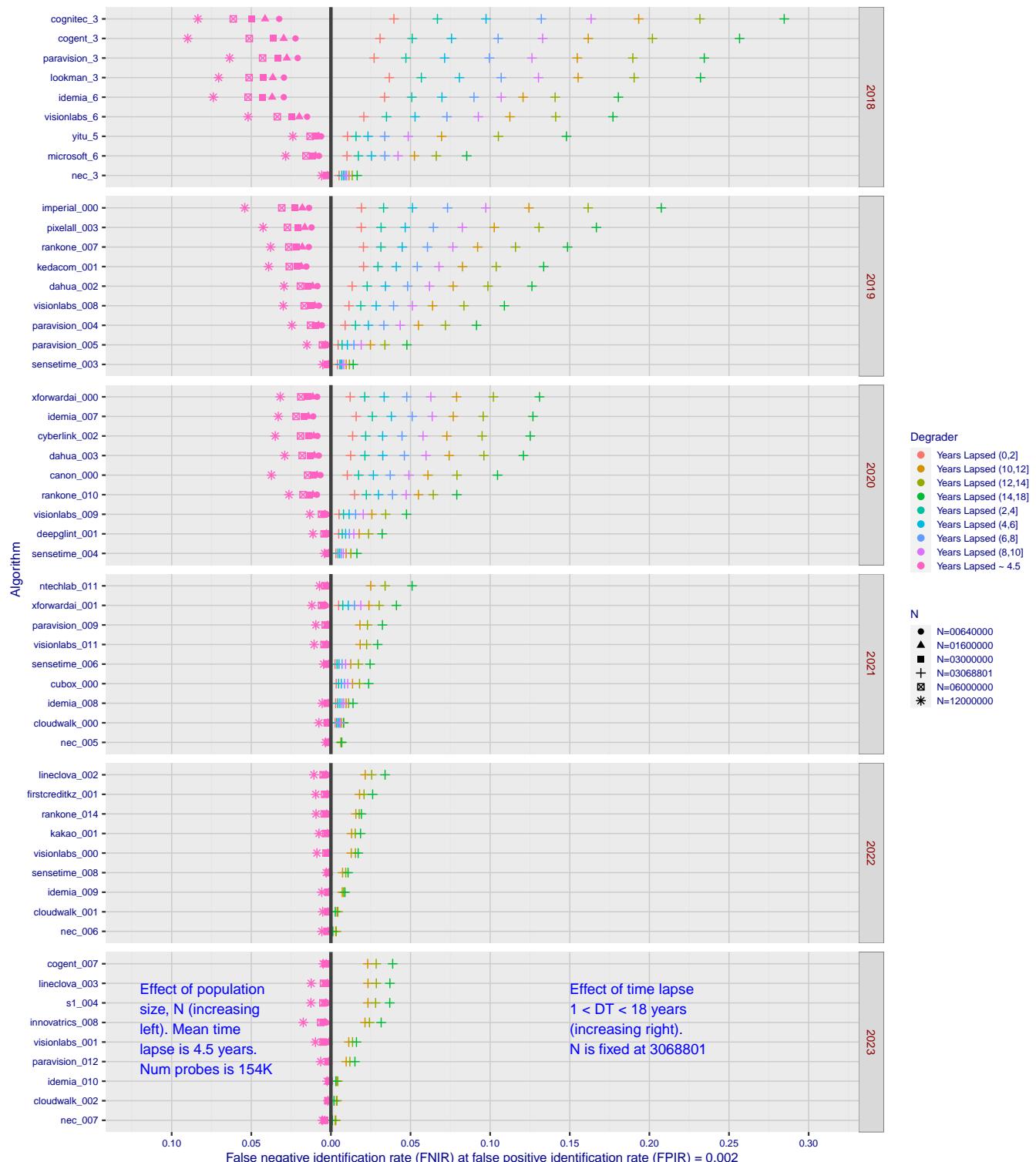


Figure 2: Identification miss rates as a function of enrolled population size, N , and time-lapse, ΔT .

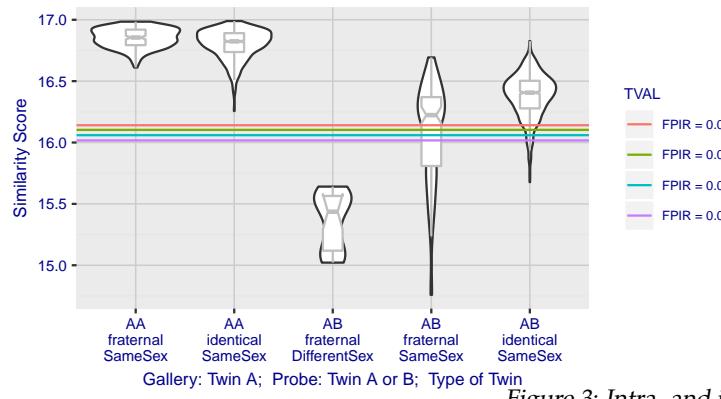


Figure 3: Intra- and inter-twin scores

▷ **False positives from twins:** By enrolling 640 000 mugshots, adding photos of one twin, and then searching photos of those subjects and their twin the inset figure shows, for one typical algorithm, the similarity is generally greater when searching twins against themselves (A) than when searching twins against their sibling (B) but very often still above even stringent thresholds i.e. those corresponding to one in one thousand searches producing a false positive. Thus twins will very often produce a high-scoring non-match on a candidate list and a false alarm in an online identification system. The plot of Fig. 3 shows that fraternal twins are sometimes correctly rejected at those thresholds - including most different sex twins (at center). Figure ?? shows substantially similar behavior for all algorithms tested. In an investigative search, a twin would typically appear at rank 1, or rank 2 if their sibling happened to also be the gallery. Twins (and triplets etc.) constituted 3.3% of all live births [17] in recent years⁵, and because that number is higher today than when the individuals in current adult databases were born, the false positives that arise from twins are now, and will increasingly be, an operational problem. Relative to the United States, twins are born with considerable regional variation. For example they are much less common in East Asia, and much more common in Sub-Saharan Africa [21].

The presence of twins in the mugshot database is inevitable given its size, around 12.3 million people. As this is not an insignificant sample of the domestic United States population, people with other familial ties will be present also. The data was collected over an extended period and because location information is not available, we are unable to estimate the proportion of the domestic population that is present in the dataset. However, if we assume twins are neither more or less disposed to arrest than the general population, we can estimate that hundreds of thousands of individuals in the dataset are twins. This will affect false positive rates because we randomly set aside 331 201 individuals for nonmate searches, and some proportion of those will be twins with siblings in the gallery.

▷ **Database integrity:** An operational error rate should be added to all false negative rates in this report reflecting the proportion of images in a real database that are un-matchable. Such anomalies arise from images that: do not contain a face; include multiple persons; cannot be decoded; are rotated by 90° or 180°; depict a face on clothing; and others introduced by a long tail of various clerical errors. While the mugshot trials in this report have been constructed to minimize such effects, they are a real problem in actual operations.

This report is being updated continuously as new algorithms are submitted to FRVT, and run on new datasets. Participation in the [one-to-many identification track](#) is independent of participation in the [one-to-one verification track](#) of FRVT.

⁵See the CDC's National Vital Statistics Report for 2017: https://www.cdc.gov/nchs/data/nvsr/nvsr67/nvsr67_08-508.pdf

Scope and Context

Audience: This report is intended for developers, integrators, end users, policy makers and others who have some familiarity with biometrics applications. The methods and metrics documented here will be of interest to organizations engaged in tests of face recognition algorithms. Some of these have been incorporated in the ISO/IEC 19795 Part 1 Biometric Testing and Reporting Framework standard, now nearing publication.

Prior benchmarks: Automated face recognition accuracy has improved massively in the two decades since initial commercialization of the various technologies. NIST has tracked that improvement through its conduct of regular independent, free, open, and public evaluations. These have fostered improvements in the state of the art. This report serves as an update to the [NIST Interagency Report 8271](#) on performance of face identification algorithms, published in September 2019.

Demographics: In December 2019, NIST published a first report on demographic dependencies in face recognition, [NIST Interagency Report 8280](#) that documented age, sex and race differentials in one-to-one and one-to-many false positive and false negative rates.

Scope: NIST IR 8271 documented recognition results for four databases containing in excess of 30.2 million still photographs of 14.4 million individuals. That constituted the largest public and independent evaluation of face recognition ever conducted. It includes results for accuracy, speed, investigative vs. identification applications, scalability to large populations, use of multiple images per person, images of cooperative and non-cooperative subjects.

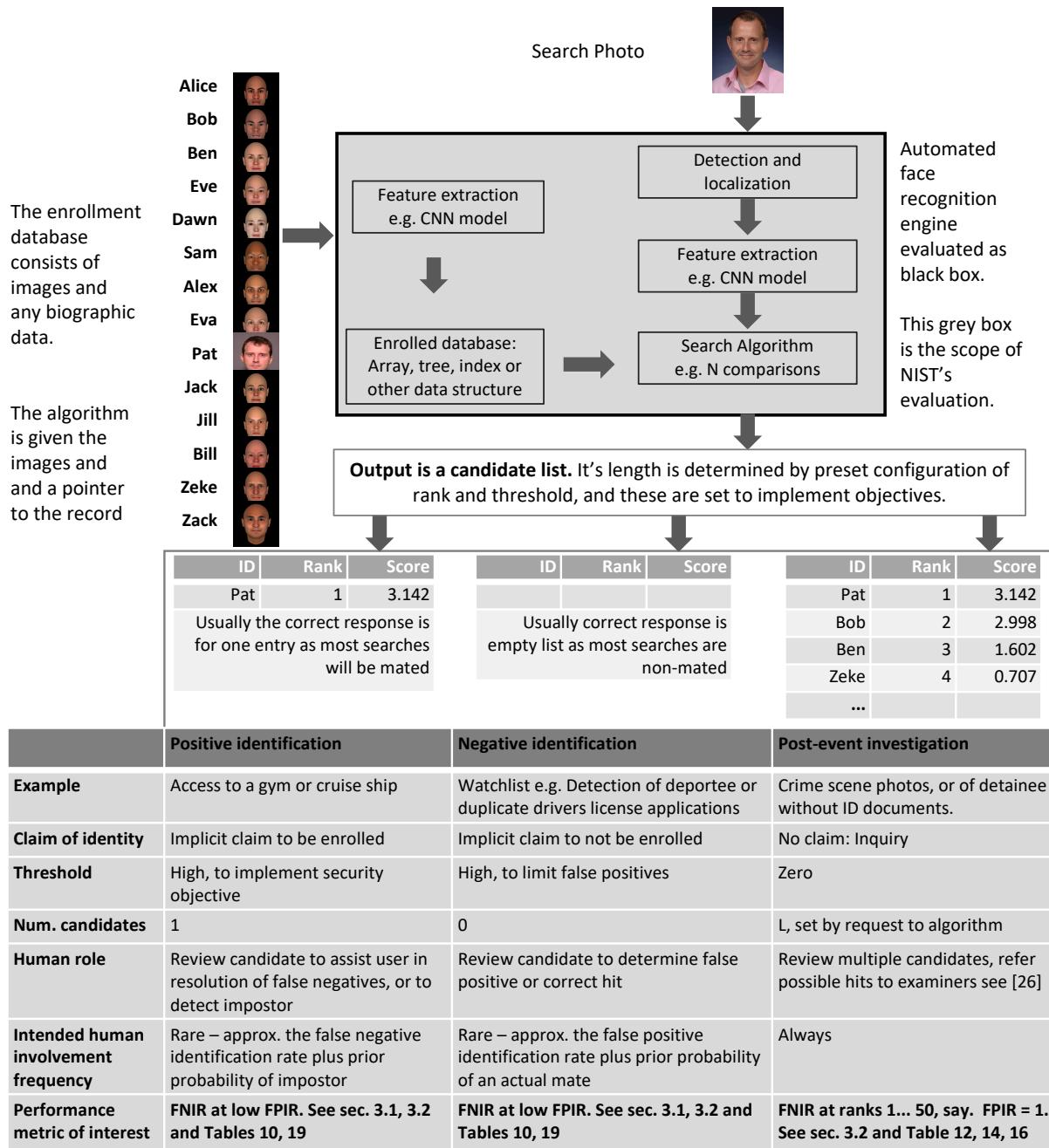
The report also includes results for ageing, recognition of twins, and recognition of profile-view images against frontal galleries. It otherwise does not address causes of recognition failure, neither image-specific problems nor subject-specific factors including demographics. Separate reports on demographic dependencies in face recognition will be published in the future. Additionally out of scope are: performance of live [human-in-the-loop transactional systems](#) like automated border control gates; human recognition accuracy as used in forensic applications; and recognition of persons in video sequences (which NIST evaluated separately [9]). Some of those applications share core matching technologies that *are* tested in this report.

Images: Five kinds of images are employed; these are either compared with images of the same kind, or against others from different capture environments as follows. The primary dataset is a set of law enforcement mugshot images (Fig. 5) which are enrolled and then searched with three kinds of images: other mugshots (i.e. within-domain); profile-view photographs (90 degree cross-view); and lower quality webcam images (Fig. 6) collected in similar detention operations (cross-domain). Additionally we compare high quality visa-like photos collected in immigration offices, with: medium quality border crossing images collected in primary immigration lanes; poor quality images collected in ATM-like registered traveller kiosks.

Participation and industry coverage: The report includes performance figures for prototype algorithms from the research laboratories of commercial developers and a few universities. This represents a substantial majority of the face recognition industry, but only a tiny minority of the academic community. Participation was open worldwide. While there is no charge for participation, developers incur some software engineering expense in implementing their algorithms behind the NIST application programming interface (API). The test is a black-box test where the function of the algorithm, and the intellectual property associated with it, is hidden inside pre-compiled libraries.

Recent technology development: Most face recognition research with deep convolutional neural networks (CNNs) has been aimed at achieving invariance to pose, illumination and expression variations that characterize photojournalism and social media images. The initial research [18, 22] employed large numbers of images of relatively few ($\sim 10^4$) individuals to learn invariance. Inevitably much larger populations ($\sim 10^7$) were employed for training [11, 20] but the benchmark, Labeled Faces in the Wild with (essentially) an equal error rate metric [12], represents an easy task,

one-to-one verification at very high false match rates. While a larger scale identification benchmark duly followed, Megaface [15], its primary metric, rank one hit rate, contrasts with the high threshold discrimination task required in most large-population applications of face recognition, namely credential de-duplication, and background checks. There, identification in galleries containing up to 10^8 individuals must be performed using a) very few images per individual and b) stringent thresholds to afford very low false positive identification rates. This track of FRVT was launched to measure the capability of the new technologies, including in these two cases. FRVT has included open-set identification tests since 2002, reporting both false negative and positive identification rates [7].



Performance metrics for applications: This report documents the performance of one-to-many face recognition algorithms. The word "performance" here refers to recognition accuracy and computational resource usage, as measured

by executing those algorithms on massive sequestered datasets.

This report includes extensive tabulation of recognition error rates germane to the main use-cases for face search technology. The Figure below, inspired by the Figure 1 in [23] differentiates different applications of the technolgy. The last row directs readers to the main tables relevant to those applications, respectively threshold-based and rank-based metrics that are special cases of the metrics given in section 3. The terms negative identification and positive identification are taken from the ISO/IEC 2382-37:2017 standardized biometrics vocabulary.

The algorithms are specifically configured for these applications by setting thresholds and candidate list lengths. Both rank-based metrics and threshold-based metrics include tradeoffs. In investigation, overall accuracy will be reduced if labor is only available to review a few candidates from the automated system. Note that when a fixed number of candidates are returned, the false positive identification rate of the automated face recognition engine will be 100%, because a probe image of anyone not enrolled will still return candidates. In identification applications where false positives must be limited to satisfy reviewer labor availability or a security objective, higher false negative rates are implied. This report includes extensive quantification of this threshold-based tradeoff.

See Sec. 3

Template diversity: The FRVT is designed to evaluate black-box technologies with the consequence that the templates that hold features extracted from face images are entirely proprietary opaque binary data that embed considerable intellectual property of the developer. Despite migration to CNN-based technologies there is no consensus on the optimal feature vector dimension. This is evidenced by template sizes ranging from below 100 bytes to more than four kilobytes. This diversity of approaches, suggests there is no prospect of a standard template something that would require a common feature set to be extracted from faces. Interoperability in automated face recognition remains solidly based on images and documentary standards for those, in particular the ICAO portrait [27] specification deriving from the ISO/IEC 19794-5 Token frontal [24] standard, which are similar to certain ANSI/NIST Type 10 [26] formats.

Training: The algorithms submitted to NIST have been developed using image datasets that developers do not disclose. The development will often include application of machine learning techniques and will additionally involve iterative training and testing cycles. NIST itself does not perform any training and does not refine or alter the algorithm in any way. Thus the model, data files, and libraries that define an algorithm are fixed for the duration of the tests. This reflects typical operational reality where recognition software, once installed, is fixed and constant until upgraded. This situation persists because on-site training of algorithms on customer data is atypical essentially because training is not a turnkey process.

Automated search and human review: Virtually all applications using automated face search require human review of the outputs at some frequency: Always for investigational applications; rarely in positive identification applications, after rejection (false or otherwise); and rarely in negative identification applications, after an alarm (false or otherwise). The human role is usually to compare a reference image with the query image or the live-subject if present, to render either a definitive decision on “exclusion” (different subjects), or “identification” (same subject), or a declaration that one or both images have “no value” and that no decision can be made. Note that automated face recognition algorithms are not built to do exclusion - low scores from a face comparison arise from different faces *and* poor quality images of the same face.

Human reviewers make recognition errors [5, 19, 25] and are sensitive to image acquisition and quality. Accurate human review is supported by high resolution - as specified in the Type 50, 51 acquisition profiles of the ANSI/NIST Type 10 record [26], and by multiple non-frontal views as specified in the same standard. These often afford views of the ear. Organizations involved in image collection should consider supporting human adjudication by collecting high-resolution frontal and non-frontal views, preparing low resolution versions for automated face recognition [24], and retaining both for any subsequent resolution of candidate matches. Along these lines, the ISO/IEC Joint Technical

Committee 1 subcommittee 37 on biometrics has just initiated projects on image quality assessment and face-aware capture.

Release Notes

FRVT Activities: Since February 2017, NIST has been evaluating one-to-one verification algorithms on an ongoing basis. NIST then restarted FRVT's one-to-many track in February 2018, inviting participants to send up to prototype algorithms. Both tracks allows developers to submit updated algorithms to NIST at any time but no more frequently than four calendar months. This more closely aligns development and evaluation schedules. Results are posted to the web within a few weeks of submission. Details and full report are linked from the [Ongoing FRVT site](#).

FRVT Reports: The results of the FRVT appear in the series NIST Interagency Reports tabulated below. The reports were developed separately and released on different schedules. In prior years NIST has mostly reported FRVT results as a single report; this had the disadvantage that results from completed sub-studies were not published until all other studies were complete.

Date	Link	Title	No.
2014-03-20	PDF	FRVT Performance of Automated Age Estimation Algorithms	7995
2015-04-20	PDF	Face Recognition Vendor Test (FRVT) Performance of Automated Gender Classification Algorithms	8052
2014-05-21	PDF	FRVT Performance of face identification algorithms	8009
2017-03-07	PDF	Face In Video Evaluation (FIVE) Face Recognition of Non-Cooperative Subjects	8173
2017-11-23	PDF	The 2017 IARPA Face Recognition Prize Challenge (FRPC)	8197
2018-11-27	PDF	Face Recognition Vendor Test - Part 2: Identification	8271
2019-09-11	PDF	Face Recognition Vendor Test - Part 2: Identification	8271
2019-12-11	PDF	Face Recognition Vendor Test - Part 3: Demographic Effects	8280
2020-01-03	WWW	Face Recognition Vendor Test (FRVT) - Part 1 Verification	Draft

Details appear on pages linked from <https://www.nist.gov/programs-projects/face-projects>.

Appendices: This report is accompanied by appendices which present exhaustive results on a per-algorithm basis. These are machine-generated and are included because the authors believe that visualization of such data is broadly informative and vital to understanding the context of the report.

Typesetting: Virtually all of the tabulated content in this report was produced automatically. This involved the use of scripting tools to generate directly type-settable L^AT_EX content. This improves timeliness, flexibility, maintainability, and reduces transcription errors.

Graphics: Many of the Figures in this report were produced using the **ggplot2** package running under **R**, the capabilities of which extend beyond those evident in this document.

Contents

Release Notes	1
Disclaimer	6
Institutional Review Board	6
Acknowledgments	6
Executive Summary	7
Scope and Context	13
Release Notes	17
1 Introduction	19
2 Evaluation datasets	20
3 Performance metrics	26
4 Results	42
Appendices	86
A Accuracy on large-population FRVT 2018 mugshots	86
B Effect of time-lapse: Accuracy after face ageing	131
C Effect of enrolling multiple images	209
D Accuracy with poor quality webcam images	216
E Accuracy for profile-view to frontal recognition	226
F Search duration	230
G Gallery Insertion Timing	264

1 Introduction

One-to-many identification represents the largest market for face recognition technology. Algorithms are used across the world in a diverse range of biometric applications: detection of duplicates in databases, detection of fraudulent applications for credentials such as passports and driving licenses, token-less access control, surveillance, social media tagging, lookalike discovery, criminal investigation, and forensic clustering.

This report contains a breadth of performance measurements relevant to many applications. Performance here refers to accuracy and resource consumption. In most applications, the core accuracy of a facial recognition algorithm is the most important performance variable. Resource consumption will be important also as it drives the amount of hardware, power, and cooling necessary to accommodate high volume workflows. Algorithms consume processing time, they require computer memory, and their static template data requires storage space. This report documents these variables.

1.1 Open-set searches

FRVT tested open-set identification algorithms. Real-world applications are almost always “open-set”, meaning that some searches have an enrolled mate, but some do not. For example, some subjects have truly not been issued a visa or drivers license before; some law enforcement searches are from first-time arrestees⁶. In an “open-set” application, algorithms make no prior assumption about whether or not to return a high-scoring result, and for a mated search, the ideal behaviour is that the search produces the correct mate at high score and first rank. For a non-mate search, the ideal behavior is that the search produces zero high-scoring candidates.

Many academic benchmarks execute only closed-set searches. The proportion of mates found in the rank one position is the default accuracy metric. This hit rate metric ignores the score with which a mate is found; weak hits count as much as strong hits. This ignores the real-world imperative that in many applications it is necessary to elevate a threshold to reduce the number of false positives.

⁶Operationally closed-set applications are rare because it is usually not the case that all searches have an enrolled mate. One counter-example, however, is a cruise ship in which all passengers are enrolled and all searches should produce exactly one identity. Another example is forensic identification of dental records from an aircraft crash.

2 Evaluation datasets

This report documents accuracy for four kinds of images - mugshots, webcam, profiles and wild - as described in the following sections.

2.1 Immigration-related images

This report includes benchmark tests sharing a common enrollment of high quality frontal portrait images collected while subject make applications for various immigration benefits. We then search that with two kinds of images, webcam images collected during in-bound immigration and also images collected from registered travelers using a ATM-style kiosk. These are described below and depicted in Figure 4.



Figure 4: Example photos.

- ▷ **Application reference photos:** The images are collected in an attended interview setting using dedicated capture equipment and lighting. The images, at size 300x300 pixels, are smaller than normally indicated by ISO. The images are all high-quality frontal portraits collected in immigration offices and with a white background. As such, potential quality related drivers of high false match rates (such as blur) can be expected to be absent. The images are encoded as ISO/IEC 10918-1 i.e. JPEG. Older images had a compression ration of about 16:1, while newer images, since 2010, are more lightly compressed at 4:1. When these images are provided as input into the algorithm, they are labeled with the type "iso". This report enrols 1 600 000 application images, one per person.
- ▷ **Border crossing photos:** Most images are have width 320 and height 240 pixels. They are JPEG compressed at 16:1 i.e. filesize just below 15KB. The images present challenges for face recognition in that subjects often exhibit non-zero yaw and pitch (associated with the rotational degrees of freedom of the camera mount), low contrast (due to varying and intense background lights), and poor spatial resolution (due to inexpensive cameras). There are often subjects standing in the background, usually at very low resolution (see Figure 4b). In such cases, algorithms should detect all faces and determine which is the largest and most centered. When these images are provided as input into the algorithm, they are labeled with the type "wild".
- ▷ **Kiosk photos:** These photos were collected from subjects whose attention was focused on interaction with an immigration kiosk. They images were not intended for use with automated face recognition. The camera is situated above a display which the user touches, and is triggered either without directing the subject to look at it, or without waiting for the subject to comply. The images are therefore characterized by pitch-down pose, sometimes exceeding 45 degrees, as in Figure 4c. Yaw-angle variation is mild, with most images close to frontal. The images

have width 320 pixels and height 240 pixels and therefore tall individuals are sometimes cropped. This is often just above the eyes and can occur at the nose or mouth. Conversely, short individuals are sometimes cropped such that only the top part of the face is visible. In a quite small number of cases, there other subjects standing just behind the primary subject such that algorithms should detect all faces and determine which is the largest and most centered. Background ceiling lighting is often visible and this sometimes leads to under-exposure of the face. When these images are provided as input into the algorithm, they are labeled with the type "wild".

2.2 Law enforcement images

The main mugshot dataset used is referred to as the FRVT 2018 set. This set was collected over the period 2002 to 2017 in routine United States law enforcement operations. This set yields three subsets

- ▷ **Mugshots:** Mugshots comprise about 86% of the database. They have reasonable compliance with the ANSI/NIST ITL1-2011 Type 10 standard's subject acquisition profiles levels 10-20 for frontal images [26]. The most common departure from the standard's requirements is the presence of mild pose variations around frontal - the images of Figure 5 are typical. The images vary in size, with many being 480x600 pixels with JPEG compression applied to produce filesizes of between 18 and 36KB with many images outside this range, implying that about 0.5 bits are being encoded per pixel. When these images are provided as input into the algorithm, they are labeled with the type "mugshot".

Example images appear in Fig. 5

[NIST Interagency Report 8238](#) includes a comparison of this set of mugshots with the smaller and easier sets of mugshots used in tests run in 2010 and 2014.

- ▷ **Profile images:** Profile-view images have been collected in law enforcement for more than 100 years, as human capability is improved with orthogonal information. The profile images used in this report were collected during the same session as the frontal mugshot photograph, in the same standardized photographic setup. These would not therefore be used with automated face recognition. A small subset, 200 000 images, were set aside for testing. When these images are provided as input into the algorithm, they are labeled with the type "wild".

Example images appear in Fig. 7

- ▷ **Webcam images:** The remaining 14% of the images were collected using an inexpensive webcam attached to a flexible operator-directed mount. These images are all of size 240x240 pixels, that are in considerable violation of most quality-related clauses of all face recognition standards. As evident in the figure, the most common defects are non-frontal pose (associated with the rotational degrees of freedom of the camera mount), low contrast (due to varying and intense background lights), and poor spatial resolution (due to inexpensive camera optics) - see examples in Fig 6. The images are overly JPEG compressed, to between 4 and 7KB, implying that only 0.5 to 1 bits are being encoded per color pixel. When these images are provided as input into the algorithm, they are labeled with the type "wild".

Example images appear in Fig. 6

These are drawn from NIST Special Database 32 which may be downloaded [here](#).

These images were partitioned in galleries and probesets for the various experiment listed in Table 1.

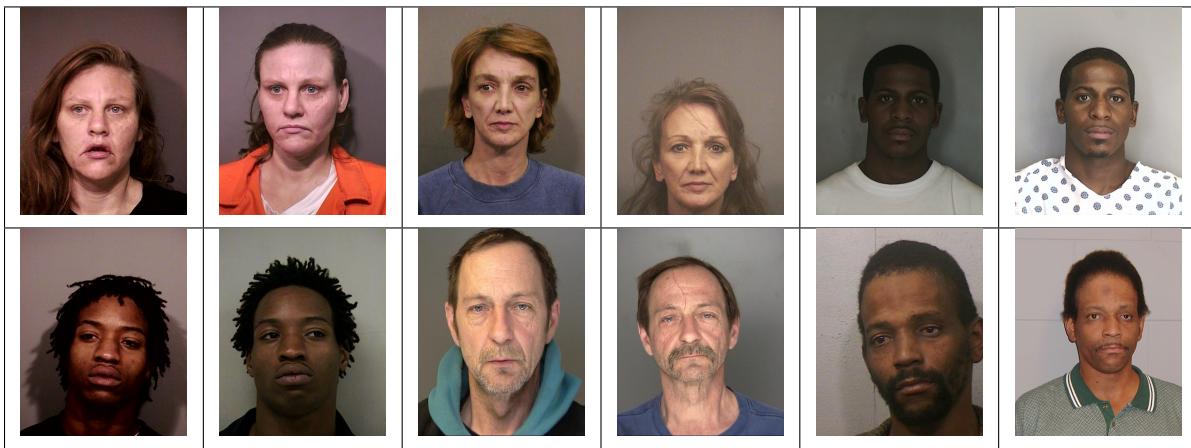


Figure 5: Six mated mugshot pairs representative of the FRVT-2014 (LEO) and FRVT-2018 datasets. The images are collected live, i.e. not scanned from paper. Image source: NIST Special Database 32 the Multiple Encounter Deceased Subjects dataset.



Figure 6: Twelve webcam images representative of probes against the FRVT-2018 mugshot gallery. The first eight images are four mated pairs. Such images present challenges to recognition including pose, non-uniform illumination, low contrast, compression, cropping, and low spatial sampling rate. Image source: NIST Special Database 32 the Multiple Encounter Deceased Subjects dataset.



Figure 7: **[Profile views]** The three images are a frontal enrollment, subsequent frontal probe, and same-session ninety degree profile view. While collection of both frontal and profile views has been typical in law enforcement for more than a century, the recognition of profile to frontal views has essentially been impossible. However, reasonably high accuracy results is now possible - see section E.

Image				
Encounter	1	...	$K_i - 1$	K_i
Capture Time	T_1	...	$T_{K_i - 1}$	T_{K_i}
Role RECENT	Not used	Not used	Enrolled	Search
Role LIFETIME	Enrolled	Enrolled	Enrolled	Search

Figure 8: Depiction of the “recent” and “lifetime” enrollment types. Image source: NIST Special Database 32

2.3 Enrollment strategies

Many operational applications include collection and enrollment of biometric data from subjects on more than one occasion. This might be done on a regular basis, as might occur in credential (re-)issuance, or irregularly, as might happen in a criminal recidivist situation [4]. The number of images per person will depend on the application area. In civil identity credentialing (e.g. passports, driver’s licenses), the images will be acquired approximately uniformly over time (e.g. ten years for a passport). While the distribution of dates for such images of a person might be assumed uniform, a number of factors might undermine this assumption⁷. In criminal applications, the number of images would depend on the number of arrests. The distribution of dates for arrest records for a person (i.e. the recidivism distribution) has been modeled using the exponential distribution but is recognized to be more complicated⁸.

In any case, the 2010 NIST evaluation of face recognition showed that considerable accuracy benefits accrue with retention and use of *all* historical images [6].

To this end, the FRVT API document provides $K \geq 1$ images of an individual to the enrollment software. The software is tasked with producing a single proprietary undocumented “black-box” template⁹ from the K images. This affords the algorithm an ability to generate a *model* of the individual, rather than to simply extract features from each image on a sequential basis.

As depicted in Figure 8, the i -th individual in the FRVT 2018 dataset has K_i images. These are labelled as x_k for $k = 1 \dots K_i$ in chronological order of capture date. To measure the utility of having multiple enrollment images, this report evaluates three kinds of enrollment:

- ▷ **Recent:** Only the second most recent image, $x_{K_i - 1}$ is enrolled. This strategy of enrollment mimics the operational policy of retaining the imagery from the most recent encounter. This might be done operationally to ameliorate the effects of face ageing. Obviously retaining only the most recent image should only be done if the identity of the person is trusted to be correct. For example, in an access control situation retention of the most recent successful *authentication* image would be hazardous if it could be a false positive.
- ▷ **Lifetime-consolidated:** All but the most recent image are enrolled, $x_1 \dots x_{K_i - 1}$. This subject-centric strategy might be adopted if quality variations exist where an older image might be more suitable for matching, despite the ageing effect.

⁷For example, a person might skip applying for a passport for one cycle, letting it expire. In addition, a person might submit identical images (from the same photography session) to consecutive passport applications at five year intervals.

⁸A number of distributions have been considered to model recidivism, see for example [3].

⁹There are no formal face template standards. Template standards only exist for fingerprint minutiae - see ISO/IEC 19794-2:2011.

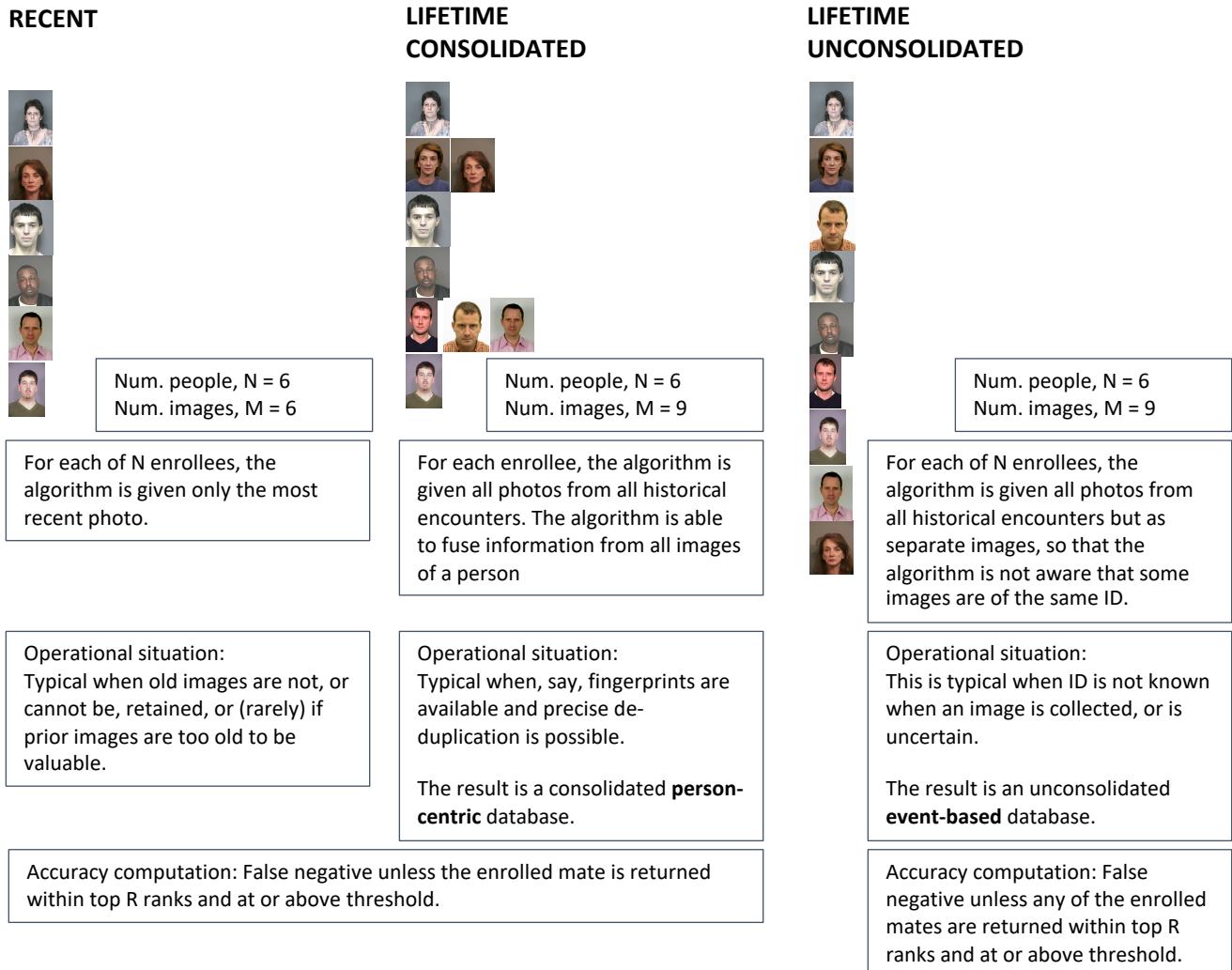


Figure 9: Enrollment strategies. The figure shows the three kinds of enrollment databases examined in this report. Image source: NIST Special Database 32

	ENROLLMENT				SEARCH			
	TYPE SEE SECTION 2.3	POPULATION FILTER	N-SUBJECTS	N-IMAGES	MATE N-SUBJECTS	NON-MATE N-IMAGES	N-SUBJECTS	N-IMAGES
Mugshot trials from enrollment of single images								
1	RECENT	NATURAL	640 000	640 000	154 549	154 549	331 254	331 254
2	RECENT	NATURAL	1 600 000	1 600 000				
3	RECENT	NATURAL	3 000 000	3 000 000				
4	RECENT	NATURAL	6 000 000	6 000 000				
5	RECENT	NATURAL	12 000 000	12 000 000				
Cross-domain								
13	MUGSHOTS AS ON ROW 2				82 106 WEBCAM	82 106 WEBCAM	331 254 WEBCAM	331 254 WEBCAM
Cross-view								
14	MUGSHOTS AS ON ROW 2				100 000 PROFILE	100 000 PROFILE	100 000 PROFILE	100 000 PROFILE
Mugshot ageing								
17	OLDEST	NATURAL	3 068 801	3 068 801	2 853 221	10 951 064	0	0
Border crossing ageing								
18	OLDEST	NATURAL	1 600 000	1 600 000	903 655	1 922 393	1 393 076	1 680 000
Visa-border								
19	PRIOR	NATURAL	1 600 000 VISA	1 600 000 VISA	577 444 BORDER	1 212 892 BORDER	79 769 BORDER	80 000 BORDER
20	VISA AS ON ROW 18				14 004 BORDER	31 579 BORDER	42 474 BORDER	45 460 BORDER

Table 1: Enrollment and search sets. Each row summarizes one identification trial. Unless stated otherwise, all entries refer to mugshot images. The term “natural” means that subjects were selected without heed to demographics, i.e. in the distribution native to this dataset. The probe images were collected in a different calendar year to the enrollment image. Missing values in rows 2-12 are the same as in row 1.

▷ **Lifetime-unconsolidated:** Again all but the most recent image are enrolled $x_1 \dots x_{K_i-1}$ but now separately, with different identifiers, such that the algorithm is not aware that the images are from the same face. This kind of event- or encounter-centric enrollment is very common when operational constraints preclude reliable consolidation of the historical encounters into a single identity. This aspect also prevents the recognition algorithm from a) building a holistic model of identity (as is common in speaker recognition systems) and b) implementing fusion, for example template-level fusion of feature vectors, or post-search score-level fusion. The result is that searches will typically yield more than one image of a person in the top ranks. This has consequences for appropriate metrics, as detailed in section 3.2.1

NIST first evaluated this kind of enrollment in mid 2018, and the results tables include some comparison of accuracy available from all three enrollment styles.

In all cases, the most recent image, x_{K_i} , is reserved as the search image. For the 1.6 million subject enrollment partition of the FRVT 2018 data, $1 \leq K_i \leq 33$ with $K_i = 1$ in 80.1% of the individuals, $K_i = 2$ in 13.4%, $K_i = 3$ in 3.7%, $K_i = 4$ in 1.4%, $K_i = 5$ in 0.6%, $K_i = 6$ in 0.3%, and $K_i > 6$ is 0.2% for everyone else. This distribution is substantially dependent on United States recidivism rates.

We did not evaluate the case of retaining only the highest quality image, since automated quality assessment is out of scope for this report. We do not anticipate that such strategies will prove beneficial when the quality assessment apparatus is imperfect and unvalidated.

3 Performance metrics

This section gives specific definitions for accuracy and timing metrics. Tests of open-set biometric algorithms must quantify frequency of two error conditions:

- ▷ **False positives:** Type I errors occur when search data from a person who has never been seen before is incorrectly associated with one or more enrollees' data.
- ▷ **Misses:** Type II errors arise when a search of an enrolled person's biometric does not return the correct identity.

Many practitioners prefer to talk about "hit rates" instead of "miss rates" - the first is simply one minus the other as detailed below. Sections 3.1 and 3.2 define metrics for the Type I and Type II performance variables.

Additionally, because recognition algorithms sometimes fail to produce a template from an image, or fail to execute a one-to-many search, the occurrence of such events must be recorded. Further because algorithms might elect to not produce a template from, for example, a poor quality image, these failure rates must be combined with the recognition error rates to support algorithm comparison. This is addressed in section 3.5.

Finally, section 3.7 discusses measurement of computation duration, and section 3.8 addresses the uncertainty associated with various measurements. Template size measurement is included with the results.

3.1 Quantifying false positives

It is typical for a search to be conducted into an enrolled population of N identities, and for the algorithm to be configured to return the closest L candidate identities. These candidates are ranked by their score, in descending order, with all scores required to be greater than or equal to zero. A human analyst might examine either all L candidates, or just the top $R \leq L$ identities, or only those with score greater than threshold, T . The workload associated with such examination is discussed later, in 3.6.

False alarm performance is quantified in two related ways. These express how many searches produces false positives, and then, how many false positives are produced in a search.

False positive identification rate: The first quantity, FPIR, is the proportion of non-mate searches that produce an adverse outcome:

$$\text{FPIR}(N, T) = \frac{\text{Num. non-mate searches where one or more enrolled candidates are returned with score at or above threshold}}{\text{Num. non-mate searches attempted.}} \quad (1)$$

Under this definition, FPIR can be computed from the highest non-mate candidate produced in a search - it is not necessary to consider candidates at rank 2 and above. FPIR is the primary measure of Type I errors in this report.

Selectivity: However, note that in any given search, several non-mate may be returned above threshold. In order to quantify such events, a second quantity, selectivity (SEL), is defined as the *number* of non-mates returned on a candidate list, averaged over all searches.

$$\text{SEL}(N, T) = \frac{\text{Num. non-mate enrolled candidates returned with score at or above threshold}}{\text{Num. non-mate searches attempted.}} \quad (2)$$

where $0 \leq \text{SEL}(N, T) \leq L$. Both of these metrics are useful operationally. FPIR is useful for targeting how often an

adverse false positive outcome can occur, while SEL as a number is related to workload associated with adjudicating candidate lists. The relationship between the two quantities is complicated - it depends on whether an algorithm concentrates the false alarms in the results of a few searches or whether it disburses them across many. This was detailed in FRVT 2014, NISTIR 8009. It has not yet been detailed in FRVT 2018.

3.2 Quantifying hits and misses

If L candidates are returned in a search, a shorter candidate list can be prepared by taking the top $R \leq L$ candidates for which the score is above some threshold, $T \geq 0$. This reduction of the candidate list is done because thresholds may be applied, and only short lists might be reviewed (according to policy or labor availability, for example). It is useful then to state accuracy in terms of R and T , so we define a “miss rate” with the general name **false negative identification rate** (FNIR), as follows:

$$\text{FNIR}(N, R, T) = \frac{\text{Num. mate searches with enrolled mate found outside top } R \text{ ranks or score below threshold}}{\text{Num. mate searches attempted.}} \quad (3)$$

This formulation is simple for evaluation in that it does not distinguish between causes of misses. Thus a mate that is not reported on a candidate list is treated the same as a miss arising from face finding failure, algorithm intolerance of poor quality, or software crashes. Thus if the algorithm fails to produce a candidate list, either because the search failed, or because a search template was not made, the result is regarded as a miss, adding to FNIR.

Hit rates, and true positive identification rates: While FNIR states the “miss rate” as how often the correct candidate is either not above threshold or not at good rank, many communities prefer to talk of “hit rates”. This is simply the **true positive identification rate**(TPIR) which is the complement of FNIR giving a positive statement of how often mated searches are successful:

$$\text{TPIR}(N, R, T) = 1 - \text{FNIR}(N, R, T) \quad (4)$$

This report does not report true positive “hit” rates, preferring false negative miss rates for two reasons. First, costs rise linearly with error rates. For example, if we double FNIR in an access control system, then we double user inconvenience and delay. If we express that as decrease of TPIR from, say 98.5% to 97%, then we mentally have to invert the scale to see a doubling in costs. More subtly, readers don’t perceive differences in numbers near 100% well, becoming inured to the “high nineties” effect where numbers close to 100 are perceived indifferently.

Reliability is a corresponding term, typically being identical to TPIR, and often cited in automated (fingerprint) identification system (AFIS) evaluations.

An important special case is the **cumulative match characteristic**(CMC) which summarizes accuracy of mated-searches only. It ignores similarity scores by relaxing the threshold requirement, and just reports the fraction of mated searches returning the mate at rank R or better.

$$\text{CMC}(N, R) = 1 - \text{FNIR}(N, R, 0) \quad (5)$$

We primarily cite the complement of this quantity, $\text{FNIR}(N, R, 0)$, the fraction of mates *not* in the top R ranks.

The **rank one hit rate** is the fraction of mated searches yielding the correct candidate at best rank, i.e. $\text{CMC}(N, 1)$. While this quantity is the most common summary indicator of an algorithm’s efficacy, it is not dependent on similarity scores, so it does not distinguish between strong (high scoring) and weak hits. It also ignores that an adjudicating reviewer is often willing to look at many candidates.

3.2.1 False negative rates for unconsolidated galleries

As detailed in section 2.3 a common type of gallery, here referred to as the lifetime unconsolidate type, is populated with all images of an individual without any association between them. That is, the gallery construction algorithm is not provided with any ID labels that would support processing of a person's images jointly. This contrasts with the lifetime consolidate type where an algorithm may explicitly fuse features from multiple images of a person, or select a best image. In such cases, where the number of enrolled images is a random variable, we define two false negative rates as follows.

The first demands that the algorithm place any of the K_i mates in the top $R \geq 1$ ranks. The proportion of searches for which this does not occur forms a false negative identification rate:

$$\text{FNIR}_{\text{any}}(N, R, T) = 1 - \frac{\text{Num. mate searches where any enrolled mate is found in the top } R \text{ ranks and at-or-above threshold}}{\text{Num. mate searches attempted.}} \quad (6)$$

The second demands that the algorithm place all K_i mates in the top $R \geq K_i$ ranks. The proportion of searches for which this does not occur forms a false negative identification rate:

$$\text{FNIR}_{\text{all}}(N, R, T) = 1 - \frac{\text{Num. mate searches where all enrolled mates are found in the top } R \text{ ranks and at-or-above threshold}}{\text{Num. mate searches attempted.}} \quad (7)$$

Placing all mates in the top ranks is a more difficult task than correctly retrieving any image, so it holds that: $\text{FNIR}_{\text{all}} \geq \text{FNIR}_{\text{any}}$. This is evident in the results presented for November 2018 algorithms in Tables starting at ??.

The information retrieval community might prefer to compute and plot *precision* and *recall*; this is a valid approach, but we advance the two metrics above because they relate to our normal definition of consolidated FNIR, and they cover the two extreme use-cases of wanting any hit vs. all hits.

3.3 DET interpretation

In biometrics, a false negative occurs when an algorithm fails to match two samples of one person – a Type II error. Correspondingly, a false positive occurs when samples from two persons are improperly associated – a Type I error.

Matches are declared by a biometric system when the native comparison score from the recognition algorithm meets some threshold. Comparison scores can be either similarity scores, in which case higher values indicate that the samples are more likely to come from the same person, or dissimilarity scores, in which case higher values indicate different people. Similarity scores are traditionally computed by fingerprint and face recognition algorithms, while dissimilarities are used in iris recognition. In some cases, the dissimilarity score is a distance possessing metric properties. In any case, scores can be either mate scores, coming from a comparison of one person's samples, or nonmate scores, coming from comparison of different persons' samples.

The words "genuine" or "authentic" are synonyms for mate, and the word "impostor" is used as a synonym for non-mate. The words "mate" and "nonmate" are traditionally used in identification applications (such as law enforcement search, or background checks) while genuine and impostor are used in verification applications (such as access control).

An error tradeoff characteristic represents the tradeoff between Type II and Type I classification errors. For identification this plots false negative vs. false positive identification rates i.e. FNIR vs. FPIR parametrically with T. Such plots

are often called detection error tradeoff (DET) characteristics or receiver operating characteristic (ROC). These serve the same function – to show error tradeoff – but differ, for example, in plotting the complement of an error rate (e.g. $TPIR = 1 - FNIR$) and in transforming the axes, most commonly using logarithms, to show multiple decades of FPIR. More rarely, the function might be the inverse of the Gaussian cumulative distribution function.

The slides of Figures 10 through 15 discuss presentation and interpretation of DETs used in this document for reporting face identification accuracy. Further detail is provided in formal biometrics testing standards, see the various parts of ISO/IEC 19795 Biometrics Testing and Reporting. More terms, including and beyond those to do with accuracy, appear in ISO/IEC 2382-37 Information technology – Vocabulary – Part 37: Harmonized biometric vocabulary.

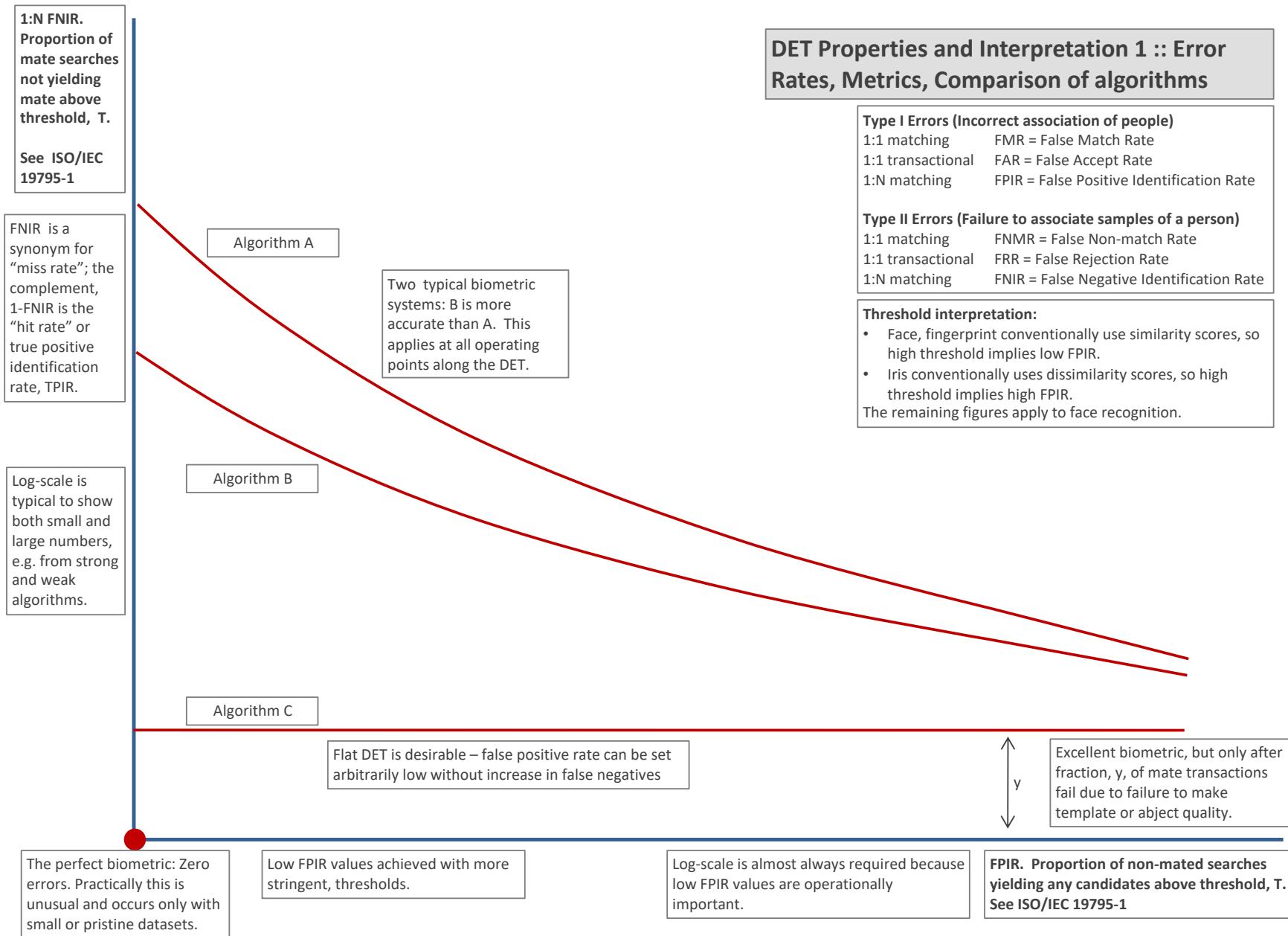


Figure 10: DET as the primary performance reporting mechanism.

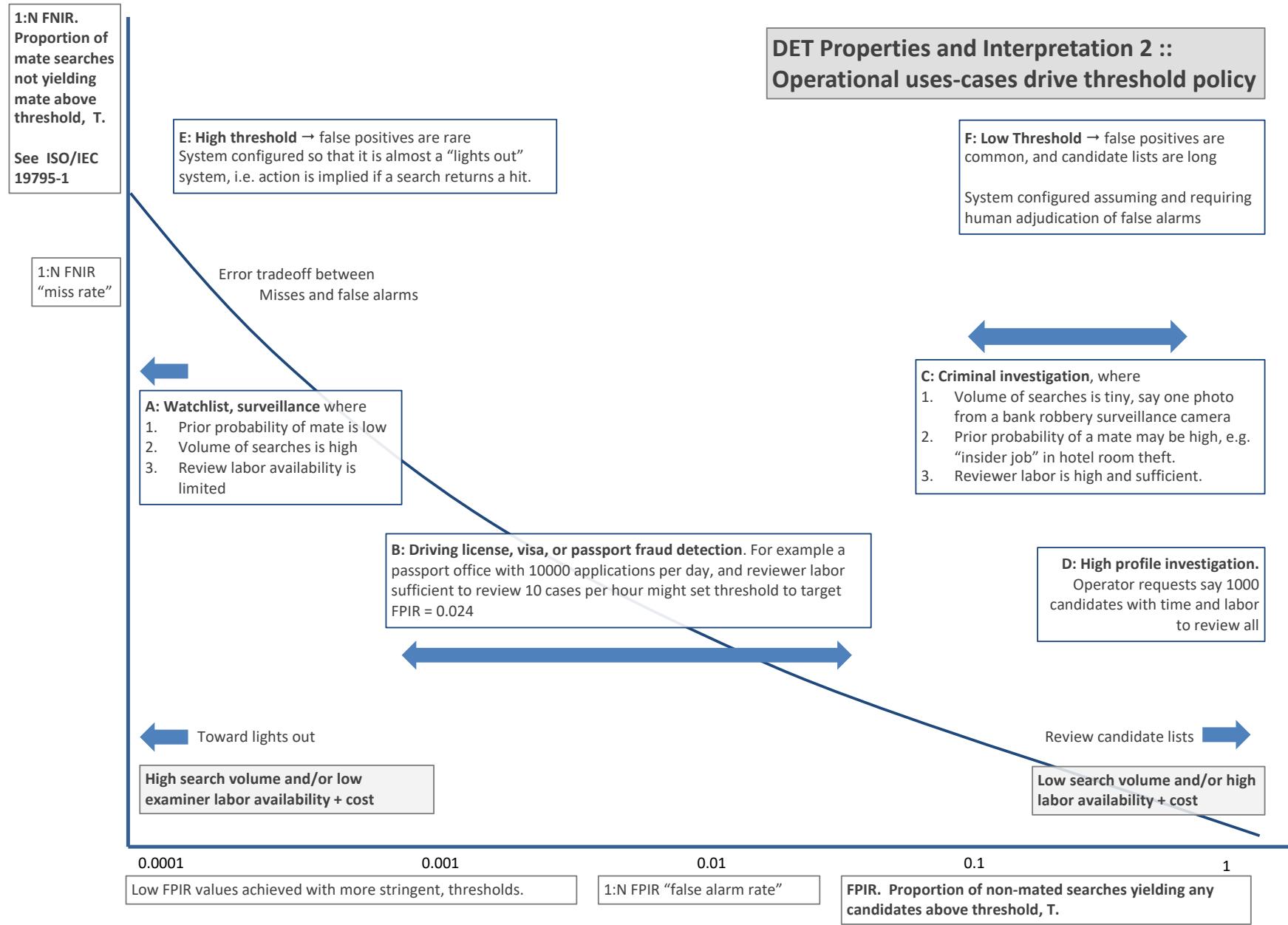


Figure 11: DET as the primary performance reporting mechanism.

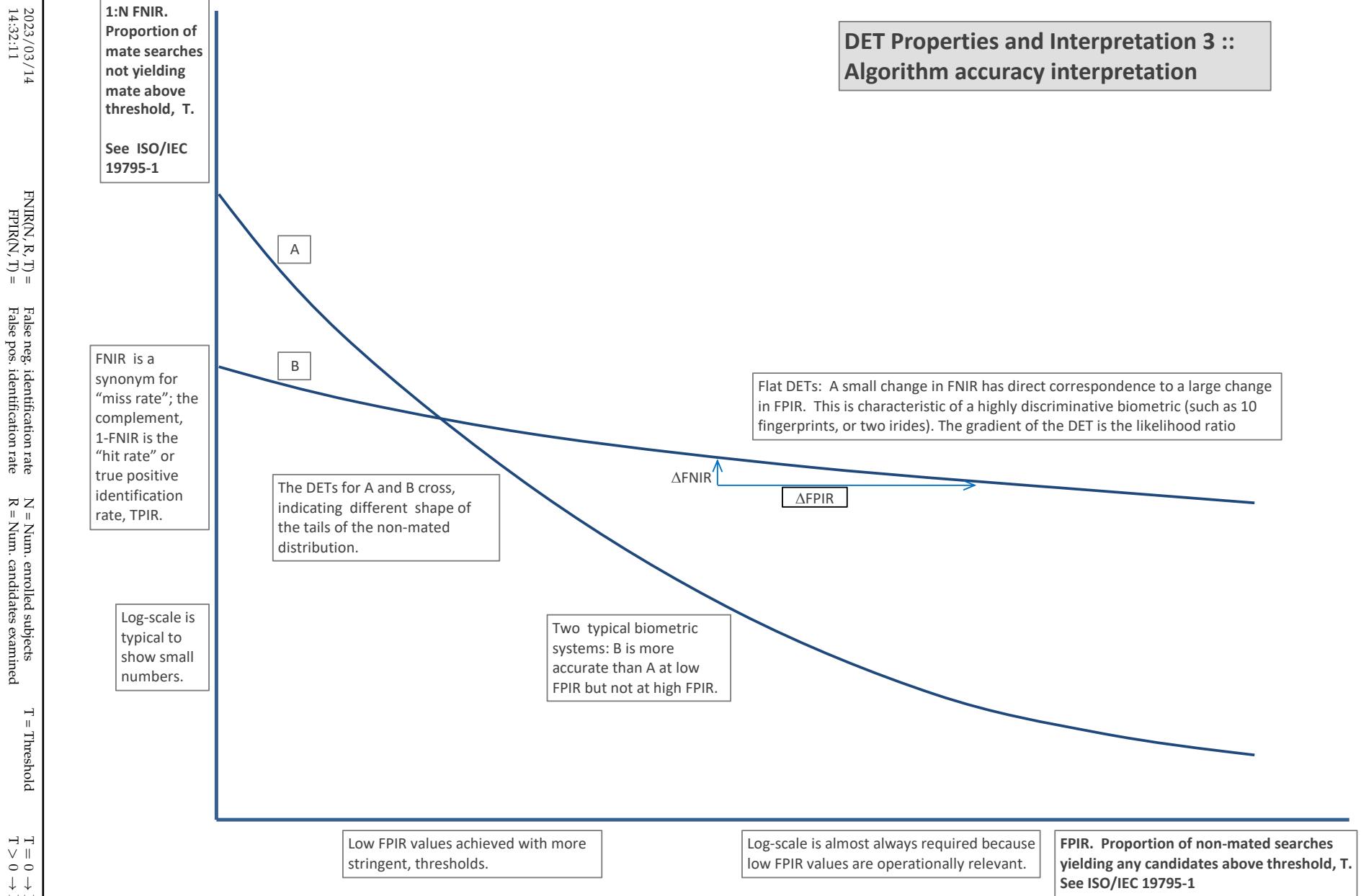


Figure 12: DET as the primary performance reporting mechanism.

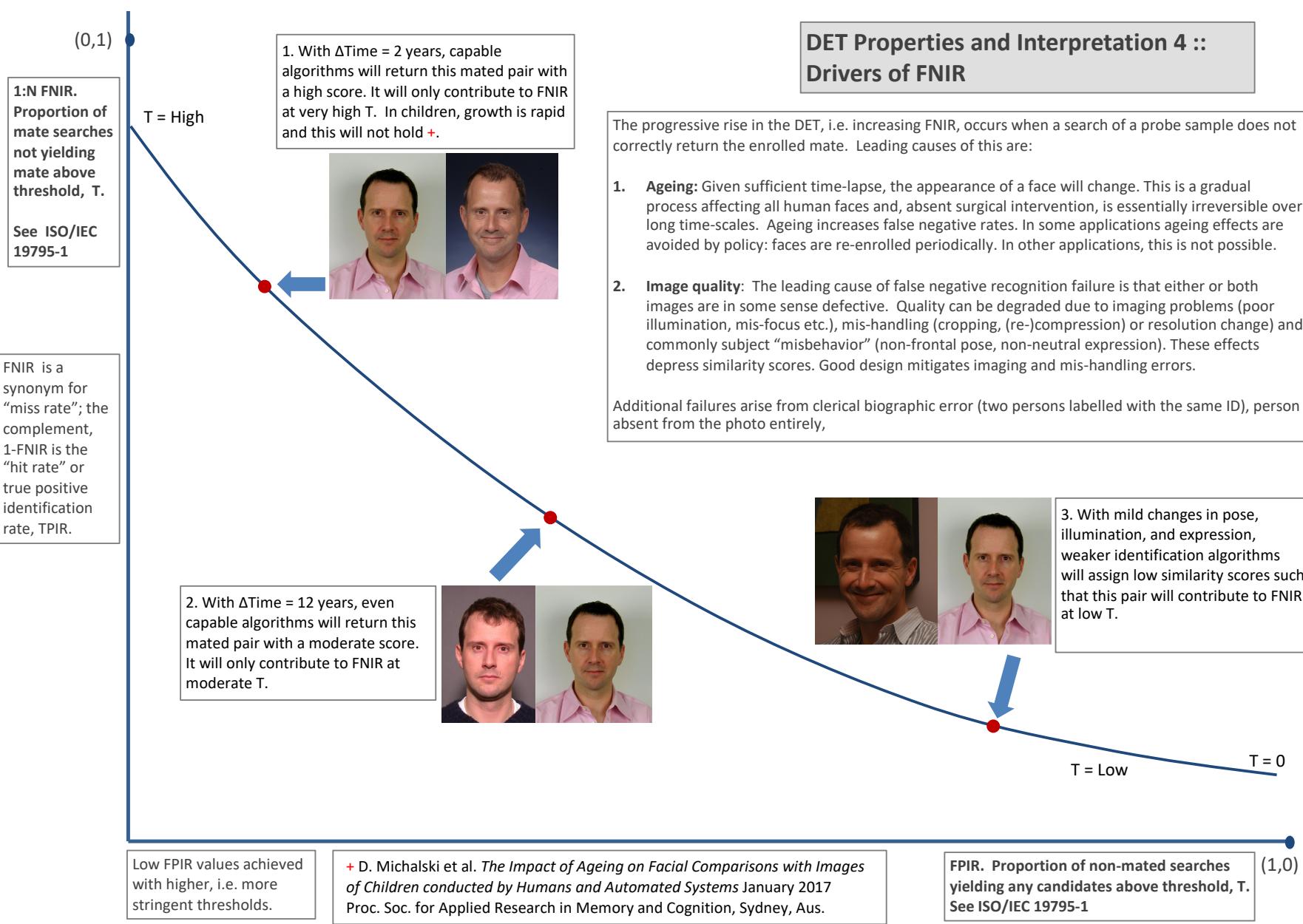


Figure 13: DET as the primary performance reporting mechanism.

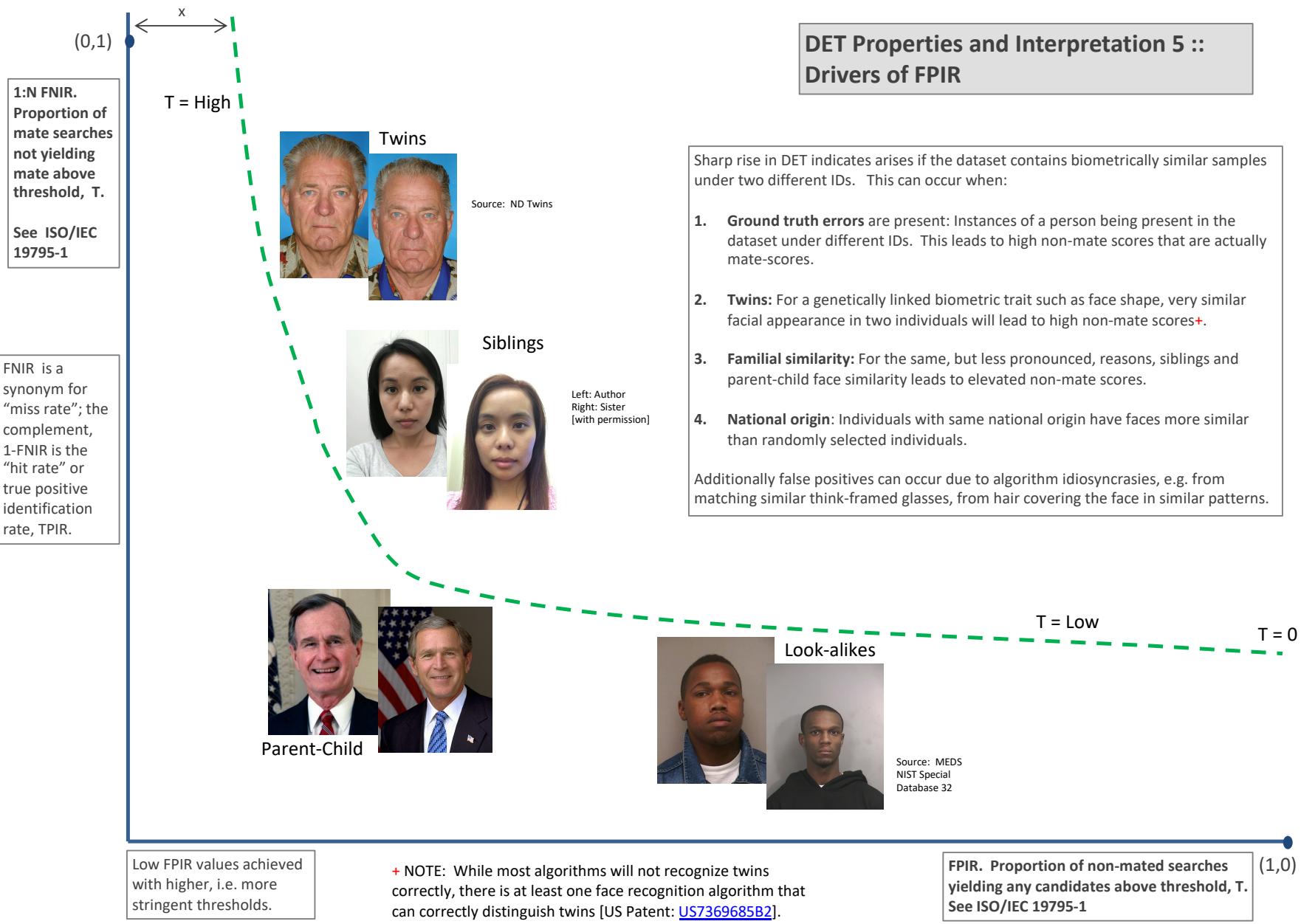


Figure 14: DET as the primary performance reporting mechanism.

DET Properties and Interpretation 6 :: Fixed thresholds, change in image properties or demographics

2023/03/14
14:32:11

$\text{FNIR}(N, R, T) =$
False neg. identification rate
 $\text{FPIR}(N, T) =$
False pos. identification rate

$N = \text{Num. enrolled subjects}$
 $R = \text{Num. candidates examined}$

$T = \text{Threshold}$

$T = 0 \rightarrow \text{Investigation}$
 $T > 0 \rightarrow \text{Identification}$

1:N FNIR.
Proportion of mate searches not yielding mate above threshold, T .
See ISO/IEC 19795-1

Algorithm X,
Condition 1

Algorithm X,
Condition 2

If system X is used with images of different properties, say from different imaging systems, or from different populations, generally both FNIR and FPIR will change. The dotted line joins points of the same threshold. Horizontal (vertical) lines indicate change in FPIR (FNIR) only. Two cases concerning population size are shown below (A and B), for the blue curves.

FNIR is a synonym for "miss rate"; the complement, 1-FNIR is the "hit rate" or true positive identification rate, TPIR.

Log-scale is typical to show small numbers.

Algorithm Y,
Condition 1

Algorithm Y,
Condition 2

If DETs are computed for two categories (men and women) or (cameras A and B) or (indoor vs. outdoor), generally the Type I and Type II errors will differ and the line of constant threshold will be neither horizontal nor vertical.

The ideal situation in most applications is that a fixed threshold yields a fixed FPIR so that system owners see no change in false alarms across populations or conditions.

Low FPIR values achieved with higher, i.e. more stringent, thresholds.

Log-scale is often required because low FPIR values are operationally relevant.

FPIR. Proportion of non-mated searches yielding any candidates above threshold, T . See ISO/IEC 19795-1

Figure 15: DET as the primary performance reporting mechanism.

2023/03/14

FNIR(N, R, T) =

FPIR(N, T) =
False neg. identification rate
FPIR(N, T) =N = Num. enrolled subjects
R = Num. candidates examined

T = Threshold

T = 0 → Investigation
T > 0 → Identification

DET Properties and Interpretation 7 :: Effect of enrolled population size.

1:N FNIR.
Proportion of mate searches not yielding mate above threshold, T.
See ISO/IEC 19795-1

FNIR is a synonym for "miss rate"; the complement, 1-FNIR is the "hit rate" or true positive identification rate, TPIR.

Log-scale is typical to show small numbers.

A: Typical case: In theory, and often in practice, a 1:N search is implemented by executing N 1:1 comparisons independently and then sorting by similarity score:

Mate scores: A mate comparison score is independent of the rest of enrollment data, and so independent of N. This implies the horizontal line above $\text{FNIR}(T, N) = \text{FNMR}(T, 1)$.

Non-mate scores: FPIR increases linearly with N from binomial theory: $\text{FPIR}(N, T) = 1 - (1 - \text{FMR}(T))^N \rightarrow N \text{ FMR}(T)$ for small FPIR.

Pop. N1

Pop. N2 > N1

B: Special case: An enrollment database is not just a linear data structure, it could be an index, or tree, then search is not simply N 1:1 comparisons and a sort. In that case:

Mate scores become dependent on the enrollment data, either its size or actual content, then generally $\text{FNIR}(T, N) \neq \text{FNIR}(T, 1)$.

Non-mate scores are normally no longer just the highest 1:1 comparison score. Instead, for example, scores may be normalized as the implementation attempts to make FPIR independent of N will yield the vertical line linking points of equal threshold.

Low FPIR values achieved with higher, i.e. more stringent, thresholds.

Log-scale is often required because low FPIR values are operationally important.

FPIR. Proportion of non-mated searches yielding any candidates above threshold, T.
See ISO/IEC 19795-1

Figure 16: DET as the primary performance reporting mechanism.

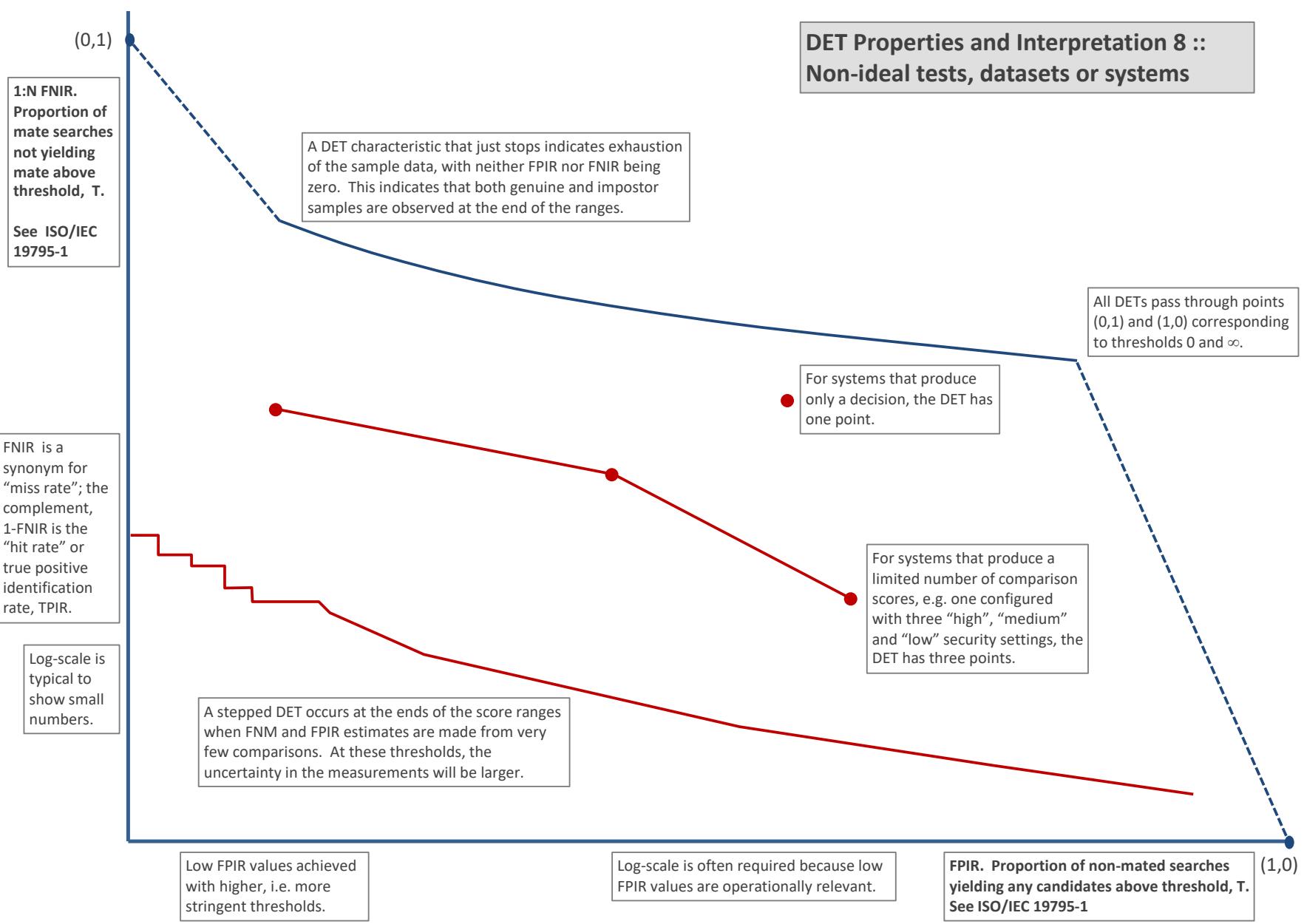


Figure 17: DET as the primary performance reporting mechanism.

3.4 Best practice testing requires execution of searches with and without mates

FRVT embeds 1:N searches of two kinds: Those for which there is an enrolled mate, and those for which there is not. The respective numbers for these types of searches appear in Table 1. However, it is common to conduct only mated searches¹⁰. The cumulative match characteristic is computed from candidate lists produced in mated searches. Even if the CMC is the only metric of interest, the actual trials executed in a test should nevertheless include searches for which no mate exists. As detailed in Table 1 the FRVT reserved disjoint populations of subjects for executing true non-mate searches.

3.5 Failure to extract features

During enrollment some algorithms fail to convert a face image to a template. The proportion of failures is the failure-to-enroll rate, denoted by FTE. Similarly, some search images are not converted to templates. The corresponding proportion is termed failure-to-extract, denoted by FTX.

We do not report FTX because we assume that the same underlying algorithm is used for template generation for enrollment and search.

Failure to extract rates are incorporated into FNIR and FPIR measurements as follows.

- ▷ **Enrollment templates:** Any failed enrollment is regarded as producing a zero length template. Algorithms are required by the API [10] to transparently process zero length templates. The effect of template generation failure on search accuracy depends on whether subsequent searches are mated, or non-mated: Mated searches will fail giving elevated FNIR; non-mated searches will not produce false positives so, to first order, FPIR will be reduced by a factor of $1 - \text{FTE}$.
- ▷ **Search templates and 1:N search:** In cases where the algorithm fails to produce a search template from input imagery, the result is taken to be a candidate list whose entries have no hypothesized identities and zero score. The effect of template generation failure on search accuracy depends on whether searches are mated, or non-mated: Mated searches will fail giving elevated FNIR; Non-mated searches will not produce false positives, so FPIR will be reduced. Thus given a measurement of false negative and positive rates made over only those where failures-to-extract did not occur, those rates - call them FNIR^\dagger and FPIR^\dagger - could be adjusted by an explicit measurement of FTX as follows

$$\text{FNIR} = \text{FTX} + (1 - \text{FTX})\text{FNIR}^\dagger \quad (8)$$

$$\text{FPIR} = (1 - \text{FTX})\text{FPIR}^\dagger \quad (9)$$

This approach is the correct treatment for positive-identification applications such as access control where cooperative users are enrolled and make attempts at recognition. This approach is not appropriate to negative identification applications, such as visa fraud detection, in which hostile individuals may attempt to evade detection by submitting poor quality samples. In those cases, template generation failures should be investigated as though a false alarm had occurred.

¹⁰For example, the [Megaface benchmark](#). This is bad practice for several reasons: First, if a developer knows, or can reasonably assume, that a mate always exists, then unrealistic gaming of the test is possible. A second reason is that it does not put FPIR on equal footing with FNIR and that matters because in most applications, not all searches have mates - not everyone has been previously enrolled in a driving license issuance or a criminal justice system - so addressing between-class separation becomes necessary.

3.6 Fixed length candidate lists, threshold independent workload

Suppose an automated face identification algorithm returns L candidates, and a human reviewer is retained to examine up to R candidates, where $R \leq L$ might be set by policy, preference or labor availability. For now, assume also that the reviewer is not provided with, or ignores, similarity scores, and thresholds are not applied. Given the algorithm typically places mates at low (good) ranks, the number of candidates a reviewer can be expected to review can be derived as follows. Note that the reviewer will:

- ▷ Always inspect the first ranked image Frac. reviewed = 1
- ▷ Then inspect those candidates where mate not confirmed at rank 1 Frac. reviewed = 1-CMC(1)
- ▷ Then inspect those candidates where mate not confirmed at rank 1 or 2 Frac. reviewed = 1-CMC(2)

etc. Thus if the reviewer will stop after a maximum of R candidates, the expected number of candidate reviews is

$$M(R) = 1 + (1 - CMC(1)) + (1 - CMC(2)) + \dots + (1 - CMC(R - 1)) \quad (10)$$

$$= R - \sum_{r=1}^{R-1} CMC(r) \quad (11)$$

A recognition algorithm that front-loads the cumulative match characteristic will offer reduced workload for the reviewer. This workload is defined only over the searches for which a mate exists. In the cases where there truly is no mate, the reviewer would review all R candidates. Thus, if the proportion of searches for which a mate does exist is β , which in the law enforcement context would be the recidivism rate [3], the full expression for workload becomes:

$$M(R) = \beta \left(R - \sum_{r=1}^{R-1} CMC(r) \right) + (1 - \beta)R \quad (12)$$

$$= R - \beta \sum_{r=1}^{R-1} CMC(r) \quad (13)$$

3.7 Timing measurement

Algorithms were submitted to NIST as implementations of the application programming interface(API) specified by NIST in the Evaluation Plan [10]. The API includes functions for initialization, template generation, finalization, search, gallery insert, and gallery delete. Two template generation functions are required, one for the preparation of an enrollment template, and one for a search template.

In NIST's test harness, all functions were wrapped by calls to the C++ std::chrono::high_resolution_clock which on the dedicated timing machine counts 1ns clock ticks. Precision is somewhat worse than that however.

3.8 Uncertainty estimation

3.8.1 Random error

This study leverages operational datasets for measurement of recognition error rates. This affords several advantages. First, large numbers of searches are conducted (see Table 1) giving precision to the measurements. Moreover, for the two mugshot datasets, these do not involve reuse of individuals so binomial statistics can be expected to apply to recognition error counts. In that case, an observed count of a particular recognition outcome (i.e. a false negative or false positive) in M trials will sustain 95% confidence that the actual error rate is no larger than some value.

As an example, the minimum number of mugshot searches conducted in this report is $M = 154\,549$, and for an observed FNIR around 0.002, the measurement supports a conclusion that the actual FNIR is no higher than 0.00228 at 99% confidence level. On the false positive side, we tabulate FNIR at FPIR values as low as 0.001. Given estimates based on 331 254 non-mate trials, the actual FPIR values will be below 0.00115 at 99% confidence. In conclusion, large scale evaluation, without reuse of subjects, supports tight uncertainty bounds on the measured error rates.

3.8.2 Systematic error

The FRVT 2018 dataset includes anomalies discovered as a result of inspecting images involved in recognition failures from the most accurate algorithms. Two kinds of failure occur: False negatives (which, for the purpose here, include failures to make templates) and false positives.

False negative errors: We reviewed 600 false negative pairs for which either or both of the leading two algorithms did not put the correct mate in the top 50 candidates. Given 154 549 searches, this number represents 0.39% of the total, resulting in $\text{FNIR} \sim 0.0039$. Of the 600 pairs:

- ▷ **A: Poor quality:** About 20% of the pairs included images of very low quality, often greyscale, low resolution, blurred, low contrast, partially cropped, interlaced, or noisy scans of paper images. Additionally, in a few cases, the face is injured or occluded by bandages or heavy cosmetics.
- ▷ **B: Ground truth identity label bugs:** About 15% of the pairs are not actually mated. We only assigned this outcome when a pair is clearly not mated.
- ▷ **C: Profile views:** About 35% included an image of a profile (side) view of the face, or, more rarely, an image that was rotated 90 degrees in-plane (roll).
- ▷ **D: Tattoos:** About 30% included an image of a tattoo that contained a face image. These arise from mis-labelling in the parent dataset metadata.
- ▷ **E: Ageing:** There is considerable time-lapse between the two captures.

All these estimates are approximate. Of these, the tattoo and mislabelled images can never be matched. These constitute an accuracy floor in the sample implying that FNIR cannot be below 0.0018¹¹. The profile-views, low-quality images, and images with considerable ageing can, in principle, be successfully matched - indeed some algorithms do so - so are not part of the accuracy floor.

¹¹This value is the sum of two partial false negative rates: $\text{FNIR}_B = 0.15 * 0.0039$ plus $\text{FNIR}_D = 0.3 * 0.0039$

For the microsoft-4 algorithm the lowest miss rate from (recent entry in Table 28) is $\text{FNIR}(640\,000, 50, 0) = 0.0018$. This is close to the value estimated from the inspection of misses. It is below the 0.0039 figure because the algorithm does match some profile and poor quality images, that the yitu-2 algorithm does not.

For many tables (e.g. Table 28), the FNIR values obtained for the FRVT-2018 mugshots could be corrected by reducing them by 0.0018. The best values would then be indistinct from zero. The results in this report *were not* adjusted to account for this systematic error.

False positive errors: As shown in Figure 1 and discussed in Figure 14 many of the DET characteristics in this report exhibit a pronounced turn upward at low false positive rates. The shape can be caused by identity labelling errors in the ground truth of a dataset, specifically persons present in the database under two IDs such that some proportion of non-mate pairs are actually mated. To look for such possibilities, we merged the highest 1000 non-mate pairs produced by three different algorithms which resulted in 1839 unique pairs. This constitutes 0.56% of all non-mate searches. We assert that it is *very* difficult for human reviewers to assign the pairs into the following three categories: twins; doppelgangers; or ground-truth errors (instances of the same person under two IDs). Given this difficulty we made no attempt to correct any possible ground truth errors except by removing 57 pairs in the following categories:

- ▷ **A: Profile views:** Thirteen pairs included one or two profile-view images. As described in Figure 150, these can cause false positives.
- ▷ **B: Same-session photographs:** For twelve pairs, the images were identical or trivially altered (e.g. cropped) versions of the same photo. These were present under a different ID likely due to some clerical or procedural mistake.
- ▷ **C: Tattoos of faces:** There were fourteen instances of tattoo photographs that contained faces causing false matches.
- ▷ **D: T-shirt faces:** There were six instances of T-shirt photographs (of Bob Marley and Che Guevara) being detected instead of the face and causing false positives.
- ▷ **E: Background faces:** There were twelve instances of one subject appearing in the background of two otherwise correct portrait photos.

Note we did not remove any images where there was a chance that the pair was actually a different person.

In any case, the results in this report have not been adjusted for this systematic error.

4 Results

This section gives extensive results for algorithms submitted to FRVT 2018. Three page “report cards” for each algorithm are contained in a [separate supplement](#). Performance metrics were described in section 3. The main results are summarized in tabular form with more exhaustive data included as DET, CMC and related graphs in appendices as follows:

- ▷ The three tables 2-4 list algorithms alongside full developer names, acceptance date, size of the provided configuration data, template size and generation time, and search duration data.
 - The **template generation duration** is most important to applications that require fast response. For example, an eGate taking more than two seconds to produce a template might be unacceptable. Note that GPUs may be of utility in expediting this operation for some algorithms, though at additional expense. Two additional factors should be considered¹²¹³.
 - The **search duration** is the time taken for a search of a search template into a gallery of N enrollment templates. This performance variable, together with the volume of searches, is influential on the amount of hardware needed to sustain an operational deployment. This is measured here with the algorithm running on a single core of a contemporary CPU. Search is most simply implemented as N computations of a distance metric followed by a sort operation to find the closest enrollments. However, considerable optimization of this process is possible, up to and including fast-search algorithms that, by various means, avoid computation of all N distances.
 - The **template size** is the size of the extracted feature vector (or vectors) and any needed header information. Large template sizes may be influential on bus or network bandwidth, storage requirements, and on search duration. While the template itself is an opaque data blob, the feature dimensionality might be estimated by assuming a four-bytes-per-float encoding. There is a wide range of encodings. For the more accurate algorithm, sizes range from 256 bytes to about 2KB bytes, indicating essentially no consensus on face modeling and template design.
 - The **template size multiplier** column shows how, given k input images, the size of the template grows. Most implementations internally extract features from each image and concatenate them, and implement some score-level fusion logic during search. Other implementations, including many of the most accurate algorithms, produce templates whose size does not grow with k . This could be achieved via selection of the best quality image - but this is not optimal in handling ageing where the oldest image could be the best quality. Another mechanism would be feature-level fusion where information is fused from all k inputs. In any case, as a black-box test, the fusion scheme is proprietary and unknown.
 - The size of the **configuration data** is the total size of all files resident in a vendor-provided directory that contains arbitrary read-only files such as parameters, recognition models (e.g caffe). Generally a large value for this quantity may prohibit the use of the algorithm on a resource-constrained device.

¹²The FRVT 2018 API prohibited threading, so some gains from parallelism may be available on multiple-cores or multiple processors, if the feature extraction code could be distributed across them.

¹³Note also that factors of two or more may be realizable by exploiting modern vector processing instructions on CPUs. It is not clear in our measurements whether all developers exploited Intel’s AVX2 instructions, for example. Our machine was so equipped, but we insisted that the same compiled library should also run on older machines lacking that instruction. The more sophisticated implementations may have detected AVX2 presence and branched accordingly. The less sophisticated may be defaulted to the reduced instruction set. Readers should see the FRVT 2018 API document for the specific chip details.

▷ Tables 28-29 report core rank-based accuracy for mugshot images. The population size is limited to $N = 1.6$ million identities because this is the largest gallery size on which all algorithms were executed. Notable observations from these tables are as follows:

- **Accuracy gains since 2018:** NIST Interagency Report 8238 documented massive gains over those reported in the FRVT 2014 report, NIST Interagency Report 8009. Further gains are documented in this report. Comparing the most accurate algorithm in November 2018, NEC-3, the value of $\text{FNIR}(N, L, T)$ reduced from 0.0031 to 0.0024 for the Sensetime-004 algorithm with $N = 12$ million recent images. The tables show broader gains: many developers have made advances since 2018 with between two and five-fold reduction in errors.
- **Wide range in accuracy:** The rank-1 miss rates vary from $\text{FNIR}(N, 1, 0) = 0.0012$ for sensetime-004 up to about 0.5 for the very fast but inaccurate microfocus-x algorithms. Among the developers who are superior to NEC in 2013, the range is from 0.002 to 0.035 for camvi-3. This large accuracy range is consistent with the buyer-beware maxim, and indicates that face recognition software is far from being commoditized.

▷ Tables 33-34 report threshold-based error rates, $\text{FNIR}(N, L, T)$, for $N = 1.6$ million for mugshot-mugshot accuracy on FRVT 2014, FRVT 2018, and also (in pink) mugshot-webcam accuracy using FRVT 2018 enrollments. Notable observations from these tables are as follows:

- **Order of magnitude accuracy gains since 2014:** As with rank-based results, the gains in accuracy are substantial, though somewhat reduced. At $\text{FPIR} = 0.01$, the best improvement over NEC in 2014 is a 27 fold reduction in FNIR using the NEC_2 algorithm. At $\text{FPIR} = 0.001$, the largest gain is a six-fold reduction in FNIR via the NEC_3 algorithm.
- **Broad gains across the industry:** About 19 companies realize accuracy better than the NEC benchmark from 2014. This is somewhat lower than the 28 developers who succeeded on the rank-1 metric. This may be due to the ubiquity of, and emphasis on, the rank-1 metric in many published algorithm development papers.
- **Webcam images:** Searches of webcam images give $\text{FNIR}(N, T)$ values around 2 to 3 times higher than mugshot searches. Notably the leading developers with mugshots are approximately the same with poorer quality webcams. But some developers e.g. Camvi, Megvii, TongYi, and Neurotechnology do improve their relative rankings on webcams, perhaps indicating their algorithms were tailored to less constrained images.

▷ Tables 20, 24, 25 and show, respectively, high-threshold, rank 1, and rank 50 FNIR values for all algorithms performing searches into five different gallery sizes, $N = 640\,000$, $N = 1\,600\,000$, $N = 3\,000\,000$, $N = 6\,000\,000$ and $12\,000\,000$. The $\text{FPIR} = 0.001$ table is included to inform high-volume duplicate detection applications. The Rank-1 table is included as a primary accuracy indicator. The Rank-50 table is included to inform agencies who routinely produce 50 candidates for human-review. The notable results are:

- **Slow growth in rank-based miss rates:** $\text{FNIR}(N, R)$ generally grows as a power law, aN^b . From the straight lines of many graphs of Figure 20 this is clearly a reasonable model for most, but not all, algorithms. The coefficient a can be interpreted as FNIR in a gallery of size 1. The more important coefficient b indicates scalability, and often, $b \ll 1$, implies very benign growth in FNIR. The coefficients of the models appear in the Tables 24 and 25.
- **Slow growth in threshold-based miss rates:** $\text{FNIR}(N, T)$ also generally grows as a power law, aN^b except at the high threshold values corresponding to low FPIR values. This is visible in the plots of Figure 36 which

show straight lines except for $FPIR = 0.001$, which increase more rapidly with N above 3 000 000. Each trace in those figures shows $FNIR(N, T)$ at fixed $FPIR$ with both N and T varying. Thus at large N , it is usually necessary to elevate T to maintain fixed $FPIR$. This causes increased $FNIR$. Why that would no-longer obey a power-law is not known. However, if we expect large galleries to contain individuals with familial relations to the non-mate search images - in the most extreme case, twins - then suppression of false positives becomes more difficult. This is discussed in the Figures starting at Fig. 10

▷ Figure ?? shows false positives from twins against their enrolled siblings, broken out by type of twin: fraternal or identical. The Figure is based on the enrollment of 104 single images on one of a pair of twins, and then the search of 2354 second images. Note that the dataset is heavily skewed towards identical twins which is not representative of the true population. There is also a skew towards same sex fraternal twin pairs compared to different sex fraternal twin pairs again not representative of the true population.

The notable results are:

- For all algorithms tested, the 1087 mated searches (Twin A vs. Twin A) produce scores almost always above typical operational thresholds, with (not shown) matches at rank 1. The images are of good quality, so this is the result expected from the rest of this report.
- For the 1066 identical twin searches (AB), almost all produce the twin at rank 1, with a few producing the mate at further down the candidate lists rank and low score.
- For the 169 fraternal searches (AB) from same sex pairs, most algorithms give a large number of very high scores, implying false positives at all thresholds. However, there are long tails containing lower scores that are correctly below threshold. In general, scores that are higher in this distribution are all rank 1 whereas the lower scores have much higher ranks.
- (Not shown) Of the 169, there are 24 fraternal searches (AB) involving different sex twins. Here most algorithms correctly report scores well below the lowest threshold, and usually not on the candidate list at all.

2023/03/14
14:32:11
 $\text{FNIR}(N, R, T) = \text{False neg. identification rate}$
 $\text{FPIR}(N, T) = \text{False pos. identification rate}$
 $N = \text{Num. enrolled subjects}$
 $R = \text{Num. candidates examined}$
 $T = \text{Threshold}$
 $T = 0 \rightarrow \text{Investigation}$
 $T > 0 \rightarrow \text{Identification}$

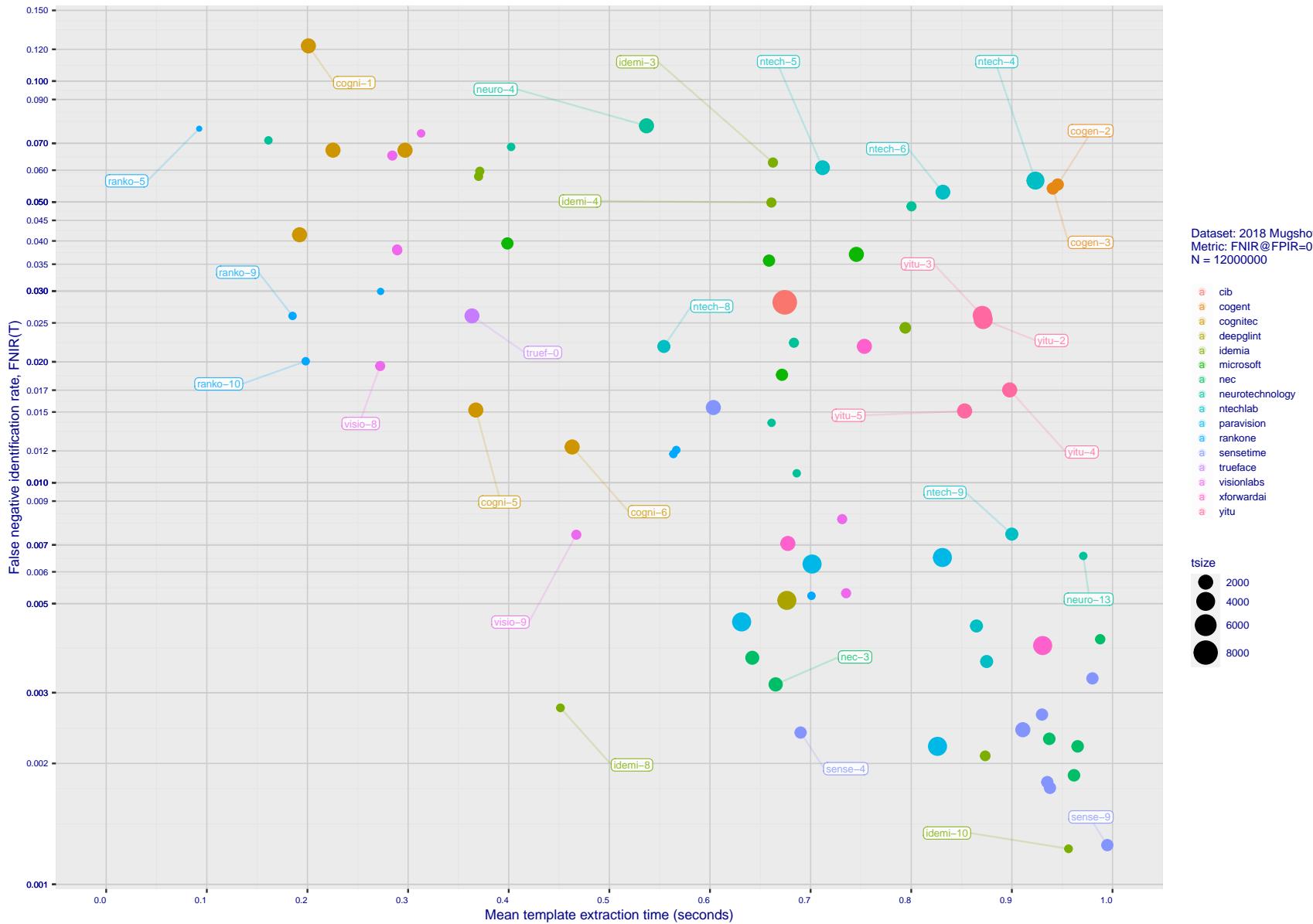


Figure 18: [Mugshot Dataset] Speed-accuracy tradeoff. For developers of the more accurate algorithms the plot shows the tradeoff of high-threshold recognition miss-rates, $\text{FNIR}(N, N, T)$ for $\text{FPIR}(N, T) = 0.003$, and template generation time. Developers are coded by color. Template size is encoded by the size of the circle. Some labels are quite distant from the respective point, to avoid superposing text. Without any other influences, the assumption would be that taking time to localize the face, and extract features, would lead to better accuracy. The most notable result, for NEC, is that their slower algorithms are much more accurate than the version that extract features in fewer than 90 milliseconds.

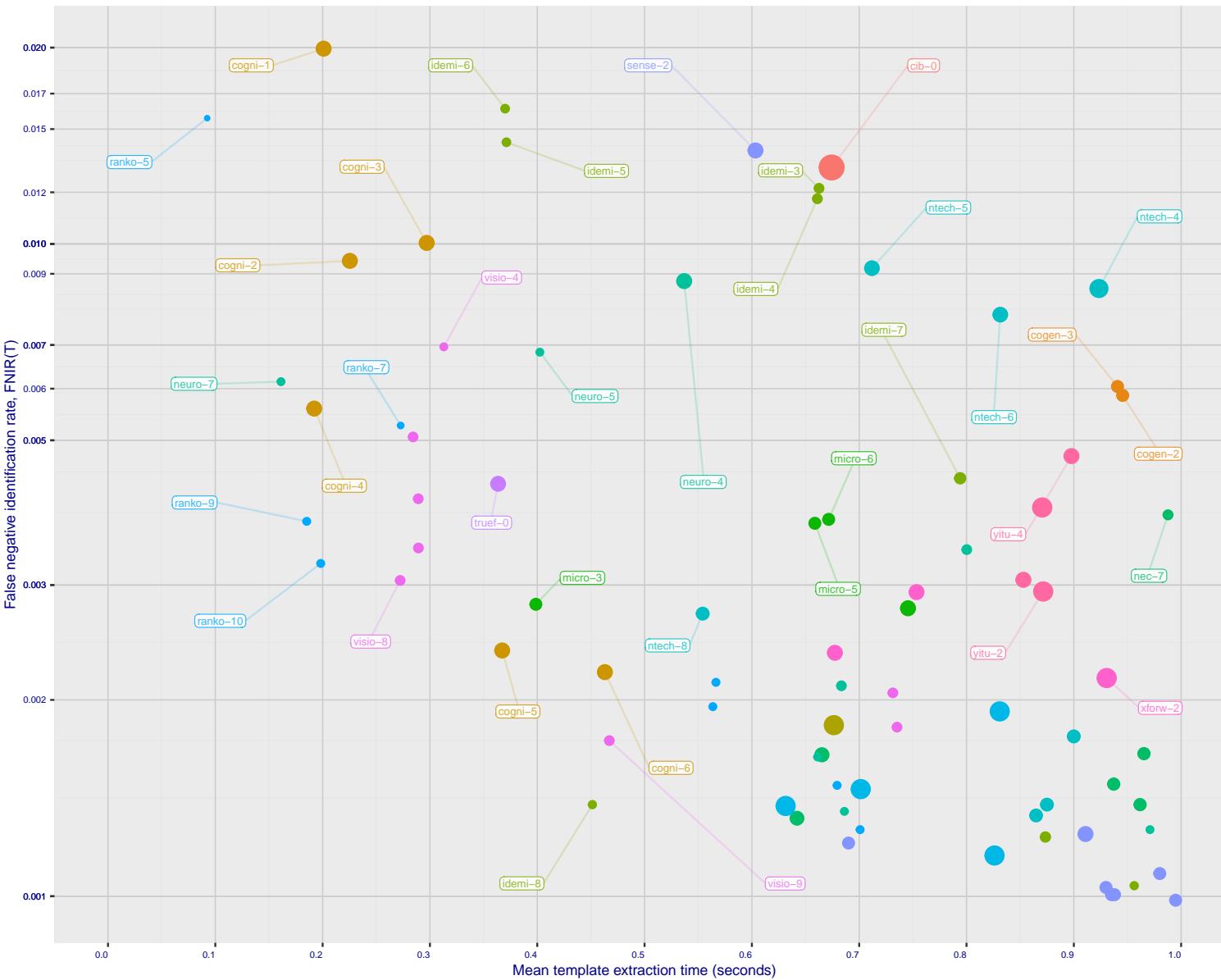
2023/03/14
14:32:11

Figure 19: [Mugshot Dataset] Speed-accuracy tradeoff. For developers of the more accurate algorithms the plot shows the tradeoff of rank-one recognition miss-rates, $\text{FNIR}(N, 1, 0)$, and template generation time. Developers are coded by color. Template size is encoded by the size of the circle. Some labels are quite distant from the respective point, to avoid superposing text. Without any other influences, the assumption would be that taking time to localize the face, and extract features, would lead to better accuracy. This occurs for NEC with their slower algorithm being much accurate than the version that extract features in fewer than 90 milliseconds.

Notes	1 Configuration size does not capture static data present in libraries. Libraries are included but the size also includes any ancillary libraries for image processing (e.g. openCV) or numerical computation (e.g. blas).
2	Finalization is the processing of converting $N = 1600000$ templates into a searchable data structure an operation which can be a simple copy, or the building of an index or tree, for example. The duration of the operation may be data dependent, and may not be linear in the number of input templates.
3	This multiplier expresses the increase in template size when k images are passed to the template generation function.
4	All durations are measured on Intel®Xeon®CPU E5-2630 v4 @ 2.20GHz processors. Estimates are made by wrapping the API function call in calls to std::chrono::high_resolution_clock which on the machine in (3) counts 1ns clock ticks. Precision is somewhat worse than that however.
5	Search durations are measured as in the prior note. The power-law model in the final column mostly fits the empirical results in Figure 151. However in certain cases the model is not correct and should not be used numerically.

Table 2: Summary of algorithms and properties included in this report. The blue superscripts give ranking for the quantity in that column. Missing search durations, denoted by “-”, are absent because those runs were not executed, usually because we did not run on the larger galleries. Caution: The power-law model is sometimes an incorrect model. It is included here only to show broad sublinear behavior, which is flagged in green. The models should not be used for prediction.

	DEVELOPER	DEVELOPER	LOCATION	SHORT NAME	SEQ. NUM.	VALIDATION DATE	CONFIG ¹ DATA (MB)	LIB ¹ DATA (MB)	TEMPLATE GENERATION			FINALIZE ² TIME (S)	SEARCH DURATION ³ MILLISEC						POWER LAW (μ s)
									SIZE (B)	MULT ³	TIME (MS) ⁴		L=1 N=1.6M	L=50 N=1.6M	L=50 N=3M	L=50 N=6M	L=50 N=12M		
53	Dermalog	DE	dermalog	008	2021-01-25	0	531	35 512	-	47 370	25 4	(61) 335	(57) 246	(45) 462	(46) 924	(44) 1849	49	0.15N ^{1.0}	
54	Dermalog	DE	dermalog	009	2021-11-09	0	318	33 512	-	40 347	18 3	(62) 253	(58) 246	(44) 461	(45) 923	(43) 1846	44	0.16N ^{1.0}	
55	Dermalog	DE	dermalog	010	2022-07-25	0	514	32 512	-	117 633	21 3	(56) 241	(56) 242	(43) 454	(44) 910	(42) 1823	47	0.15N ^{1.0}	
56	Dermalog	DE	dermalog	011	2022-12-12	0	272	5 128	-	39 342	2 1	(22) 87	(21) 88	(18) 165	(18) 331	(18) 664	64	0.05N ^{1.0}	
57	Digidata	IN	didata	000	2022-06-03	248	33	129 2048	-	98 560	255 2444	(2) 0	(23) 95	-	-	-	-	-	
58	DiluSense Technology	CN	dilusense	000	2022-05-26	311	56	128 2048	-	24 247	204 26	(203) 1904	(203) 1898	(174) 3597	(170) 7256	(173) 14689	103	0.88N ^{1.0}	
59	DiluSense Technology	CN	dilusense	001	2022-12-24	599	5	247 4096	-	225 883	22 38	(226) 3026	(229) 3042	(192) 4738	(190) 9473	(191) 19026	25	5.36N ^{0.9}	
60	FarBar Inc	TW	f8	001	2019-10-03	266	19	179 2048	k	191 810	142 14	-	-	-	-	-	-	-	
61	Fincore Ltd	UK	fincore	000	2021-08-18	250	224	147 2048	-	81 475	70 9	(122) 562	(119) 560	-	-	-	-	-	
62	First Credit Bureau Kazakhstan	KZ	firstcreditkz	001	2022-11-22	548	24	24 288	-	187 799	6 2	(20) 46	(18) 46	(16) 87	(16) 179	(16) 354	71	0.03N ^{1.0}	
63	Fujitsu Research and Development Center	CN	fujitsulab	000	2021-10-12	497	337	66 1032	-	295 945	35 5	(194) 1668	(192) 1657	(165) 3140	(163) 6320	(162) 12723	101	0.78N ^{1.0}	
64	Fujitsu Research and Development Center	CN	fujitsulab	001	2022-03-15	675	386	72 1032	-	224 882	71 9	(201) 1854	(202) 1817	(170) 3451	(169) 6986	(170) 14166	121	0.72N ^{1.0}	
65	Gorilla Technology	TW	gorilla	2	2018-10-29	91	1252	85 1132	k	38 338	202 24	(39) 145	(40) 146	(33) 293	(32) 612	(35) 1509	178	0.02N ^{1.1}	
66	Gorilla Technology	TW	gorilla	3	2018-10-26	94	1252	232 2156	k	97 559	263 12020	-	(20) 2047	-	-	-	-	-	
67	Gorilla Technology	TW	gorilla	004	2020-01-06	182	1244	233 2192	k	53 388	230 41	(74) 286	(72) 285	(99) 1191	(102) 2416	(95) 5036	220	0.00N ^{1.3}	
68	Gorilla Technology	TW	gorilla	005	2021-02-22	306	1420	269 6288	-	483 78	(142) 802	(142) 799	(116) 1514	(134) 4454	(128) 8820	206	0.05N ^{1.2}		
69	Gorilla Technology	TW	gorilla	006	2021-09-30	377	691	272 8336	-	174 767	251 99	(190) 1626	(189) 1612	(144) 2422	(133) 4422	(133) 9363	108	0.59N ^{1.0}	
70	Gorilla Technology	TW	gorilla	007	2022-02-16	392	322	270 6290	-	93 526	259 89	(140) 765	(137) 745	(110) 1408	(111) 2823	(104) 5764	79	0.42N ^{1.0}	
71	Gorilla Technology	TW	gorilla	008	2022-10-31	321	290	263 4242	-	249 938	240 54	(111) 513	(107) 500	(84) 949	(100) 2402	(107) 6006	203	0.03N ^{1.2}	
72	Griaule	US	griaule	000	2021-11-01	0	584	207 2052	-	63 417	52 8	(248) 582	(252) 6150	(213) 11473	(211) 22952	(208) 46070	41	3.89N ^{1.0}	
73	Griaule	US	griaule	001	2022-07-26	0	615	206 2052	-	272 1102	105 12	(249) 5866	(253) 6181	(215) 11629	(212) 23175	(209) 46504	59	3.74N ^{1.0}	
74	Guangzhou Pixel Solutions Co Ltd	CN	pixelall	002	2019-07-01	0	165	236 2560	k	15 190	160 15	(178) 1296	(180) 1334	(151) 2526	(147) 5136	(151) 11045	127	0.52N ^{1.0}	
75	Guangzhou Pixel Solutions Co Ltd	CN	pixelall	003	2019-11-05	0	690	237 2560	k	152 703	199 22	(175) 1273	(176) 1307	(148) 2474	(148) 5198	(152) 11141	140	0.46N ^{1.0}	
76	Guangzhou Pixel Solutions Co Ltd	CN	pixelall	004	2020-07-02	0	538	234 2560	k	69 449	181 17	(174) 1259	(175) 1300	(147) 2465	(154) 5492	(153) 11443	154	0.34N ^{1.1}	
77	Guangzhou Pixel Solutions Co Ltd	CN	pixelall	005	2021-03-23	0	717	235 2560	-	204 840	100 11	(187) 1606	(187) 1528	(153) 2609	(149) 4926	(156) 11770	91	0.73N ^{1.0}	
78	Hangzhou Allu Network Information Technology	CN	hzailu	000	2022-03-18	855	97	60 1024	-	124 649	101 11	(221) 2609	(225) 2551	(194) 4813	(193) 9702	(192) 19338	69	1.50N ^{1.0}	
79	Hangzhou Allu Network Information Technology	CN	hzailu	001	2022-08-18	273	162	165 2048	-	179 777	107 12	(239) 4537	(241) 4637	(206) 8666	(204) 17109	(205) 39805	129	1.79N ^{1.0}	
80	Hangzhou Allu Network Information Technology	CN	hzailu	002	2023-01-12	302	293	164 2048	-	208 845	111 12	(230) 4579	(242) 4652	(207) 8705	(205) 17192	(205) 39864	126	1.82N ^{1.0}	
81	Hikvision Research Institute	CN	hikvision	5	2018-10-29	593	9	91 1408	1	108 607	166 16	(153) 883	(153) 895	(129) 1908	(124) 3792	(135) 9387	186	0.10N ^{1.1}	
82	Hikvision Research Institute	CN	hikvision	6	2018-10-29	593	9	90 1408	1	106 598	169 16	(151) 871	(152) 877	-	-	-	-	-	
83	HyperVerge Inc	IN	hyperverge	001	2021-08-11	1791	212	61 1024	-	207 845	31 5	(135) 705	(130) 681	(105) 1346	(108) 2681	(102) 5680	113	0.32N ^{1.0}	
84	HyperVerge Inc	IN	hyperverge	002	2022-04-13	1140	1118	64 1024	-	244 934	75 9	(130) 661	(129) 659	(103) 1292	(94) 2188	(49) 2181	20	11.29N ^{0.8}	
85	Idemia	FR	idemia	5	2018-10-29	417	48	30 352	1	48 371	32 5	(35) 137	(37) 138	(40) 437	(37) 724	(38) 1630	212	0.01N ^{1.2}	
86	Idemia	FR	idemia	6	2018-10-29	417	48	28 352	1	46 370	29 4	(36) 137	(36) 138	(41) 442	(42) 827	(39) 1646	214	0.01N ^{1.2}	
87	Idemia	FR	idemia	007	2020-01-17	738	113	58 860	1	188 794	143 14	(40) 151	(41) 152	(66) 683	(72) 1481	(69) 3022	223	0.00N ^{1.4}	
88	Idemia	FR	idemia	008	2021-03-15	378	65	27 300	-	71 451	19 3	(34) 132	(35) 131	(30) 247	(29) 501	(28) 1013	82	0.07N ^{1.0}	
89	Idemia	FR	idemia	009	2022-03-01	735	68	56 636	-	219 873	44 7	(52) 211	(51) 205	(39) 389	(41) 787	(37) 1615	108	0.10N ^{1.0}	
90	Idemia	FR	idemia	010	2023-01-11	942	71	28 300	-	257 956	11 2	(80) 194	(48) 195	(37) 369	(36) 732	(34) 1488	70	0.11N ^{1.0}	
91	Imagus Technology Pty Ltd	AU	imagus	005	2021-01-15	222	311	143 2048	-	182 786	141 14	(55) 236	(77) 313	(63) 651	(67) 1361	(54) 2461	184	0.03N ^{1.1}	
92	Imagus Technology Pty Ltd	AU	imagus	006	2021-05-27	248	369	154 2048	-	235 904	84 9	(79) 317	(54) 234	(49) 499	(63) 1273	(50) 2727	209	0.01N ^{1.2}	
93	Imagus Technology Pty Ltd	AU	imagus	007	2021-11-16	248	366	192 2048	-	109 609	65 9	(54) 234	(55) 238	(42) 442	(43) 881	(41) 1765	36	0.16N ^{1.0}	
94	Imagus Technology Pty Ltd	AU	imagus	008	2022-05-26	204	335	190 2048	-	68 445	179 17	(120) 560	(122) 565	-	-	-	-	-	
95	Imperial College London	GB	imperial	000	2019-08-28	461	15	161 2048	1	102 577	116 13	(65) 360	(91) 379	(120) 1626	(128) 4057	(149) 10291	228	0.00N ^{1.5}	
96	Incode Technologies Inc	US	incode	2	2018-10-29	71	31	108 2048	1	29 289	165 15	(95) 411	(93) 404	-	-	-	-	-	
97	Incode Technologies Inc	US	incode	3	2018-10-29	133	31	184 2048	1	148 697	155 15	(94) 408	(97) 412	(75) 847	(76) 1608	(88) 4486	179	0.05N ^{1.1}	
98	Incode Technologies Inc	US	incode	004	2019-06-24	254	50	157 2048	1	82 475	106 12	(86) 365	(90) 378	(113) 1482	(79) 1660	(67) 2954	152	0.12N ^{1.1}	
99	Incode Technologies Inc	US	incode	005	2021-07-29	259	21	145 2048	-	87 500	89 10	(78) 316	(102) 454	(81) 890	(86) 1843	(80) 3640	168	0.07N ^{1.1}	
100	Innovatrics	SK	innovatrics	4	2018-10-30	0	400	81 1076	k	54 399	260 10902	(7) 8	(4) 11	(2) 9	(3) 13	9 668.38N ^{0.2}			
101	Innovatrics	SK	innovatrics	005	2019-09-30	0	455	48 538	1	200 827	262 11897	(6) 8	(5) 8	(3) 9	(3) 9	(2) 9	1 4055.65N ^{0.1}		
102	Innovatrics	SK	innovatrics	007	2021-08-16	175	58	48 538	-	176 777	144 14	(25) 97	(31) 100	(23) 188	(26) 378	(25) 788	31	0.09N ^{1.0}	
103	Innovatrics	SK	innovatrics	008	2023-01-12	609	102	261 4136	-	239 959	234 42	(149) 846	(154) 908	(122) 1671	(122) 3351	(117) 6635	33	0.72N ^{1.0}	
104	Intellivision	IN	intellivision	001	2022-03-08	62	130	223 2056	-	60 406	193 20	(89) 388							

	DEVELOPER FULL NAME	DEVELOPER LOCATION	SHORT NAME	SEQ. NUM.	VALIDATION DATE	CONFIG ¹ DATA (MB)	LIB ¹ DATA (MB)	TEMPLATE GENERATION			FINALIZE ² TIME (S)	SEARCH DURATION ⁵ MILLISEC							
								SIZE (B)	MULT ³	TIME (MS) ⁴		L=1 N=1.6M	L=50 N=1.6M	L=50 N=3M	L=50 N=6M	L=50 N=12M	POWER LAW (μ s)		
105	Intellivision	IN	intellivision	002	2022-07-28	114	128	219	2056	-	34	331	122	13	(264) 20542	(269) 20448	-	-	
106	Intema-LGL Group	LU	intema	000	2022-08-24	1042	20	31	512	-	165	737	267	1809	(15) 27	(13) 31	(10) 36	(12) 44	(10) 54
107	Intema-LGL Group	LU	intema	001	2023-02-22	723	20	43	512	-	249	938	258	4808	(14) 26	(9) 26	(14) 49	(13) 57	(11) 66
108	IrexAI	US	irex	000	2021-02-09	724	46	238	3080	-	206	844	189	19	(127) 616	(124) 600	(94) 1120	(104) 2477	(105) 5863
109	Kakao Enterprise	KR	kakao	000	2021-06-23	404	124	260	2052	-	203	835	98	8	(53) 213	(52) 215	(50) 510	(49) 971	(46) 1955
110	Kakao Enterprise	KR	kakao	001	2022-06-08	615	102	187	2048	-	260	961	183	18	(103) 469	(103) 471	(86) 952	(88) 1887	(81) 3870
111	Kedacom International Pte	SG	kedacom	001	2019-09-16	239	36	25	292	1	89	507	8	2	(139) 764	(139) 760	(130) 1940	(115) 2983	(116) 6623
112	Kneron	US	kneron	000	2020-03-03	366	13	122	2048	k	92	523	121	13	(220) 2535	(223) 2506	(193) 4752	(192) 6969	(194) 20926
113	Kneron	US	kneron	001	2021-06-10	270	69	183	2048	-	80	472	72	9	(222) 2690	(226) 2642	-	-	-
114	Line Corporation	JP	line	000	2021-06-02	138	397	150	2048	-	84	481	98	8	(242) 5433	(247) 5418	(210) 10144	-	-
115	Line Corporation	JP	line	001	2021-11-21	471	396	115	2048	-	238	907	60	8	(202) 1872	(206) 1934	(176) 3647	(178) 7675	-
116	Line Corporation	JP	lineclova	002	2022-07-29	560	72	172	2048	-	198	824	126	13	(63) 262	(64) 257	(48) 488	(51) 977	(47) 1963
117	Line Corporation	JP	lineclova	003	2023-01-19	574	397	188	2048	-	188	799	45	7	(42) 158	(33) 103	(47) 487	(50) 972	(60) 2731
118	Lomonosov Moscow State University	RU	instsysmsu	000	2019-08-19	375	168	118	2048	1	111	614	127	13	(98) 430	(100) 431	(78) 860	(80) 1730	(98) 5353
119	Lookman Electroplast Industries	IN	lookman	3	2018-10-28	203	24	26	292	1	37	336	173	3	(138) 739	(136) 745	(109) 1394	(110) 2817	(123) 8286
120	Lookman Electroplast Industries	IN	lookman	4	2018-10-28	184	24	52	548	1	33	320	28	4	(157) 981	(158) 998	-	-	-
121	Lookman Electroplast Industries	IN	lookman	005	2019-09-16	239	36	51	548	1	88	506	24	4	(150) 1005	(160) 1008	(152) 2597	(152) 5446	(129) 8939
122	Mantra Softech India	IN	mantra	000	2021-10-28	460	61	194	2052	-	62	412	88	10	(155) 916	(159) 910	(124) 1714	(123) 3411	(119) 6841
123	Maxvision	CN	maxvision	000	2022-06-17	167	60	123	2048	-	11	183	273	10	(241) 5044	(245) 5188	(209) 9663	(209) 19358	(203) 39552
124	Maxvision	CN	maxvision	001	2022-10-28	228	63	148	2048	-	74	457	125	13	(169) 1173	(169) 1177	(138) 2233	(138) 4589	(134) 9371
125	Megvii/Face++	CN	megvii	1	2018-10-28	1703	41	243	4096	1	115	631	221	32	(117) 552	(120) 561	(102) 2321	(106) 5968	(178) 0.08N ^{1.1}
126	Megvii/Face++	CN	megvii	2	2018-10-28	1735	42	246	4096	1	119	635	219	31	(118) 553	(117) 558	-	-	-
127	MicroFocus	GB	microfocus	5	2018-10-29	94	26	16	256	k	28	262	14	2	(47) 182	(46) 186	(36) 354	(36) 708	(32) 1425
128	MicroFocus	GB	microfocus	6	2018-10-29	94	26	13	256	k	25	262	14	2	(48) 183	(45) 186	-	-	-
129	Microsoft	US	microsoft	5	2018-10-29	381	155	62	1024	1	127	658	103	11	(186) 1606	(193) 1673	(164) 3076	(162) 6302	(167) 13160
130	Microsoft	US	microsoft	6	2018-10-29	478	155	65	1024	1	132	671	159	15	(191) 1642	(191) 1618	(178) 3710	(165) 6401	(164) 12892
131	Mukh Technologies	US	mukh	002	2022-09-16	693	442	191	2048	-	273	1278	257	4261	(4) 5	(20) 83	(17) 106	(17) 313	(17) 628
132	N-Tech Lab	RU	ntech	5	2018-10-30	1685	113	102	1940	k	156	711	241	55	(59) 243	(60) 246	(52) 534	(54) 1100	(63) 2867
133	N-Tech Lab	RU	ntech	6	2018-10-30	1686	117	103	1940	k	202	831	243	63	(58) 243	(59) 246	(54) 546	(55) 1104	(64) 2873
134	N-Tech Lab	RU	ntechlab	007	2019-06-25	2450	51	240	3348	k	189	795	246	73	(91) 393	(98) 427	(72) 780	(80) 1768	(78) 3499
135	N-Tech Lab	RU	ntechlab	008	2020-01-06	1111	51	89	1300	k	96	554	228	36	(46) 179	(43) 184	(35) 341	(35) 683	(31) 1395
136	N-Tech Lab	RU	ntechlab	009	2021-03-01	1208	42	88	1300	-	235	899	226	35	(45) 178	(44) 184	(34) 336	(34) 676	(40) 1704
137	N-Tech Lab	RU	ntechlab	010	2021-06-24	351	213	87	1280	-	220	874	36	6	(99) 440	(101) 435	(74) 821	(73) 3337	(92) 223N ^{1.0}
138	N-Tech Lab	RU	ntechlab	011	2021-12-07	679	208	86	1280	-	214	864	39	6	(106) 488	(105) 483	(82) 912	(87) 1869	(93) 5003
139	NFC	JP	nec	2	2018-10-30	705	35	98	1616	k	123	642	186	18	(92) 405	(95) 409	(92) 1072	(81) 1755	(88) 4255
140	NFC	JP	nec	3	2018-10-30	774	110	99	1712	k	130	665	194	21	(5) 7	(3) 7	(5) 14	(9) 40	(12) 82
141	NFC	JP	nec	004	2021-07-19	971	63	83	1104	-	262	965	40	7	(82) 349	(83) 351	(64) 662	(64) 1330	(56) 2685
142	NFC	JP	nec	005	2021-12-13	922	88	84	1104	-	261	961	41	7	(104) 473	(115) 551	(90) 1017	(92) 2091	(86) 4242
143	NFC	JP	nec	006	2022-08-10	701	54	82	1104	-	247	937	69	9	(83) 358	(84) 354	(65) 666	(65) 1331	(57) 2707
144	NFC	JP	nec	007	2023-03-03	632	56	55	560	-	270	987	37	6	(51) 200	(49) 200	-	(39) 752	(36) 1527
145	Neurotechnology	LT	neurotech	5	2018-10-30	266	53	11	256	k	98	402	132	12	(146) 835	(148) 839	(123) 1690	(121) 3219	(130) 8955
146	Neurotechnology	LT	neurotech	6	2018-10-30	564	53	10	256	k	160	726	102	2	(147) 839	(149) 842	-	-	-
147	Neurotechnology	LT	neurotech	007	2019-10-03	57	51	12	256	k	761	161	72	2	(165) 1118	(165) 1110	(136) 2143	(132) 4397	(131) 9045
148	Neurotechnology	LT	neurotechnology	008	2021-03-22	355	49	46	514	-	189	800	27	4	(168) 1167	(168) 1149	(139) 2266	(137) 4573	(139) 9586
149	Neurotechnology	LT	neurotechnology	009	2021-09-01	246	82	44	513	-	139	683	15	3	(162) 1035	(162) 1049	(132) 1977	(130) 4270	(126) 8756
150	Neurotechnology	LT	neurotechnology	010	2022-01-07	247	83	9	256	-	129	661	3	2	(158) 988	(156) 984	(127) 1897	(127) 3977	(122) 8048
151	Neurotechnology	LT	neurotechnology	012	2022-06-07	247	84	15	256	-	142	686	16	3	(163) 1036	(164) 1063	(133) 2046	(129) 4179	(125) 8624
152	Neurotechnology	LT	neurotechnology	013	2023-02-03	364	87	14	256	-	265	970	4	2	(247) 5779	(246) 5231	(212) 10886	(219) 27551	(220) 76318
153	Newland Computer Co Ltd	CN	newland	2	2018-10-30	96	27	156	2048	-	211	855	161	15	(26) 8741	(265) 8854	(227) 17892	(226) 39356	-
154	Nobilis	US	nobilis	1	2018-10-30	114	176	159	2048	1	18	206	15	176	(172) 1273	(173) 1272	-	-	-
155	Nobilis	US	nobilis	2	2018-10-30	153	176	264	6144	1	91	517	23	43	(219) 2513	(224) 2522	(195) 5649	(197) 12432	(207) 44262
156	NotionTag Technologies Private Limited	IN	notiontag	000	2022-01-14	265	945	231	2120	-	72	453	92	10	(259) 8619	(264) 8705	(226) 16652	(225) 38794	(222) 90607

Notes

1 Configuration size does not capture static data present in libraries. Libraries are included but the size also includes any ancillary libraries for image processing (e.g. openCV) or numerical computation (e.g. blas).

2 Finalization is the processing of converting $N = 1600000$ templates into a searchable data structure an operation which can be a simple copy, or the building of an index or tree, for example. The duration of the operation may be data dependent, and may not be linear in the number of input templates.3 This multiplier expresses the increase in template size when k images are passed to the template generation function.

4 All durations are measured on Intel®Xeon®CPU E5-2630 v4 @ 2.20GHz processors. Estimates are made by wrapping the API function call in calls to std::chrono::high_resolution_clock which on the machine in (3) counts 1ns clock ticks. Precision is somewhat worse than that however.

5 Search durations are measured as in the prior note. The power-law model in the final column mostly fits the empirical results in Figure 151. However in certain cases the model is not correct and should not be used numerically.

2023 / 03 / 14

FNR(N, R, T) =

False neg. identification rate

N = Num. enrolled subjects

R = Num. candidates examined

T = Threshold

T = 0 → Investigation

T √

	DEVELOPER	DEVELOPER	SHORT	SEQ.	VALIDATION	CONFIG ¹	LIB ¹	TEMPLATE GENERATION			FINALIZE ²	SEARCH DURATION ⁵ MILLISEC														
								NUM.	DATE	DATA (MB)	DATA (MB)	SIZE (B)	MULT ³	TIME (MS) ⁴	L=1	L=50	L=50	L=50	L=50	POWER LAW						
															N=1.6M	N=1.6M	N=3M	N=6M	N=12M	(μ s)						
157	Pangiam	US	pangiam	000	2022-02-22	453	23	130	2048	-	120	636	180	17	(67)	276	(78)	319	(59)	601	(60)	1210	(53)	2443	75	0.18N ^{1.0}
158	Pangiam	US	pangiam	001	2022-11-17	991	36	176	2048	-	263	966	139	14	(66)	275	(79)	323	(80)	885	(84)	1771	(79)	3592	207	0.02N ^{1.2}
159	Paravision (EverAI)	US	everai	2	2018-10-30	224	304	174	2048	1	43	366	210	30	(69)	278	(71)	283	-	-	-	-	-	-	-	
160	Paravision (EverAI)	US	everai	3	2018-10-30	438	304	153	2048	1	157	717	209	28	(68)	278	(70)	281	(56)	572	(56)	1146	(50)	2278	122	0.12N ^{1.0}
161	Paravision (EverAI)	US	everai-paravision	004	2019-06-19	527	128	248	4096	1	133	672	236	45	(119)	559	(118)	559	(154)	2611	(167)	6445	(171)	14519	226	0.00N ^{1.5}
162	Paravision (EverAI)	US	paravision	005	2019-12-11	543	154	241	4096	1	201	830	238	48	(121)	561	(121)	564	(91)	1056	(96)	2298	(92)	4966	150	0.16N ^{1.1}
163	Paravision (EverAI)	US	paravision	007	2021-02-01	529	235	250	4096	-	150	701	239	48	(123)	569	(116)	558	(93)	1086	(93)	2111	(87)	4254	27	1.11N ^{0.9}
164	Paravision	US	paravision	009	2021-12-14	672	300	256	4100	-	116	631	246	82	(232)	3690	(237)	4230	(203)	8037	(203)	16532	(199)	31422	124	1.62N ^{1.0}
165	Paravision	US	paravision	012	2023-02-07	762	182	255	4100	-	198	826	249	85	(234)	4475	(239)	4466	(205)	8552	(207)	17349	(200)	33950	131	1.66N ^{1.0}
166	Qnap Security	TW	qnap	000	2021-07-28	182	15	146	2048	-	73	457	77	9	(171)	1231	(199)	1763	-	-	-	-	-	-	-	
167	Qnap Security	TW	qnap	001	2021-12-09	191	13	110	2048	-	110	613	55	8	(193)	1666	(184)	1429	(171)	3472	(175)	7375	(178)	15159	198	0.11N ^{1.2}
168	Qnap Security	TW	qnap	002	2022-04-15	338	32	185	2048	-	195	822	177	17	(176)	958	(170)	1179	(141)	2312	(141)	4789	(146)	9791	162	0.24N ^{1.1}
169	Qnap Security	TW	qnap	003	2022-12-09	239	60	160	2048	-	52	387	136	13	(195)	1671	(182)	1396	(173)	3567	(174)	7350	(176)	15014	206	0.09N ^{1.2}
170	Quantasoft	CZ	quantasoft	1	2018-10-30	276	452	193	2048	k	51	385	38	6	(262)	15422	(267)	14858	(224)	14717	-	(184)	18323	-	-	-
171	Rank One Computing	US	rankone	4	2018-10-09	0	101	101	85	k	36	427	30	101	(32)	101	(26)	190	-	-	-	-	37	0.07N ^{1.0}		
172	Rank One Computing	US	rankone	5	2018-10-24	0	101	6	133	k	92	437	(37)	140	(38)	144	(31)	266	(30)	525	(29)	1049	34	0.11N ^{1.0}		
173	Rank One Computing	US	rankone	006	2019-06-03	0	133	7	165	k	23	245	33	8	-	-	-	-	-	-	-	-	-			
174	Rank One Computing	US	rankone	007	2019-11-12	0	137	8	165	k	27	272	47	7	(33)	116	(34)	115	(28)	215	(28)	439	(26)	877	73	0.07N ^{1.0}
175	Rank One Computing	US	rankone	009	2020-06-26	0	105	18	260	k	13	185	99	11	(24)	95	(27)	96	(21)	181	(22)	727	48	0.06N ^{1.0}		
176	Rank One Computing	US	rankone	010	2020-11-05	0	135	19	261	-	16	198	93	10	(25)	95	(22)	95	(19)	178	(20)	714	43	0.06N ^{1.0}		
177	Rank One Computing	US	rankone	011	2021-08-27	0	175	20	261	-	100	566	61	8	(27)	96	(24)	95	(22)	183	(19)	714	58	0.06N ^{1.0}		
178	Rank One Computing	US	rankone	012	2021-12-27	0	257	20	261	-	99	563	49	8	(26)	95	(20)	179	(21)	361	(21)	718	46	0.06N ^{1.0}		
179	Rank One Computing	US	rankone	013	2022-07-21	0	223	21	261	-	138	679	177	16	(31)	101	(30)	100	(24)	188	(24)	376	(24)	784	26	0.20N ^{0.9}
180	Rank One Computing	US	rankone	014	2022-12-21	0	237	21	261	-	149	700	51	8	(32)	101	(29)	100	(25)	188	(25)	376	(23)	775	84	0.06N ^{1.0}
181	Realnetworks Inc	US	realnetworks	2	2018-10-30	105	104	259	4104	k	22	241	208	28	(204)	2008	(210)	2048	(181)	4194	(181)	8642	(177)	15035	90	1.08N ^{1.0}
182	Realnetworks Inc	US	realnetworks	003	2019-06-12	93	102	101	1848	k	10	173	115	13	(167)	1145	(166)	1132	(135)	2142	(149)	5241	(150)	10495	166	0.21N ^{1.1}
183	Realnetworks Inc	US	realnetworks	004	2019-10-17	94	102	100	1848	1	9	171	98	11	(166)	1143	(167)	1137	(137)	2149	(140)	4740	(142)	9693	145	0.36N ^{1.0}
184	Realnetworks Inc	US	realnetworks	005	2021-06-23	168	209	220	2056	-	35	332	68	9	(192)	1654	(190)	1616	(163)	3030	(160)	6068	(159)	12134	53	1.01N ^{1.0}
185	Realnetworks Inc	US	realnetworks	006	2021-12-02	250	56	217	2056	-	41	348	56	8	(116)	543	(113)	531	(89)	996	(91)	1998	(85)	3991	51	0.33N ^{1.0}
186	Realnetworks Inc	US	realnetworks	007	2022-04-11	455	99	222	2056	-	118	634	178	17	(145)	815	(145)	812	(117)	1559	(118)	3159	(114)	6361	141	0.27N ^{1.0}
187	Realnetworks Inc	US	realnetworks	008	2022-08-29	557	99	213	2056	-	264	968	108	12	(115)	538	(112)	525	(88)	986	(90)	1967	(100)	5559	167	0.09N ^{1.1}
188	Remark Holdings	CN	remarkai	000	2019-06-12	234	1092	109	2048	k	125	650	114	12	(246)	5776	(249)	5703	(214)	11604	(223)	32133	(223)	91436	219	0.05N ^{1.3}
189	Remark Holdings	CN	remarkai	0	2018-10-30	187	847	149	2048	k	104	593	148	14	(245)	5685	(250)	5723	-	-	-	-	-	-	-	
190	Remark Holdings	CN	remarkai	1	2018-10-30	187	847	172	2048	k	65	427	153	14	(244)	5680	(251)	5761	(218)	12475	(221)	28726	(218)	59618	204	0.37N ^{1.2}
191	Rendip	SG	rendip	000	2021-05-21	0	416	134	2048	-	228	890	80	9	(60)	249	(86)	368	(68)	697	(71)	1452	(66)	2926	157	0.08N ^{1.1}
192	Reveal Media Ltd	UK	revealmedia	000	2022-02-02	287	196	209	2052	-	50	383	87	10	(208)	2322	(207)	2019	(180)	3838	(179)	7816	(181)	16559	128	0.78N ^{1.0}
193	SQLsoft	KR	sqlsoft	001	2021-12-20	271	377	221	2056	-	77	462	78	9	(179)	1310	(178)	1319	(146)	2456	(143)	4906	(145)	9755	38	0.90N ^{1.0}
194	SQLsoft	KR	sqlsoft	002	2022-10-26	354	593	215	2056	-	128	661	124	13	(184)	1480	(185)	1456	(156)	2712	(153)	5487	(160)	12210	120	0.59N ^{1.0}
195	Samsung S1 Corp	KR	s1	000	2021-06-03	257	196	254	4096	-	215	865	191	20	(255)	6715	(260)	6794	(222)	13032	(218)	26372	(216)	55723	118	2.82N ^{1.0}
196	Samsung S1 Corp	KR	s1	001	2021-11-01	240	198	138	2048	-	192	813	62	8	(210)	2415	(222)	2491	(191)	4718	(191)	9614	(195)	24472	161	0.53N ^{1.1}
197	Samsung S1 Corp	KR	s1	002	2022-05-04	244	93	152	2048	-	258	958	167	6	(172)	1234	(174)	1285	(144)	2411	(142)	4805	(143)	9705	62	0.77N ^{1.0}
198	Samsung S1 Corp	KR	s1	003	2022-09-27	471	93	177	2048	-	267	977	133	13	(189)	1620	(194)	1697	(167)	3187	(164)	6400	(163)	12792	68	0.99N ^{1.0}
199	Samsung S1 Corp	KR	s1	004	2023-02-03	471	58	163	2048	-	256	955	123	13	(188)	1617	(195)	1703	(168)	3194	(166)	6418	(165)	12999	83	0.94N ^{1.0}
200	Scanova Ltd	IL	scanovate	000	2020-01-15	250	446	142	2048	-	153	705	151	14	(183)	1419	(183)	1412	(162)	3008	(194)	11616	(157)	12012	205	0.10N ^{1.2}
201	Scanova Ltd	IL	scanovate	001	2020-09-10	250	446	119	2048	-	135	675	120	13	(180)	1321	(179)	1320	(149)	2502	(146)	5047	(147)	10163</td		

	DEVELOPER FULL NAME	DEVELOPER LOCATION	SHORT NAME	SEQ. NUM.	VALIDATION DATE	CONFIG ¹ DATA (MB)	LIB ¹ DATA (MB)	TEMPLATE GENERATION SIZE (B) MULT ³ TIME (MS) ⁴	FINALIZE ² TIME (S)	SEARCH DURATION ⁵ MILLISEC						POWER LAW (μ s)
										L=1 N=1.6M	L=50 N=1.6M	L=50 N=3M	L=50 N=6M	L=50 N=12M		
209	Sensetime Group	CN	sensetime	007	2022-01-15	526	37	70 1032 - 245 935	83 8	(211) 2432 (215) 2406 (183) 4513 (182) 8998 (188) 18796	88 1.28 $N^{1.0}$					
210	Sensetime Group	CN	sensetime	008	2022-08-17	567	37	67 1032 - 246 937	71 9	(212) 2444 (216) 2419 (184) 4525 (184) 9114 (183) 18279	67 1.43 $N^{1.0}$					
211	Sensetime Group	CN	sensetime	009	2023-01-04	883	59	69 1032 - 271 994	64 9	(213) 2446 (214) 2398 (186) 4540 (183) 9040 (182) 18167	66 1.42 $N^{1.0}$					
212	Shaman Software	US	shaman	6	2018-10-26	0	200	111 2048 k	154 14	(126) 603 (125) 612	- - -					
213	Shaman Software	US	shaman	7	2018-10-26	0	200	107 2048 k	157 14	(125) 602 (126) 614 (97) 1187 (103) 2448 (97) 5083	123 0.25 $N^{1.0}$					
214	Shanghai Yitu Technology	CN	yitu	4	2018-10-30	2119	136	227 2070 1	231 897	238 45 (177) 1288 (172) 1203 (145) 2440 (150) 5241 (141) 9671	117 0.52 $N^{1.0}$					
215	Shanghai Yitu Technology	CN	yitu	5	2018-10-30	2043	136	228 2070 1	218 853	234 44 (173) 1237 (171) 1199 (150) 2513 (148) 5013 (140) 9620	113 0.55 $N^{1.0}$					
216	Smilart	DE	smilart	4	2018-10-30	65	89	36 512 k	8 167	26 4 (263) 16137 (268) 15633	- - -					
217	Smilart	DE	smilart	5	2018-10-30	562	89	178 2048 k	70 450	146 14 - - -	- - -					
218	Staqua Technologies	IN	staqua	000	2021-08-30	1018	690	244 4096 -	198 826	203 24 (240) 4950 (243) 4933	- - -					
219	Synesis	RU	synesis	3	2018-10-30	237	150	247 4096 k	5 99	212 29 (141) 789 (143) 801 (131) 1941 (126) 3888 (127) 8810	191 0.07 $N^{1.1}$					
220	Synesis	RU	synesis	003	2019-07-04	143	17	135 2048 k	19 211	109 12 (110) 507 (110) 502 (140) 2297 (136) 4564 (136) 9452	224 0.00 $N^{1.4}$					
221	Synesis	RU	synesis	005	2020-09-08	494	24	257 4104 -	171 756	201 24 (152) 877 (150) 865 (166) 3182 (139) 4658 (144) 9750	208 0.06 $N^{1.2}$					
222	T4iSB	BR	t4isb	000	2022-08-17	228	15	131 2048 -	167 741	129 13 (61) 250 (62) 250	- - -					
223	Tech5 SA	CH	tech5	001	2019-08-19	1394	116	92 1536 k	227 887	86 10 (87) 383 (140) 766 (157) 2767	(161) 6149 (110) 6178					
224	Tech5 SA	CH	tech5	002	2021-04-07	727	112	45 513 -	259 940	22 4 (238) 4682 (258) 6689 (219) 12541 (215) 25145 (213) 50239	50 4.18 $N^{1.0}$					
225	Tencent Deepsea Lab	CN	deepsea	001	2019-07-29	250	323	158 2048 1	166 737	112 12 (161) 1021 (161) 1020 (158) 2774	(157) 5767 (161) 12341					
226	Tevian	RU	tevian	5	2018-10-30	773	15	118 2048 1	59 405	158 15 (93) 405 (94) 408 (76) 854	(82) 1757 (77) 3380					
227	Tevian	RU	tevian	006	2021-04-16	769	19	75 1032 -	105 597	85 10 (76) 295 (74) 295 (57) 578	(58) 1187 (61) 2741					
228	Tevian	RU	tevian	007	2021-10-12	703	19	71 1032 -	178 777	30 4 (77) 297 (75) 298 (56) 579	(57) 1179 (52) 2418					
229	Thales Group	US	cogent	2	2018-10-30	681	39	78 1043 k	253 945	206 27 (205) 2017 (212) 2144 (182) 4298 (180) 8472 (180) 16429	95 1.08 $N^{1.0}$					
230	Thales Group	US	cogent	3	2018-10-30	681	39	79 1043 k	259 940	82 9 (170) 1230 (177) 1311 (155) 2687 (151) 3398 (148) 10184	108 0.62 $N^{1.0}$					
231	Thales Group	US	cogent	004	2021-02-10	1376	59	212 2053 -	254 947	138 14 (223) 2903 (204) 1911 (172) 3566 (176) 7498 (179) 16370	143 0.64 $N^{1.0}$					
232	Thales Group	US	cogent	005	2021-09-13	1043	56	80 1062 -	175 769	34 5 (154) 912 (157) 996 (126) 1872 (125) 3845 (120) 7555	110 0.44 $N^{1.0}$					
233	Thales Group	US	cogent	006	2022-05-14	508	70	54 550 -	205 843	50 8 (124) 587 (146) 820 (118) 1564 (119) 3173 (124) 8290	165 0.16 $N^{1.1}$					
234	Thales Group	US	cogent	007	2023-01-30	597	72	53 550 -	269 984	20 3 (148) 843 (151) 868 (121) 1631 (78) 1649 (95) 3341	17 25.73 $N^{0.7}$					
235	TigerIT Americas LLC	US	tiger	2	2018-10-29	416	518	198 2052 k	76 461	161 15 (200) 1816 (205) 1921 (179) 3833 (177) 7526 (174) 14820	115 0.83 $N^{1.0}$					
236	TigerIT Americas LLC	US	tiger	3	2018-10-30	416	518	201 2052 k	76 461	27 37431 (49) 191 (47) 189 - - -	- - -					
237	Toshiba	JP	toshiba	0	2018-10-30	961	105	97 1548 k	227 876	104 12 (252) 6153 (254) 6236 (216) 12221 (216) 25355 (212) 49448	199 0.36 $N^{1.2}$					
238	Toshiba	JP	toshiba	1	2018-10-30	961	105	225 2060 k	221 875	272 44701 (251) 6007 (256) 6355 - - -	- - -					
239	Tripleze	JP	aize	001	2021-08-06	262	150	12 2048 -	50 402	71 9 (227) 3087 (230) 3080 - - -	- - -					
240	Trueface.ai	US	trueface	000	2021-01-27	247	119	104 2000 -	42 363	118 13 (64) 271 (82) 327 (61) 614 (61) 1239 (55) 2678	105 0.15 $N^{1.0}$					
241	TuringTech.vip	CN	turingtechvip	001	2022-09-29	151	161	178 2048 -	198 817	135 13 (265) 22085 (220) 22044 - - -	- - -					
242	Veridas Digital Authentication Solutions S.L.	ES	veridas	001	2021-03-05	347	875	133 2048 -	218 872	119 13 (243) 5493 (248) 5469 (211) 10350 (210) 20655 (206) 41264	54 3.40 $N^{1.0}$					
243	Veridas Digital Authentication Solutions S.L.	ES	veridas	002	2021-07-06	347	870	134 2048 -	223 877	95 10 (80) 322 (80) 325 (67) 685 (68) 1365 (59) 2730	151 0.09 $N^{1.1}$					
244	Veridas Digital Authentication Solutions S.L.	ES	veridas	003	2021-11-09	346	870	141 2048 -	216 867	66 9 (101) 440 (81) 327 (69) 699 (69) 1401 (84) 3954	202 0.02 $N^{1.2}$					
245	Veridas Digital Authentication Solutions S.L.	ES	veridas	004	2023-02-03	1074	608	144 2048 -	212 856	131 13 (102) 466 (104) 474 (85) 951 (48) 953 (82) 3881	30 0.49 $N^{1.0}$					
246	Verijelas	ID	verijelas	000	2022-10-11	248	11	158 2048 -	36 334	140 14 (20) 20 (10) 27 - - -	- - -					
247	Vietnam Posts and Telecommunications Group	VN	vnpt	001	2022-05-05	361	235	173 2048 -	230 892	192 20 (144) 813 (144) 804 (115) 1514 (116) 3037 (108) 6128	52 0.50 $N^{1.0}$					
248	Vietnam Posts and Telecommunications Group	VN	vnpt	002	2022-09-08	547	235	108 2048 -	198 808	176 16 (150) 857 (147) 835 (119) 1576 (120) 3183 (115) 6412	87 0.44 $N^{1.0}$					
249	Viettel Group	VN	vts	000	2021-03-12	250	257	171 2048 -	86 492	254 2295 (3) 4 (2) 4 (2) 6 (4) 11 - 15 0.61 $N^{0.6}$						
250	Viettel Group	VN	vts	001	2021-07-16	352	600	188 2048 -	229 891	197 21 (215) 2477 (221) 2487 (187) 4644 (187) 9313 (187) 18713	56 1.53 $N^{1.0}$					
251	Viettel Group	VN	vts	002	2022-02-08	244	600	117 2048 -	234 903	213 29 (217) 2485 (220) 2485 (190) 4678 (188) 9370 (189) 18833	65 1.49 $N^{1.0}$					
252	Viettel Group	VN	vts	003	2022-07-14	493	468	139 2048 -	151 702	223 34 (216) 2482 (219) 2480 (188) 4649 (186) 9302 (186) 18651	57 1.52 $N^{1.0}$					
253	Vigilant Solutions	US	vigilant	5	2018-10-30	335	122	95 1544 k	762 189	19 1720 - - -	- - -					
254	Vigilant Solutions	US	vigilant	6	2018-10-30	337	122	96 1544 k	816 195	21 (196) 1713 - - -	- - -					
255	Vigilant Solutions	US	vigilantsolutions	007	2021-01-08	340	51	94 1544 -	112 616	175 16 (182) 1354 (181) 1352 (160) 2911 (159) 5966 (154) 11466	164 0.27 $N^{1.1}$					
256	Vigilant Solutions	US	vigilantsolutions	008	2021-07-23	340	51	95 1544 -	57 403	128 13 (164) 1062 (163) 1061 (142) 2330 (155) 5520 (137) 9499	187 0.11 $N^{1.1}$					
257	Visidon	FI	visidon	1	2018-10-30	166	42	198 2052 k	136 667	164 15 (233) 4370 (240) 4472 (204) 8454 (206) 17262 (203) 34288	86 2.40 $N^{1.0}$					
258	Visidon	FI	vd	002	2021-05-18	248	42	198 2052 -	143 687	69 9 (206) 2089 (213) 2336 - - -	- - -					
259	Visidon	FI	vd	003	2021-10-12	497	43	198 2052 -	146 692	58 7 (207) 2095 (211) 2082 - - -	- - -					
260	Vision-Box	PT	visionbox	000	2021-09-17	252	274	224 2059 -	83 481	174 16 (96) 422 (85) 359 (77) 855 (33) 631 (48) 2096	21 2.46 $N^{0.8}$					

Notes

- Configuration size does not capture static data present in libraries. Libraries are included but the size also includes any ancillary libraries for image processing (e.g. openCV) or numerical computation (e.g. blas).
- Finalization is the processing of converting $N = 1600000$ templates into a searchable data structure an operation which can be a simple copy, or the building of an index or tree, for example. The duration of the operation may be data dependent, and may not be linear in the number of input templates.
- This multiplier expresses the increase in template size when k images are passed to the template generation function.
- All durations are measured on Intel®Xeon®CPU E5-2630 v4 @ 2.20GHz processors. Estimates are made by wrapping the API function call in calls to std::chrono::high_resolution_clock which on the machine in (3) counts 1ns clock ticks. Precision is somewhat worse than that however.
- Search durations are measured as in the prior note. The power-law model in the final column mostly fits the empirical results in Figure 151. However in certain cases the model is not correct and should not be used numerically.

Table 6: Summary of algorithms and properties included in this report. The blue superscripts give ranking for the quantity in that column. Missing search durations, denoted by “-”, are absent because those runs were not executed, usually because we did not run on the larger galleries. Caution: The power-law model is sometimes an incorrect model. It is included here only to show broad sublinear behavior, which is flagged in green. The models should not be used for prediction.

2023/03/14

FNIR(N, R, T) =

FPFR(N, T) =

N = Num. enrolled subjects

T = Threshold

T = 0 → Investigation

T √ 0 → Identification

	DEVELOPER FULL NAME	DEVELOPER LOCATION	SHORT NAME	SEQ. NUM.	VALIDATION DATE	CONFIG ¹ DATA (MB)	LIB ¹ DATA (MB)	TEMPLATE GENERATION			FINALIZE ² TIME (S)	SEARCH DURATION ⁵ MILLISEC						POWER LAW (μ s)				
								SIZE (B)	MULT ³	TIME (MS) ⁴		L=1	L=50	L=50	L=50	L=50						
												N=1.6M	N=1.6M	N=1.6M	N=3M	N=6M	N=12M					
2023/03/14 14:32:11	FNIR(N, R, T) FPFR(N, T) =	False neg. identification rate False pos. identification rate	N = Num. enrolled subjects R = Num. candidates examined	T = Threshold T = 0 → Investigation T > 0 → Identification	261	VisionLabs	RU	visionlabs	6	2018-10-30	360	17	³⁷ 512	1	³⁰ 289	²⁶⁸ 20290	⁽¹⁹⁾ 36	⁽¹⁷⁾ 36	⁽¹³⁾ 39	⁽¹¹⁾ 44	⁽⁹⁾ 53	⁸ 3211.93N ^{0.2}
					262	VisionLabs	RU	visionlabs	7	2018-10-30	360	17	⁴² 512	1	³¹ 289	²⁷⁰ 34666	⁽²¹⁾ 63	⁽¹⁹⁾ 63	⁽¹⁵⁾ 72	⁽¹⁵⁾ 80	⁽¹³⁾ 115	¹⁰ 2076.32N ^{0.2}
					263	VisionLabs	RU	visionlabs	008	2019-06-18	348	17	⁴¹ 512	1	²⁸ 272	²⁶⁵ 12747	⁽¹²⁾ 23	⁽⁸⁾ 24	⁽⁷⁾ 26	⁽⁶⁾ 29	⁽⁵⁾ 33	⁶ 2539.61N ^{0.2}
					264	VisionLabs	RU	visionlabs	009	2020-08-04	689	20	³⁹ 512	-	⁷⁹ 467	²⁶⁶ 13245	⁽¹³⁾ 23	⁽¹¹⁾ 29	⁽⁹⁾ 34	⁽¹⁴⁾ 61	⁽¹⁴⁾ 145	¹⁴ 8.88N ^{0.6}
					265	VisionLabs	RU	visionlabs	010	2021-02-05	1042	20	³⁴ 512	-	¹⁶² 731	²⁶¹ 11837	⁽¹⁰⁾ 21	⁽¹⁴⁾ 32	⁽¹¹⁾ 36	⁽⁸⁾ 39	⁽⁶⁾ 43	⁷ 3183.79N ^{0.2}
					266	VisionLabs	RU	visionlabs	011	2021-10-20	1042	20	³⁸ 512	-	¹⁶⁴ 735	²⁶⁴ 12255	⁽¹¹⁾ 21	⁽⁷⁾ 23	⁽⁸⁾ 26	⁽⁷⁾ 34	⁽⁸⁾ 51	¹² 301.26N ^{0.3}
					267	Vixvizon	AU	vixvizion	009	2022-11-28	580	460	¹⁸² 2048	-	²³⁹ 907	¹³⁷ 14	⁽⁹⁰⁾ 389	⁽⁷⁶⁾ 312	⁽⁷¹⁾ 714	⁽⁷³⁾ 1530	⁽⁷⁰⁾ 3105	¹⁹⁷ 0.02N ^{1.2}
					268	Vocord	RU	vocord	5	2018-10-30	1035	185	⁵⁷ 768	k	¹⁸⁰ 780	⁴⁶ 7	⁽⁴³⁾ 158	⁽⁵⁰⁾ 204	⁽³⁸⁾ 383	⁽⁴⁰⁾ 767	⁽³³⁾ 1466	⁶⁰ 0.12N ^{1.0}
					269	Vocord	RU	vocord	6	2018-10-30	1035	185	²⁷³ 10240	k	¹⁸¹ 785	²⁵³ 243	⁽⁴⁴⁾ 170	⁽⁵³⁾ 216	-	-	-	-
					270	Xforward AI Technology	CN	xforwardai	000	2020-07-24	236	171	¹⁶² 2048	-	¹⁶⁹ 753	¹³² 13	⁽²³⁷⁾ 4603	⁽²⁶³⁾ 7647	⁽²²⁵⁾ 15723	⁽²¹³⁾ 23900	⁽²¹⁵⁾ 53729	¹⁸⁸ 0.56N ^{1.1}
					271	Xforward AI Technology	CN	xforwardai	001	2021-01-21	332	50	¹²⁵ 2048	-	¹³² 677	¹⁷² 16	⁽²⁵⁰⁾ 5887	⁽²²⁸⁾ 4384	⁽²⁰⁸⁾ 8798	⁽²⁰⁶⁾ 18553	⁽²¹⁰⁾ 48993	¹⁹⁵ 0.32N ^{1.1}
					272	Xforward AI Technology	CN	xforwardai	002	2021-05-24	691	50	²⁵³ 4096	-	²⁴³ 930	¹⁸⁵ 18	⁽²⁵⁷⁾ 6957	⁽²⁵⁷⁾ 6400	⁽²²⁰⁾ 12659	⁽²²²⁾ 31077	⁽²¹⁹⁾ 65158	¹⁹³ 0.52N ^{1.1}
					273	verihubs-inteligensia	ID	verihubs-inteligensia	000	2022-09-29	204	75	¹¹⁴ 2048	-	¹⁰¹ 575	¹⁴⁷ 14	⁽²⁶¹⁾ 7175	⁽²⁶⁶⁾ 9670	⁽²²⁸⁾ 18711	⁽²²⁴⁾ 38110	⁽²²¹⁾ 79675	⁹⁹ 4.77N ^{1.0}

Notes

- 1 Configuration size does not capture static data present in libraries. Libraries are included but the size also includes any ancillary libraries for image processing (e.g. openCV) or numerical computation (e.g. blas).
- 2 Finalization is the processing of converting N = 1600000 templates into a searchable data structure an operation which can be a simple copy, or the building of an index or tree, for example. The duration of the operation may be data dependent, and may not be linear in the number of input templates.
- 3 This multiplier expresses the increase in template size when k images are passed to the template generation function.
- 4 All durations are measured on Intel®Xeon®CPU E5-2630 v4 @ 2.20GHz processors. Estimates are made by wrapping the API function call in calls to std::chrono::high_resolution_clock which on the machine in (3) counts 1ns clock ticks. Precision is somewhat worse than that however.
- 5 Search durations are measured as in the prior note. The power-law model in the final column mostly fits the empirical results in Figure 151. However in certain cases the model is not correct and should not be used numerically.

Table 7: Summary of algorithms and properties included in this report. The blue superscripts give ranking for the quantity in that column. Missing search durations, denoted by “-”, are absent because those runs were not executed, usually because we did not run on the larger galleries. Caution: The power-law model is sometimes an incorrect model. It is included here only to show broad sublinear behavior, which is flagged in green. The models should not be used for prediction.

#	ALGORITHM	INVESTIGATION, FNIR(N, R = 1, T = 0)								IDENTIFICATION, FNIR(N, R = L, T ≥ 0) FOR FPIR = 0.001							
		(0, 2]	(2, 4]	(4, 6]	(6, 8]	(8, 10]	(10, 12]	(12, 14]	(14, 18]	(0, 2]	(2, 4]	(4, 6]	(6, 8]	(8, 10]	(10, 12]	(12, 14]	(14, 18]
1	3DIVI-005	⁹⁷ 0.0207	⁹⁷ 0.0304	⁹⁷ 0.0415	⁹⁷ 0.0533	⁹⁷ 0.0646	¹⁵⁴ 0.0735	¹⁵⁴ 0.0884	¹⁵⁵ 0.1148	¹⁰⁷ 0.1580	⁹⁸ 0.2316	⁹⁸ 0.3033	⁹⁸ 0.3740	⁹⁸ 0.4285	¹⁵³ 0.4742	¹⁵³ 0.5329	¹⁵³ 0.5975
2	ANKE-000	⁹⁵ 0.0162	⁹⁵ 0.0245	⁹⁵ 0.0333	⁹⁵ 0.0428	⁹⁵ 0.0515	¹⁵² 0.0615	¹⁵² 0.0780	¹⁵¹ 0.1028	⁹⁶ 0.1132	⁹⁶ 0.1761	⁹⁶ 0.2402	⁹⁵ 0.3057	⁹⁵ 0.3640	¹⁵⁰ 0.4200	¹⁵⁰ 0.4928	¹⁵⁰ 0.5680
3	ANKE-002	⁴⁷ 0.0055	⁵⁰ 0.0074	⁵⁰ 0.0090	⁴⁹ 0.0103	⁴⁸ 0.0116	¹⁰⁵ 0.0135	¹⁰² 0.0162	¹⁰¹ 0.0202	⁵⁴ 0.0329	⁵⁴ 0.0560	⁵⁶ 0.0843	⁵⁷ 0.1169	⁵⁷ 0.1481	¹¹¹ 0.1820	¹¹¹ 0.2280	¹¹¹ 0.2831
4	AWARE-005	¹⁰⁶ 0.0328	¹⁰⁶ 0.0519	¹⁰⁶ 0.0712	¹⁰⁹ 0.0910	¹⁰⁴ 0.1078	¹⁶¹ 0.1235	¹⁶¹ 0.1457	¹⁶² 0.1831	¹⁰⁸ 0.3605	¹⁰⁷ 0.4949	¹⁰⁷ 0.5948	¹⁰⁷ 0.6783	¹⁰⁸ 0.7393	¹⁶³ 0.7905	¹⁶³ 0.8408	¹⁶³ 0.8831
5	AWARE-006	¹¹⁰ 0.0702	¹¹¹ 0.1110	¹¹¹ 0.1502	¹¹¹ 0.1899	¹¹¹ 0.2253	¹⁷⁶ 0.2614	¹⁶⁹ 0.3045	¹⁶⁹ 0.3659								
6	AYONIX-002	¹¹³ 0.3360	¹¹⁴ 0.4389	¹¹⁴ 0.5144	¹¹⁴ 0.5814	¹¹⁴ 0.6340	¹⁷³ 0.6818	¹⁷³ 0.7297	¹⁷⁴ 0.7774	¹¹⁶ 0.8288	¹¹¹ 0.9013	¹¹¹ 0.9375	¹¹¹ 0.9603	¹¹¹ 0.9744	¹⁶⁸ 0.9837	¹⁶⁸ 0.9893	¹⁶⁸ 0.9927
7	CAMVI-004	¹⁰⁹ 0.0623	¹⁰⁹ 0.0944	¹⁰⁹ 0.1243	¹⁰⁸ 0.1548	¹⁰⁸ 0.1812	¹⁶⁷ 0.2056	¹⁶⁷ 0.2344	¹⁶⁵ 0.2672	⁹¹ 0.0810	⁹¹ 0.1267	⁸⁸ 0.1721	⁸⁸ 0.2203	⁸⁸ 0.2619	¹⁴¹ 0.3040	¹⁴⁰ 0.3543	¹³⁶ 0.4124
8	CAMVI-005	¹¹¹ 0.0849	¹¹¹ 0.1255	¹¹¹ 0.1631	¹¹¹ 0.1989	¹¹¹ 0.2298	¹⁶⁸ 0.2585	¹⁶⁸ 0.2915	¹⁶⁸ 0.3246								
9	CANON-001						⁴⁷ 0.0052	⁴⁶ 0.0057	⁴⁶ 0.0042						⁵³ 0.0491	⁵³ 0.0606	⁵⁵ 0.0826
10	CANON-002						⁶² 0.0061	⁶² 0.0070	⁶¹ 0.0070						⁵⁰ 0.0472	⁵⁰ 0.0582	⁵³ 0.0792
11	CIB-000	¹⁴ 0.0022	¹⁴ 0.0030	¹⁵ 0.0037	¹⁵ 0.0044	¹⁷ 0.0049	⁵⁷ 0.0057	⁶⁰ 0.0069	⁵⁹ 0.0062	²⁵ 0.0139	²⁶ 0.0240	²⁷ 0.0373	²⁸ 0.0525	²⁸ 0.0689	⁷² 0.0859	⁷³ 0.1109	⁷³ 0.1454
12	CLEARVIEW1-000	⁴ 0.0017	⁴ 0.0023	⁴ 0.0028	⁹ 0.0034	¹¹ 0.0039	³⁷ 0.0046	⁴⁵ 0.0056	⁴⁹ 0.0047	¹⁶ 0.0066	¹⁸ 0.0121	¹⁸ 0.0194	¹⁹ 0.0287	¹⁹ 0.0385	⁵⁴ 0.0493	⁵⁹ 0.0662	⁵⁹ 0.0873
13	CLOUDWALK-MT-000	¹⁰ 0.0019	⁷ 0.0024	⁸ 0.0029	⁶ 0.0032	⁵ 0.0032	⁸ 0.0036	¹² 0.0041	⁷ 0.0020	¹ 0.0029	¹ 0.0041	¹ 0.0054	¹ 0.0064	⁴ 0.0073	⁹ 0.0085	⁹ 0.0102	⁹ 0.0112
14	CLOUDWALK-MT-000						¹³ 0.0037	¹⁶ 0.0038	¹⁴ 0.0013						⁶ 0.0065	⁶ 0.0072	⁶ 0.0075
15	CLOUDWALK-MT-001						¹⁰ 0.0037	¹⁰ 0.0037	¹⁰ 0.0012						³ 0.0045	⁴ 0.0051	⁴ 0.0042
16	CLOUDWALK-MT-002						⁹ 0.0036	¹⁰ 0.0038	¹⁰ 0.0012						³ 0.0037	³ 0.0041	³ 0.0025
17	COGENT-000	⁹⁰ 0.0128	⁹¹ 0.0184	⁹³ 0.0250	⁹³ 0.0327	⁹³ 0.0407	¹⁴⁶ 0.0488	¹⁴⁵ 0.0611	¹⁴⁵ 0.0794	⁷⁸ 0.0559	⁷⁸ 0.0923	⁷⁶ 0.1342	⁷⁷ 0.1812	⁷⁶ 0.2243	¹³⁰ 0.2675	¹³² 0.3240	¹³² 0.3992
18	COGENT-001	⁹¹ 0.0128	⁹⁰ 0.0184	⁹² 0.0250	⁹² 0.0327	⁹² 0.0407	¹⁴⁷ 0.0488	¹⁴⁶ 0.0611	¹⁴⁴ 0.0794	⁷⁷ 0.0559	⁷⁹ 0.0923	⁷⁷ 0.1342	⁷⁸ 0.1812	⁷⁸ 0.2243	¹²⁹ 0.2675	¹³⁰ 0.3240	¹³⁰ 0.3992
19	COGENT-002	⁶⁹ 0.0081	⁶⁶ 0.0105	⁶³ 0.0123	⁶⁴ 0.0137	⁶² 0.0157	¹¹⁷ 0.0175	¹¹⁵ 0.0215	¹¹⁵ 0.0280	⁶⁹ 0.0499	⁶⁸ 0.0827	⁶⁷ 0.1207	⁶⁷ 0.1639	⁶⁷ 0.2037	¹²¹ 0.2432	¹²² 0.2972	¹²³ 0.3638
20	COGENT-003	⁷¹ 0.0082	⁶⁷ 0.0108	⁶⁵ 0.0128	⁶⁷ 0.0145	⁶⁶ 0.0168	¹²³ 0.0191	¹²⁴ 0.0239	¹²¹ 0.0312	⁸⁰ 0.0582	⁸⁰ 0.0971	⁸¹ 0.1417	⁸¹ 0.1918	⁸⁰ 0.2380	¹³¹ 0.2836	¹³⁴ 0.3400	¹³⁵ 0.4207
21	COGENT-004	⁵⁹ 0.0066	⁵³ 0.0080	⁴⁵ 0.0085	³⁹ 0.0080	³¹ 0.0083	⁸¹ 0.0092	⁸¹ 0.0106	⁸⁵ 0.0130	⁶³ 0.0410	⁶⁵ 0.0720	⁶⁵ 0.1099	⁶⁵ 0.1539	⁶⁴ 0.1974	¹²² 0.2443	¹²⁵ 0.3757	
22	COGENT-006						³⁵ 0.0045	³⁵ 0.0049	³⁶ 0.0038						⁴³ 0.0370	³⁹ 0.0448	³⁹ 0.0602
23	COGENT-007						³⁰ 0.0044	²⁹ 0.0049	³² 0.0036						³⁴ 0.0332	³⁴ 0.0415	³⁴ 0.0566
24	COGNITEC-000	¹⁰⁵ 0.0265	¹⁰³ 0.0423	¹⁰³ 0.0588	¹⁰³ 0.0757	¹⁰² 0.0894	¹⁵⁹ 0.1014	¹⁵⁸ 0.1381	¹⁰⁰ 0.1522	⁹⁹ 0.2330	⁹⁹ 0.3051	⁹⁹ 0.3751	⁹⁹ 0.4300	¹⁵¹ 0.4779	¹⁵¹ 0.5307	¹⁵¹ 0.5913	
25	COGNITEC-001	⁹³ 0.0149	⁹⁴ 0.0228	⁹⁴ 0.0312	⁹⁴ 0.0399	⁹⁴ 0.0479	¹⁴⁹ 0.0546	¹⁴⁸ 0.0656	¹⁴⁶ 0.0806	⁹³ 0.0963	⁹³ 0.1562	⁹³ 0.2157	⁹³ 0.2771	⁹³ 0.3287	¹⁴⁸ 0.3771	¹⁴⁷ 0.4343	¹⁴⁶ 0.4959
26	COGNITEC-002	⁷¹ 0.0101	⁸⁶ 0.0138	⁸¹ 0.0170	⁸¹ 0.0201	⁸¹ 0.0237	¹³⁵ 0.0264	¹³³ 0.0309	¹³² 0.0389	⁷² 0.0517	⁷¹ 0.0879	⁷² 0.1269	⁷¹ 0.1707	⁷¹ 0.2098	¹²³ 0.2463	¹²³ 0.2919	¹²³ 0.3535
27	COGNITEC-003	⁷⁰ 0.0104	⁸¹ 0.0140	⁸² 0.0174	⁸² 0.0205	⁸² 0.0238	¹³⁶ 0.0266	¹³⁴ 0.0311	¹³⁴ 0.0401	⁷¹ 0.0504	⁷⁰ 0.0855	⁶⁹ 0.1235	⁶⁹ 0.1662	⁶⁹ 0.2045	¹²³ 0.2403	¹¹⁷ 0.3451	
28	COGNITEC-004	⁶⁴ 0.0073	⁶³ 0.0099	⁶² 0.0118	⁵⁹ 0.0130	⁵⁹ 0.0147	¹¹⁶ 0.0163	¹¹¹ 0.0189	¹¹¹ 0.0239	⁵³ 0.0325	⁵³ 0.0548	⁵² 0.0798	⁵¹ 0.1074	¹⁰² 0.1325	¹⁰² 0.1591	⁹⁸ 0.1952	⁹⁸ 0.2414
29	COGNITEC-006						⁷⁴ 0.0081	⁷² 0.0086	⁷⁰ 0.0090						⁶⁹ 0.0777	⁶⁹ 0.0926	⁶⁹ 0.1274
30	CUBOX-000	⁷ 0.0019	⁵ 0.0024	⁵ 0.0028	⁴ 0.0031	⁴ 0.0032	¹¹ 0.0037	¹⁹ 0.0044	¹⁹ 0.0027	⁶ 0.0039	⁶ 0.0059	⁷ 0.0083	⁸ 0.0111	⁸ 0.0141	²² 0.0185	²³ 0.0252	²⁴ 0.0339
31	CYBERLINK-002	⁵¹ 0.0055	⁴⁸ 0.0068	⁴¹ 0.0075	³⁵ 0.0078	³² 0.0084	⁸² 0.0094	⁸² 0.0107	⁸⁰ 0.0114	³² 0.0180	³³ 0.0302	³³ 0.0460	³¹ 0.0643	³¹ 0.0837	⁸¹ 0.1058	⁸⁰ 0.1370	⁸⁰ 0.1787
32	CYBERLINK-003	³⁵ 0.0041	³⁴ 0.0052	²⁷ 0.0057	²⁵ 0.0058	²⁵ 0.0061	⁷⁰ 0.0068	⁶⁷ 0.0078	⁶⁹ 0.0078	¹⁹ 0.0109	¹⁹ 0.0175	²⁰ 0.0259	²¹ 0.0356	⁶² 0.0594	⁶⁵ 0.0787	⁶⁷ 0.1072	
33	DAHUA-002	³ 0.0035	²⁸ 0.0047	²⁸ 0.0058	²⁷ 0.0067	²⁸ 0.0074	⁷⁵ 0.0082	⁷⁸ 0.0100	⁷⁰ 0.0108	³⁰ 0.0169	³² 0.0294	³¹ 0.0449	³⁰ 0.0635	³⁰ 0.0817	⁷⁸ 0.1013	⁷⁷ 0.1291	⁷⁶ 0.1638
34	DAHUA-003	¹⁹ 0.0026	¹⁹ 0.0036	¹⁹ 0.0043	²⁰ 0.0050	²⁰ 0.0055	⁶¹ 0.0062	⁶⁹ 0.0080	⁶⁸ 0.0073	²⁹ 0.0160	³⁰ 0.0280	²⁹ 0.0432	²⁹ 0.0615	²⁹ 0.0794	⁷⁶ 0.0987	⁷⁴ 0.1270	⁷⁴ 0.1587
35	DEEPEGLINT-001	¹ 0.0024	¹⁶ 0.0032	¹⁴ 0.0037	¹³ 0.0040	¹³ 0.0043	⁴⁵ 0.0049	⁵² 0.0060	⁵² 0.0052	¹² 0.0058	¹⁰ 0.0087	¹¹ 0.0119	¹¹ 0.0155	¹¹ 0.0199	²⁸ 0.0249	³⁰ 0.0338	³⁰ 0.0463
36	DEEPSA-001	⁷⁰ 0.0081	⁷⁰ 0.0116	⁷³ 0.0149	⁷⁶ 0.0182	⁷⁶ 0.0216	¹³⁴ 0.0260	¹³⁶ 0.0332	¹³⁶ 0.0432	⁶⁶ 0.0458	⁶⁶ 0.0752	⁶⁴ 0.1086	⁶³ 0.1460	⁶³ 0.1812	¹¹⁸ 0.2186	¹¹⁸ 0.2663	¹¹⁷ 0.3213
37	DERMALOG-006	⁸ 0.0113	⁸² 0.0142	⁷⁸ 0.0163	⁷⁷ 0.0183	⁷⁴ 0.0200	¹²⁸ 0.0218	¹²⁶ 0.0251	¹²⁴ 0.0329	⁷⁵ 0.0545	⁷⁵ 0.0889	⁷³ 0.1271	⁷² 0.1697	⁷¹ 0.2090	¹²² 0.2498	¹²² 0.3028	¹²² 0.3670
38	DERMALOG-007	⁸⁸ 0.0125	⁸⁸ 0.0170	⁸⁸ 0.0214	⁸⁸ 0.0264	⁸⁷ 0.0309	¹⁴¹ 0.0356	¹⁴² 0.0432</td									

MISS RATES		INVESTIGATION, FNIR(N, R = 1, T = 0)								IDENTIFICATION, FNIR(N, R = L, T ≥ 0) FOR FPIR = 0.001							
#	ALGORITHM	(0, 2]	(2, 4]	(4, 6]	(6, 8]	(8, 10]	(10, 12]	(12, 14]	(14, 18]	(0, 2]	(2, 4]	(4, 6]	(6, 8]	(8, 10]	(10, 12]	(12, 14]	(14, 18]
45	FUJITSULAB-001																
46	GORILLA-002	100.0213	108.0359	101.0528	102.0716	103.0895	100.1088	100.1367	100.1765	103.01828	104.02787	104.03654	104.04485	104.05168	105.05823	105.06508	107.07180
47	GORILLA-005	38.0044	47.0070	38.0102	62.0136	6.0170	126.0204	129.0272	13.0373	70.0566	81.0973	82.01432	81.01937	81.02398	138.02862	137.03437	107.04150
48	GORILLA-007																
49	GORILLA-008																
50	GRIAULE-001																
51	HZAILU-001																
52	HZAILU-002																
53	IDEMIA-003	81.00110	86.0151	86.0196	85.0238	84.0281	139.0313	138.0368	138.0504	87.0717	86.1147	86.1614	86.2113	85.2553	140.2976	139.3537	140.4334
54	IDEMIA-004	80.0107	84.0148	85.0192	84.0233	81.0277	138.0312	138.0367	139.0512	86.0373	85.0587	84.0833	83.1100	82.1340	101.1580	98.1911	96.2482
55	IDEMIA-005	84.0118	87.0167	90.0218	89.0270	88.0317	142.0357	141.0425	141.0579	63.0440	64.0689	60.0964	59.1254	58.1513	108.1762	103.2113	106.2698
56	IDEMIA-006	87.0124	89.0171	89.0218	89.0263	89.0302	140.0321	139.0356	137.0471	62.0409	59.0620	57.0850	52.1097	49.1309	93.1486	91.1738	90.2200
57	IDEMIA-007	47.0050	48.0071	48.0089	50.0106	51.0124	105.0142	105.0171	107.0220	36.0202	36.0335	34.0491	33.0663	31.0825	77.0999	74.1240	77.1645
58	IDEMIA-008	5.0018	6.0024	6.0029	7.0032	7.0035	15.0039	23.0046	29.0033	3.0034	3.0051	5.0069	5.0087	5.0102	14.0123	15.0146	15.0186
59	IDEMIA-009																
60	IDEMIA-010																
61	IMAGUS-005	33.0039	33.0052	31.0061	29.0067	30.0077	78.0088	79.0103	78.0109	39.0212	39.0357	40.0539	40.0755	38.0967	86.1183	85.1485	85.1893
62	IMAGUS-008																
63	IMPERIAL-000	34.0040	35.0054	36.0067	38.0079	40.0093	92.0112	91.0139	95.0178	48.0286	51.0503	51.0779	54.1116	56.1455	112.1844	115.2341	114.2951
64	INCODE-003	94.0155	96.0247	96.0348	96.0463	96.0571	153.0674	153.0856	154.1114	102.1627	102.2507	103.322	103.4122	108.4772	156.5368	156.6059	156.6766
65	INCODE-004	56.0061	59.0087	59.0110	61.0136	61.0161	119.0185	122.0236	120.0309	79.0532	79.0908	75.1809	75.2245	131.2675	130.3249	129.3932	
66	INNOVATRICS-004	113.3594	113.3629	113.3688	112.3754	112.3813	171.3870	171.3960	171.4135	107.4243	106.4642	106.5073	106.5522	106.5902	160.6274	158.6736	158.7253
67	INNOVATRICS-005	41.0046	41.0063	42.0078	45.0092	45.0106	99.0124	96.0149	96.0178	39.0343	36.0590	38.0886	38.1222	39.1544	113.1881	114.2321	112.2874
68	INNOVATRICS-008																
69	INTELLIVISION-002																
70	INTEMA-000																
71	INTEMA-001																
72	IREX-000	24.0031	24.0042	25.0051	26.0060	26.0068	73.0080	73.0095	76.0107	52.0313	53.0539	53.0815	56.1137	55.1442	107.1755	110.2181	108.2718
73	ISYSTEMS-002	76.0101	79.0135	80.0169	79.0197	80.0228	132.0256	132.0304	133.0398	96.0779	96.1258	91.1759	90.2299	90.2758	144.3204	144.3763	142.4401
74	ISYSTEMS-003	75.0089	69.0115	69.0139	69.0158	70.0177	125.0198	121.0234	118.0303	84.0647	84.1056	84.1502	84.1986	83.2402	134.2819	133.3351	131.3976
75	KAKAO-001																
76	KEDACOM-001	83.0116	78.0130	67.0135	60.0133	57.0135	104.0141	97.0151	94.0176	41.0241	41.0360	39.0513	34.0689	34.0866	82.1060	78.1327	78.1694
77	LINECLOVA-002																
78	LINECLOVA-003																
79	LOOKMAN-003	86.0123	83.0144	77.0158	70.0168	71.0178	121.0188	114.0212	111.0260	64.0438	62.0687	61.0978	61.1296	60.1581	114.1879	113.2294	110.2756
80	LOOKMAN-005	85.0118	77.0134	70.0142	66.0144	61.0150	114.0160	106.0176	104.0213	51.0310	49.0480	46.0698	46.0954	46.1216	95.1491	97.1890	97.2381
81	MAXVISION-000																
82	MAXVISION-001																
83	MICROFOCUS-005	113.4269	115.5527	115.6355	116.7024	116.7503	175.7876	172.8234	174.8601	111.8338	112.9113	112.9468	112.9667	112.9771	167.9836	167.9880	167.9924
84	MICROSOFT-003	28.0034	32.0050	33.0064	36.0078	38.0092	88.0107	90.0135	92.0166	39.0288	50.0503	50.0763	50.1067	54.1359	104.1680	105.2116	104.2644
85	MICROSOFT-004	25.0032	27.0047	29.0060	32.0075	33.0087	89.0103	89.0131	90.0159	42.0268	43.0470	45.0716	45.1007	46.1291	103.1610	102.2052	101.2590
86	MICROSOFT-005	22.0031	29.0047	35.0066	43.0084	43.0103	100.0131	103.0164	99.0185	43.0243	44.0432	44.0658	44.0913	45.1172	92.1476	96.1874	92.2272
87	MICROSOFT-006	26.0032	31.0049	34.0065	42.0081	42.0096	93.0117	92.0144	91.0160	24.0134	24.0233	25.0346	25.0462	22.0578	68.0713	68.0903	68.1156
88	MUKH-002																

Table 9: Accuracy for the FRVT 2018 mugshot sets under ageing. The second row shows the time lapse between gallery and subsequent probe images, in years. The first two columns identify the algorithm. The next 8 values give rank-based FNIR with $R = 1$, $T = 0$ and $\text{FPIR} = 1$. All these are relevant to investigational uses where candidates from all searches would need human review. The second 8 values give threshold-based FNIR with $T \geq 0$, $\text{FPIR} = 0.001$ and no rank criterion. The shaded cells indicate the three most accurate algorithms for that elapsed time. The gallery size is 3068801. The total number of searches is 10951064.

2023/03/14

14:32:11

FNIR(N, R, T)

FPIR(N, T)

False neg. identification rate

False pos. identification rate

N = Num. enrolled subjects

R = Num. candidates examined

T = Threshold

T = 0 → Investigation

T > 0 → Identification

MISS RATES		INVESTIGATION, FNIR(N, R = 1, T = 0)								IDENTIFICATION, FNIR(N, R = L, T ≥ 0) FOR FPIR = 0.001							
#	ALGORITHM	(0, 2]	(2, 4]	(4, 6]	(6, 8]	(8, 10]	(10, 12]	(12, 14]	(14, 18]	(0, 2]	(2, 4]	(4, 6]	(6, 8]	(8, 10]	(10, 12]	(12, 14]	(14, 18]
89	NEC-000	⁹⁷ 0.0195	⁹⁹ 0.0316	⁹⁹ 0.0445	⁹⁹ 0.0581	⁹⁸ 0.0699	¹⁵⁸ 0.0817	¹⁵⁸ 0.0998	¹⁵⁸ 0.1237	⁸⁹ 0.0759	⁸⁹ 0.1245	⁸⁹ 0.1729	⁸⁹ 0.2240	⁸⁹ 0.2671	¹⁴³ 0.3117	¹⁴¹ 0.3639	¹⁴¹ 0.4348
90	NEC-001	¹⁰⁴ 0.0246	¹⁰² 0.0382	¹⁰⁰ 0.0524	¹⁰⁸ 0.0672	¹⁰¹ 0.0793	¹⁵⁸ 0.0904	¹⁵⁷ 0.1076	¹⁵⁷ 0.1317	⁹⁴ 0.1019	⁹⁴ 0.1623	⁹⁴ 0.2214	⁹⁴ 0.2834	⁹⁴ 0.3341	¹⁴⁹ 0.3844	¹⁴⁹ 0.4440	¹⁴⁸ 0.5183
91	NEC-002	²⁹ 0.0033	²² 0.0041	¹⁸ 0.0043	¹⁶ 0.0044	¹⁵ 0.0045	⁴² 0.0049	⁴⁴ 0.0056	³⁹ 0.0041	¹⁵ 0.0066	¹¹ 0.0090	¹⁰ 0.0111	¹⁰ 0.0131	¹⁰ 0.0149	¹⁸ 0.0171	²⁰ 0.0207	²⁰ 0.0267
92	NEC-003	³¹ 0.0036	²⁶ 0.0046	²⁴ 0.0051	²⁴ 0.0055	²⁴ 0.0059	⁶⁵ 0.0067	⁶⁵ 0.0077	⁶⁷ 0.0073	⁹ 0.0056	⁹ 0.0076	⁹ 0.0091	⁷ 0.0105	⁶ 0.0119	¹⁷ 0.0137	¹⁵ 0.0162	¹⁵ 0.0209
93	NEC-004	³² 0.0039	²⁵ 0.0045	²² 0.0047	¹⁸ 0.0046	¹⁴ 0.0044	⁴⁰ 0.0046	⁴¹ 0.0052	³⁴ 0.0036	⁷ 0.0046	⁵ 0.0057	² 0.0063	² 0.0066	¹ 0.0069	⁷ 0.0076	⁷ 0.0090	⁷ 0.0105
94	NEC-005														⁸ 0.0080	⁸ 0.0091	⁸ 0.0107
95	NEC-006														¹ 0.0030	¹ 0.0033	¹ 0.0012
96	NEC-007														¹ 0.0027	¹ 0.0031	¹ 0.0010
97	NEUROTECHNOLOGY-003	¹⁰¹ 0.0234	¹⁰¹ 0.0379	¹⁰² 0.0549	¹⁰¹ 0.0682	¹⁰⁰ 0.0720	¹⁵⁸ 0.0747	¹⁵⁸ 0.0886	¹⁵¹ 0.1066	¹⁰⁹ 0.6802	¹⁰⁸ 0.8187	¹¹⁰ 0.8920	¹¹⁰ 0.9355	¹¹⁰ 0.9594	¹⁶⁵ 0.9738	¹⁶⁵ 0.9828	¹⁶⁵ 0.9885
98	NEUROTECHNOLOGY-004	⁷⁹ 0.0104	⁷⁸ 0.0134	⁷⁹ 0.0156	⁷³ 0.0173	⁷² 0.0195	¹² 0.0212	¹² 0.0245	¹² 0.0320	⁸³ 0.0642	⁸² 0.1015	⁸¹ 0.1426	⁷⁹ 0.1881	⁷⁸ 0.2299	¹³² 0.2722	¹³¹ 0.3269	¹³² 0.3943
99	NEUROTECHNOLOGY-005	⁷⁴ 0.0089	⁷¹ 0.0116	⁶⁸ 0.0136	⁶⁸ 0.0152	⁶⁹ 0.0173	¹²⁴ 0.0196	¹²⁰ 0.0233	¹¹⁹ 0.0306	⁷⁶ 0.0556	⁷⁶ 0.0913	⁷⁴ 0.1315	⁷⁴ 0.1766	⁷⁴ 0.2192	¹²⁸ 0.2617	¹²⁷ 0.3174	¹²⁷ 0.3843
100	NEUROTECHNOLOGY-007	⁶⁶ 0.0078	⁶⁵ 0.0103	⁶⁹ 0.0124	⁶⁹ 0.0140	⁶³ 0.0161	¹¹⁸ 0.0185	¹¹⁷ 0.0225	¹¹⁶ 0.0290	⁸² 0.0641	⁸⁵ 0.1069	⁸⁵ 0.1546	⁸⁵ 0.2075	⁸⁶ 0.2572	¹⁴² 0.3081	¹⁴³ 0.3713	¹⁴ 0.4421
101	NEUROTECHNOLOGY-011														⁷³ 0.0863	⁷¹ 0.1050	⁷¹ 0.1333
102	NEUROTECHNOLOGY-012														⁶⁹ 0.0636	⁶⁴ 0.0783	⁶⁵ 0.1027
103	NEUROTECHNOLOGY-013														⁴ 0.0406	⁴ 0.0498	⁴ 0.0654
104	NOBLIS-002	¹¹² 0.1520	¹¹² 0.2419	¹¹² 0.3296	¹¹³ 0.4114	¹¹³ 0.4855	¹⁷² 0.5528	¹⁷² 0.6061	¹⁷² 0.6532	¹¹³ 0.9984	¹¹³ 0.9996	¹¹³ 0.9998	¹¹³ 0.9999	¹¹³ 0.9999	¹⁶⁹ 1.0000	¹⁷⁵ 1.0000	¹⁷⁶ 1.0000
105	NTECHLAB-003	⁶⁵ 0.0078	⁷⁸ 0.0131	⁸⁹ 0.0202	⁹⁰ 0.0295	⁹¹ 0.0405	¹⁴⁸ 0.0543	¹⁵¹ 0.0761	¹⁵² 0.1035	⁶⁸ 0.0491	⁷² 0.0881	⁷⁹ 0.1384	⁸³ 0.1985	⁸⁷ 0.2594	¹⁴⁵ 0.3270	¹⁴⁵ 0.4065	¹⁴⁵ 0.4891
106	NTECHLAB-004	⁶² 0.0068	⁶⁸ 0.0110	⁷⁹ 0.0167	⁸⁶ 0.0239	⁸⁹ 0.0330	¹⁴⁵ 0.0447	¹⁴⁷ 0.0641	¹⁴⁹ 0.0891	⁶¹ 0.0379	⁶³ 0.0688	⁶⁶ 0.1108	⁶⁶ 0.1629	⁷³ 0.2192	¹³⁷ 0.2846	¹⁴² 0.3657	¹⁴⁴ 0.4524
107	NTECHLAB-006	⁸¹ 0.0056	⁶⁹ 0.0095	⁷⁷ 0.0148	⁸³ 0.0218	⁸⁵ 0.0301	¹⁴⁴ 0.0413	¹⁴⁴ 0.0591	¹⁴⁷ 0.0814	⁵⁶ 0.0349	⁶⁰ 0.0636	⁶³ 0.1023	⁶⁴ 0.1506	⁶⁶ 0.2024	¹²⁷ 0.2617	¹³⁴ 0.3374	¹³⁵ 0.4185
108	NTECHLAB-007	³⁷ 0.0044	⁴³ 0.0066	⁴⁹ 0.0089	⁵⁷ 0.0118	⁶⁰ 0.0150	¹²⁹ 0.0189	¹²² 0.0255	¹²² 0.0342	⁴⁵ 0.0256	⁴⁶ 0.0450	⁴⁸ 0.0705	⁴⁹ 0.1012	⁵¹ 0.1334	¹⁰⁵ 0.1692	¹⁰⁷ 0.2170	¹⁰⁹ 0.2752
109	NTECHLAB-008	¹⁸ 0.0025	²¹ 0.0038	²⁸ 0.0052	³¹ 0.0074	⁴⁴ 0.0104	¹⁰⁸ 0.0146	¹²² 0.0236	¹²⁸ 0.0348	²⁶ 0.0143	²⁸ 0.0267	³² 0.0459	³⁷ 0.0733	⁴⁰ 0.1062	⁹¹ 0.1469	¹⁰¹ 0.2044	¹⁰⁵ 0.2698
110	NTECHLAB-009	¹³ 0.0022	¹⁵ 0.0031	¹⁶ 0.0038	¹⁷ 0.0045	¹⁹ 0.0055	⁶⁷ 0.0067	⁷³ 0.0088	⁷⁵ 0.0100	¹⁸ 0.0073	¹⁷ 0.0117	¹⁷ 0.0170	¹⁷ 0.0238	¹⁸ 0.0319	⁴⁷ 0.0419	⁴⁸ 0.0577	⁵⁶ 0.0833
111	NTECHLAB-011														³⁷ 0.0351	⁴⁶ 0.0475	⁴⁶ 0.0724
112	PANGIAM-000														³⁶ 0.0503	³⁵ 0.0617	³⁴ 0.0810
113	PANGIAM-001														⁶¹ 0.0545	⁶¹ 0.0685	⁶¹ 0.0894
114	PARAVISION-002	³³ 0.0058	³⁸ 0.0083	⁶⁹ 0.0111	⁶³ 0.0137	⁶⁵ 0.0162	¹²⁹ 0.0187	¹¹⁹ 0.0229	¹¹⁷ 0.0295								
115	PARAVISION-003	⁴⁴ 0.0048	⁴⁴ 0.0067	⁵¹ 0.0090	⁵² 0.0109	⁵⁴ 0.0128	¹⁰⁷ 0.0148	¹⁰⁷ 0.0178	¹⁰⁵ 0.0219	⁵⁷ 0.0354	⁵⁸ 0.0618	⁵⁹ 0.0931	⁶⁰ 0.1290	⁶¹ 0.1625	¹¹⁶ 0.1964	¹¹⁶ 0.2408	¹¹³ 0.2924
116	PARAVISION-004	¹⁶ 0.0024	¹⁷ 0.0032	¹⁹ 0.0040	¹⁹ 0.0047	¹⁸ 0.0053	⁶⁰ 0.0061	⁶³ 0.0073	⁶³ 0.0079	²⁰ 0.0118	²³ 0.0209	²⁴ 0.0327	²⁴ 0.0465	²⁴ 0.0613	²⁶ 0.0779	²⁶ 0.1008	²⁶ 0.1285
117	PARAVISION-005	¹² 0.0021	¹³ 0.0028	¹³ 0.0035	¹⁴ 0.0041	¹⁶ 0.0046	⁵² 0.0054	⁵⁸ 0.0067	⁶² 0.0070	¹¹ 0.0057	¹² 0.0093	¹² 0.0144	¹⁴ 0.0207	¹⁵ 0.0278	⁴¹ 0.0368	⁴⁵ 0.0508	⁴³ 0.0715
118	PARAVISION-007	⁴ 0.0019	⁸ 0.0025	⁷ 0.0029	⁸ 0.0033	⁸ 0.0036	²⁵ 0.0042	³² 0.0049	²⁴ 0.0030	¹⁰ 0.0057	¹³ 0.0094	¹⁴ 0.0144	¹⁵ 0.0206	¹⁴ 0.0275	³⁷ 0.0357	⁴¹ 0.0485	⁴¹ 0.0652
119	PARAVISION-009														³⁰ 0.0283	³² 0.0371	³³ 0.0525
120	PARAVISION-012														¹⁶ 0.0137	¹⁶ 0.0167	¹⁶ 0.0219
121	PIXELALL-002	⁷² 0.0085	⁷³ 0.0119	⁷¹ 0.0147	⁷² 0.0172	⁷³ 0.0198	¹²⁹ 0.0225	¹²⁸ 0.0270	¹²⁹ 0.0349	⁹⁷ 0.1193	⁹⁷ 0.1900	⁹⁷ 0.2601	⁹⁷ 0.3332	⁹⁷ 0.3955	¹⁵² 0.4565	¹⁵² 0.5268	¹⁵³ 0.6030
122	PIXELALL-003	⁴⁶ 0.0050	⁴⁹ 0.0063	³⁹ 0.0072	³⁴ 0.0077	³³ 0.0085	⁸³ 0.0095	⁸⁴ 0.0113	⁸¹ 0.0119	⁴⁴ 0.0248	⁴³ 0.0418	⁴⁵ 0.0622	⁴³ 0.0861	⁴³ 0.1104	⁸⁸ 0.1364	⁸⁷ 0.1723	⁸⁸ 0.2167
123	PIXELALL-004	⁴⁵ 0.0049	⁴⁰ 0.0063	⁴⁰ 0.0072	³⁷ 0.0079	³⁶ 0.0089	⁸⁷ 0.0103	⁸⁷ 0.0127	⁸⁷ 0.0146	³⁸ 0.0211	⁴⁰ 0.0360	⁴² 0.0553	⁴² 0.0792	³⁹ 0.1045	⁸⁷ 0.1317	⁹¹ 0.2246	
124	PTAKURATSATU-000	⁵⁴ 0.0061	⁵⁵ 0.0082	⁵⁶ 0.0097	⁵⁵ 0.0109	⁴⁵ 0.0120	⁹⁹ 0.0131	⁹⁴ 0.0146	⁹⁹ 0.0180	⁵⁹ 0.0375	⁵⁷ 0.0596	⁵⁸ 0.0842	⁵⁵ 0.1116	⁵⁵ 0.1357	⁹⁹ 0.1553	⁹⁹ 0.1820	⁹⁵ 0.2326
125	RANKONE-002	⁹⁹ 0.0212	⁹⁸ 0.0313	⁹⁸ 0.0431	⁹⁸ 0.0562	⁹⁹ 0.0712	¹⁵⁸ 0.0881	¹⁵⁸ 0.1130	¹⁵⁹ 0.1543	⁹⁵ 0.1111	⁹⁵ 0.1707	⁹⁵ 0.2305	⁹⁵ 0.2968	⁹⁶ 0.3646	¹⁵¹ 0.4345	¹⁵¹ 0.5172	¹⁵⁴ 0.6110
126	RANKONE-004	¹⁰⁸ 0.0424	¹⁰⁷ 0.0643	¹⁰⁷ 0.0875	¹⁰⁷ 0.1127	¹⁰⁷ 0.1364	¹⁶³ 0.1579	¹⁶⁴ 0.1914	¹⁶⁴ 0.2378	¹⁰⁴ 0.1855	¹⁰³ 0.2681	¹⁰³ 0.3431	¹⁰¹ 0.4155	¹⁰¹ 0.4785	¹⁵⁵ 0.5350	¹⁵⁵ 0.5980	¹⁵⁵ 0.6722
127	RANKONE-005	⁹² 0.0136	⁹³ 0.0192	⁹¹ 0.0246	⁹¹ 0.0303	⁹⁰ 0.0362	¹⁴⁴ 0.0422	¹⁴⁴ 0.0521	¹⁴³ 0.0694	⁸¹ 0.0582	⁷⁵ 0.0910	⁷¹ 0.1260	⁶⁸ 0.1645	⁶⁵ 0.2005	¹¹⁹ 0.2353	¹¹⁹ 0.2816	¹²⁰ 0.3522
128	RANKONE-007	⁶⁷ 0.0078	⁶⁴ 0.0099	⁶¹ 0.0113	⁵⁸ 0.0123	⁵⁸ 0.0139	¹¹³ 0.0156	¹¹³ 0.0191	¹¹² 0.0242	⁴² 0.0242	⁴² 0.0376	<					

MISS RATES		INVESTIGATION, FNIR(N, R = 1, T = 0)								IDENTIFICATION, FNIR(N, R = L, T ≥ 0) FOR FPIR = 0.001							
#	ALGORITHM	(0, 2]	(2, 4]	(4, 6]	(6, 8]	(8, 10]	(10, 12]	(12, 14]	(14, 18]	(0, 2]	(2, 4]	(4, 6]	(6, 8]	(8, 10]	(10, 12]	(12, 14]	(14, 18]
133	RANKONE-013						46.0051	38.0051	31.0035						31.0306	31.0355	21.0405
134	RANKONE-014					29.0044	24.0047	21.0029							21.0222	21.0255	21.0287
135	REALNETWORKS-002	107.0381	108.0687	108.1062	108.1495	109.1963	168.2513	170.3206	170.3927	105.02153	108.03323	108.04444	105.05485	106.06355	161.07132	162.07855	162.08437
136	REALNETWORKS-003	103.0245	105.0437	105.0686	106.0975	108.1312	168.01719	168.02294	167.02907	98.01468	108.02370	101.03313	103.04269	103.05142	159.05979	160.06815	161.07567
137	REALNETWORKS-004	102.0244	104.0428	104.0663	105.0939	105.1251	165.01634	168.02170	166.02785	99.01484	101.02377	100.03303	102.04249	102.05106	158.05924	159.06758	159.07534
138	REALNETWORKS-006						71.0069	66.0077	70.0080						71.01022	71.01253	71.01622
139	REALNETWORKS-008						44.0049	42.0054	48.0047						40.0462	40.0577	40.0745
140	S1-002						38.0046	37.0051	38.0038						31.0482	32.0597	31.0788
141	S1-003						56.0057	54.0063	57.0056						69.0681	67.0839	66.1061
142	S1-004						23.0042	20.0045	27.0032						40.0360	38.0448	38.0598
143	SCANOVATE-001	68.0079	72.00117	78.0151	78.0185	78.0221	135.0259	135.0321	135.0427	88.00727	88.01169	87.01650	87.02115	81.02528	139.02925	136.03437	135.04084
144	SENSETIME-002	96.0186	92.0191	84.0183	79.0179	68.0173	102.0133	74.0089	58.0059	40.0220	25.0236	19.0237	18.0240	12.0245	24.0219	19.0195	17.0222
145	SENSETIME-003	71.0021	12.0028	11.0031	7.0033	6.0035	19.0040	26.0047	28.0033	8.0046	8.0064	6.0076	4.0086	4.0101	13.0122	14.0155	14.0196
146	SENSETIME-004	3.0016	3.0022	3.0025	3.0028	3.0030	7.0035	18.0043	17.0025	4.0036	4.0052	3.0066	3.0081	3.0099	15.0126	17.0169	18.0230
147	SENSETIME-005	0.0015	~0.0020	~0.0024	2.0026	2.0029	6.0035	15.0043	20.0028	5.0036	7.0059	8.0089	9.00128	10.0177	29.0240	31.0345	31.0493
148	SENSETIME-006	1.0015	1.0019	1.0022	1.0025	1.0027	1.0033	9.0040	13.0021	2.0031	2.0049	4.0068	6.0097	7.0132	21.0184	29.0262	29.0359
149	SENSETIME-007						3.0035	5.0038	5.0015						12.0112	12.0140	12.0176
150	SENSETIME-008						4.0034	7.0039	7.0017						11.0103	11.0127	11.0163
151	SIAT-002	117.08309	117.08310	117.08311	117.08306	117.08296	176.08302	176.08300	175.08301	112.08340	110.08368	109.08404	109.08445	109.08480	164.08532	164.08593	163.08691
152	SYNESIS-003	89.00125	89.0151	89.0174	89.0199	79.0223	139.0240	139.0279	125.0331	85.00658	83.01052	83.01483	82.01968	82.02399	135.02834	135.03405	134.04046
153	SYNESIS-005	40.0044	37.0058	37.0070	40.0080	37.0091	86.0103	86.0125	88.0152	46.0262	45.0444	45.0666	45.0923	44.1156	89.01399	90.01736	89.02185
154	T4ISB-000						15.00606	15.0748	150.0970								
155	TECH5-001	57.0061	61.0093	66.0128	71.0171	77.0221	137.0289	140.0412	140.0560	86.0660	87.01156	90.1733	91.2385	91.2998	146.3629	148.4424	149.5284
156	TOSHIBA-001	73.0086	79.0119	79.0150	79.0178	79.0209	131.0241	131.0292	130.0365								
157	TRUEFACE-000	36.0043	36.0057	39.0061	28.0067	27.0073	76.0084	76.0097	74.0099	35.0200	37.0338	38.0504	35.0705	35.0904	83.1112	81.1401	81.1792
158	VERIDAS-001	58.0063	58.0083	58.0099	56.0113	56.0132	108.0148	108.0184	106.0219	61.0403	61.0684	62.1012	62.1386	62.1741	117.2113	117.2611	118.3233
159	VERIDAS-004						48.0052	51.0059	43.0043						57.0506	57.0634	57.0836
160	VISIONLABS-004	43.0048	48.0069	52.0091	55.0111	55.0130	111.0152	116.0187	113.0242	74.0540	77.0916	78.01358	78.01855	79.02303	133.02745	132.03312	132.03913
161	VISIONLABS-005	39.0044	39.0063	43.0081	46.0095	46.0109	96.0125	98.0151	100.0187	67.0479	67.0812	68.01212	70.01664	69.02078	124.02473	123.02999	123.03577
162	VISIONLABS-006	27.0035	39.0048	36.0061	36.0069	29.0077	77.0087	80.0105	83.0120	48.0273	47.0465	47.0702	47.0970	47.1228	96.01486	96.01847	95.02295
163	VISIONLABS-008	21.0028	20.0037	21.0047	22.0053	23.0058	66.0067	71.0081	71.00885	27.0143	27.0241	28.0373	27.0519	27.0677	71.0850	72.1104	72.1444
164	VISIONLABS-009	10.0020	10.0026	10.0030	10.0034	10.0038	31.0044	40.0052	46.0046	14.0065	15.0105	15.0156	15.0217	16.0289	46.0368	44.0499	44.0681
165	VISIONLABS-010	9.0020	9.0025	9.0030	11.0034	9.0036	27.0043	35.0051	47.0047	17.0069	16.0113	16.0170	16.0238	17.0316	46.0411	47.0557	48.0740
166	VISIONLABS-011						24.0042	22.0046	33.0036						29.0270	27.0337	28.0432
167	VIXVIZION-009						11.0161	11.0190	110.0238						109.01787	108.02116	102.02595
168	VNPPT-002						50.0053	50.0059	44.0044						60.0534	60.0670	60.0882
169	VTS-000	116.05878	116.06312	116.06602	115.06863	113.07073	174.07246	174.07458	173.07747	108.05929	108.06397	108.06729	108.07034	107.07279	162.07493	161.07739	160.08076
170	VTS-003						51.0054	47.0059	55.0054						63.0597	62.0731	62.0950
171	XFORWARDAI-000	20.00027	18.00034	20.00044	21.00052	21.00058	69.0067	68.0079	68.0076	28.0157	31.0281	30.0443	31.0635	32.0834	89.01050	79.01330	79.01714
172	XFORWARDAI-001	15.00023	11.00028	12.00034	12.00037	12.00039	34.0045	39.0052	42.0043	13.0060	14.0096	13.0144	12.0200	13.0260	35.0334	36.0435	36.0586
173	YITU-002	60.0066	59.0083	59.0094	48.0101	50.0121	111.0150	116.0223	123.0328	33.0189	34.0317	35.0494	39.0750	41.0166	96.01494	108.02171	111.02958
174	YITU-003	63.0072	60.0089	59.0100	51.0107	52.0125	112.0153	118.0226	126.0334	34.0194	35.0321	36.0500	41.0756	42.1071	97.01500	109.02177	116.02964
175	YITU-004	50.0061	51.0075	49.0081	41.0081	39.0092	89.0107	101.0154	103.0207	22.0204	23.0204	23.0314	25.0469	26.0671	79.00955	84.01421	86.02006
176	YITU-005	61.0067	54.0080	47.0087	44.0085	41.0094	90.0108	99.0151	102.0204	21.0124	21.0198	22.0308	22.0462	25.0667	74.00953	83.01418	84.01930

Table 11: **Accuracy for the FRVT 2018 mugshot sets under ageing.** The second row shows the time lapse between gallery and subsequent probe images, in years. The first two columns identify the algorithm. The next 8 values give rank-based FNIR with $R = 1$, $T = 0$ and FPIR = 1. All these are relevant to investigational uses where candidates from all searches would need human review. The second 8 values give threshold-based FNIR with $T \geq 0$, FPIR = 0.001 and no rank criterion. The shaded cells indicate the three most accurate algorithms for that elapsed time. The gallery size is 3068801. The total number of searches is 10951064.

#	ALGORITHM	INVESTIGATION MODE						IDENTIFICATION MODE						FAILURE TO EXTRACT FEATURES						FEATURES								
		RANK ONE MISS RATE, FNIR(N, 0, 1)						HIGH T → FPIR = 0.001, FNIR(N, T, L)						N=1.6M						FEATURES								
		GALLERY		MUGSHOT	MUGSHOT	MUGSHOT	VISA	BORDER	BOR _L 10YR	KIOSK	MUGSHOT	MUGSHOT	MUGSHOT	VISA	BORDER	BOR _L 10YR	KIOSK	MUGSHOT	MUGSHOT	MUGSHOT	VISA	BORDER	BOR _L 10YR	KIOSK				
1	20FACE-000	29 ^{0.055}	28 ^{0.085}	19 ^{0.736}	22 ^{0.056}	14 ^{0.239}	21 ^{0.243}	29 ^{0.348}	28 ^{0.450}	26 ^{1.000}	22 ^{0.424}	13 ^{0.772}	21 ^{0.938}	0.000	0.000	0.000	0.000	0.000	0.000	0.000	0.000	0.000	0.000	0.000	0.000			
2	3DIVI-003	30 ^{0.083}	30 ^{0.206}	23 ^{0.141}	24 ^{0.474}	30 ^{0.400}	30 ^{0.626}	23 ^{0.605}	19 ^{0.821}	0.002	0.005	17 ^{0.607}	17 ^{0.277}	17 ^{0.607}	0.002	0.005	0.005	0.005	0.005	0.005	0.005	0.005	0.005	0.005	0.005			
3	3DIVI-004	26 ^{0.018}	27 ^{0.062}	21 ^{0.035}	22 ^{0.279}	27 ^{0.169}	27 ^{0.343}	22 ^{0.277}	26 ^{0.166}	27 ^{0.339}	18 ^{0.996}	24 ^{0.864}	17 ^{0.597}	0.002	0.005	0.442	0.002	0.005	0.442	0.002	0.005	0.442	0.002	0.005	0.442			
4	3DIVI-005	26 ^{0.018}	27 ^{0.062}	24 ^{0.930}	25 ^{0.821}	22 ^{0.279}	26 ^{0.166}	27 ^{0.339}	18 ^{0.996}	24 ^{0.864}	17 ^{0.597}	0.002	0.005	0.442	0.002	0.005	0.442	0.002	0.005	0.442	0.002	0.005	0.442	0.002	0.005			
5	3DIVI-006	27 ^{0.024}	27 ^{0.074}	21 ^{0.047}	23 ^{0.312}	27 ^{0.168}	27 ^{0.342}	21 ^{0.283}	21 ^{0.283}	17 ^{0.283}	17 ^{0.615}	0.002	0.005	0.442	0.002	0.005	0.442	0.002	0.005	0.442	0.002	0.005	0.442	0.002	0.005			
6	ACER-000	24 ^{0.011}	23 ^{0.036}	22 ^{0.827}	20 ^{0.025}	20 ^{0.146}	20 ^{0.209}	26 ^{0.146}	25 ^{0.246}	12 ^{0.981}	20 ^{0.201}	14 ^{0.490}	0.000	0.000	0.042	0.000	0.000	0.042	0.000	0.000	0.042	0.000	0.000	0.042	0.000	0.000		
7	ACER-001	19 ^{0.005}	18 ^{0.020}	14 ^{0.422}	16 ^{0.008}	12 ^{0.050}	10 ^{0.098}	20 ^{0.056}	17 ^{0.109}	19 ^{0.999}	16 ^{0.068}	11 ^{0.406}	15 ^{0.479}	0.001	0.001	0.041	0.001	0.001	0.041	0.001	0.001	0.041	0.000	0.000	0.041	0.000	0.000	
8	AIZE-001	19 ^{0.006}	19 ^{0.022}	18 ^{0.683}	18 ^{0.016}	12 ^{0.050}	18 ^{0.165}	22 ^{0.077}	20 ^{0.143}	15 ^{0.994}	17 ^{0.101}	10 ^{0.364}	13 ^{0.387}	0.001	0.001	0.047	0.001	0.001	0.047	0.001	0.001	0.047	0.000	0.000	0.047	0.000	0.000	
9	ALCHERA-000	26 ^{0.016}	25 ^{0.047}	23 ^{0.870}	21 ^{0.046}	22 ^{0.292}	25 ^{0.138}	23 ^{0.216}	19 ^{0.999}	20 ^{0.176}	19 ^{0.803}	0.006	0.014	0.328	0.006	0.014	0.328	0.006	0.014	0.328	0.006	0.014	0.328	0.006	0.014	0.328		
10	ALCHERA-001	33 ^{0.987}	33 ^{1.000}	25 ^{1.000}	32 ^{1.000}	33 ^{0.999}	33 ^{1.000}	26 ^{1.000}	28 ^{1.000}	26 ^{1.000}	28 ^{1.000}	26 ^{1.000}	28 ^{1.000}	0.006	0.013	0.324	0.006	0.013	0.324	0.006	0.013	0.324	0.006	0.013	0.324	0.006	0.013	0.324
11	ALCHERA-002	30 ^{0.095}	29 ^{0.166}	28 ^{0.954}	25 ^{0.668}	24 ^{0.446}	30 ^{0.486}	29 ^{0.591}	22 ^{1.000}	24 ^{0.827}	20 ^{0.172}	14 ^{0.464}	14 ^{0.464}	0.001	0.001	0.106	0.001	0.001	0.106	0.001	0.001	0.106	0.001	0.001	0.106	0.001	0.001	0.106
12	ALCHERA-003	23 ^{0.010}	23 ^{0.035}	19 ^{0.741}	18 ^{0.016}	20 ^{0.088}	21 ^{0.144}	20 ^{0.394}	20 ^{0.529}	15 ^{0.991}	22 ^{0.424}	12 ^{0.708}	16 ^{0.546}	0.001	0.001	0.046	0.001	0.001	0.046	0.001	0.001	0.046	0.000	0.000	0.046	0.000	0.000	0.046
13	ALCHERA-004	24 ^{0.011}	23 ^{0.038}	13 ^{0.345}	19 ^{0.017}	14 ^{0.088}	17 ^{0.144}	20 ^{0.394}	20 ^{0.529}	15 ^{0.991}	22 ^{0.424}	12 ^{0.708}	16 ^{0.546}	0.001	0.001	0.046	0.001	0.001	0.046	0.001	0.001	0.046	0.000	0.000	0.046	0.000	0.000	0.046
14	ALLGOVISION-000	24 ^{0.011}	23 ^{0.033}	23 ^{0.894}	19 ^{0.021}	22 ^{0.282}	23 ^{0.088}	22 ^{0.166}	14 ^{0.990}	18 ^{0.117}	16 ^{0.526}	0.002	0.003	0.122	0.002	0.003	0.122	0.002	0.003	0.122	0.002	0.003	0.122	0.002	0.003	0.122		
15	ALLGOVISION-001	22 ^{0.009}	24 ^{0.038}	18 ^{0.661}	19 ^{0.021}	21 ^{0.241}	24 ^{0.102}	23 ^{0.221}	13 ^{0.986}	19 ^{0.150}	15 ^{0.491}	0.001	0.001	0.042	0.001	0.001	0.042	0.001	0.001	0.042	0.001	0.001	0.042	0.001	0.001	0.042		
16	ANKE-000	25 ^{0.013}	24 ^{0.036}	24 ^{0.931}	31 ^{1.000}	29 ^{0.100}	24 ^{0.117}	27 ^{0.220}	15 ^{0.994}	32 ^{1.000}	26 ^{0.100}	16 ^{0.546}	16 ^{0.546}	0.000	0.000	0.080	0.000	0.000	0.080	0.000	0.000	0.080	0.000	0.000	0.080			
17	ANKE-001	25 ^{0.013}	23 ^{0.038}	25 ^{0.946}	26 ^{1.000}	33 ^{1.000}	25 ^{0.119}	28 ^{0.220}	16 ^{0.994}	29 ^{1.000}	31 ^{1.000}	16 ^{0.546}	16 ^{0.546}	0.000	0.000	0.080	0.000	0.000	0.080	0.000	0.000	0.080	0.000	0.000	0.080			
18	ANKE-002	15 ^{0.003}	14 ^{0.016}	16 ^{0.522}	12 ^{0.005}	14 ^{0.119}	16 ^{0.032}	14 ^{0.079}	9 ^{0.948}	12 ^{0.034}	9 ^{0.245}	0.001	0.001	0.049	0.001	0.001	0.049	0.001	0.001	0.049	0.000	0.000	0.049	0.000	0.000	0.049		
19	AWARE-003	28 ^{0.031}	28 ^{0.090}	27 ^{0.966}	24 ^{0.316}	22 ^{0.290}	25 ^{0.128}	26 ^{0.298}	13 ^{0.984}	22 ^{0.428}	16 ^{0.530}	0.004	0.003	0.874	0.004	0.003	0.874	0.004	0.003	0.874	0.004	0.003	0.874	0.004	0.003	0.874		
20	AWARE-004	30 ^{0.068}	30 ^{0.176}	27 ^{0.976}	24 ^{0.122}	28 ^{0.414}	28 ^{0.269}	28 ^{0.509}	22 ^{1.000}	20 ^{0.397}	19 ^{0.816}	0.003	0.003	0.776	0.003	0.003	0.776	0.003	0.003	0.776	0.003	0.003	0.776	0.003	0.003	0.776		
21	AWARE-005	28 ^{0.031}	27 ^{0.067}	28 ^{0.978}	22 ^{0.048}	23 ^{0.308}	29 ^{0.364}	23 ^{0.253}	23 ^{1.000}	21 ^{0.255}	21 ^{0.916}	0.001	0.001	0.189	0.001	0.001	0.189	0.001	0.001	0.189	0.001	0.001	0.189	0.001	0.001	0.189		
22	AWARE-006	30 ^{0.070}	29 ^{0.128}	28 ^{0.983}	23 ^{0.111}	23 ^{0.421}	28 ^{0.276}	27 ^{0.398}	22 ^{0.999}	22 ^{1.000}	18 ^{0.368}	18 ^{0.749}	0.001	0.001	0.189	0.001	0.001	0.189	0.001	0.001	0.189	0.001	0.001	0.189	0.001	0.001	0.189	
23	AYONIX-000	32 ^{0.450}	32 ^{0.685}	29 ^{0.996}	29 ^{0.607}	24 ^{0.867}	32 ^{0.811}	19 ^{0.939}	18 ^{0.998}	24 ^{0.954}	22 ^{0.982}	0.010	0.031	0.939	0.010	0.031	0.939	0.010	0.031	0.939	0.010	0.031	0.939	0.010	0.031	0.939		
24	AYONIX-001	32 ^{0.341}	31 ^{0.527}	28 ^{0.993}	25 ^{0.694}	25 ^{0.778}	32 ^{0.824}	31 ^{0.920}	22 ^{0.999}	25 ^{0.999}	22 ^{0.969}	0.010	0.031	0.939	0.010	0.031	0.939	0.010	0.031	0.939	0.010	0.031	0.939	0.010	0.031	0.939		
25	AYONIX-002	32 ^{0.341}	31 ^{0.527}	28 ^{0.993}	24 ^{0.464}	25 ^{0.778}	32 ^{0.824}	31 ^{0.920}	21 ^{0.999}	24 ^{0.915}	22 ^{0.969}	0.010	0.031	0.939	0.010	0.031	0.939	0.010	0.031	0.939	0.010	0.031	0.939	0.010	0.031	0.939		
26	CAMVI-003	29 ^{0.052}	28 ^{0.090}	23 ^{0.911}	23 ^{0.093}	23 ^{0.360}	21 ^{0.071}	19 ^{0.132}	10 ^{0.970}	18 ^{0.114}	13 ^{0.402}	0.006	0.006	0.675	0.006	0.006	0.675	0.006	0.006	0.675	0.006	0.006	0.675	0.006	0.006	0.675		
27	CAMVI-004	29 ^{0.047}	28 ^{0.077}	20 ^{0.744}	22 ^{0.072}	25 ^{0.296}	21 ^{0.072}	10 ^{0.136}	21 ^{0.099}	17 ^{0.100}	19 ^{0.787}	0.000	0.000	0.000	0.000	0.000	0.000	0.000	0.000	0.000	0.000	0.000	0.000	0.000	0.000	0.000	0.000	
28	CAMVI-005	30 ^{0.065}	29 ^{0.103}	20 ^{0.746}	23 ^{0.098}	22 ^{0.066}	22 ^{0.057}	18 ^{0.002}	17 ^{0.013}	6 ^{0.133}	21 ^{0.005}	10 ^{0.033}	20 ^{0.099}	0.001	0.001	0.042	0.001	0.001	0.042	0.001	0.001	0.042	0.001	0.001	0.042			
29	CANON-001	2 ^{0.001}	5 ^{0.006}	5 ^{0.088}	3 ^{0.001}	2 ^{0.007}	3 ^{0.062}	2 ^{0.005}	2 ^{0.023}	26 ^{0.365} </																		

#	ALGORITHM	INVESTIGATION MODE										IDENTIFICATION MODE										FAILURE TO EXTRACT FEATURES										
		RANK ONE MISS RATE, FNIR(N, 0, 1)					N=1.6M					HIGH T → FPIR = 0.001, FNIR(N, T, L)					N=1.6M															
		GALLERY	MUGSHOT	MUGSHOT	MUGSHOT	VISA	BORDER	BOR _L 10YR	KIOSK	MUGSHOT	MUGSHOT	MUGSHOT	VISA	BORDER	BOR _L 10YR	KIOSK	MUGSHOT	MUGSHOT	MUGSHOT	VISA	BORDER	BOR _L 10YR	KIOSK									
47	COGNITEC-002	208	0.006	212	0.025	235	0.949			195	0.053	228	0.178	241	1.000						0.003	0.002	0.924									
48	COGNITEC-003	208	0.006	211	0.025	246	0.930			191	0.053	229	0.162	246	1.000						0.004	0.002	0.878									
49	COGNITEC-004	161	0.003	153	0.016	221	0.813	180	0.013	133	0.057	175	0.143	162	0.031	166	0.097	144	0.990	163	0.068	108	0.316	111	0.288	0.002	0.001	0.635	0.006			
50	COGNITEC-005	79	0.002	74	0.010	194	0.713	197	0.021	124	0.037	144	0.115	77	0.010	80	0.041	36	1.000	135	0.041	72	0.157	77	0.179	0.002	0.001	0.614	0.017			
51	COGNITEC-006	74	0.002	61	0.010	191	0.703	154	0.007	102	0.024	136	0.111	68	0.008	76	0.040	279	1.000	111	0.030	78	0.171	181	0.681	0.002	0.001	0.568	0.003			
52	CUBOX-000	58	0.001	6	0.010	12	0.058	41	0.002	12	0.004	6	0.049	27	0.003	27	0.019	10	0.168	17	0.004	14	0.028	7	0.073	0.001	0.000	0.042	0.000			
53	CYBERLINK-000	173	0.004	180	0.020	195	0.717	157	0.007	168	0.134	203	0.056	182	0.116	175	0.995	161	0.063	128	0.339	0.001	0.001	0.063								
54	CYBERLINK-001	166	0.004	16	0.018	196	0.731	150	0.007	167	0.133	196	0.054	170	0.109	168	0.995	158	0.062	17	0.652	0.000	0.000	0.040								
55	CYBERLINK-002	145	0.003	103	0.012	174	0.577	105	0.004	128	0.107	101	0.015	109	0.053	142	0.988	98	0.024	112	0.288	0.001	0.000	0.042								
56	CYBERLINK-003	73	0.002	49	0.009	151	0.474	85	0.003	64	0.012	76	0.082	69	0.008	67	0.035	112	0.972	64	0.012	51	0.100	129	0.368	0.000	0.000	0.039	0.000			
57	CYBERLINK-004	81	0.002	97	0.011	142	0.423	84	0.003	61	0.011	117	0.104	65	0.007	69	0.036	269	1.000	66	0.013	54	0.109	227	0.954	0.000	0.000	0.011	0.000			
58	CYBERLINK-005	94	0.002	80	0.011	95	0.209	65	0.002	51	0.010	105	0.098	81	0.010	77	0.041	232	1.000	70	0.014	49	0.089	216	0.926	0.000	0.000	0.034	0.000			
59	DAHUA-000	231	0.009	215	0.026					230	0.086	199	0.135								0.004	0.003										
60	DAHUA-001	208	0.007	206	0.024	192	0.703			220	0.073	190	0.122	125	0.980						0.002	0.002	0.346									
61	DAHUA-002	99	0.002	10	0.012	121	0.304	80	0.003	79	0.084	102	0.015	86	0.046	38	0.638	77	0.017	65	0.159	0.001	0.000	0.099								
62	DAHUA-003	32	0.001	21	0.007	93	0.206	56	0.002	50	0.009	52	0.073	96	0.014	79	0.041	31	0.579	65	0.013	46	0.081	47	0.134	0.000	0.000	0.000	0.000			
63	DAHUA-004	21	0.001	26	0.008	78	0.144	42	0.002	32	0.007	43	0.069	64	0.007	47	0.026	44	0.485	48	0.008	26	0.051	38	0.113	0.000	0.000	0.000	0.000			
64	DAON-000	176	0.004	161	0.017	163	0.530	126	0.005	92	0.020	159	0.125	133	0.023	111	0.061	231	1.000	99	0.025	80	0.173	203	0.846	0.002	0.002	0.108	0.001			
65	DECATUR-000	119	0.002	101	0.011	103	0.229	115	0.004	89	0.019	132	0.109	136	0.023	120	0.066	61	0.675	103	0.027	79	0.173	93	0.239	0.001	0.000	0.044	0.001			
66	DEEPLINT-001	62	0.001	1	0.007	91	0.200	71	0.002	59	0.073	33	0.003	19	0.014	234	1.000	31	0.006	64	0.159	0.000	0.000	0.038								
67	DEEPSA-001	181	0.004	151	0.016	222	0.814	167	0.010	174	0.140	183	0.046	170	0.101	134	0.985	168	0.077	122	0.326	0.000	0.001	0.047								
68	DERMALOG-003	312	0.126	303	0.217	241	0.296	24	0.560	307	0.482	309	0.655					241	0.677			206	0.870	0.002	0.002	0.103						
69	DERMALOG-004	311	0.125	302	0.215	245	0.930	235	0.135	241	0.467	306	0.480	303	0.657	174	0.995	235	0.603	204	0.856	0.001	0.002	0.107								
70	DERMALOG-005	259	0.015	27	0.037	190	0.701	240	0.242	239	0.384	233	0.088	219	0.154	146	0.990	214	0.300	171	0.614	0.001	0.002	0.102								
71	DERMALOG-006	222	0.008	210	0.024	180	0.619	168	0.010	183	0.155	190	0.052	173	0.105	128	0.981	156	0.059	121	0.318	0.003	0.006	0.181								
72	DERMALOG-007	230	0.009	21	0.027	185	0.675	184	0.014	189	0.170	231	0.086	217	0.152	14	0.990	176	0.099	168	0.557	0.001	0.002	0.102								
73	DERMALOG-008	154	0.003	144	0.015	158	0.516	147	0.007	116	0.029	173	0.139	181	0.045	159	0.094	259	1.000	153	0.057	112	0.382	218	0.940	0.000	0.000	0.002	0.000			
74	DERMALOG-009	153	0.003	150	0.014	86	0.167	135	0.007	150	0.999	122	0.106	125	0.021	121	0.066	24	1.000	113	0.031	144	0.999	20	0.840	0.001	0.001	0.018	0.003			
75	DERMALOG-010	122	0.002	96	0.011	30	0.066	215	0.038	144	0.124	144	0.113	63	0.007	105	0.055	207	0.999	174	0.089	148	1.000	160	0.522	0.001	0.001	0.018	0.003			
76	DERMALOG-011	77	0.002	74	0.010	61	0.096	94	0.003	118	0.031	93	0.092	128	0.022	108	0.087	194	0.998	184	0.129	141	0.991	187	0.764	0.000	0.000	0.013	0.000			
77	DIGIDATA-000	331	0.590	318	0.548	235	0.895	251	0.642	151	0.707	259	0.813	313	0.610	294	0.577	162	0.994	239	0.646	131	0.789	199	0.824	0.002	0.001	0.070	0.001			
78	DILUSENSE-000	125	0.002	103	0.012	119	0.297	160	0.008	113	0.028	109	0.099	160	0.030	140	0.078	57	0.655	130	0.039	122	0.664	86	0.203	0.001	0.001	0.219	0.006			
79	DILUSENSE-001	63	0.001	59	0.010	109	0.250	140	0.006	80	0.016	88	0.088	71	0.009	69	0.034	35	0.456	73	0.015	119	0.511	48	0.137	0.001	0.001	0.219	0.007			
80	EYEDEA-003	308	0.080	266	0.148	264	0.960	232	0.101	226	0.379	297	0.388	292	0.543	165	0.994	230	0.570	193	0.792	0.001	0.003	0.161								
81	F8-001	257	0.012	184	0.669	259	1.000			328	1.000	267	0.166			197	0.998					0.004	1.000	1.058								
82	FINCORE-000	243	0.011	231	0.034	208	0.767	208	0.032	143	0.117	198	0.191	256	0.134	236	0.217	256	1.000	202	0.187	121	0.598	146	0.458	0.000	0.001	0.043	0.000			
83	FIRSTCREDITKZ-001	39	0.001	41	0.008	60	0.094	50	0.002	30	0.010	36	0.065	29	0.003	25	0.019	38	0.007	34	0.061	22	0.097	0.000	0.001	0.047	0.001					
84	FUJITSULAB-000	126	0.002	131	0.014	145	0.440	110	0.004	96	0.023	106	0.098	126	0.021	107	0.056	96	0.024	81	0.177	98	0.240	0.000	0.001	0.016	0.000					
85	FUJITSULAB-001	101	0.002	124	0.013	147	0.455	112	0.004	108	0.026	120	0.106	115	0.018	109	0.058	153	0.992	97												

#	ALGORITHM	INVESTIGATION MODE						IDENTIFICATION MODE						FAILURE TO EXTRACT FEATURES					
		RANK ONE MISS RATE, FNIR(N, 0, 1)						HIGH T → FPIR = 0.001, FNIR(N, T, L)											
		N=1.6M						N=1.6M											
GALLERY	MUGSHOT	MUGSHOT	MUGSHOT	VISA	BORDER	VISA	MUGSHOT	MUGSHOT	MUGSHOT	VISA	BORDER	VISA	MUGSHOT	MUGSHOT	MUGSHOT	VISA	BORDER	KIOSK	
PROBE	MUGSHOT	WEBCAM	PROFILE	BORDER	BOR _E 10YR	KIOSK	MUGSHOT	WEBCAM	PROFILE	BORDER	BOR _E 10YR	KIOSK	MUGSHOT	WEBCAM	PROFILE	BORDER	BOR _E 10YR	KIOSK	
93 GORILLA-006	⁸⁷ 0.002	¹⁰⁵ 0.012	⁷⁰ 0.122	⁹³ 0.003	⁸⁴ 0.018	¹²¹ 0.105	¹⁵¹ 0.027	¹⁵³ 0.089	⁴⁹ 0.531	¹⁰⁴ 0.028	⁷⁶ 0.166	⁸⁷ 0.218	0.000	0.000	0.041	0.000	0.000	0.000	
94 GORILLA-007	⁸¹ 0.002	⁷⁹ 0.011	⁶⁸ 0.114	⁶⁹ 0.002	⁸¹ 0.016	⁸³ 0.088	¹⁴⁹ 0.027	¹³⁹ 0.077	⁵⁰ 0.534	¹⁰⁰ 0.026	⁹⁵ 0.264	⁷⁷ 0.178	0.000	0.000	0.041	0.000	0.000	0.000	
95 GORILLA-008	⁶⁷ 0.001	⁶³ 0.010	⁵¹ 0.085	⁴⁷ 0.002	⁶⁸ 0.012	⁷⁷ 0.082	¹³⁷ 0.024	¹⁴⁶ 0.083	³⁸ 0.463	¹¹⁰ 0.030	¹⁰⁷ 0.319	⁷³ 0.178	0.000	0.000	0.041	0.000	0.000	0.000	
96 GRIAULE-000	¹⁴⁷ 0.002	¹²⁵ 0.014	¹²⁷ 0.327	¹⁷¹ 0.011	¹² 0.031	¹⁵⁹ 0.126	¹²³ 0.020	¹¹⁷ 0.063	¹⁷¹ 0.995	¹²⁰ 0.033	⁸¹ 0.185	⁸⁴ 0.198	0.000	0.002	0.090	0.001	0.000	0.000	
97 GRIAULE-001	³⁶ 0.001	³⁴ 0.008	⁷⁵ 0.132	¹⁴ 0.001	⁹⁸ 0.023	³⁷ 0.065	⁴⁸ 0.005	⁵² 0.028	⁸⁴ 0.865	³⁵ 0.007	¹⁴² 0.995	²⁵ 0.099	0.000	0.000	0.000	0.000	0.000	0.000	
98 HIK-003	²⁴⁷ 0.012	²²⁰ 0.027	¹⁸⁸ 0.689	¹⁷⁶ 0.012	¹⁸⁰ 0.151	²⁴¹ 0.103	²¹⁸ 0.158	¹⁰⁷ 0.969	¹⁹¹ 0.142	¹⁴⁴ 0.445	0.000	0.000	0.048						
99 HIK-004	²⁴⁶ 0.011	²¹⁸ 0.027	¹⁹⁹ 0.743	¹⁷⁴ 0.012	¹⁸² 0.152	²³⁷ 0.099	²¹² 0.153	¹¹⁵ 0.976	¹⁸⁹ 0.137	¹⁴¹ 0.434	0.000	0.000	0.048						
100 HIK-005	¹⁸⁷ 0.005	¹⁵⁵ 0.017	¹⁶⁵ 0.535	¹⁵² 0.007	¹³⁰ 0.111	¹⁷⁶ 0.044	¹³⁰ 0.077	²²² 0.999	¹⁶² 0.068	¹⁶ 0.541	0.000	0.000	0.000						
101 HIK-006	¹⁸⁸ 0.005	¹⁵⁵ 0.017	¹⁶⁶ 0.535				¹⁸⁰ 0.047	¹⁴⁹ 0.086	²⁵⁸ 1.000				0.000	0.000	0.000				
102 HYPERVERGE-001	⁵⁵ 0.001	⁹¹ 0.011	³³ 0.067	⁴⁰ 0.002	³⁰ 0.007	³⁰ 0.061	⁴⁴ 0.004	⁵⁹ 0.031	¹⁷ 0.220	³⁶ 0.007	²⁸ 0.053	³⁰ 0.101	0.001	0.000	0.041	0.000	0.000	0.000	
103 HYPERVERGE-002	⁵¹ 0.001	⁸⁵ 0.011	¹⁹ 0.063	²⁹ 0.001	²⁰ 0.006	²⁷ 0.058	³⁹ 0.004	⁵⁰ 0.027	¹⁵ 0.210	²⁵ 0.006	²⁹ 0.048	¹⁹ 0.093	0.001	0.000	0.041	0.000	0.000	0.000	
104 HZAILU-000	¹²⁴ 0.002	¹²³ 0.013	¹⁰⁷ 0.244	⁸⁶ 0.003	⁷⁸ 0.015	⁸⁹ 0.090	¹²² 0.020	⁹¹ 0.051	¹⁰⁵ 0.967	⁸⁷ 0.020	¹⁰⁴ 0.316	⁵⁹ 0.153	0.001	0.001	0.054	0.001	0.000	0.000	
105 HZAILU-001	¹⁰⁸ 0.002	⁸⁹ 0.011	⁶⁶ 0.106	⁶⁹ 0.002	¹⁴¹ 0.113	⁹² 0.092	⁷² 0.009	²³⁸ 0.183	¹³⁹ 0.986	²⁰⁶ 0.196	²⁴¹ 1.000	¹⁸⁰ 0.679	0.000	0.000	0.039	0.000	0.000	0.000	
106 HZAILU-002	¹¹¹ 0.002	⁹⁰ 0.011	⁷¹ 0.122	⁵¹ 0.002	⁵⁶ 0.010	⁵⁹ 0.076	⁷⁰ 0.008	⁷⁵ 0.039	⁶⁴ 0.704	⁶² 0.012	³⁸ 0.066	¹²⁴ 0.330	0.001	0.000	0.041	0.000	0.000	0.000	
107 IDEMIA-003	²¹⁷ 0.007	²²⁷ 0.034	²⁵⁹ 0.958	¹⁹² 0.018	²⁰⁶ 0.210	¹⁸⁶ 0.047	²² 0.165	¹⁸³ 0.123	¹⁹ 0.766	0.000	0.000	0.041							
108 IDEMIA-004	²⁰⁷ 0.007	²²⁷ 0.032	²⁵⁴ 0.947	¹⁹³ 0.018	²⁰⁵ 0.210	¹⁷² 0.037	¹⁸⁶ 0.118	¹¹³ 0.973	¹⁸² 0.123	¹⁹⁰ 0.766	0.000	0.000	0.041						
109 IDEMIA-005	²² 0.008	²⁴⁵ 0.039	²⁵⁷ 0.954	¹⁹⁹ 0.021	²¹⁰ 0.217	¹⁷⁸ 0.044	²¹⁸ 0.150	¹¹⁸ 0.978	¹⁸⁵ 0.130	²⁰ 0.879	0.000	0.000	0.041						
110 IDEMIA-006	²³⁵ 0.010	²⁷⁷ 0.072	²⁷³ 0.969	²⁰⁴ 0.030	²¹⁸ 0.253	¹⁷⁵ 0.043	²⁴¹ 0.226	¹³⁰ 0.982	¹⁹² 0.144	¹⁸⁵ 0.733	0.000	0.000	0.041						
111 IDEMIA-007	¹⁴⁷ 0.003	¹⁴⁸ 0.015	³²⁹ 1.000	¹⁴¹ 0.006	¹²³ 0.036	¹⁶⁴ 0.131	¹⁴¹ 0.018	¹⁰⁷ 0.055	²⁸ 1.000	¹⁴⁷ 0.052	⁸³ 0.182	³³ 1.000	0.000	0.000	0.040	0.000	0.000	0.000	
112 IDEMIA-008	²⁹ 0.001	¹² 0.007	⁴⁷ 0.079	³⁹ 0.001	³⁰ 0.007	³⁶ 0.075	¹⁴ 0.002	¹⁰³ 0.013	¹⁴ 0.204	²⁰ 0.005	¹⁹ 0.036	³⁶ 0.106	0.000	0.000	0.040	0.000	0.000	0.000	
113 IDEMIA-009	⁹ 0.001	¹¹ 0.006	²⁷ 0.065	¹⁶ 0.001	¹⁷ 0.005	¹² 0.051	⁷ 0.002	⁶ 0.011	⁷ 0.141	¹⁰ 0.003	¹² 0.027	¹⁰ 0.074	0.000	0.000	0.040	0.000	0.000	0.000	
114 IDEMIA-010	⁷ 0.001	¹³ 0.006	¹⁵³ 0.058	⁶ 0.001	⁸ 0.004	⁶ 0.049	² 0.001	⁷ 0.008	³ 0.131	⁵ 0.002	¹⁷ 0.028	⁷ 0.070	0.000	0.000	0.037	0.000	0.000	0.000	
115 IMAGUS-002	³¹⁹ 0.220	³⁰⁷ 0.301	²⁸⁴ 0.988				³¹ 0.749	³⁰⁹ 0.816	²⁶⁸ 1.000				0.004	0.008	0.550				
116 IMAGUS-003	³² 0.356	³¹⁴ 0.513	²⁸⁸ 0.993				³¹⁹ 0.807	³¹⁰ 0.909	²⁴⁸ 1.000				0.004	0.008	0.550				
117 IMAGUS-005	¹⁰⁶ 0.002	¹⁰⁴ 0.012	¹²⁴ 0.319	¹³⁸ 0.006	⁹⁴ 0.022	¹⁶⁶ 0.132	¹¹⁸ 0.018	¹¹⁹ 0.066	⁸² 0.838	¹⁰⁶ 0.029	⁷⁸ 0.161	⁹² 0.231	0.000	0.000	0.000	0.000	0.000	0.000	
118 IMAGUS-006	¹¹ 0.002	¹² 0.014	¹¹⁸ 0.293	¹¹⁵ 0.004	⁹¹ 0.019	¹³⁸ 0.112	¹²¹ 0.019	¹² 0.069	⁹² 0.897	¹⁰⁵ 0.028	⁷⁷ 0.161	¹⁰ 0.260	0.000	0.000	0.000	0.000	0.000	0.000	
119 IMAGUS-007	¹¹⁹ 0.002	¹²¹ 0.013	¹²⁵ 0.321	¹⁰⁶ 0.004	⁹² 0.022	¹⁴⁶ 0.117	¹³⁸ 0.023	¹³¹ 0.073	⁹⁰ 0.893	¹¹⁴ 0.031	⁷⁷ 0.169	¹⁰⁸ 0.265	0.000	0.000	0.000	0.000	0.000	0.000	
120 IMAGUS-008	³⁰⁷ 0.086	²⁸⁷ 0.093	¹²² 0.305	¹⁹⁸ 0.021	¹³⁹ 0.081	¹⁴⁸ 0.119	³² 0.074	³⁶ 0.774	¹⁷⁶ 0.996	²³¹ 0.520	¹⁴⁶ 1.000	¹⁵⁹ 0.518	0.000	0.000	0.000	0.000	0.000	0.000	
121 IMPERIAL-000	¹⁴⁸ 0.002	¹⁴⁵ 0.015	¹¹⁵ 0.280	¹²¹ 0.004	¹⁰¹ 0.097	¹⁴³ 0.026	¹²⁰ 0.068	²⁰² 0.999	¹³⁶ 0.042	⁹⁸ 0.245	0.000	0.000							
122 INCODE-000	²⁹⁵ 0.049	²⁹⁰ 0.100	²⁵⁶ 0.951				²⁸⁰ 0.310	²⁸⁰ 0.420	¹⁹² 0.998				0.001	0.004	0.173				
123 INCODE-001	²⁶ 0.017	²⁵⁸ 0.046	²⁰⁵ 0.762				²⁷ 0.212	²⁶ 0.296	²⁶⁵ 1.000				0.001	0.004	0.173				
124 INCODE-002	²⁶⁶ 0.018	²⁵⁰ 0.048	²²⁶ 0.843				²⁷³ 0.184	²⁶¹ 0.269	¹⁵⁶ 0.993				0.000	0.001	0.066				
125 INCODE-003	²⁵ 0.013	²⁴⁷ 0.040	²⁰⁶ 0.764				²⁶⁹ 0.167	²⁵ 0.264	²¹⁸ 0.999				0.000	0.001	0.066				
126 INCODE-004	¹⁶⁷ 0.004	¹⁶⁶ 0.017	¹⁵² 0.475	¹⁶⁸ 0.008	¹⁷⁰ 0.135	¹⁹⁹ 0.054	¹⁸⁰ 0.120	¹⁶⁶ 0.995	¹⁶⁰ 0.063	¹¹⁷ 0.313	0.000	0.001	0.066						
127 INCODE-005	⁸⁰ 0.002	⁷⁷ 0.011	⁸¹ 0.147	⁷² 0.002	⁷¹ 0.013	⁷⁰ 0.079	⁸⁹ 0.011	⁸⁴ 0.043	⁴⁷ 0.528	⁷⁹ 0.017	⁶⁶ 0.145	⁶² 0.155	0.000	0.000	0.042	0.000	0.000	0.000	
128 INNOVATRICS-002	²⁹³ 0.045	²⁷⁸ 0.074	²²⁹ 0.853				²⁸² 0.234	²⁶⁸ 0.310	²⁴⁹ 1.000				0.000	0.001	0.046				
129 INNOVATRICS-003	²⁷ 0.026	²⁶³ 0.055	²²⁸ 0.845				²⁷⁸ 0.221	²⁶ 0.297	²³⁰ 1.000				0.000	0.001	0.046				
130 INNOVATRICS-004	²⁵ 0.012	²⁴⁹ 0.040	²⁶¹ 0.958				²⁵⁴ 0.132	²⁴⁰ 0.222	¹²⁴ 0.980				0.000	0.001	0.046				
131 INNOVATRICS-005	¹⁴¹ 0.002	¹³⁷ 0.014	¹⁴⁰ 0.407	¹²⁴ 0.005	¹³¹ 0.109	¹⁶³ 0.034	¹⁵⁴ 0.089	⁸³ 0.846	¹⁴³ 0.047	¹⁰⁰ 0.251	0.000	0.001	0.041						
132 INNOVATRICS-007	⁸¹ 0.002	⁸⁵ 0.011	¹⁰⁸ 0.248																

#	ALGORITHM	INVESTIGATION MODE								IDENTIFICATION MODE								FAILURE TO EXTRACT FEATURES											
		RANK ONE MISS RATE, FNIR(N, 0, 1)								HIGH T → FPIR = 0.001, FNIR(N, T, L)								N=1.6M											
		GALLERY		MUGSHOT	MUGSHOT	MUGSHOT	VISA	BORDER	VISA	GALLERY		MUGSHOT	MUGSHOT	MUGSHOT	VISA	BORDER	VISA	GALLERY		MUGSHOT	MUGSHOT	MUGSHOT	VISA	BORDER	KIOSK				
139	INTSYSMSU-000	314	0.146	204	0.023	177	0.562	228	0.072		165	0.132	330	0.998	324	1.000	228	1.000	235	0.999	0.000	0.000	0.050						
140	IREE-000	182	0.004	56	0.010	186	0.681	70	0.002	66	0.012	74	0.082	155	0.028	113	0.060	99	0.957	139	0.044	103	0.302	71	0.170	0.000	0.042	0.000	
141	ISYSTEMS-002	206	0.006	214	0.026	227	0.844						224	0.078	193	0.126	188	0.998					0.002	0.002	0.142				
142	ISYSTEMS-003	194	0.005	201	0.023	211	0.791						208	0.059	177	0.107	234	1.000					0.002	0.002	0.142				
143	KAKAO-000	65	0.001	78	0.011	67	0.119	75	0.002	70	0.013	65	0.078	104	0.015	106	0.056	46	0.468	81	0.019	61	0.141	63	0.158	0.000	0.041	0.000	
144	KAKAO-001	54	0.001	50	0.009	70	0.058	11	0.001	14	0.004	4	0.047	24	0.003	25	0.017	9	0.159	16	0.004	22	0.042	9	0.074	0.000	0.040	0.000	
145	KEDACOM-001	217	0.008	233	0.036	270	0.972	210	0.034		212	0.237	134	0.023	129	0.072	137	0.986	152	0.055		115	0.305	0.000	0.000				
146	KNERON-000	201	0.006	219	0.027	177	0.552	203	0.028		199	0.195										0.000	0.000	0.000					
147	KNERON-001	282	0.030	325	0.621	102	0.237	229	0.144	147	0.207	223	0.280									0.000	0.000	0.000	0.000				
148	LINE-000	127	0.002	129	0.014	102	0.223	131	0.005	114	0.029	126	0.107	161	0.031	163	0.095	141	0.046	98	0.278	314	1.000	0.000	0.000	0.000			
149	LINE-001	26	0.001	25	0.007	21	0.063	32	0.002	44	0.008	84	0.085	49	0.005	48	0.027	263	1.000	3	0.009	41	0.072	281	1.000	0.000	0.000	0.000	
150	LINECLOVA-002	47	0.001	25	0.008	38	0.070	44	0.002	62	0.011	26	0.058	36	0.004	195	0.130	122	0.981	133	0.040	147	1.000	183	0.700	0.000	0.001	0.040	0.001
151	LINECLOVA-003	10	0.001	323	0.601	63	0.099	17	0.001	46	0.009	83	0.085	25	0.003	298	0.606	21	0.006	139	0.974	35	0.110	0.000	0.000	0.024	0.000		
152	LOOKMAN-003	226	0.009	243	0.038		213	0.035		214	0.239	177	0.044	181	0.112	172	0.084		127	0.355	0.000	0.000							
153	LOOKMAN-004	228	0.009	246	0.039	278	0.973					189	0.045	175	0.105	116	0.977					0.000	0.000	0.000					
154	LOOKMAN-005	220	0.008	236	0.036	277	0.972	212	0.035		213	0.237	159	0.030	148	0.086	119	0.978	159	0.062	116	0.308	0.000	0.000	0.000				
155	MANTRA-000	86	0.002	70	0.010	193	0.709	148	0.007	103	0.024	137	0.112	82	0.010	78	0.041	281	1.000	107	0.029	70	0.152	238	1.000	0.002	0.001	0.591	0.003
156	MAXVISION-000	139	0.002	141	0.015	120	0.327	116	0.004	130	0.051	111	0.101	156	0.028	244	0.237	71	0.767	193	0.149	143	0.997	167	0.557	0.000	0.000	0.042	0.000
157	MAXVISION-001	38	0.001	22	0.008	26	0.064	21	0.001	87	0.018	24	0.057	42	0.004	43	0.025	16	0.219	34	0.007	136	0.951	29	0.100	0.000	0.000	0.042	0.000
158	MEGVII-001	280	0.012	165	0.017		279	1.000					219	0.072	167	0.097							0.002	0.000					
159	MEGVII-002	251	0.012	167	0.017	146	0.450	306	1.000					223	0.077	165	0.096	196	0.998					0.002	0.000	0.033			
160	MICROFOCUS-003	333	0.594	329	0.781	257	0.708			256	0.907	325	0.931	323	0.979			250	0.982		230	0.991	0.001	0.005					
161	MICROFOCUS-004	330	0.576	328	0.758	253	0.701			255	0.904	331	0.999	321	0.975			248	0.974		228	0.989	0.001	0.005					
162	MICROFOCUS-005	326	0.424	322	0.601	248	0.494			249	0.777	322	0.835	317	0.928			249	0.935		227	0.985	0.001	0.005					
163	MICROFOCUS-006	327	0.427	320	0.583	247	0.490			252	0.782	328	0.978	316	0.923			245	0.923		224	0.971	0.001	0.005					
164	MICROSOFT-003	76	0.002	109	0.012		163	0.004			133	0.109	151	0.028	157	0.091			128	0.036	94	0.233	0.000	0.001					
165	MICROSOFT-004	68	0.001	107	0.012		97	0.004			134	0.109	144	0.026	151	0.087			122	0.033	90	0.222	0.000	0.001					
166	MICROSOFT-005	102	0.002	84	0.011	79	0.144	98	0.003		107	0.099	141	0.026	127	0.070	52	0.587	101	0.027	78	0.180	0.000	0.001	0.049				
167	MICROSOFT-006	110	0.002	100	0.011	87	0.150	101	0.004		110	0.100	87	0.012	70	0.037	30	0.386	117	0.032	74	0.178	0.000	0.001	0.049				
168	MUKH-002	278	0.026	235	0.036	181	0.638	172	0.012	137	0.079	160	0.129	311	0.594	250	0.242	242	1.000	198	0.170	126	0.741	133	0.389	0.000	0.000	0.042	0.000
169	NEC-000	263	0.017	251	0.041	265	0.959	200	0.025		216	0.243	226	0.079	204	0.140	122	0.979			152	0.474	0.001	0.002	0.890				
170	NEC-001	272	0.021	264	0.056	271	0.967	209	0.033		220	0.277	243	0.106	233	0.197	138	0.986	186	0.133		150	0.468	0.005	0.003	0.934			
171	NEC-002	18	0.001	47	0.009	135	0.363	96	0.003		145	0.117	23	0.003	31	0.020	215	0.999	48	0.008		179	0.676	0.000	0.001	0.041			
172	NEC-003	53	0.001	68	0.010	135	0.352	100	0.004	69	0.013	151	0.120	20	0.002	24	0.017	79	0.824	47	0.008	20	0.036	178	0.668	0.000	0.001	0.041	0.001
173	NEC-004	60	0.001	46	0.009	167	0.538	88	0.003	40	0.007	57	0.075	11	0.002	14	0.013	55	0.622	18	0.004	1	0.019	28	1.000	0.000	0.001	0.041	0.001
174	NEC-005	34	0.001	28	0.008	49	0.081	50	0.002	16	0.005	54	0.073	8	0.002	9	0.012	60	0.673	12	0.003	6	0.019	24	0.099	0.000	0.001	0.040	0.001
175	NEC-006	42	0.001	38	0.008	28	0.066	53	0.002	19	0.005	39	0.065	16	0.002	26	0.018	39	0.463	12	0.004	11	0.026	20	0.094	0.000	0.001	0.040	0.001
176	NEC-007	169	0.004	5	0.006	17	0.059	15	0.001	3	0.003	8	0.049	37	0.004	3	0.009	8	0.147	1	0.002	1	0.010	3	0.065	0.000	0.000	0.040	0.000
177	NEUROTECHNOLOGY-003	273	0.022	252	0.042	265	0.961						315	0.636	259	0.266	313	1.000					0.000	0.001	0.131				
178	NEUROTECHNOLOGY-004	196	0.006	179	0.020	277	0.970						213	0.063	183	0.117	161	0.994					0.000	0.001	0.131				
179	NEUROTECHNOLOGY-005	180	0.004	209	0.024	233	0.893						208	0.054	196	0.130	188	0.998					0.000	0.000	0.030				
180	NEUROTECHNOLOGY-006	267	0.018</																										

#	ALGORITHM	INVESTIGATION MODE								IDENTIFICATION MODE								FAILURE TO EXTRACT FEATURES									
		RANK ONE MISS RATE, FNIR(N, 0, 1)								HIGH T → FPIR = 0.001, FNIR(N, T, L)								N=1.6M									
		GALLERY		MUGSHOT	MUGSHOT	MUGSHOT	VISA	BORDER	BOR;10YR	KIOSK	MUGSHOT	MUGSHOT	MUGSHOT	VISA	BORDER	VISA	MUGSHOT	MUGSHOT	MUGSHOT	VISA	BORDER	KIOSK					
	PROBE	MUGSHOT	WEBCAM	PROFILE	BORDER	BOR;10YR	KIOSK				MUGSHOT	WEBCAM	PROFILE	BORDER	BOR;10YR	KIOSK	MUGSHOT	WEBCAM	PROFILE	BORDER	BOR;10YR	KIOSK					
185	NEUROTECHNOLOGY-012	15.001	32.008	20.063	3.001	20.005	23.057	62.007	63.032	101.059	31.008	33.061	212.016	0.000	0.000	0.039	0.000	0.000	0.000	0.000	0.000	0.000	0.000	0.000	0.000		
186	NEUROTECHNOLOGY-013	16.001	31.008	17.058	8.001	15.004	20.056	41.004	36.023	22.034	30.006	23.046	176.041	0.000	0.000	0.039	0.000	0.000	0.000	0.000	0.000	0.000	0.000	0.000	0.000		
187	NEWLAND-002	304.079	293.117	248.0936				304.0438	286.0466	208.0999							0.007	0.012	0.200								
188	NOBLIS-001	321.0249	315.0522	289.0993				333.1000	325.1000	266.1000							0.000	0.000	0.000								
189	NOBLIS-002	317.0179	312.0392	281.0982				329.0997	327.1000	261.1000							0.000	0.000	0.000								
190	NOTIONTAG-000	142.002	116.012	97.0204	109.004	79.016	98.095	109.017	112.059	94.0611	91.021	69.150	72.0176	0.000	0.000	0.000	0.000	0.000	0.000	0.000	0.000	0.000	0.000	0.000	0.000		
191	NTECHLAB-003	202.006	198.023	154.0504				198.054	184.118	81.0837							0.000	0.000	0.040								
192	NTECHLAB-004	189.005	174.019	151.0506	159.008	161.0129	173.041	174.0105	80.0833	150.053		105.0263	0.000	0.000	0.040												
193	NTECHLAB-005	187.005	170.018	137.0367	163.008	147.0118	174.0042	172.0102	72.0771	166.073		113.0294	0.000	0.000	0.040												
194	NTECHLAB-006	177.004	160.017	134.0347	156.007	145.0113	168.037	160.0094	70.0754	151.057		104.260	0.000	0.000	0.040												
195	NTECHLAB-007	146.003	113.012	120.0326	120.004	125.0107	140.026	122.0067	69.0750	118.032		91.0223	0.000	0.000	0.042												
196	NTECHLAB-008	85.002	57.010	85.0157	95.003	80.084	98.014	85.045	48.0529	122.033		79.0183	0.000	0.000	0.044												
197	NTECHLAB-009	44.001	33.008	70.138	61.002	74.013	56.074	81.005	35.022	34.0430	70.015	35.0109	33.0142	0.000	0.000	0.041	0.001										
198	NTECHLAB-010	25.001	40.008	32.085	48.002	43.008	25.057	22.003	21.015	21.025	32.007	32.059	23.098	0.001	0.001	0.043	0.000										
199	NTECHLAB-011	17.001	15.007	46.072	30.001	42.007	13.051	28.003	20.015	18.0228	31.009	43.074	17.091	0.000	0.000	0.040	0.000										
200	PANGIAM-000	33.001	29.008	42.074	55.002	41.007	38.065	59.006	57.030	26.0318	58.009	60.136	32.0105	0.000	0.001	0.044	0.001										
201	PANGIAM-001	212.007	118.013	47.078	22.001	52.009	35.064	26.011	56.030	29.0383	31.009	133.0860	52.0141	0.003	0.000	0.040	0.000										
202	PARAVISION-000	268.019	242.038	164.0534	245.0423	244.0529	235.089	223.170	210.0999	229.0470		215.0926	0.000	0.000	0.000	0.000											
203	PARAVISION-001	170.004	184.020	129.0329	24.0414	245.0484	18.049	194.128	20.099	22.0444		186.0739	0.000	0.000	0.000	0.000											
204	PARAVISION-002	175.004	191.022	131.0335	186.0015	191.0175	188.050	187.0119	131.0983	166.080		156.0497	0.000	0.000	0.032												
205	PARAVISION-003	159.003	176.019	110.0252	187.0015	188.0167	166.035	164.0096	161.0994	153.058		114.0296	0.000	0.000	0.032												
206	PARAVISION-004	78.002	73.010	61.0104	136.0006	139.0112	84.010	74.038	251.000	81.018		210.0908	0.000	0.000	0.032												
207	PARAVISION-005	72.002	62.010	46.079	151.007	123.0106	40.004	39.024	121.0980	40.0111		45.0132	0.000	0.000	0.038												
208	PARAVISION-007	32.001	36.008	29.066	12.005	57.010	112.0101	38.004	42.025	257.0000	51.009	56.0113	296.0000	0.000	0.000	0.000	0.000										
209	PARAVISION-009	14.001	22.007	31.067	32.001	11.004	17.054	25.003	29.019	66.0735	11.003	16.0033	8.073	0.000	0.001	0.025	0.000										
210	PARAVISION-012	8.001	18.007	17.061	30.001	10.004	14.052	6.002	12.012	41.0475	7.002	10.025	4.068	0.000	0.001	0.025	0.000										
211	PIXELLALL-002	184.005	194.022	219.0810	170.011	196.0187	242.0105	226.0388	231.0000	234.0602		325.0000	0.000	0.000	0.000	0.000											
212	PIXELLALL-003	120.002	135.014	157.0515	146.006	179.0151	130.022	130.073	225.0000	128.037		166.0554	0.000	0.000	0.000	0.000											
213	PIXELLALL-004	117.002	142.015	161.0523	135.0005	181.0152	117.018	142.079	248.0000	145.051		231.0994	0.000	0.000	0.000	0.000											
214	PIXELLALL-005	104.002	83.011	112.0264	175.012	110.028	177.0146	89.0129	194.050	254.0000	102.027	87.0203	237.0000	0.000	0.000	0.000	0.000										
215	PTAKURATSATU-000	157.003	159.017	177.0605	132.0005	108.027	120.0105	167.037	192.0124	95.0924		140.0466	89.0206	93.0232	0.000	0.001	0.039	0.000									
216	QNAP-000	218.008	222.027	193.0522	182.013	131.054	184.0158	233.0129	246.0238	270.0000	203.0191	120.0539	233.098	0.001	0.000	0.054	0.000										
217	QNAP-001	178.004	192.022	152.0498	140.006	126.041	140.0112	197.0054	201.037	96.0928	170.0881	110.0368	125.0331	0.000	0.000	0.004	0.000										
218	QNAP-002	190.005	186.021	88.0172	114.004	120.031	156.0125	145.026	176.0106	73.0772	149.052	99.0281	110.0272	0.001	0.004	0.057	0.001										
219	QNAP-003	151.003	163.017	84.0152	161.008	134.061	96.093	120.019	311.0835	152.0992	230.0502	330.0000	205.0865	0.000	0.001	0.002	0.001										
220	QUANTASOFT-001	318.0218	322.0727																								
221	RANKONE-002	270.019	276.071																								
222	RANKONE-003	269.019	274.068																								
223	RANKONE-004	292.041	295.0141																								
224	RANKONE-005	232.009	250.041	283.0986																							
225	RANKONE-006	192.005	210.0797																								
226	RANKONE-007	163.003	172.019	217.0796																							
227	RANKONE-009	135.002	115.013	168.0549	135.0006	169.0134	112.0018	134.0076	108.0969	157.0062		123.0328	0.000	0.000	0.000	0.000											
228	RANKONE-010	128.002	64.010	135.0374	12.0005	106.027	158.0126	95.0014	110.058	77.0802	148.0052	90.0208	102.0259	0.000	0.000	0.000	0.000										
229	RANKONE-011	69.002	98.011	101.0223	99.004	78.019	73.0009	87.0048	80.048	128.0357	82.0182	225.0977	0.000	0.000	0.000	0.000											

#	ALGORITHM	INVESTIGATION MODE										IDENTIFICATION MODE										FAILURE TO EXTRACT FEATURES											
		RANK ONE MISS RATE, FNIR(N, 0, 1)					N=1.6M					HIGH T → FPIR = 0.001, FNIR(N, T, L)					N=1.6M																
		GALLERY	MUGSHOT	MUGSHOT	MUGSHOT	VISA	BORDER	BOR _L 10YR	KIOSK	MUGSHOT	MUGSHOT	MUGSHOT	VISA	BORDER	VISA	MUGSHOT	MUGSHOT	MUGSHOT	VISA	BORDER	BOR _L 10YR	KIOSK											
231	RANKONE-013	¹⁹ 0.001	¹⁴ 0.007	⁴¹ 0.076	²⁴ 0.001	⁴⁵ 0.008	¹⁶ 0.054	³⁵ 0.005	⁶⁵ 0.034	¹⁷ 0.996	⁸² 0.018	⁶³ 0.141	⁵⁴ 0.142	0.000	0.000	0.033	0.000	0.000	0.000	0.000	0.000	0.000	0.000	0.000	0.000	0.000	0.000	0.000	0.000				
232	RANKONE-014	¹¹ 0.001	⁷ 0.006	³⁸ 0.067	¹³ 0.001	²¹ 0.005	⁹ 0.050	³¹ 0.003	⁴⁰ 0.024	⁵⁶ 0.009	⁴⁷ 0.081	³¹³ 1.000	0.000	0.000	0.000	0.000	0.000	0.000	0.000	0.000	0.000	0.000	0.000	0.000	0.000	0.000	0.000	0.000					
233	REALNETWORKS-000	²⁹ 0.040	²⁸ 0.078						²⁸ 0.234	²⁷ 0.319									0.001	0.000													
234	REALNETWORKS-001	²⁹ 0.040	²⁸ 0.078						²⁸ 0.234	²⁷ 0.319									0.001	0.000													
235	REALNETWORKS-002	²⁸ 0.039	²⁸ 0.078						²⁷ 0.231	²⁶ 0.315									0.001	0.000													
236	REALNETWORKS-003	²⁷ 0.024	²⁷ 0.062	²⁰ 0.771	²⁰ 0.031		²⁰ 0.209	²⁶ 0.159	²⁸ 0.266	¹⁹ 0.998	¹⁹ 0.164	¹⁵ 0.500	0.001	0.000	0.009																		
237	REALNETWORKS-004	²⁷ 0.024	²⁸ 0.059	²¹ 0.797	²⁰ 0.031		²⁰ 0.213	²⁶ 0.158	²⁶ 0.263	²¹ 0.999	¹⁹ 0.170	¹⁷ 0.613	0.001	0.000	0.009																		
238	REALNETWORKS-005	¹³ 0.002	¹² 0.013	¹⁴ 0.433	¹¹ 0.004	⁹² 0.023	¹¹⁶ 0.102	¹⁵² 0.028	¹³² 0.074	¹¹⁰ 0.971	¹² 0.037	⁹¹ 0.223	⁸⁸ 0.215	0.000	0.000	0.006	0.000	0.000	0.000	0.000	0.000	0.000	0.000	0.000	0.000	0.000	0.000	0.000					
239	REALNETWORKS-006	³⁶ 0.001	⁶⁶ 0.010	¹¹⁷ 0.287	⁷ 0.002	³⁸ 0.010	⁶⁶ 0.078	³⁹ 0.015	⁹⁸ 0.053	¹²⁶ 0.980	⁷ 0.016	³⁷ 0.120	⁶¹ 0.154	0.000	0.000	0.009	0.000	0.000	0.000	0.000	0.000	0.000	0.000	0.000	0.000	0.000	0.000	0.000					
240	REALNETWORKS-007	⁴⁸ 0.001	⁵⁴ 0.009	¹¹³ 0.267	⁴⁵ 0.002	⁴⁷ 0.009	⁵⁰ 0.072	⁷⁸ 0.010	⁸³ 0.043	¹²¹ 0.979	⁶³ 0.012	¹¹⁸ 0.463	⁵¹ 0.140	0.000	0.000	0.009	0.000	0.000	0.000	0.000	0.000	0.000	0.000	0.000	0.000	0.000	0.000	0.000					
241	REALNETWORKS-008	²⁹ 0.001	³⁰ 0.008	⁵⁴ 0.089	⁴⁹ 0.002	³⁷ 0.007	⁹⁰ 0.091	⁶⁰ 0.006	⁵⁵ 0.029	¹⁰⁶ 0.968	⁴⁷ 0.008	⁴⁰ 0.068	⁴⁵ 0.129	0.000	0.000	0.042	0.000	0.000	0.000	0.000	0.000	0.000	0.000	0.000	0.000	0.000	0.000	0.000	0.000				
242	REMARKAI-000	²² 0.009	²² 0.030						²⁵ 0.128	²³ 0.203									0.000	0.001													
243	REMARKAI-000	¹⁶ 0.003	¹⁷ 0.018	¹⁸ 0.660	¹⁵ 0.008		¹⁷ 0.148	²⁰ 0.055	¹⁸ 0.120	²⁰ 0.999	¹⁶ 0.069	¹⁸ 0.717	0.000	0.000	0.000	0.000	0.000	0.000	0.000	0.000	0.000	0.000	0.000	0.000	0.000	0.000	0.000	0.000					
244	REMARKAI-002	²² 0.008	²² 0.029	²¹ 0.802					²⁵ 0.124	²³ 0.196	¹⁴ 0.991								0.000	0.001	0.017												
245	RENDIP-000	⁷ 0.002	¹⁴ 0.015	¹⁴ 0.424	¹⁴ 0.006	¹⁰ 0.028	⁸¹ 0.084	²⁸ 0.012	¹¹ 0.059	⁹¹ 0.894	⁹² 0.022	⁸⁴ 0.185	⁶⁹ 0.167	0.000	0.000	0.041	0.000	0.000	0.000	0.000	0.000	0.000	0.000	0.000	0.000	0.000	0.000	0.000	0.000	0.000			
246	REVEALMEDIA-000	¹⁰⁰ 0.002	⁶⁰ 0.010	¹¹⁴ 0.275	⁶² 0.002	⁶⁷ 0.012	⁵⁵ 0.074	⁹⁰ 0.012	⁸¹ 0.042	⁶² 0.680	⁹⁰ 0.021	⁵² 0.093	³⁵ 0.143	0.000	0.000	0.041	0.000	0.000	0.000	0.000	0.000	0.000	0.000	0.000	0.000	0.000	0.000	0.000	0.000				
247	S1-000	¹³⁷ 0.002	¹⁵⁸ 0.017	¹¹¹ 0.258	¹³ 0.005	¹⁰⁴ 0.025	⁸⁸ 0.090	¹⁵⁴ 0.028	¹⁴⁷ 0.085	²⁷¹ 1.000	¹⁴ 0.047	²⁴⁵ 1.000	³¹⁵ 1.000	0.000	0.000	0.040	0.000	0.000	0.000	0.000	0.000	0.000	0.000	0.000	0.000	0.000	0.000	0.000	0.000	0.000			
248	S1-001	¹³⁸ 0.003	¹³² 0.014	⁹⁹ 0.215	⁸² 0.003	⁸⁵ 0.018	⁶⁰ 0.077	¹⁰⁶ 0.016	⁹⁵ 0.052	¹³⁵ 0.985	⁸ 0.019	³⁹ 0.136	³⁷ 0.148	0.001	0.000	0.035	0.000	0.000	0.000	0.000	0.000	0.000	0.000	0.000	0.000	0.000	0.000	0.000	0.000	0.000			
249	S1-002	⁵⁹ 0.001	⁵² 0.009	⁵⁹ 0.093	²⁰ 0.001	⁵⁹ 0.010	¹⁹ 0.055	⁵⁶ 0.006	⁵⁸ 0.031	¹⁵ 0.196	³⁷ 0.007	¹³² 0.792	²⁰² 0.841	0.000	0.000	0.028	0.000	0.000	0.000	0.000	0.000	0.000	0.000	0.000	0.000	0.000	0.000	0.000	0.000	0.000			
250	S1-003	⁶⁴ 0.001	⁵⁸ 0.010	⁶¹ 0.114	³⁹ 0.001	³⁶ 0.007	²⁹ 0.060	⁷⁴ 0.009	⁷¹ 0.037	²³⁸ 1.000	⁷ 0.014	¹¹⁵ 0.396	²⁹⁵ 1.000	0.000	0.000	0.033	0.000	0.000	0.000	0.000	0.000	0.000	0.000	0.000	0.000	0.000	0.000	0.000	0.000	0.000			
251	S1-004	⁴⁹ 0.001	⁵¹ 0.009	²³ 0.064	¹² 0.001	¹⁸ 0.005	⁷ 0.049	³⁹ 0.004	⁴¹ 0.025	¹⁸² 0.997	²⁷ 0.006	³⁶ 0.064	³²³ 1.000	0.000	0.000	0.033	0.000	0.000	0.000	0.000	0.000	0.000	0.000	0.000	0.000	0.000	0.000	0.000	0.000	0.000			
252	SCANOVATE-000	¹⁹ 0.005	²⁴ 0.045	¹⁷ 0.560	²¹ 0.035		²⁰ 0.211	²¹⁶ 0.067	²⁴⁹ 0.240	⁸⁹ 0.893	²⁰ 0.215	¹³⁵ 0.400	0.000	0.001	0.057																		
253	SCANOVATE-001	¹⁹ 0.005	²⁴ 0.040	¹⁷ 0.585	²⁰ 0.031		¹⁹⁴ 0.178	²²⁷ 0.081	²⁴² 0.227	⁹⁴ 0.911	²⁰⁴ 0.192	¹³⁸ 0.404	0.000	0.001	0.044																		
254	SENSETIME-000	¹³³ 0.002	¹⁵⁰ 0.016	¹⁶ 0.528				¹² 0.021	¹¹⁶ 0.063	²⁹⁸ 1.000									0.004	0.000	0.042												
255	SENSETIME-001	¹³⁴ 0.002	¹⁴⁹ 0.016					¹³¹ 0.022	¹¹⁸ 0.064										0.004	0.000													
256	SENSETIME-002	²⁷ 0.014	¹⁷ 0.020	¹³⁹ 0.384	¹⁶ 0.011		¹¹⁸ 0.104	¹⁶ 0.015	³³ 0.028	¹⁵⁹ 0.994	¹¹⁶ 0.032	¹⁶¹ 0.523	0.009	0.000	0.040																		
257	SENSETIME-003	¹³ 0.001	¹³ 0.007	⁸² 0.150	⁸¹ 0.003		⁹¹ 0.091	¹² 0.002	¹⁰ 0.012	⁴² 0.477	⁴ 0.008	⁴⁶ 0.133	0.000	0.000	0.041																		
258	SENSETIME-004	¹² 0.001	¹⁶ 0.007	⁴¹ 0.072	⁶⁸ 0.002		⁸² 0.084	⁹ 0.002	¹³ 0.013	¹⁹ 0.229	²⁶ 0.006	³⁷ 0.113	0.000	0.000	0.041																		
259	SENSETIME-005	⁶ 0.001	⁶ 0.006	¹⁶ 0.059	⁶ 0.002	³⁵ 0.007	⁷³ 0.082	¹⁹ 0.002	¹⁹ 0.014	¹¹ 0.173	³¹ 0.007	²⁷ 0.051	³¹ 0.104	0.000	0.000	0.041	0.000	0.000	0.000	0.000	0.000	0.000	0.000	0.000	0.000	0.000	0.000	0.000	0.000	0.000	0.000		
260	SENSETIME-006	⁵ 0.001	⁴ 0.006	⁷ 0.055	¹⁰ 0.001	⁷ 0.004	³⁴ 0.064	¹⁰ 0.002	¹¹ 0.012	¹⁹³ 0.998	¹⁵ 0.004	¹⁷ 0.034	¹⁸ 0.093	0.000	0.000	0.025	0.000	0.000	0.000	0.000	0.000	0.000	0.000	0.000	0.000	0.000	0.000	0.000	0.000	0.000	0.000		
261	SENSETIME-007	⁴ 0.001	³ 0.006	³ 0.052	³ 0.001	⁶ 0.003	^{31</sup}																										

#	ALGORITHM	INVESTIGATION MODE						IDENTIFICATION MODE						FAILURE TO EXTRACT FEATURES									
		RANK ONE MISS RATE, FNIR(N, 0, 1)						HIGH T → FPIR = 0.001, FNIR(N, T, L)															
		N=1.6M						N=1.6M															
	GALLERY	MUGSHOT	MUGSHOT	MUGSHOT	VISA	BORDER	BOR _i 10YR	KIOSK	MUGSHOT	MUGSHOT	MUGSHOT	VISA	BORDER	BOR _i 10YR	KIOSK	MUGSHOT	MUGSHOT	MUGSHOT	VISA	BORDER	BOR _i 10YR	KIOSK	
PROBE	MUGSHOT	WEBCAM	PROFILE	BORDER	BOR _i 10YR	KIOSK			MUGSHOT	WEBCAM	PROFILE	BORDER	BOR _i 10YR	KIOSK	MUGSHOT	WEBCAM	PROFILE	BORDER	BOR _i 10YR	KIOSK			
323 VOCORD-004	219 0.008	185 0.021	212 0.792	177 0.012	159 0.127	294 0.355	224 0.173	240 1.000	205 0.193	229 0.991	0.000	0.000	0.000	0.000									
324 VOCORD-005	213 0.007	205 0.023	225 0.812	221 0.055	201 0.206	263 0.158	197 0.130	188 0.997	190 0.138	131 0.381	0.001	0.009	0.554										
325 VOCORD-006	336 1.000	337 1.000	300 1.000	329 1.000	271 1.000	337 1.000	326 1.000	324 1.000	309 1.000	247 1.000	0.001	0.009	0.554										
326 VTS-000	332 0.594	322 0.608	236 0.099	249 0.607	152 0.724	248 0.739	312 0.598	299 0.619	217 0.999	237 0.613	129 0.760	188 0.761	0.000	0.001	0.047						0.000		
327 VTS-001	70 0.002	67 0.010	87 0.167	137 0.006	86 0.018	63 0.077	94 0.013	93 0.051	160 0.994	93 0.022	64 0.141	83 0.192	0.000	0.000	0.040							0.000	
328 VTS-002	107 0.002	117 0.013	106 0.233	185 0.014	125 0.038	154 0.125	142 0.026	133 0.075	222 1.000	140 0.045	92 0.231	139 0.417	0.000	0.000	0.029							0.000	
329 VTS-003	30 0.001	29 0.007	43 0.074	43 0.002	48 0.009	15 0.053	66 0.007	64 0.033	244 1.000	69 0.014	137 0.954	175 0.635	0.000	0.001	0.029							0.000	
330 XFORWARDAI-000	130 0.002	131 0.014	95 0.089	104 0.004	77 0.015	92 0.094	103 0.015	102 0.053	35 0.440	89 0.021	73 0.159	70 0.169	0.000	0.000	0.000							0.000	
331 XFORWARDAI-001	118 0.002	115 0.013	32 0.067	87 0.003	49 0.009	79 0.082	50 0.005	54 0.028	36 0.448	46 0.008	35 0.062	41 0.123	0.000	0.000	0.000							0.000	
332 XFORWARDAI-002	109 0.002	106 0.012	14 0.059	74 0.002	31 0.007	62 0.077	30 0.003	22 0.016	46 0.525	23 0.005	21 0.041	27 0.099	0.000	0.000	0.000							0.000	
333 YISHENG-001	280 0.027	269 0.060	224 0.058	229 0.287	291 0.346	307 0.808	240 0.666	213 0.919	0.002	0.005													
334 YITU-002	98 0.002	71 0.010					111 0.018	88 0.049					0.000	0.000									
335 YITU-003	155 0.003	155 0.016					119 0.019	97 0.052					0.003	0.001									
336 YITU-004	43 0.001	43 0.008	230 0.866				76 0.010	49 0.027	97 0.936				0.000	0.000	0.000								
337 YITU-005	132 0.002	140 0.014					83 0.010	62 0.032					0.003	0.001									

Table 19: **Miss rates by dataset:** At left, rank 1 miss rates relevant to investigations; at right, with threshold set to target FPIR = 0.01 for higher volume, low prior, uses. Yellow indicates most accurate algorithm. Throughout blue superscripts indicate the rank of the algorithm for that column.

2023 / 03 / 14

14:32:11

FNIR(N, R, T) = False neg. identification rate
FPIR(N, T) = False pos. identification rateN = Num. enrolled subjects
R = Num. candidates examined

T = Threshold

T = 0 → Investigation
T > 0 → Identification

#	ALGORITHM	MISSES BELOW THRESHOLD, T					ENROL, MOST RECENT				
		FNIR(N, T > 0, R > L)					DATASET: FRVT 2018 MUGSHOTS				
		N=0.64M	N=1.6M	N=3.0M	N=6.0M	N=12.0M					
1	3DIVI-005	²⁶⁸ 0.1358	²⁶⁸ 0.1664	²³⁹ 0.1915	²³⁹ 0.2370	²²¹ 0.3054					
2	ACER-000	²⁶¹ 0.1185	²⁶⁰ 0.1455	²³³ 0.1714	²²³ 0.2074	²¹⁴ 0.2537					
3	ALCHERA-003	²⁵⁹ 0.1176	²⁶² 0.1553	²³⁸ 0.1853	²³⁰ 0.2409	²²⁵ 0.3553					
4	ALLGOVISION-000	²³³ 0.0688	²³⁴ 0.0881	²¹⁶ 0.1084	²⁰⁷ 0.1389	¹⁹⁴ 0.2129					
5	ALLGOVISION-001	²³⁷ 0.0785	²⁴⁰ 0.1017	²²² 0.1218	²¹⁴ 0.1584	²⁰¹ 0.2273					
6	ANKE-000	²⁴⁶ 0.0942	²⁴⁴ 0.1169	²²⁸ 0.1404	²¹⁹ 0.1776	²¹⁵ 0.2559					
7	ANKE-002	¹⁶³ 0.0229	¹⁶³ 0.0318	¹⁶² 0.0406	¹⁵⁵ 0.0605	¹⁴⁴ 0.1466					
8	AWARE-003	²⁵⁶ 0.1098	²⁵² 0.1283	²²⁹ 0.1447	²¹⁷ 0.1768	²⁰⁶ 0.2364					
9	AWARE-005	²⁵⁹ 0.3389	²⁹⁵ 0.3643	²⁴⁶ 0.3993	²³⁸ 0.4526	²¹⁷ 0.2531					
10	AYONIX-002	³²¹ 0.7862	³²¹ 0.8242	²⁵³ 0.8508	²⁴⁴ 0.8704	²³⁸ 0.8939					
11	CAMVI-004	¹⁸⁹ 0.0367	²¹⁸ 0.0716	²¹¹ 0.0983	²³² 0.2508	²¹⁸ 0.2701					
12	CANON-001	⁵⁵ 0.0039	⁵⁵ 0.0054	⁵⁵ 0.0074	⁵⁰ 0.0158	⁶⁰ 0.0924					
13	CANON-002	⁴⁸ 0.0036	⁴⁷ 0.0047	⁴⁶ 0.0061	⁴¹ 0.0124	³⁹ 0.0808					
14	CIB-000	⁸⁷ 0.0086	⁹¹ 0.0125	⁹¹ 0.0160	⁹⁴ 0.0303	¹¹³ 0.1251					
15	CLEARVIEWAI-000	⁵⁹ 0.0040	⁵⁸ 0.0058	⁵⁸ 0.0078	⁵² 0.0159	⁶⁶ 0.0971					
16	CLOUDWALK-HR-000	¹⁸ 0.0019	¹⁸ 0.0020	¹⁴ 0.0023	²¹ 0.0072	²⁸ 0.0701					
17	CLOUDWALK-MT-000	¹⁹ 0.0019	¹⁷ 0.0020	¹⁵ 0.0022	⁹ 0.0049	¹³ 0.0466					
18	CLOUDWALK-MT-001	¹⁷ 0.0018	¹⁵ 0.0019	¹⁰ 0.0020	¹¹ 0.0052	²¹ 0.0555					
19	CLOUDWALK-MT-002	¹⁶ 0.0018	¹³ 0.0019	⁷ 0.0019	¹⁰ 0.0019	¹ 0.0051					
20	COGENT-000	²⁰⁷ 0.0430	¹⁹³ 0.0527	¹⁹¹ 0.0695	¹⁹³ 0.1133	¹⁸² 0.1960					
21	COGENT-001	²⁰⁸ 0.0430	¹⁹² 0.0527	¹⁹³ 0.0695	¹⁹² 0.1133	¹⁸³ 0.1960					
22	COGENT-002	¹⁷ 0.0322	¹⁷⁹ 0.0444	¹⁷⁸ 0.0610	¹⁹⁰ 0.1116	¹⁹⁴ 0.2180					
23	COGENT-003	¹⁷⁶ 0.0328	¹⁸⁴ 0.0463	¹⁹⁰ 0.0683	²⁰⁰ 0.1294	²⁰⁸ 0.2445					
24	COGENT-004	¹⁶¹ 0.0210	¹⁶⁴ 0.0331	¹⁷³ 0.0527	¹⁹⁵ 0.1138	¹⁹¹ 0.2119					
25	COGENT-005	⁷⁵ 0.0064	⁷⁵ 0.0091	⁷⁸ 0.0123	⁹⁵ 0.0303	¹⁰⁹ 0.1233					
26	COGENT-006	⁴² 0.0032	⁴³ 0.0044	⁴² 0.0057	³⁷ 0.0120	⁴⁸ 0.0830					
27	COGENT-007	³⁵ 0.0028	³⁴ 0.0036	³⁷ 0.0049	¹⁰ 0.0049	² 0.0111					
28	COGNITEC-000	²⁷⁰ 0.1377	²⁶⁶ 0.1606	²³⁸ 0.1870	²²⁴ 0.2176	²²⁰ 0.2831					
29	COGNITEC-001	²⁴¹ 0.0807	²³⁹ 0.1017	²²² 0.1214	²¹⁰ 0.1513	¹⁹⁹ 0.2238					
30	COGNITEC-002	²⁰⁰ 0.0406	¹⁹⁵ 0.0531	¹⁸⁶ 0.0666	¹⁷⁸ 0.0935	¹⁷⁸ 0.1874					
31	COGNITEC-003	¹⁹ 0.0400	¹⁹¹ 0.0526	¹⁸¹ 0.0650	¹⁷³ 0.0895	¹⁷ 0.1772					
32	COGNITEC-004	¹⁶² 0.0222	¹⁶² 0.0313	¹⁵⁸ 0.0388	¹⁴⁶ 0.0540	⁸⁷ 0.1103					
33	COGNITEC-005	⁷ 0.0063	⁷⁷ 0.0096	⁸⁴ 0.0144	⁸⁸ 0.0287	⁶² 0.0967					
34	COGNITEC-006	⁶⁶ 0.0053	⁶⁸ 0.0077	⁷¹ 0.0117	⁷⁵ 0.0254	⁵⁶ 0.0919					
35	CYBERLINK-000	²⁶² 0.0414	²⁰⁵ 0.0565	¹⁹⁷ 0.0707	¹⁸⁶ 0.1031	¹⁸ 0.2050					
36	CYBERLINK-001	¹⁹³ 0.0392	¹⁹⁶ 0.0536	¹⁹² 0.0695	¹⁸³ 0.0973	¹⁷² 0.1794					
37	CYBERLINK-002	⁹⁸ 0.0105	¹⁰¹ 0.0148	¹⁰⁶ 0.0202	¹¹⁷ 0.0399	¹¹⁴ 0.1255					
38	CYBERLINK-003	⁶⁸ 0.0056	⁶⁹ 0.0077	⁶⁹ 0.0100	⁷¹ 0.0235	¹¹⁰ 0.1237					
39	CYBERLINK-004	⁶⁴ 0.0051	⁶⁵ 0.0071	⁶⁹ 0.0102	⁶⁹ 0.0199	¹¹⁷ 0.1269					
40	CYBERLINK-005	⁷⁸ 0.0067	⁸¹ 0.0099	⁸² 0.0138	¹¹⁴ 0.0394	¹⁵ 0.1566					
41	DAHUA-001	²²² 0.0569	²²⁰ 0.0727	²⁰⁵ 0.0878	¹⁹⁶ 0.1148	¹⁷⁷ 0.1867					
42	DAHUA-002	¹⁰³ 0.0108	¹⁰² 0.0151	¹⁰¹ 0.0191	⁹⁰ 0.0291	⁹⁹ 0.1153					
43	DAHUA-003	⁹⁵ 0.0100	⁹⁶ 0.0139	⁹⁷ 0.0180	⁹¹ 0.0296	⁹³ 0.1130					
44	DAHUA-004	⁶² 0.0048	⁶⁴ 0.0069	⁶² 0.0090	⁵⁵ 0.0164	⁴⁴ 0.0853					
45	DAON-000	¹³³ 0.0161	¹³³ 0.0226	¹³⁴ 0.0293	¹³⁴ 0.0562	¹⁶⁵ 0.1702					
46	DECATUR-000	¹³⁶ 0.0173	¹³⁶ 0.0229	¹³⁸ 0.0305	¹³⁸ 0.0464	¹³⁹ 0.1433					
47	DEEPLINT-001	³³ 0.0027	³³ 0.0033	³¹ 0.0043	³⁹ 0.0121	³⁹ 0.0922					
48	DEEPSSEA-001	¹⁸⁷ 0.0347	¹⁸³ 0.0462	¹⁷⁷ 0.0586	¹⁷¹ 0.0802	¹⁶ 0.1708					
49	DERMALOG-005	²³⁷ 0.0700	²³³ 0.0880	²¹⁸ 0.1144	²¹³ 0.1578	²⁰⁹ 0.2451					
50	DERMALOG-006	¹⁹³ 0.0395	¹⁹⁰ 0.0517	¹⁸⁶ 0.0659	¹⁸² 0.0973	¹⁷² 0.1745					
51	DERMALOG-007	²³⁴ 0.0691	²³¹ 0.0863	²¹⁷ 0.1107	²⁰⁹ 0.1504	²⁰¹ 0.2299					
52	DERMALOG-008	¹⁸¹ 0.0338	¹⁸¹ 0.0455	¹⁸¹ 0.0626	¹⁸⁷ 0.1060	²⁰² 0.2276					
53	DERMALOG-009	¹² 0.0148	¹²⁵ 0.0206	¹²² 0.0268	¹²¹ 0.0416	¹³ 0.1374					
54	DERMALOG-010	⁶⁵ 0.0052	⁶³ 0.0069	⁶² 0.0088	⁶² 0.0207	⁶⁴ 0.0971					
55	DERMALOG-011	¹² 0.0149	¹²⁸ 0.0215	¹³¹ 0.0279	¹²⁷ 0.0461	¹⁰⁶ 0.1192					
56	DILUSENSE-000	¹⁵⁹ 0.0208	¹⁶⁰ 0.0305	¹⁵⁸ 0.0377	¹⁵⁰ 0.0543	¹³⁷ 0.1429					
57	DILUSENSE-001	⁷¹ 0.0061	⁷¹ 0.0085	⁷¹ 0.0109	⁷¹ 0.0161						
58	FIRSTCREDITKZ-001	²⁷ 0.0023	²⁹ 0.0030	²⁸ 0.0039	²⁸ 0.0093	³⁵ 0.0760					
59	FUJITSULAB-000	¹² 0.0148	¹²⁶ 0.0206	¹²⁸ 0.0277	¹⁴⁸ 0.0541	¹⁶ 0.1739					
60	FUJITSULAB-001	¹⁰⁸ 0.0126	¹¹⁵ 0.0182	¹²⁰ 0.0251	¹⁵⁸ 0.0646	¹⁹⁰ 0.2079					
61	GORILLA-002	²²⁴ 0.1539	²⁷⁴ 0.1880	²⁴² 0.2184	²³³ 0.2596	²²⁸ 0.3398					
62	GORILLA-004	²³⁶ 0.0699	²³⁶ 0.0892	²¹⁸ 0.1048	²⁰⁵ 0.1370	¹⁸⁶ 0.1969					
63	GORILLA-005	²¹² 0.0453	²⁰⁷ 0.0583	¹⁹⁸ 0.0704	¹⁸⁴ 0.0974	¹⁴³ 0.1474					
64	GORILLA-006	¹⁵ 0.0196	¹⁵¹ 0.0275	¹⁴⁷ 0.0331	¹³⁸ 0.0516	⁹⁹ 0.1113					
65	GORILLA-007	¹⁴⁸ 0.0190	¹⁴⁹ 0.0271	¹⁴⁸ 0.0348	¹⁴² 0.0520	⁹² 0.1129					
66	GORILLA-008	¹³⁵ 0.0170	¹³⁷ 0.0238	¹³⁶ 0.0308	¹²⁹ 0.0469	⁹¹ 0.1120					
67	GRIAULE-000	¹²² 0.0145	¹²³ 0.0201	¹²¹ 0.0253	¹¹⁹ 0.0407	¹⁴⁰ 0.1440					
68	GRIAULE-001	⁴ 0.0033	⁴⁸ 0.0047	⁵⁴ 0.0064	⁴⁸ 0.0153	³⁶ 0.0910					
69	HIK-003	²⁴² 0.0828	²⁴¹ 0.1028	²²¹ 0.1202	²¹² 0.1525	²¹¹ 0.2480					
70	HIK-004	²⁴ 0.0796	²³⁷ 0.0988	²¹⁸ 0.1147	²⁰⁸ 0.1474	²¹ 0.2483					
71	HIK-005	¹⁷ 0.0312	¹⁷⁶ 0.0436	¹⁷⁶ 0.0560	¹⁷⁵ 0.0911	¹⁹⁵ 0.2129					
72	HYPERVERGE-001	⁴³ 0.0033	⁴⁴ 0.0045	⁴⁴ 0.0059	³⁴ 0.0117	⁴⁷ 0.0872					

Table 20: Identification-mode: Effect of N on FNIR at high threshold. Values are threshold-based miss rates i.e. FNIR at FPIR = 0.001 for five enrollment population sizes, N. The right six columns apply for enrollment of one image. Missing entries usually apply because another algorithm from the same developer was run instead. Some developers are missing because less accurate algorithms were not run on galleries with $N \geq 3\,000\,000$. Throughout blue superscripts indicate the rank of the algorithm for that column.

#	ALGORITHM	MISSES BELOW THRESHOLD, T FNIR(N, T > 0, R > L)					ENROL MOST RECENT DATASET: FRVT 2018 MUGSHOTS				
		N=0.64M	N=1.6M	N=3.0M	N=6.0M	N=12.0M	N=0.64M	N=1.6M	N=3.0M	N=6.0M	N=12.0M
73	HYPERVERGE-002	³⁶ 0.0028	³⁵ 0.0037	³³ 0.0046	¹⁷ 0.0064	¹⁸ 0.0538					
74	HZAILU-000	¹²¹ 0.0143	¹²² 0.0197	¹²² 0.0255	¹²⁰ 0.0411	¹⁰³ 0.1174					
75	HZAILU-001	⁷⁷ 0.0066	⁷² 0.0086	²⁰ 0.0109	⁶³ 0.0207	²⁹ 0.1052					
76	HZAILU-002	⁷¹ 0.0061	⁷⁰ 0.0080	⁶⁶ 0.0101	⁵⁸ 0.0187	⁵⁹ 0.0914					
77	IDEMIA-003	¹⁸³ 0.0346	¹⁸⁶ 0.0471	²⁰⁶ 0.0892	²³⁵ 0.2789	²³² 0.4311					
78	IDEMIA-004	¹⁷ 0.0300	¹⁷² 0.0373	¹⁶⁵ 0.0447	¹⁸⁶ 0.0617	¹⁶¹ 0.1635					
79	IDEMIA-005	¹⁸⁸ 0.0360	¹⁷⁸ 0.0440	¹⁷¹ 0.0537	¹⁷⁰ 0.0764	¹⁷⁹ 0.1915					
80	IDEMIA-006	¹⁸⁵ 0.0351	¹⁷⁵ 0.0433	¹⁷⁴ 0.0525	¹⁶⁶ 0.0734	¹⁹⁷ 0.2201					
81	IDEMIA-007	¹¹⁶ 0.0136	¹¹⁴ 0.0181	¹⁰⁸ 0.0228	¹¹⁶ 0.0357	¹³³ 0.1402					
82	IDEMIA-008	¹³ 0.0016	¹⁴ 0.0019	¹⁶ 0.0024	¹² 0.0053	¹⁶ 0.0470					
83	IDEMIA-009	¹ 0.0013	⁷ 0.0016	³ 0.0018	¹⁶ 0.0061	²⁹ 0.0550					
84	IDEMIA-010	² 0.0010	² 0.0011	¹ 0.0012	³ 0.0027	³ 0.0193					
85	IMAGUS-005	¹¹ 0.0137	¹¹⁸ 0.0185	¹¹⁴ 0.0237	¹¹⁸ 0.0368	⁸⁴ 0.1067					
86	IMAGUS-006	¹¹⁸ 0.0137	¹²¹ 0.0190	¹¹⁸ 0.0244	¹¹⁵ 0.0396	¹⁰⁰ 0.1159					
87	IMAGUS-007	¹³ 0.0160	¹³⁵ 0.0228	¹³⁶ 0.0284	¹²⁴ 0.0444	¹⁶¹ 0.1179					
88	IMPERIAL-000	¹⁴⁴ 0.0187	¹⁴³ 0.0259	¹⁵⁴ 0.0358	¹⁶⁵ 0.0733	¹⁷³ 0.1794					
89	INCODE-003	²⁶ 0.1324	²⁶⁹ 0.1672	²⁴⁶ 0.1961	²²⁷ 0.2345	²²² 0.3123					
90	INCODE-004	¹⁹⁸ 0.0403	¹⁹⁹ 0.0538	¹⁸⁸ 0.0662	¹⁷⁷ 0.0917	¹⁶¹ 0.1619					
91	INCODE-005	⁸⁵ 0.0083	⁸⁵ 0.0113	⁸⁰ 0.0145	⁷² 0.0247	⁵³ 0.0912					
92	INNOVATRICS-007	⁹¹ 0.0093	⁹² 0.0125	⁹⁰ 0.0159	⁷⁷ 0.0259	⁸⁴ 0.1092					
93	INNOVATRICS-008	⁵¹ 0.0037	⁵² 0.0050	⁵² 0.0066	⁶¹ 0.0206	⁸⁴ 0.1093					
94	INTEMA-000	²⁰ 0.0019	²¹ 0.0024	²¹ 0.0032	²⁹ 0.0098	³³ 0.0745					
95	INTEMA-001	⁷ 0.0014	⁵ 0.0014	³⁸ 0.0049	³¹ 0.0098	²⁹ 0.0703					
96	INTSYSMSU-000	³³² 0.9982	³³⁰ 0.9984	²⁵⁷ 0.9985	²⁴⁷ 0.9987	²⁴² 0.9988					
97	IREX-000	¹⁴⁹ 0.0190	¹⁵⁵ 0.0280	¹⁵⁹ 0.0391	¹⁶¹ 0.0677	¹⁴⁶ 0.1479					
98	ISYSTEMS-002	²² 0.0584	²²⁴ 0.0783	²¹⁹ 0.0973	²¹⁶ 0.1373	²⁰¹ 0.2295					
99	ISYSTEMS-003	²¹⁰ 0.0438	²⁰⁸ 0.0590	²⁰³ 0.0807	¹⁹⁸ 0.1259	²⁰⁵ 0.2357					
100	KAKAO-000	¹⁰⁴ 0.0109	¹⁰⁴ 0.0151	¹⁰⁵ 0.0196	¹⁰¹ 0.0324	²⁰¹ 0.1010					
101	KAKAO-001	²⁵ 0.0021	²⁴ 0.0026	²² 0.0032	²⁶ 0.0085	²⁷ 0.0693					
102	KEDACOM-001	¹³ 0.0181	¹³⁴ 0.0227	¹²² 0.0265	¹²³ 0.0422	¹²⁰ 0.1340					
103	LINELICOVA-002	³⁴ 0.0028	³⁶ 0.0040	³⁶ 0.0049	³⁸ 0.0120	⁴¹ 0.0824					
104	LINELICOVA-003	³¹ 0.0026	²⁶ 0.0026	³⁴ 0.0049	³¹ 0.0158	⁶⁵ 0.0989					
105	LOOKMAN-003	¹⁸⁴ 0.0346	¹⁷⁷ 0.0437	¹⁷⁰ 0.0514	¹⁶⁴ 0.0724	¹⁶² 0.1620					
106	LOOKMAN-005	¹⁶ 0.0240	¹⁵⁹ 0.0301	¹⁵⁰ 0.0356	¹³⁷ 0.0512	¹²² 0.1334					
107	MANTRA-000	⁷⁶ 0.0065	⁸² 0.0101	⁸⁶ 0.0151	⁹⁶ 0.0308	⁷⁵ 0.1035					
108	MAXVISION-000	¹⁵⁸ 0.0206	¹⁵⁶ 0.0282	¹⁵⁹ 0.0355	¹⁵⁹ 0.0517	¹² 0.1340					
109	MAXVISION-001	⁴⁰ 0.0031	⁴² 0.0043	³⁸ 0.0055	⁴⁰ 0.0122	³¹ 0.0895					
110	MEGVI-001	²²⁰ 0.0562	²¹⁹ 0.0722	²⁰⁹ 0.0872	²⁰² 0.1309	²¹⁹ 0.2713					
111	MICROFOCUS-005	³²⁹ 0.9732	³²³ 0.8354	²⁵⁴ 0.8555	²⁴⁵ 0.8755	²³⁹ 0.8954					
112	MICROSOFT-003	¹⁵ 0.0198	¹⁵³ 0.0278	¹⁵⁶ 0.0356	¹⁴⁵ 0.0538	¹⁵² 0.1539					
113	MICROSOFT-004	¹⁴² 0.0185	¹⁴⁴ 0.0259	¹⁴⁴ 0.0333	¹⁴⁰ 0.0517	¹⁵⁰ 0.1510					
114	MICROSOFT-005	¹⁴⁰ 0.0181	¹⁴¹ 0.0256	¹⁴⁶ 0.0320	¹³⁶ 0.0512	¹⁴⁸ 0.1491					
115	MICROSOFT-006	⁹⁰ 0.0091	⁸⁷ 0.0120	⁹² 0.0162	⁹³ 0.0301	¹⁴ 0.1482					
116	MUKH-002	³¹¹ 0.5041	³¹¹ 0.5942	²⁵¹ 0.6674	²⁴² 0.7314	²³⁷ 0.8276					
117	NEC-000	²²⁸ 0.0637	²²⁶ 0.0789	²⁰⁹ 0.0933	¹⁹⁷ 0.1163	¹⁸¹ 0.1941					
118	NEC-001	²⁴³ 0.0863	²⁴³ 0.1055	²²⁴ 0.1249	²¹¹ 0.1519	²⁰¹ 0.2253					
119	NEC-002	²⁹ 0.0020	²³ 0.0026	²⁵ 0.0033	⁴⁴ 0.0135	²⁴ 0.0653					
120	NEC-003	²⁴ 0.0021	²⁰ 0.0024	¹⁸ 0.0028	¹⁵ 0.0059	¹⁹ 0.0540					
121	NEC-004	¹⁴ 0.0017	¹¹ 0.0018	⁹ 0.0020	⁶ 0.0037	¹⁰ 0.0329					
122	NEC-005	⁹ 0.0015	⁸ 0.0017	⁸ 0.0019	¹⁸ 0.0065	⁸ 0.0307					
123	NEC-006	¹⁵ 0.0018	¹⁶ 0.0020	¹⁷ 0.0026	³² 0.0103	²² 0.0573					
124	NEC-007	³⁴ 0.0039	³⁷ 0.0040	²⁹ 0.0041	¹⁴ 0.0055	⁷ 0.0294					
125	NEUROTECHNOLOGY-003	³¹⁴ 0.5698	³¹⁵ 0.6362	²⁵² 0.7035	²⁴³ 0.7602	²³⁶ 0.8224					
126	NEUROTECHNOLOGY-004	²¹ 0.0466	²¹³ 0.0629	¹⁹⁸ 0.0779	¹⁹⁴ 0.1135	¹⁹² 0.2102					
127	NEUROTECHNOLOGY-005	¹⁹⁵ 0.0396	²⁰⁰ 0.0538	¹⁸⁸ 0.0675	¹⁸¹ 0.0950	¹⁸⁵ 0.1966					
128	NEUROTECHNOLOGY-007	²⁰⁹ 0.0432	²¹² 0.0623	²⁰⁸ 0.0802	²⁰³ 0.1320	²⁰⁷ 0.2393					
129	NEUROTECHNOLOGY-008	¹⁸² 0.0339	¹⁹⁴ 0.0530	²⁰⁷ 0.0893	²¹⁸ 0.1769	²²⁶ 0.3288					
130	NEUROTECHNOLOGY-009	¹⁶ 0.0108	¹⁰⁵ 0.0152	¹⁰⁴ 0.0196	⁹⁹ 0.0324	⁸⁹ 0.1102					
131	NEUROTECHNOLOGY-010	⁸¹ 0.0069	⁸⁰ 0.0099	⁸³ 0.0138	¹²⁶ 0.0449	¹⁶⁸ 0.1727					
132	NEUROTECHNOLOGY-012	⁶¹ 0.0047	⁶² 0.0068	⁶³ 0.0097	⁸¹ 0.0265	¹²⁹ 0.1343					
133	NEUROTECHNOLOGY-013	³⁹ 0.0029	⁴¹ 0.0043	⁴³ 0.0057	⁶⁴ 0.0208	¹⁰ 0.1202					
134	NOTIONTAG-000	¹⁶⁹ 0.0128	¹⁰⁹ 0.0175	¹⁰⁹ 0.0228	¹⁰⁷ 0.0357	¹¹⁸ 0.1270					
135	NTECHLAB-003	²⁰⁴ 0.0421	¹⁹⁸ 0.0537	¹⁸⁷ 0.0674	¹⁷⁴ 0.0907	¹⁵⁸ 0.1582					
136	NTECHLAB-004	¹⁷⁴ 0.0312	¹⁷³ 0.0405	¹⁷¹ 0.0519	¹⁶³ 0.0722	¹⁴⁹ 0.1503					
137	NTECHLAB-005	¹⁷⁸ 0.0334	¹⁷⁴ 0.0424	¹⁷⁵ 0.0537	¹⁶⁹ 0.0760	¹⁵⁹ 0.1543					
138	NTECHLAB-006	¹⁷⁰ 0.0288	¹⁶⁸ 0.0367	¹⁶⁸ 0.0471	¹⁶⁰ 0.0670	¹⁵¹ 0.1523					
139	NTECHLAB-007	¹⁴⁸ 0.0188	¹⁴⁰ 0.0256	¹³⁸ 0.0317	¹³⁴ 0.0495	¹²⁴ 0.1306					
140	NTECHLAB-008	¹⁰⁰ 0.0107	⁹⁸ 0.0145	⁹⁹ 0.0187	⁸⁷ 0.0286	⁶⁸ 0.0995					
141	NTECHLAB-009	⁵⁰ 0.0037	⁵¹ 0.0049	⁴⁹ 0.0062	⁴² 0.0125	³² 0.0735					
142	NTECHLAB-010	²¹ 0.0020	²² 0.0025	¹⁹ 0.0030	²⁴ 0.0077	³¹ 0.0710					
143	NTECHLAB-011	²⁶ 0.0022	²⁸ 0.0030	²⁷ 0.0038	²² 0.0075	²³ 0.0625					
144	PANGIAM-000	⁵⁹ 0.0042	⁵⁹ 0.0060	⁵⁹ 0.0080	⁵³ 0.0160	⁴⁹ 0.0876					

Table 21: Identification-mode: Effect of N on FNIR at high threshold. Values are threshold-based miss rates i.e. FNIR at FPIR = 0.001 for five enrollment population sizes, N. The right six columns apply for enrollment of one image. Missing entries usually apply because another algorithm from the same developer was run instead. Some developers are missing because less accurate algorithms were not run on galleries with $N \geq 3\,000\,000$. Throughout blue superscripts indicate the rank of the algorithm for that column.

MISSES BELOW THRESHOLD, T FNIR(N, T > 0, R > L)		ENROL MOST RECENT DATASET: FRVT 2018 MUGSHOTS				
#	ALGORITHM	N=0.64M	N=1.6M	N=3.0M	N=6.0M	N=12.0M
145	PANGIAM-001	⁹⁴ 0.0098	⁸⁶ 0.0113	⁷⁹ 0.0134	⁶⁷ 0.0232	⁴⁶ 0.0865
146	PARAVISION-003	¹⁶⁶ 0.0260	¹⁶⁶ 0.0351	¹⁶⁸ 0.0447	¹⁵⁹ 0.0657	¹⁶³ 0.1630
147	PARAVISION-004	⁸² 0.0074	⁸⁴ 0.0101	⁸¹ 0.0136	⁸² 0.0267	¹¹⁵ 0.1256
148	PARAVISION-005	⁴¹ 0.0032	⁴⁰ 0.0041	⁴¹ 0.0057	³⁷ 0.0174	⁷⁸ 0.1037
149	PARAVISION-007	³⁸ 0.0030	³⁸ 0.0040	³⁹ 0.0055	⁶⁵ 0.0211	⁸⁵ 0.1097
150	PARAVISION-009	²⁸ 0.0020	²⁵ 0.0026	²⁸ 0.0038	³⁰ 0.0098	⁴⁸ 0.0857
151	PARAVISION-012	⁵ 0.0013	⁶ 0.0015	⁸ 0.0018	¹⁹ 0.0065	³⁶ 0.0770
152	PIXELALL-002	²³ 0.0716	²⁴² 0.1052	²³ 0.1475	²³¹ 0.2489	²³ 0.3904
153	PIXELALL-003	¹³⁰ 0.0158	¹³⁰ 0.0218	¹³⁰ 0.0288	¹³⁰ 0.0474	⁹⁷ 0.1138
154	PIXELALL-004	¹¹² 0.0129	¹¹⁷ 0.0183	¹¹⁹ 0.0245	¹⁰⁹ 0.0378	¹³² 0.1375
155	PIXELALL-005	⁸⁸ 0.0087	⁸⁹ 0.0121	⁹⁰ 0.0171	⁷⁴ 0.0250	⁷⁸ 0.1052
156	PTAKURATSATU-000	¹⁶⁷ 0.0275	¹⁶⁷ 0.0366	¹⁶⁷ 0.0458	¹⁴³ 0.0523	¹⁷ 0.0523
157	QNAP-001	¹⁹⁹ 0.0404	¹⁹⁷ 0.0536	¹⁸⁸ 0.0661	¹⁷⁶ 0.0916	¹⁵⁹ 0.1595
158	QNAP-002	¹⁵³ 0.0200	¹⁴⁵ 0.0265	¹⁴¹ 0.0327	¹³² 0.0490	¹²⁸ 0.1341
159	QNAP-003	¹²⁸ 0.0139	¹²⁰ 0.0189	¹¹⁸ 0.0239	¹¹⁰ 0.0379	¹³⁷ 0.1414
160	QUANTASOFT-001	³¹⁶ 0.6387	³¹⁶ 0.6387	²⁵⁰ 0.6387		²³⁴ 0.6387
161	RANKONE-002	²⁵ 0.0973	²⁴⁶ 0.1175	²²⁹ 0.1359	²¹⁵ 0.1718	²¹⁷ 0.2613
162	RANKONE-003	²⁵² 0.0973	²⁴⁷ 0.1175	²²⁵ 0.1359	²¹⁶ 0.1718	²¹⁶ 0.2613
163	RANKONE-005	²¹ 0.0473	²⁰⁹ 0.0592	¹⁹⁴ 0.0700	¹⁷⁷ 0.0944	¹⁸ 0.1998
164	RANKONE-007	¹³⁴ 0.0168	¹³² 0.0222	¹²⁴ 0.0266	¹¹² 0.0381	⁹⁴ 0.1132
165	RANKONE-009	¹¹³ 0.0132	¹¹² 0.0177	¹¹¹ 0.0230	¹⁰³ 0.0344	⁵⁸ 0.0921
166	RANKONE-010	⁹⁰ 0.0106	⁹⁵ 0.0136	⁹⁹ 0.0174	⁸⁰ 0.0265	³⁷ 0.0785
167	RANKONE-011	⁷³ 0.0063	⁷³ 0.0087	⁷² 0.0115	⁸³ 0.0269	⁹⁶ 0.1135
168	RANKONE-012	⁶⁹ 0.0058	⁶⁷ 0.0077	⁶⁷ 0.0100	⁶⁶ 0.0220	⁸⁰ 0.1111
169	RANKONE-013	⁴⁶ 0.0034	⁴⁵ 0.0046	⁴⁵ 0.0059	⁴³ 0.0127	⁴⁸ 0.0875
170	RANKONE-014	²⁸ 0.0025	³¹ 0.0033	³⁶ 0.0043	³³ 0.0106	²⁸ 0.0656
171	REALNETWORKS-002	²⁸⁰ 0.1943	²⁷⁹ 0.2314	²⁴⁸ 0.2656	²³⁷ 0.3134	²²⁵ 0.3208
172	REALNETWORKS-003	²⁶ 0.1300	²⁶⁵ 0.1594	²⁵⁹ 0.1858	²²⁵ 0.2246	²² 0.3076
173	REALNETWORKS-004	²⁸⁵ 0.1279	²⁶⁴ 0.1581	²³⁸ 0.1857	²²⁶ 0.2329	²²⁴ 0.3179
174	REALNETWORKS-005	¹⁵⁴ 0.0202	¹⁵² 0.0277	¹⁵¹ 0.0355	¹⁵³ 0.0560	¹³⁸ 0.1431
175	REALNETWORKS-006	⁹³ 0.0097	⁹⁹ 0.0145	⁹⁸ 0.0182	⁹⁷ 0.0308	⁶⁷ 0.0991
176	REALNETWORKS-007	⁸⁰ 0.0068	⁷⁸ 0.0097	⁷⁶ 0.0125	⁶⁹ 0.0233	⁵⁵ 0.0917
177	REALNETWORKS-008	⁶⁰ 0.0044	⁶⁰ 0.0062	⁶⁰ 0.0082	⁴⁵ 0.0139	⁴⁰ 0.0824
178	REMARKAI-000	²⁰¹ 0.0406	²⁰¹ 0.0552	¹⁸⁹ 0.0676	¹⁸⁵ 0.1028	¹⁸⁸ 0.2003
179	RENDIP-000	⁸⁸ 0.0085	⁸⁸ 0.0121	⁸⁸ 0.0156	⁸⁶ 0.0277	¹⁰ 0.1182
180	REVEALMEDIA-000	⁸⁹ 0.0090	⁹⁰ 0.0122	⁸⁹ 0.0158	⁸⁵ 0.0277	⁷² 0.1019
181	S1-000	¹⁵ 0.0204	¹⁵⁴ 0.0279	¹⁵⁷ 0.0382	¹⁵⁷ 0.0630	¹⁶ 0.1707
182	S1-001	¹⁰⁵ 0.0115	¹⁰⁶ 0.0156	¹⁰⁸ 0.0199	¹¹³ 0.0392	¹¹⁶ 0.1256
183	S1-002	⁵⁶ 0.0040	⁵⁶ 0.0056	⁵⁶ 0.0077	⁷⁹ 0.0264	¹²⁰ 0.1285
184	S1-003	⁷² 0.0061	⁷⁴ 0.0088	⁷³ 0.0116	⁸⁴ 0.0277	¹²¹ 0.1298
185	S1-004	³⁹ 0.0030	³⁹ 0.0040	⁴⁰ 0.0056	⁵⁴ 0.0162	⁶⁶ 0.0989
186	SCANOVATE-000	²¹⁶ 0.0498	²¹⁶ 0.0667	²⁰⁷ 0.0804	¹⁸⁹ 0.1097	⁸⁸ 0.1109
187	SCANOVATE-001	²²⁷ 0.0630	²²⁷ 0.0815	²¹² 0.0993	¹⁹⁹ 0.1292	¹⁸⁴ 0.1960
188	SENSETIME-000	¹² 0.0158	¹²⁷ 0.0208	¹²² 0.0270	¹¹⁶ 0.0398	¹⁰ 0.1232
189	SENSETIME-001	¹³² 0.0161	¹³¹ 0.0219	¹³⁰ 0.0277	¹²² 0.0420	¹²³ 0.1304
190	SENSETIME-002	¹² 0.0146	¹⁰⁰ 0.0148	⁸⁷ 0.0153	⁷⁰ 0.0234	²⁶ 0.0657
191	SENSETIME-003	¹¹ 0.0016	¹² 0.0018	¹² 0.0021	¹³ 0.0054	¹³ 0.0451
192	SENSETIME-004	¹⁰ 0.0015	⁹ 0.0018	¹¹ 0.0021	⁷ 0.0040	¹⁰ 0.0354
193	SENSETIME-005	¹² 0.0016	¹⁹ 0.0022	²⁹ 0.0031	²⁷ 0.0089	¹⁴ 0.0454
194	SENSETIME-006	⁸ 0.0014	¹⁰ 0.0018	¹⁵ 0.0023	⁸ 0.0047	¹² 0.0372
195	SENSETIME-007	⁴ 0.0012	⁴ 0.0014	⁴ 0.0016	⁵ 0.0036	³ 0.0316
196	SENSETIME-008	³ 0.0011	³ 0.0013	³ 0.0015	⁴ 0.0031	⁶ 0.0288
197	SENSETIME-009	¹ 0.0010	¹ 0.0011	² 0.0012	² 0.0024	³ 0.0238
198	SHAMAN-007	²⁶³ 0.1212	²⁵⁹ 0.1413	²³² 0.1587	²²⁰ 0.1879	²¹⁰ 0.2460
199	SIAT-001	¹¹⁵ 0.0136	¹¹⁰ 0.0176	¹¹⁵ 0.0230	¹⁰² 0.0344	⁷⁴ 0.1035
200	SIAT-002	¹²⁸ 0.0154	¹²⁹ 0.0216	¹²⁸ 0.0273	¹¹⁸ 0.0404	¹¹⁹ 0.1283
201	SQISOFT-001	²⁴ 0.0921	²⁵⁵ 0.1322	²³⁴ 0.1781	²²⁸ 0.2348	²⁴ 0.9271
202	SQISOFT-002	¹³⁷ 0.0177	¹⁵⁸ 0.0290	¹⁶³ 0.0415	¹⁶⁷ 0.0739	¹³⁰ 0.1351
203	SYNESIS-003	²¹⁷ 0.0499	²¹⁴ 0.0652	²⁰⁸ 0.0804	¹⁸⁸ 0.1095	¹⁸⁴ 0.1916
204	SYNESIS-003	³¹² 0.5341	³¹⁰ 0.5821	²⁴⁹ 0.6113	²⁴¹ 0.6479	²³⁵ 0.6822
205	SYNESIS-005	¹³⁸ 0.0181	¹³⁹ 0.0248	¹³⁹ 0.0319	¹⁴¹ 0.0518	¹³⁷ 0.1580
206	TECH5-001	²⁰ 0.0420	²⁰⁴ 0.0574	²⁰⁸ 0.0911	²²³ 0.2106	²³ 0.3725
207	TECH5-002	¹⁵⁰ 0.0194	¹⁴⁸ 0.0269	¹⁴⁷ 0.0346	¹⁴⁴ 0.0537	¹⁶⁰ 0.1607
208	TEVIAN-005	²³ 0.0692	²³² 0.0873	²¹⁷ 0.1066	²⁰¹ 0.1301	¹⁷ 0.1840
209	TEVIAN-006	⁸⁴ 0.0078	⁷⁹ 0.0098	⁷⁸ 0.0130	⁷⁸ 0.0261	¹²³ 0.1305
210	TEVIAN-007	⁵⁸ 0.0038	⁵⁴ 0.0052	⁵¹ 0.0065	⁴⁹ 0.0154	⁶¹ 0.0957
211	TIGER-002	²³⁰ 0.0647	²²⁹ 0.0861	²¹³ 0.1036	²⁰⁴ 0.1332	¹⁹⁸ 0.2231
212	TOSHIBA-000	²¹³ 0.0460	²¹¹ 0.0620	¹⁹⁹ 0.0780	¹⁹¹ 0.1117	¹⁹ 0.2082
213	TRUEFACE-000	¹¹⁴ 0.0134	¹¹⁶ 0.0182	¹¹⁵ 0.0238	¹¹¹ 0.0380	¹³⁴ 0.1385
214	VD-001	²⁶ 0.1642	²⁶ 0.2015	²⁴ 0.2351	²⁴ 0.2736	²² 0.3293
215	VERIDAS-001	¹⁶⁹ 0.0278	¹⁷⁰ 0.0373	¹⁶⁹ 0.0491	¹⁶⁸ 0.0753	¹⁵³ 0.1541
216	VERIDAS-002	¹⁶⁸ 0.0278	¹⁷¹ 0.0373	¹⁵⁹ 0.0373	¹⁵³ 0.0491	³⁴ 0.0753

Table 22: **Identification-mode: Effect of N on FNIR at high threshold.** Values are threshold-based miss rates i.e. FNIR at FPIR = 0.001 for five enrollment population sizes, N. The right six columns apply for enrollment of one image. Missing entries usually apply because another algorithm from the same developer was run instead. Some developers are missing because less accurate algorithms were not run on galleries with $N \geq 3\ 000\ 000$. Throughout blue superscripts indicate the rank of the algorithm for that column.

#	ALGORITHM	ENROL MOST RECENT				
		DATASET: FRVT 2018 MUGSHOTS				
		N=0.64M	N=1.6M	N=3.0M	N=6.0M	N=12.0M
217	VERIDAS-003	¹⁰⁶ 0.0117	¹⁰⁸ 0.0166	¹⁰⁹ 0.0219	¹²⁵ 0.0446	¹⁵⁴ 0.1543
218	VERIDAS-004	⁵⁸ 0.0042	⁵⁷ 0.0058	⁵⁷ 0.0077	²³ 0.0077	⁴ 0.0232
219	VIDILANTSOLUTIONS-008	¹²⁴ 0.0146	¹²⁴ 0.0205	¹²⁹ 0.0269	¹³¹ 0.0489	¹⁰² 0.1164
220	VISIONBOX-000	¹⁰⁷ 0.0122	¹¹³ 0.0177	¹¹⁷ 0.0239	²⁴¹ 0.9538	
221	VISIONLABS-004	²⁰⁶ 0.0427	²⁰⁵ 0.0578	¹⁹⁹ 0.0703	¹⁸⁰ 0.0949	¹⁷⁶ 0.1853
222	VISIONLABS-005	¹⁹⁷ 0.0369	¹⁸⁹ 0.0502	¹⁷⁹ 0.0626	¹⁷² 0.0847	¹⁷⁴ 0.1815
223	VISIONLABS-006	¹⁴ 0.0188	¹⁴⁷ 0.0267	¹⁴⁸ 0.0336	¹⁴⁹ 0.0542	¹⁴ 0.1478
224	VISIONLABS-007	¹⁴⁶ 0.0188	¹⁴⁶ 0.0266	¹⁴⁴ 0.0335	¹⁴⁷ 0.0540	¹⁴⁵ 0.1479
225	VISIONLABS-008	⁹² 0.0096	⁹³ 0.0131	⁹ 0.0166	⁸⁹ 0.0291	¹¹² 0.1247
226	VISIONLABS-009	⁴⁷ 0.0034	⁴⁶ 0.0046	⁴⁶ 0.0060	⁴⁶ 0.0140	⁵⁰ 0.0881
227	VISIONLABS-010	⁵³ 0.0038	⁵³ 0.0051	⁵¹ 0.0070	⁴⁷ 0.0149	⁵⁷ 0.0920
228	VISIONLABS-011	³⁰ 0.0025	³² 0.0033	³⁰ 0.0044	³⁶ 0.0120	⁴² 0.0825
229	VIXVIZION-009	¹⁵⁶ 0.0203	¹⁵⁰ 0.0273	¹⁴⁹ 0.0348	¹⁵¹ 0.0545	¹⁵³ 0.1377
230	VNPT-001	⁹⁷ 0.0104	⁹⁷ 0.0143	¹⁰⁸ 0.0190	⁹² 0.0296	⁷³ 0.1028
231	VNPT-002	⁶³ 0.0051	⁶¹ 0.0065	⁶¹ 0.0083	⁵⁶ 0.0172	⁶⁹ 0.1005
232	VOCORD-005	²⁶⁰ 0.1179	²⁶³ 0.1577	²⁴¹ 0.2183	²³⁶ 0.3122	²³³ 0.4490
233	VTS-001	⁹⁶ 0.0102	⁹⁴ 0.0133	⁹⁸ 0.0175	⁹⁸ 0.0322	¹¹¹ 0.1243
234	VTS-002	¹⁴¹ 0.0185	¹⁴² 0.0259	¹⁴⁶ 0.0344	¹⁵² 0.0549	¹⁴ 0.1447
235	VTS-003	⁶⁷ 0.0053	⁶⁶ 0.0073	⁶⁴ 0.0096	⁵⁹ 0.0188	⁷¹ 0.1017
236	XFORWARDAI-000	¹⁰¹ 0.0107	¹⁰³ 0.0151	¹⁰⁸ 0.0195	¹⁰⁰ 0.0324	⁸⁰ 0.1057
237	XFORWARDAI-001	⁴⁹ 0.0037	⁵⁰ 0.0049	⁴⁷ 0.0060	³⁵ 0.0120	³⁸ 0.0800
238	XFORWARDAI-002	³² 0.0026	³⁰ 0.0030	²⁹ 0.0035	²⁵ 0.0078	³⁰ 0.0706
239	YITU-002	¹¹¹ 0.0129	¹¹¹ 0.0177	¹¹⁰ 0.0228	¹⁰⁴ 0.0345	⁹⁵ 0.1133
240	YITU-003	¹¹ 0.0138	¹¹⁹ 0.0185	¹¹ 0.0236	¹⁰⁵ 0.0353	⁹⁶ 0.1148
241	YITU-004	⁷⁹ 0.0067	⁷⁶ 0.0096	⁷⁷ 0.0129	⁶⁸ 0.0232	⁷⁷ 0.1046
242	YITU-005	⁸³ 0.0074	⁸³ 0.0101	⁸⁰ 0.0135	⁷⁶ 0.0255	⁸¹ 0.1057

Table 23: Identification-mode: Effect of N on FNIR at high threshold. Values are threshold-based miss rates i.e. FNIR at FPIR = 0.001 for five enrollment population sizes, N. The right six columns apply for enrollment of one image. Missing entries usually apply because another algorithm from the same developer was run instead. Some developers are missing because less accurate algorithms were not run on galleries with $N \geq 3\,000\,000$. Throughout blue superscripts indicate the rank of the algorithm for that column.

MISSES AT GIVEN RANK		ENROL MOST RECENT											
FNIR(N, T= 0, R)		RANK 1					RANK 50						
#	ALGORITHM	N=0.64M	N=1.6M	N=3.0M	N=6.0M	N=12.0M	aN ^b	N=0.64M	N=1.6M	N=3.0M	N=6.0M	N=12.0M	aN ^b
217	VERIDAS-002	¹⁴⁶ 0.0023	¹⁴⁹ 0.0028	¹³⁹ 0.0028	¹³⁸ 0.0032	¹³⁰ 0.0037	¹⁴¹ 0.0003 N ^{0.1158} 116	¹³⁸ 0.0014	¹³⁵ 0.0015	¹²³ 0.0015	¹¹⁸ 0.0015	¹¹² 0.0016	¹⁵⁰ 0.0007 N ^{0.047} 102
218	VERIDAS-003	⁹⁵ 0.0017	⁹⁵ 0.0018	⁹¹ 0.0020	⁹¹ 0.0022	⁹⁹ 0.0026	¹¹⁷ 0.0002 N ^{0.150} 109	¹¹⁸ 0.0013	¹⁰⁷ 0.0013	¹⁰¹ 0.0013	⁹⁵ 0.0014	⁸⁹ 0.0014	¹³³ 0.0007 N ^{0.043} 105
219	VERIDAS-004	⁵⁷ 0.0013	⁵⁰ 0.0014	⁴⁵ 0.0014	³⁵ 0.0014	³¹ 0.0015	²⁰⁸ 0.0007 N ^{0.043} 11	⁹³ 0.0012	⁸⁷ 0.0012	⁷⁹ 0.0012	⁶⁹ 0.0012	⁶² 0.0012	¹⁹⁶ 0.0011 N ^{0.008} 22
220	VIGILANTSOLUTIONS-008	¹⁵³ 0.0025	¹⁵⁶ 0.0029	¹⁵⁶ 0.0034	¹⁵⁶ 0.0040	¹⁴⁸ 0.0047	⁵⁷ 0.0001 N ^{0.224} 168	⁸⁰ 0.0012	⁹⁹ 0.0013	¹¹⁷ 0.0014	¹²⁰ 0.0015	¹¹⁹ 0.0017	⁵⁶ 0.0002 N ^{0.130} 180
221	VISIONBOX-000	¹⁰³ 0.0017	¹⁰⁵ 0.0019	¹¹¹ 0.0022	³⁰⁶ 1.0000	²⁴³ 0.9526	¹ 0.0000 N ^{-2.57} 0 243	¹⁰³ 0.0012	⁹⁸ 0.0013	¹⁰⁴ 0.0013	²⁴⁹ 1.0000	²⁴³ 0.9525	¹ 0.0000 N ^{-2.719} 243
222	VISIONLABS-004	¹⁴² 0.0022	¹⁴⁸ 0.0027	¹⁵³ 0.0032	¹⁵⁶ 0.0044	¹⁶⁹ 0.0070	⁸ 0.0000 N ^{-0.387} 235	¹⁰⁵ 0.0012	¹²⁵ 0.0014	¹⁴⁵ 0.0017	¹⁷⁷ 0.0025	¹⁹² 0.0045	⁷ 0.0000 N ^{0.435} 234
223	VISIONLABS-005	¹²⁶ 0.0020	¹³⁶ 0.0024	¹⁴⁴ 0.0029	¹⁴⁵ 0.0037	¹⁵⁵ 0.0051	¹² 0.0000 N ^{-0.322} 232	⁹⁷ 0.0012	¹⁰⁴ 0.0013	¹³⁸ 0.0016	¹⁵³ 0.0019	¹⁷³ 0.0029	¹⁵ 0.0000 N ^{0.298} 222
224	VISIONLABS-006	⁹² 0.0016	⁹⁷ 0.0018	¹¹⁷ 0.0022	¹²¹ 0.0028	¹⁴⁴ 0.0041	¹¹ 0.0000 N ^{0.314} 230	⁹⁶ 0.0012	¹⁰⁰ 0.0013	¹²⁵ 0.0015	¹⁴⁷ 0.0019	¹⁶⁸ 0.0027	¹⁵ 0.0000 N ^{0.275} 215
225	VISIONLABS-007	⁹⁰ 0.0016	⁹¹ 0.0018	⁹⁴ 0.0020	¹⁰⁸ 0.0023	¹²² 0.0034	²¹ 0.0001 N ^{0.248} 190	⁸⁸ 0.0012	⁸⁴ 0.0012	⁸³ 0.0013	⁸³ 0.0013	¹⁴¹ 0.0020	⁴⁵ 0.0001 N ^{0.152} 186
226	VISIONLABS-008	¹¹⁷ 0.0019	¹¹⁴ 0.0020	¹⁰⁶ 0.0021	¹⁰⁹ 0.0025	¹⁰⁹ 0.0030	⁹⁸ 0.0002 N ^{0.169} 128	¹⁶⁷ 0.0016	¹⁶³ 0.0017	¹⁵¹ 0.0017	¹⁵⁷ 0.0020	¹⁵⁸ 0.0023	⁷⁵ 0.0003 N ^{0.114} 169
227	VISIONLABS-009	³² 0.0011	²⁸ 0.0011	²⁶ 0.0012	³⁰ 0.0014	⁴⁸ 0.0017	⁵¹ 0.0001 N ^{0.160} 121	⁴⁷ 0.0010	⁴⁰ 0.0010	⁴³ 0.0010	³² 0.0011	⁸⁶ 0.0014	⁶¹ 0.0002 N ^{0.109} 165
228	VISIONLABS-010	⁶³ 0.0014	⁵⁷ 0.0014	⁵⁷ 0.0015	⁵⁷ 0.0017	⁶⁴ 0.0021	¹⁰⁶ 0.0002 N ^{0.137} 98	¹⁰⁹ 0.0013	⁹² 0.0013	¹⁰⁵ 0.0013	¹⁰⁶ 0.0014	¹¹⁶ 0.0017	⁷⁹ 0.0004 N ^{0.090} 155
229	VISIONLABS-011	³³ 0.0011	³⁵ 0.0012	³⁴ 0.0013	³⁶ 0.0014	³⁵ 0.0018	⁵⁰ 0.0001 N ^{0.162} 124	⁵⁶ 0.0010	⁵⁶ 0.0011	⁵⁸ 0.0011	⁶⁴ 0.0012	⁹⁸ 0.0015	⁵⁸ 0.0002 N ^{0.114} 170
230	VIXVIZION-009	¹²³ 0.0019	¹²⁹ 0.0023	¹³⁴ 0.0026	¹³⁶ 0.0032	¹²⁶ 0.0037	³⁹ 0.0001 N ^{-0.226} 170	⁶² 0.0011	⁸¹ 0.0012	⁹⁰ 0.0013	⁹⁴ 0.0013	⁹¹ 0.0015	⁶⁷ 0.0003 N ^{0.106} 163
231	VNPPT-001	¹³² 0.0020	¹²¹ 0.0022	¹¹⁵ 0.0023	¹⁰⁹ 0.0025	⁹⁷ 0.0028	¹⁹³ 0.0005 N ^{0.101} 60	¹⁷⁹ 0.0018	¹⁷⁰ 0.0018	¹⁶⁵ 0.0018	¹⁴⁴ 0.0018	¹²⁹ 0.0019	²⁶⁹ 0.0014 N ^{0.18} 53
232	VNPPT-002	¹¹³ 0.0018	¹⁰³ 0.0019	⁹⁰ 0.0020	⁸⁵ 0.0021	⁷⁷ 0.0023	²⁰³ 0.0007 N ^{0.072} 31	¹⁷⁰ 0.0017	¹⁶⁶ 0.0017	¹⁵³ 0.0018	¹³⁵ 0.0018	¹²⁵ 0.0018	²¹³ 0.0015 N ^{0.09} 28
233	VOCORD-005	²¹³ 0.0060	²¹³ 0.0070	²⁰³ 0.0082	²⁰¹ 0.0097	¹⁹⁵ 0.0117	¹³⁴ 0.0003 N ^{0.232} 179	²³ 0.0033	²³¹ 0.0035	²¹² 0.0037	¹⁹⁹ 0.0040	¹⁹⁰ 0.0043	¹⁸⁷ 0.0010 N ^{0.090} 154
234	VTS-001	⁶² 0.0014	⁷⁰ 0.0015	⁷¹ 0.0017	⁷⁶ 0.0019	⁸⁰ 0.0023	⁵² 0.0001 N ^{-0.179} 158	⁴⁴ 0.0010	⁴² 0.0010	⁴⁵ 0.0010	⁴² 0.0011	⁴⁶ 0.0011	⁹³ 0.0005 N ^{0.051} 119
235	VTS-002	⁹⁶ 0.0017	¹⁰⁷ 0.0019	¹¹³ 0.0022	¹¹⁵ 0.0026	¹¹⁷ 0.0032	³⁶ 0.0001 N ^{-0.215} 162	⁶⁶ 0.0011	⁶⁷ 0.0011	⁷² 0.0012	⁷² 0.0013	⁷⁹ 0.0013	⁸¹ 0.0004 N ^{0.079} 147
236	VTS-003	²⁸ 0.0011	³⁰ 0.0011	²⁶ 0.0012	²⁹ 0.0013	³³ 0.0015	¹⁰³ 0.0002 N ^{0.124} 89	²⁰ 0.0009	²¹ 0.0009	¹⁹ 0.0009	²⁰ 0.0009	¹¹³ 0.0006 N ^{0.026} 75	
237	XFORWARDAI-000	¹³⁷ 0.0021	¹³⁰ 0.0023	¹³⁰ 0.0024	¹¹⁸ 0.0027	¹⁶⁸ 0.0029	¹⁸⁵ 0.0005 N ^{0.111} 72	¹⁸⁰ 0.0019	¹⁷⁹ 0.0019	¹⁷¹ 0.0019	¹⁵⁹ 0.0020	¹⁴³ 0.0020	²¹¹ 0.0015 N ^{0.18} 56
238	XFORWARDAI-001	¹³⁰ 0.0020	¹¹⁸ 0.0020	¹⁰³ 0.0021	⁸⁹ 0.0022	⁸¹ 0.0024	²¹² 0.0009 N ^{0.055} 18	¹⁸¹ 0.0019	¹⁷⁸ 0.0019	¹⁶⁹ 0.0019	¹⁵¹ 0.0019	¹³⁵ 0.0019	²²⁰ 0.0018 N ^{0.04} 14
239	XFORWARDAI-002	¹²⁴ 0.0019	¹⁰⁹ 0.0020	⁹⁷ 0.0020	⁸⁴ 0.0021	⁷¹ 0.0022	²¹⁶ 0.0001 N ^{0.038} 10	¹⁸³ 0.0019	¹⁷⁷ 0.0019	¹⁶⁸ 0.0019	¹⁵⁹ 0.0019	¹³¹ 0.0019	²¹⁹ 0.0018 N ^{0.03} 12
240	YITU-002	⁸⁷ 0.0016	⁹⁸ 0.0018	¹⁰⁴ 0.0021	¹⁰⁹ 0.0024	¹⁰⁶ 0.0029	³⁶ 0.0001 N ^{0.213} 161	³⁹ 0.0009	⁴⁸ 0.0010	⁴⁴ 0.0010	⁴³ 0.0011	⁴⁹ 0.0012	⁷⁸ 0.0004 N ^{0.073} 143
241	YITU-003	¹⁵⁸ 0.0026	¹⁵⁵ 0.0029	¹⁴⁹ 0.0031	¹⁴⁰ 0.0035	¹³⁸ 0.0039	¹⁷⁰ 0.0004 N ^{0.141} 101	¹⁹⁴ 0.0020	¹⁸⁸ 0.0021	¹⁸⁰ 0.0022	¹⁷¹ 0.0023	¹⁶¹ 0.0024	¹⁸⁸ 0.0010 N ^{0.054} 120
242	YITU-004	³⁵ 0.0011	⁴³ 0.0013	³⁶ 0.0015	⁵⁹ 0.0017	¹⁴⁹ 0.0047	⁶ 0.0000 N ^{0.438} 236	¹⁷ 0.0008	¹⁶ 0.0009	¹⁶ 0.0009	¹⁵ 0.0009	¹⁷⁸ 0.0036	⁸ 0.0000 N ^{0.395} 233
243	YITU-005	¹⁴⁴ 0.0022	¹³² 0.0023	¹²⁵ 0.0025	¹¹⁵ 0.0027	¹¹⁰ 0.0031	¹⁸⁸ 0.0005 N ^{0.113} 74	¹⁸⁷ 0.0020	¹⁸² 0.0020	¹⁶⁰ 0.0020	¹⁴⁵ 0.0020	²¹⁴ 0.0017 N ^{0.012} 34	

Table 27: Investigation-mode: Effect of N on FNIR on recent images For five enrollment population sizes, N , with $T = 0$ and $FPIR = 1$. The left five columns are rank 1 miss rates The right five columns are rank 50 miss rates Missing entries usually apply because another algorithm from the same developer was run instead. Some developers are missing because less accurate algorithms were not run on galleries with $N > 1\,600\,000$. Throughout blue superscripts indicate the rank of the algorithm for that column, and yellow highlighting indicates the most accurate value. Caution: The Power-low models are mostly intended to draw attention to the kind of behavior, not as a model to be used for prediction.

MISSES OUTSIDE RANK R		RESOURCE USAGE		ENROL MOST RECENT, N = 1.6M					
#	ALGORITHM	BYTES	MSEC	R=1	R=5	R=10	R=20	R=50	WORK=10
1	20FACE-000	18 ¹ 2048	41 ² 247	29 ³ 0.0552	29 ¹ 0.0269	29 ⁹ 0.0198	28 ⁷ 0.0146	28 ¹⁰ 0.0099	29 ² 1.275
2	3DIVI-003	49 ⁵ 512	153 ⁶ 625	30 ⁶ 0.0833	30 ¹ 0.0444	30 ¹ 0.0349	29 ⁷ 0.0270	29 ⁷ 0.0191	30 ² 1.447
3	3DIVI-004	311 ⁴ 4096	154 ⁵ 628	26 ⁶ 0.0175	25 ⁵ 0.0091	25 ⁷ 0.0075	24 ⁹ 0.0061	24 ⁴ 0.0049	26 ⁴ 1.092
4	3DIVI-005	303 ³ 4096	166 ⁴ 653	26 ⁵ 0.0176	25 ⁶ 0.0091	25 ¹ 0.0074	24 ⁸ 0.0061	24 ⁵ 0.0049	26 ¹ 1.092
5	3DIVI-006	64 ² 528	167 ³ 653	27 ⁴ 0.0240	28 ² 0.0171	28 ⁶ 0.0160	28 ⁹ 0.0154	29 ³ 0.0148	28 ¹ 1.162
6	ACER-000	42 ¹ 512	31 ⁰ 201	24 ¹ 0.0106	22 ² 0.0051	21 ⁸ 0.0041	21 ⁵ 0.0034	20 ⁷ 0.0026	22 ³ 1.053
7	ACER-001	142 ⁰ 2048	22 ¹ 184	19 ² 0.0051	19 ⁴ 0.0032	19 ² 0.0028	19 ² 0.0025	19 ¹ 0.0022	19 ³ 1.031
8	AIZE-001	19 ⁵ 2048	86 ⁴ 403	19 ⁰ 0.0056	19 ⁹ 0.0037	20 ¹ 0.0033	21 ⁴ 0.0030	21 ¹ 0.0027	20 ⁸ 1.035
9	ALCHERA-000	14 ¹ 2048	46 ² 263	26 ⁰ 0.0161	26 ⁹ 0.0124	27 ⁵ 0.0117	28 ⁰ 0.0111	28 ³ 0.0105	26 ⁸ 1.116
10	ALCHERA-001	21 ⁰ 2048	8 ⁶ 66	33 ⁵ 0.9869	33 ⁵ 0.9782	33 ⁵ 0.9735	33 ⁵ 0.9679	33 ⁴ 0.9590	33 ⁸ 9.811
11	ALCHERA-002	23 ⁵ 2048	14 ¹¹ 115	30 ⁸ 0.0949	30 ⁶ 0.0555	30 ⁴ 0.0443	30 ⁴ 0.0354	29 ⁹ 0.0254	30 ⁶ 1.544
12	ALCHERA-003	17 ¹ 2048	135 ⁴ 548	23 ⁰ 0.0104	22 ⁵ 0.0054	22 ⁹ 0.0045	22 ⁰ 0.0038	22 ³ 0.0032	22 ⁷ 1.055
13	ALCHERA-004	18 ⁸ 2048	26 ⁶ 854	24 ⁴ 0.0110	21 ¹ 0.0049	21 ⁴ 0.0038	20 ⁷ 0.0032	20 ⁴ 0.0025	22 ¹ 1.051
14	ALLGOVISION-000	22 ⁸ 2048	97 ⁴ 425	24 ¹ 0.0114	25 ⁰ 0.0084	25 ⁹ 0.0078	25 ⁷ 0.0073	26 ¹ 0.0067	25 ⁹ 1.079
15	ALLGOVISION-001	15 ² 2048	23 ⁶ 792	22 ⁷ 0.0090	21 ⁹ 0.0048	21 ⁷ 0.0040	21 ⁴ 0.0033	21 ² 0.0027	21 ⁹ 1.048
16	ANKE-000	28 ¹ 2072	99 ⁴ 431	25 ⁰ 0.0132	24 ¹ 0.0073	23 ⁹ 0.0060	23 ⁸ 0.0050	23 ⁷ 0.0040	24 ⁶ 1.072
17	ANKE-001	28 ² 2072	101 ⁴ 433	25 ⁶ 0.0132	24 ² 0.0073	24 ¹ 0.0061	23 ⁹ 0.0050	23 ⁸ 0.0040	24 ⁷ 1.073
18	ANKE-002	26 ¹ 2056	159 ⁶ 641	15 ⁰ 0.0028	15 ¹ 0.0020	14 ⁷ 0.0018	15 ⁷ 0.0018	15 ⁸ 0.0017	15 ¹ 1.019
19	AWARE-003	28 ³ 2076	20 ⁷ 716	28 ³ 0.0306	28 ⁰ 0.0162	27 ⁷ 0.0127	27 ³ 0.0100	26 ⁹ 0.0075	28 ¹ 1.163
20	AWARE-004	29 ² 2076	20 ³ 712	30 ¹ 0.0679	28 ⁹ 0.0348	29 ³ 0.0274	29 ⁵ 0.0208	29 ² 0.0145	29 ⁸ 1.354
21	AWARE-005	29 ¹ 3100	250 ² 827	28 ¹ 0.0311	28 ¹ 0.0167	27 ⁶ 0.0134	27 ⁶ 0.0107	27 ⁵ 0.0082	28 ¹ 1.167
22	AWARE-006	3 ¹ 124	24 ³ 818	30 ³ 0.0697	30 ⁰ 0.0369	29 ⁶ 0.0288	29 ⁶ 0.0223	29 ⁴ 0.0158	30 ¹ 1.371
23	AYONIX-000	10 ⁶ 1036	1 ¹⁰ 10	32 ⁴ 0.4505	32 ⁹ 0.3540	32 ⁹ 0.3176	32 ⁹ 0.2834	32 ⁸ 0.2381	32 ⁹ 4.288
24	AYONIX-001	10 ¹ 1036	3 ¹² 12	32 ³ 0.3414	32 ² 0.2338	32 ³ 0.1977	32 ³ 0.1652	32 ² 0.1274	32 ³ 3.226
25	AYONIX-002	10 ⁴ 1036	2 ¹¹ 11	32 ⁴ 0.3414	32 ⁵ 0.2338	32 ⁴ 0.1977	32 ² 0.1652	32 ² 0.1274	32 ³ 3.226
26	CAMVI-003	86 ¹⁰²⁴	19 ⁹ 707	29 ⁶ 0.0520	30 ⁵ 0.0517	30 ⁶ 0.0517	30 ⁹ 0.0517	30 ⁹ 0.0517	30 ⁴ 1.466
27	CAMVI-004	89 ¹⁰²⁴	20 ⁹ 718	29 ⁴ 0.0468	30 ³ 0.0465	30 ⁶ 0.0465	30 ⁸ 0.0464	30 ⁸ 0.0464	30 ¹ 1.419
28	CAMVI-005	88 ¹⁰²⁴	22 ⁶ 769	30 ¹ 0.0652	30 ⁷ 0.0648	31 ¹ 0.0648	31 ² 0.0648	31 ⁴ 0.0647	30 ⁷ 1.584
29	CANON-001	30 ¹ 4096	28 ⁷ 893	28 ¹ 0.0011	32 ⁰ 0.0010	27 ¹ 0.0010	28 ⁶ 0.0009	27 ⁰ 0.0009	28 ¹ 1.009
30	CANON-002	32 ² 6200	30 ³ 932	31 ⁰ 0.0012	27 ² 0.0010	29 ⁵ 0.0009	23 ⁵ 0.0009	25 ⁰ 0.0009	25 ¹ 1.009
31	CIB-000	33 ⁵ 8196	17 ⁵ 674	21 ⁰ 0.0015	74 ⁴ 0.0013	72 ⁰ 0.0012	74 ⁰ 0.0012	73 ⁰ 0.0012	76 ¹ 1.012
32	CLEARVIEWAI-000	30 ⁹ 4096	22 ³ 765	23 ⁰ 0.0011	31 ⁰ 0.0010	32 ⁰ 0.0010	26 ⁰ 0.0009	26 ⁰ 0.0009	26 ¹ 1.009
33	CLOUDWALK-HR-000	138 ²⁰⁴⁸	29 ⁶ 908	6 ⁰ 0.0015	96 ⁴ 0.0014	10 ⁸ 0.0014	11 ⁷ 0.0014	12 ⁶ 0.0014	9 ¹ 1.013
34	CLOUDWALK-MT-000	14 ⁶ 2048	27 ⁴ 870	9 ⁰ 0.0018	129 ¹ 0.0018	14 ¹ 0.0018	153 ¹ 0.0018	167 ¹ 0.0018	12 ⁶ 1.016
35	CLOUDWALK-MT-001	19 ⁸ 2048	31 ⁵ 955	8 ⁰ 0.0018	132 ¹ 0.0018	139 ¹ 0.0018	149 ¹ 0.0018	169 ¹ 0.0018	12 ⁴ 1.016
36	CLOUDWALK-MT-002	23 ⁸ 2048	32 ⁷ 979	8 ⁰ 0.0018	130 ¹ 0.0018	140 ¹ 0.0018	154 ¹ 0.0018	168 ¹ 0.0018	12 ⁵ 1.016
37	COGENT-000	60 ⁵²⁵	136 ⁵⁵¹	23 ⁹ 0.0105	26 ¹ 0.0096	26 ⁷ 0.0095	20 ⁹ 0.0032	20 ¹ 0.0024	25 ⁸ 1.088
38	COGENT-001	61 ⁵²⁵	137 ⁵⁵²	24 ¹ 0.0105	26 ² 0.0096	26 ⁸ 0.0095	20 ⁸ 0.0032	20 ¹ 0.0024	25 ⁷ 1.088
39	COGENT-002	10 ⁶ 1043	330 ⁹⁸⁷	16 ⁸ 0.036	16 ³ 0.0222	16 ⁰ 0.0200	15 ⁵ 0.0018	14 ⁷ 0.0015	16 ¹ 1.021
40	COGENT-003	10 ⁸ 1043	319 ⁹⁶⁰	17 ¹ 0.0038	17 ⁴ 0.0024	16 ⁷ 0.0021	17 ¹ 0.0019	15 ⁹ 0.0017	17 ² 1.023
41	COGENT-004	26 ² 2053	312 ⁹⁵²	112 ⁰ 0.0020	113 ¹ 0.0016	113 ⁰ 0.0015	121 ¹ 0.0015	124 ⁰ 0.0014	10 ⁹ 1.015
42	COGENT-005	10 ⁷ 1062	22 ⁹ 774	8 ¹ 0.0017	94 ¹ 0.0014	97 ¹ 0.0014	108 ¹ 0.0014	115 ⁰ 0.0013	9 ⁴ 1.013
43	COGENT-006	72 ⁵⁵⁰	24 ² 850	41 ⁰ 0.0012	49 ¹ 0.0011	47 ¹ 0.0011	52 ¹ 0.0011	61 ¹ 0.0011	46 ¹ 1.010
44	COGENT-007	73 ⁵⁵⁰	331 ⁹⁹¹	24 ¹ 0.0011	33 ¹ 0.0010	34 ¹ 0.0010	35 ¹ 0.0010	37 ¹ 0.0010	31 ¹ 1.009
45	COGNITEC-000	26 ¹ 2052	19 ¹⁷ 16	27 ⁵ 0.0125	27 ⁵ 0.0136	27 ¹ 0.0107	27 ⁰ 0.0085	25 ⁹ 0.0065	27 ⁶ 1.136
46	COGNITEC-001	246 ²⁰⁵²	32 ²⁰²	248 ⁰ 0.0117	233 ⁰ 0.0062	233 ⁰ 0.0051	233 ⁰ 0.0042	229 ⁰ 0.0034	234 ¹ 1.062
47	COGNITEC-002	26 ² 2052	37 ²²⁷	20 ⁰ 0.0057	19 ⁸ 0.0037	19 ⁸ 0.0032	20 ⁰ 0.0029	20 ⁹ 0.0026	19 ¹ 1.035
48	COGNITEC-003	25 ² 2052	56 ²⁹⁷	20 ⁴ 0.0062	20 ⁷ 0.0040	20 ⁷ 0.0036	21 ³ 0.0033	22 ¹ 0.0030	20 ⁶ 1.039
49	COGNITEC-004	24 ¹ 2052	28 ¹⁹²	16 ¹ 0.0032	154 ¹ 0.0020	147 ¹ 0.0018	152 ¹ 0.0015	128 ¹ 0.0014	15 ⁸ 1.020
50	COGNITEC-005	24 ² 2052	367 ¹⁶	27 ⁰ 0.0016	69 ¹ 0.0013	67 ¹ 0.0012	68 ¹ 0.0011	68 ¹ 0.0011	70 ¹ 1.012
51	COGNITEC-006	25 ¹ 2052	411 ⁴⁶³	27 ¹ 0.0016	68 ¹ 0.0013	62 ¹ 0.0012	63 ¹ 0.0012	66 ¹ 0.0011	66 ¹ 1.012
52	CUBOX-000	18 ² 2048	259 ⁹¹⁸	58 ¹ 0.0014	85 ¹ 0.0014	99 ¹ 0.0014	109 ¹ 0.0014	119 ¹ 0.0014	82 ¹ 1.012
53	CYBERLINK-000	25 ⁹ 2052	192 ⁶⁹⁹	123 ⁰ 0.0040	184 ⁰ 0.0028	188 ⁰ 0.0026	191 ⁰ 0.0024	192 ⁰ 0.0022	183 ¹ 1.027
54	CYBERLINK-001	25 ¹ 2052	102 ⁴³³	166 ⁰ 0.0035	169 ¹ 0.0023	168 ¹ 0.0021	161 ¹ 0.0018	165 ¹ 0.0017	167 ¹ 1.022
55	CYBERLINK-002	32 ⁶ 4140	217 ⁷³⁸	145 ⁰ 0.0026	165 ⁰ 0.0023	176 ⁰ 0.0022	182 ⁰ 0.0021	186 ⁰ 0.0021	162 ¹ 1.021
56	CYBERLINK-003	33 ¹ 6212	190 ⁶⁹⁶	75 ¹ 0.0016	75 ¹ 0.0013	74 ¹ 0.0013	73 ¹ 0.0012	72 ¹ 0.0012	79 ¹ 1.012
57	CYBERLINK-004	33 ¹ 6212	216 ⁷³⁸	81 ⁰ 0.0017	102 ¹ 0.0015	112 ¹ 0.0015	118 ¹ 0.0014	129 ¹ 0.0014	98 ¹ 1.014
58	CYBERLINK-005	33 ² 6212	218 ⁷³⁹	91 ⁰ 0.0018	112 ¹ 0.0016	115 ¹ 0.0015	128 ¹ 0.0015	131 ¹ 0.0014	108 ¹ 1.015
59	DAHUA-000	17 ¹ 2048	79 ³⁷⁸	231 ⁰ 0.0093	236 ⁰ 0.0066	240 ¹ 0.0061	246 ⁰ 0.0057	249 ⁰ 0.0054	235 ¹ 1.062
60	DAHUA-001	23 ¹ 2048	371 ²⁷¹	20 ⁶ 0.0067	208 ⁰ 0.0040	206 ¹ 0.0036	211 ⁰ 0.0033	215 ⁰ 0.0029	208 ¹ 1.040
61	DAHUA-002	21 ² 2048	191 ⁶⁹⁹	99 ¹ 0.0018	100 ¹ 0.0015	109 ¹ 0.0014	113 ¹ 0.0014	11	

MISSES OUTSIDE RANK R		RESOURCE USAGE		ENROL MOST RECENT, N = 1.6M						
#	ALGORITHM	BYTES	MSEC	R=1	R=5	R=10	R=20	R=50	WORK-10	
73	DERMALOG-008	512	370	154	0.0029	150	0.0020	146	0.0018	
74	DERMALOG-009	512	347	153	0.0028	172	0.0024	181	0.0023	
75	DERMALOG-010	512	634	123	0.0022	158	0.0021	167	0.0021	
76	DERMALOG-011	128	343	77	0.0016	61	0.0012	59	0.0011	
77	DIGIDATA-000	2048	138	561	331	0.5897	332	0.5891	332	0.5891
78	DILUSENSE-000	177	2048	42	249	125	0.0022	108	0.0014	
79	DILUSENSE-001	4096	281	885	63	0.0015	66	0.0013	63	0.0012
80	EYEDEA-003	103	1036	80	385	305	0.0800	302	0.0451	
81	F8-001	205	2048	260	851	252	0.0120	264	0.0105	
82	FINCORE-000	213	2048	116	477	243	0.0108	224	0.0052	
83	FIRSTCREDITKZ-001	32	288	239	799	39	0.0012	55	0.0012	
84	FUJITSULAB-000	94	1032	311	950	126	0.0022	120	0.0016	
85	FUJITSULAB-001	96	1032	283	890	101	0.0019	106	0.0015	
86	GLORY-000	39	418	15	160	316	0.1781	318	0.1391	
87	GLORY-001	131	1726	88	405	313	0.1268	313	0.0967	
88	GORILLA-001	285	2156	18	169	288	0.0603	293	0.0304	
89	GORILLA-002	112	1132	67	341	271	0.0197	257	0.0092	
90	GORILLA-003	286	2156	140	563	285	0.0361	278	0.0146	
91	GORILLA-004	287	2192	84	395	205	0.0063	193	0.0032	
92	GORILLA-005	333	6288	119	483	160	0.0032	139	0.0019	
93	GORILLA-006	336	8336	225	768	87	0.0017	65	0.0013	
94	GORILLA-007	334	6290	122	527	83	0.0017	60	0.0012	
95	GORILLA-008	327	4242	308	940	67	0.0015	52	0.0012	
96	GRIAULE-000	247	2052	96	419	143	0.0025	147	0.0020	
97	GRIAULE-001	256	2052	335	1103	36	0.0012	40	0.0011	
98	HIK-003	118	1408	155	633	249	0.0117	231	0.0060	
99	HIK-004	113	1152	124	510	246	0.0113	229	0.0059	
100	HIK-005	119	1408	152	619	188	0.0046	177	0.0025	
101	HIK-006	120	1408	148	610	186	0.0046	176	0.0025	
102	HYPERVERGE-001	87	1024	262	846	35	0.0014	72	0.0013	
103	HYPERVERGE-002	81	1024	305	935	51	0.0014	71	0.0013	
104	HZAILU-000	84	1024	162	650	124	0.0022	117	0.0016	
105	HZAILU-001	227	2048	230	778	108	0.0020	126	0.0017	
106	HZAILU-002	157	2048	261	847	111	0.0020	125	0.0017	
107	IDEMIA-003	62	528	183	689	211	0.0069	215	0.0045	
108	IDEMIA-004	63	528	173	669	207	0.0066	204	0.0038	
109	IDEMIA-005	38	352	77	374	221	0.0081	213	0.0044	
110	IDEMIA-006	37	352	76	373	235	0.0096	223	0.0052	
111	IDEMIA-007	7	860	240	807	144	0.0026	115	0.0016	
112	IDEMIA-008	35	300	105	451	20	0.0011	18	0.0009	
113	IDEMIA-009	7	636	276	874	9	0.0010	17	0.0009	
114	IDEMIA-010	36	300	316	957	7	0.0009	7	0.0009	
115	IMAGUS-002	48	512	76	76	319	0.2203	317	0.1342	
116	IMAGUS-003	40	512	57	325	0.3559	324	0.2491	324	0.1791
117	IMAGUS-005	181	2048	239	788	105	0.0019	116	0.0016	
118	IMAGUS-006	237	2048	293	905	115	0.0020	121	0.0016	
119	IMAGUS-007	186	2048	142	590	116	0.0020	103	0.0015	
120	IMAGUS-008	160	2048	100	432	307	0.0860	308	0.0701	
121	IMPERIAL-000	166	2048	168	654	140	0.0024	141	0.0019	
122	INCODE-000	83	1024	295	489	290	0.0261	29	0.0204	
123	INCODE-001	149	2048	188	690	262	0.0166	251	0.0084	
124	INCODE-002	212	2048	53	291	266	0.0178	254	0.0090	
125	INCODE-003	236	2048	199	704	254	0.0129	238	0.0064	
126	INCODE-004	173	2048	125	508	167	0.0035	170	0.0024	
127	INCODE-005	161	2048	122	500	80	0.0017	86	0.0014	
128	INNOVATRICS-002	65	530	43	255	293	0.0451	240	0.0342	
129	INNOVATRICS-003	63	530	44	255	279	0.0263	270	0.0126	
130	INNOVATRICS-004	108	1076	90	406	253	0.0123	234	0.0063	
131	INNOVATRICS-005	67	538	259	842	141	0.0024	135	0.0018	
132	INNOVATRICS-007	68	538	234	785	84	0.0017	91	0.0014	
133	INNOVATRICS-008	323	4136	982	45	0.0013	47	0.0011		
134	INTELIGENSIA-000	208	2048	143	576	113	0.0020	98	0.0015	
135	INTELLIVISION-001	267	2056	95	417	286	0.0365	281	0.0199	
136	INTELLIVISION-002	271	2056	63	333	234	0.0107	227	0.0055	
137	INTEMA-000	41	512	219	739	27	0.0011	38	0.0011	
138	INTEMA-001	54	512	306	940	1	0.0008	1	0.0008	
139	INTSYSMSU-000	210	2048	176	675	314	0.1457	316	0.1320	
140	IREX-000	294	3080	337	2379	182	0.0044	298	0.0043	
141	ISYSTEMS-002	204	2048	61	316	218	0.0064	210	0.0043	
142	ISYSTEMS-003	185	2048	267	856	194	0.0052	205	0.0039	
143	KAKAO-000	239	2052	257	840	65	0.0015	45	0.0011	
144	KAKAO-001	174	2048	324	976	54	0.0014	78	0.0013	
								85	0.0013	
								100	0.0013	
								105	0.0012	

Table 29: **Rank-based accuracy for the FRVT 2018 mugshot sets.** In columns 3 and 4 are template size and template generation duration. Thereafter values are rank-based FNIR with $T = 0$ and FPIR = 1. This is appropriate to investigational uses but not those with higher volumes where candidates from all searches would need review. The next column is a workload statistic, a small value shows an algorithm front-loads mates into the first 10 candidates. Throughout, blue superscripts indicate the rank of the algorithm for that column, and the best value is highlighted in yellow.

MISSES OUTSIDE RANK R FNIR(N, T=0, R)			RESOURCE USAGE TEMPLATE		ENROL MOST RECENT, N = 1.6M FRVT 2018 MUGSHOTS					
#	ALGORITHM		BYTES	MSEC	R=1	R=5	R=10	R=20	R=50	WORK-10
145	KEDACOM-001		³⁴ 292	¹³ 537	217.0077	²⁴ 0.0074	²⁴ 0.0073	²⁵ 0.0072	²⁶ 0.0072	²⁴ 1.067
146	KNERON-000		²²⁴ 2048	¹²⁸ 530	201.0059	²³⁰ 0.0059	²³⁰ 0.0059	²⁴ 0.0059	²⁵⁴ 0.0059	²²⁴ 1.053
147	KNERON-001		²⁰ 2048	¹¹⁷ 468	282.00295	²⁹ 0.0295	²⁹ 0.0295	²⁹ 0.0295	³⁰ 0.0295	²⁹¹ 1.266
148	LINE-000		²²⁸ 2048	¹¹⁸ 482	127.0022	¹⁰⁹ 0.0015	⁹⁹ 0.0014	⁸⁰ 0.0013	⁷⁴ 0.0012	¹⁰⁸ 1.015
149	LINE-001		¹⁵ 2048	²⁹ 910	26.00011	³⁶ 0.0010	³⁵ 0.0010	³⁶ 0.0009	³¹ 0.0009	²⁹ 1.009
150	LINECLOVA-002		¹⁶⁸ 2048	²⁴⁸ 825	47.00013	⁵⁷ 0.0012	⁶¹ 0.0012	⁷¹ 0.0012	⁷⁸ 0.0012	⁵⁶ 1.011
151	LINECLOVA-003		¹⁹ 2048	²³⁸ 801	10.00010	⁸ 0.0009	¹⁰ 0.0008	¹² 0.0008	¹⁸ 0.0008	⁸ 1.008
152	LOOKMAN-003		³³ 292	⁶⁸ 342	228.0088	²⁴⁷ 0.0078	²⁵³ 0.0076	²⁶¹ 0.0075	²⁶⁸ 0.0074	²⁴⁴ 1.071
153	LOOKMAN-004		⁷⁰ 548	⁶² 325	228.0091	²⁴⁶ 0.0079	²⁵⁴ 0.0076	²⁶⁰ 0.0075	²⁶ 0.0073	²⁴⁵ 1.072
154	LOOKMAN-005		⁷¹ 548	¹² 514	220.0080	²⁴⁸ 0.0075	²⁵² 0.0074	²⁵⁸ 0.0073	²⁶⁶ 0.0072	²⁴² 1.068
155	MANTRA-000		²⁵⁷ 2052	⁹² 412	86.00017	⁸¹ 0.0013	⁷⁸ 0.0013	⁷⁸ 0.0012	⁸² 0.0012	⁸⁴ 1.013
156	MAXVISION-000		¹⁶⁹ 2048	²¹ 184	139.0024	¹²⁹ 0.0017	¹²⁵ 0.0016	¹²² 0.0015	¹²⁰ 0.0014	¹³² 1.016
157	MAXVISION-001		¹⁵¹ 2048	¹⁰⁸ 458	38.00012	⁴⁸ 0.0011	⁵¹ 0.0011	⁵⁶ 0.0011	⁶⁰ 0.0011	⁴⁵ 1.010
158	MEGVII-001		³¹¹ 4096	¹⁶ 652	250.00118	²⁵⁹ 0.0093	²⁵⁸ 0.0087	²⁶⁸ 0.0084	²⁷ 0.0080	²⁵⁴ 1.086
159	MEGVII-002		³⁰⁰ 4096	¹⁷⁰ 656	251.00118	²⁵⁹ 0.0093	²⁶⁰ 0.0088	²⁶⁷ 0.0084	²⁷³ 0.0080	²⁵⁵ 1.087
160	MICROFOCUS-003		²¹ 256	⁴⁹ 269	333.05942	³³¹ 0.4692	³³¹ 0.4204	³³¹ 0.3724	³³¹ 0.3095	³³¹ 5.361
161	MICROFOCUS-004		¹⁷ 256	⁵⁰ 270	330.05763	³³⁰ 0.4519	³³⁰ 0.4026	³³⁰ 0.3560	³³⁰ 0.2957	³³⁰ 5.199
162	MICROFOCUS-005		¹⁴ 256	⁴⁸ 266	326.04242	³²⁸ 0.3028	³²⁵ 0.2606	³²⁵ 0.2209	³²² 0.1724	³²⁶ 3.861
163	MICROFOCUS-006		¹⁶ 256	⁴⁷ 265	327.04268	³²⁷ 0.3049	³²⁶ 0.2623	³²⁷ 0.2233	³²⁷ 0.1746	³²⁷ 3.880
164	MICROSOFT-003		⁸² 1024	⁸ 404	76.00016	²⁸ 0.0010	¹⁵ 0.0009	³ 0.0008	¹ 0.0006	³³ 1.009
165	MICROSOFT-004		¹⁴⁰ 2048	²²⁸ 773	68.00015	¹⁶ 0.0009	¹ 0.0008	¹ 0.0007	¹ 0.0006	³⁰ 1.009
166	MICROSOFT-005		⁸⁸ 1024	¹⁷ 673	102.0019	²⁹ 0.0010	⁹ 0.0008	⁷ 0.0008	⁷ 0.0006	⁴⁰ 1.010
167	MICROSOFT-006		⁸⁰ 1024	¹⁸⁸ 695	110.0020	⁴⁹ 0.0011	²⁹ 0.0010	⁵ 0.0008	⁴ 0.0007	⁵⁷ 1.011
168	MUKH-002		¹⁶⁴ 2048	³³⁶ 1283	278.0258	²⁷⁶ 0.0139	²⁷⁴ 0.0112	²⁷¹ 0.0090	²⁶⁴ 0.0070	²⁷⁷ 1.140
169	NEC-000		²⁹ 2592	⁸ 82	263.0170	²⁵⁹ 0.0086	²⁴³ 0.0066	²⁴⁰ 0.0052	²³⁶ 0.0038	²⁶ 1.087
170	NEC-001		²⁹ 2592	⁹ 88	272.0209	²⁷⁷ 0.0141	²⁷⁸ 0.0128	²⁸¹ 0.0119	²⁸⁴ 0.0113	²⁷⁵ 1.135
171	NEC-002		¹² 1616	¹⁶ 653	188.0010	¹¹ 0.0009	⁸ 0.0008	⁶ 0.0008	⁷ 0.0008	¹⁰ 1.008
172	NEC-003		¹³ 1712	¹⁸⁴ 690	53.0014	⁶⁴ 0.012	⁶⁸ 0.0012	⁷⁵ 0.0012	⁷⁶ 0.0012	⁵⁹ 1.011
173	NEC-004		¹⁰ 1104	³² 967	60.0014	⁸⁷ 0.0013	⁹³ 0.0013	⁹⁵ 0.0013	¹⁰² 0.0013	⁸⁰ 1.012
174	NEC-005		¹¹⁰ 1104	³²⁰ 964	34.0012	⁴⁴ 0.0011	⁴⁹ 0.0011	⁵⁴ 0.0011	⁵⁷ 0.0011	⁴⁴ 1.010
175	NEC-006		¹¹¹ 1104	³⁰ 940	42.0012	⁵⁶ 0.0012	⁶⁴ 0.0012	⁶⁷ 0.0012	⁶⁹ 0.0011	⁵⁴ 1.011
176	NEC-007		⁷⁴ 560	³³² 992	169.0037	¹⁹⁶ 0.0036	²⁰⁸ 0.0036	²¹⁹ 0.0036	²³² 0.0036	¹⁹⁴ 1.033
177	NEUROTECHNOLOGY-003		¹³⁷ 2048	¹³⁴ 547	273.0225	²⁷¹ 0.0126	²⁶⁸ 0.0100	²⁶⁵ 0.0078	²⁵² 0.0057	²⁷² 1.125
178	NEUROTECHNOLOGY-004		¹³⁹ 2048	¹³⁵ 543	196.0056	¹⁹⁷ 0.0036	²⁰¹ 0.0032	²⁰³ 0.0029	²⁰² 0.0025	¹⁹⁸ 1.035
179	NEUROTECHNOLOGY-005		²⁵ 256	⁹¹ 412	180.0043	¹⁸⁶ 0.0029	¹⁹⁰ 0.0027	¹⁹⁰ 0.0024	¹⁹⁶ 0.0023	¹⁸⁷ 1.028
180	NEUROTECHNOLOGY-006		¹⁵ 256	²² 746	267.00180	²⁴⁷ 0.0079	²³⁶ 0.0059	²³⁶ 0.0046	²²² 0.0033	²⁵¹ 1.083
181	NEUROTECHNOLOGY-007		²³ 256	¹⁷ 169	172.0039	¹⁸¹ 0.0027	¹⁸⁶ 0.0025	¹⁸⁰ 0.0023	¹⁸⁹ 0.0022	¹⁷⁹ 1.026
182	NEUROTECHNOLOGY-008		⁵⁹ 514	²³ 804	122.0022	¹⁰⁸ 0.0015	¹⁰⁸ 0.0014	¹¹⁰ 0.0014	¹¹¹ 0.0013	¹⁰⁷ 1.015
183	NEUROTECHNOLOGY-009		⁵⁷ 513	¹⁸⁰ 886	61.0014	⁵⁸ 0.0012	⁶⁰ 0.0012	⁶⁴ 0.0011	⁵⁸ 0.0011	⁵⁸ 1.011
184	NEUROTECHNOLOGY-010		²⁴ 256	¹⁷ 663	40.0012	³⁶ 0.0011	³⁸ 0.0010	³⁸ 0.0010	⁴ 0.0010	³⁸ 1.010
185	NEUROTECHNOLOGY-012		¹⁸ 256	²⁰² 711	150.0010	²⁹ 0.0010	³⁰ 0.0010	³¹ 0.0009	³⁴ 0.0009	²⁰ 1.009
186	NEUROTECHNOLOGY-013		¹⁹ 256	³²⁸ 980	16.0010	²⁴ 0.0010	³¹ 0.0010	³⁴ 0.0010	³⁶ 0.0010	¹⁹ 1.009
187	NEWLAND-002		²³⁸ 2048	²⁷ 868	304.00786	³⁰¹ 0.0480	³⁰³ 0.0397	³⁰³ 0.0332	³⁰¹ 0.0263	³⁰⁵ 1.468
188	NOBLIS-001		¹⁷⁹ 2048	³⁵ 211	321.02492	³²¹ 0.1772	³²¹ 0.1542	³²¹ 0.1339	³¹⁹ 0.1112	³²¹ 2.679
189	NOBLIS-002		³² 6144	¹³ 535	317.01794	³¹⁷ 0.1108	³¹⁴ 0.0903	³¹³ 0.0722	³¹¹ 0.0535	³¹⁴ 2.077
190	NOTIONTAG-000		²⁸⁴ 2120	¹¹⁰ 461	142.0024	¹⁶⁰ 0.021	¹⁶⁶ 0.0021	¹⁷⁷ 0.0020	¹⁸¹ 0.0019	¹⁵⁵ 1.019
191	NTECHLAB-003		²⁹⁸ 3484	²⁵ 831	202.0062	¹⁸⁹ 0.0029	¹⁸² 0.0023	¹⁷² 0.0019	¹⁵² 0.0016	¹⁹² 1.030
192	NTECHLAB-004		²⁹⁷ 3484	³⁰⁰ 929	189.0048	¹⁶⁷ 0.0023	¹⁵⁴ 0.0019	¹⁴¹ 0.0016	¹¹⁶ 0.0013	¹⁷⁸ 1.024
193	NTECHLAB-005		¹³ 1940	²⁰ 717	187.0047	¹⁶⁷ 0.0022	¹⁷⁸ 0.0017	⁹⁹ 0.0013	⁹³ 0.0011	¹⁷⁰ 1.023
194	NTECHLAB-006		¹³⁵ 1940	²⁵ 841	177.0041	¹⁴⁰ 0.0019	¹¹⁵ 0.0015	⁶⁹ 0.0012	⁵⁰ 0.0009	¹⁵⁷ 1.019
195	NTECHLAB-007		²⁹ 3348	²⁵ 834	146.00207	¹²⁴ 0.0017	¹⁰⁷ 0.0014	¹⁰⁴ 0.0013	⁸⁷ 0.0012	¹²⁸ 1.016
196	NTECHLAB-008		¹¹⁶ 1300	¹³⁹ 562	85.0017	⁵⁶ 0.0012	⁵⁶ 0.0012	⁵⁵ 0.0011	⁴⁹ 0.0010	⁶⁵ 1.012
197	NTECHLAB-009		¹¹⁷ 1300	²⁹¹ 900	44.0013	³⁹ 0.0011	³⁶ 0.0010	³⁶ 0.0010	³⁵ 0.0009	⁴² 1.010
198	NTECHLAB-010		¹¹¹ 1280	²⁷ 875	25.0011	²¹ 0.0010	³⁶ 0.0010	³⁹ 0.0010	⁴⁶ 0.0010	³² 1.009
199	NTECHLAB-011		¹¹⁵ 1280	²⁷ 865	17.0010	¹⁵ 0.0009	¹⁸ 0.0009	²¹ 0.0009	²² 0.0009	¹⁵ 1.008
200	PANGIAM-000		¹⁵ 2048	¹⁵ 637	33.00112	⁴¹ 0.0011	⁴³ 0.0011	⁴³ 0.0010	⁴¹ 0.0010	⁴¹ 1.010
201	PANGIAM-001		¹⁷² 2048	³²² 968	212.0069	²³⁸ 0.0068	²⁴⁶ 0.0068	²⁵² 0.0068	²⁶² 0.0068	²³³ 1.061
202	PARAVISION-000		²³ 2048	¹⁰¹ 438	268.00188	²⁸¹ 0.0171	²⁸⁸ 0.0167	²⁹¹ 0.0165	²⁹⁶ 0.0164	²⁹ 1.156
203	PARAVISION-001		¹⁴⁸ 2048	¹⁴⁶ 590	170.0038	¹⁷³ 0.0024	¹⁷³ 0.0022	¹⁷⁸ 0.0020	¹⁷⁵ 0.0019	¹⁷³ 1.023
204	PARAVISION-002		¹⁶ 2048	⁷ 377	175.00404	¹⁷⁰ 0.0025	¹⁷⁹ 0.0022	¹⁸¹ 0.0021	¹⁷⁶ 0.0019	¹⁷⁶ 1.025
205	PARAVISION-003		¹⁵ 2048	²¹⁴ 735	159.0031	¹⁶⁰ 0.0022	¹⁶⁵ 0.0020	¹⁶² 0.0019	¹⁶² 0.0017	¹⁶¹ 1.021
206	PARAVISION-004		³¹⁸ 4096	²¹ 720	78.0016	⁸⁹ 0.0014	⁹² 0.0013	¹⁰¹ 0.0013	¹⁰⁶ 0.0013	⁸⁸ 1.013
207	PARAVISION-005		³⁰ 4096	²⁶ 858	72.0015	⁸⁷ 0.0014	⁹¹ 0.0013	¹⁰² 0.0013	¹¹⁵ 0.0013	⁸³ 1.013
208	PARAVISION-007		³¹³ 4096	¹⁹⁸ 706	32.0012	⁴² 0.0011	⁴⁰ 0.0010	⁴¹ 0.0010	⁴³ 0.0010	³⁷ 1.010
209	PARAVISION-009		³¹⁷ 4100	¹⁵ 638	140.0010	²¹ 0.0010	²⁶ 0.0010	³² 0.0009	³⁵ 0.0009	¹⁸ 1.009
210</td										

MISSES OUTSIDE RANK R		RESOURCE USAGE		ENROL MOST RECENT, N = 1.6M					
#	ALGORITHM	BYTES	MSEC	R=1	R=5	R=10	R=20	R=50	WORK-10
217	QNAP-001	¹⁷⁵ 2048	¹⁴ 615	0.0041	¹⁸⁷ 0.0029	¹⁹¹ 0.0027	¹⁹³ 0.0025	¹⁹⁵ 0.0023	¹⁸⁵ 1.028
218	QNAP-002	²⁰⁷ 2048	²⁴⁶ 825	¹⁹⁰ 0.0049	²¹² 0.0044	²²⁴ 0.0043	²³⁴ 0.0043	²⁴⁰ 0.0042	²⁰⁹ 1.040
219	QNAP-003	¹⁹⁷ 2048	⁸ 387	¹⁵¹ 0.0028	¹⁵⁶ 0.0021	¹⁵² 0.0019	¹⁴³ 0.0017	¹⁵⁰ 0.0015	¹⁵⁶ 1.019
220	QUANTASOFT-001	²¹⁹ 2048	⁸⁸ 396	³¹⁸ 0.2177	³²⁰ 0.1643	³²⁰ 0.1468	³²⁰ 0.1312	³²⁰ 0.1116	³²⁰ 2.539
221	RANKONE-002	¹¹ 133	¹² 113	²⁷⁰ 0.0194	²⁶⁴ 0.0112	²⁶³ 0.0093	²⁶³ 0.0077	²⁵⁹ 0.0060	²⁶⁶ 1.111
222	RANKONE-003	⁹ 133	¹³ 114	²⁶⁹ 0.0194	²⁶⁶ 0.0112	²⁶² 0.0093	²⁶² 0.0077	²⁵⁷ 0.0060	²⁶⁵ 1.111
223	RANKONE-004	¹⁸⁵	⁴ 36	0.0415	²⁸⁷ 0.0226	²⁸⁹ 0.0177	²⁸⁵ 0.0141	²⁸⁷ 0.0102	²⁸⁹ 1.225
224	RANKONE-005	¹⁰ 133	¹⁰ 94	²³² 0.0094	²²⁹ 0.0054	²²⁷ 0.0046	²²⁸ 0.0039	²²⁴ 0.0032	²²⁶ 1.054
225	RANKONE-006	¹² 165	⁴⁵ 261	¹⁹² 0.0050	¹⁹² 0.0030	¹⁹² 0.0027	¹⁸⁹ 0.0024	¹⁸⁴ 0.0021	¹⁹¹ 1.030
226	RANKONE-007	¹³ 165	⁵ 278	¹⁶³ 0.0034	¹⁶⁸ 0.0023	¹⁷⁰ 0.0021	¹⁶⁴ 0.0018	¹⁵⁷ 0.0017	¹⁶⁵ 1.022
227	RANKONE-009	²⁶ 260	²⁷ 191	¹³⁵ 0.0024	¹¹⁹ 0.0016	¹²³ 0.0015	¹²⁶ 0.0015	¹²⁷ 0.0014	¹²¹ 1.015
228	RANKONE-010	³⁰ 261	³⁰ 200	¹²⁸ 0.0022	¹³⁴ 0.0018	¹³⁰ 0.0016	¹³⁴ 0.0015	¹³² 0.0015	¹³¹ 1.016
229	RANKONE-011	²⁷ 261	¹⁴² 567	⁶⁹ 0.0015	⁶³ 0.0012	⁶⁶ 0.0012	⁶⁸ 0.0012	⁷¹ 0.0012	⁶³ 1.011
230	RANKONE-012	²⁸ 261	¹⁴ 563	⁵² 0.0014	⁵⁴ 0.0012	⁵⁵ 0.0011	⁵⁹ 0.0011	⁶⁰ 0.0011	⁵¹ 1.011
231	RANKONE-013	²⁹ 261	¹⁷ 680	¹⁹ 0.0011	¹⁴ 0.0009	¹⁶ 0.0009	¹⁸ 0.0009	¹⁹ 0.0009	¹⁴ 1.008
232	RANKONE-014	³¹ 261	¹⁹ 702	¹¹ 0.0010	¹² 0.0009	¹⁵ 0.0009	¹⁷ 0.0009	²⁰ 0.0009	¹² 1.008
233	REALNETWORKS-000	³¹ 4100	³⁹ 244	²⁹⁰ 0.0402	²⁸⁷ 0.0195	²⁸² 0.0149	²⁷⁸ 0.0111	²⁷⁴ 0.0077	²⁸⁷ 1.201
234	REALNETWORKS-001	³² 4104	³⁸ 243	²⁹¹ 0.0402	²⁸⁶ 0.0195	²⁸³ 0.0149	²⁷⁹ 0.0111	²⁷¹ 0.0077	²⁸⁸ 1.201
235	REALNETWORKS-002	³² 4104	⁴⁰ 245	²⁸⁷ 0.0393	²⁸⁷ 0.0189	²⁸¹ 0.0142	²⁷⁷ 0.0108	²⁷⁷ 0.0076	²⁸⁵ 1.195
236	REALNETWORKS-003	¹³² 1848	²⁰ 178	²⁷⁶ 0.0242	²⁶⁸ 0.0177	²⁶¹ 0.0090	²⁵⁵ 0.0070	²⁵⁰ 0.0054	²⁷⁰ 1.120
237	REALNETWORKS-004	¹³³ 1848	²¹ 185	²⁷⁴ 0.0236	²⁶⁷ 0.0112	²⁵⁹ 0.0087	²⁵³ 0.0068	²⁴⁶ 0.0050	²⁶⁷ 1.116
238	REALNETWORKS-005	²⁷³ 2056	⁶⁵ 337	¹³¹ 0.0023	¹¹¹ 0.0016	¹⁰¹ 0.0014	¹⁰⁸ 0.0013	⁸⁶ 0.0012	¹¹³ 1.015
239	REALNETWORKS-006	²⁶ 2056	⁷¹ 350	⁵⁶ 0.0014	⁵³ 0.0012	⁵³ 0.0011	⁴⁷ 0.0011	⁴¹ 0.0010	⁵² 1.011
240	REALNETWORKS-007	²⁷ 2056	¹⁶ 645	⁴⁸ 0.0013	⁵⁰ 0.0012	⁴⁶ 0.0011	⁴⁵ 0.0011	³⁹ 0.0010	⁴⁹ 1.011
241	REALNETWORKS-008	²⁶ 2056	³² 977	²⁹ 0.0011	²⁰ 0.0010	²⁴ 0.0009	²⁷ 0.0009	¹⁷ 0.0009	²² 1.009
242	REMARKAI-000	¹⁵⁹ 2048	⁶¹ 515	²²⁵ 0.0086	²¹⁷ 0.0044	²⁰⁶ 0.0036	²⁰⁶ 0.0031	²⁰⁷ 0.0025	²¹⁶ 1.045
243	REMARKAI-000	¹⁹⁴ 2048	⁶⁸ 691	¹⁶⁵ 0.0034	¹⁵⁷ 0.0021	¹⁵¹ 0.0019	¹⁴⁴ 0.0017	¹⁴⁹ 0.0015	¹⁶⁰ 1.020
244	REMARKAI-002	¹⁴ 2048	¹⁰ 434	²²³ 0.0081	²⁰⁸ 0.0040	¹⁹⁷ 0.0031	¹⁹⁴ 0.0026	¹⁸⁵ 0.0021	²¹⁰ 1.041
245	RENDIP-000	²¹¹ 2048	²⁸⁸ 894	⁷³ 0.0015	⁷⁶ 0.0013	⁷⁰ 0.0012	⁷² 0.0012	⁸⁰ 0.0012	⁷⁵ 1.012
246	REVEALMEDIA-000	²⁵ 2052	⁸¹ 385	¹⁰⁰ 0.0019	⁷⁹ 0.0013	⁸³ 0.0013	⁸³ 0.0013	⁸⁷ 0.0012	⁸⁷ 1.013
247	S1-000	³¹² 4096	²⁰ 865	¹³⁷ 0.0024	¹²⁸ 0.0018	¹³² 0.0017	¹³⁵ 0.0016	¹⁴² 0.0015	¹³⁴ 1.017
248	S1-001	²¹ 2048	²⁴ 814	¹⁵⁸ 0.0031	¹⁷³ 0.0025	¹⁸⁵ 0.0024	¹⁸⁸ 0.0024	¹⁹⁵ 0.0023	¹⁷¹ 1.023
249	S1-002	²⁰ 2048	³¹⁸ 660	⁵⁹ 0.0014	⁸⁰ 0.0013	⁸⁸ 0.0013	⁹⁸ 0.0013	¹¹² 0.0013	⁷⁸ 1.012
250	S1-003	²³ 2048	³² 979	⁶⁴ 0.0015	⁷⁷ 0.0013	⁷⁹ 0.0013	⁸⁰ 0.0013	⁹¹ 0.0013	⁷⁷ 1.012
251	S1-004	¹⁹ 2048	³¹ 957	⁴⁹ 0.0013	⁷⁰ 0.0013	⁷⁶ 0.0013	⁸⁵ 0.0013	⁹⁵ 0.0013	⁶⁷ 1.012
252	SCANOVATE-000	²²⁰ 2048	²⁰ 712	¹⁹¹ 0.0050	¹⁸⁰ 0.0026	¹⁷⁵ 0.0022	¹⁶² 0.0018	¹⁴⁸ 0.0015	¹⁸² 1.026
253	SCANOVATE-001	¹⁴ 2048	¹⁷ 675	¹⁹⁵ 0.0053	¹⁸⁷ 0.0027	¹⁷⁸ 0.0022	¹⁶³ 0.0018	¹⁴⁶ 0.0015	¹⁸⁶ 1.028
254	SENSETIME-000	³² 4104	²⁰ 715	¹³³ 0.0023	¹⁵² 0.0020	¹⁵⁷ 0.0019	¹⁵⁹ 0.0018	¹⁶⁴ 0.0017	¹⁴⁷ 1.018
255	SENSETIME-001	³¹ 4104	¹⁶ 656	¹³⁴ 0.0023	¹⁴⁷ 0.0020	¹⁵⁵ 0.0019	¹⁴⁸ 0.0017	¹⁵³ 0.0016	¹⁴⁴ 1.018
256	SENSETIME-002	²⁶ 2056	¹⁶ 650	²⁵⁷ 0.0137	²⁷⁴ 0.0136	²⁸⁰ 0.0136	²⁸⁴ 0.0136	²⁹⁰ 0.0136	²⁷¹ 1.122
257	SENSETIME-003	²⁶ 2056	³⁰ 940	¹³ 0.0010	²⁵ 0.0010	²⁸ 0.0010	²⁹ 0.0009	³¹ 0.0009	¹⁷ 1.009
258	SENSETIME-004	⁹¹ 1032	²⁰ 710	¹² 0.0010	¹⁰ 0.0009	¹⁴ 0.0009	¹⁵ 0.0009	¹³ 0.0009	¹¹ 1.008
259	SENSETIME-005	¹⁰³ 1032	³³ 1007	⁶ 0.0009	⁷ 0.0008	⁷ 0.0008	⁷ 0.0008	⁷ 0.0008	⁵³ 1.008
260	SENSETIME-006	⁹⁷ 1032	³¹ 956	⁵ 0.0009	⁷ 0.0008	⁷ 0.0008	¹¹ 0.0008	¹¹ 0.0008	⁶¹ 1.008
261	SENSETIME-007	⁹³ 1032	³¹ 958	⁴ 0.0008	⁴ 0.0008	⁵ 0.0008	⁹ 0.0008	¹² 0.0008	⁴¹ 1.007
262	SENSETIME-008	⁹² 1032	³² 969	³ 0.0008	² 0.0008	⁴ 0.0008	⁸ 0.0008	⁷ 0.0008	²¹ 1.007
263	SENSETIME-009	⁹⁹ 1032	³³⁴ 1023	² 0.0008	³ 0.0008	⁶ 0.0008	¹⁰ 0.0008	⁹ 0.0008	³ 1.007
264	SHAMAN-003	¹⁶ 2048	⁷⁰ 704	³⁰⁹ 0.1243	³¹⁸ 0.0823	³¹² 0.0708	³¹¹ 0.0616	³¹¹ 0.0518	³¹² 1.789
265	SHAMAN-004	¹⁹⁰ 2048	¹⁶⁰ 642	³²⁰ 0.2221	³¹⁹ 0.1473	³¹⁷ 0.1241	³¹⁷ 0.1049	³¹⁶ 0.0825	³¹⁹ 2.411
266	SHAMAN-006	²² 2048	⁷⁰ 706	²⁸⁹ 0.0398	²⁹⁷ 0.0344	³⁰⁰ 0.0332	³⁰² 0.0323	³⁰ 0.0315	²⁹⁶ 1.316
267	SHAMAN-007	²¹⁸ 2048	²⁰ 709	²⁸⁸ 0.0396	²⁹⁹ 0.0342	²⁹⁹ 0.0331	³⁰¹ 0.0322	³⁰⁴ 0.0314	²⁹⁴ 1.315
268	SIAT-001	²⁴ 2052	²⁶⁰ 842	⁹³ 0.0018	⁹⁰ 0.0014	⁷⁷ 0.0013	⁷⁰ 0.0012	⁶⁷ 0.0011	⁹⁰ 1.013
269	SIAT-002	²⁴⁸ 2052	²⁹ 906	⁹⁶ 0.0018	⁸⁸ 0.0014	⁹⁴ 0.0013	⁹¹ 0.0013	⁸⁵ 0.0012	⁹³ 1.013
270	SMILART-004	³² 512	¹⁶ 167	³³⁴ 0.9648	³³⁴ 0.9641	³³⁴ 0.9640	³³⁴ 0.9639	³³⁵ 0.9638	³³⁴ 9.678
271	SMILART-005	¹⁹¹ 2048	¹¹ 464	²² 0.0042	²² 0.0042	²² 0.0042	²² 0.0042	²² 0.0042	³³ 10.000
272	SQISOFT-001	²²² 2056	¹⁰⁹ 460	¹⁷⁹ 0.0042	⁹⁷ 0.0014	⁷³ 0.0013	⁶¹ 0.0012	⁵⁷ 0.0010	¹²⁹ 1.016
273	SQISOFT-002	²⁶ 2056	¹⁶ 661	⁴⁶ 0.0013	³⁹ 0.0010	³⁵ 0.0010	³³ 0.0010	²⁹ 0.0009	³⁵ 1.010
274	STAQU-000	³⁰² 4096	²⁴⁹ 827	²¹⁴ 0.0071	²³² 0.0060	²³⁴ 0.0057	²⁴² 0.0055	²⁴⁷ 0.0053	²²⁹ 1.056
275	SYNESIS-003	¹⁴ 2048	³⁶ 215	²⁶¹ 0.0162	²⁷⁹ 0.0160	²⁸⁵ 0.0160	²⁹⁰ 0.0160	²⁹ 0.0160	²⁸ 1.144
276	SYNESIS-003	³⁰⁴ 4096	¹¹ 103	³¹⁵ 0.1700	³¹⁵ 0.1172	³¹⁵ 0.1047	³¹⁶ 0.0953	³¹⁷ 0.0869	³¹⁵ 2.120
277	SYNESIS-005	³¹⁹ 4104	²² 772	²²⁴ 0.0085	²⁵⁹ 0.0085	²⁵⁷ 0.0085	²⁶⁹ 0.0085	²⁷⁶ 0.0085	²⁴⁹ 1.076
278	T4ISB-000	¹⁸⁹ 2048	²²¹ 752	²³⁷ 0.0104	²⁶³ 0.0103	²⁷¹ 0.0103	²⁷⁵ 0.0103	²⁸² 0.0103	²⁶² 1.093
279	TECH-001	¹²¹ 1536	²⁹⁸ 898	¹⁷⁴ 0.0040	¹⁷¹ 0.0024	¹⁷¹ 0.0021	¹⁶⁵ 0.0018	¹⁶⁴ 0.0017	¹⁷⁴ 1.024
280	TECH-002	⁵⁸ 513	³¹⁰ 941	¹⁴⁷ 0.0027	⁹⁵ 0.0014	⁶⁹ 0.0012	⁵⁷ 0.0011	⁴⁴ 0.0010	¹⁰⁴ 1.014
281	TEVIAN-003	²¹⁴ 2048	⁵⁶ 300	²⁵⁸ 0.0147	²⁴⁶ 0.0074	²³⁵ 0.0059	²³⁷ 0.0047	²³⁵ 0.0037	²⁴⁸ 1.075
282	TEVIAN-004	¹⁶ 2048</							

MISSES OUTSIDE RANK R		RESOURCE USAGE		ENROL MOST RECENT, N = 1.6M					
FNIR(N, T=0, R)		TEMPLATE		FRVT 2018 MUGSHOTS					
#	ALGORITHM	BYTES	MSEC	R=1	R=5	R=10	R=20	R=50	WORK=10
289	TONGYITRANS-000	²⁷⁹ 2070	²⁶ 190	²⁰³ 0.0069	²⁰¹ 0.0038	²⁰² 0.0032	²⁰² 0.0029	²⁰⁶ 0.0026	²⁰³ 1.038
290	TONGYITRANS-001	²⁸⁰ 2070	²⁴ 189	²¹⁰ 0.0069	²⁰⁹ 0.0038	²⁰⁰ 0.0032	²⁰¹ 0.0029	²⁰⁸ 0.0026	²⁰⁴ 1.038
291	TOSHIBA-000	¹²⁸ 1548	³⁰¹ 930	¹⁸³ 0.0045	¹⁷⁹ 0.0026	¹⁷⁷ 0.0022	¹⁷³ 0.0020	¹⁷³ 0.0018	¹⁸⁰ 1.026
292	TOSHIBA-001	²⁷⁵ 2060	³⁰² 631	¹⁸⁸ 0.0048	¹⁸⁷ 0.0027	¹⁸⁰ 0.0023	¹⁷⁹ 0.0020	¹⁷² 0.0018	¹⁸⁴ 1.027
293	TRUEFACE-000	¹³⁶ 2000	⁷² 365	¹⁶² 0.0033	¹⁸⁵ 0.0028	¹⁹⁴ 0.0028	¹⁹⁶ 0.0026	²⁰⁵ 0.0026	¹⁸¹ 1.026
294	TURINGTECHVIP-001	¹⁵⁴ 2048	²⁴ 823	²³³ 0.0095	²⁶⁹ 0.0093	²⁶⁴ 0.0093	²⁷⁷ 0.0093	²³² 1.084	
295	VD-000	⁹⁰ 1028	⁶⁶ 337	³²⁹ 0.4737	³²⁸ 0.3204	³²² 0.2695	³²⁶ 0.2215	³²⁵ 0.1678	³²⁸ 4.058
296	VD-001	²⁴¹ 2052	¹⁸⁷ 695	²⁸¹ 0.2076	²⁸⁷ 0.0181	²⁸⁷ 0.0162	²⁸⁶ 0.0146	²⁸⁵ 0.0130	²⁸⁴ 1.174
297	VD-002	²⁵⁰ 2052	¹⁸² 689	²³⁴ 0.0095	²⁴⁶ 0.0077	²⁵⁰ 0.0073	²⁵⁴ 0.0070	²⁶³ 0.0068	²⁴³ 1.071
298	VD-003	²⁴⁰ 2052	¹⁸ 693	²¹⁶ 0.0076	²³⁹ 0.0069	²⁴⁵ 0.0067	²⁵¹ 0.0066	²⁶⁰ 0.0066	²³⁷ 1.063
299	VERIDAS-001	²³² 2048	²⁸⁰ 885	¹⁵⁰ 0.0028	¹⁴⁵ 0.0019	¹³⁶ 0.0017	¹³³ 0.0015	¹³⁷ 0.0015	¹⁴⁵ 1.018
300	VERIDAS-002	¹⁵⁵ 2048	²⁸ 888	¹⁴⁹ 0.0028	¹⁴⁴ 0.0019	¹³³ 0.0017	¹³¹ 0.0015	¹³⁵ 0.0015	¹⁴³ 1.018
301	VERIDAS-003	¹⁹² 2048	²⁷⁹ 877	⁹⁵ 0.0018	¹⁰¹ 0.0015	¹⁰³ 0.0014	¹⁰⁸ 0.0013	¹⁰⁷ 0.0013	⁹⁷ 1.014
302	VERIDAS-004	¹⁷⁶ 2048	²⁸ 891	⁵⁰ 0.0014	⁶⁷ 0.0013	⁷¹ 0.0012	⁷⁷ 0.0012	⁶⁷ 0.0012	⁶¹ 1.011
303	VERIJELAS-000	²²¹ 2048	⁶⁴ 335	³²⁴ 0.3547	³²⁸ 0.2975	³²⁸ 0.2805	³²⁸ 0.2655	³²⁹ 0.2489	³²⁵ 3.744
304	VIGILANTSOLUTIONS-003	¹²⁷ 1544	²⁵³ 832	³⁰² 0.0694	²⁹⁹ 0.0349	²⁹⁴ 0.0262	²⁹⁴ 0.0201	²⁹¹ 0.0140	²⁹⁹ 1.355
305	VIGILANTSOLUTIONS-004	¹²⁴ 1544	²⁵ 830	³¹⁰ 0.1249	³⁰⁹ 0.0706	³⁰⁷ 0.0557	³⁰⁹ 0.0434	³⁰³ 0.0305	³⁰⁹ 1.699
306	VIGILANTSOLUTIONS-005	¹²⁶ 1544	²³¹ 778	²²⁹ 0.0092	²¹⁶ 0.0045	²⁰⁴ 0.0036	¹⁹⁹ 0.0029	¹⁹⁰ 0.0022	²¹⁷ 1.046
307	VIGILANTSOLUTIONS-006	¹²⁵ 1544	²⁵ 834	²³⁶ 0.0099	²¹⁹ 0.0048	²¹³ 0.0038	²⁰⁹ 0.0030	¹⁹⁵ 0.0022	²²⁰ 1.049
308	VIGILANTSOLUTIONS-007	¹²² 1544	¹⁵¹ 618	¹⁶⁴ 0.0034	¹⁴⁸ 0.0020	¹³⁷ 0.0017	¹³⁰ 0.0015	¹¹⁰ 0.0013	¹⁵⁴ 1.019
309	VIGILANTSOLUTIONS-008	¹²³ 1544	⁸⁹ 405	¹⁵⁶ 0.0029	¹³⁸ 0.0018	¹²⁷ 0.0016	¹²² 0.0015	⁹⁹ 0.0013	¹⁴² 1.018
310	VISIONBOX-000	²⁰⁴ 2059	¹¹⁷ 482	¹⁰⁵ 0.0019	¹⁰⁵ 0.0015	¹¹⁰ 0.0014	¹⁰⁷ 0.0013	⁹⁸ 0.0013	¹⁰² 1.014
311	VISIONLABS-004	²⁵ 256	⁶⁰ 315	¹⁴⁸ 0.0027	¹³⁴ 0.0018	¹²⁸ 0.0016	¹²⁹ 0.0015	¹²⁵ 0.0014	¹³⁸ 1.017
312	VISIONLABS-005	⁴⁵ 512	⁵⁹ 300	¹³⁶ 0.0024	¹²³ 0.0017	¹¹⁸ 0.0015	¹¹¹ 0.0014	¹⁰⁴ 0.0013	¹²⁷ 1.016
313	VISIONLABS-006	⁵¹ 512	⁵⁹ 292	⁹⁷ 0.0018	⁹⁹ 0.0015	⁹⁶ 0.0014	⁹⁶ 0.0013	¹⁰³ 0.0013	⁹⁶ 1.014
314	VISIONLABS-007	⁴⁵ 512	⁵⁵ 293	⁹¹ 0.0018	⁹⁹ 0.0014	⁸⁴ 0.0013	⁸¹ 0.0013	⁸⁴ 0.0012	⁹² 1.013
315	VISIONLABS-008	⁵⁵ 512	⁵¹ 277	¹¹⁴ 0.0020	¹²⁷ 0.0018	¹⁴⁵ 0.0018	¹⁵² 0.0018	¹⁶³ 0.0017	¹³³ 1.017
316	VISIONLABS-009	⁴ 512	¹² 494	²⁸ 0.0011	³ 0.0011	³⁹ 0.0010	⁴⁰ 0.0010	⁴⁰ 0.0010	³⁴ 1.010
317	VISIONLABS-010	⁴¹ 512	²¹³ 732	⁵⁷ 0.0014	⁷³ 0.0013	⁸² 0.0013	⁸⁴ 0.0013	⁹² 0.0013	⁷² 1.012
318	VISIONLABS-011	⁴ 512	²¹ 736	³⁵ 0.0012	⁴ 0.0011	⁵⁰ 0.0011	⁴⁹ 0.0011	⁵⁶ 0.0011	⁴³ 1.010
319	VIXVIZION-009	²⁰⁶ 2048	²⁸⁹ 896	¹²⁹ 0.0023	¹¹⁰ 0.0016	¹⁰² 0.0014	⁹³ 0.0013	⁸¹ 0.0012	¹¹² 1.015
320	VNPT-001	¹⁸⁰ 2048	²⁸ 892	¹²¹⁰ 0.0022	¹⁴ 0.0019	¹⁵⁰ 0.0018	¹⁶⁰ 0.0018	¹⁷⁰ 0.0018	¹³⁹ 1.017
321	VNPT-002	¹⁹³ 2048	²⁴¹ 810	¹⁰³ 0.0019	¹³⁵ 0.0018	¹⁴⁴ 0.0018	¹⁵⁰ 0.0018	¹⁶⁶ 0.0017	¹³⁰ 1.016
322	VOCORD-003	⁷ 896	²⁶ 714	²⁰³ 0.0062	¹⁹ 0.0035	¹⁹⁵ 0.0030	¹⁹⁵ 0.0026	¹⁹ 0.0023	¹⁹⁷ 1.035
323	VOCORD-004	⁷⁸ 896	¹³² 538	²¹⁹ 0.0079	²²⁰ 0.0049	²²² 0.0043	²²⁷ 0.0038	²²⁸ 0.0034	²¹⁸ 1.048
324	VOCORD-005	⁷⁶ 768	²⁴¹ 822	²¹³ 0.0070	²¹⁷ 0.0046	²¹⁹ 0.0041	²²⁶ 0.0038	²³¹ 0.0035	²¹⁴ 1.044
325	VOCORD-006	³³⁷ 10240	²⁴ 825	³³⁶ 1.0000	³³⁸ 1.0000	³³⁷ 1.0000	³³⁶ 1.0000	³³⁷ 1.0000	
326	VTS-000	¹⁷⁰ 2048	¹²⁰ 492	³³² 0.5937	³³³ 0.5936	³³³ 0.5936	³³³ 0.5936	³³³ 0.5936	³³³ 6.343
327	VTS-001	¹⁴⁴ 2048	²⁸ 891	⁷⁰ 0.0015	⁵¹ 0.0012	⁴⁵ 0.0011	⁴⁶ 0.0011	⁴² 0.0010	³⁵ 1.011
328	VTS-002	²⁰² 2048	²⁹² 903	¹⁰² 0.0019	⁹² 0.0014	⁷⁵ 0.0013	⁷⁶ 0.0012	⁶⁷ 0.0011	⁹⁵ 1.013
329	VTS-003	²⁰⁰ 2048	¹⁹ 703	³⁰ 0.0011	²⁹ 0.0010	²³ 0.0009	²⁶ 0.0009	²¹ 0.0009	²⁴ 1.009
330	XFORWARDAI-000	¹⁸⁷ 2048	²²⁴ 768	¹³⁰ 0.0023	¹⁵³ 0.0020	¹⁶¹ 0.0020	¹⁷³ 0.0019	¹⁷⁹ 0.0019	¹⁴⁸ 1.018
331	XFORWARDAI-001	¹⁵⁸ 2048	¹⁷ 681	¹¹⁸ 0.0020	¹⁴⁹ 0.0019	¹⁵⁸ 0.0019	¹⁷⁰ 0.0019	¹⁷⁸ 0.0019	¹⁴⁰ 1.018
332	XFORWARDAI-002	³⁰⁵ 4096	³⁰⁴ 935	¹⁰⁹ 0.0020	¹⁴³ 0.0019	¹⁵⁶ 0.0019	¹⁶⁹ 0.0019	¹⁷⁷ 0.0019	¹³⁷ 1.017
333	YISHENG-001	²⁹⁹ 3704	⁸ 387	²⁸⁰ 0.0265	²⁷⁸ 0.0130	²⁶⁹ 0.0102	²⁶⁶ 0.0080	²⁵ 0.0059	²⁴ 1.134
334	YITU-002	³²⁴ 4138	²⁷³ 870	⁹⁸ 0.0018	⁶² 0.0012	⁵⁴ 0.0011	⁴⁸ 0.0011	⁴⁸ 0.0010	⁷¹ 1.012
335	YITU-003	³²⁵ 4138	²⁷ 871	¹⁵⁵ 0.0029	¹⁶¹ 0.0023	¹⁷⁴ 0.0022	¹⁸³ 0.0021	¹⁶³ 0.0021	¹⁶³ 1.021
336	YITU-004	²⁷⁷ 2070	²⁹⁸ 910	⁴³ 0.0013	³⁷ 0.0009	¹⁷ 0.0009	¹⁶ 0.0009	¹⁶ 0.0009	²⁷ 1.009
337	YITU-005	²⁷⁸ 2070	²⁶⁹ 861	¹³² 0.0023	¹²⁵ 0.0021	¹⁶⁴ 0.0020	¹⁷⁶ 0.0020	¹⁸² 0.0020	¹⁵⁰ 1.019

Table 32: **Rank-based accuracy for the FRVT 2018 mugshot sets.** In columns 3 and 4 are template size and template generation duration. Thereafter values are rank-based FNIR with $T = 0$ and FPIR = 1. This is appropriate to investigational uses but not those with higher volumes where candidates from all searches would need review. The next column is a workload statistic, a small value shows an algorithm front-loads mates into the first 10 candidates. Throughout, blue superscripts indicate the rank of the algorithm for that column, and the best value is highlighted in yellow.

MISSSES BELOW THRESHOLD, T		ENROL RECENT MUGSHOT, N = 1.6M												ENROL APPLICATION PORTRAIT, N = 1.6M																	
#	ALGORITHM	ENROL: MUGSHOT			ENROL: MUGSHOT			ENROL: WEBCAM			ENROL: PROFILE			ENROL: VISA			ENROL: BORDER			PROBE: BORDER 10+YR			ENROL: KIOSK								
		FPIR=0.0003	FPIR=0.001	FPIR=0.01	FPIR=0.0003	FPIR=0.001	FPIR=0.01	FPIR=0.0003	FPIR=0.001	FPIR=0.01	FPIR=0.0003	FPIR=0.001	FPIR=0.01	FPIR=0.001	FPIR=0.001	FPIR=0.01	FPIR=0.001	FPIR=0.001	FPIR=0.01	FPIR=0.001	FPIR=0.001	FPIR=0.01	FPIR=0.001	FPIR=0.001	FPIR=0.01						
1	20FACE-000	282	0.462	292	0.348	300	0.230	293	0.763	284	0.450	286	0.301	242	1.000	267	1.000	268	1.000	223	0.424	225	0.255	130	0.772	141	0.599	217	0.938	233	0.836
2	3DIVI-003	284	0.482	301	0.400	306	0.282	288	0.685	300	0.626	302	0.497					236	0.605	239	0.445					198	0.821	222	0.717		
3	3DIVI-004	254	0.256	271	0.169	276	0.093	253	0.400	274	0.343	280	0.237					212	0.277	218	0.172					171	0.607	203	0.485		
4	3DIVI-005	253	0.255	268	0.166	277	0.093	252	0.395	277	0.339	279	0.234	169	0.998	180	0.996	199	0.990	243	0.864	248	0.846					170	0.597	205	0.484
5	3DIVI-006	252	0.253	270	0.168	278	0.096	256	0.403	273	0.342	281	0.238					213	0.283	219	0.174					174	0.615	204	0.490		
6	ACER-000	238	0.208	260	0.146	265	0.074	256	0.300	251	0.246	254	0.157	113	0.987	129	0.981	161	0.955	207	0.201	211	0.114			154	0.490	189	0.363		
7	ACER-001	184	0.109	202	0.056	207	0.026	169	0.136	178	0.109	185	0.069	205	1.000	219	0.999	247	0.998	164	0.068	167	0.036	115	0.406	128	0.250	153	0.479	131	0.206
8	AIZE-001	195	0.127	222	0.077	224	0.034	200	0.187	206	0.143	208	0.087	142	0.995	157	0.994	188	0.983	178	0.101	181	0.052	108	0.364	124	0.216	132	0.387	167	0.289
9	ALCHERA-000	245	0.231	257	0.138	259	0.070	225	0.259	235	0.216	247	0.146	182	0.999	198	0.999	229	0.996	201	0.176	212	0.111			194	0.803	197	0.456		
10	ALCHERA-001	332	1.000	332	0.999	332	0.999	332	1.000	336	1.000									269	1.000	298	1.000			282	1.000	274	1.000		
11	ALCHERA-002	307	0.807	308	0.486	309	0.302	287	0.685	295	0.591	297	0.442	225	1.000	226	1.000	252	0.999	242	0.827	243	0.770			195	0.811	219	0.705		
12	ALCHERA-003	278	0.450	262	0.155	260	0.070	237	0.304	247	0.239	252	0.152	217	1.000	212	0.999	234	0.997	200	0.172	208	0.097			148	0.464	184	0.362		
13	ALCHERA-004	289	0.520	300	0.394	299	0.211	284	0.642	290	0.529	291	0.327	143	0.995	150	0.991	122	0.813	224	0.424	222	0.232	123	0.708	135	0.515	165	0.546	194	0.398
14	ALLGOVISION-000	204	0.138	234	0.088	241	0.045	212	0.202	222	0.166	232	0.106	129	0.993	147	0.990	185	0.982	181	0.117	189	0.066			162	0.526	193	0.396		
15	ALLGOVISION-001	213	0.155	240	0.102	249	0.053	230	0.275	230	0.221	246	0.141	133	0.993	136	0.986	144	0.933	194	0.150	209	0.081			135	0.491	192	0.389		
16	ANKE-000	224	0.184	244	0.117	256	0.063	223	0.256	237	0.220	250	0.151	139	0.995	158	0.994	197	0.990	329	1.000	273	1.000			264	1.000	300	1.000		
17	ANKE-001	222	0.183	248	0.119	259	0.063	224	0.256	238	0.220	251	0.151	144	0.995	164	0.994	208	0.992	291	1.000	322	1.000			316	1.000	251	1.000		
18	ANKE-002	147	0.062	163	0.032	163	0.014	133	0.103	141	0.079	147	0.050	89	0.975	98	0.948	118	0.795	123	0.034	128	0.018			92	0.245	128	0.190		
19	AWARE-003	221	0.174	252	0.128	268	0.082	248	0.351	266	0.298	273	0.204	110	0.987	133	0.984	181	0.977	225	0.428	231	0.378			163	0.530	196	0.443		
20	AWARE-004	270	0.355	284	0.269	295	0.175	280	0.619	289	0.509	295	0.375	222	1.000	229	1.000	256	0.999	220	0.397	227	0.279			196	0.816	214	0.631		
21	AWARE-005	269	0.608	295	0.364	274	0.085	248	0.342	259	0.253	256	0.163	216	1.000	233	1.000	259	0.999	211	0.255	218	0.122			211	0.916	221	0.714		
22	AWARE-006	283	0.475	285	0.276	296	0.175	266	0.466	277	0.398	284	0.283	201	1.000	221	0.999	248	0.999	218	0.368	224	0.254			187	0.749	217	0.623		
23	AYONIX-000	311	0.846	320	0.811	322	0.724	302	0.956	317	0.939	321	0.892	171	0.998	187	0.998	225	0.995	247	0.954	248	0.891			226	0.982	239	0.959		
24	AYONIX-001	313	0.875	322	0.824	324	0.701	302	0.946	314	0.920	317	0.845	215	1.000	220	0.999	230	0.996	252	0.999	252	0.998			222	0.969	238	0.926		
25	AYONIX-002	314	0.876	321	0.824	325	0.702	303	0.946	315	0.920	316	0.845	215	1.000	217	0.999	231	0.996	244	0.915	244	0.821			223	0.969	235	0.926		
26	CAMVI-003	173	0.094	217	0.071	252	0.058	180	0.152	198	0.132	233	0.108	97	0.979	109	0.970	15	0.940	180	0.114	209	0.100			136	0.402	189	0.377		
27	CAMVI-004	182	0.107	218	0.072	250	0.054	220	0.240	200	0.136	222	0.100	201	1.000	216	0.999	238	0.998	177	0.100	199	0.081			192	0.787	205	0.507		
28	CAMVI-005	205	0.139	238	0.099	267	0.076	221	0.451	227	0.179	241	0.132	210	1.000	227	0.998	195	0.156	217	0.112			234	0.999	249	0.983				
29	CANON-001	45	0.012	55	0.005	54	0.002	37	0.031	37	0.023	38	0.015	40	0.633	28	0.365	45	0.217	40	0.008	44	0.004	39	0.068	43	0.034	49	0.139	47	0.092
30	CANON-002	33	0.010	47	0.005	47	0.002	31	0.027	32	0.020	240	0.013	240	0.487	32	0.407	42	0.253	68	0.013	47	0.004	51	0.046	82	0.188	54	0.106		
31	CIB-000	111	0.044	91	0.012	85	0.005	102	0.077	84	0.045	83	0.025	245	1.000	247	1.000	264	1.000	80	0.017	72	0.008	62	0.141	66	0.068	208	0.894	206	0.521
32	CLEARVIEWAI-000	49	0.013	58	0.006	55	0.002	49	0.036	47	0.025	44	0.016	185	0.999	114	0.974	21	0.149	41	0.008	36	0.004	30	0.057	37	0.027	109	0.268	24	0.080
33	CLOUDWALK-HR-000	15	0.004	18	0.002	23	0.002	14	0.015	17	0.013	20	0.012	5	0.188	6	0.133	11	0.095	21	0.005	27	0.003	15	0.033	19	0.018	26	0.099	16	0.075
34	CLOUDWALK-MT-000	10	0.003	17	0.002	31	0.002	11	0.015	16	0.013	22	0.012	4	0.169	4	0.109	7	0.077	7	0.002	10	0.002	5	0.018	7	0.009	6	0.072	10	0.063
35	CLOUDWALK-MT-001	7	0.003	15	0.002	29	0.002	8	0.013	8	0.012	19	0.011	2	0.104	2	0.070	2	0.060	2	0.001	2	0.001	4	0.015	3	0.006	2	0.056	2	0.049
36	CLOUDWALK-MT-002	6	0.003	13	0.002	28	0.002	6	0.012	7	0.011	18	0.011	1	0.081	1	0.063	1	0.056	1	0.001	1	0.001	2	0.013	1	0.005	1	0.055	1	0.047
37	COGENT-000	209	0.143	193	0.053	215	0.029	191	0.175	202	0.140	224																			

Table 35: **Threshold-based accuracy**. Values are FNIR(N, T, L) with N = 1.6 million with thresholds set to produce FPIR = 0.0003, 0.001, and 0.01 in non-mate searches. Throughout blue superscripts indicate the rank of the algorithm for that column. Caution: The Power-low models are mostly intended to draw attention to the kind of behavior, not as a model to be used for prediction.

2023/03/14
14:32:11

FNIR(N, K, I) = False neg. identification rate
FPIR(N, T) = False pos. identification rate

N = Num. enrolled subjects
R = Num. candidates examined

Threshold

$T > 0 \rightarrow$ Identification

MISSES BELOW THRESHOLD, T		ENROL RECENT MUGSHOT, N = 1.6M									ENROL APPLICATION PORTRAIT, N = 1.6M									ENROL: VISA					
#	ALGORITHM	ENROL: MUGSHOT			ENROL: MUGSHOT			ENROL: WEBCAM			ENROL: PROFILE			ENROL: VISA			ENROL: BORDER			ENROL: BORDER 10+YR			ENROL: VISA		
		FPIR=0.0003	FPIR=0.001	FPIR=0.01	FPIR=0.0003	FPIR=0.001	FPIR=0.01	FPIR=0.0003	FPIR=0.001	FPIR=0.01	FPIR=0.0003	FPIR=0.001	FPIR=0.01	FPIR=0.001	FPIR=0.01	FPIR=0.001	FPIR=0.01	FPIR=0.0003	FPIR=0.001	FPIR=0.01	FPIR=0.0003	FPIR=0.001	FPIR=0.01		
323	VOCORD-004	³⁹ 0.826	²⁹⁴ 0.355	²⁴⁴ 0.051	²⁵⁴ 0.401	²²⁸ 0.173	²¹³ 0.093	²⁴³ 1.000	²⁴⁰ 1.000	²⁵⁰ 0.999	²⁰⁵ 0.193	¹⁸⁸ 0.065	¹⁹⁰ 0.138	²⁰⁴ 0.090	²²⁹ 0.991	²²⁷ 0.776	¹³¹ 0.381	¹⁶⁶ 0.287	²⁴⁷ 1.000	³³¹ 1.000					
324	VOCORD-005	³⁰² 0.689	³⁶³ 0.158	²³⁶ 0.044	¹⁸⁵ 0.161	¹⁹⁷ 0.130	²⁰² 0.080	¹⁸⁶ 0.999	¹⁸³ 0.997	¹⁶⁷ 0.968	¹⁹⁰ 0.138	²⁰⁴ 0.090													
325	VOCORD-006	³³⁷ 1.000	³³⁷ 1.000	³³⁷ 1.000	³²⁴ 1.000	³²⁶ 1.000	³²⁹ 1.000	²⁹⁴ 1.000	³²⁴ 1.000	³⁰¹ 1.000	³⁰⁹ 1.000	²⁶¹ 1.000													
326	VTS-000	²⁹⁴ 0.605	³¹² 0.598	³²⁰ 0.595	²⁸¹ 0.624	²⁹⁹ 0.619	³¹⁰ 0.613	¹⁹⁶ 0.999	²¹³ 0.999	²⁴⁶ 0.998	²³⁷ 0.613	²⁴⁰ 0.609	¹²⁹ 0.760	¹⁴⁵ 0.739	¹⁸⁸ 0.761	²²⁴ 0.749									
327	VTS-001	⁹⁵ 0.035	⁹⁴ 0.013	⁹¹ 0.006	⁸⁹ 0.067	⁹³ 0.051	⁹⁴ 0.031	¹⁶⁶ 0.998	¹⁶⁰ 0.994	⁷⁹ 0.510	⁹³ 0.022	¹⁰⁸ 0.012	⁶⁴ 0.141	⁷⁸ 0.079	⁸³ 0.192	⁷⁸ 0.126									
328	VTS-002	¹³⁵ 0.053	¹⁴² 0.026	¹⁴¹ 0.010	¹²⁶ 0.098	¹³³ 0.075	¹³⁸ 0.046	²¹⁴ 1.000	²²³ 1.000	¹⁶⁰ 0.953	¹⁴⁰ 0.045	¹⁵⁰ 0.026	⁹² 0.231	¹⁰⁵ 0.133	¹³⁹ 0.417	¹²² 0.187									
329	VTS-003	⁵⁶ 0.015	⁶⁶ 0.007	⁶² 0.003	⁶⁴ 0.048	⁶⁴ 0.033	⁵⁹ 0.019	²⁵¹ 1.000	²⁴⁴ 1.000	⁹⁹ 0.632	⁶⁹ 0.014	⁹⁷ 0.005	¹³⁷ 0.954	⁶¹ 0.060	¹⁷⁵ 0.635	³⁹ 0.089									
330	XFORWARDAI-000	⁸⁶ 0.029	¹⁰³ 0.015	¹⁰⁴ 0.006	⁹⁴ 0.070	¹⁰² 0.053	¹¹¹ 0.034	⁴⁷ 0.698	³⁵ 0.440	⁴⁶ 0.250	⁸⁹ 0.021	⁸⁸ 0.011	⁷³ 0.159	⁸⁰ 0.082	⁷⁰ 0.169	⁸⁴ 0.134									
331	XFORWARDAI-001	³⁹ 0.010	⁵⁰ 0.005	⁵⁰ 0.003	⁴⁸ 0.036	⁵⁴ 0.028	⁶⁰ 0.020	⁶¹ 0.838	³⁶ 0.448	²⁸ 0.143	⁴⁶ 0.008	⁵⁶ 0.005	³⁵ 0.062	³⁶ 0.030	⁴¹ 0.123	⁵² 0.102									
332	XFORWARDAI-002	²⁵ 0.007	³⁰ 0.003	⁴⁵ 0.002	²² 0.018	²² 0.016	³⁰ 0.014	⁹¹ 0.975	⁴⁶ 0.525	⁹ 0.095	²³ 0.005	³⁰ 0.003	²¹ 0.041	²⁰ 0.018	²⁷ 0.099	³² 0.089									
333	YISHENG-001	²⁷⁹ 0.452	²⁹¹ 0.346	²⁹³ 0.206	³¹¹ 0.983	³⁰⁷ 0.808	²⁸³ 0.269				²⁴⁰ 0.666	²⁵³ 0.396				²¹³ 0.919	²¹⁰ 0.695								
334	YITU-002	⁹⁰ 0.031	¹¹¹ 0.018	¹¹⁵ 0.008	⁷⁹ 0.063	⁸⁸ 0.049	⁸⁹ 0.028																		
335	YITU-003	⁹¹ 0.032	¹¹⁹ 0.019	¹²⁶ 0.009	⁸⁷ 0.067	⁹⁷ 0.052	¹⁰⁶ 0.033																		
336	YITU-004	⁶¹ 0.019	⁷⁶ 0.010	⁸⁰ 0.004	⁴⁷ 0.035	⁴⁹ 0.027	⁵¹ 0.017	⁸³ 0.948	⁹⁷ 0.936	¹³⁸ 0.913															
337	YITU-005	⁶⁵ 0.022	⁸³ 0.010	⁸⁶ 0.005	⁵³ 0.039	⁶² 0.032	⁷³ 0.023																		

Table 40: **Threshold-based accuracy.** Values are FNIR(N , T , L) with $N = 1.6$ million with thresholds set to produce FPIR = 0.0003, 0.001, and 0.01 in non-mate searches. Throughout blue superscripts indicate the rank of the algorithm for that column. Caution: The Power-low models are mostly intended to draw attention to the kind of behavior, not as a model to be used for prediction.

2023 / 03 / 14

14:32:11

 $\text{FNIR}(N, T, L) =$

False neg. identification rate
False pos. identification rate

 $N = \text{Num. enrolled subjects}$ $T = \text{Threshold}$

$T = 0 \rightarrow \text{Investigation}$
 $T > 0 \rightarrow \text{Identification}$

Appendices

Appendix A Accuracy on large-population FRVT 2018 mugshots

2023/03/14 14:32:11	$\text{FNIR}(N, R, T) =$ $\text{FPTR}(N, T) =$	False neg. identification rate False pos. identification rate	$N =$ Num. enrolled subjects $R =$ Num. candidates examined	$T =$ Threshold $T > 0 \rightarrow$ Identification	$T = 0 \rightarrow$ Investigation
------------------------	---	--	--	---	-----------------------------------

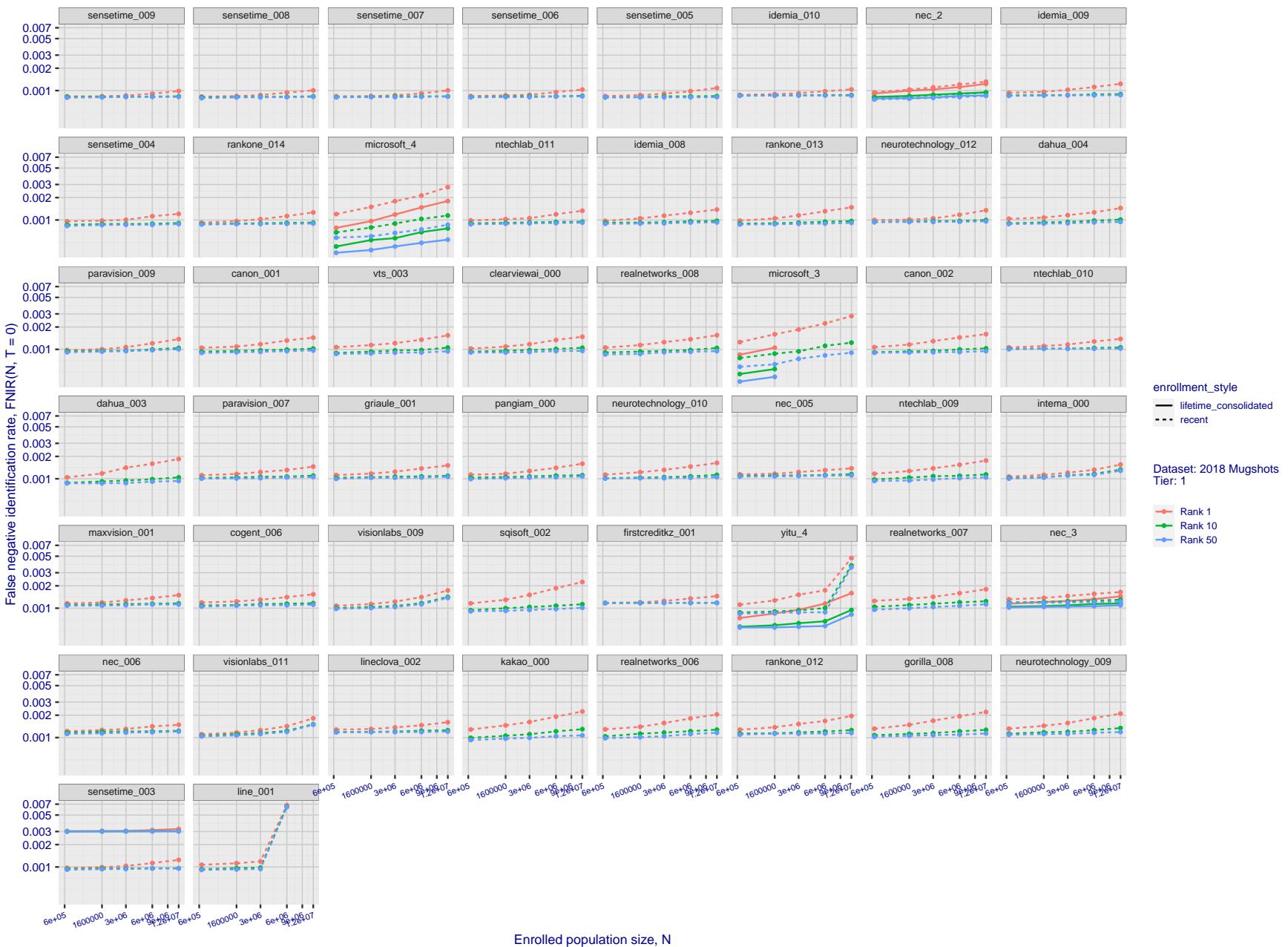


Figure 20: [FRVT-2018 Mugshot Dataset] Rank-based identification miss rates vs. number of enrolled subjects. The figure shows false negative identification rates, FNIR(N, R), across various gallery sizes and ranks 1, 10 and 50. The threshold is set to zero, so this metric rewards even weak scoring rank 1 mates. This also means FPIR = 1, so any search without an enrolled mate will return non-mated candidates. For clarity, results are sorted and reported into tiers spanning multiple pages, the tiering criteria being rank 1 hit rate on a gallery size of 640 000.

2023/03/14

14:32:11

FNIR($N, R, T = 0$)
FPIR($N, T = 0$)
False neg. identification rate
False pos. identification rateN = Num. enrolled subjects
R = Num. candidates examined

T = Threshold

T = 0 → Investigation
T > 0 → Identification

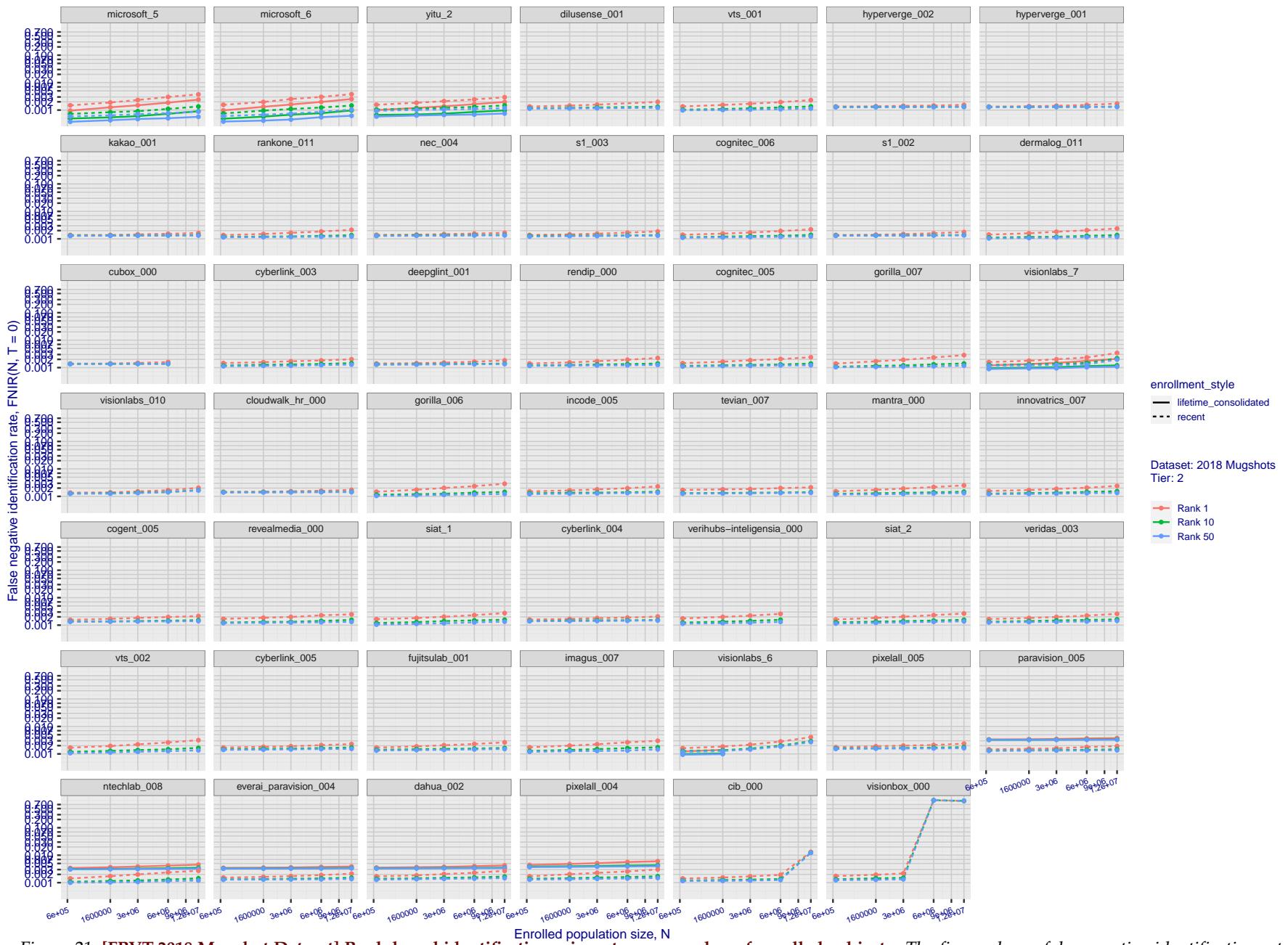


Figure 21: [FRVT-2018 Mugshot Dataset] Rank-based identification miss rates vs. number of enrolled subjects. The figure shows false negative identification rates, $\text{FNIR}(N, R)$, across various gallery sizes and ranks 1, 10 and 50. The threshold is set to zero, so this metric rewards even weak scoring rank 1 mates. This also means $\text{FPIR} = 1$, so any search without an enrolled mate will return non-mated candidates. For clarity, results are sorted and reported into tiers spanning multiple pages, the tiering criteria being rank 1 hit rate on a gallery size of 640 000.

2023/03/14

14:32:11

FNIR($N, R, T =$
False neg. identification rate
 $FPIR(N, T) =$
False pos. identification rate $N = \text{Num. enrolled subjects}$

T = Threshold

 $T = 0 \rightarrow \text{Investigation}$ $T > 0 \rightarrow \text{Identification}$

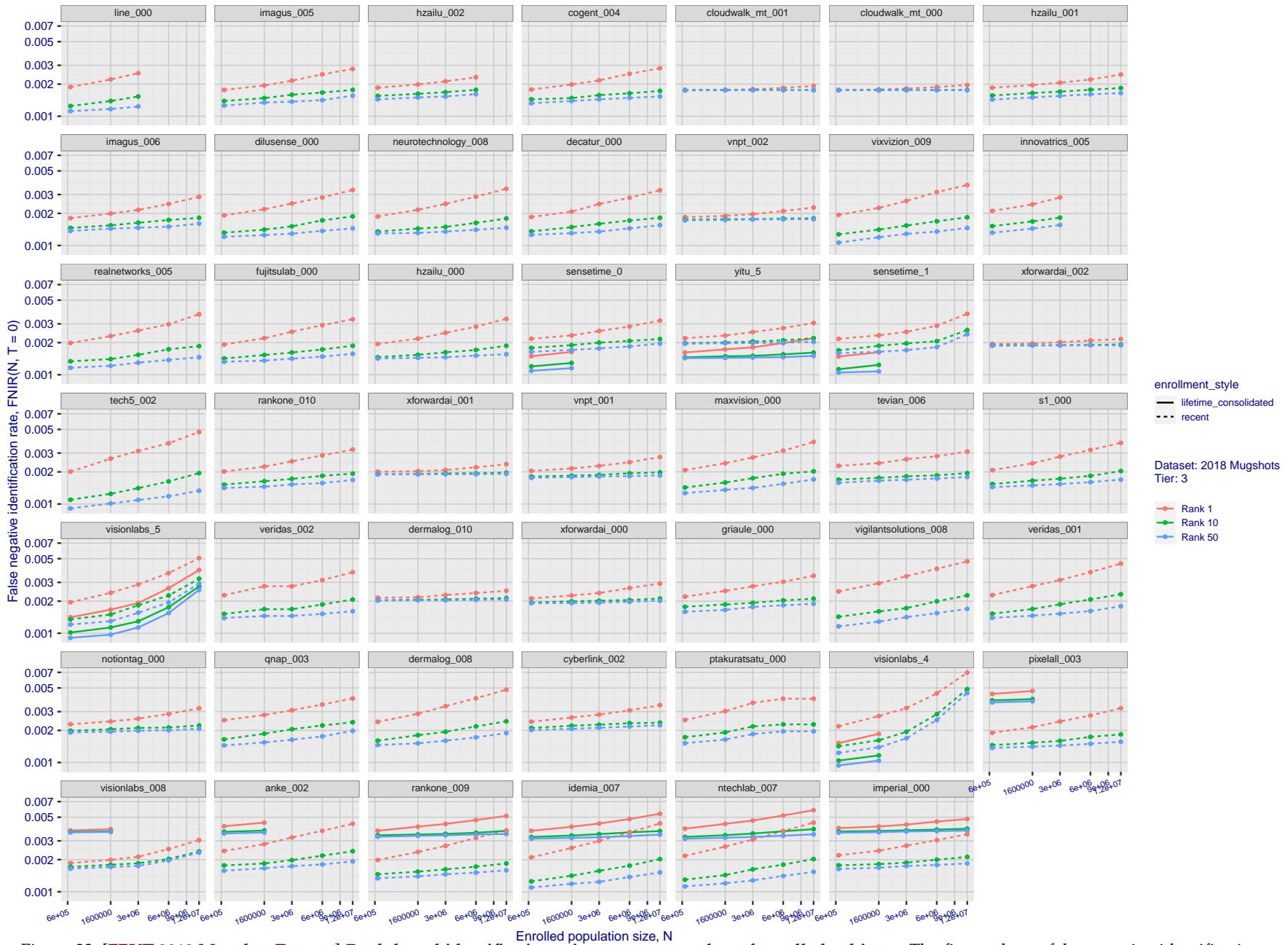
2023/03/14
14:32:11FNIR(N, R, T) = False neg. identification rate
FPIR(N, T) = False pos. identification rateN = Num. enrolled subjects
R = Num. candidates examinedT = Threshold
T = 0 → Investigation
T > 0 → Identification

Figure 22: [FRVT-2018 Mugshot Dataset] Rank-based identification miss rates vs. number of enrolled subjects. The figure shows false negative identification rates, $\text{FNIR}(N, R)$, across various gallery sizes and ranks 1, 10 and 50. The threshold is set to zero, so this metric rewards even weak scoring rank 1 mates. This also means $\text{FPIR} = 1$, so any search without an enrolled mate will return non-mated candidates. For clarity, results are sorted and reported into tiers spanning multiple pages, the tiering criteria being rank 1 hit rate on a gallery size of 640 000.

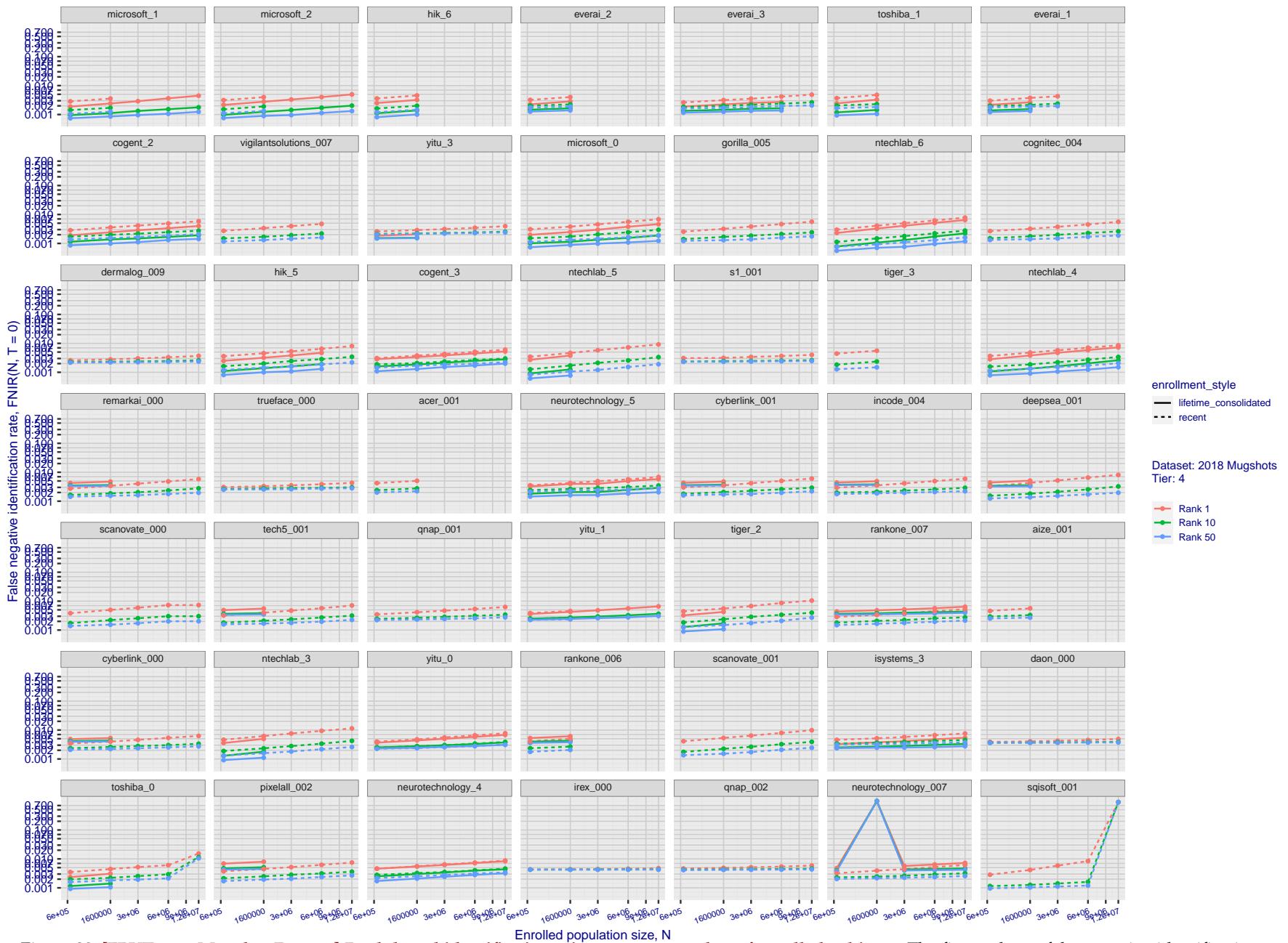


Figure 23: [FRVT-2018 Mugshot Dataset] Rank-based identification miss rates vs. number of enrolled subjects. The figure shows false negative identification rates, $\text{FNIR}(N, R)$, across various gallery sizes and ranks 1, 10 and 50. The threshold is set to zero, so this metric rewards even weak scoring rank 1 mates. This also means $\text{FPIR} = 1$, so any search without an enrolled mate will return non-mated candidates. For clarity, results are sorted and reported into tiers spanning multiple pages, the tiering criteria being rank 1 hit rate on a gallery size of 640 000.

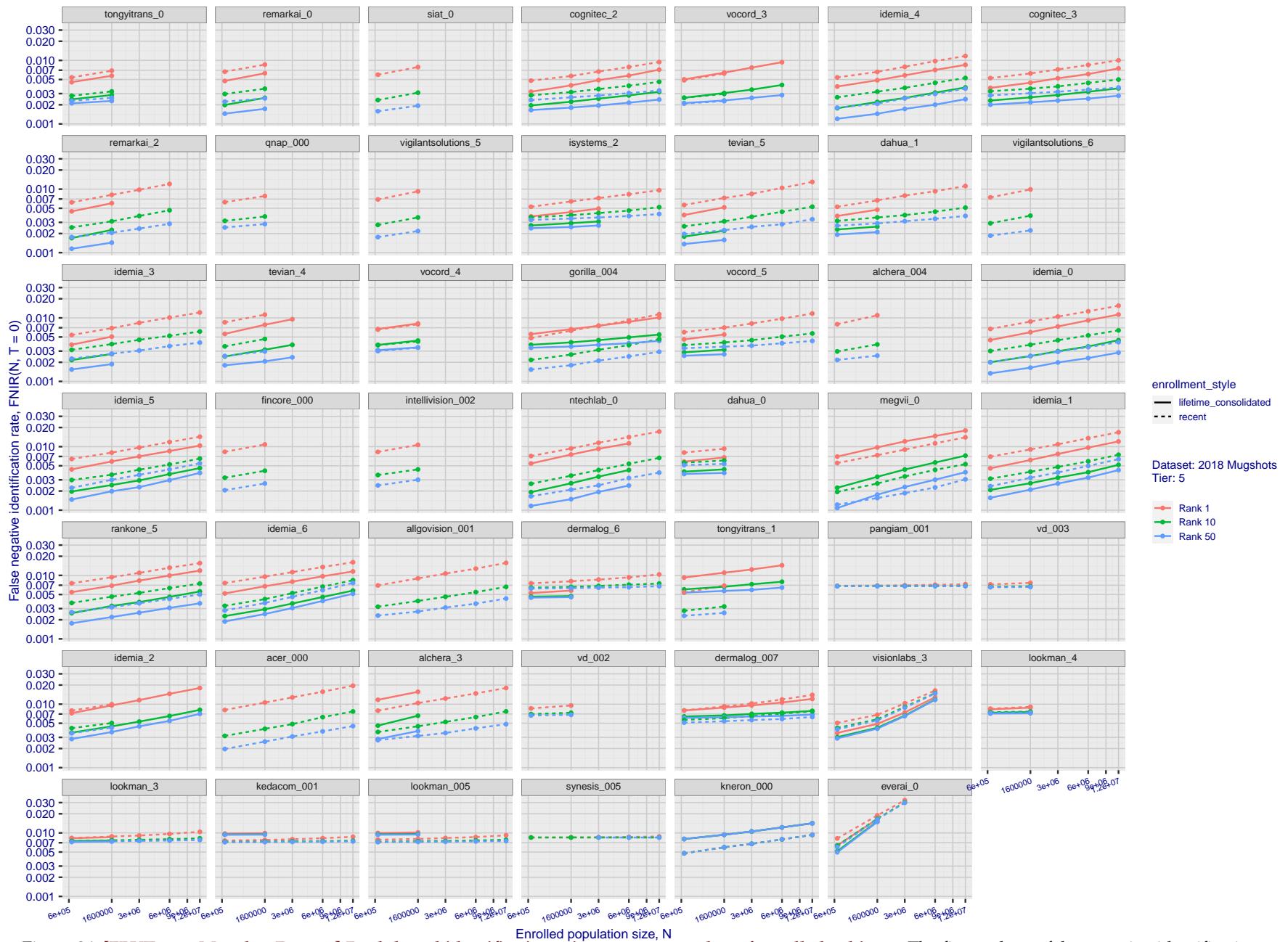


Figure 24: [FRVT-2018 Mugshot Dataset] Rank-based identification miss rates vs. number of enrolled subjects. The figure shows false negative identification rates, $\text{FNIR}(N, R)$, across various gallery sizes and ranks 1, 10 and 50. The threshold is set to zero, so this metric rewards even weak scoring rank 1 mates. This also means $\text{FPIR} = 1$, so any search without an enrolled mate will return non-mated candidates. For clarity, results are sorted and reported into tiers spanning multiple pages, the tiering criteria being rank 1 hit rate on a gallery size of 640 000.

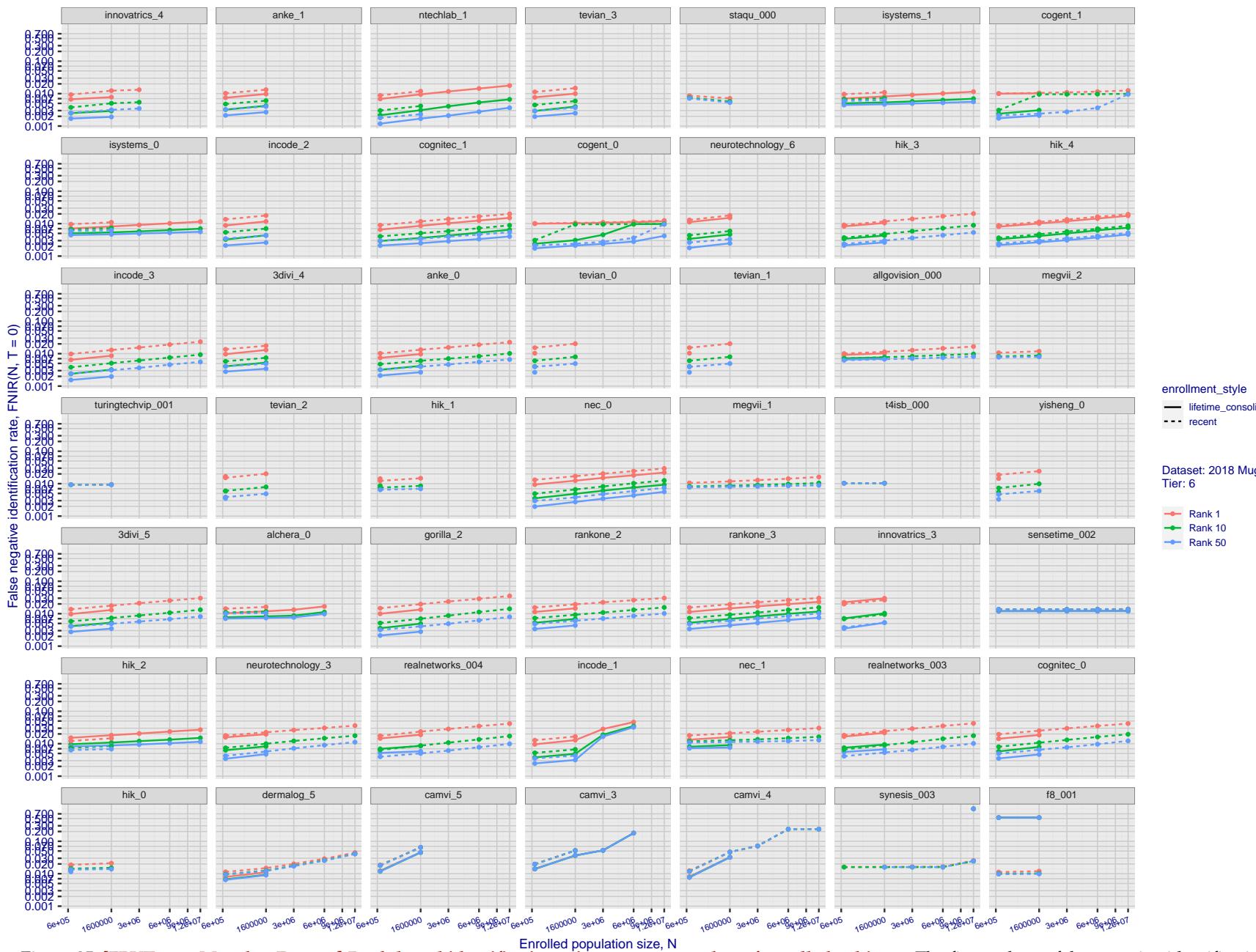


Figure 25: [FRVT-2018 Mugshot Dataset] Rank-based identification miss rates vs. number of enrolled subjects. The figure shows false negative identification rates, $\text{FNIR}(N, R)$, across various gallery sizes and ranks 1, 10 and 50. The threshold is set to zero, so this metric rewards even weak scoring rank 1 mates. This also means $\text{FPIR} = 1$, so any search without an enrolled mate will return non-mated candidates. For clarity, results are sorted and reported into tiers spanning multiple pages, the tiering criteria being rank 1 hit rate on a gallery size of 640 000.

2023/03/14

14:32:11

FNIR($N, R, T = 0$) = False neg. identification rate
FPIR($N, T = 0$) = False pos. identification rate $N = \text{Num. enrolled subjects}$ $T = \text{Threshold}$ $T = 0 \rightarrow \text{Investigation}$
 $T > 0 \rightarrow \text{Identification}$

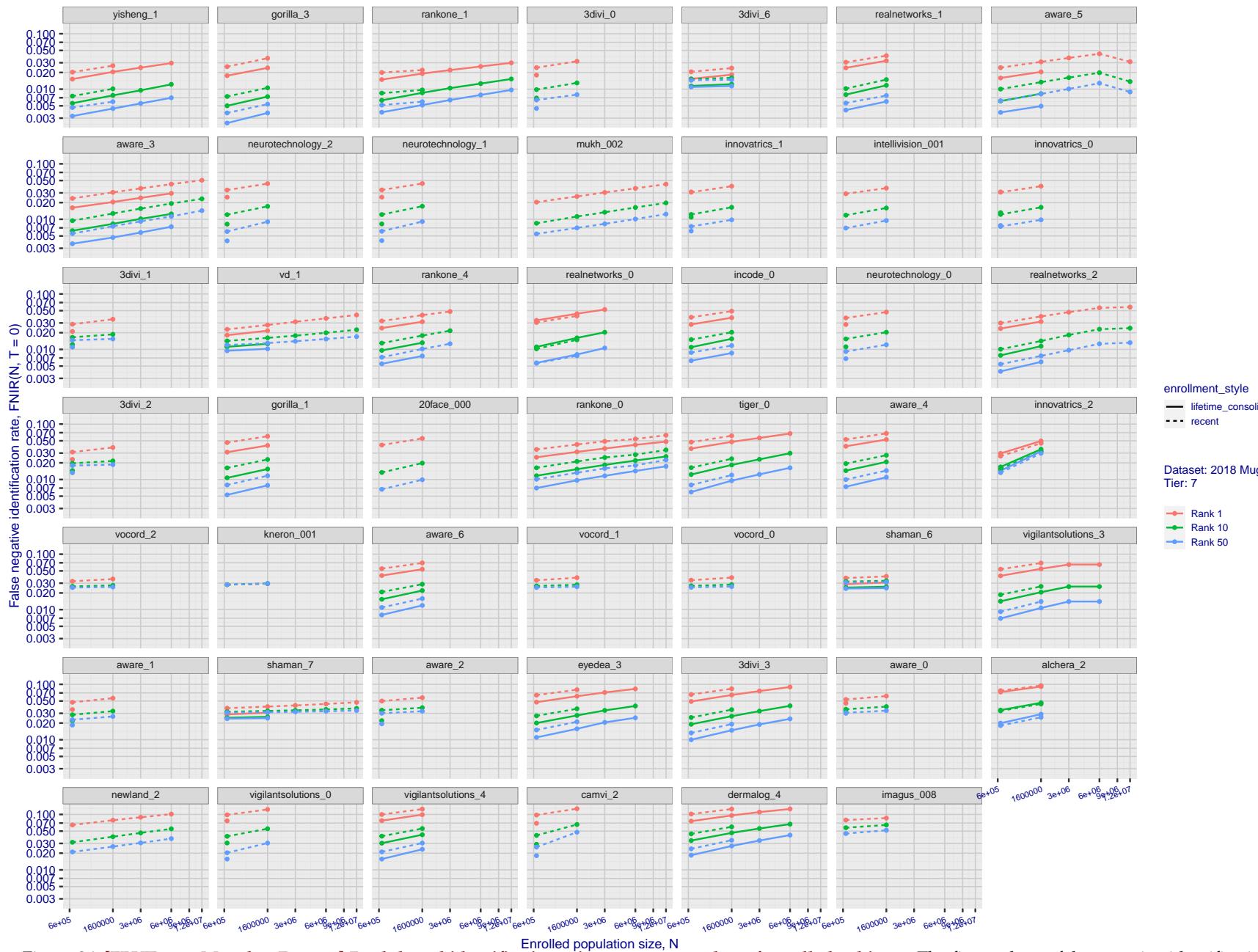


Figure 26: [FRVT-2018 Mugshot Dataset] Rank-based identification miss rates vs. number of enrolled subjects. The figure shows false negative identification rates, $\text{FNIR}(N, R)$, across various gallery sizes and ranks 1, 10 and 50. The threshold is set to zero, so this metric rewards even weak scoring rank 1 mates. This also means $\text{FPIR} = 1$, so any search without an enrolled mate will return non-mated candidates. For clarity, results are sorted and reported into tiers spanning multiple pages, the tiering criteria being rank 1 hit rate on a gallery size of 640 000.

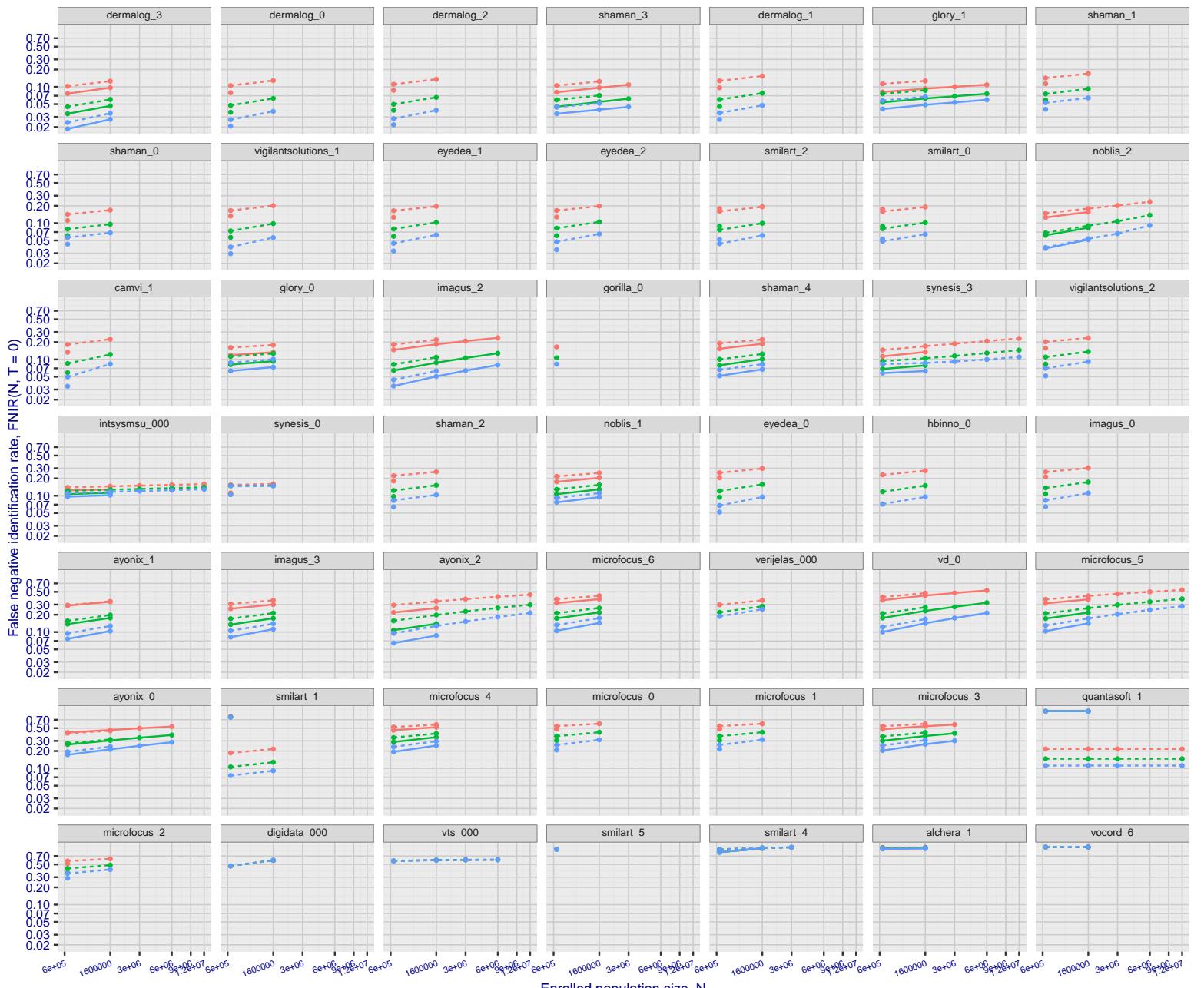


Figure 27: [FRVT-2018 Mugshot Dataset] Rank-based identification miss rates vs. number of enrolled subjects. The figure shows false negative identification rates, $\text{FNIR}(N, R)$, across various gallery sizes and ranks 1, 10 and 50. The threshold is set to zero, so this metric rewards even weak scoring rank 1 mates. This also means $\text{FPIR} = 1$, so any search without an enrolled mate will return non-mated candidates. For clarity, results are sorted and reported into tiers spanning multiple pages, the tiering criteria being rank 1 hit rate on a gallery size of 640 000.

2023/03/14
14:32:11FNIR(N, R, T) = False neg. identification rate
FPIR(N, T) = False pos. identification rateN = Num. enrolled subjects
R = Num. candidates examinedT = Threshold
 $T = 0 \rightarrow$ Investigation
 $T > 0 \rightarrow$ Identification

2023/03/14 14:32:11	$\text{FNIR}(N, R, T) =$ $\text{FPTR}(N, T) =$	False neg. identification rate False pos. identification rate	$N =$ Num. enrolled subjects $R =$ Num. candidates examined	$T =$ Threshold $T > 0 \rightarrow$ Identification	$T = 0 \rightarrow$ Investigation
------------------------	---	--	--	---	-----------------------------------

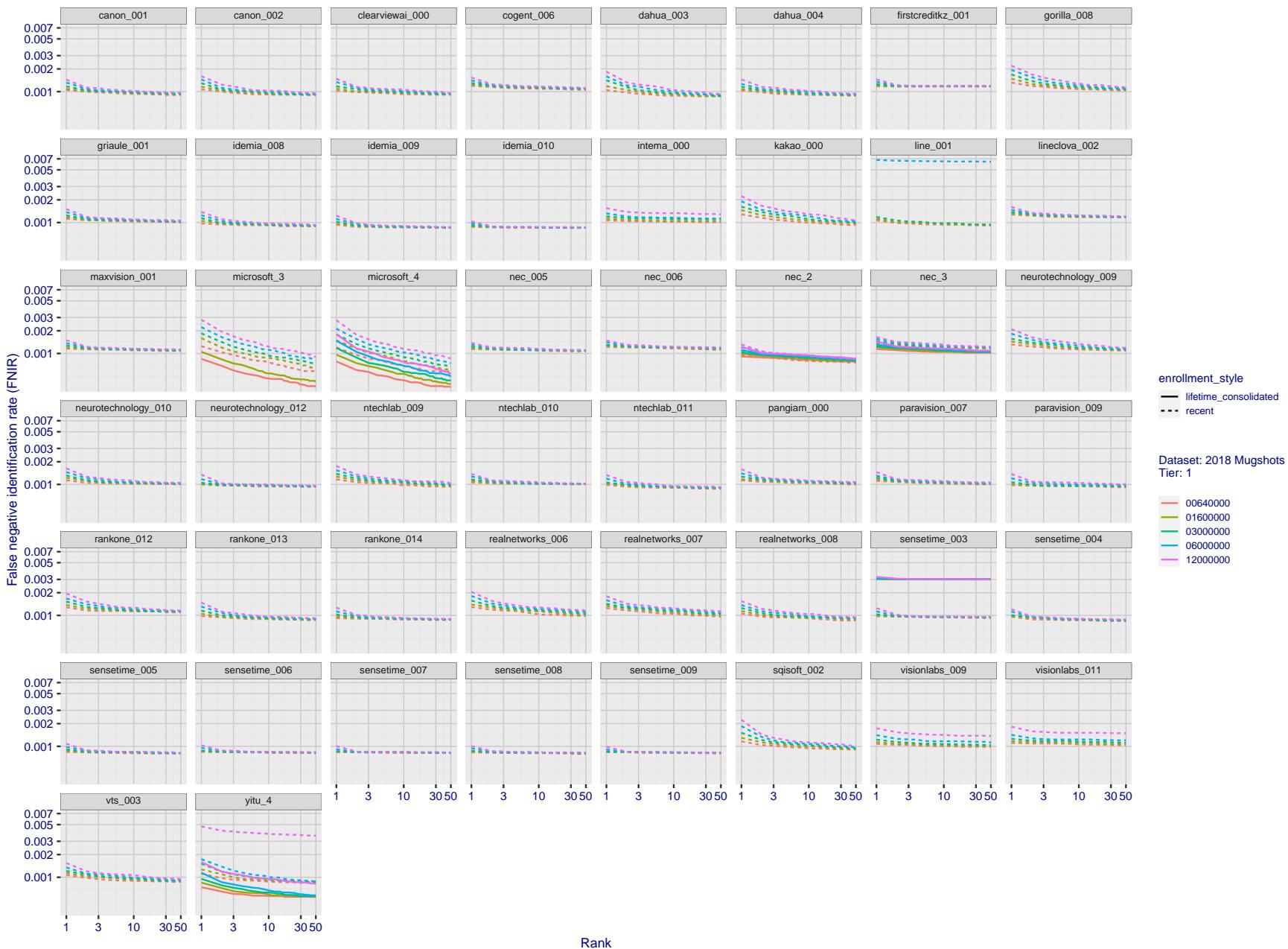


Figure 28: [FRVT-2018 Mugshot Dataset] Rank-based identification miss rates vs. rank. The figure shows false negative identification rates (FNIR) for ranks up to 50. This metric is appropriate to investigational applications where human reviewers will adjudicate sorted candidate lists. Note that with threshold set to zero, FPIR = 1, i.e. any search without an enrolled mate will return non-mated candidates. Results are sorted and reported into tiers for clarity, with the tiering criteria being rank 1 hit rate on a gallery size of $N = 640\,000$ subjects.

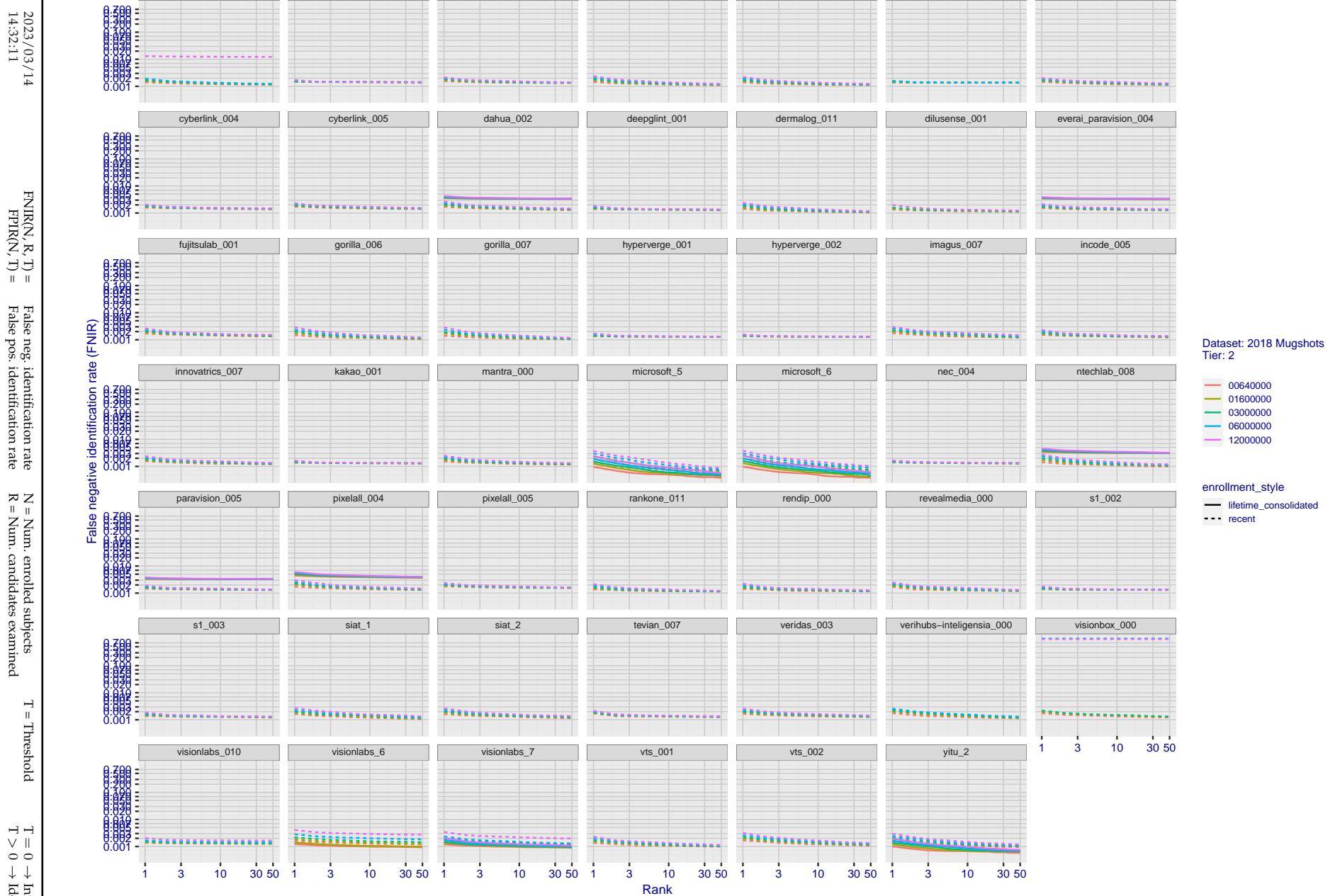


Figure 29: [FRVT-2018 Mugshot Dataset] Rank-based identification miss rates vs. rank. The figure shows false negative identification rates (FNIR) for ranks up to 50. This metric is appropriate to investigational applications where human reviewers will adjudicate sorted candidate lists. Note that with threshold set to zero, FPIR = 1, i.e. any search without an enrolled mate will return non-mated candidates. Results are sorted and reported into tiers for clarity, with the tiering criteria being rank 1 hit rate on a gallery size of N = 640 000 subjects.

2023/03/14
14:32:11FNIR(N, R, T) = False neg. identification rate
FPIR(N, T) = False pos. identification rateN = Num. enrolled subjects
R = Num. candidates examined

T = Threshold

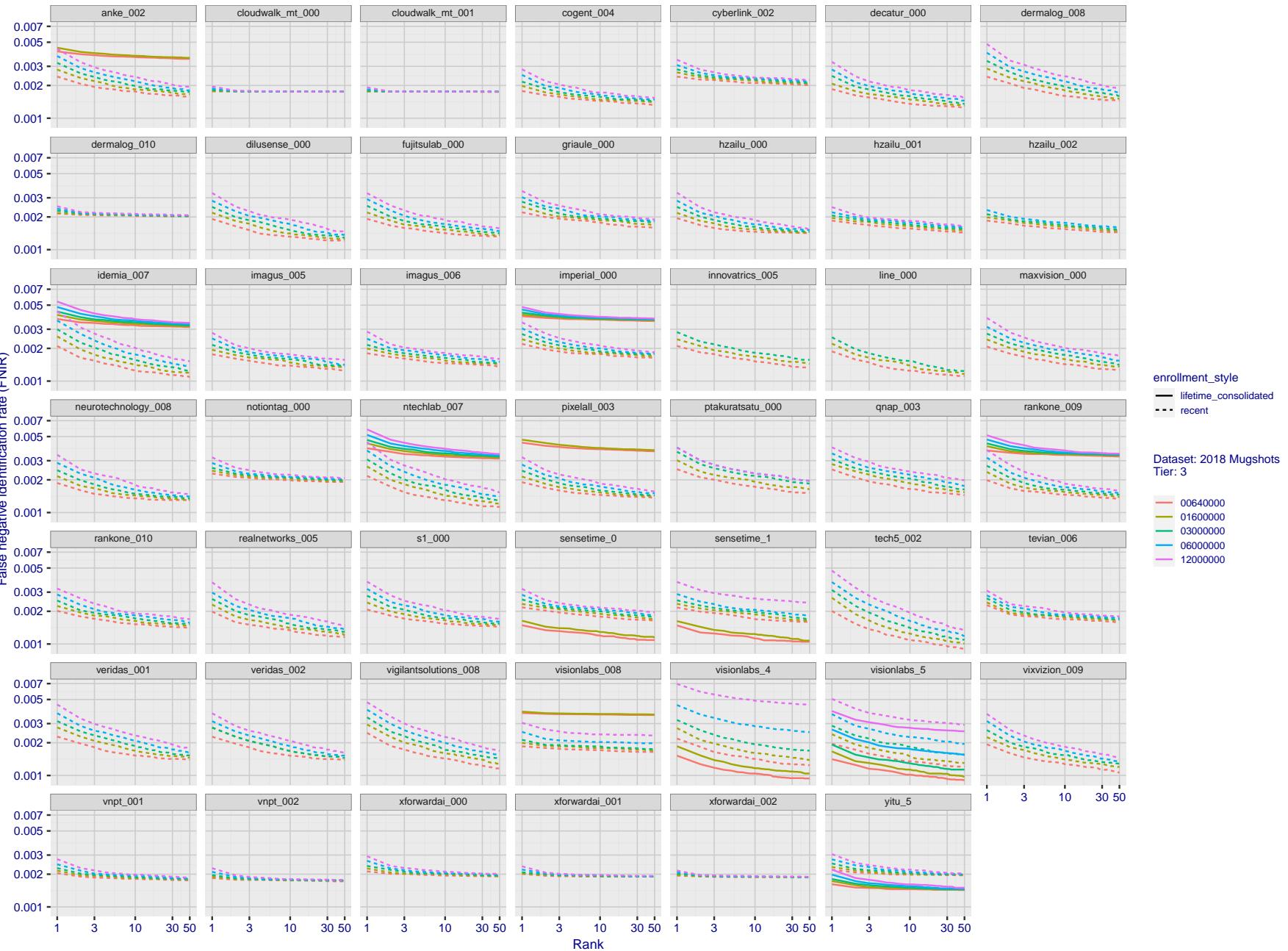
T = 0 → Investigation
T > 0 → Identification

Figure 30: [FRVT-2018 Mugshot Dataset] Rank-based identification miss rates vs. rank. The figure shows false negative identification rates (FNIR) for ranks up to 50. This metric is appropriate to investigational applications where human reviewers will adjudicate sorted candidate lists. Note that with threshold set to zero, FPIR = 1, i.e. any search without an enrolled mate will return non-mated candidates. Results are sorted and reported into tiers for clarity, with the tiering criteria being rank 1 hit rate on a gallery size of N = 640 000 subjects.

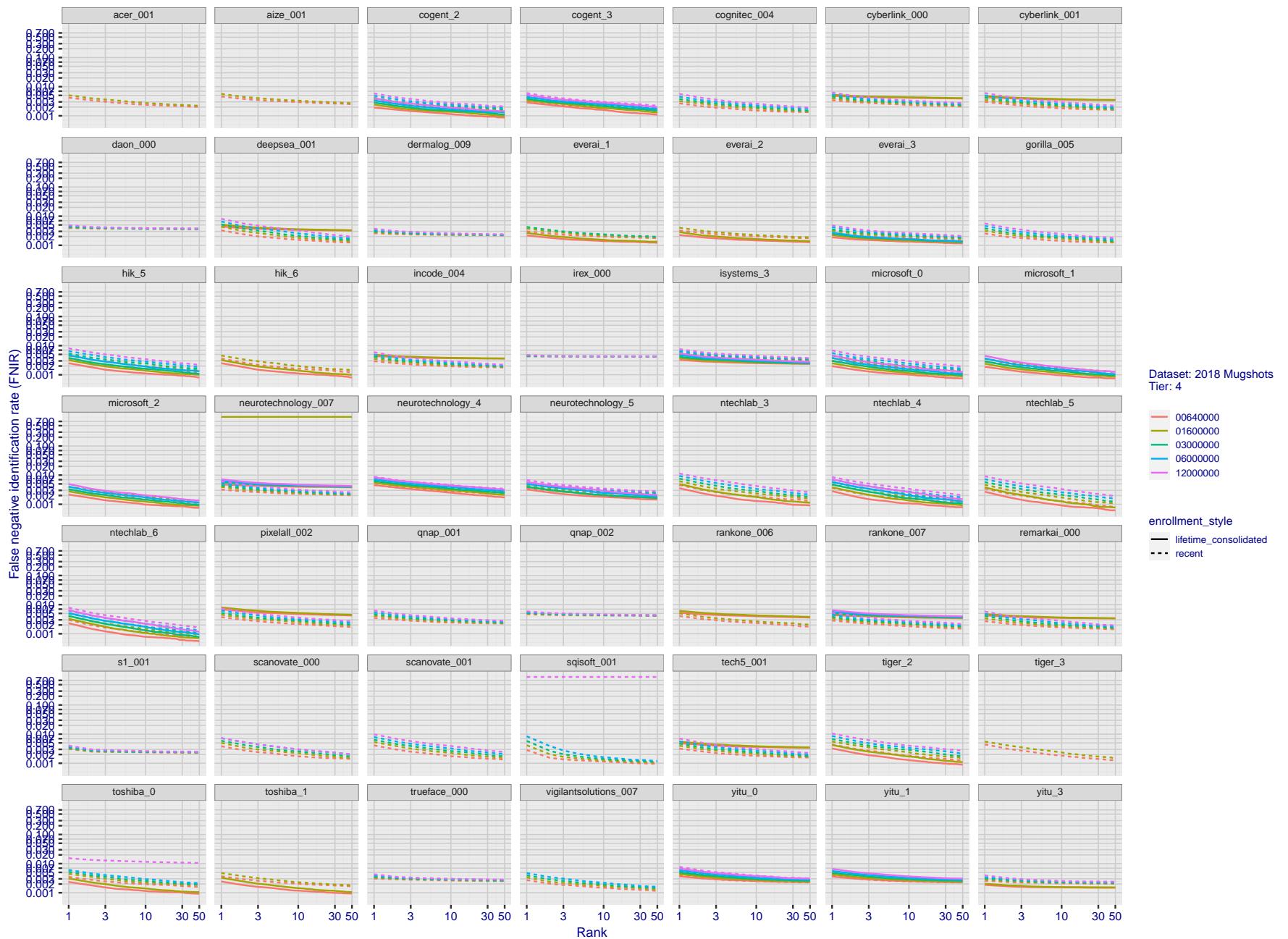


Figure 31: [FRVT-2018 Mugshot Dataset] Rank-based identification miss rates vs. rank. The figure shows false negative identification rates (FNIR) for ranks up to 50. This metric is appropriate to investigational applications where human reviewers will adjudicate sorted candidate lists. Note that with threshold set to zero, FPIR = 1, i.e. any search without an enrolled mate will return non-mated candidates. Results are sorted and reported into tiers for clarity, with the tiering criteria being rank 1 hit rate on a gallery size of $N = 640\,000$ subjects.

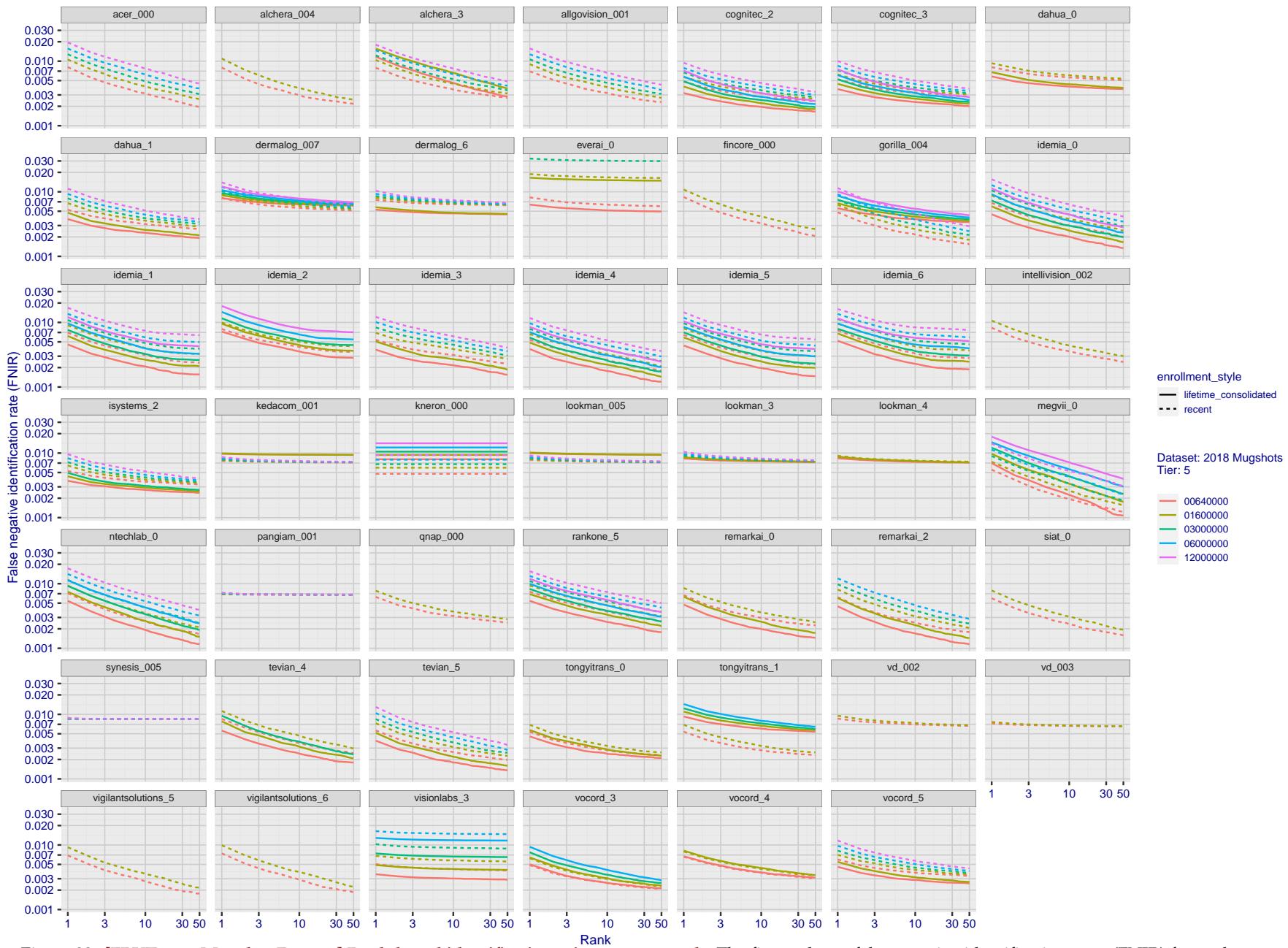


Figure 32: [FRVT-2018 Mugshot Dataset] Rank-based identification miss rates vs. rank. The figure shows false negative identification rates (FNIR) for ranks up to 50. This metric is appropriate to investigational applications where human reviewers will adjudicate sorted candidate lists. Note that with threshold set to zero, FPIR = 1, i.e. any search without an enrolled mate will return non-mated candidates. Results are sorted and reported into tiers for clarity, with the tiering criteria being rank 1 hit rate on a gallery size of $N = 640\,000$ subjects.

2023 /03 /14

FNIR(N, R, T) = False neg. identification rate

N = Num. enrolled subjects

T = Threshold

R = Num. candidates examined

FPIR(N, T) = False pos. identification rate

14:32:11

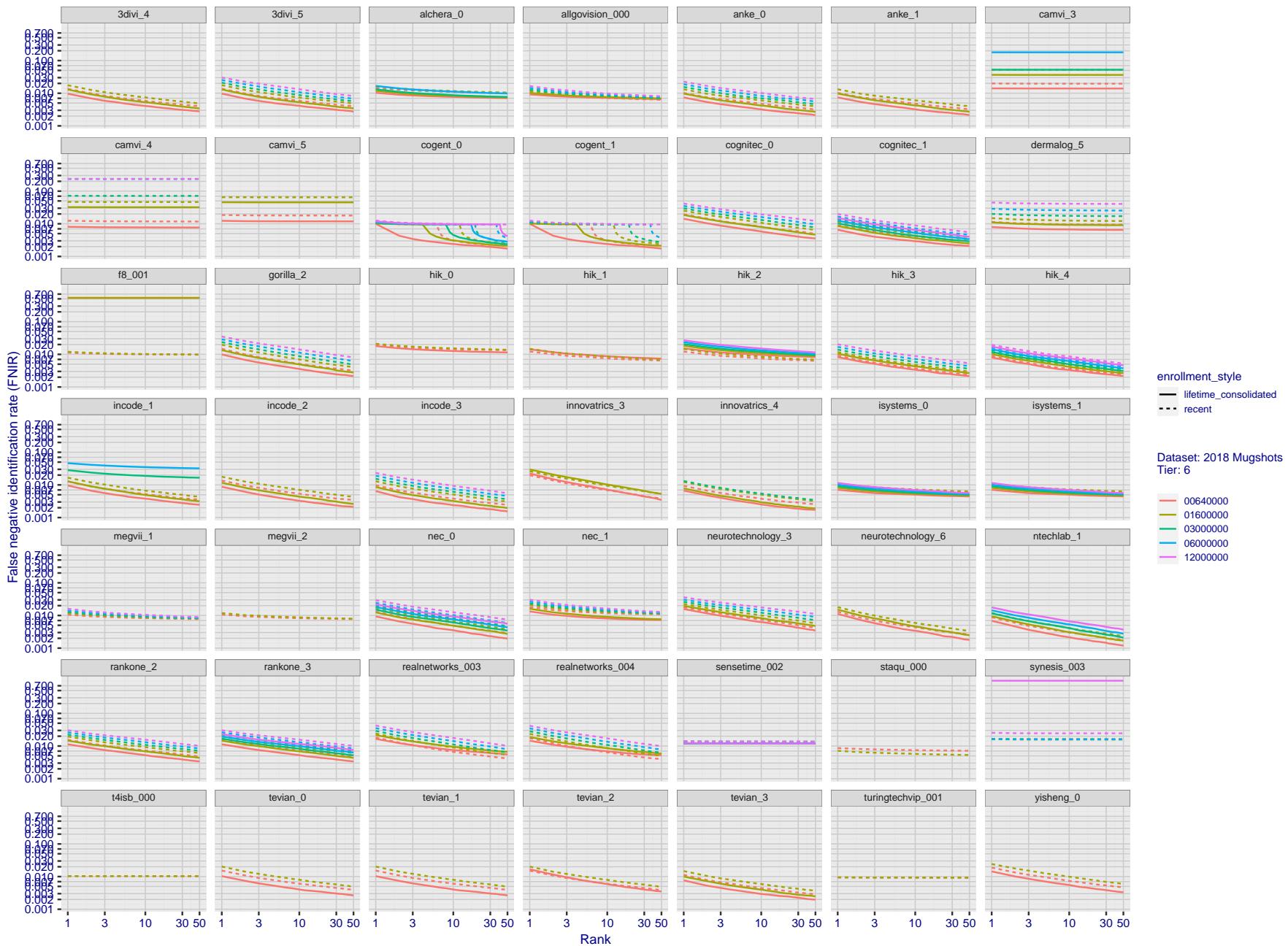


Figure 33: [FRVT-2018 Mugshot Dataset] Rank-based identification miss rates vs. rank. The figure shows false negative identification rates (FNIR) for ranks up to 50. This metric is appropriate to investigational applications where human reviewers will adjudicate sorted candidate lists. Note that with threshold set to zero, FPIR = 1, i.e. any search without an enrolled mate will return non-mated candidates. Results are sorted and reported into tiers for clarity, with the tiering criteria being rank 1 hit rate on a gallery size of $N = 640\,000$ subjects.

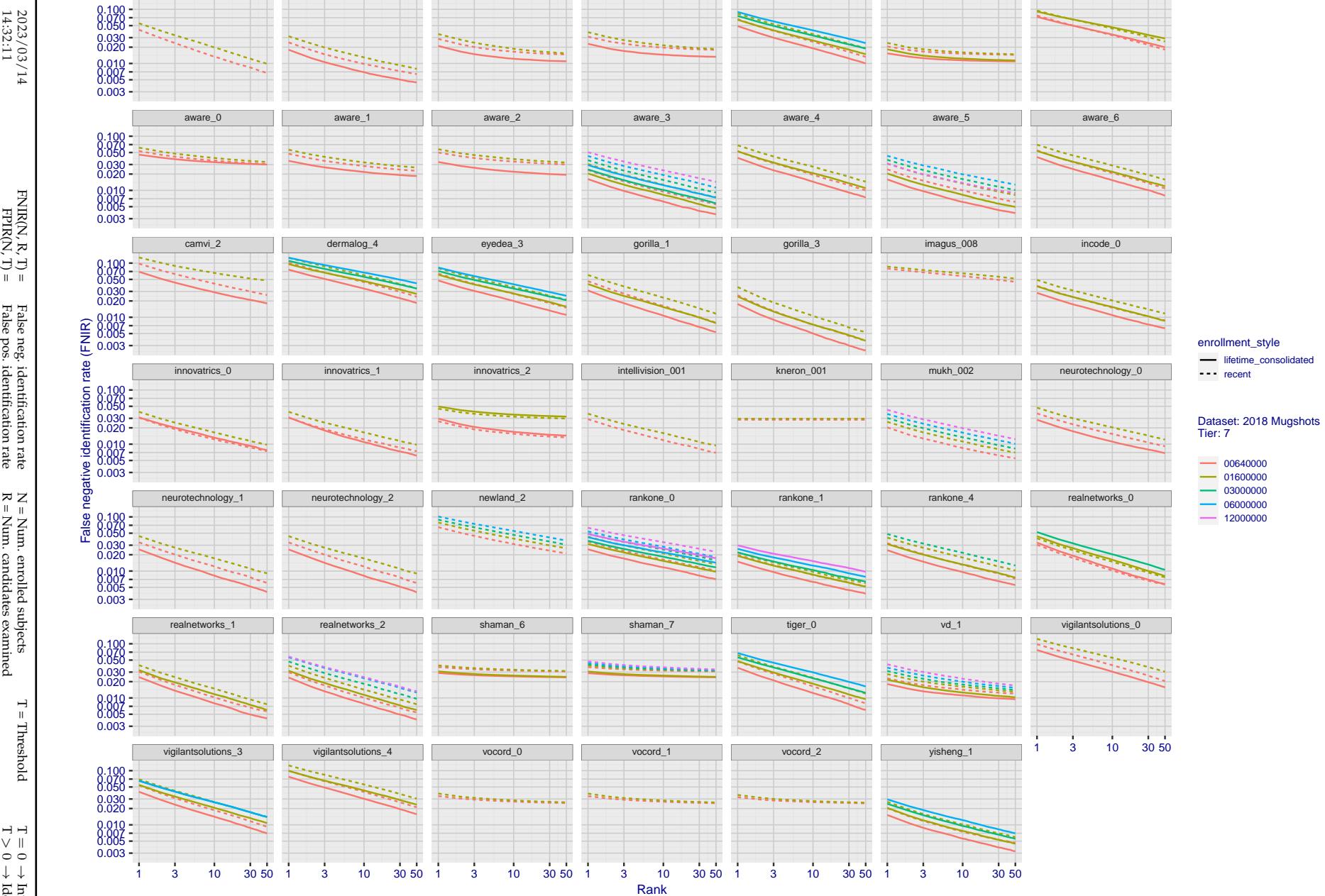


Figure 34: [FRVT-2018 Mugshot Dataset] Rank-based identification miss rates vs. rank. The figure shows false negative identification rates (FNIR) for ranks up to 50. This metric is appropriate to investigational applications where human reviewers will adjudicate sorted candidate lists. Note that with threshold set to zero, FPIR = 1, i.e. any search without an enrolled mate will return non-mated candidates. Results are sorted and reported into tiers for clarity, with the tiering criteria being rank 1 hit rate on a gallery size of N = 640 000 subjects.

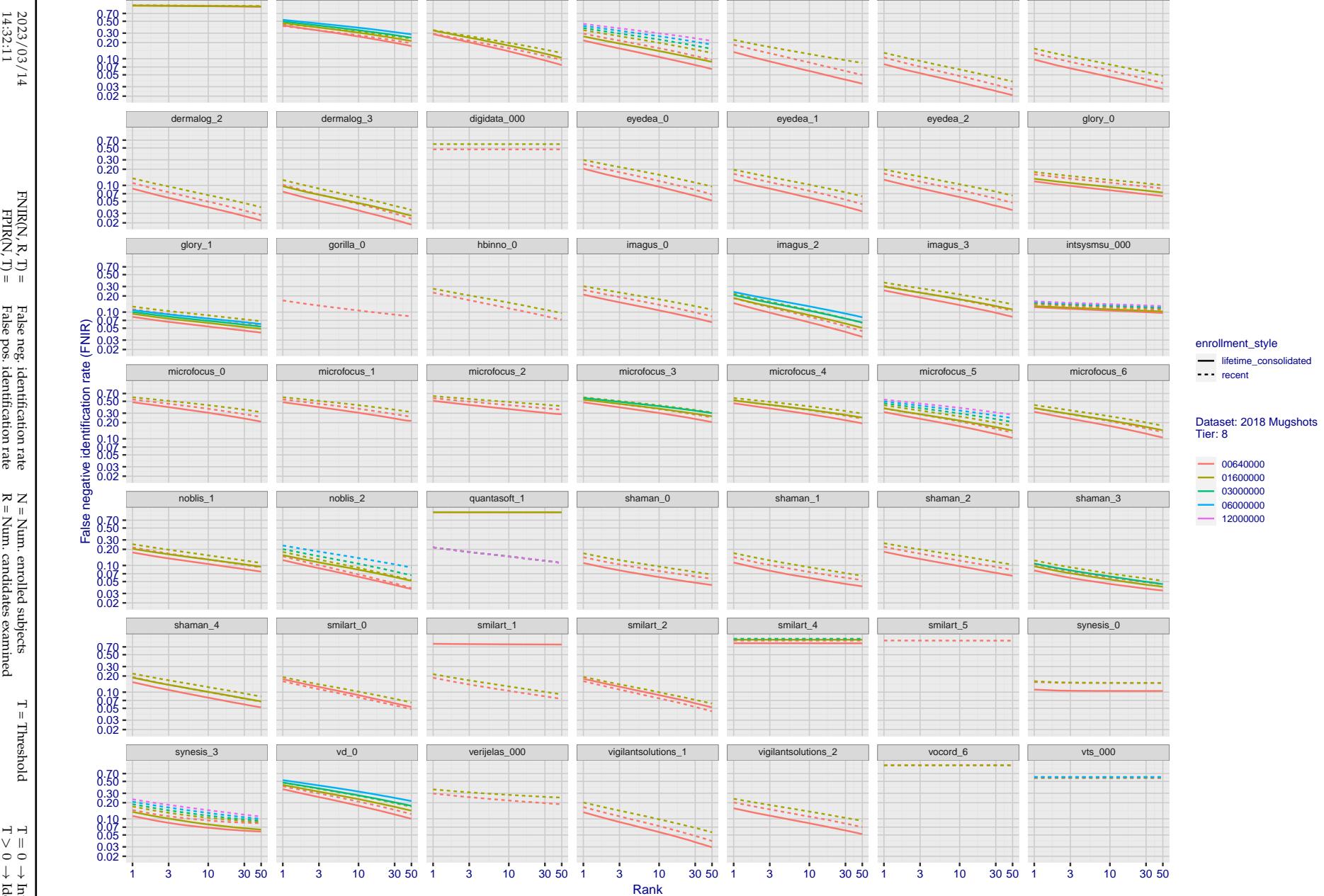


Figure 35: [FRVT-2018 Mugshot Dataset] Rank-based identification miss rates vs. rank. The figure shows false negative identification rates (FNIR) for ranks up to 50. This metric is appropriate to investigational applications where human reviewers will adjudicate sorted candidate lists. Note that with threshold set to zero, FPIR = 1, i.e. any search without an enrolled mate will return non-mated candidates. Results are sorted and reported into tiers for clarity, with the tiering criteria being rank 1 hit rate on a gallery size of N = 640 000 subjects.

2023/03/14 14:32:11	$\text{FNIR}(N, R, T) =$ $\text{FPTR}(N, T) =$	False neg. identification rate False pos. identification rate	$N =$ Num. enrolled subjects $R =$ Num. candidates examined	$T =$ Threshold $T > 0 \rightarrow$ Identification	$T = 0 \rightarrow$ Investigation
------------------------	---	--	--	---	-----------------------------------

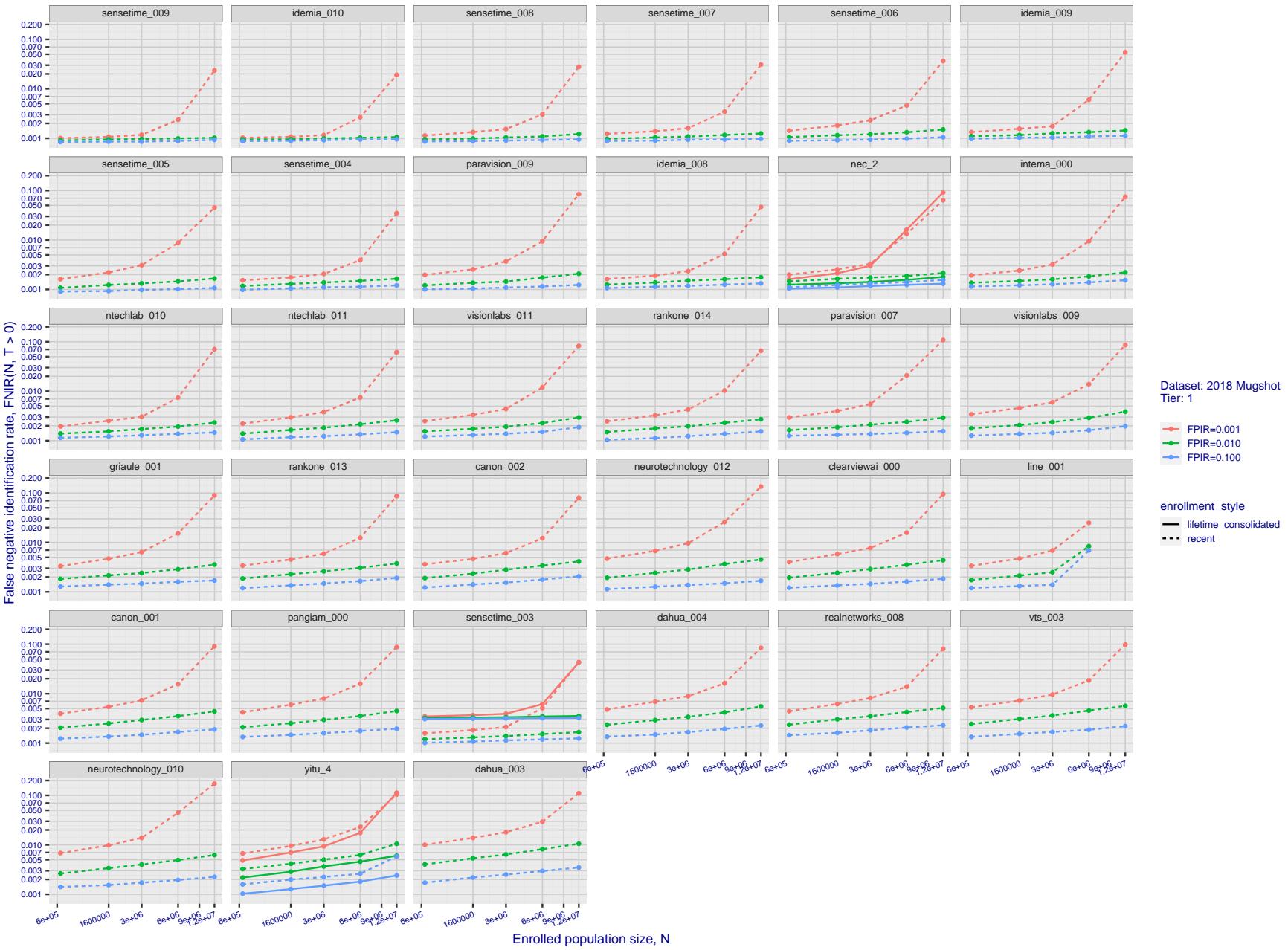
2023/03/14
14:32:11FNIR(N, R, T) = False neg. identification rate
FPIR(N, T) = False pos. identification rateN = Num. enrolled subjects
R = Num. candidates examined
T = ThresholdT = 0 → Investigation
T > 0 → Identification

Figure 36: [FRVT-2018 Mugshot Dataset] Threshold-based identification miss rates vs. number of enrolled subjects. The figure shows $\text{FNIR}(N, T)$ across various gallery sizes when the threshold is set to achieve the given FPIRs. The rank criterion is irrelevant at high thresholds as mates are always at rank 1. The results are computed from the trials listed in rows 1-10 of Table 1. Less accurate algorithms were not run on large N , so results are missing. For clarity, results are sorted and reported into tiers spanning multiple pages. The tiering criteria is complicated: First paging by $\text{FNIR}(N_b, 1, 0)$, then sorting by median $\text{FNIR}(N_b, T)$, $N_b = 640\,000$.

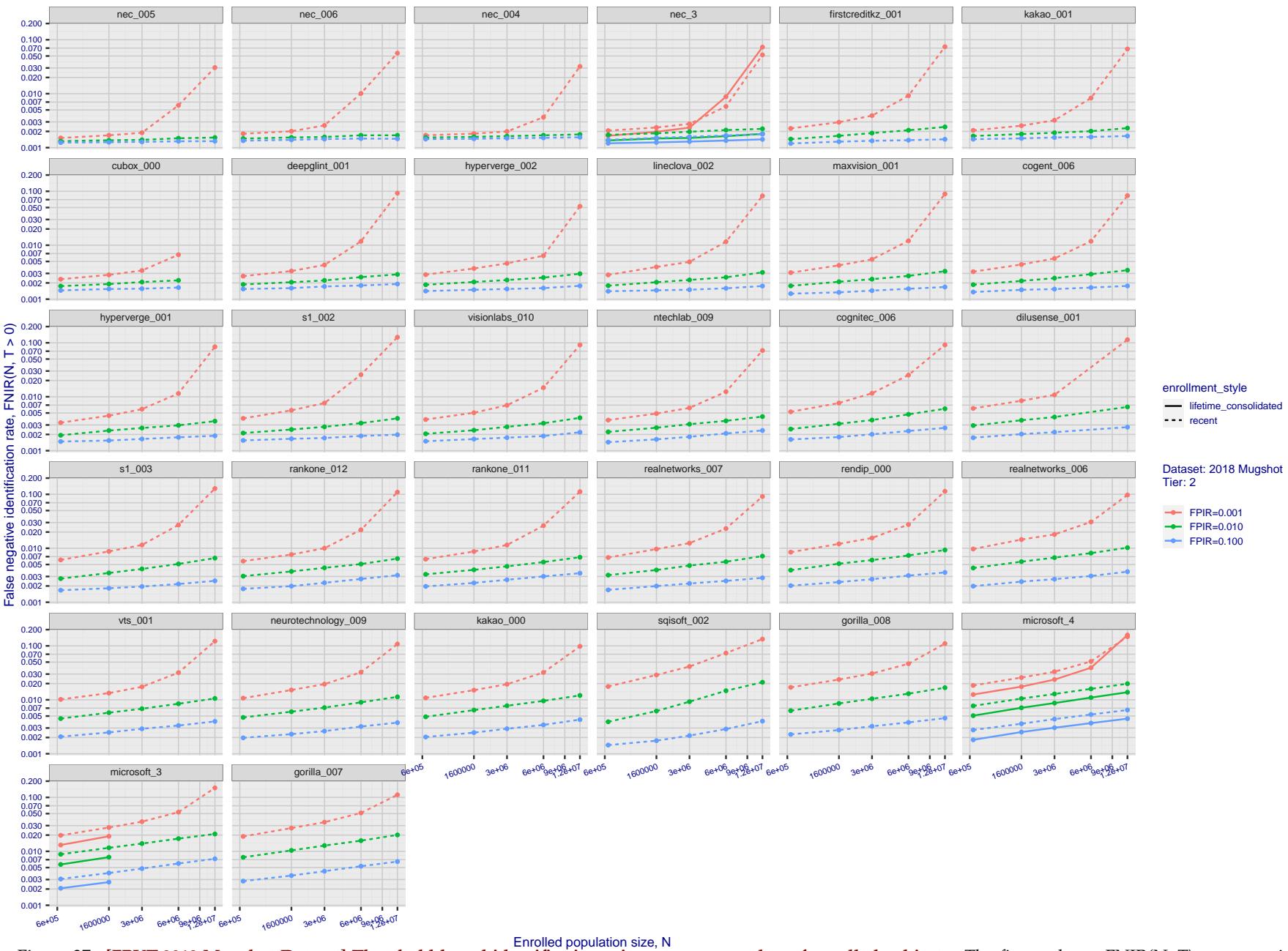
2023 / 03 / 14
14:32:11FNIR(N, R, T) = False neg. identification rate
FPFR(N, T) = False pos. identification rate
N = Num. enrolled subjects
R = Num. candidates examined
T = Threshold
T = 0 → Investigation
T > 0 → Identification

Figure 37: [FRVT-2018 Mugshot Dataset] Threshold-based identification miss rates vs. number of enrolled subjects. The figure shows FNIR(N, T) across various gallery sizes when the threshold is set to achieve the given FPIRs. The rank criterion is irrelevant at high thresholds as mates are always at rank 1. The results are computed from the trials listed in rows 1-10 of Table 1. Less accurate algorithms were not run on large N , so results are missing. For clarity, results are sorted and reported into tiers spanning multiple pages. The tiering criteria is complicated: First paging by $\text{FNIR}(N_b, 1, 0)$, then sorting by median $\text{FNIR}(N_b, T)$, $N_b = 640\,000$.

2023 /03 /14
14:32:11FNIR(N, R, T) = False neg. identification rate
FPFR(N, T) = False pos. identification rateN = Num. enrolled subjects
R = Num. candidates examined

T = Threshold

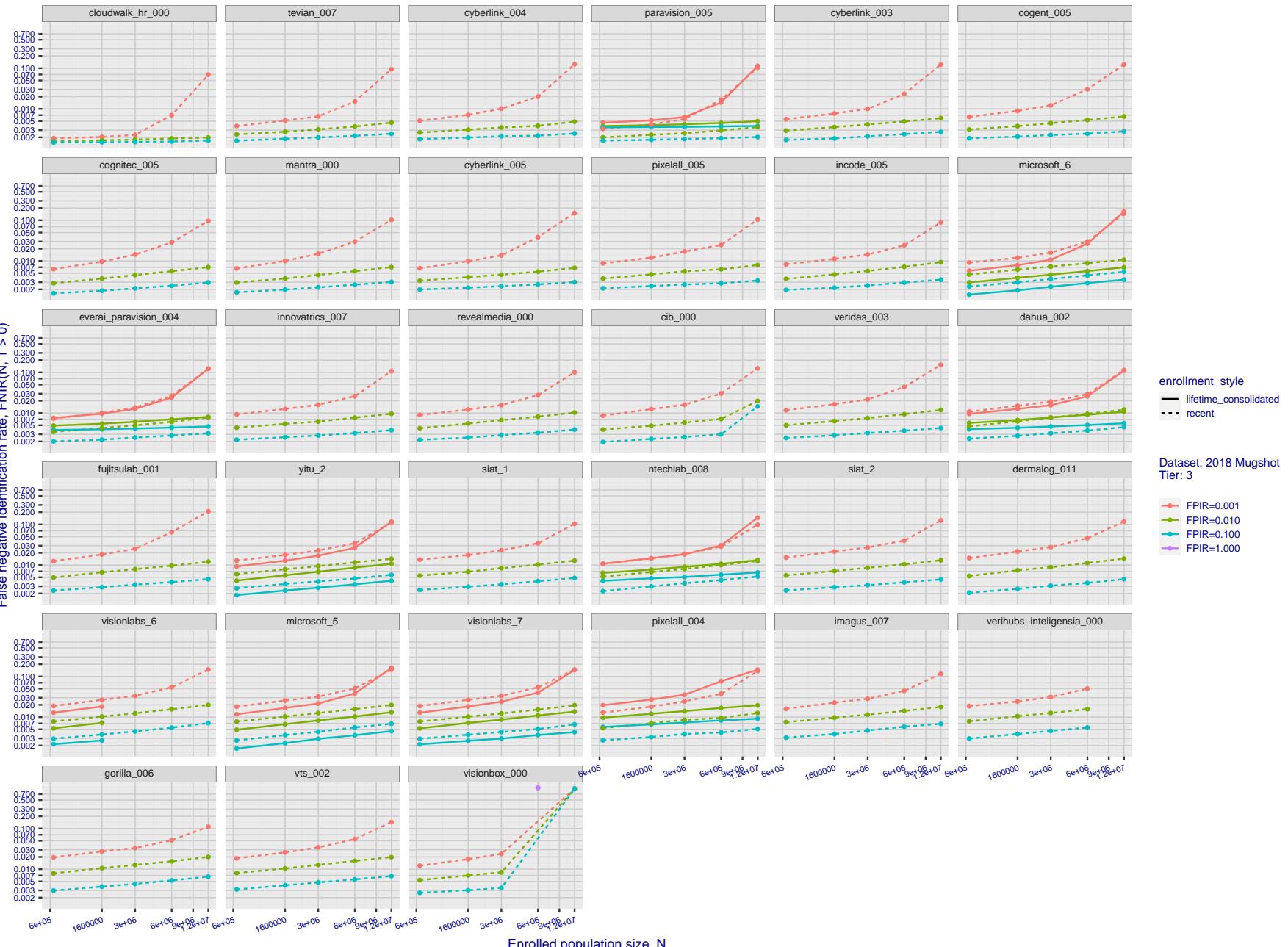
T = 0 → Investigation
T > 0 → Identification

Figure 38: [FRVT-2018 Mugshot Dataset] Threshold-based identification miss rates vs. number of enrolled subjects. The figure shows $\text{FNIR}(N, T)$ across various gallery sizes when the threshold is set to achieve the given FPIRs. The rank criterion is irrelevant at high thresholds as mates are always at rank 1. The results are computed from the trials listed in rows 1-10 of Table 1. Less accurate algorithms were not run on large N , so results are missing. For clarity, results are sorted and reported into tiers spanning multiple pages. The tiering criteria is complicated: First paging by $\text{FNIR}(N_b, 1, 0)$, then sorting by median $\text{FNIR}(N_b, T)$, $N_b = 640,000$.

2023 /03 /14
14:32:11FNIR(N, R, T) = False neg. identification rate
FPFR(N, T) = False pos. identification rateN = Num. enrolled subjects
R = Num. candidates examined

T = Threshold

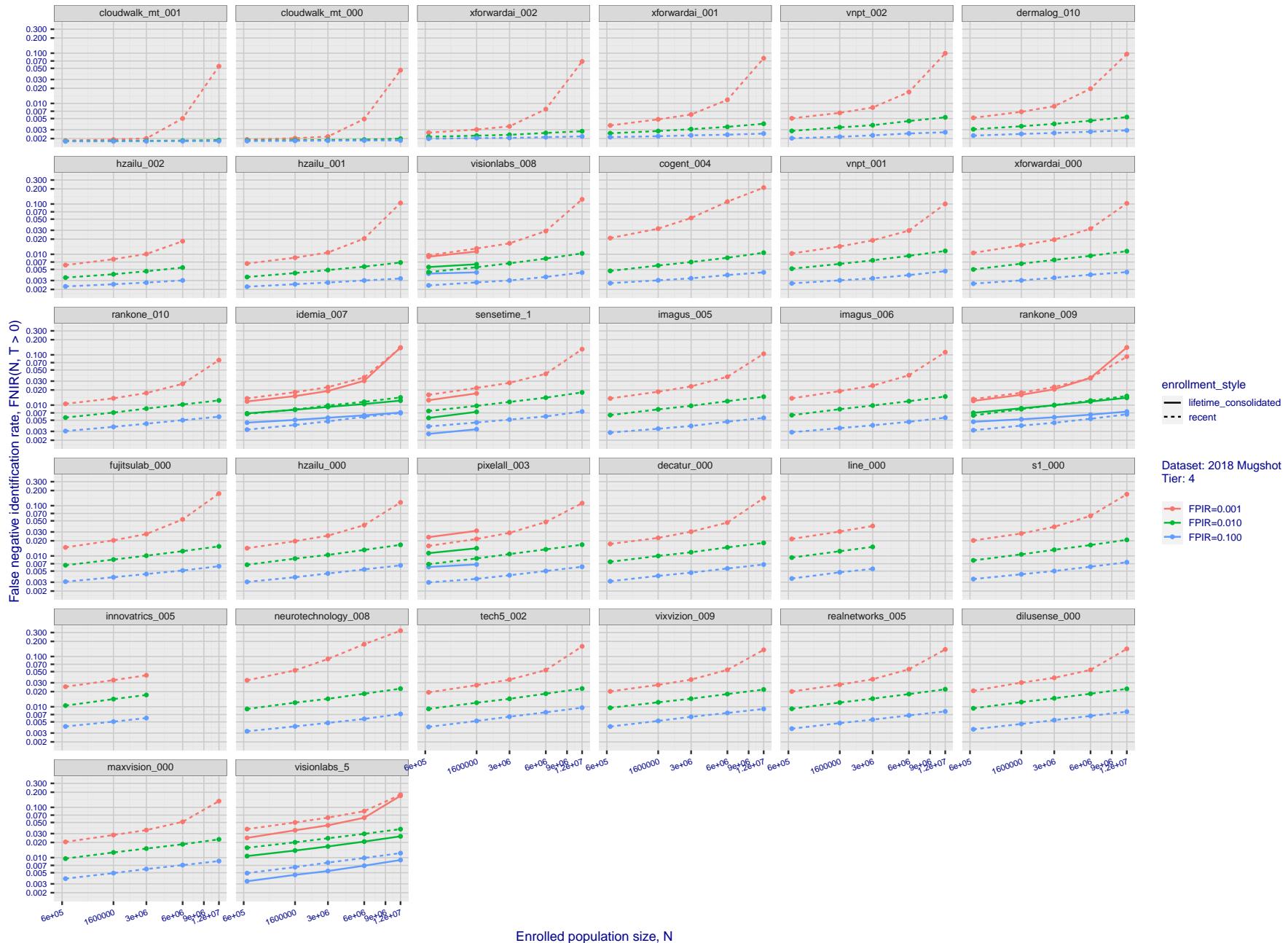
T = 0 → Investigation
T > 0 → Identification

Figure 39: [FRVT-2018 Mugshot Dataset] Threshold-based identification miss rates vs. number of enrolled subjects. The figure shows $\text{FNIR}(N, T)$ across various gallery sizes when the threshold is set to achieve the given FPIRs. The rank criterion is irrelevant at high thresholds as mates are always at rank 1. The results are computed from the trials listed in rows 1-10 of Table 1. Less accurate algorithms were not run on large N , so results are missing. For clarity, results are sorted and reported into tiers spanning multiple pages. The tiering criteria is complicated: First paging by $\text{FNIR}(N_b, 1, 0)$, then sorting by median $\text{FNIR}(N_b, T)$, $N_b = 640\,000$.

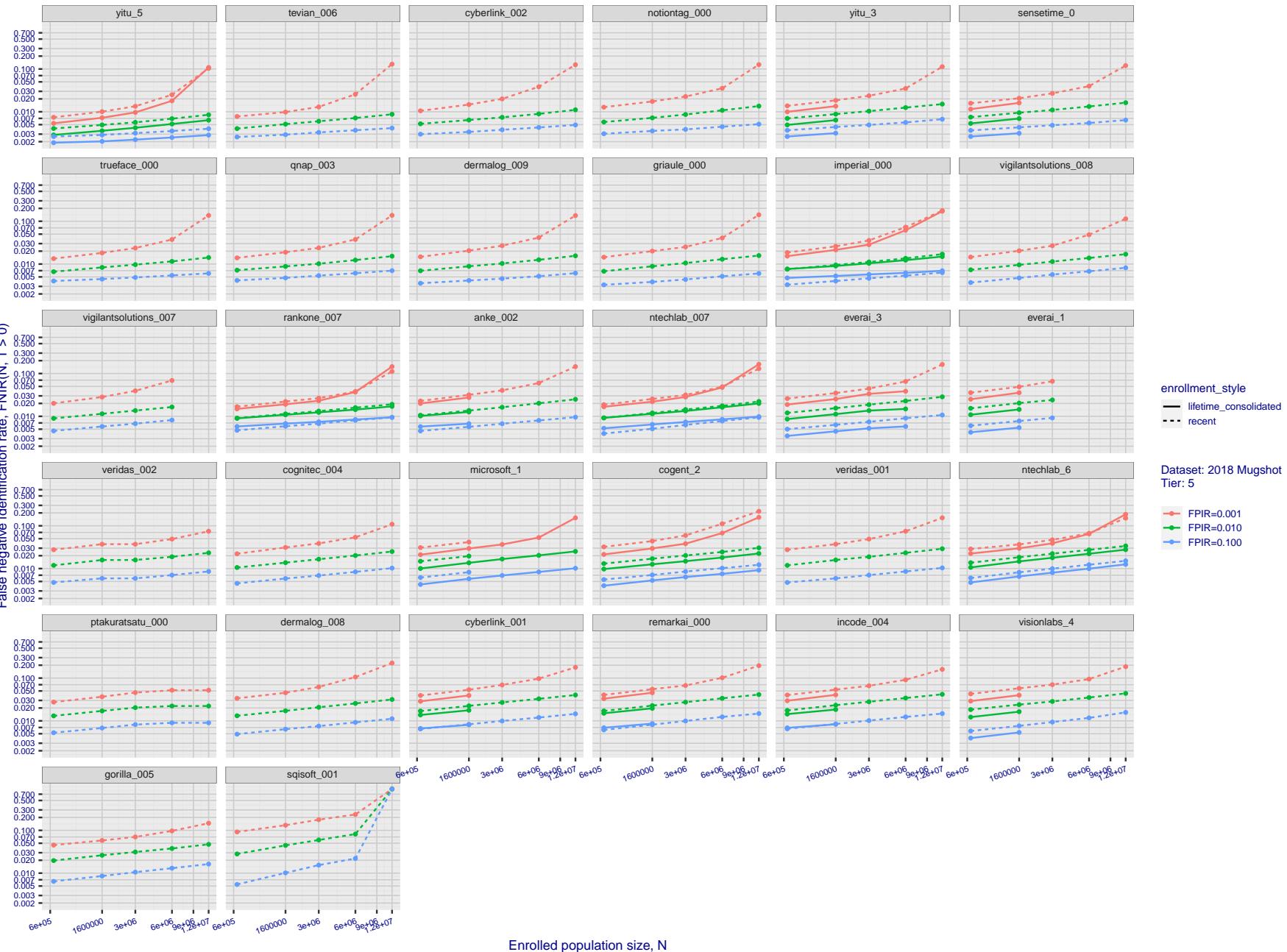
2023 /03 /14
14:32:11FNIR(N, R, T) = False neg. identification rate
FPIR(N, T) = False pos. identification rateN = Num. enrolled subjects
R = Num. candidates examined
T = ThresholdT = 0 → Investigation
T > 0 → Identification

Figure 40: [FRVT-2018 Mugshot Dataset] Threshold-based identification miss rates vs. number of enrolled subjects. The figure shows FNIR(N, T) across various gallery sizes when the threshold is set to achieve the given FPIRs. The rank criterion is irrelevant at high thresholds as mates are always at rank 1. The results are computed from the trials listed in rows 1-10 of Table 1. Less accurate algorithms were not run on large N, so results are missing. For clarity, results are sorted and reported into tiers spanning multiple pages. The tiering criteria is complicated: First paging by FNIR(N_b , 1, 0), then sorting by median FNIR(N_b , T), $N_b = 640\,000$.

2023/03/14
14:32:11FNIR(N, R, T) = False neg. identification rate
FPFR(N, T) = False pos. identification rateN = Num. enrolled subjects
R = Num. candidates examined

T = Threshold

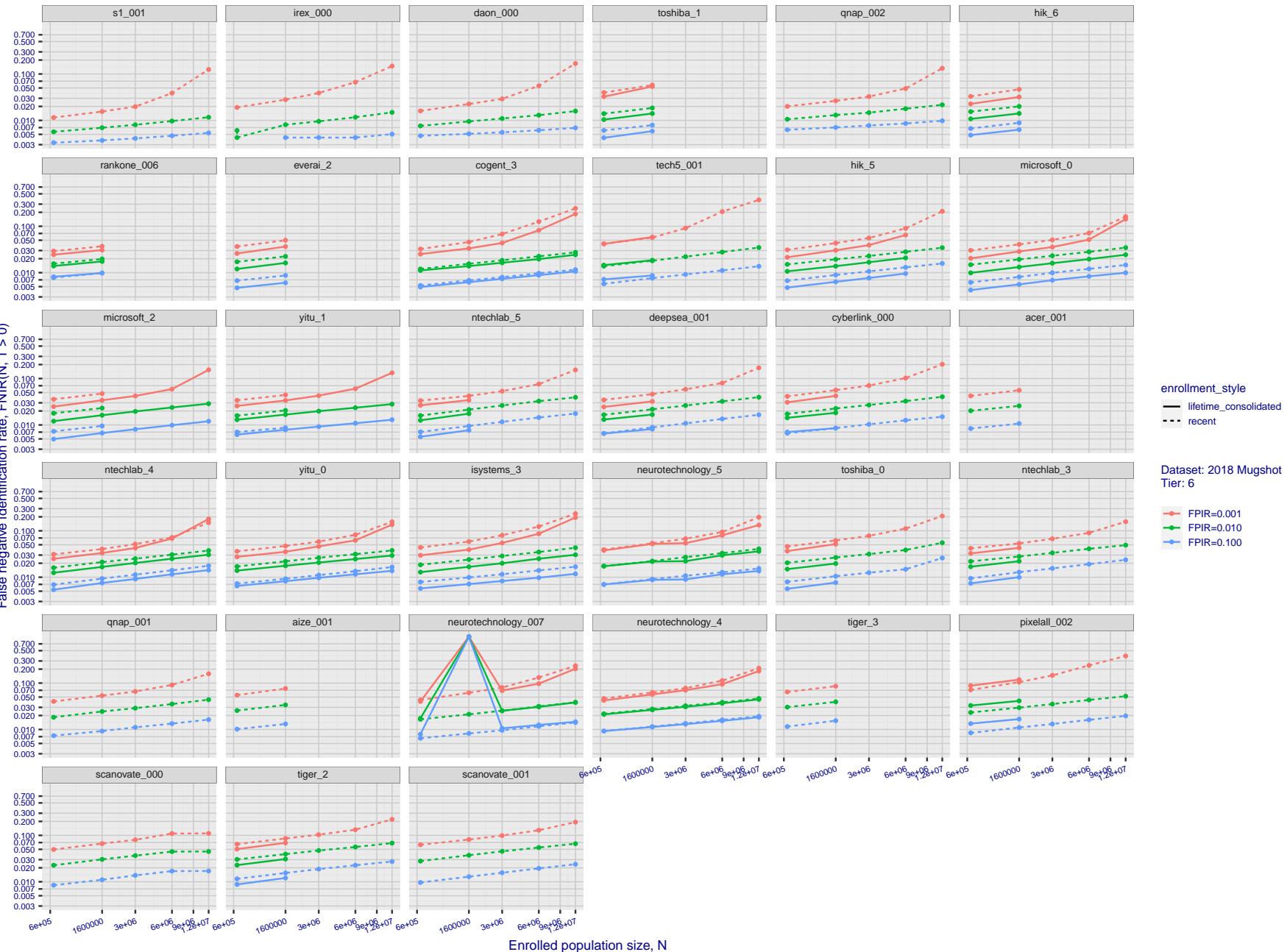
T = 0 → Investigation
T > 0 → Identification

Figure 41: [FRVT-2018 Mugshot Dataset] Threshold-based identification miss rates vs. number of enrolled subjects. The figure shows $\text{FNIR}(N, T)$ across various gallery sizes when the threshold is set to achieve the given FPIRs. The rank criterion is irrelevant at high thresholds as mates are always at rank 1. The results are computed from the trials listed in rows 1-10 of Table 1. Less accurate algorithms were not run on large N , so results are missing. For clarity, results are sorted and reported into tiers spanning multiple pages. The tiering criteria is complicated: First paging by $\text{FNIR}(N_b, 1, 0)$, then sorting by median $\text{FNIR}(N_b, T)$, $N_b = 640\,000$.

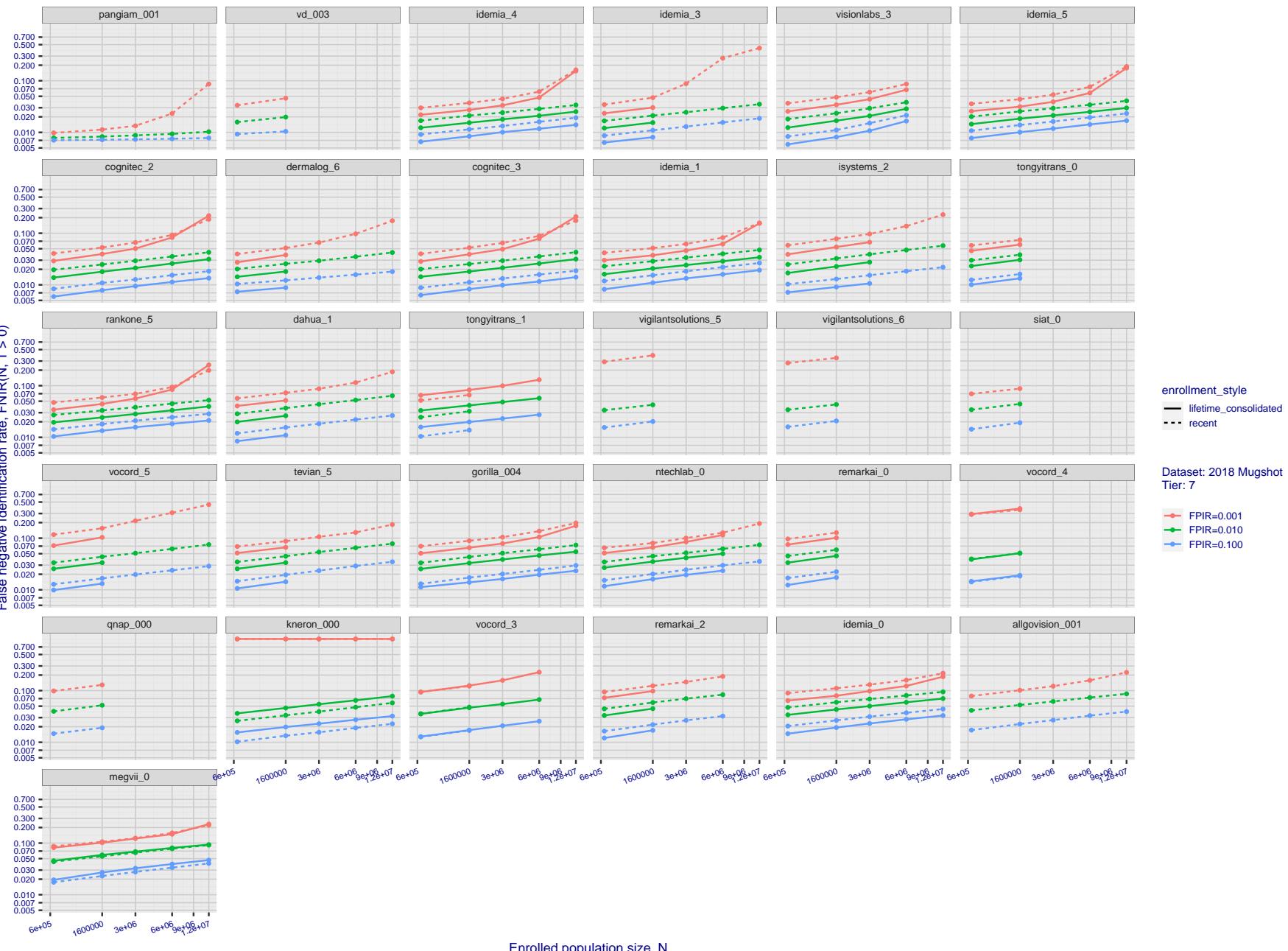
2023 / 03 / 14
14:32:11FNIR(N, R, T) = False neg. identification rate
FPIR(N, T) = False pos. identification rate
N = Num. enrolled subjects
R = Num. candidates examined
T = Threshold
T = 0 → Investigation
T > 0 → Identification

Figure 42: [FRVT-2018 Mugshot Dataset] Threshold-based identification miss rates vs. number of enrolled subjects. The figure shows $\text{FNIR}(N, T)$ across various gallery sizes when the threshold is set to achieve the given FPIRs. The rank criterion is irrelevant at high thresholds as mates are always at rank 1. The results are computed from the trials listed in rows 1-10 of Table 1. Less accurate algorithms were not run on large N , so results are missing. For clarity, results are sorted and reported into tiers spanning multiple pages. The tiering criteria is complicated: First paging by $\text{FNIR}(N_b, 1, 0)$, then sorting by median $\text{FNIR}(N_b, T)$, $N_b = 640\,000$.

2023/03/14
14:32:11FNIR(N, R, T) = False neg. identification rate
FPIR(N, T) = False pos. identification rateN = Num. enrolled subjects
R = Num. candidates examined

T = Threshold

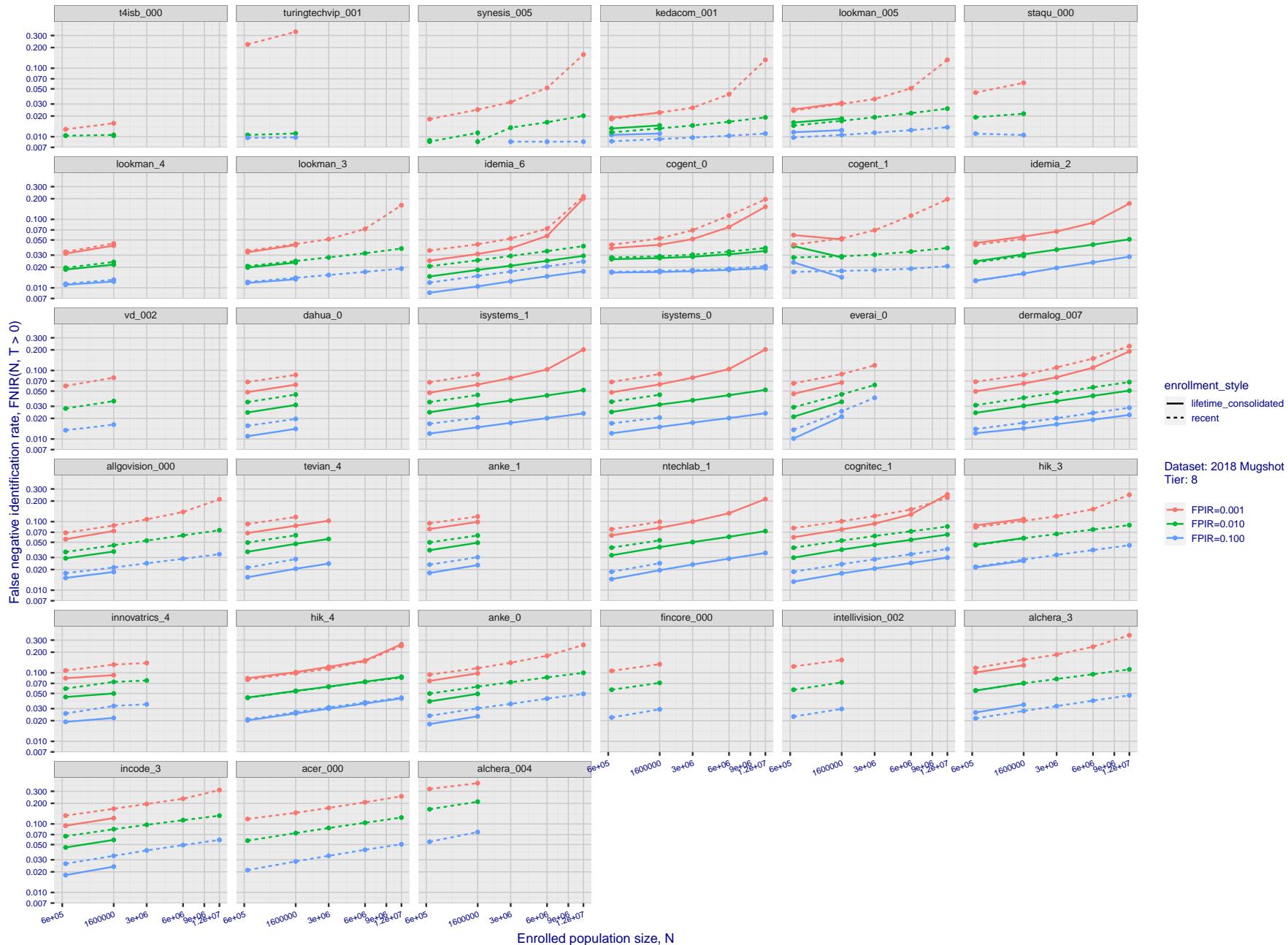
T = 0 → Investigation
T > 0 → Identification

Figure 43: [FRVT-2018 Mugshot Dataset] Threshold-based identification miss rates vs. number of enrolled subjects. The figure shows $\text{FNIR}(N, T)$ across various gallery sizes when the threshold is set to achieve the given FPIRs. The rank criterion is irrelevant at high thresholds as mates are always at rank 1. The results are computed from the trials listed in rows 1-10 of Table 1. Less accurate algorithms were not run on large N , so results are missing. For clarity, results are sorted and reported into tiers spanning multiple pages. The tiering criteria is complicated: First paging by $\text{FNIR}(N_b, 1, 0)$, then sorting by median $\text{FNIR}(N_b, T)$, $N_b = 640\,000$.

2023/03/14
14:32:11FNIR(N, R, T) = False neg. identification rate
FPFR(N, T) = False pos. identification rateN = Num. enrolled subjects
R = Num. candidates examined

T = Threshold

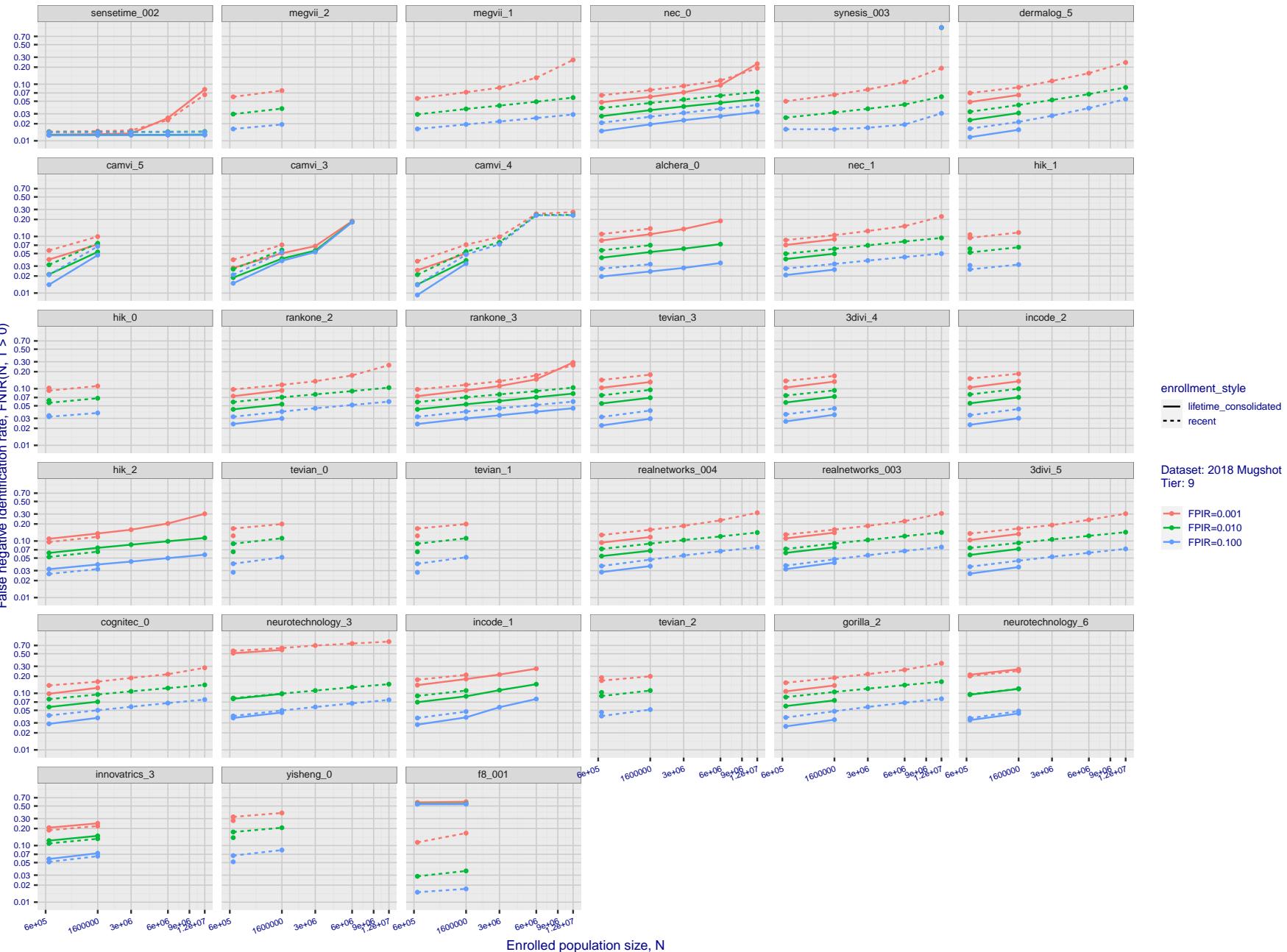
T = 0 → Investigation
T > 0 → Identification

Figure 44: [FRVT-2018 Mugshot Dataset] Threshold-based identification miss rates vs. number of enrolled subjects. The figure shows $\text{FNIR}(N, T)$ across various gallery sizes when the threshold is set to achieve the given FPIRs. The rank criterion is irrelevant at high thresholds as mates are always at rank 1. The results are computed from the trials listed in rows 1-10 of Table 1. Less accurate algorithms were not run on large N , so results are missing. For clarity, results are sorted and reported into tiers spanning multiple pages. The tiering criteria is complicated: First paging by $\text{FNIR}(N_b, 1, 0)$, then sorting by median $\text{FNIR}(N_b, T)$, $N_b = 640\,000$.

2023/03/14
14:32:11FNIR(N, R, T) = False neg. identification rate
FPFR(N, T) = False pos. identification rateN = Num. enrolled subjects
R = Num. candidates examined

T = Threshold

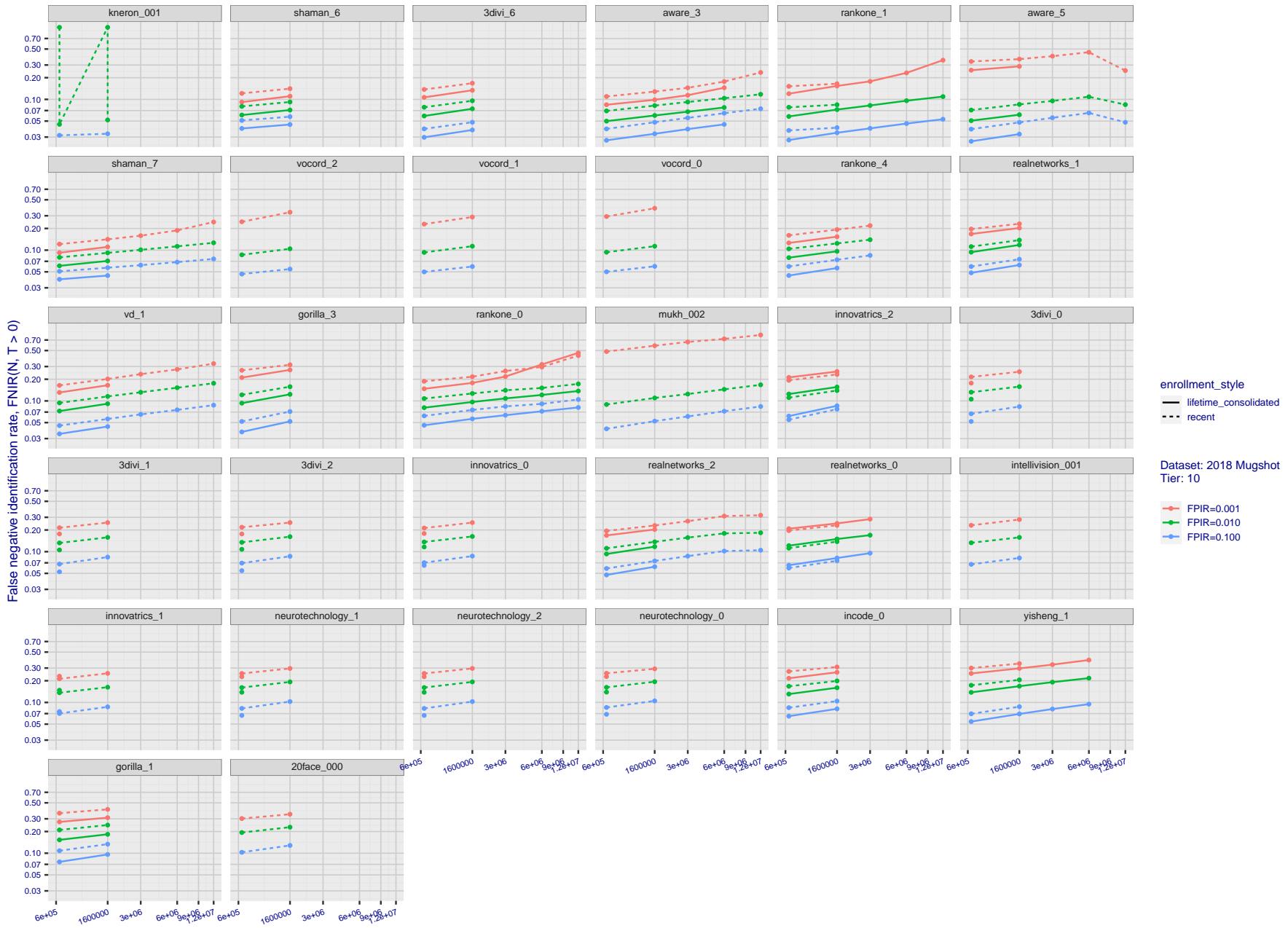
T = 0 → Investigation
T > 0 → Identification

Figure 45: [FRVT-2018 Mugshot Dataset] Threshold-based identification miss rates vs. number of enrolled subjects. The figure shows $\text{FNIR}(N, T)$ across various gallery sizes when the threshold is set to achieve the given FPIRs. The rank criterion is irrelevant at high thresholds as mates are always at rank 1. The results are computed from the trials listed in rows 1-10 of Table 1. Less accurate algorithms were not run on large N , so results are missing. For clarity, results are sorted and reported into tiers spanning multiple pages. The tiering criteria is complicated: First paging by $\text{FNIR}(N_b, 1, 0)$, then sorting by median $\text{FNIR}(N_b, T)$, $N_b = 640\,000$.

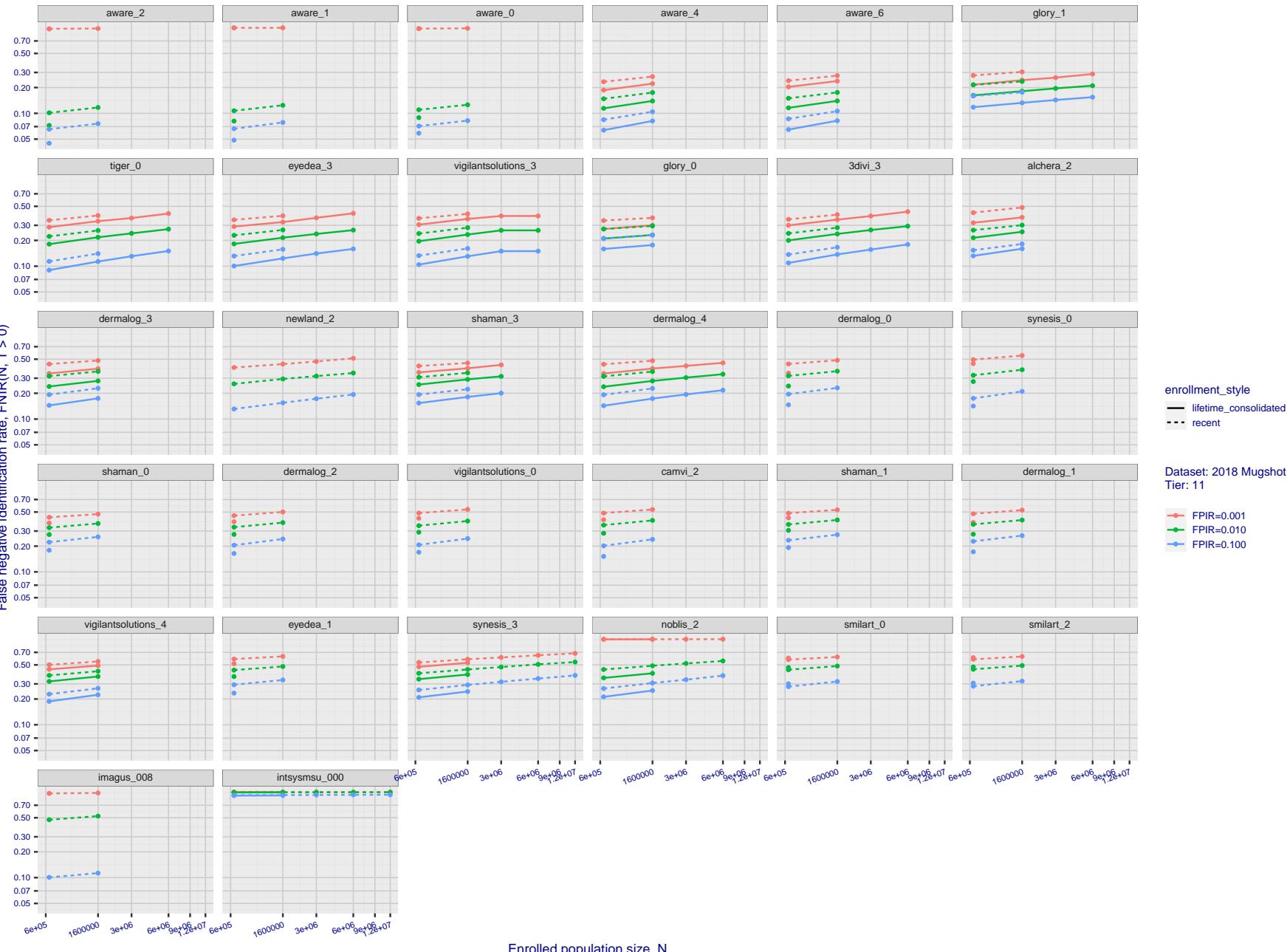
2023/03/14
14:32:11FNIR(N, R, T) = False neg. identification rate
FPFR(N, T) = False pos. identification rate
N = Num. enrolled subjects
R = Num. candidates examined
T = Threshold
T = 0 → Investigation
T > 0 → Identification

Figure 46: [FRVT-2018 Mugshot Dataset] Threshold-based identification miss rates vs. number of enrolled subjects. The figure shows $\text{FNIR}(N, T)$ across various gallery sizes when the threshold is set to achieve the given FPIRs. The rank criterion is irrelevant at high thresholds as mates are always at rank 1. The results are computed from the trials listed in rows 1-10 of Table 1. Less accurate algorithms were not run on large N , so results are missing. For clarity, results are sorted and reported into tiers spanning multiple pages. The tiering criteria is complicated: First paging by $\text{FNIR}(N_b, 1, 0)$, then sorting by median $\text{FNIR}(N_b, T)$, $N_b = 640\,000$.

2023/03/14
14:32:11

 $\text{FNIR}(N, R, T) =$
 False neg. identification rate
 $\text{FPIR}(N, T) =$
 False pos. identification rate
 $N =$ Num. enrolled subjects
 $R =$ Num. candidates examined
 $T =$ Threshold
 $T = 0 \rightarrow$ Investigation
 $T > 0 \rightarrow$ Identification

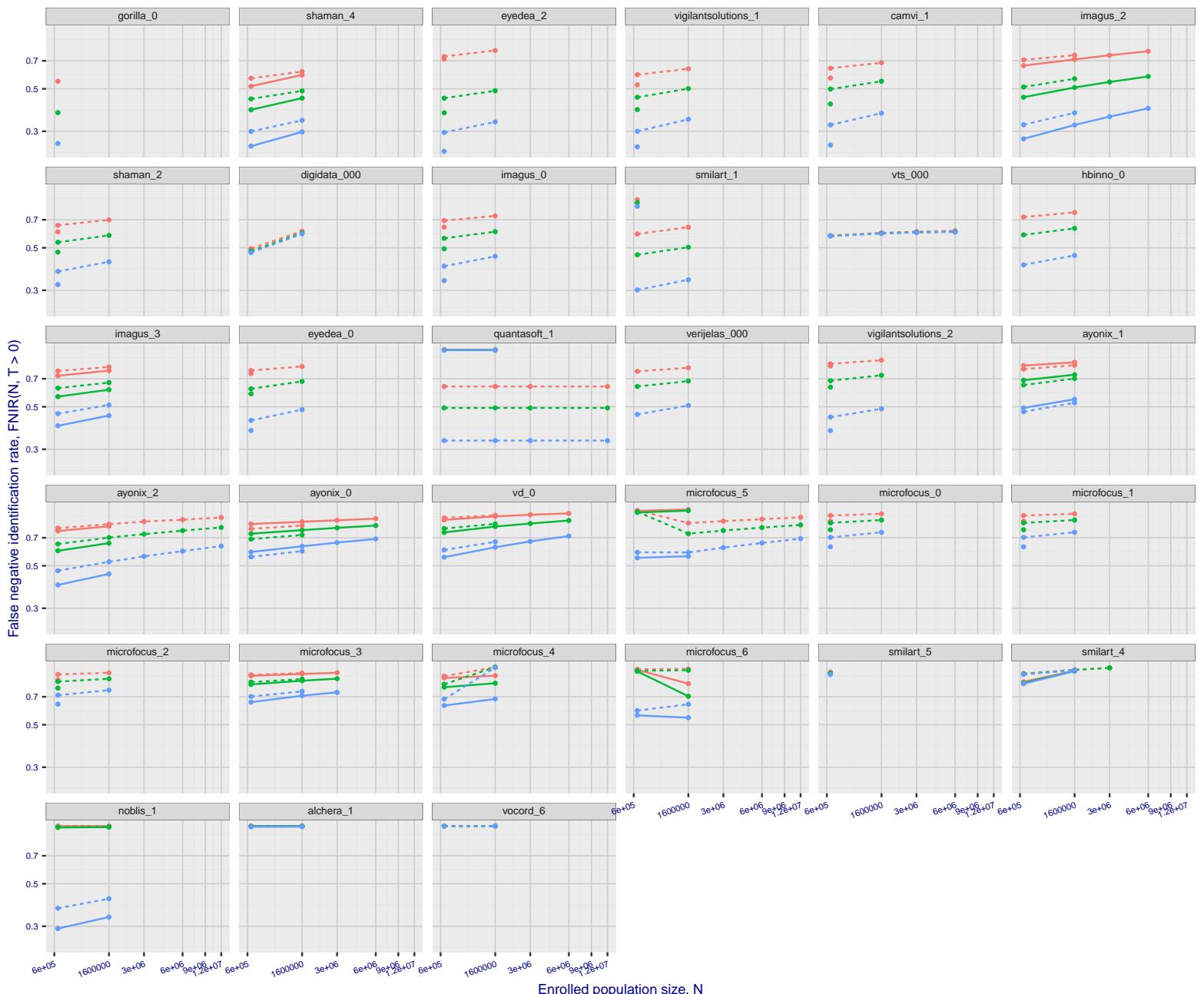


Figure 47: [FRVT-2018 Mugshot Dataset] Threshold-based identification miss rates vs. number of enrolled subjects. The figure shows $\text{FNIR}(N, T)$ across various gallery sizes when the threshold is set to achieve the given FPIRs. The rank criterion is irrelevant at high thresholds as mates are always at rank 1. The results are computed from the trials listed in rows 1-10 of Table 1. Less accurate algorithms were not run on large N , so results are missing. For clarity, results are sorted and reported into tiers spanning multiple pages. The tiering criteria is complicated: First paging by $\text{FNIR}(N_b, 1, 0)$, then sorting by median $\text{FNIR}(N_b, T)$, $N_b = 640\,000$.

2023/03/14 14:32:11	$\text{FNIR}(N, R, T) =$ $\text{FPTR}(N, T) =$	False neg. identification rate False pos. identification rate	$N =$ Num. enrolled subjects $R =$ Num. candidates examined	$T =$ Threshold $T > 0 \rightarrow$ Identification	$T = 0 \rightarrow$ Investigation
------------------------	---	--	--	---	-----------------------------------

2023/03/14

FNIR(N, R, T) = False neg. identification rate
FPIR(N, T) = False pos. identification rateN = Num. enrolled subjects
R = Num. candidates examined

T = Threshold

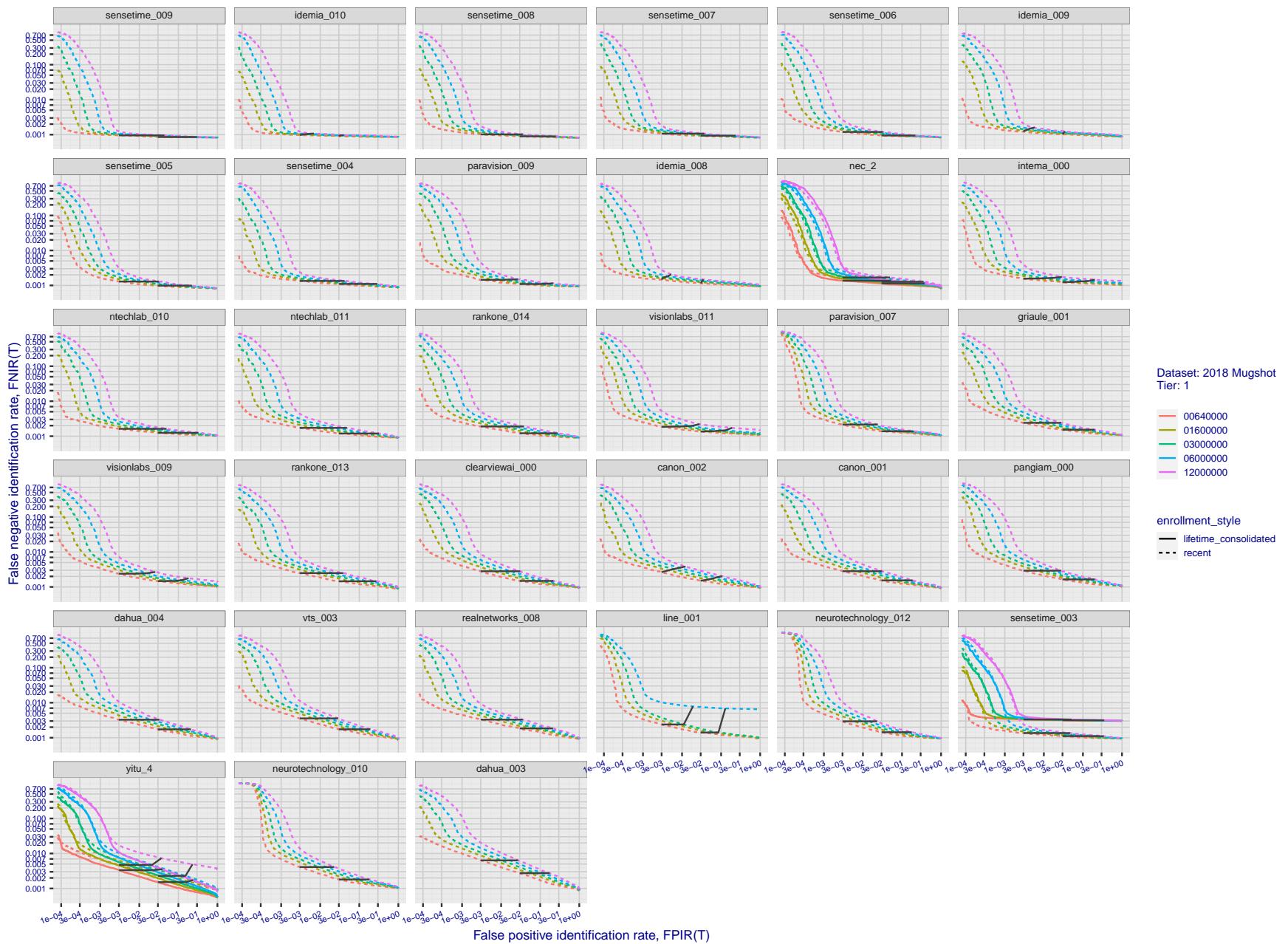
T = 0 → Investigation
T > 0 → Identification

Figure 48: [FRVT-2018 Mugshot Dataset] Identification miss rates vs. false positive rates. The figure shows miss rates $\text{FNIR}(N, L, T)$ as a function of $\text{FPIR}(N, T)$, with N ranging from 640 000 to 12 000 000 as noted in rows 1-10 of Table 1. These error tradeoff characteristics are useful for applications where a threshold must be elevated to limit false positives, such as when human reviewer labor is not matched to the volume of searches. Dark lines join points of equal threshold: If horizontal, $\text{FPIR}(T)$ rises with N , and mate scores are independent of N . Other algorithms adjust scores in an attempt to make FPIR independent of N .

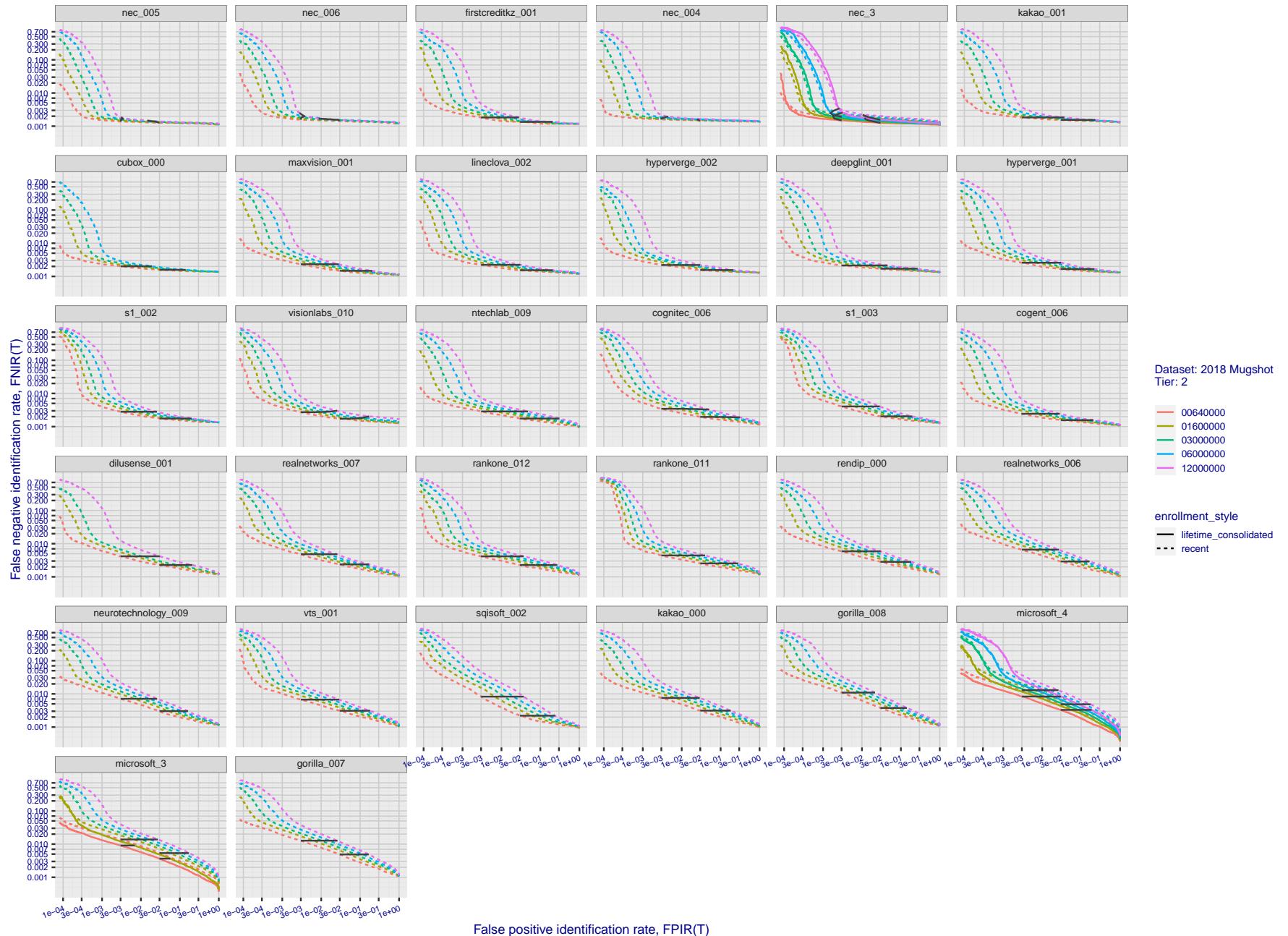


Figure 49: [FRVT-2018 Mugshot Dataset] Identification miss rates vs. false positive rates. The figure shows miss rates $\text{FNIR}(N, L, T)$ as a function of $\text{FPIR}(N, T)$, with N ranging from 640 000 to 12 000 000 as noted in rows 1-10 of Table 1. These error tradeoff characteristics are useful for applications where a threshold must be elevated to limit false positives, such as when human reviewer labor is not matched to the volume of searches. Dark lines join points of equal threshold: If horizontal, $\text{FPIR}(T)$ rises with N , and mate scores are independent of N . Other algorithms adjust scores in an attempt to make FPIR independent of N .

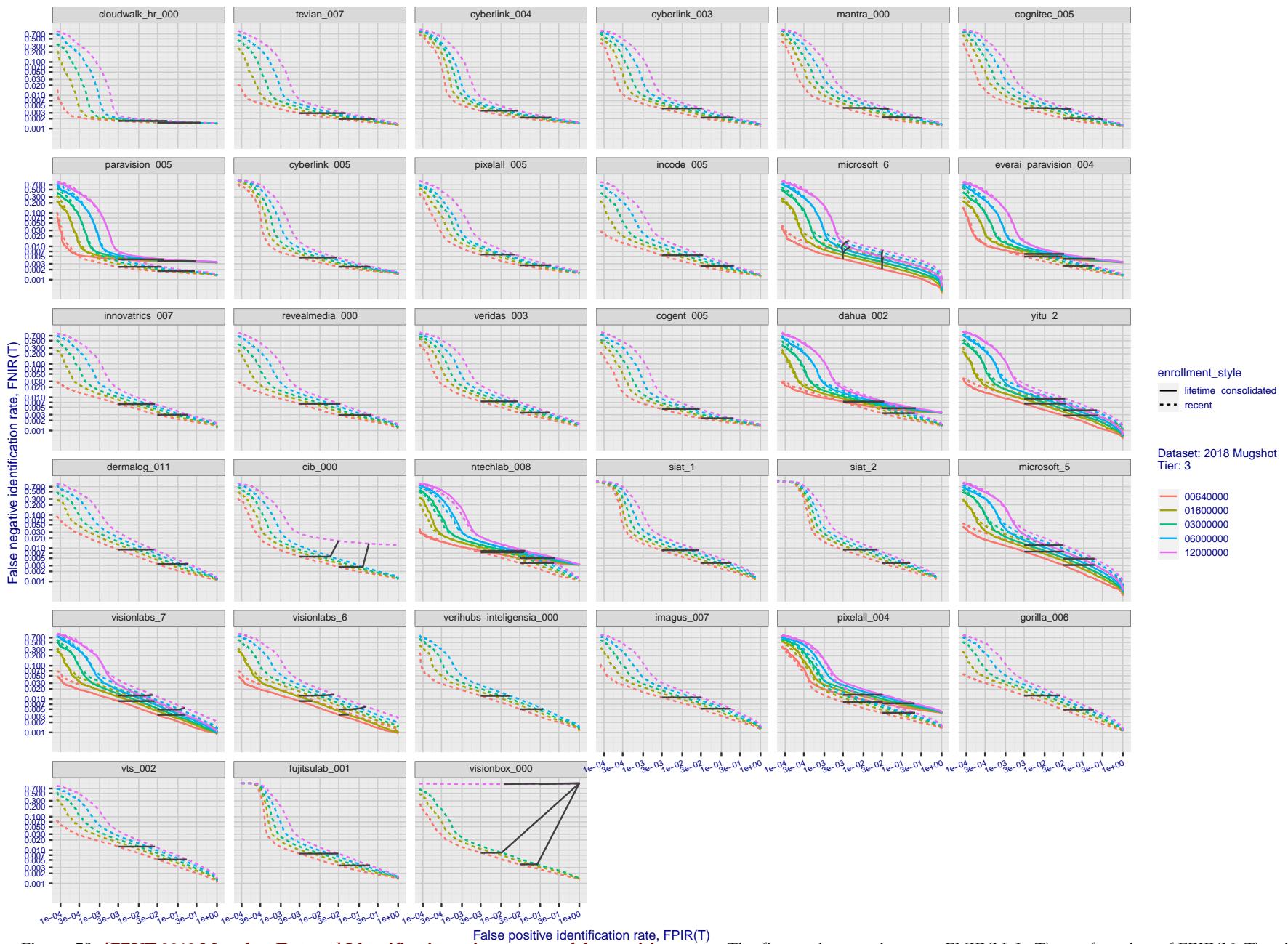


Figure 50: [FRVT-2018 Mugshot Dataset] Identification miss rates vs. false positive rates. The figure shows miss rates $\text{FNIR}(N, L, T)$ as a function of $\text{FPIR}(N, T)$, with N ranging from 640 000 to 12 000 000 as noted in rows 1-10 of Table 1. These error tradeoff characteristics are useful for applications where a threshold must be elevated to limit false positives, such as when human reviewer labor is not matched to the volume of searches. Dark lines join points of equal threshold: If horizontal, $\text{FPIR}(T)$ rises with N , and mate scores are independent of N . Other algorithms adjust scores in an attempt to make FPIR independent of N .

2023/03/14

14:32:11

FNIR(N, R, T) = False neg. identification rate
FPIR(N, T) = False pos. identification rateN = Num. enrolled subjects
R = Num. candidates examined

T = Threshold

T = 0 → Investigation
 $T > 0 \rightarrow$ Identification

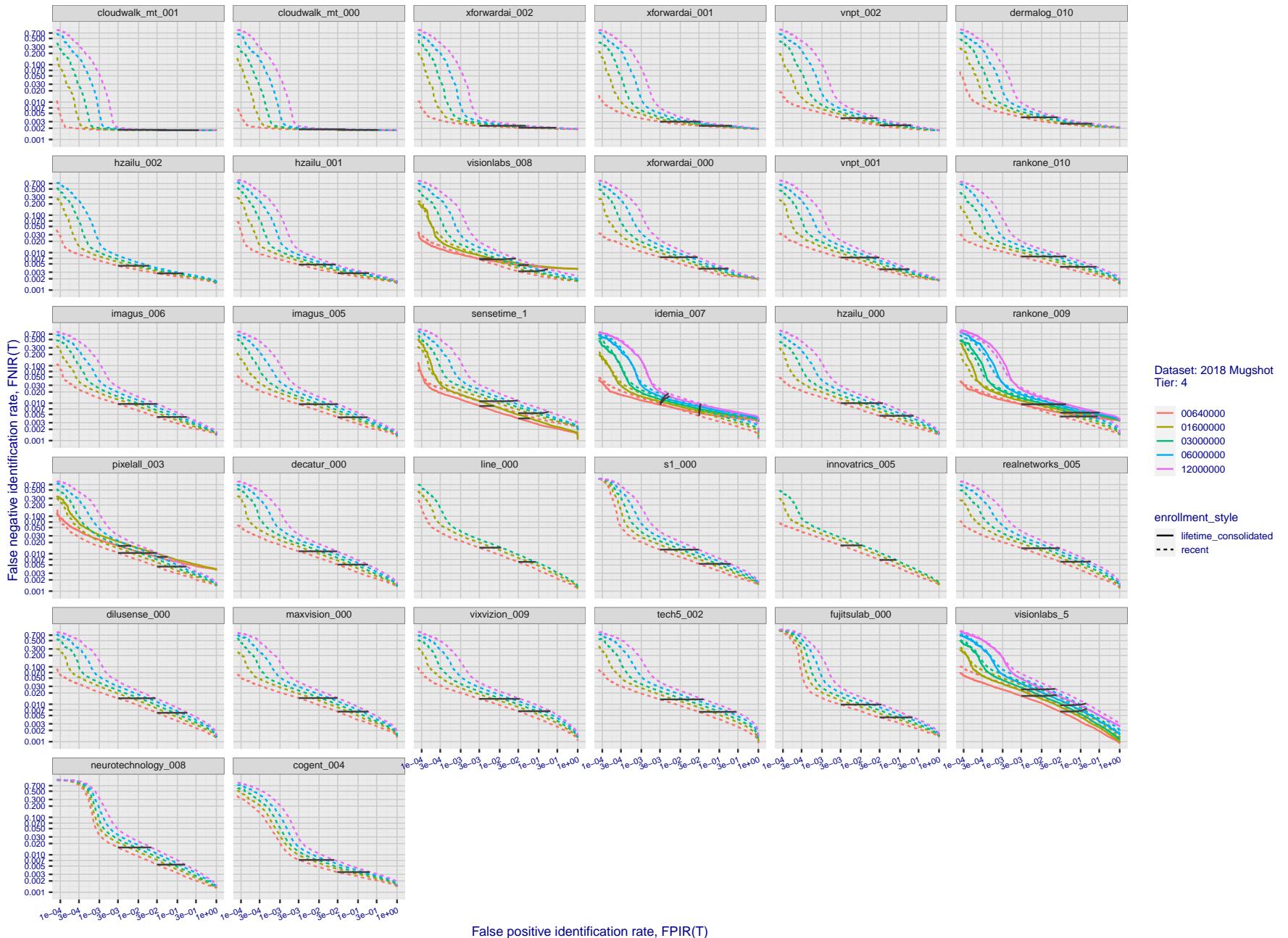


Figure 51: [FRVT-2018 Mugshot Dataset] Identification miss rates vs. false positive rates. The figure shows miss rates $\text{FNIR}(N, L, T)$ as a function of $\text{FPIR}(N, T)$, with N ranging from 640 000 to 12 000 000 as noted in rows 1-10 of Table 1. These error tradeoff characteristics are useful for applications where a threshold must be elevated to limit false positives, such as when human reviewer labor is not matched to the volume of searches. Dark lines join points of equal threshold: If horizontal, $\text{FPIR}(T)$ rises with N , and mate scores are independent of N . Other algorithms adjust scores in an attempt to make FPIR independent of N .

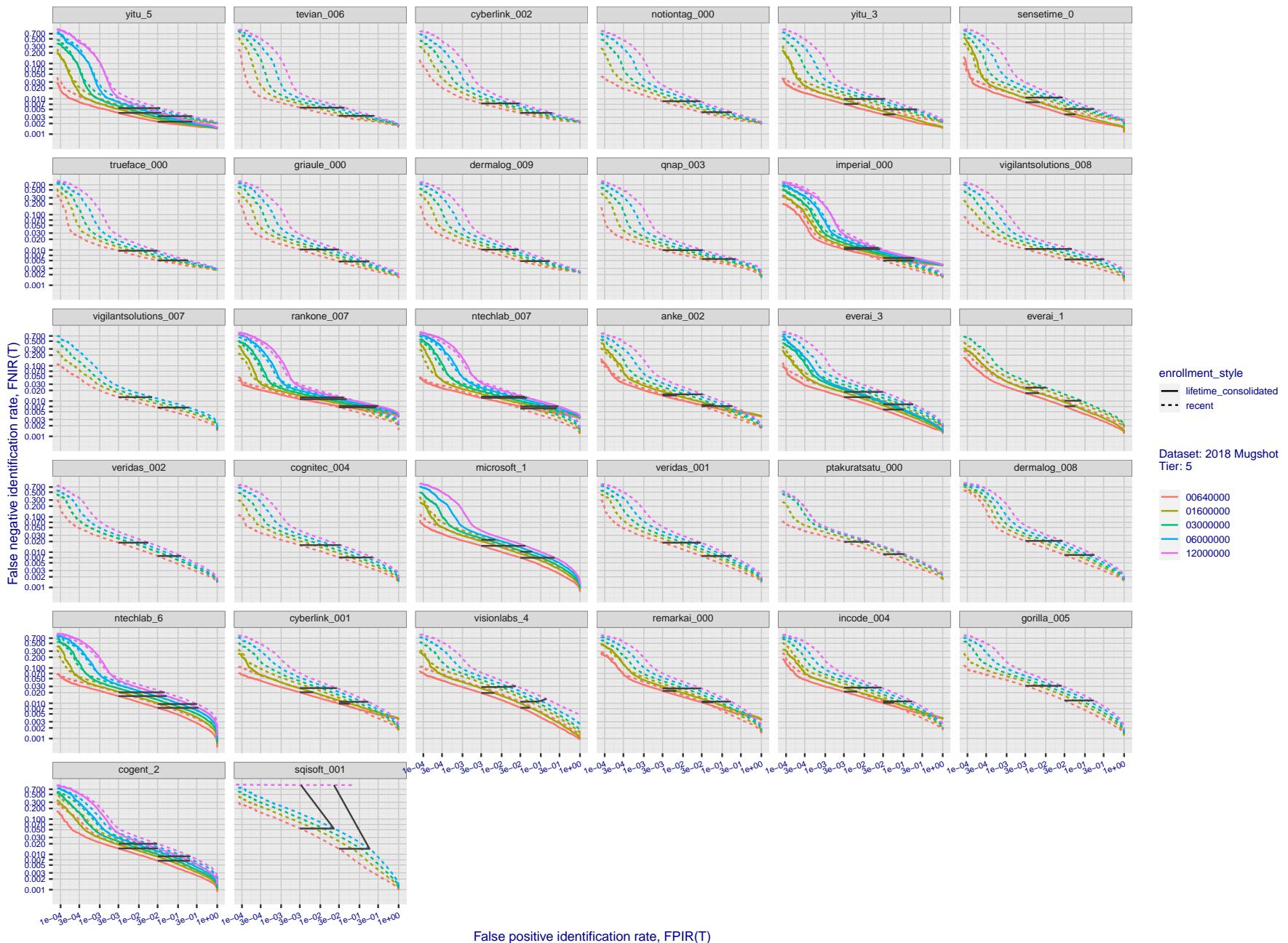


Figure 52: [FRVT-2018 Mugshot Dataset] Identification miss rates vs. false positive rates. The figure shows miss rates $\text{FNIR}(N, L, T)$ as a function of $\text{FPIR}(N, T)$, with N ranging from 640 000 to 12 000 000 as noted in rows 1-10 of Table 1. These error tradeoff characteristics are useful for applications where a threshold must be elevated to limit false positives, such as when human reviewer labor is not matched to the volume of searches. Dark lines join points of equal threshold: If horizontal, $\text{FPIR}(T)$ rises with N , and mate scores are independent of N . Other algorithms adjust scores in an attempt to make FPIR independent of N .

2023/03/14

14:32:11

 $\text{FNIR}(N, R, T) = \text{False neg. identification rate}$ $N = \text{Num. enrolled subjects}$ $T = \text{Threshold}$ $T = 0 \rightarrow \text{Investigation}$ $T > 0 \rightarrow \text{Identification}$ $\text{FPIR}(N, T) = \text{False pos. identification rate}$

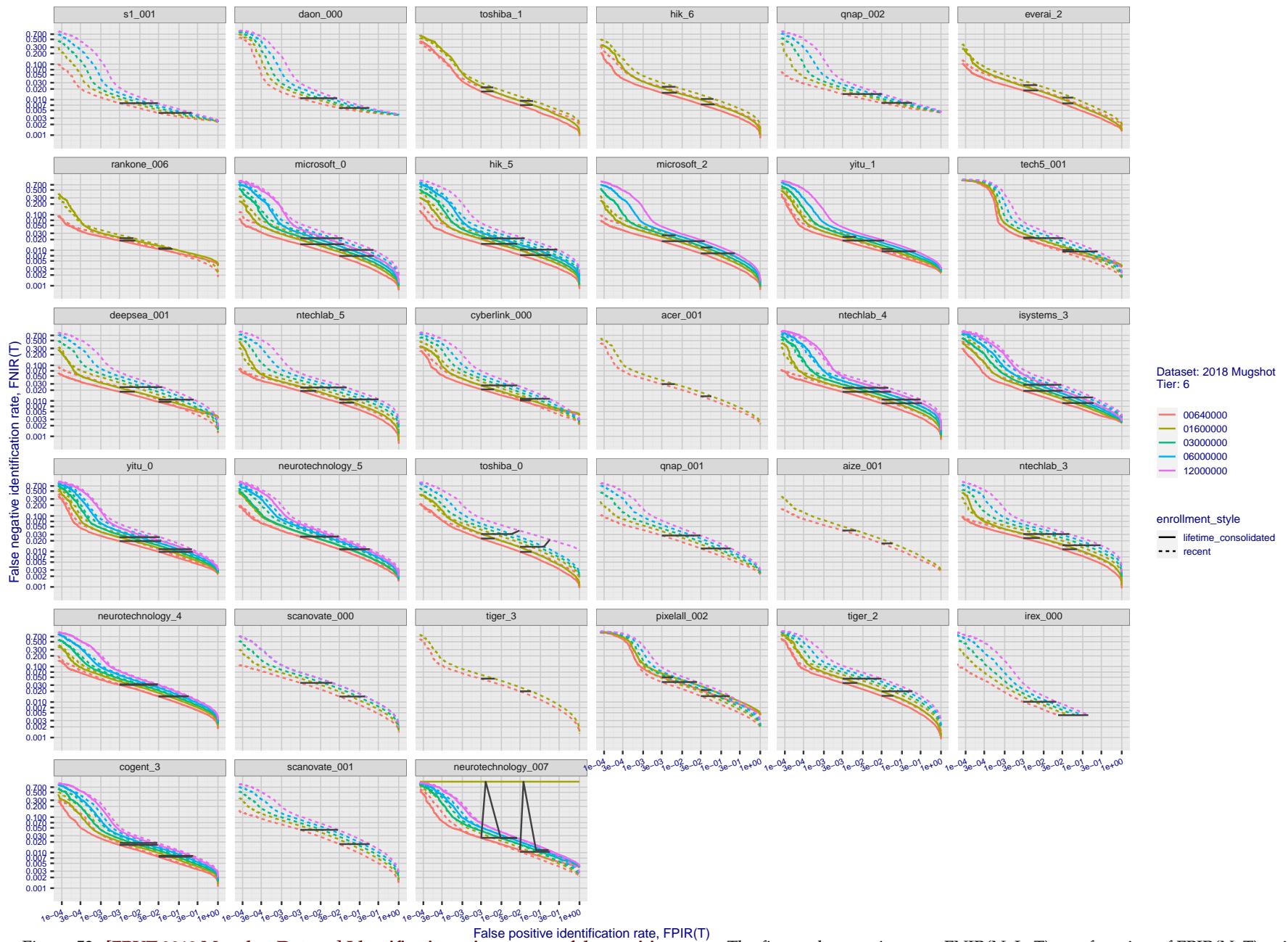


Figure 53: [FRVT-2018 Mugshot Dataset] Identification miss rates vs. false positive rates. The figure shows miss rates $\text{FNIR}(N, L, T)$ as a function of $\text{FPIR}(N, T)$, with N ranging from 640 000 to 12 000 000 as noted in rows 1-10 of Table 1. These error tradeoff characteristics are useful for applications where a threshold must be elevated to limit false positives, such as when human reviewer labor is not matched to the volume of searches. Dark lines join points of equal threshold: If horizontal, $\text{FPIR}(T)$ rises with N , and mate scores are independent of N . Other algorithms adjust scores in an attempt to make FPIR independent of N .

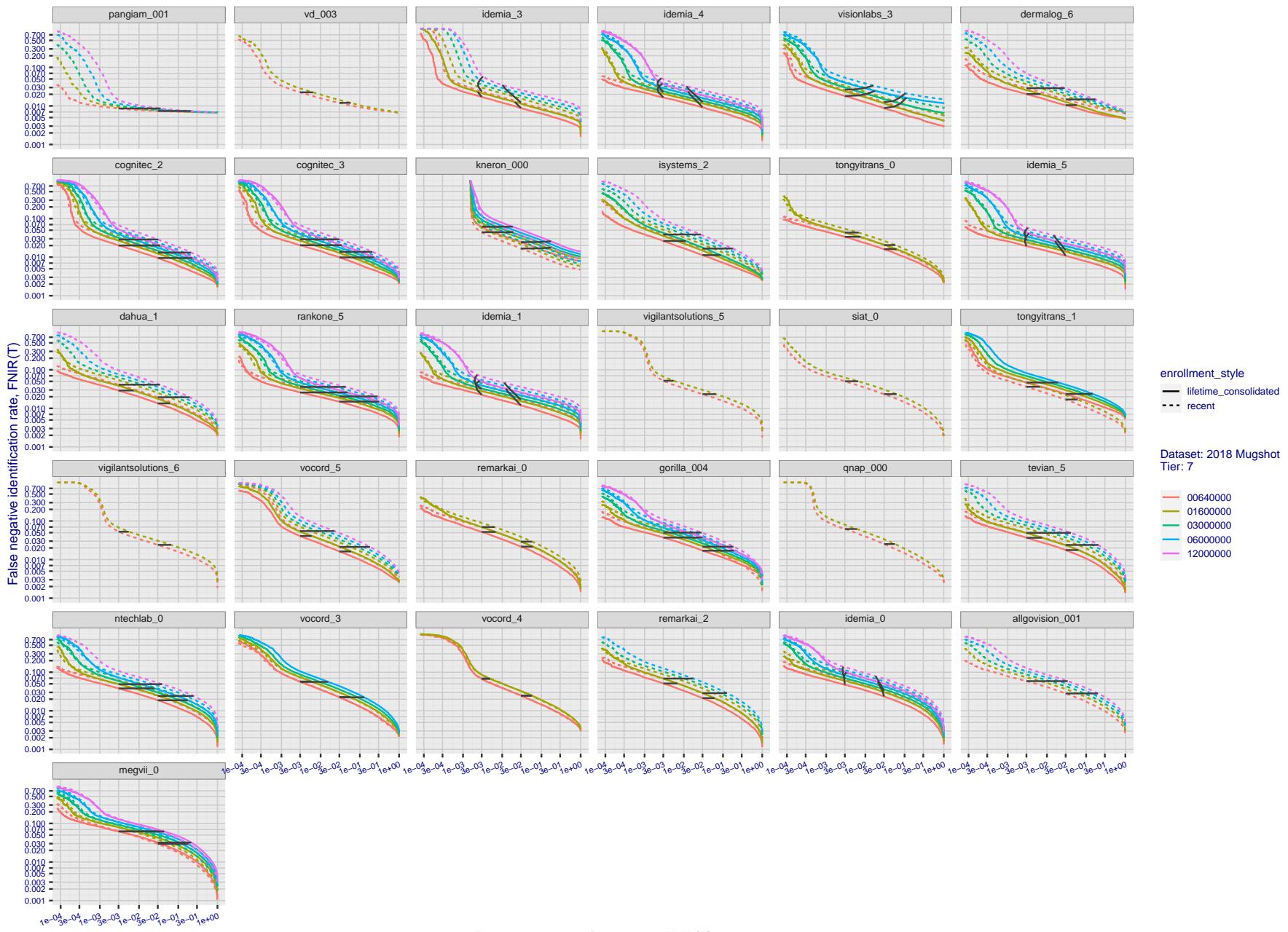


Figure 54: [FRVT-2018 Mugshot Dataset] Identification miss rates vs. false positive rates. The figure shows miss rates $\text{FNIR}(N, L, T)$ as a function of $\text{FPIR}(N, T)$, with N ranging from 640 000 to 12 000 000 as noted in rows 1-10 of Table 1. These error tradeoff characteristics are useful for applications where a threshold must be elevated to limit false positives, such as when human reviewer labor is not matched to the volume of searches. Dark lines join points of equal threshold: If horizontal, $\text{FPIR}(T)$ rises with N , and mate scores are independent of N . Other algorithms adjust scores in an attempt to make FPIR independent of N .

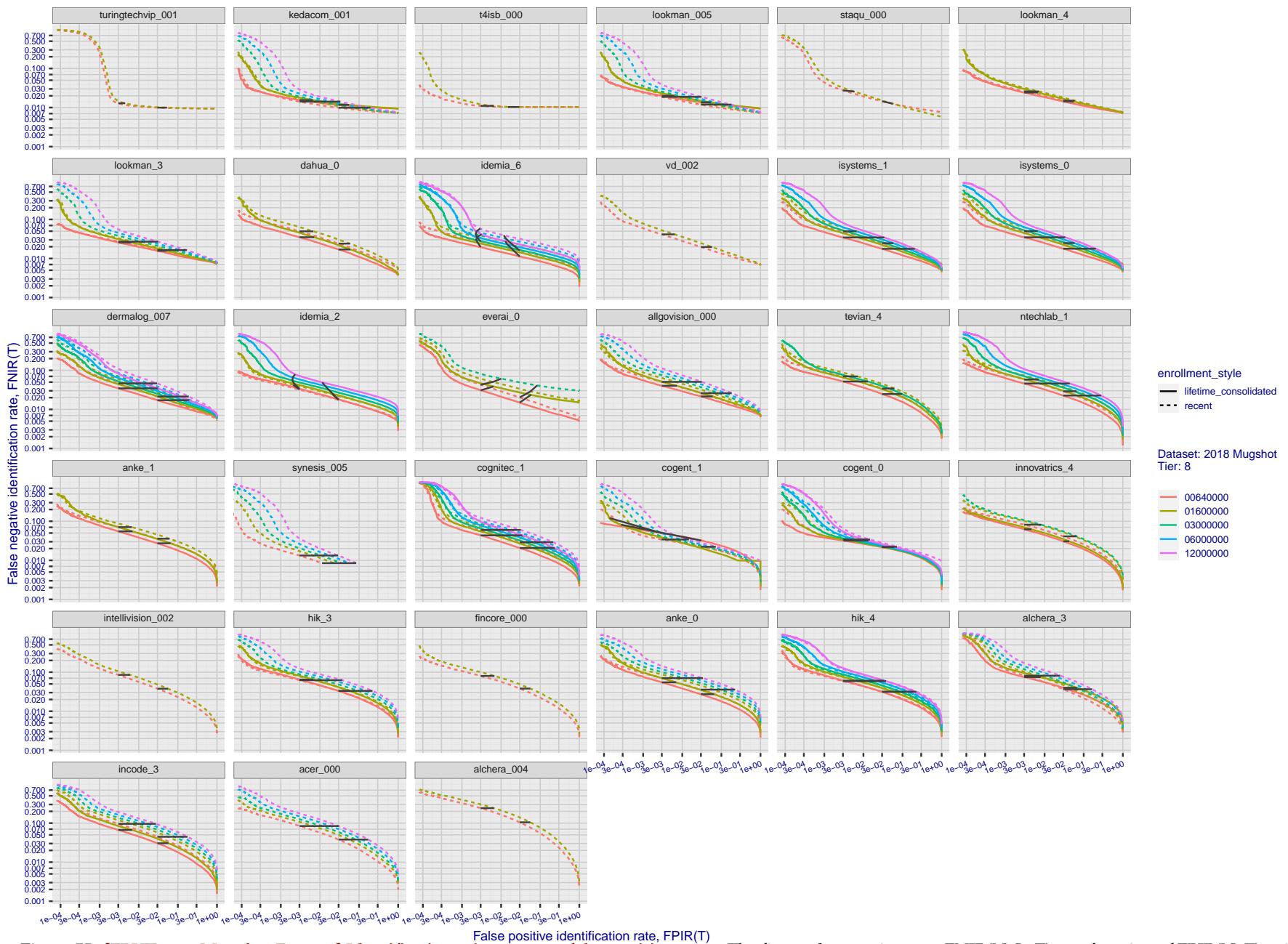


Figure 55: [FRVT-2018 Mugshot Dataset] Identification miss rates vs. false positive rates. The figure shows miss rates $\text{FNIR}(N, L, T)$ as a function of $\text{FPIR}(N, T)$, with N ranging from 640 000 to 12 000 000 as noted in rows 1-10 of Table 1. These error tradeoff characteristics are useful for applications where a threshold must be elevated to limit false positives, such as when human reviewer labor is not matched to the volume of searches. Dark lines join points of equal threshold: If horizontal, $\text{FPIR}(T)$ rises with N , and mate scores are independent of N . Other algorithms adjust scores in an attempt to make FPIR independent of N .

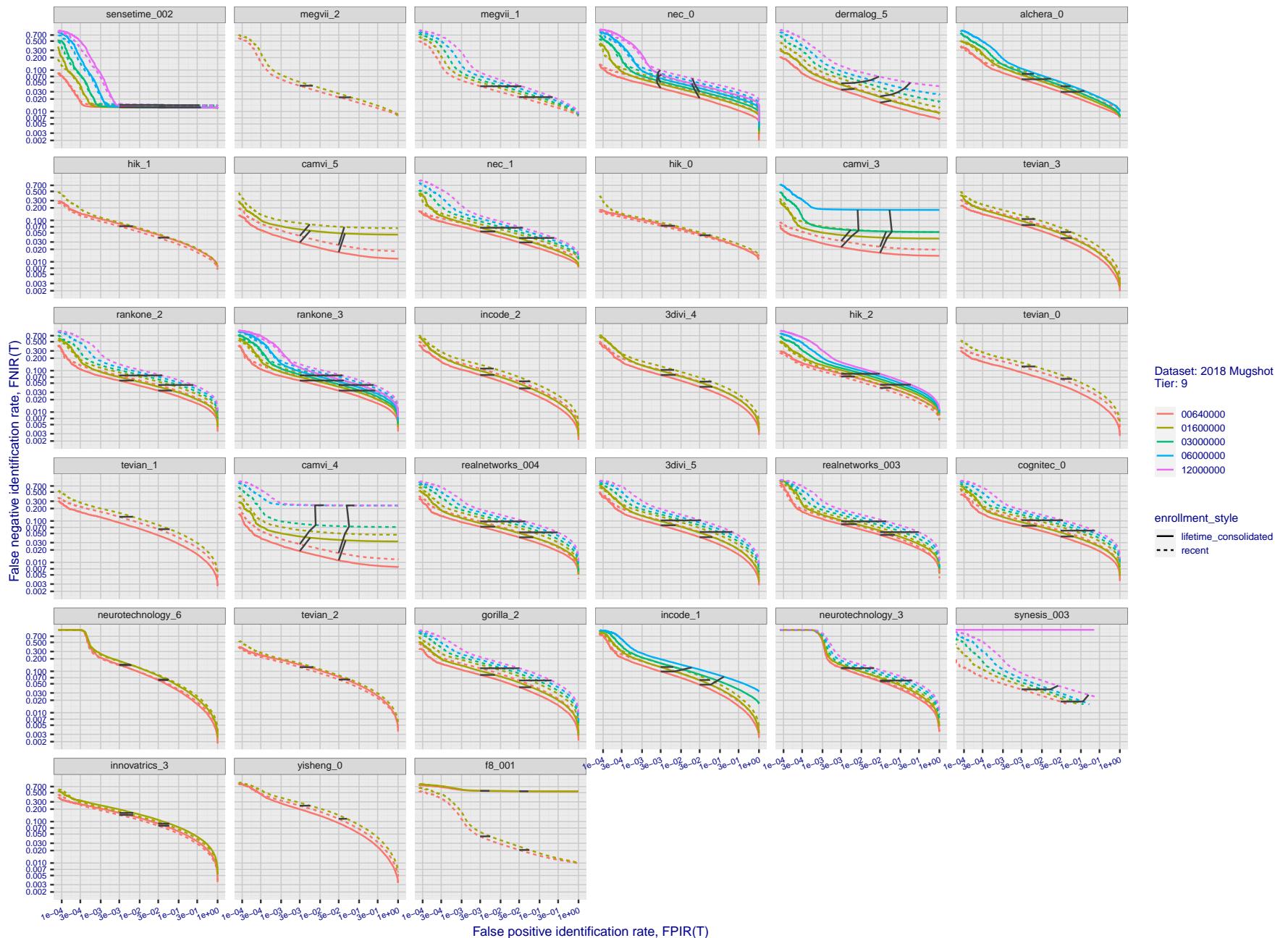


Figure 56: [FRVT-2018 Mugshot Dataset] Identification miss rates vs. false positive rates. The figure shows miss rates $\text{FNIR}(N, L, T)$ as a function of $\text{FPIR}(N, T)$, with N ranging from 640 000 to 12 000 000 as noted in rows 1-10 of Table 1. These error tradeoff characteristics are useful for applications where a threshold must be elevated to limit false positives, such as when human reviewer labor is not matched to the volume of searches. Dark lines join points of equal threshold: If horizontal, $\text{FPIR}(T)$ rises with N , and mate scores are independent of N . Other algorithms adjust scores in an attempt to make FPIR independent of N .

2023 /03 /14

14:32:11

FNIR(N, R, T) = False neg. identification rate

N = Num. enrolled subjects

T = Threshold

T = 0 → Investigation

FPIR(N, T) = False pos. identification rate

R = Num. candidates examined

T > 0 → Identification

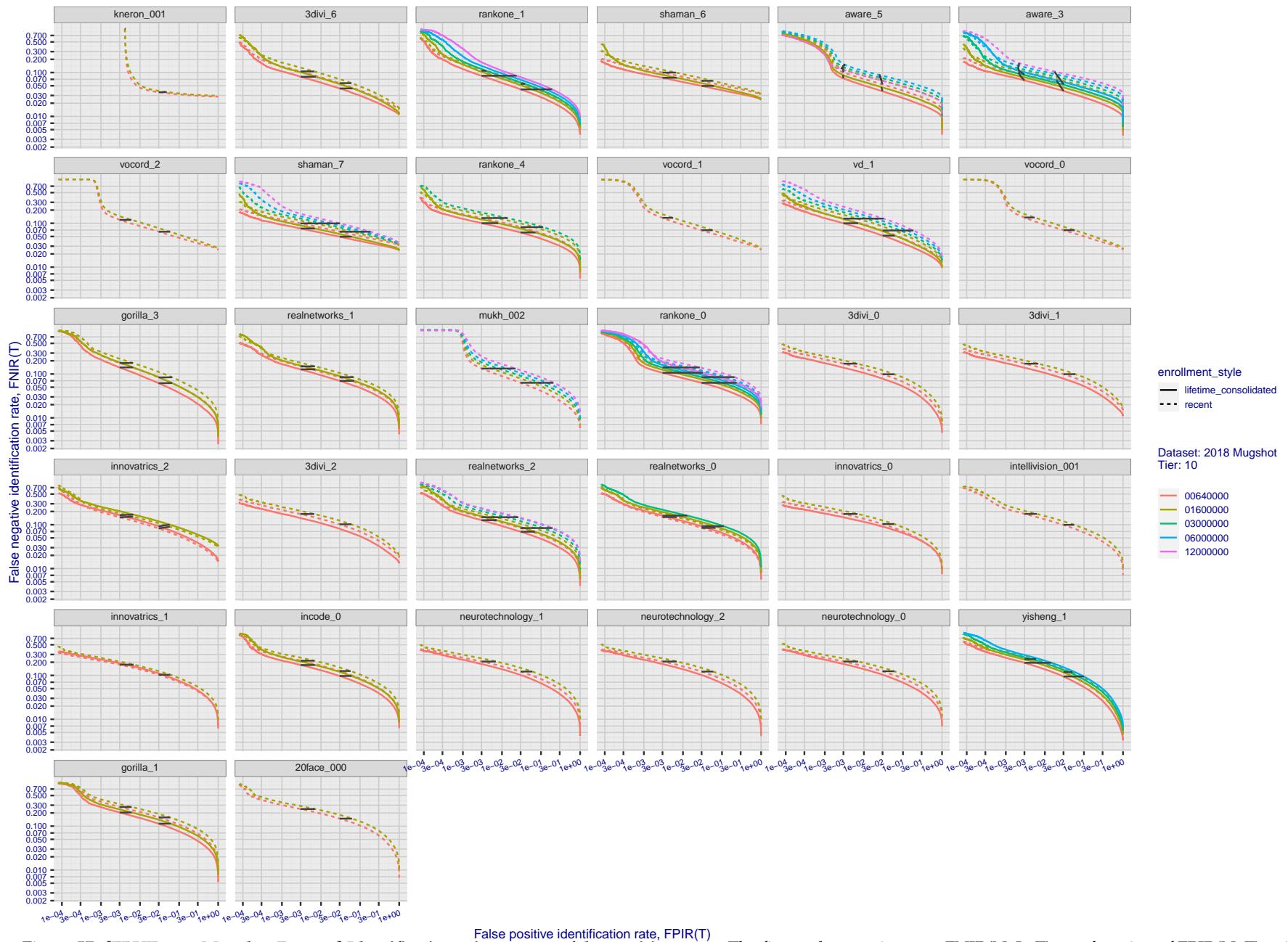


Figure 57: [FRVT-2018 Mugshot Dataset] Identification miss rates vs. false positive rates. The figure shows miss rates $\text{FNIR}(N, L, T)$ as a function of $\text{FPIR}(N, T)$, with N ranging from 640 000 to 12 000 000 as noted in rows 1-10 of Table 1. These error tradeoff characteristics are useful for applications where a threshold must be elevated to limit false positives, such as when human reviewer labor is not matched to the volume of searches. Dark lines join points of equal threshold: If horizontal, $\text{FPIR}(T)$ rises with N , and mate scores are independent of N . Other algorithms adjust scores in an attempt to make FPIR independent of N .

2023 / 03 / 14

14:32:11

FNIR(N, R, T) = False neg. identification rate
FPIR(N, T) = False pos. identification rateN = Num. enrolled subjects
R = Num. candidates examined

T = Threshold

T = 0 → Investigation
T > 0 → Identification

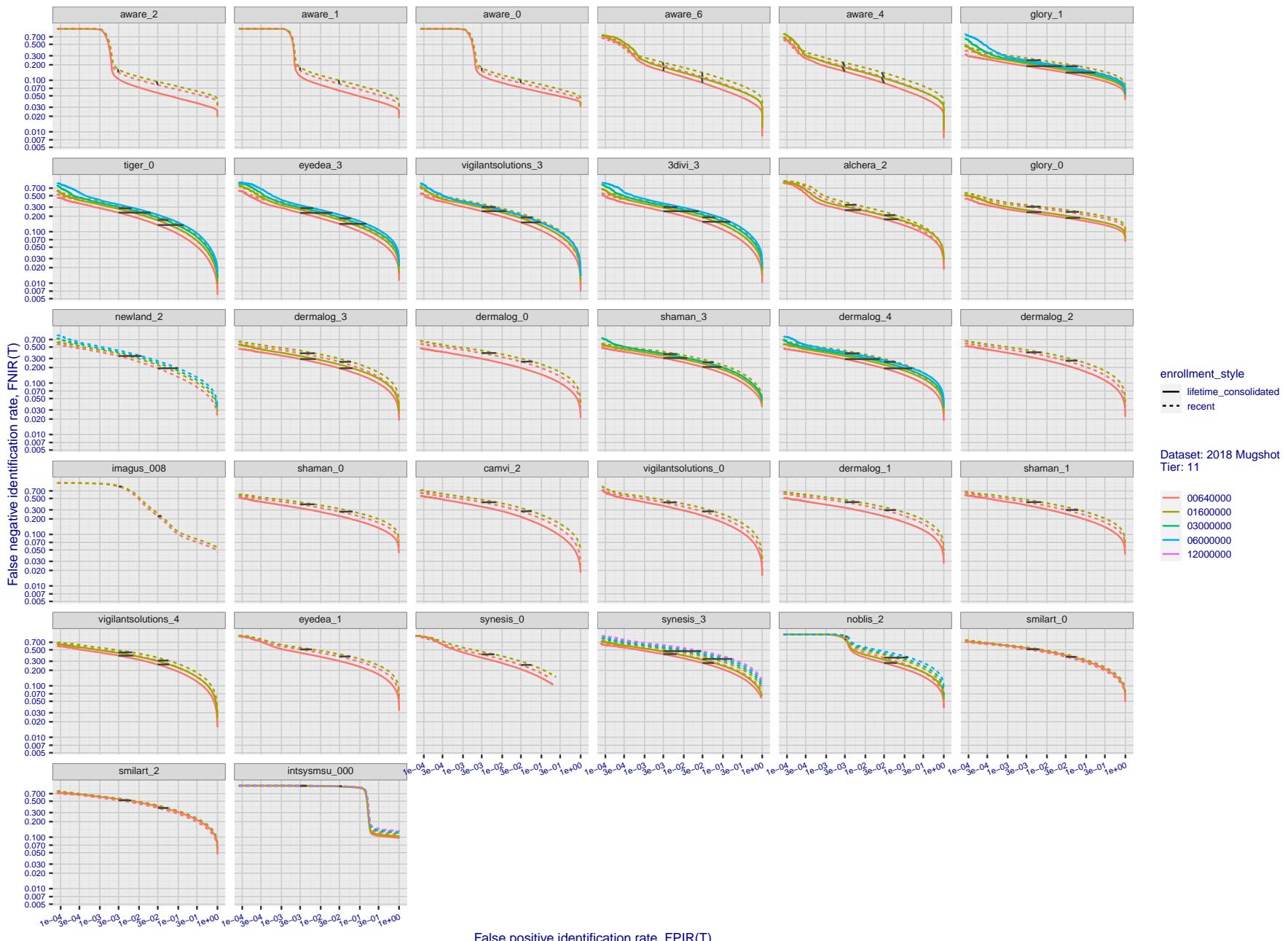


Figure 58: [FRVT-2018 Mugshot Dataset] Identification miss rates vs. false positive rates. The figure shows miss rates $\text{FNIR}(N, L, T)$ as a function of $\text{FPIR}(N, T)$, with N ranging from 640 000 to 12 000 000 as noted in rows 1-10 of Table 1. These error tradeoff characteristics are useful for applications where a threshold must be elevated to limit false positives, such as when human reviewer labor is not matched to the volume of searches. Dark lines join points of equal threshold: If horizontal, $\text{FPIR}(T)$ rises with N , and mate scores are independent of N . Other algorithms adjust scores in an attempt to make FPIR independent of N .

2023/03/14

14:32:11

FNIR(N, R, T) = False neg. identification rate N = Num. enrolled subjects T = Threshold $T = 0 \rightarrow$ Investigation R = Num. candidates examined $T > 0 \rightarrow$ Identification

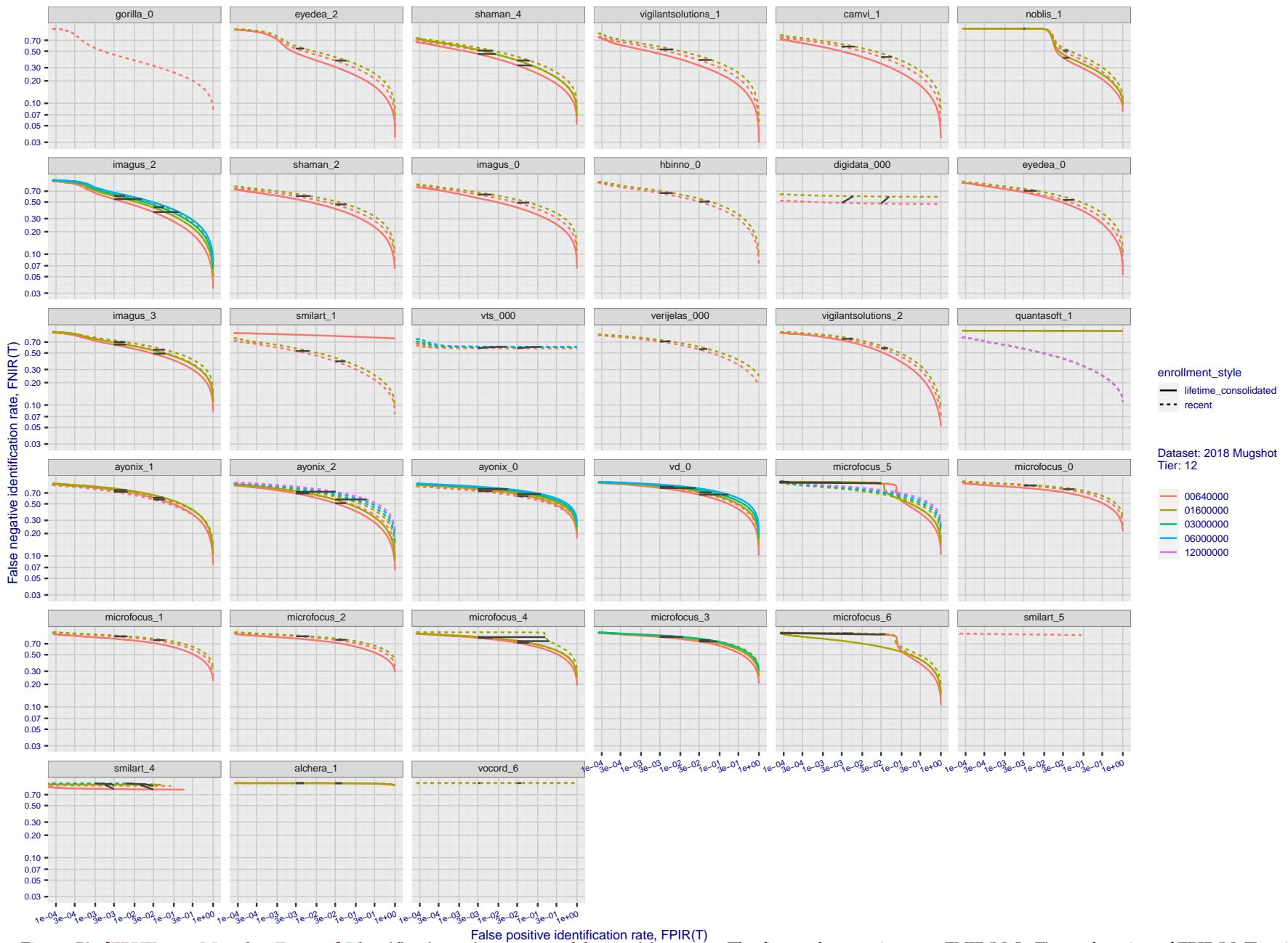


Figure 59: [FRVT-2018 Mugshot Dataset] Identification miss rates vs. false positive rates. The figure shows miss rates $\text{FNIR}(N, L, T)$ as a function of $\text{FPIR}(N, T)$, with N ranging from 640 000 to 12 000 000 as noted in rows 1-10 of Table 1. These error tradeoff characteristics are useful for applications where a threshold must be elevated to limit false positives, such as when human reviewer labor is not matched to the volume of searches. Dark lines join points of equal threshold: If horizontal, $\text{FPIR}(T)$ rises with N , and mate scores are independent of N . Other algorithms adjust scores in an attempt to make FPIR independent of N .

2023/03/14

14:32:11

 $\text{FNIR}(N, R, T) =$
False neg. identification rate
FPRI(N, T) =
False pos. identification rate $N = \text{Num. enrolled subjects}$
 $R = \text{Num. candidates examined}$ $T = \text{Threshold}$ $T = 0 \rightarrow \text{Investigation}$
 $T > 0 \rightarrow \text{Identification}$

Appendix B Effect of time-lapse: Accuracy after face ageing

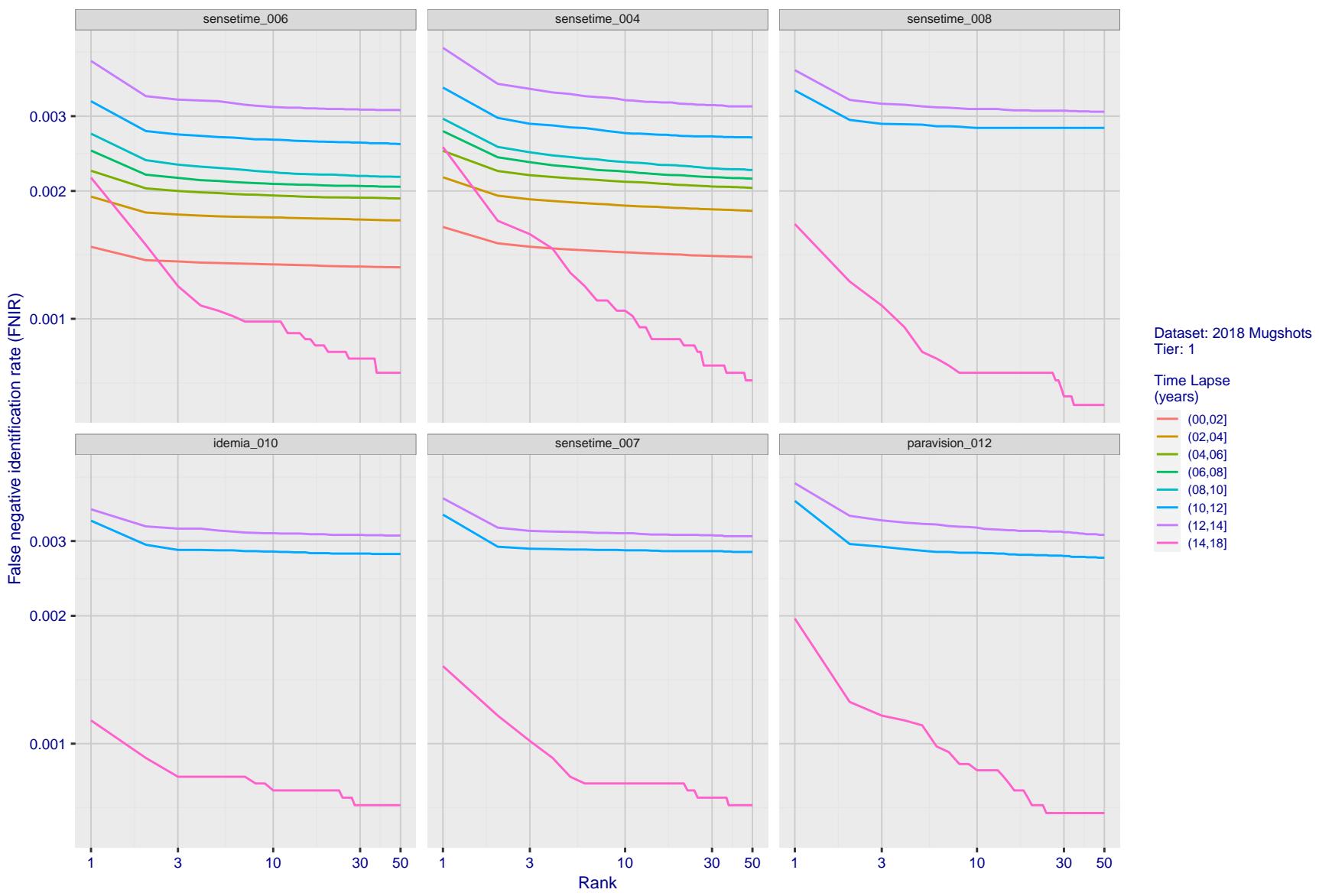


Figure 60: [FRVT-2018 Mugshot Ageing Dataset] Identification miss rates vs. rank by time-elapsed. The oldest image of each individual is enrolled. Thereafter, all more recent images are searched. Miss rates are computed over all searches noted in row 17 of Table 1 and binned by number of years between search and initial enrollment.

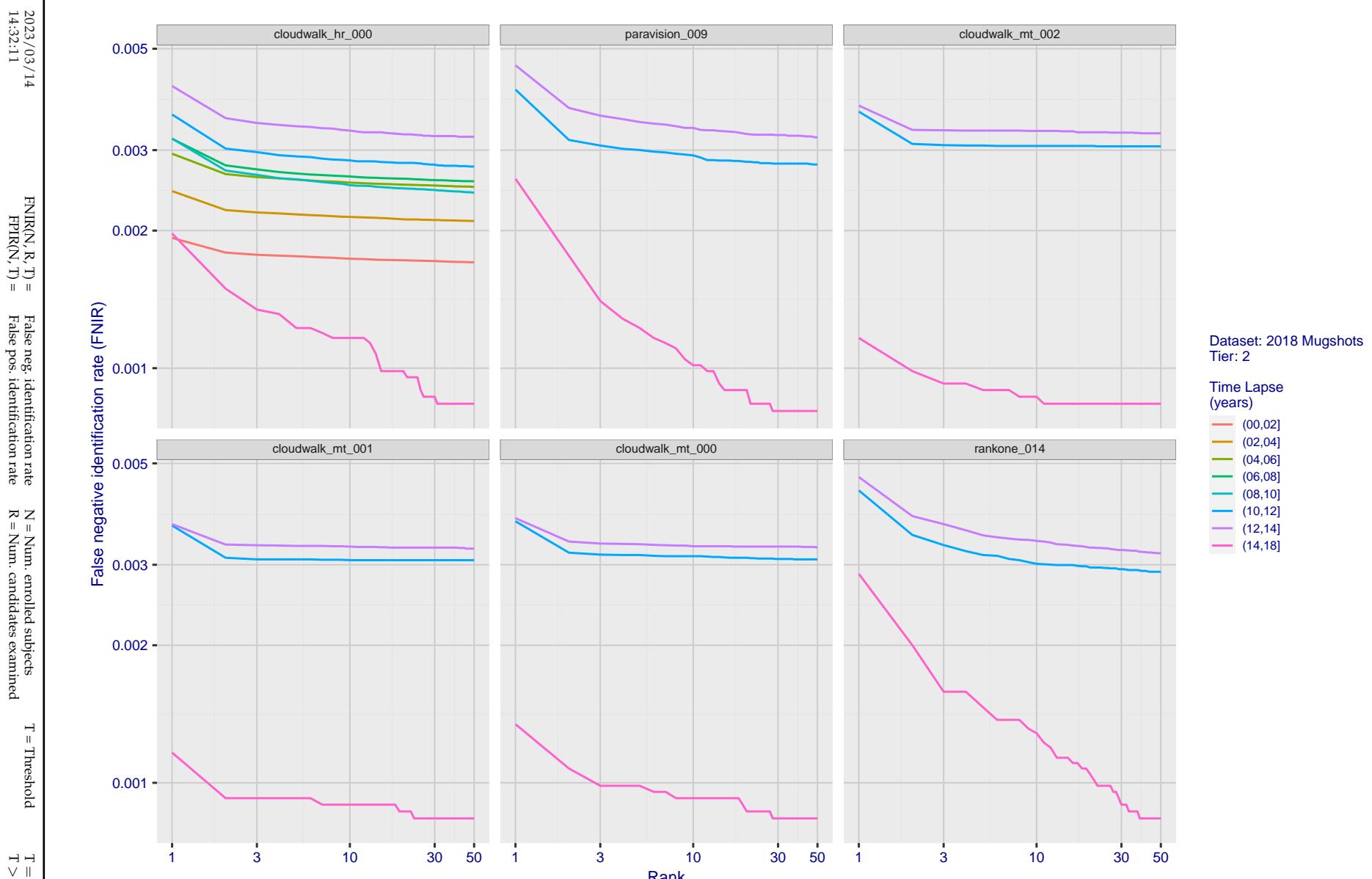


Figure 61: [FRVT-2018 Mugshot Ageing Dataset] Identification miss rates vs. rank by time-elapsed. The oldest image of each individual is enrolled. Thereafter, all more recent images are searched. Miss rates are computed over all searches noted in row 17 of Table 1 and binned by number of years between search and initial enrollment.

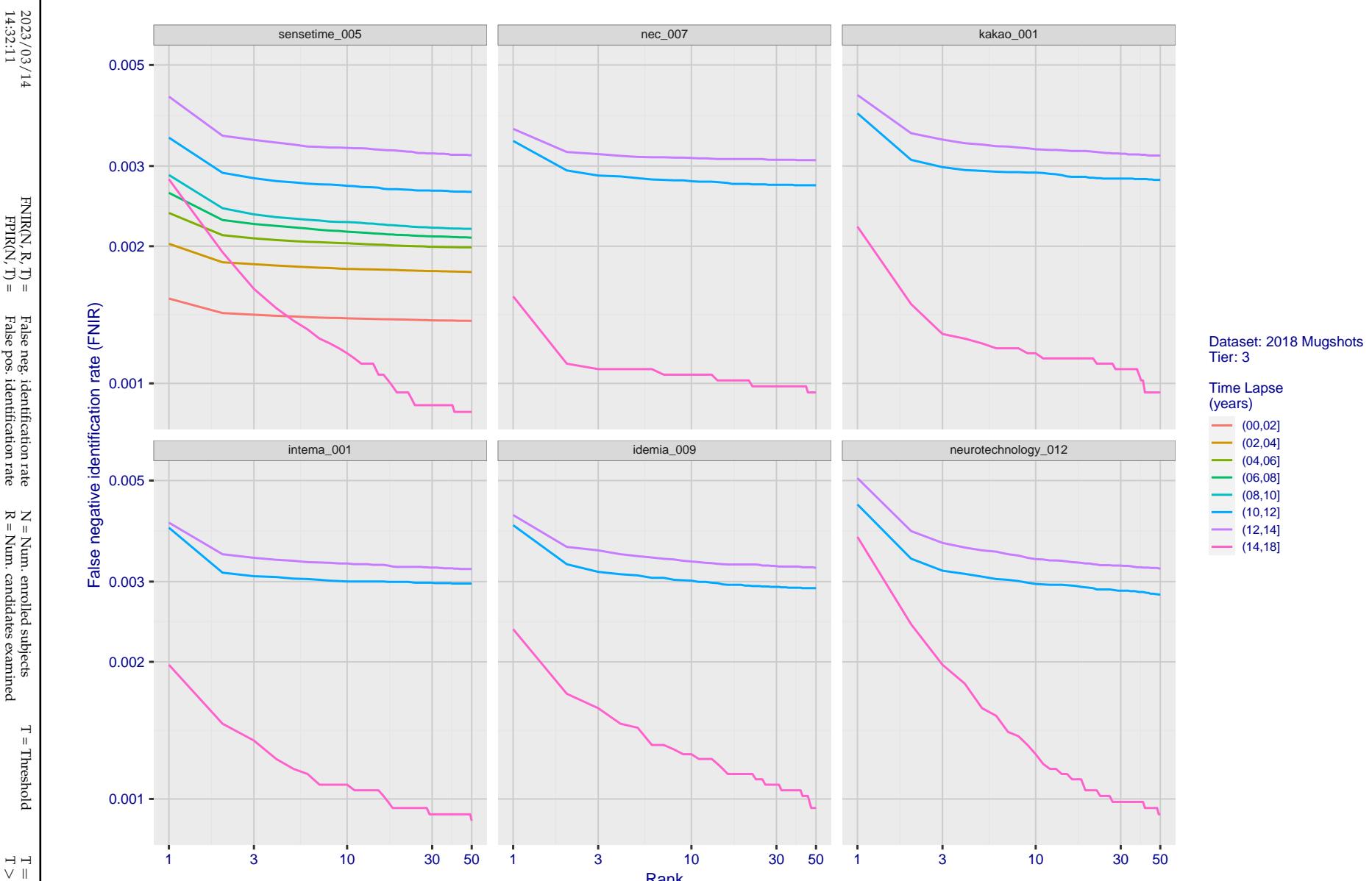


Figure 62: [FRVT-2018 Mugshot Ageing Dataset] Identification miss rates vs. rank by time-elapsed. The oldest image of each individual is enrolled. Thereafter, all more recent images are searched. Miss rates are computed over all searches noted in row 17 of Table 1 and binned by number of years between search and initial enrollment.

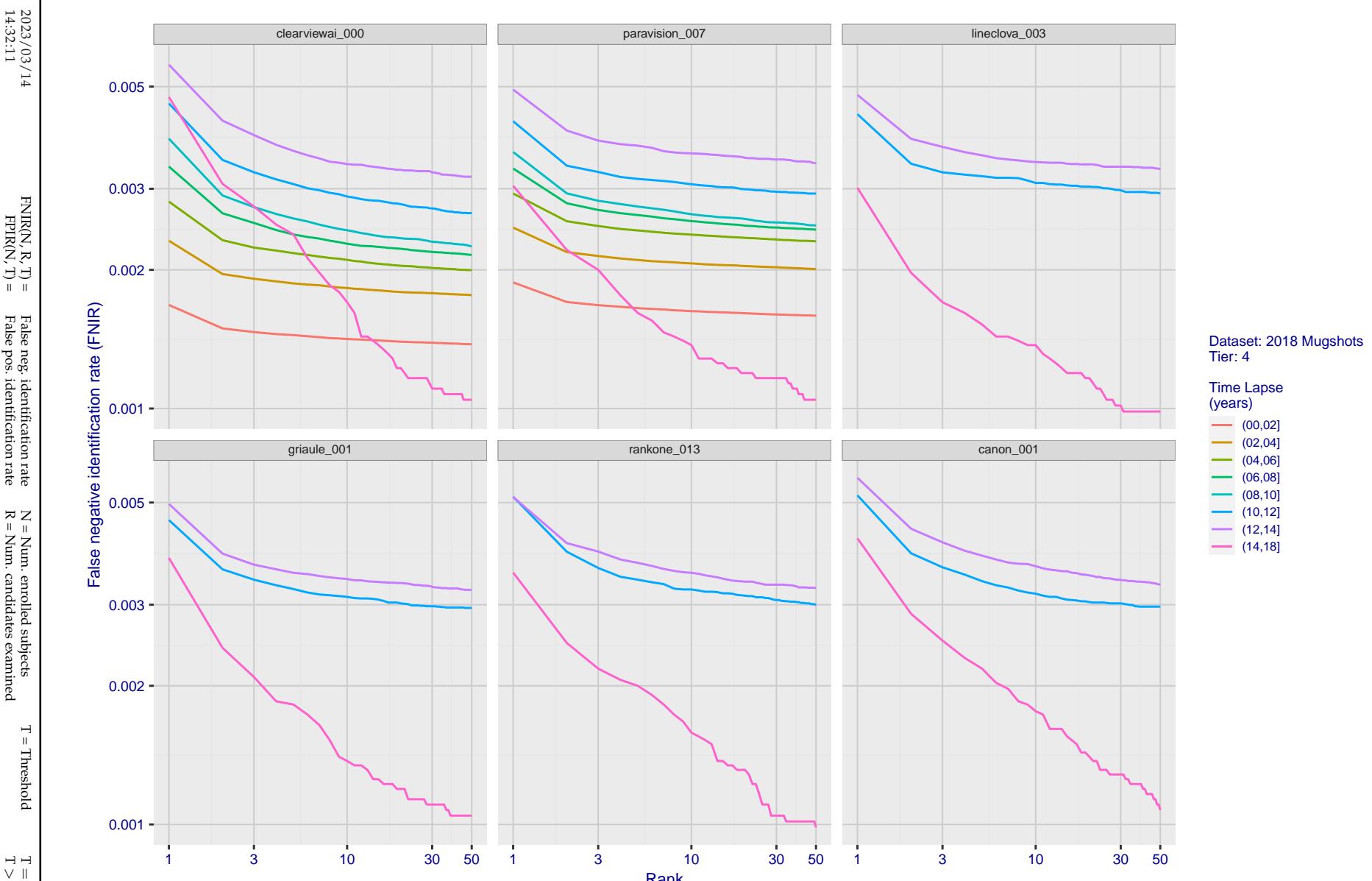


Figure 63: [FRVT-2018 Mugshot Ageing Dataset] Identification miss rates vs. rank by time elapsed. The oldest image of each individual is enrolled. Thereafter, all more recent images are searched. Miss rates are computed over all searches noted in row 17 of Table 1 and binned by number of years between search and initial enrollment.

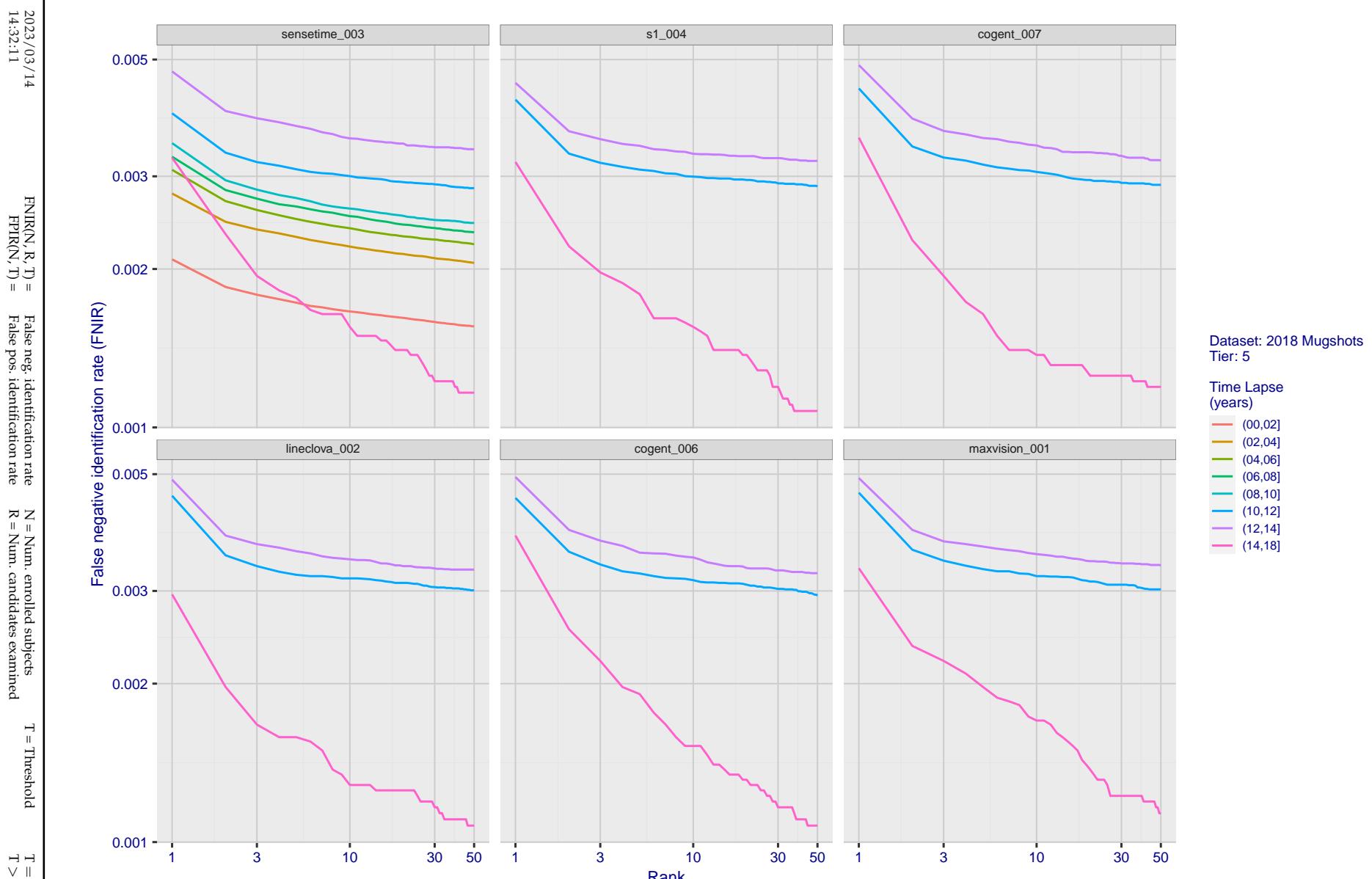


Figure 64: [FRVT-2018 Mugshot Ageing Dataset] Identification miss rates vs. rank by time-elapsed. The oldest image of each individual is enrolled. Thereafter, all more recent images are searched. Miss rates are computed over all searches noted in row 17 of Table 1 and binned by number of years between search and initial enrollment.

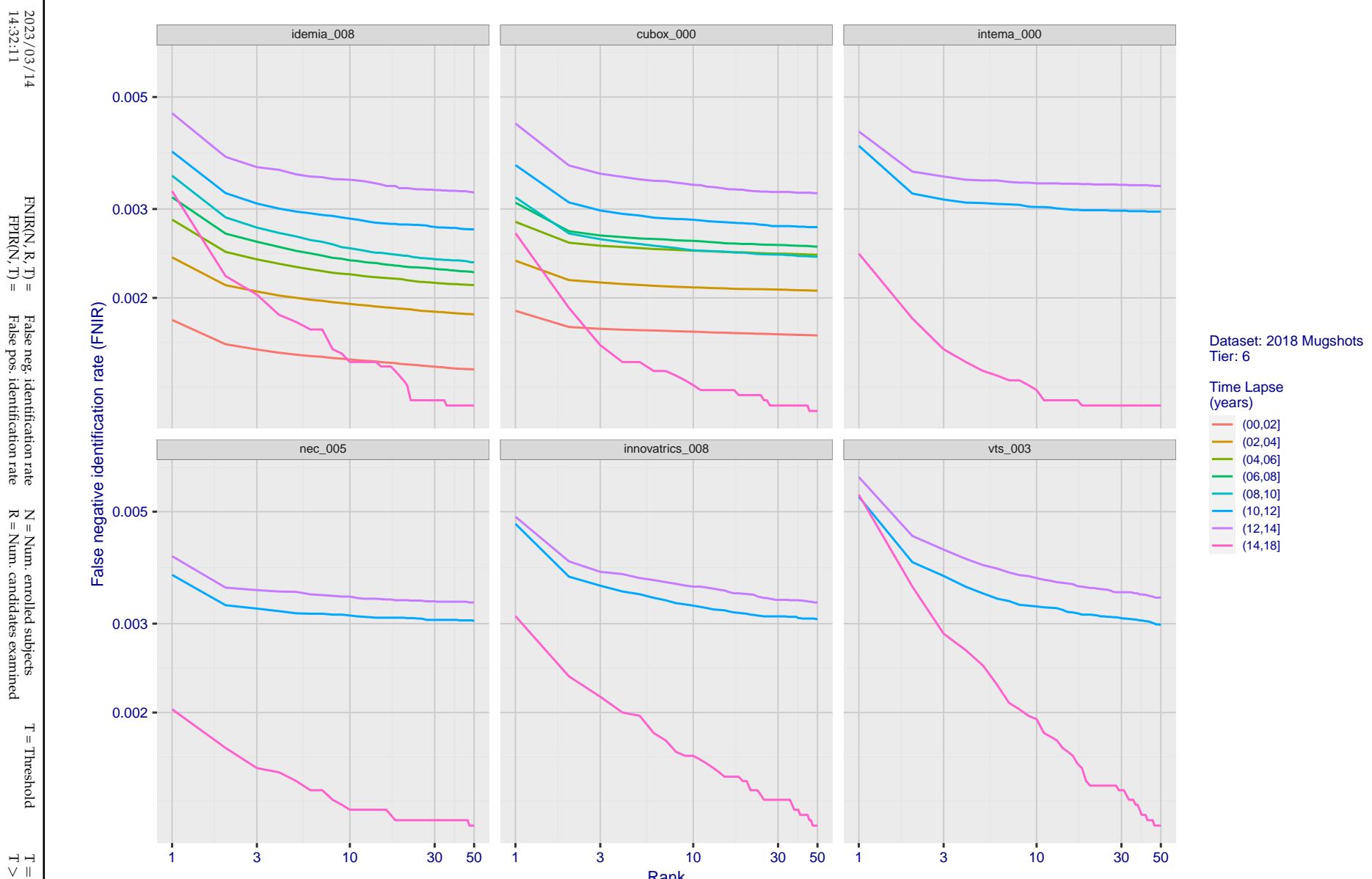


Figure 65: [FRVT-2018 Mugshot Ageing Dataset] Identification miss rates vs. rank by time-elapsed. The oldest image of each individual is enrolled. Thereafter, all more recent images are searched. Miss rates are computed over all searches noted in row 17 of Table 1 and binned by number of years between search and initial enrollment.

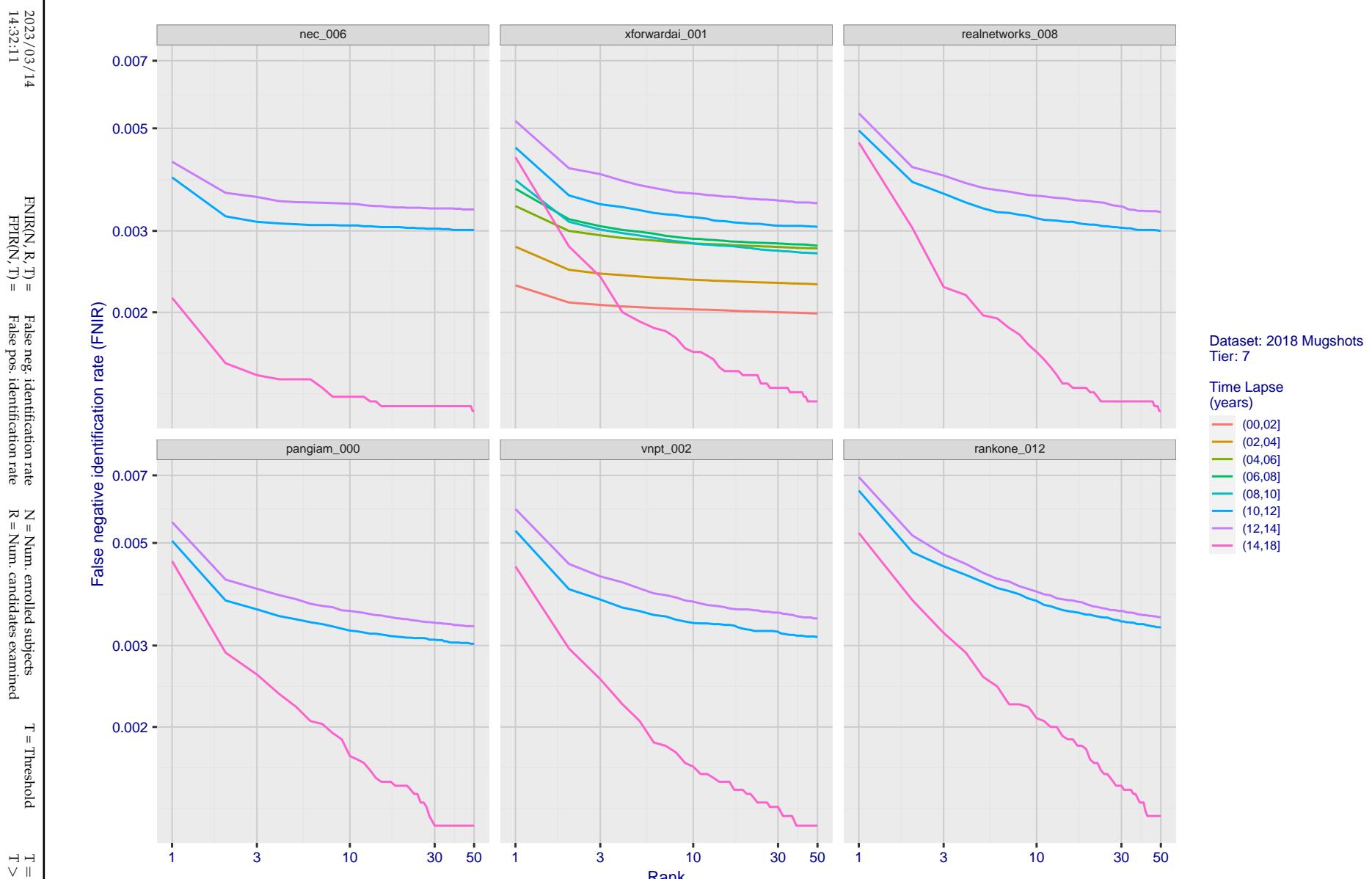


Figure 66: [FRVT-2018 Mugshot Ageing Dataset] Identification miss rates vs. rank by time elapsed. The oldest image of each individual is enrolled. Thereafter, all more recent images are searched. Miss rates are computed over all searches noted in row 17 of Table 1 and binned by number of years between search and initial enrollment.

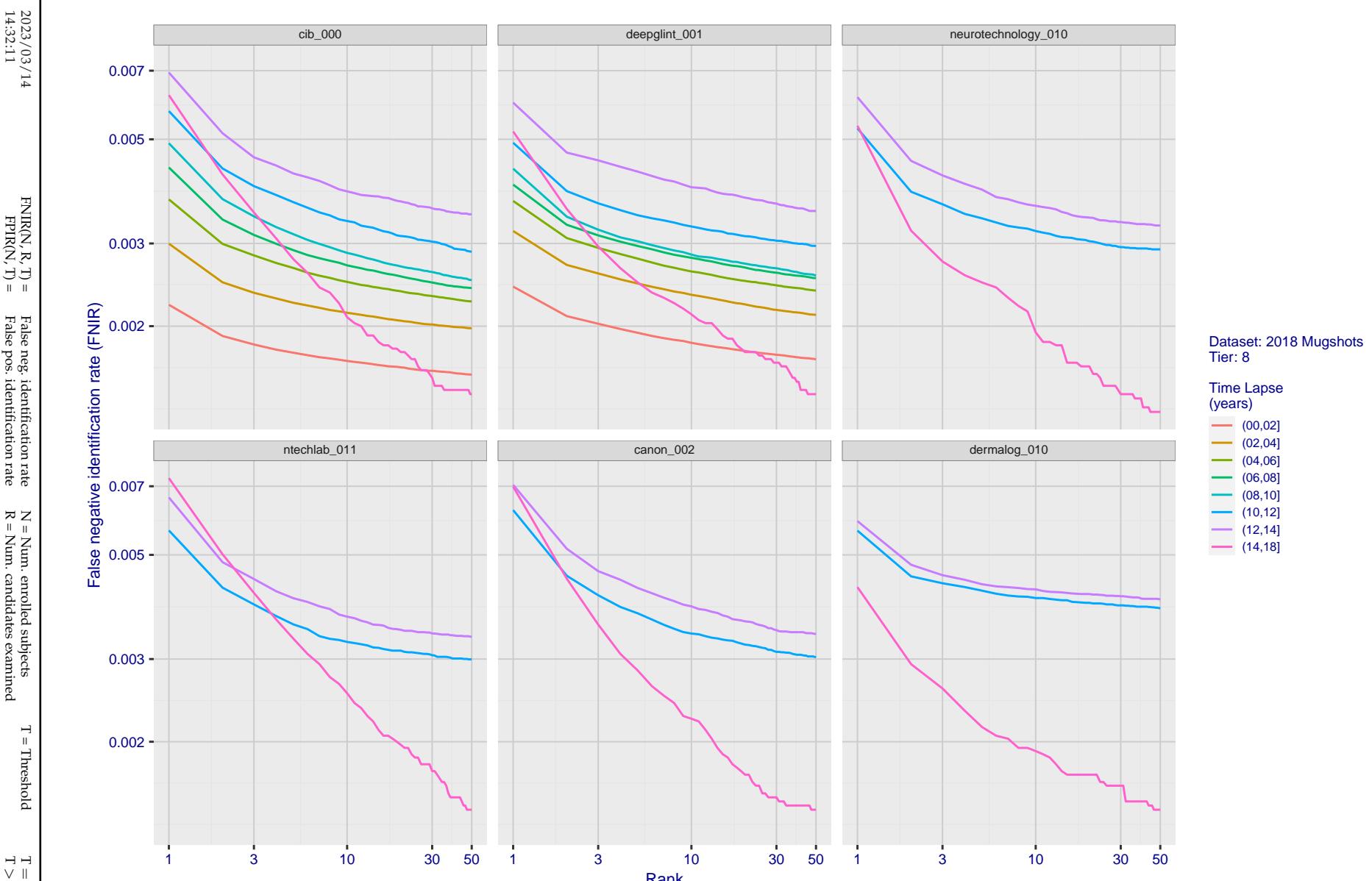


Figure 67: [FRVT-2018 Mugshot Ageing Dataset] Identification miss rates vs. rank by time-elapsed. The oldest image of each individual is enrolled. Thereafter, all more recent images are searched. Miss rates are computed over all searches noted in row 17 of Table 1 and binned by number of years between search and initial enrollment.

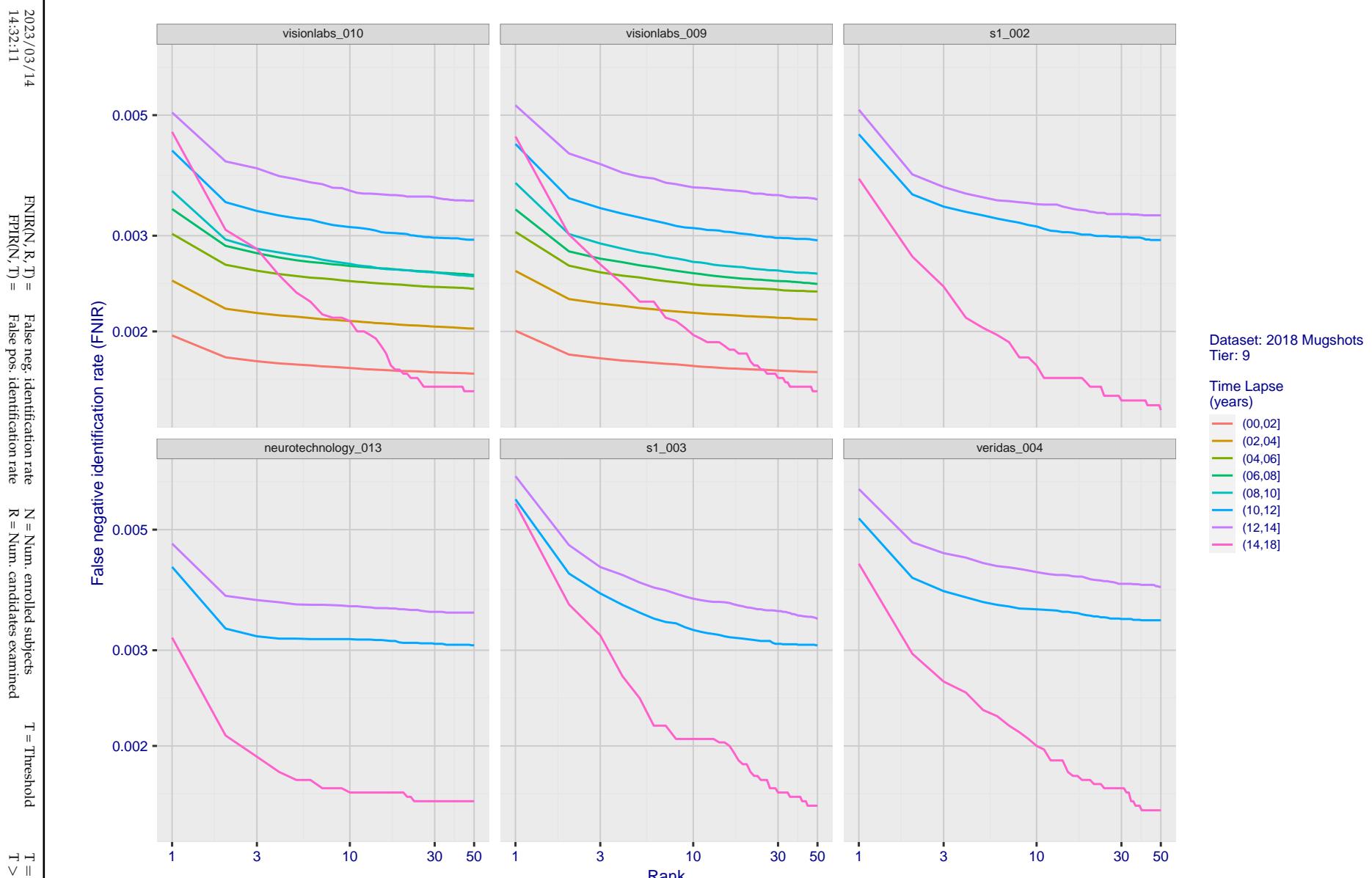


Figure 68: [FRVT-2018 Mugshot Ageing Dataset] Identification miss rates vs. rank by time-elapsed. The oldest image of each individual is enrolled. Thereafter, all more recent images are searched. Miss rates are computed over all searches noted in row 17 of Table 1 and binned by number of years between search and initial enrollment.

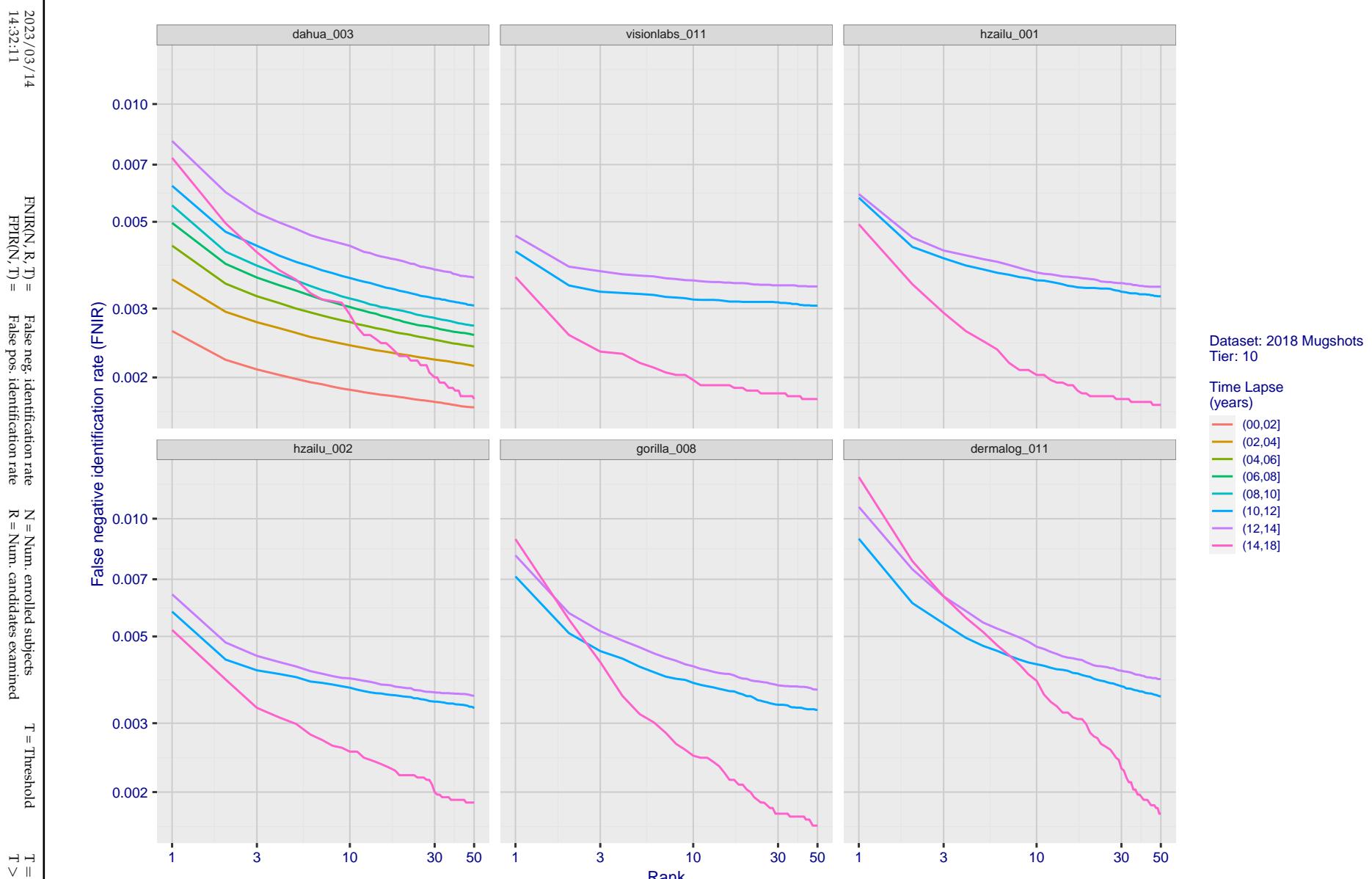


Figure 69: [FRVT-2018 Mugshot Ageing Dataset] Identification miss rates vs. rank by time-elapsed. The oldest image of each individual is enrolled. Thereafter, all more recent images are searched. Miss rates are computed over all searches noted in row 17 of Table 1 and binned by number of years between search and initial enrollment.

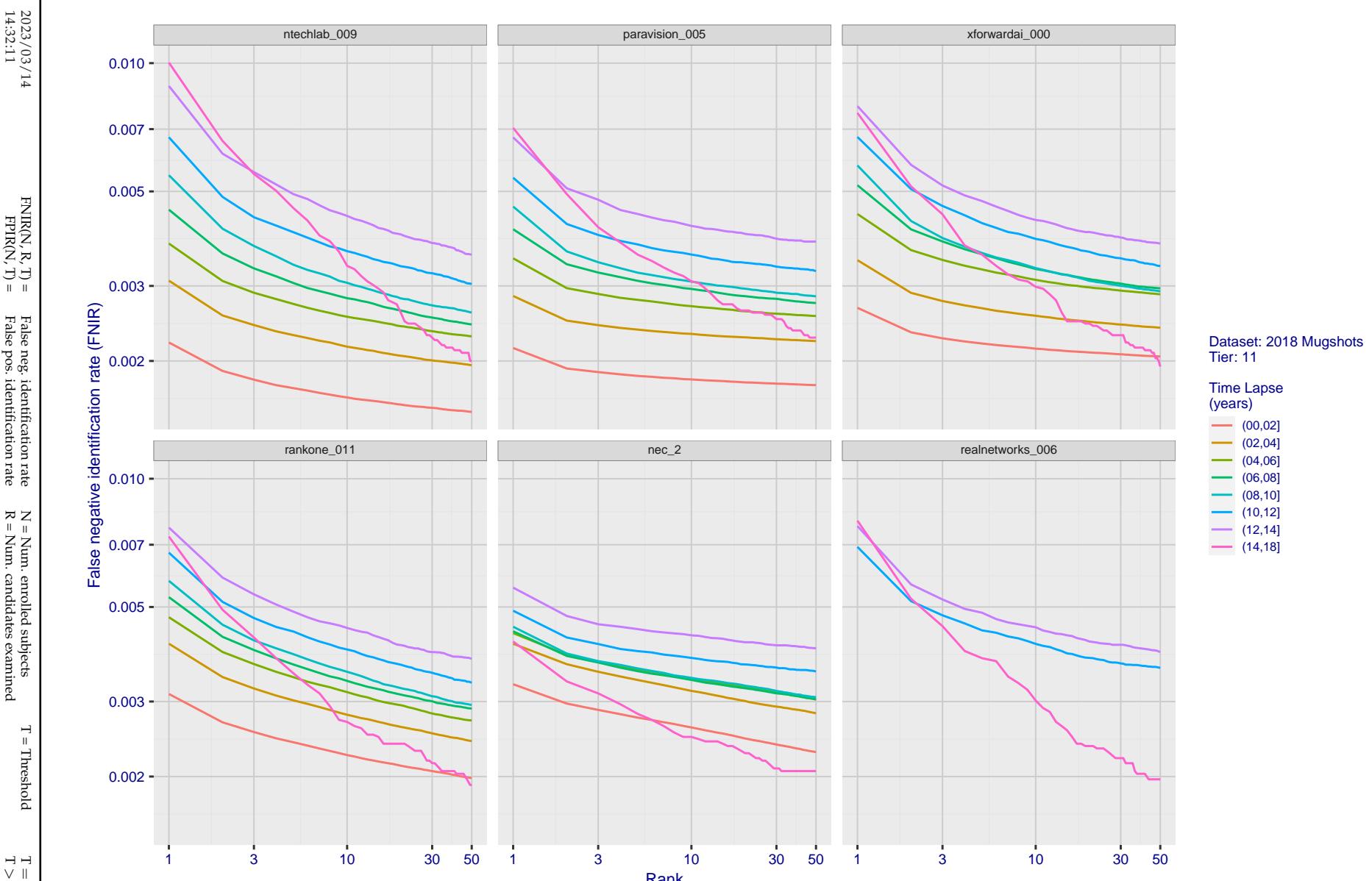


Figure 70: [FRVT-2018 Mugshot Ageing Dataset] Identification miss rates vs. rank by time-elapsed. The oldest image of each individual is enrolled. Thereafter, all more recent images are searched. Miss rates are computed over all searches noted in row 17 of Table 1 and binned by number of years between search and initial enrollment.

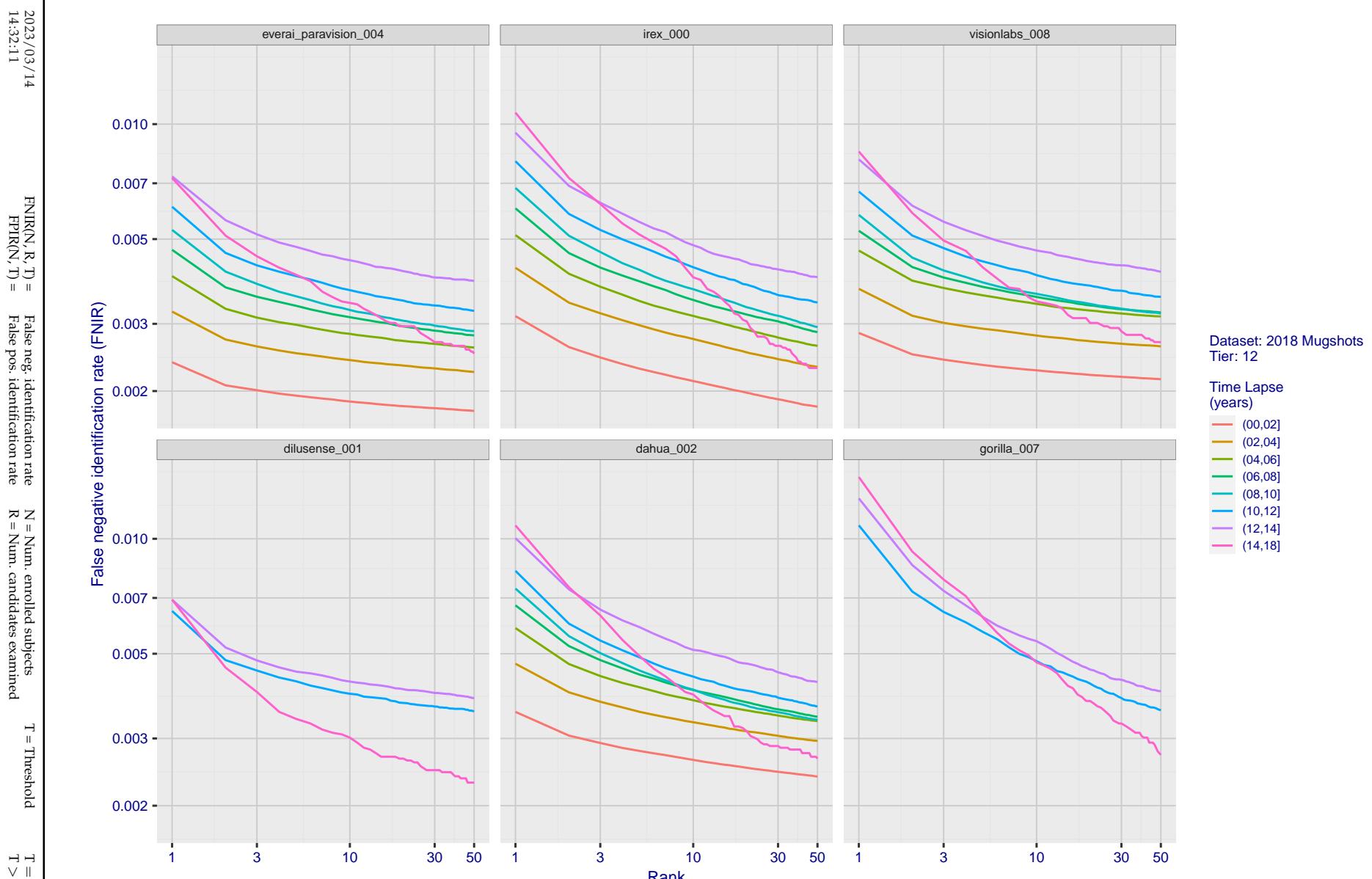


Figure 71: [FRVT-2018 Mugshot Ageing Dataset] Identification miss rates vs. rank by time-elapsed. The oldest image of each individual is enrolled. Thereafter, all more recent images are searched. Miss rates are computed over all searches noted in row 17 of Table 1 and binned by number of years between search and initial enrollment.

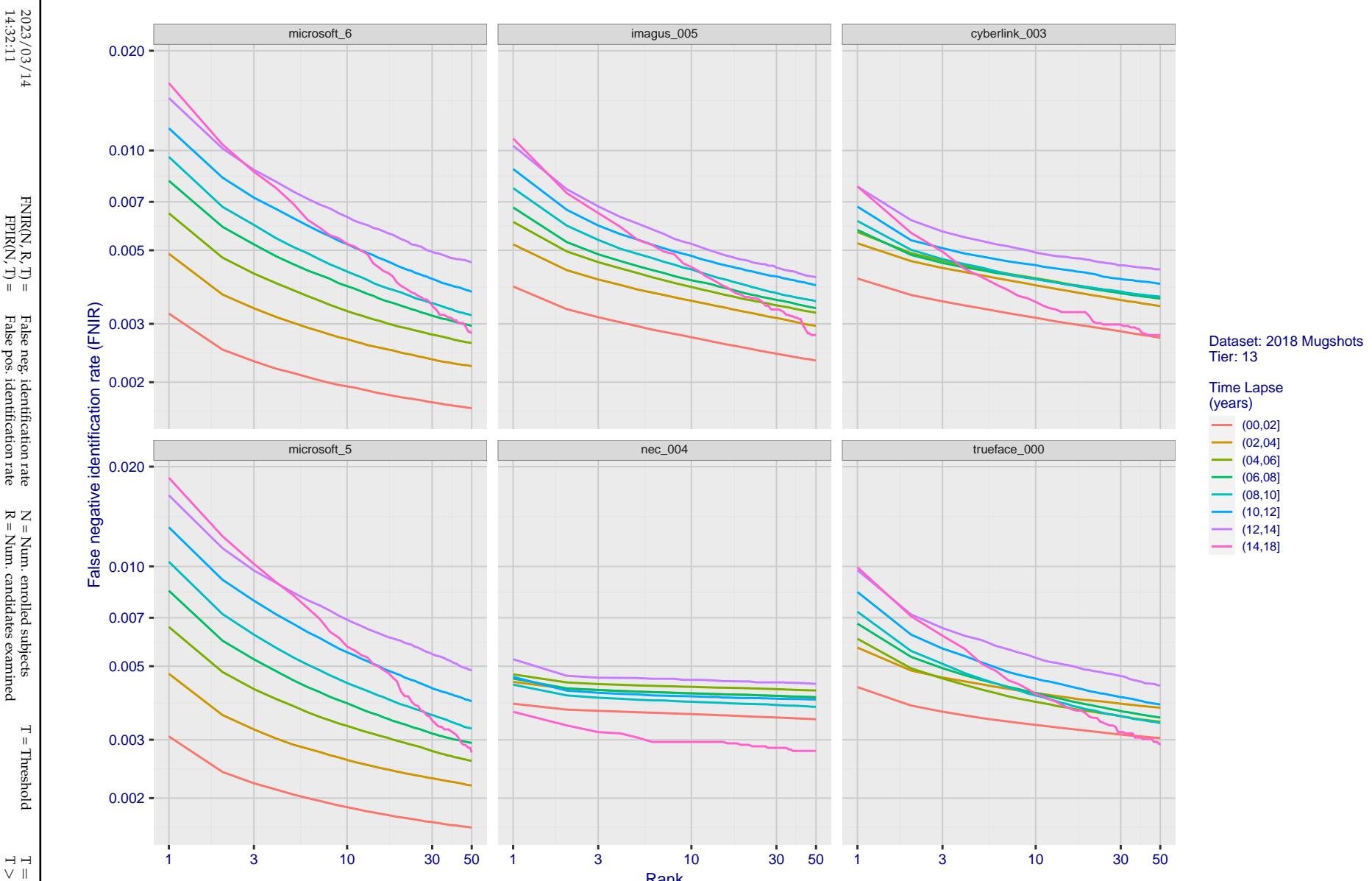


Figure 72: [FRVT-2018 Mugshot Ageing Dataset] Identification miss rates vs. rank by time-elapsed. The oldest image of each individual is enrolled. Thereafter, all more recent images are searched. Miss rates are computed over all searches noted in row 17 of Table 1 and binned by number of years between search and initial enrollment.

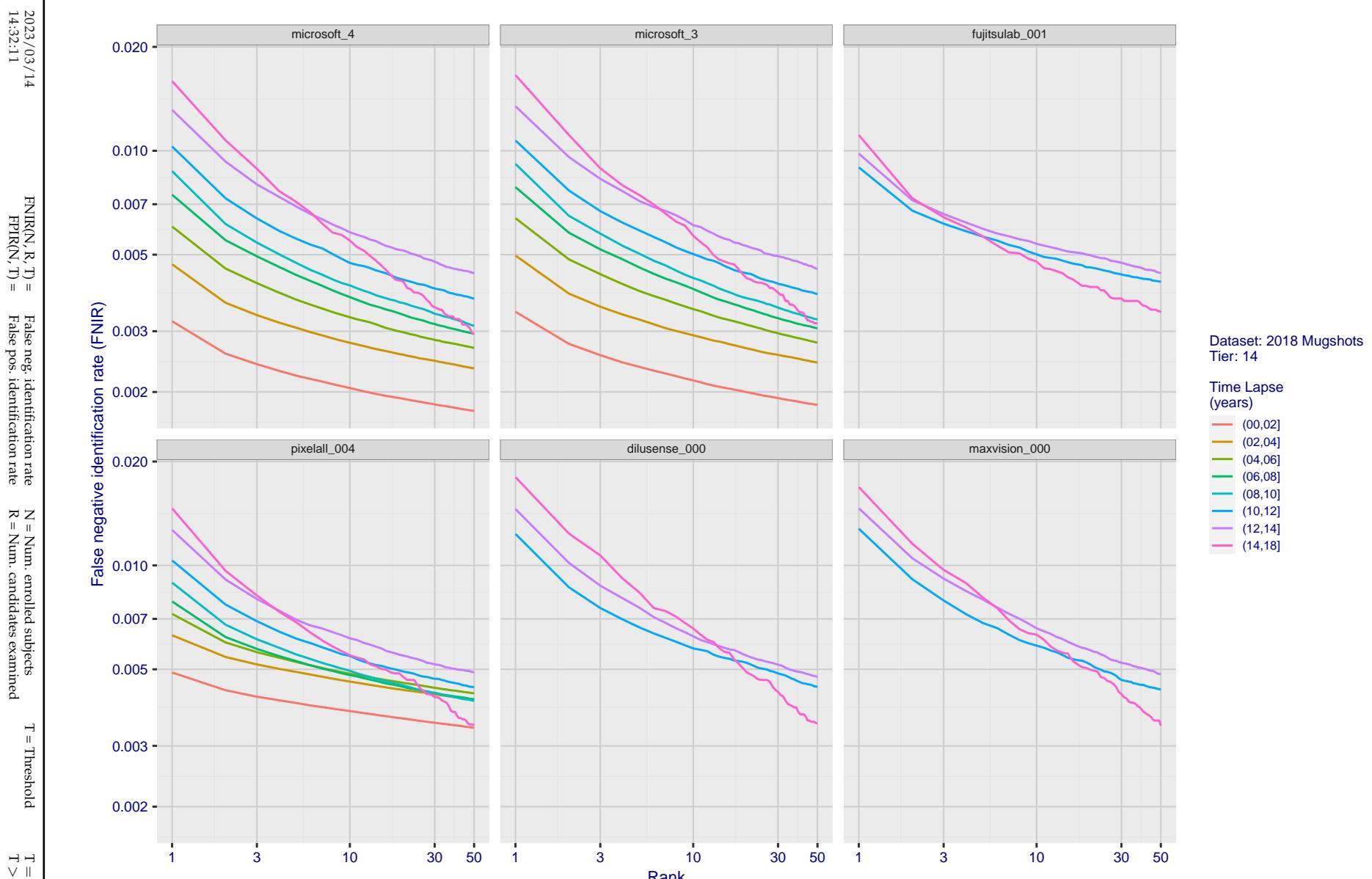


Figure 73: [FRVT-2018 Mugshot Ageing Dataset] Identification miss rates vs. rank by time-elapsed. The oldest image of each individual is enrolled. Thereafter, all more recent images are searched. Miss rates are computed over all searches noted in row 17 of Table 1 and binned by number of years between search and initial enrollment.

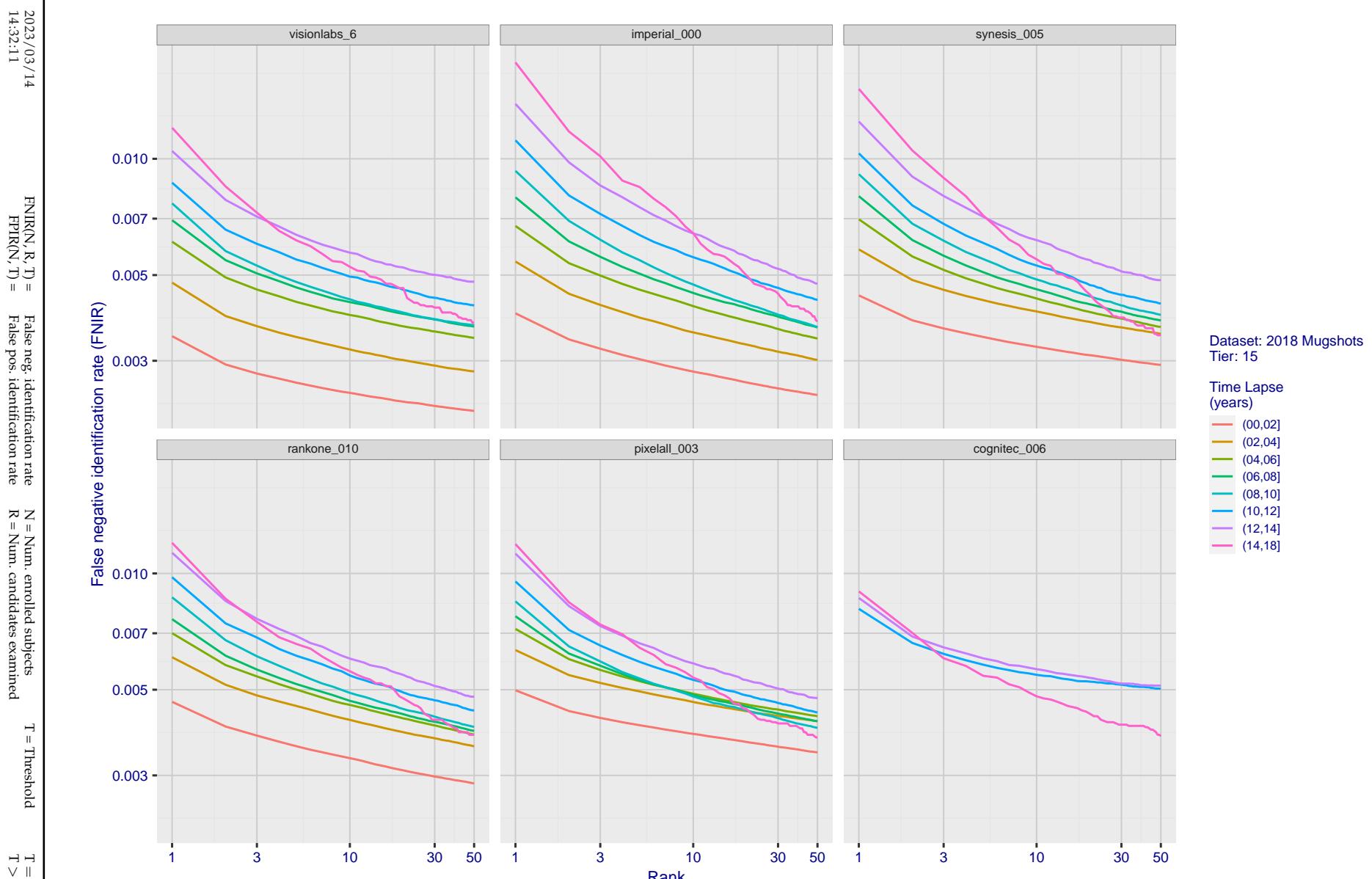


Figure 74: [FRVT-2018 Mugshot Ageing Dataset] Identification miss rates vs. rank by time-elapsed. The oldest image of each individual is enrolled. Thereafter, all more recent images are searched. Miss rates are computed over all searches noted in row 17 of Table 1 and binned by number of years between search and initial enrollment.

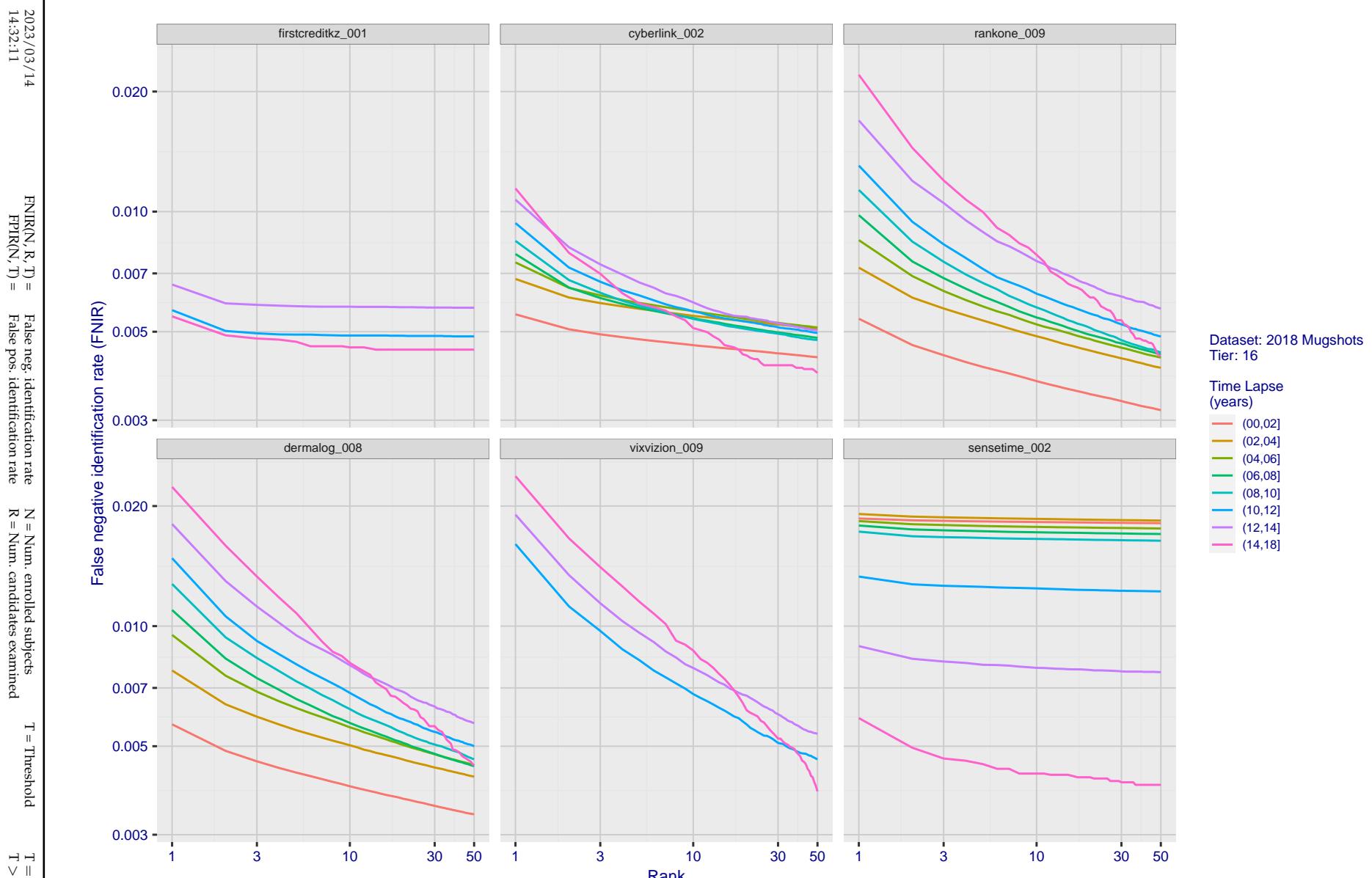


Figure 75: [FRVT-2018 Mugshot Ageing Dataset] Identification miss rates vs. rank by time-elapsed. The oldest image of each individual is enrolled. Thereafter, all more recent images are searched. Miss rates are computed over all searches noted in row 17 of Table 1 and binned by number of years between search and initial enrollment.

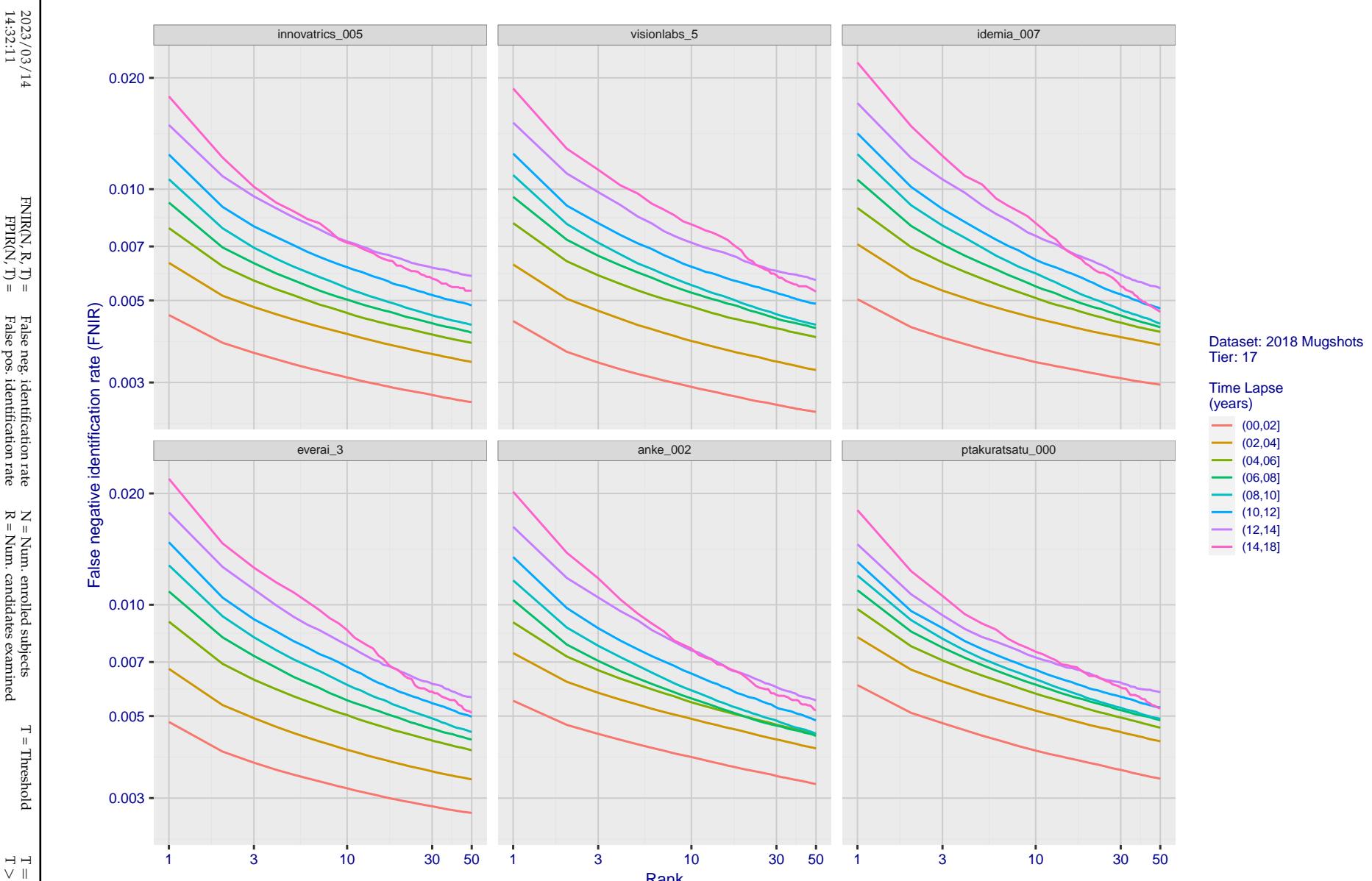


Figure 76: [FRVT-2018 Mugshot Ageing Dataset] Identification miss rates vs. rank by time elapsed. The oldest image of each individual is enrolled. Thereafter, all more recent images are searched. Miss rates are computed over all searches noted in row 17 of Table 1 and binned by number of years between search and initial enrollment.

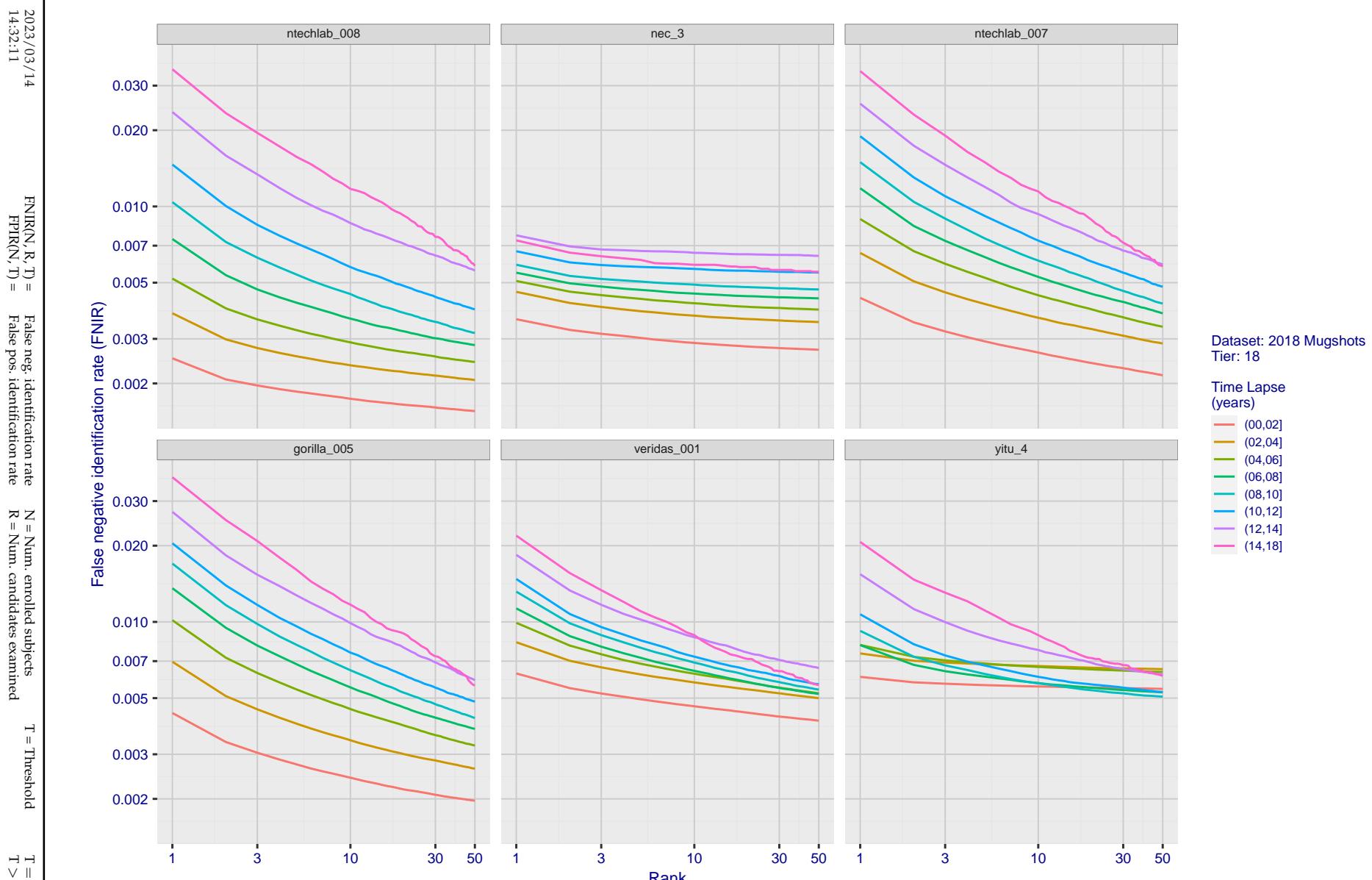


Figure 77: [FRVT-2018 Mugshot Ageing Dataset] Identification miss rates vs. rank by time-elapsed. The oldest image of each individual is enrolled. Thereafter, all more recent images are searched. Miss rates are computed over all searches noted in row 17 of Table 1 and binned by number of years between search and initial enrollment.

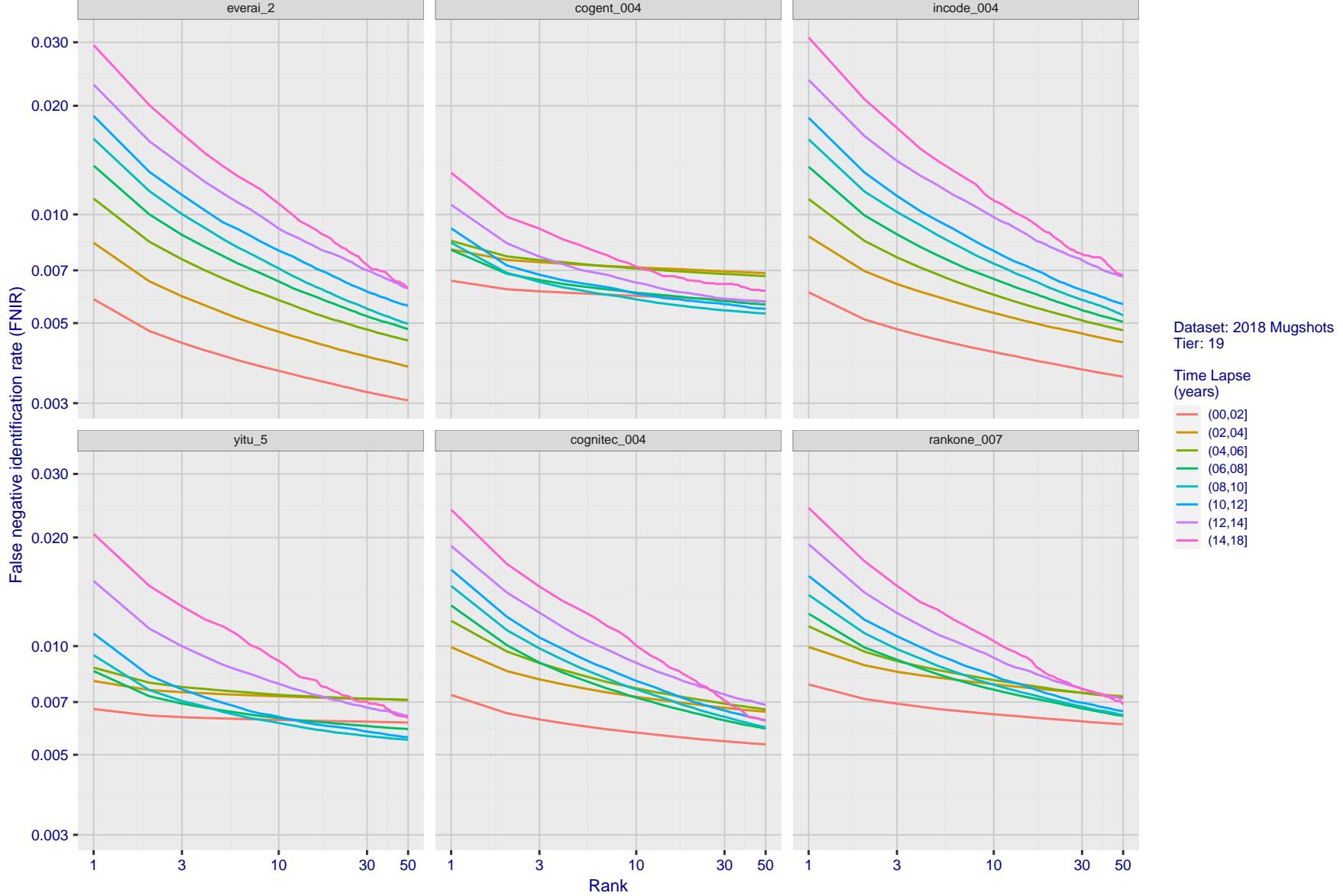


Figure 78: [FRVT-2018 Mugshot Ageing Dataset] Identification miss rates vs. rank by time elapsed. The oldest image of each individual is enrolled. Thereafter, all more recent images are searched. Miss rates are computed over all searches noted in row 17 of Table 1 and binned by number of years between search and initial enrollment.

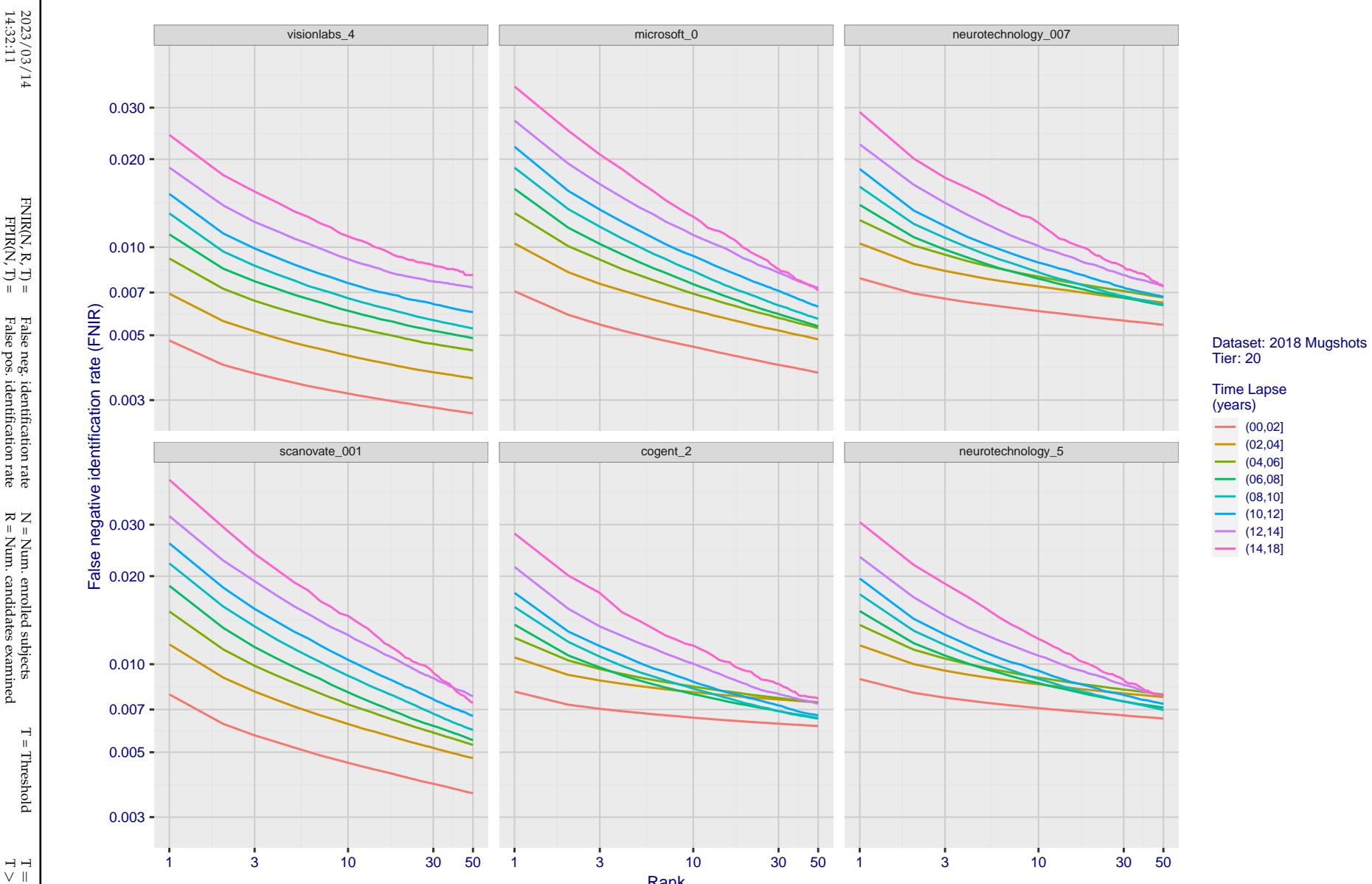


Figure 79: [FRVT-2018 Mugshot Ageing Dataset] Identification miss rates vs. rank by time-elapsed. The oldest image of each individual is enrolled. Thereafter, all more recent images are searched. Miss rates are computed over all searches noted in row 17 of Table 1 and binned by number of years between search and initial enrollment.

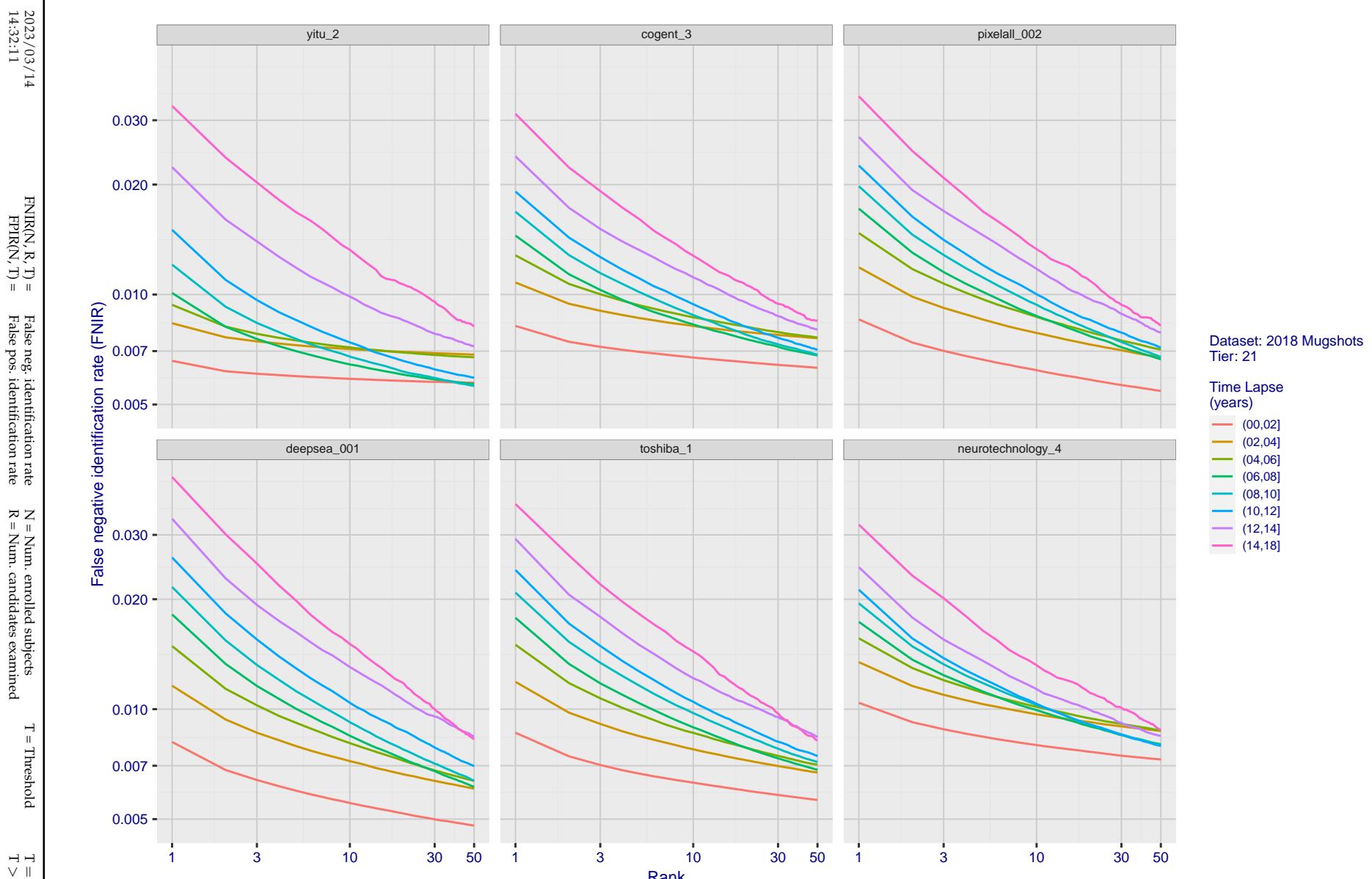


Figure 80: [FRVT-2018 Mugshot Ageing Dataset] Identification miss rates vs. rank by time-elapsed. The oldest image of each individual is enrolled. Thereafter, all more recent images are searched. Miss rates are computed over all searches noted in row 17 of Table 1 and binned by number of years between search and initial enrollment.

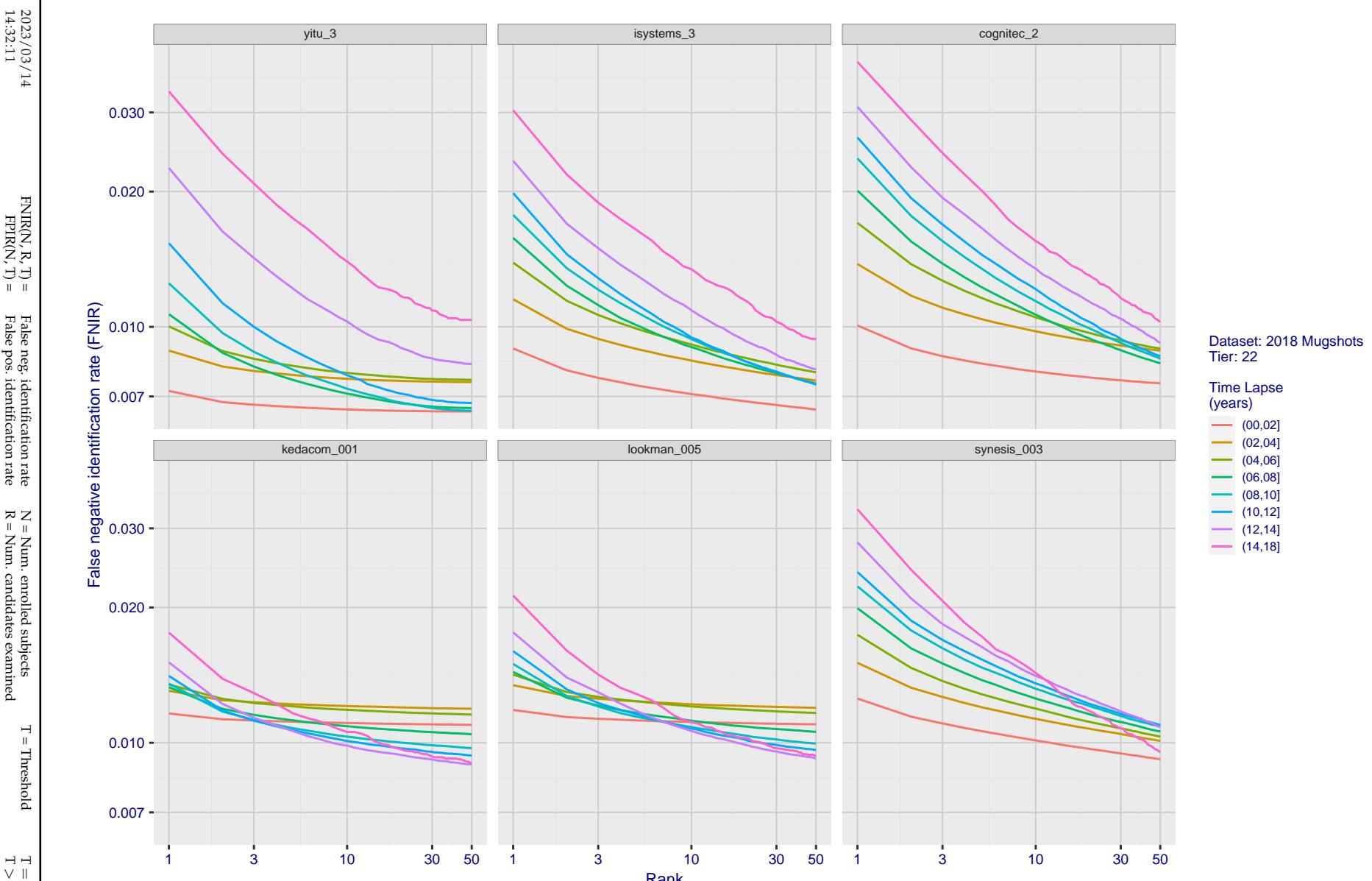


Figure 81: [FRVT-2018 Mugshot Ageing Dataset] Identification miss rates vs. rank by time-elapsed. The oldest image of each individual is enrolled. Thereafter, all more recent images are searched. Miss rates are computed over all searches noted in row 17 of Table 1 and binned by number of years between search and initial enrollment.

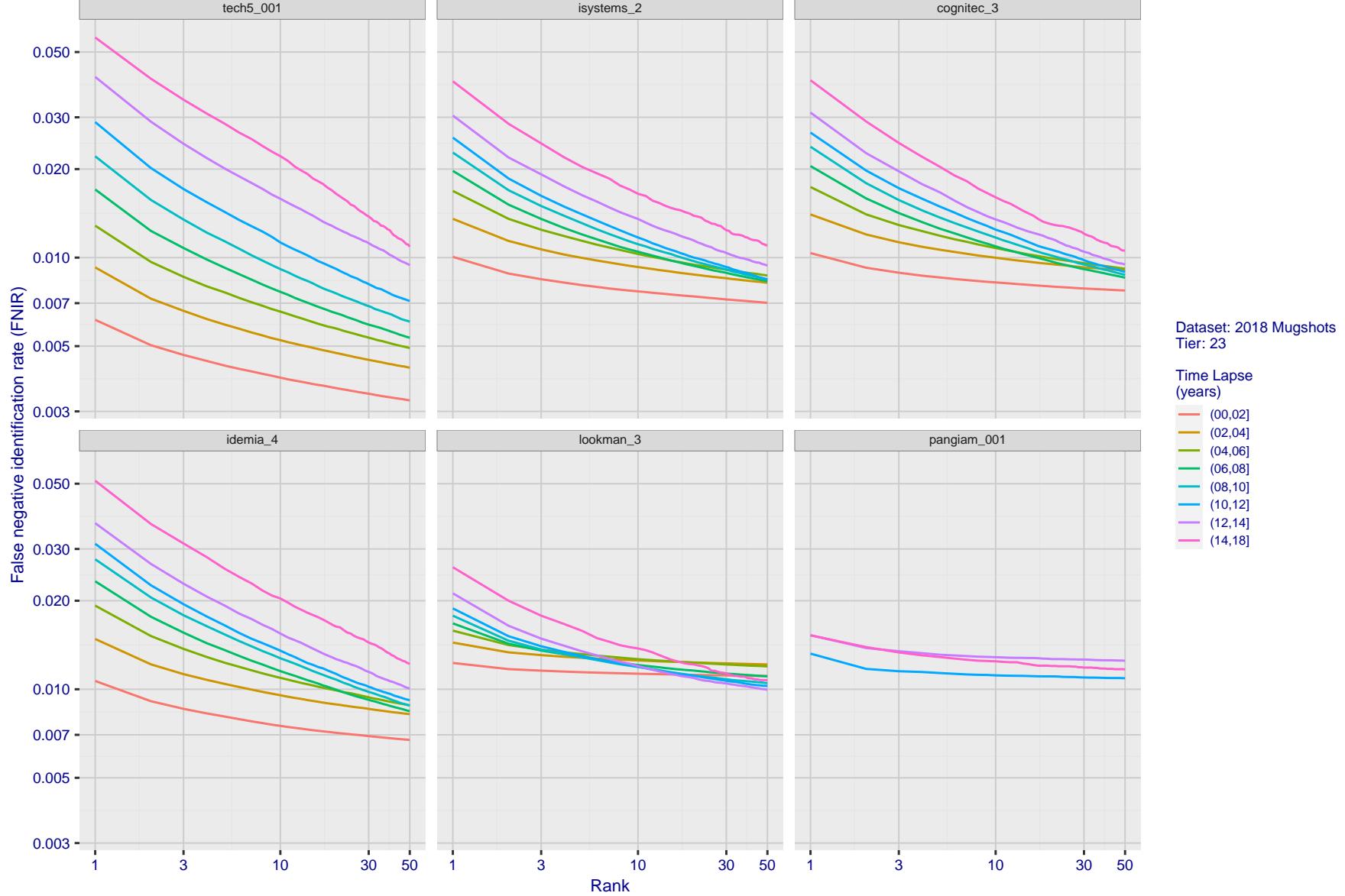


Figure 82: [FRVT-2018 Mugshot Ageing Dataset] Identification miss rates vs. rank by time-elapsed. The oldest image of each individual is enrolled. Thereafter, all more recent images are searched. Miss rates are computed over all searches noted in row 17 of Table 1 and binned by number of years between search and initial enrollment.

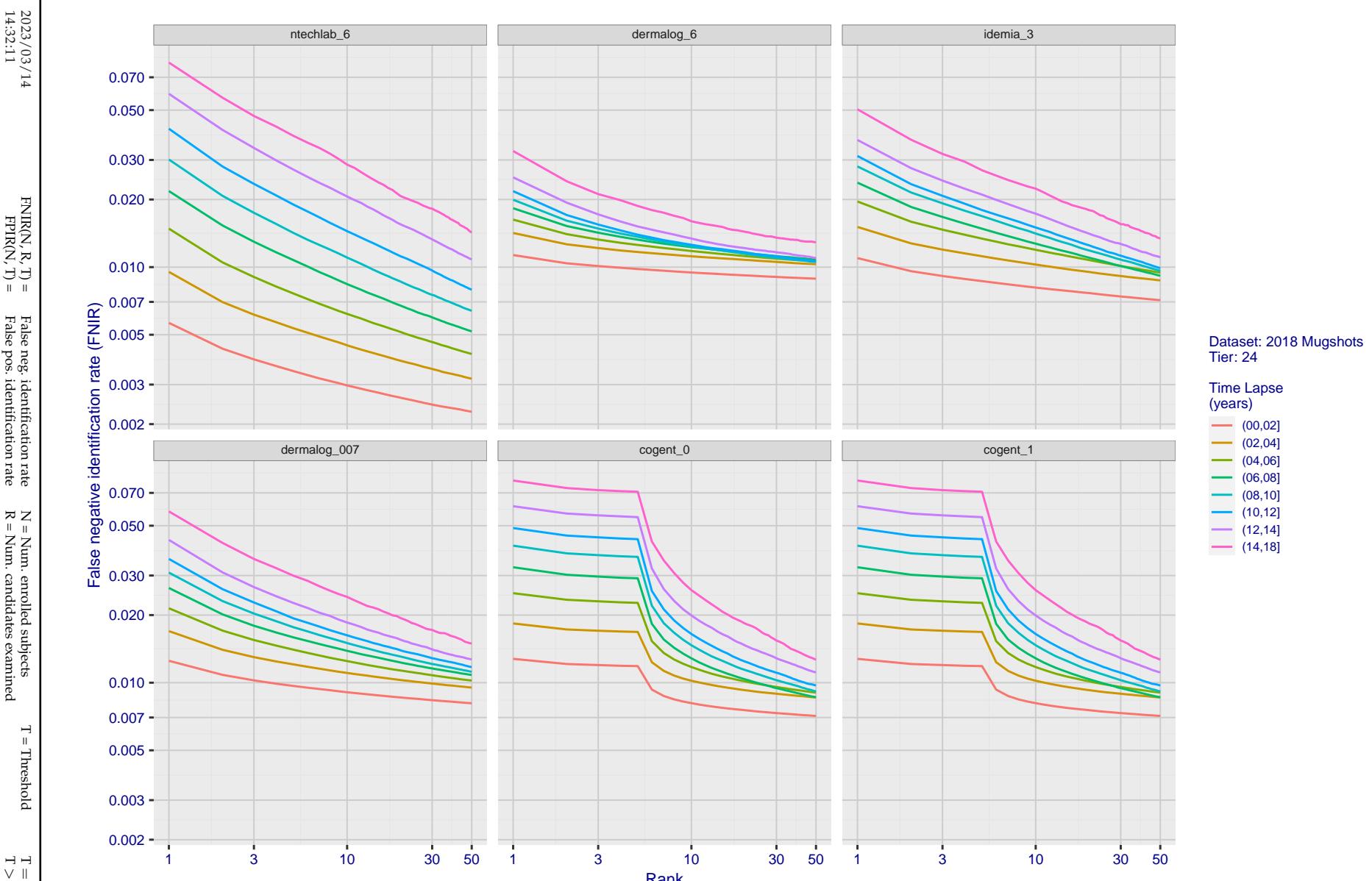


Figure 83: [FRVT-2018 Mugshot Ageing Dataset] Identification miss rates vs. rank by time-elapsed. The oldest image of each individual is enrolled. Thereafter, all more recent images are searched. Miss rates are computed over all searches noted in row 17 of Table 1 and binned by number of years between search and initial enrollment.

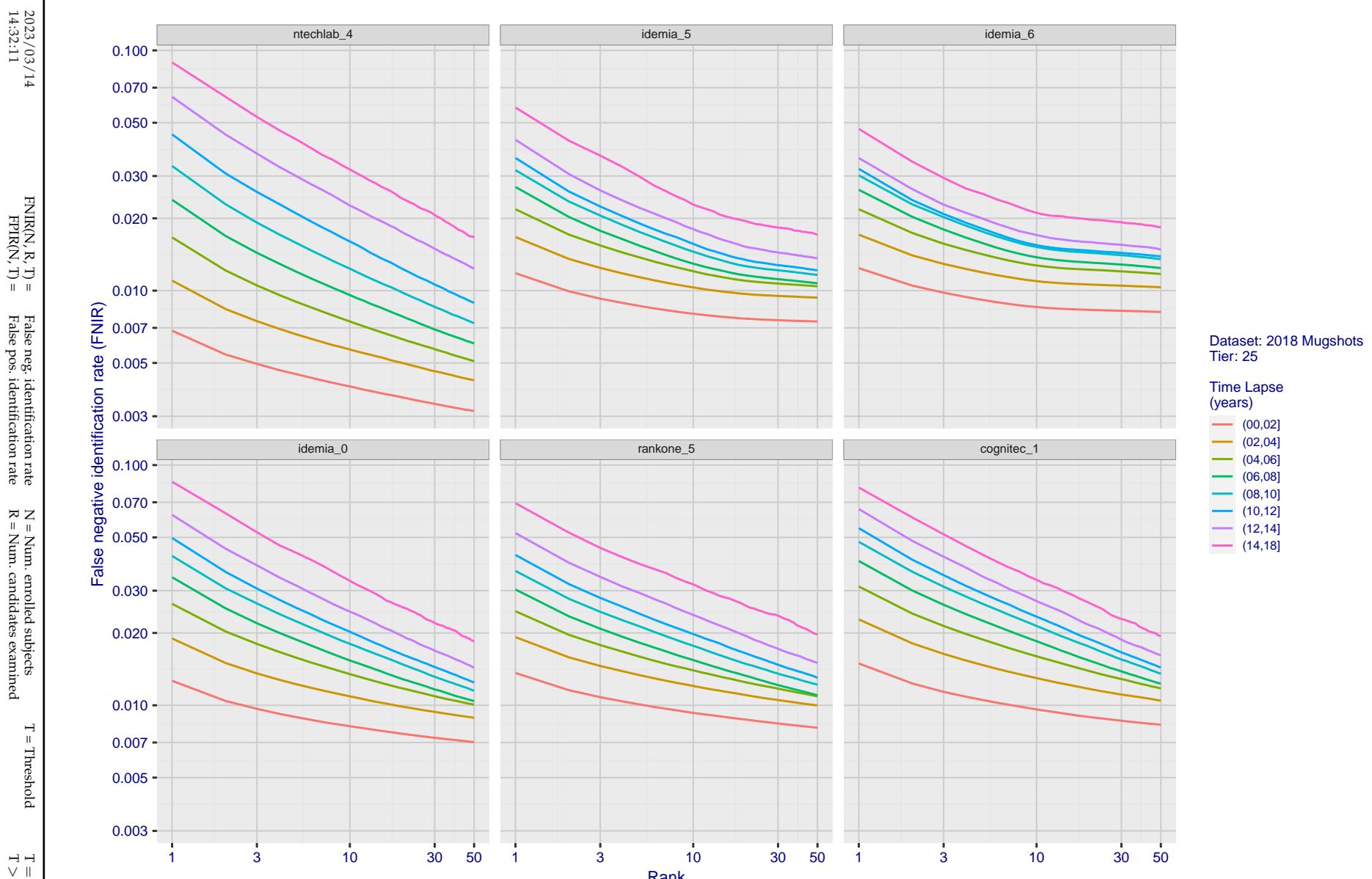


Figure 84: [FRVT-2018 Mugshot Ageing Dataset] Identification miss rates vs. rank by time elapsed. The oldest image of each individual is enrolled. Thereafter, all more recent images are searched. Miss rates are computed over all searches noted in row 17 of Table 1 and binned by number of years between search and initial enrollment.

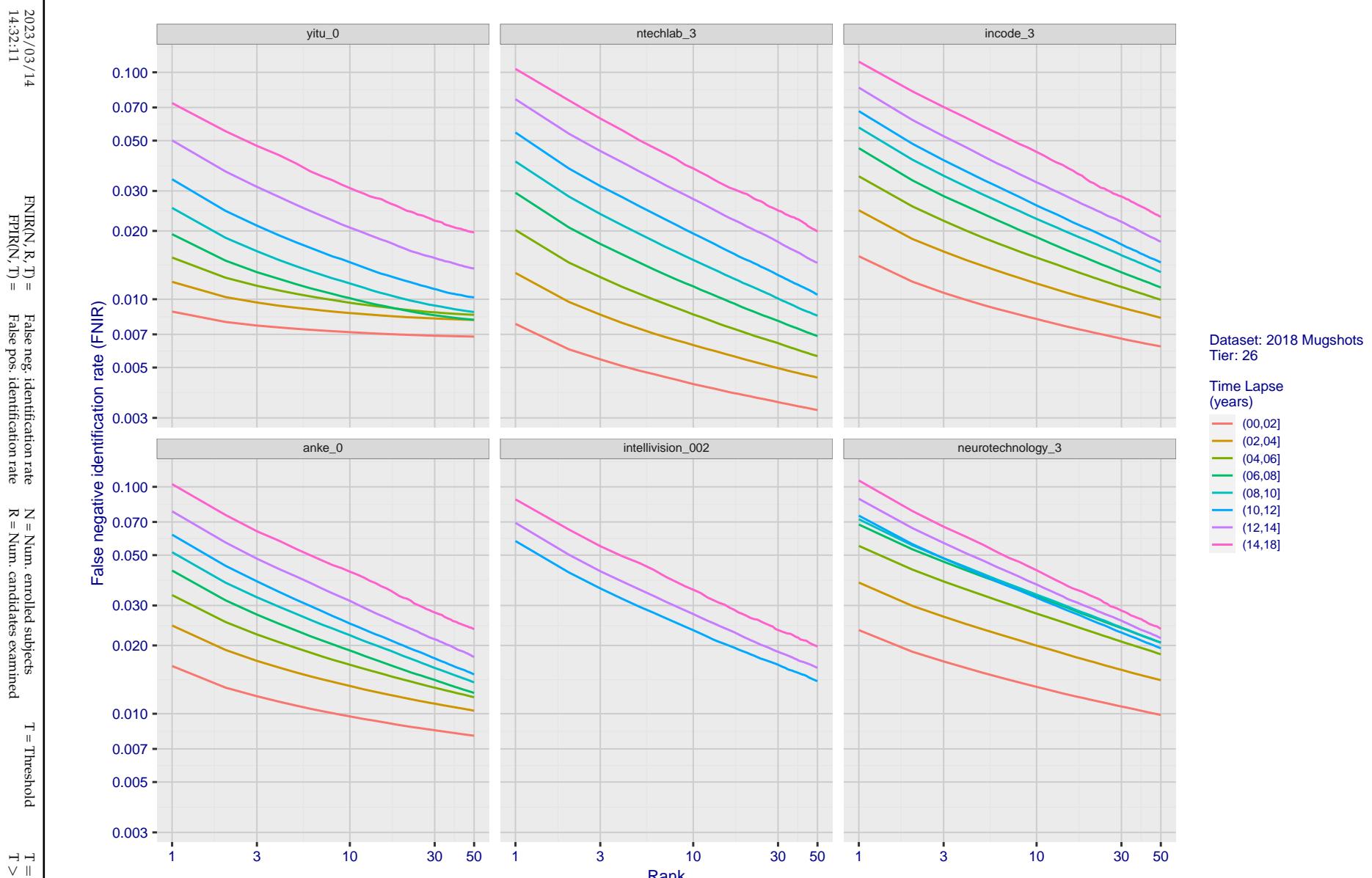


Figure 85: [FRVT-2018 Mugshot Ageing Dataset] Identification miss rates vs. rank by time elapsed. The oldest image of each individual is enrolled. Thereafter, all more recent images are searched. Miss rates are computed over all searches noted in row 17 of Table 1 and binned by number of years between search and initial enrollment.

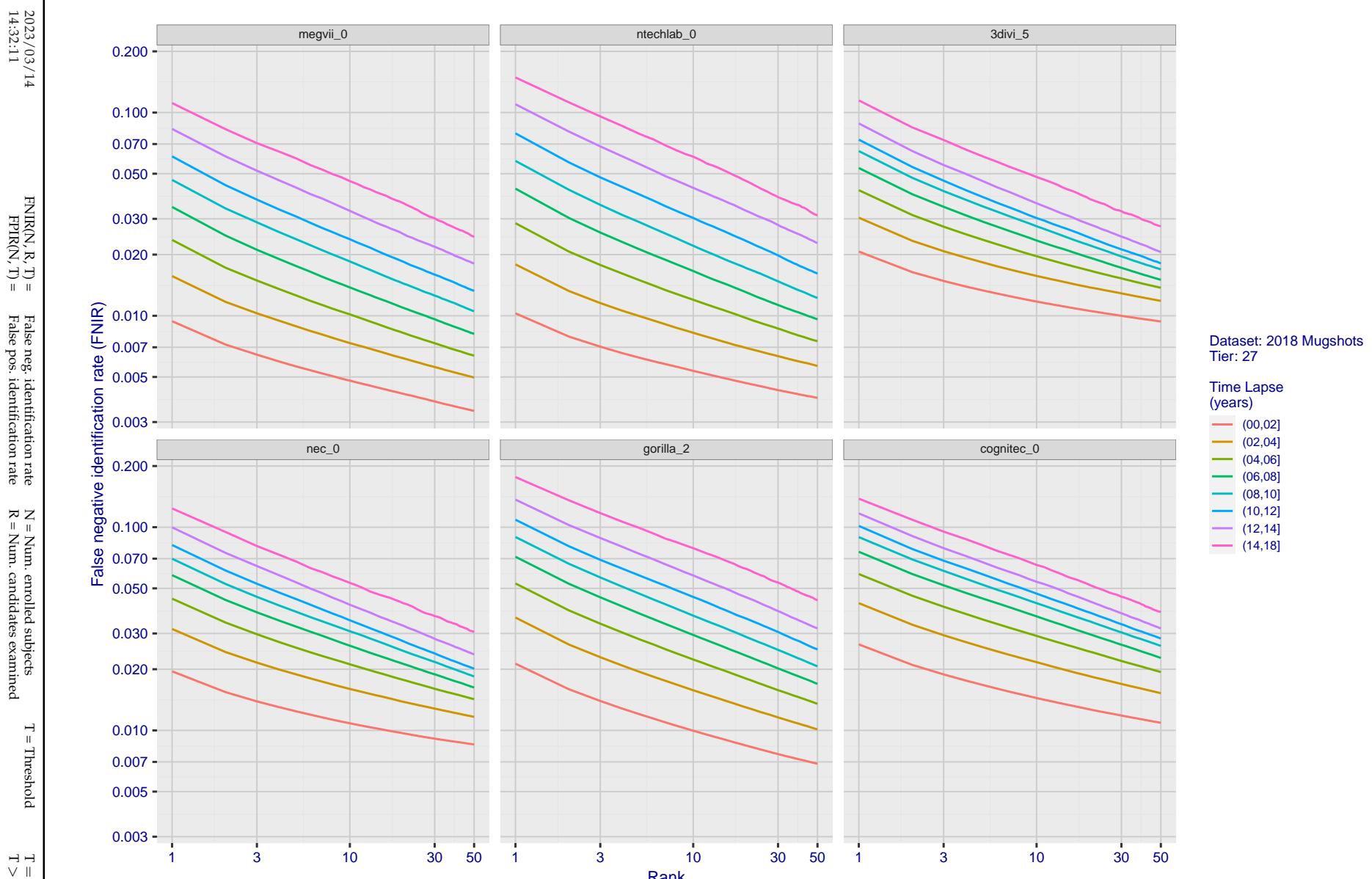


Figure 86: [FRVT-2018 Mugshot Ageing Dataset] Identification miss rates vs. rank by time-elapsed. The oldest image of each individual is enrolled. Thereafter, all more recent images are searched. Miss rates are computed over all searches noted in row 17 of Table 1 and binned by number of years between search and initial enrollment.

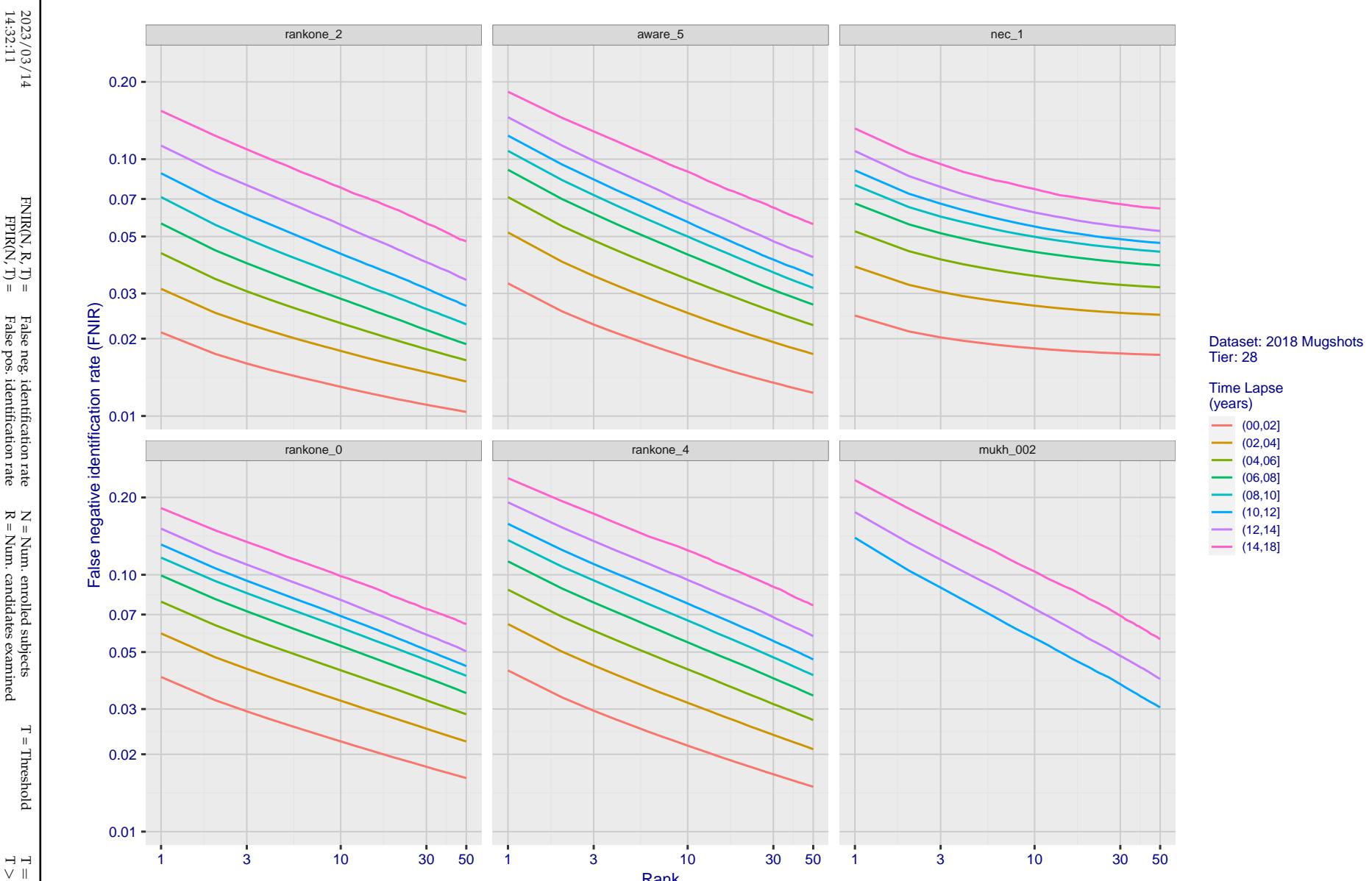


Figure 87: [FRVT-2018 Mugshot Ageing Dataset] Identification miss rates vs. rank by time-elapsed. The oldest image of each individual is enrolled. Thereafter, all more recent images are searched. Miss rates are computed over all searches noted in row 17 of Table 1 and binned by number of years between search and initial enrollment.

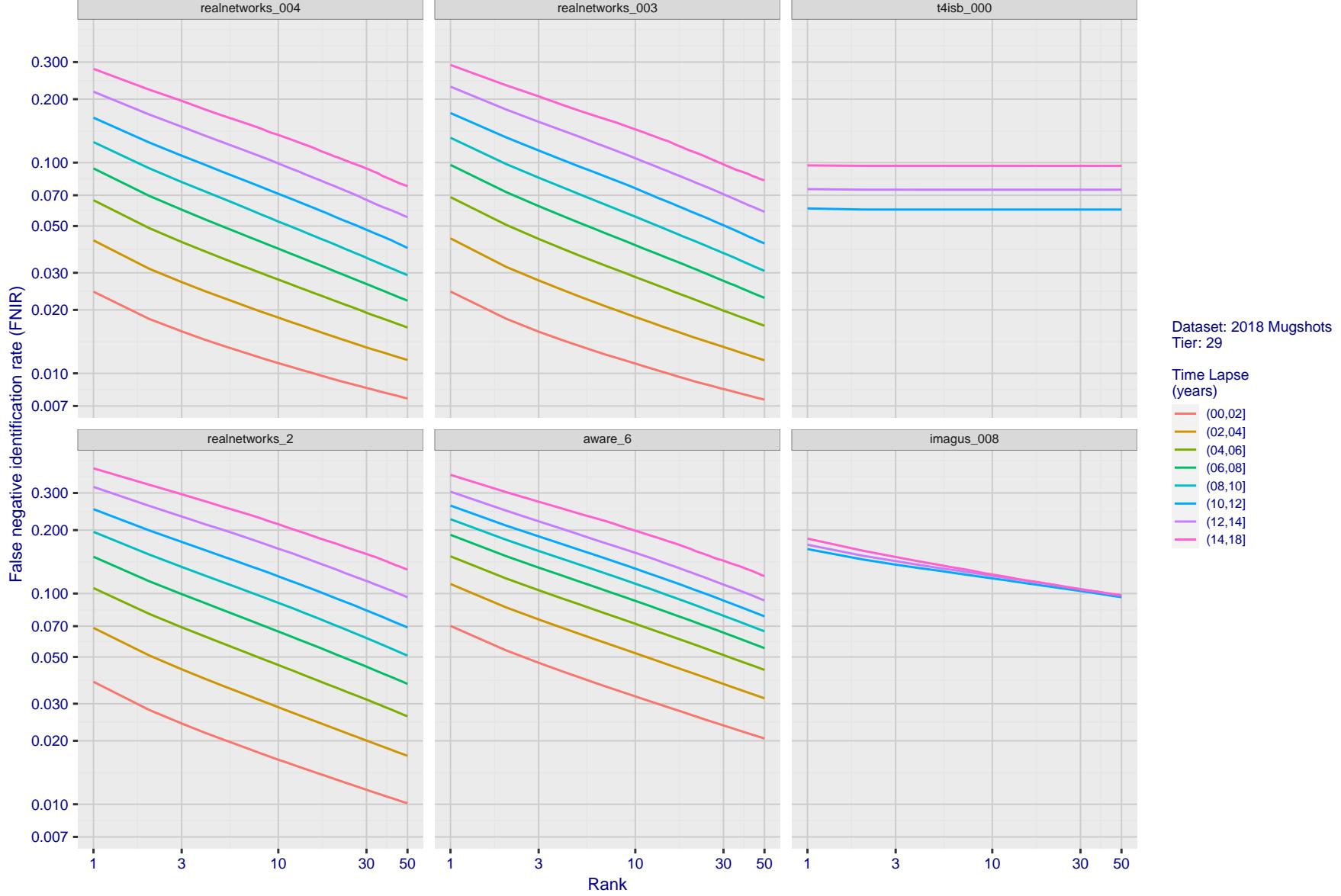


Figure 88: [FRVT-2018 Mugshot Ageing Dataset] Identification miss rates vs. rank by time-elapsed. The oldest image of each individual is enrolled. Thereafter, all more recent images are searched. Miss rates are computed over all searches noted in row 17 of Table 1 and binned by number of years between search and initial enrollment.

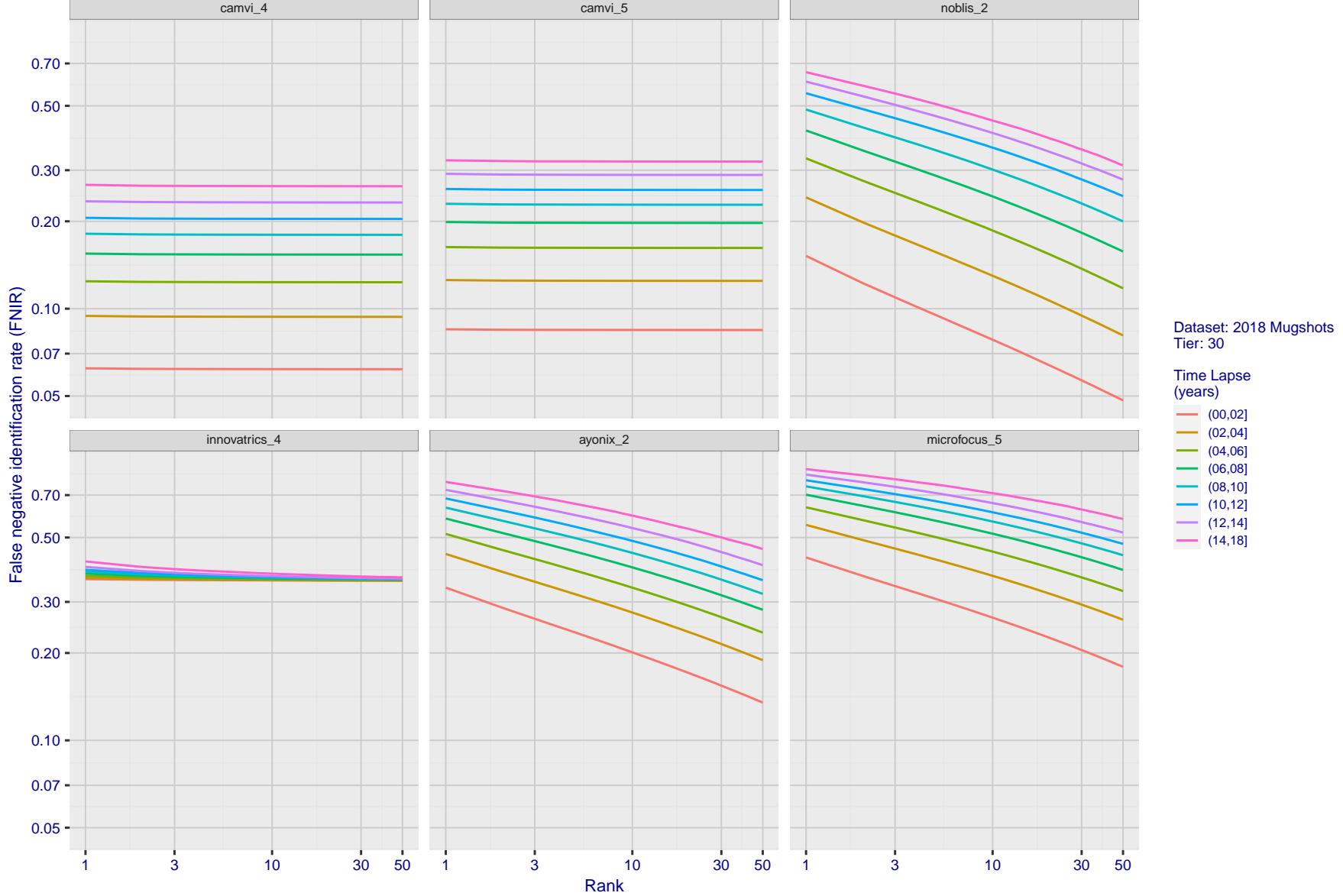


Figure 89: [FRVT-2018 Mugshot Ageing Dataset] Identification miss rates vs. rank by time-elapsed. The oldest image of each individual is enrolled. Thereafter, all more recent images are searched. Miss rates are computed over all searches noted in row 17 of Table 1 and binned by number of years between search and initial enrollment.

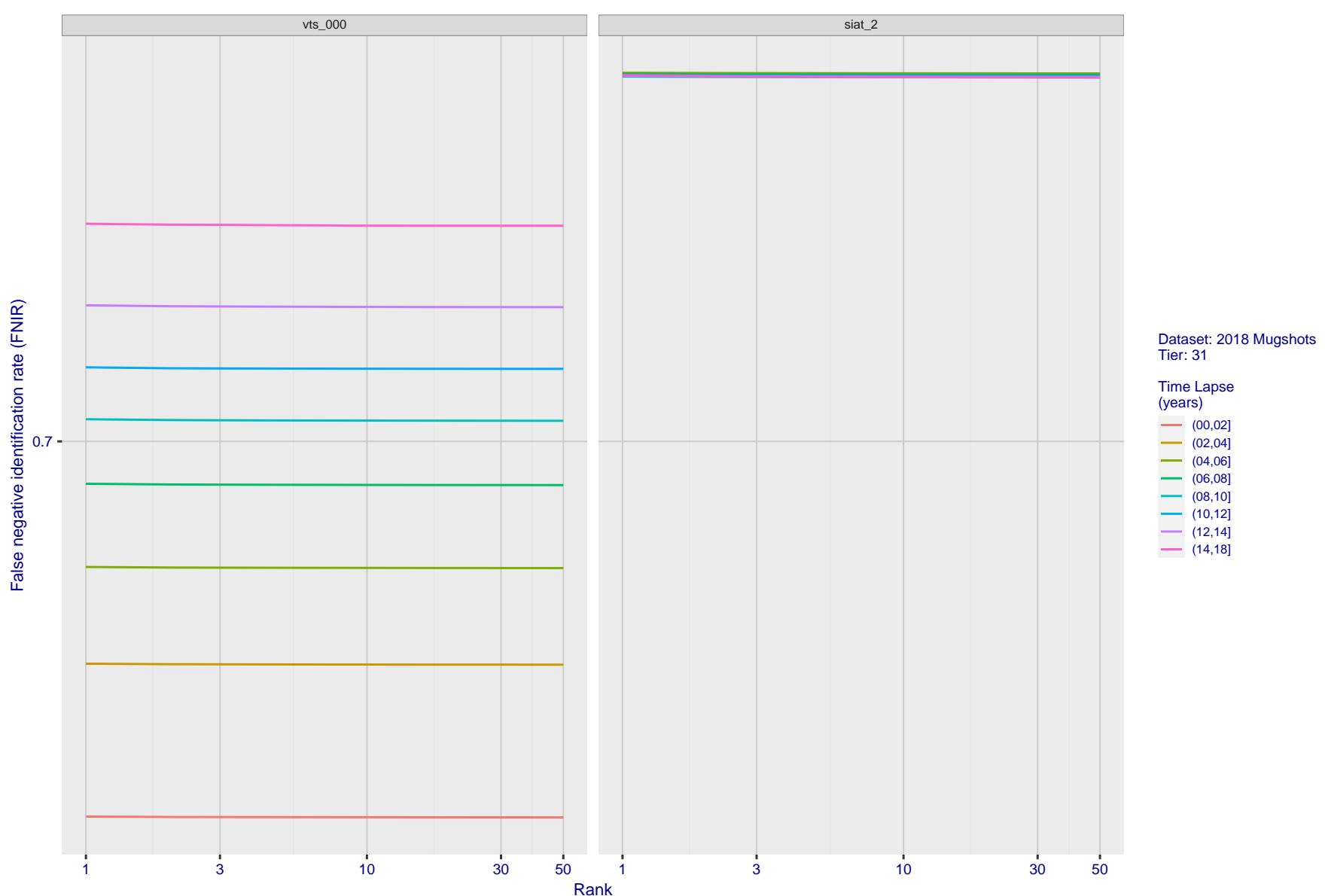


Figure 90: [FRVT-2018 Mugshot Ageing Dataset] Identification miss rates vs. rank by time-elapsed. The oldest image of each individual is enrolled. Thereafter, all more recent images are searched. Miss rates are computed over all searches noted in row 17 of Table 1 and binned by number of years between search and initial enrollment.

2023/03/14 14:32:11	$\text{FNIR}(N, R, T) =$ $\text{FPTR}(N, T) =$	False neg. identification rate False pos. identification rate	$N =$ Num. enrolled subjects $R =$ Num. candidates examined	$T =$ Threshold $T > 0 \rightarrow$ Identification	$T = 0 \rightarrow$ Investigation
------------------------	---	--	--	---	-----------------------------------

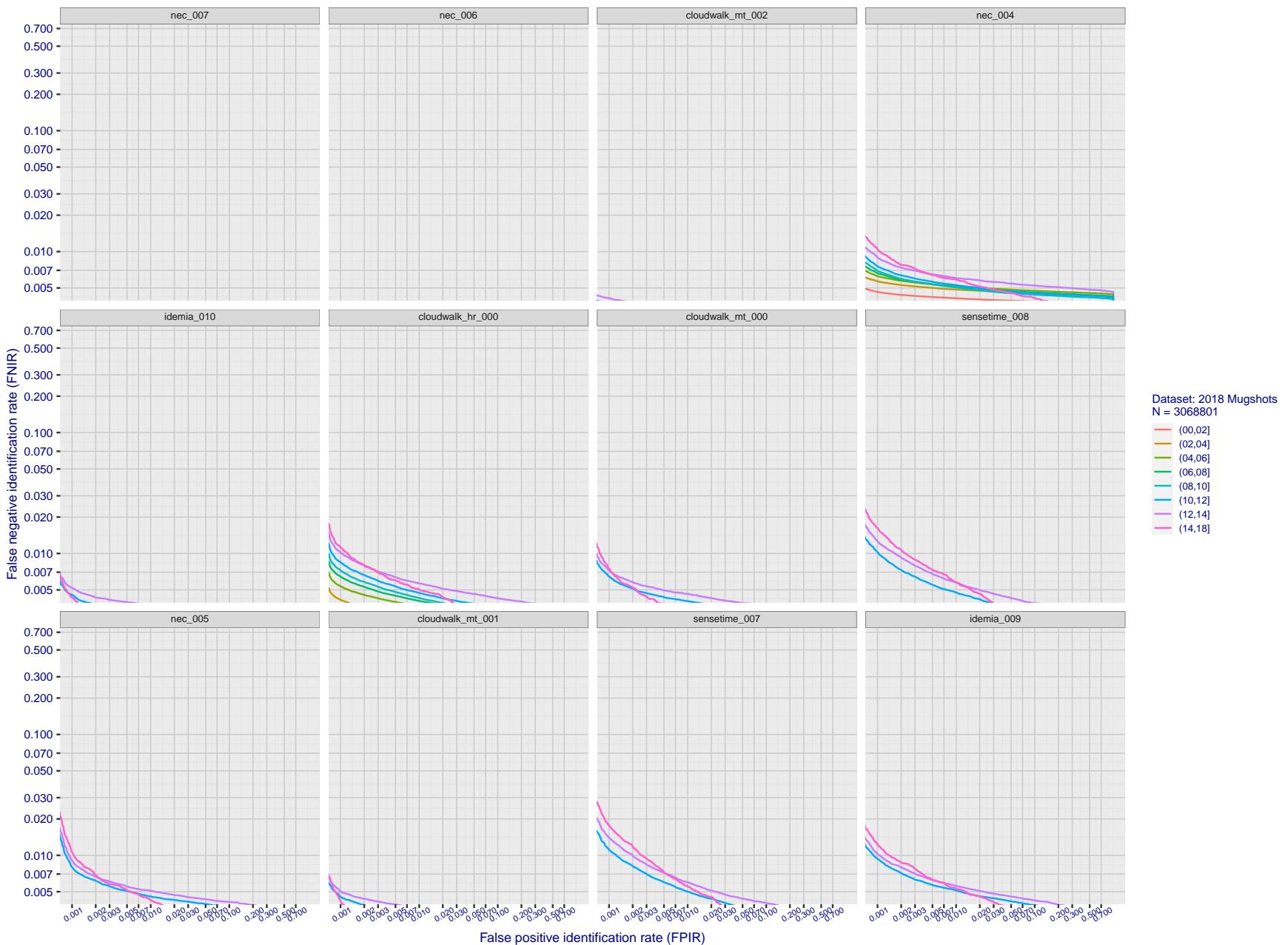


Figure 91: [FRVT-2018 Mugshot Ageing Dataset] Identification miss rates vs. FPIR by time-elapsed. The oldest image of each individual is enrolled. Thereafter, all more recent images are searched. Miss rates are computed over all searches noted in row 17 of Table 1 and binned by number of years between search and initial enrollment. FPIR is computed from the same FRVT 2018 non-mates noted in row 3 of Table 1 with $N = 3000\,000$.

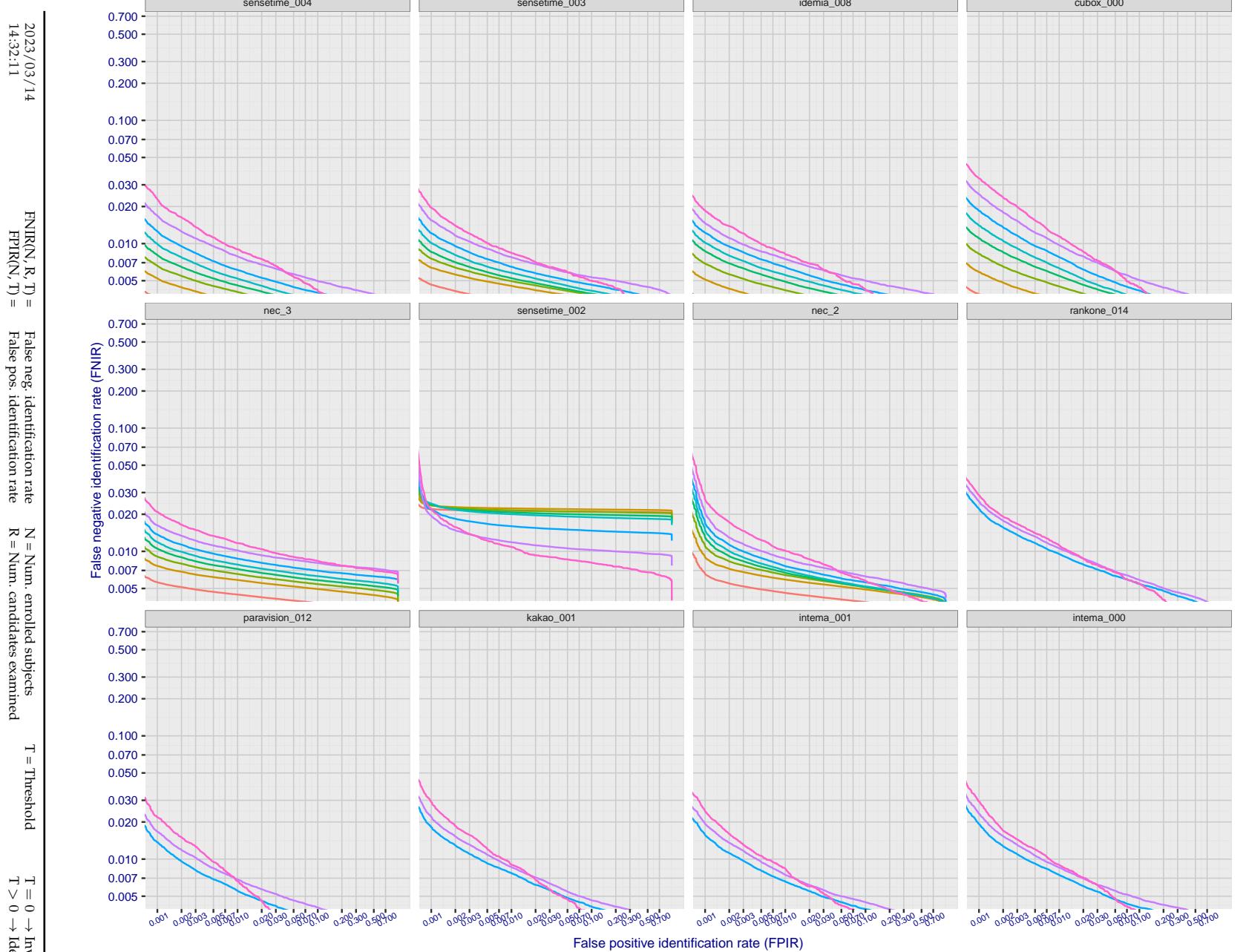


Figure 92: [FRVT-2018 Mugshot Ageing Dataset] Identification miss rates vs. FPIR by time-elapsed. The oldest image of each individual is enrolled. Thereafter, all more recent images are searched. Miss rates are computed over all searches noted in row 17 of Table 1 and binned by number of years between search and initial enrollment. FPIR is computed from the same FRVT 2018 non-mates noted in row 3 of Table 1 with $N = 3\,000\,000$.

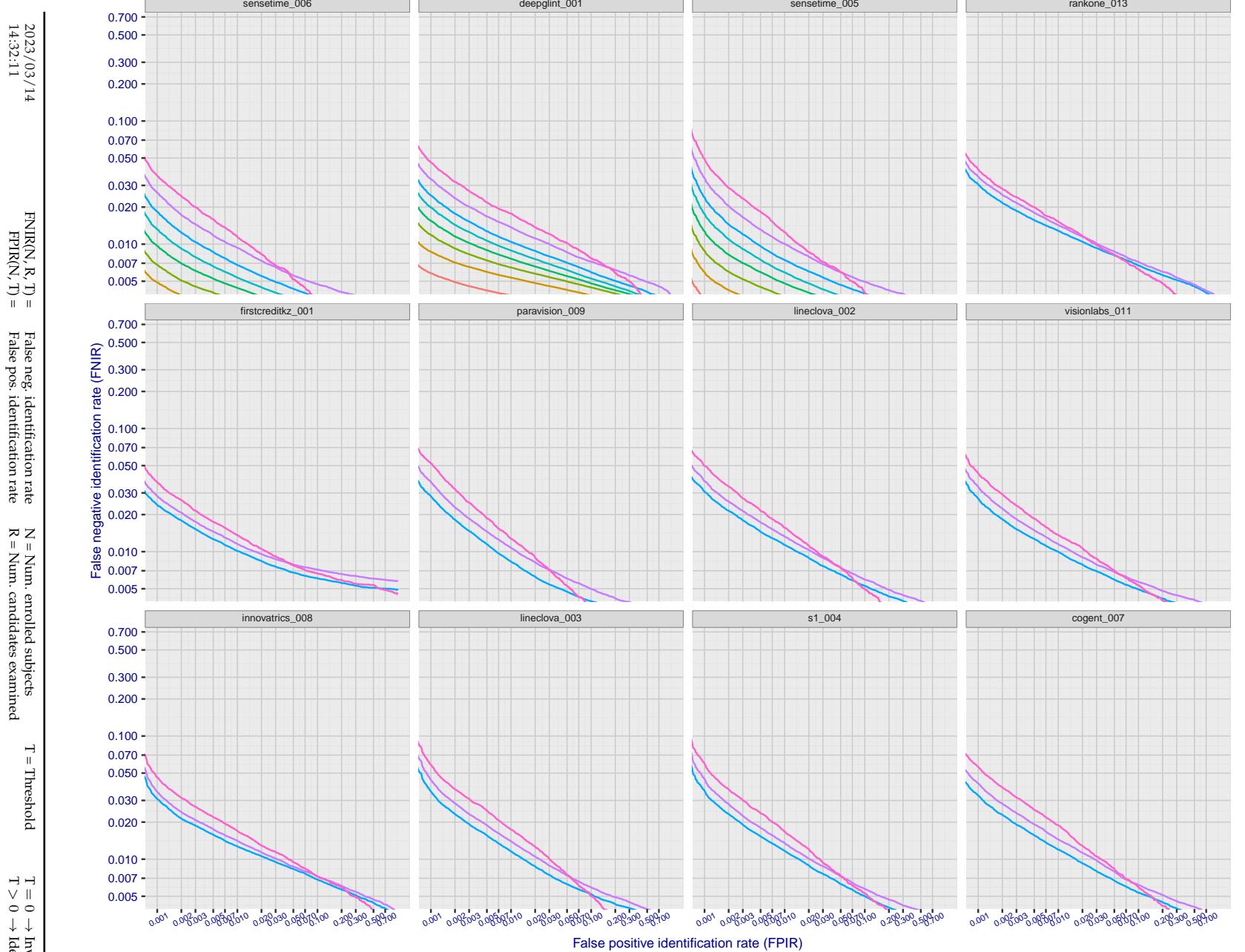


Figure 93: [FRVT-2018 Mugshot Ageing Dataset] Identification miss rates vs. FPIR by time-elapsed. The oldest image of each individual is enrolled. Thereafter, all more recent images are searched. Miss rates are computed over all searches noted in row 17 of Table 1 and binned by number of years between search and initial enrollment. FPIR is computed from the same FRVT 2018 non-mates noted in row 3 of Table 1 with $N = 3\,000\,000$.

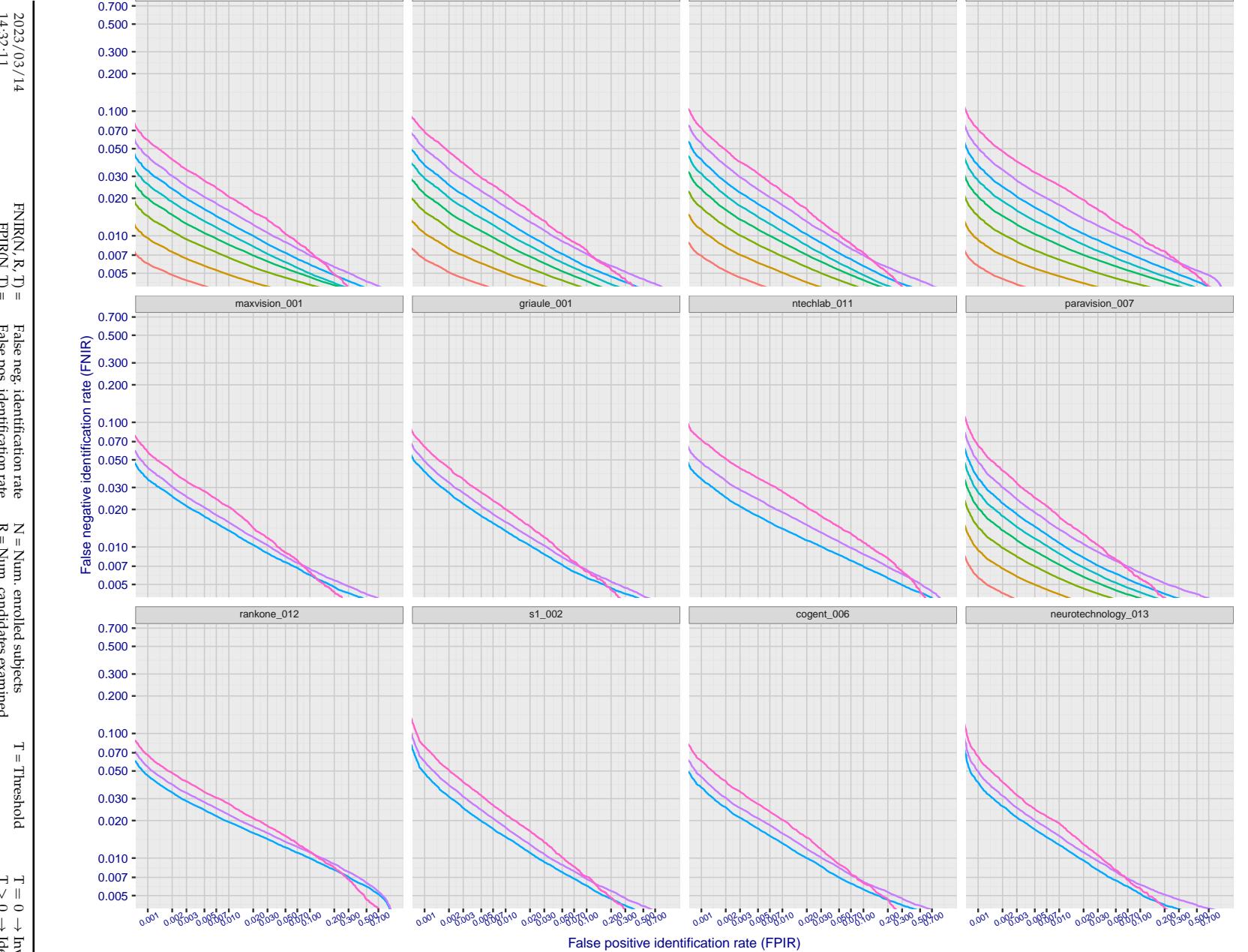


Figure 94: [FRVT-2018 Mugshot Ageing Dataset] Identification miss rates vs. FPIR by time-elapsed. The oldest image of each individual is enrolled. Thereafter, all more recent images are searched. Miss rates are computed over all searches noted in row 17 of Table 1 and binned by number of years between search and initial enrollment. FPIR is computed from the same FRVT 2018 non-mates noted in row 3 of Table 1 with $N = 3\,000\,000$.

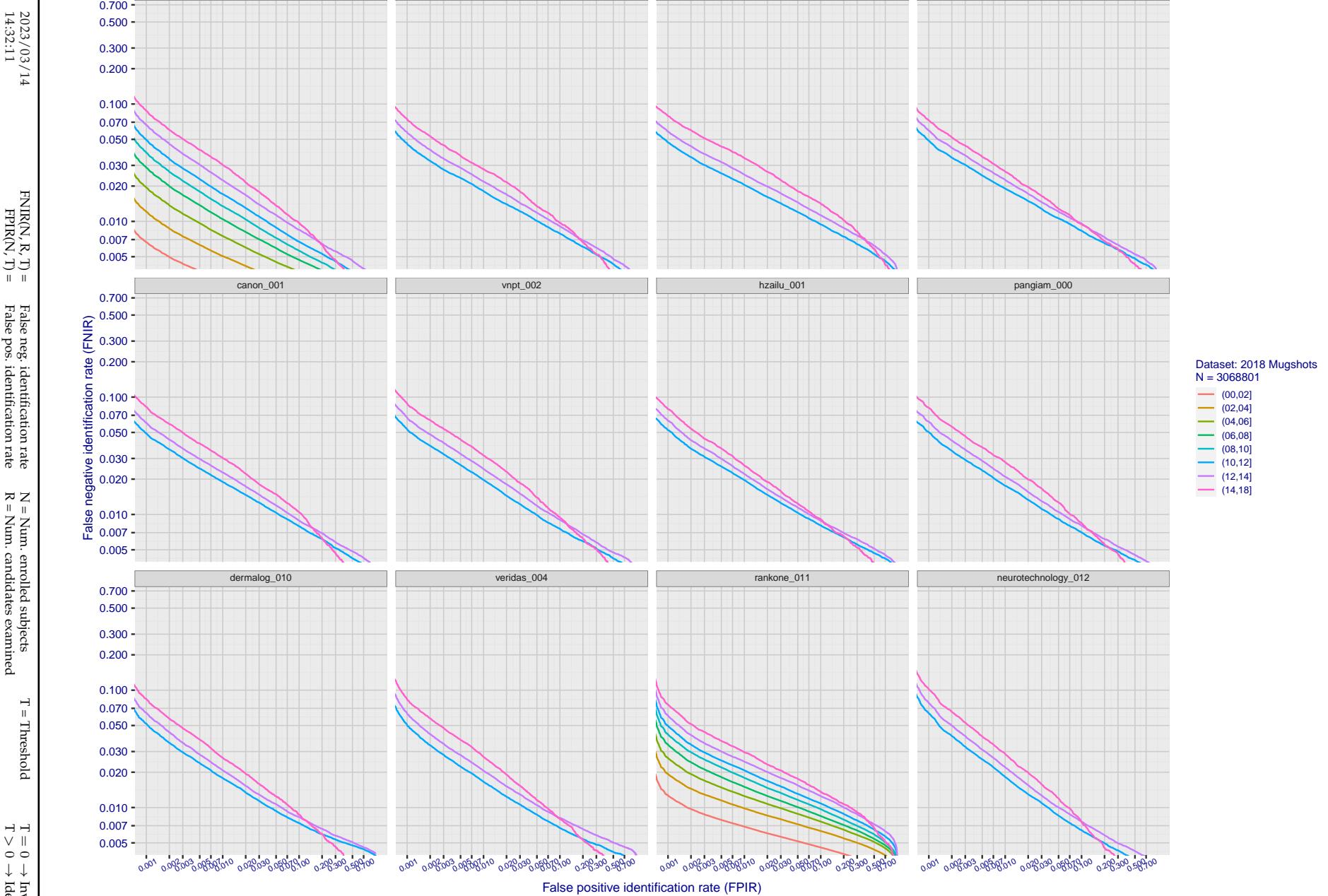


Figure 95: [FRVT-2018 Mugshot Ageing Dataset] Identification miss rates vs. FPIR by time-elapsed. The oldest image of each individual is enrolled. Thereafter, all more recent images are searched. Miss rates are computed over all searches noted in row 17 of Table 1 and binned by number of years between search and initial enrollment. FPIR is computed from the same FRVT 2018 non-mates noted in row 3 of Table 1 with $N = 3\,000\,000$.

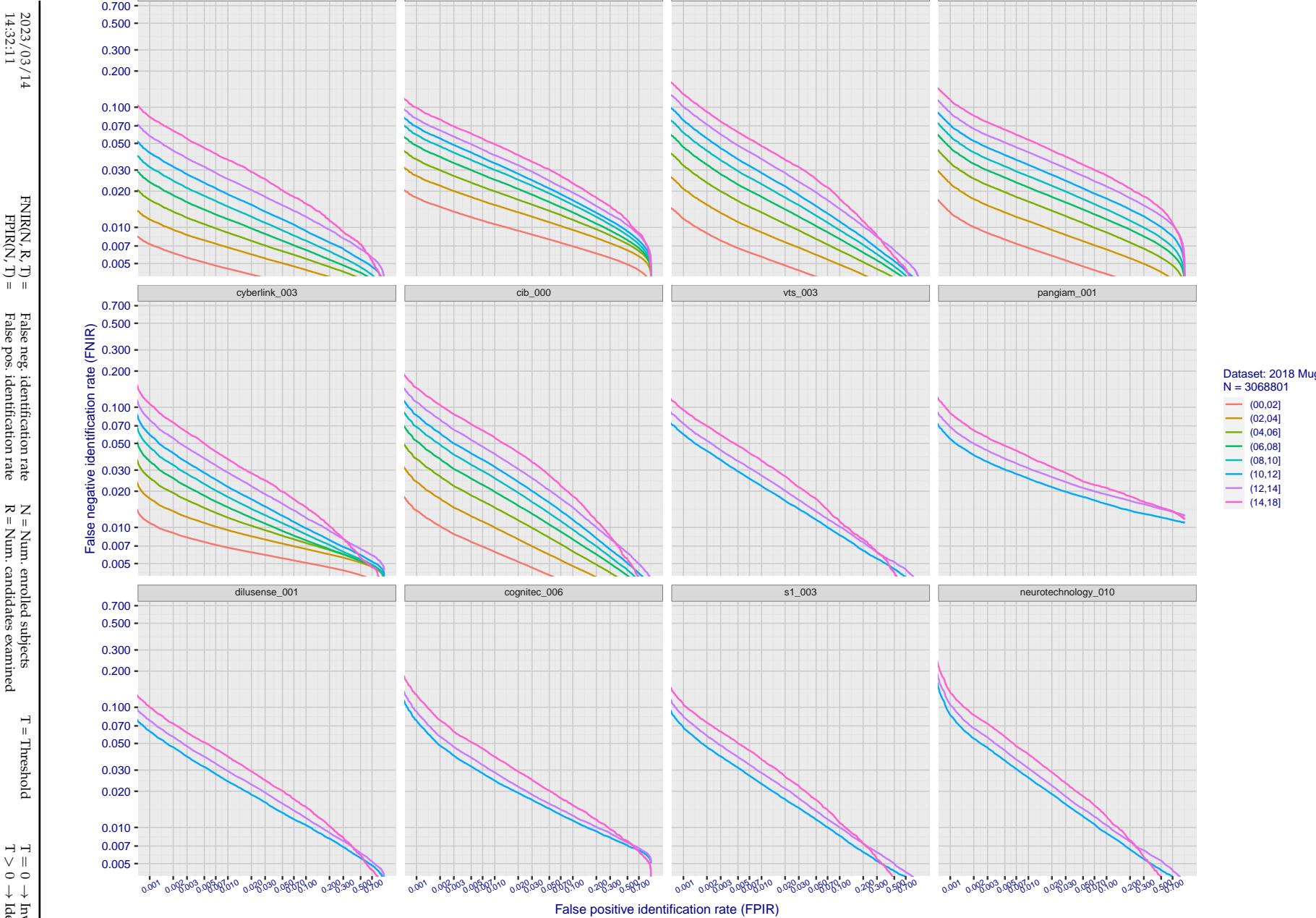


Figure 96: [FRVT-2018 Mugshot Ageing Dataset] Identification miss rates vs. FPIR by time elapsed. The oldest image of each individual is enrolled. Thereafter, all more recent images are searched. Miss rates are computed over all searches noted in row 17 of Table 1 and binned by number of years between search and initial enrollment. FPIR is computed from the same FRVT 2018 non-mates noted in row 3 of Table 1 with $N = 3\,000\,000$.

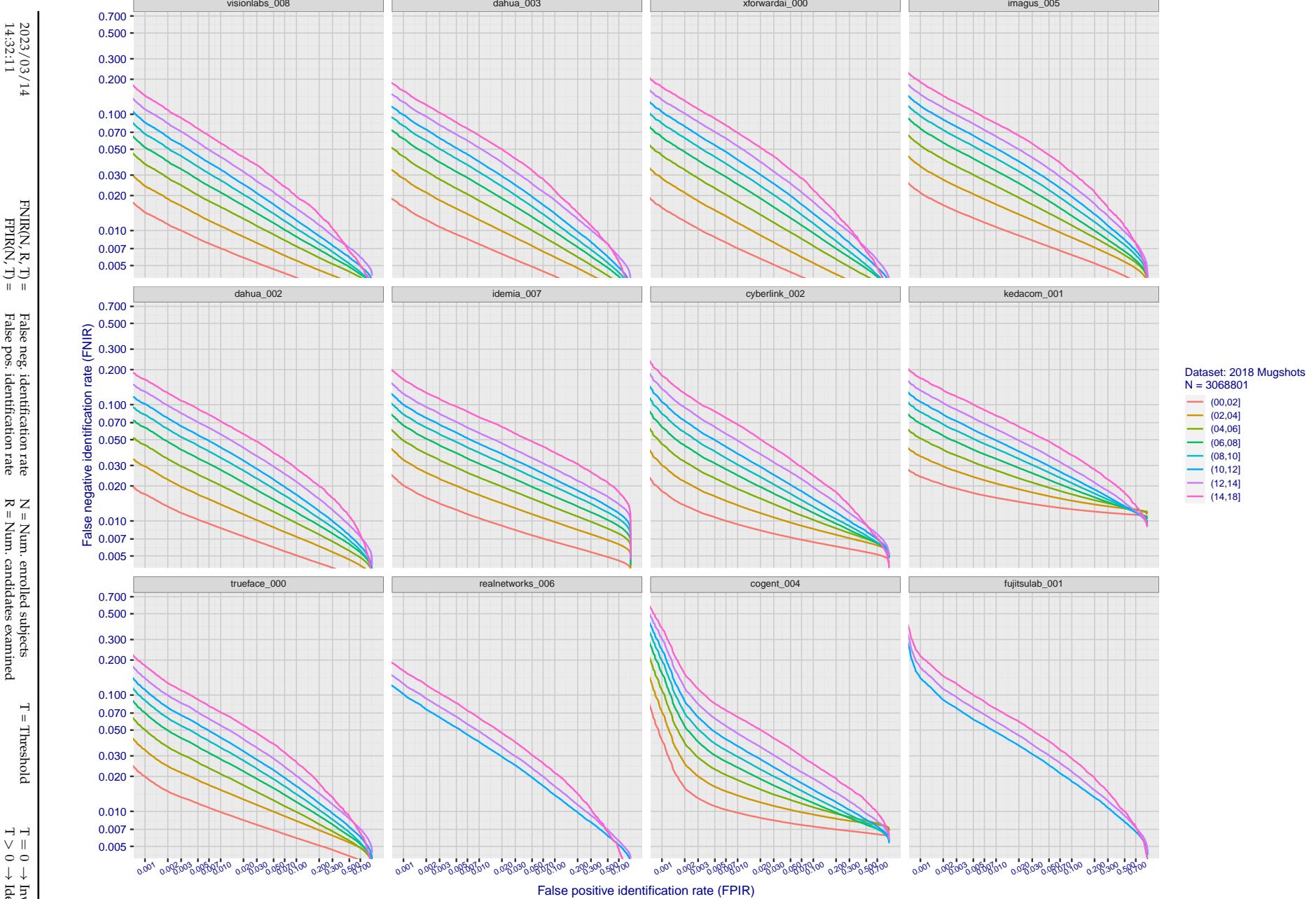


Figure 97: [FRVT-2018 Mugshot Ageing Dataset] Identification miss rates vs. FPIR by time-elapsed. The oldest image of each individual is enrolled. Thereafter, all more recent images are searched. Miss rates are computed over all searches noted in row 17 of Table 1 and binned by number of years between search and initial enrollment. FPIR is computed from the same FRVT 2018 non-mates noted in row 3 of Table 1 with N = 3 000 000.

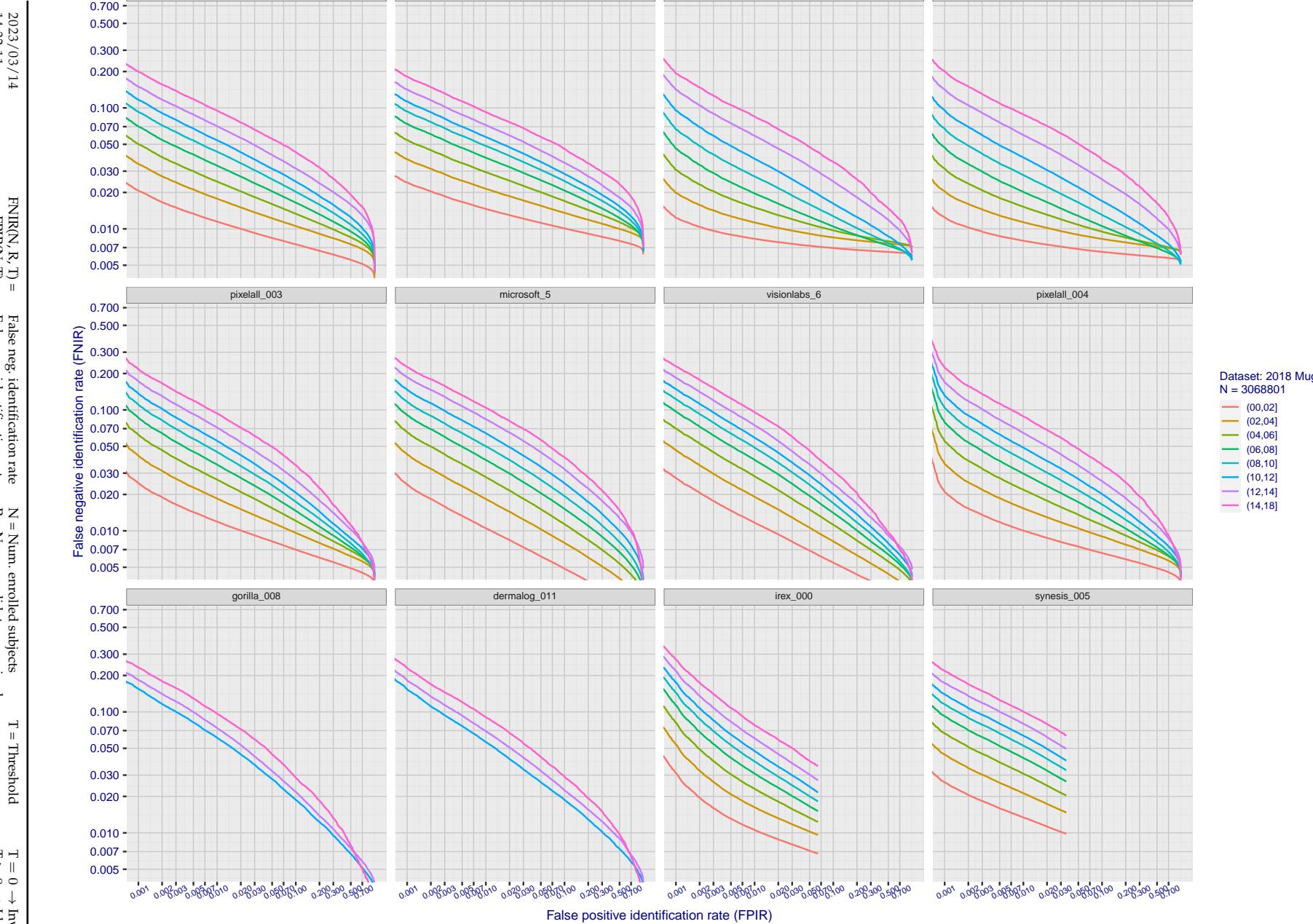


Figure 98: [FRVT-2018 Mugshot Ageing Dataset] Identification miss rates vs. FPIR by time-elapsed. The oldest image of each individual is enrolled. Thereafter, all more recent images are searched. Miss rates are computed over all searches noted in row 17 of Table 1 and binned by number of years between search and initial enrollment. FPIR is computed from the same FRVT 2018 non-mates noted in row 3 of Table 1 with $N = 3\,000\,000$.

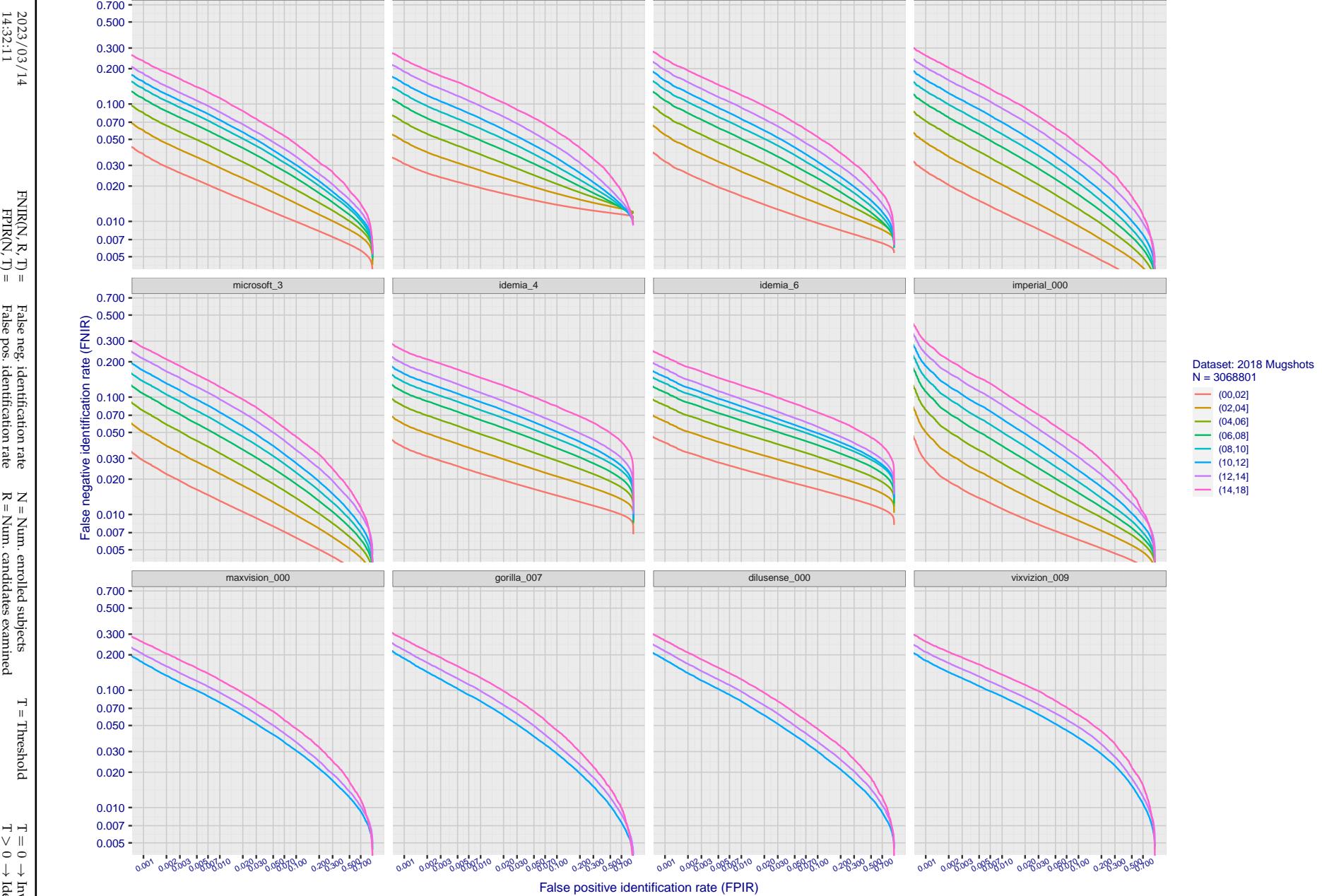


Figure 99: [FRVT-2018 Mugshot Ageing Dataset] Identification miss rates vs. FPIR by time-elapsed. The oldest image of each individual is enrolled. Thereafter, all more recent images are searched. Miss rates are computed over all searches noted in row 17 of Table 1 and binned by number of years between search and initial enrollment. FPIR is computed from the same FRVT 2018 non-mates noted in row 3 of Table 1 with $N = 3\,000\,000$.

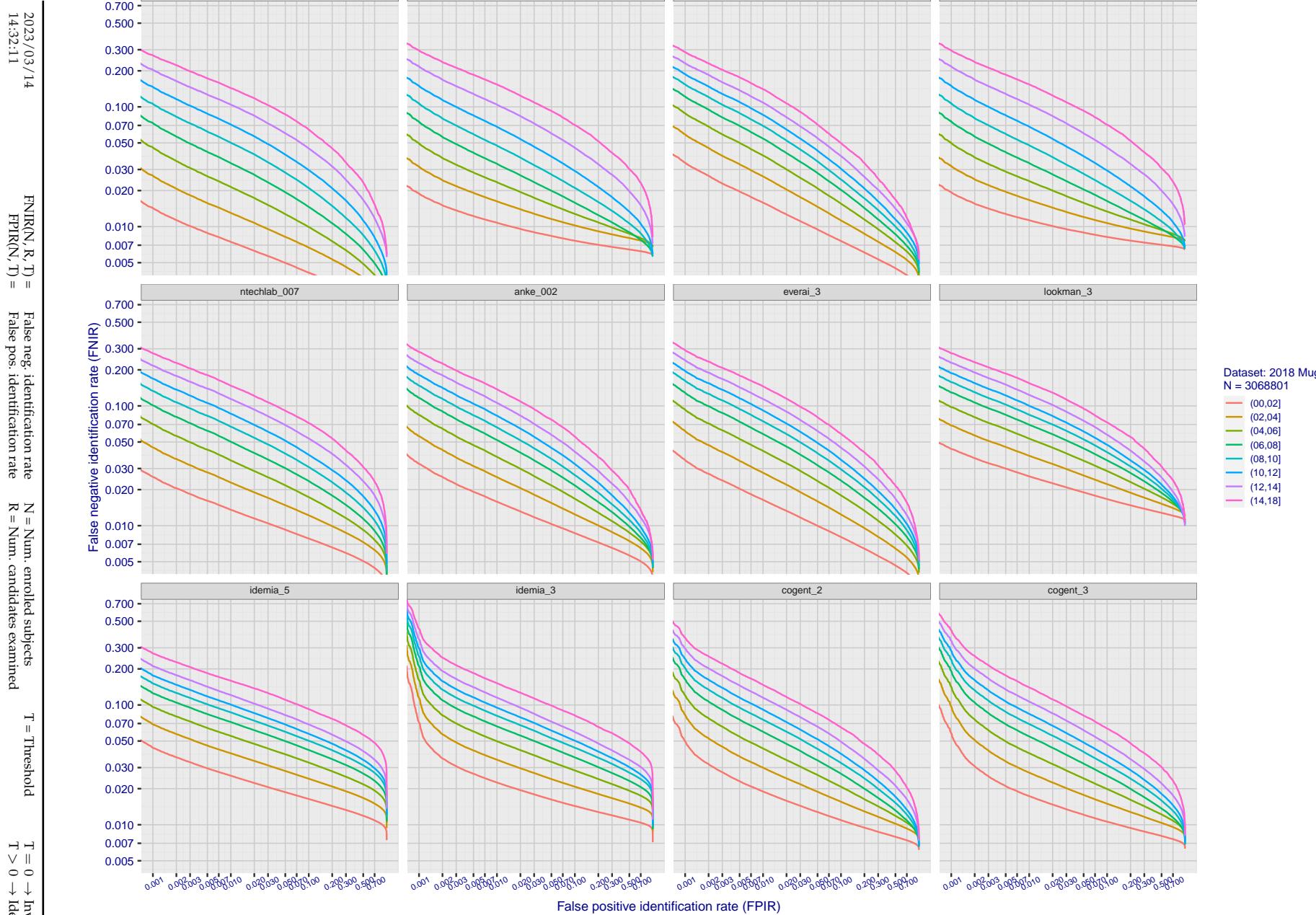


Figure 100: [FRVT-2018 Mugshot Ageing Dataset] Identification miss rates vs. FPIR by time-elapsed. The oldest image of each individual is enrolled. Thereafter, all more recent images are searched. Miss rates are computed over all searches noted in row 17 of Table 1 and binned by number of years between search and initial enrollment. FPIR is computed from the same FRVT 2018 non-mates noted in row 3 of Table 1 with $N = 3\,000\,000$.

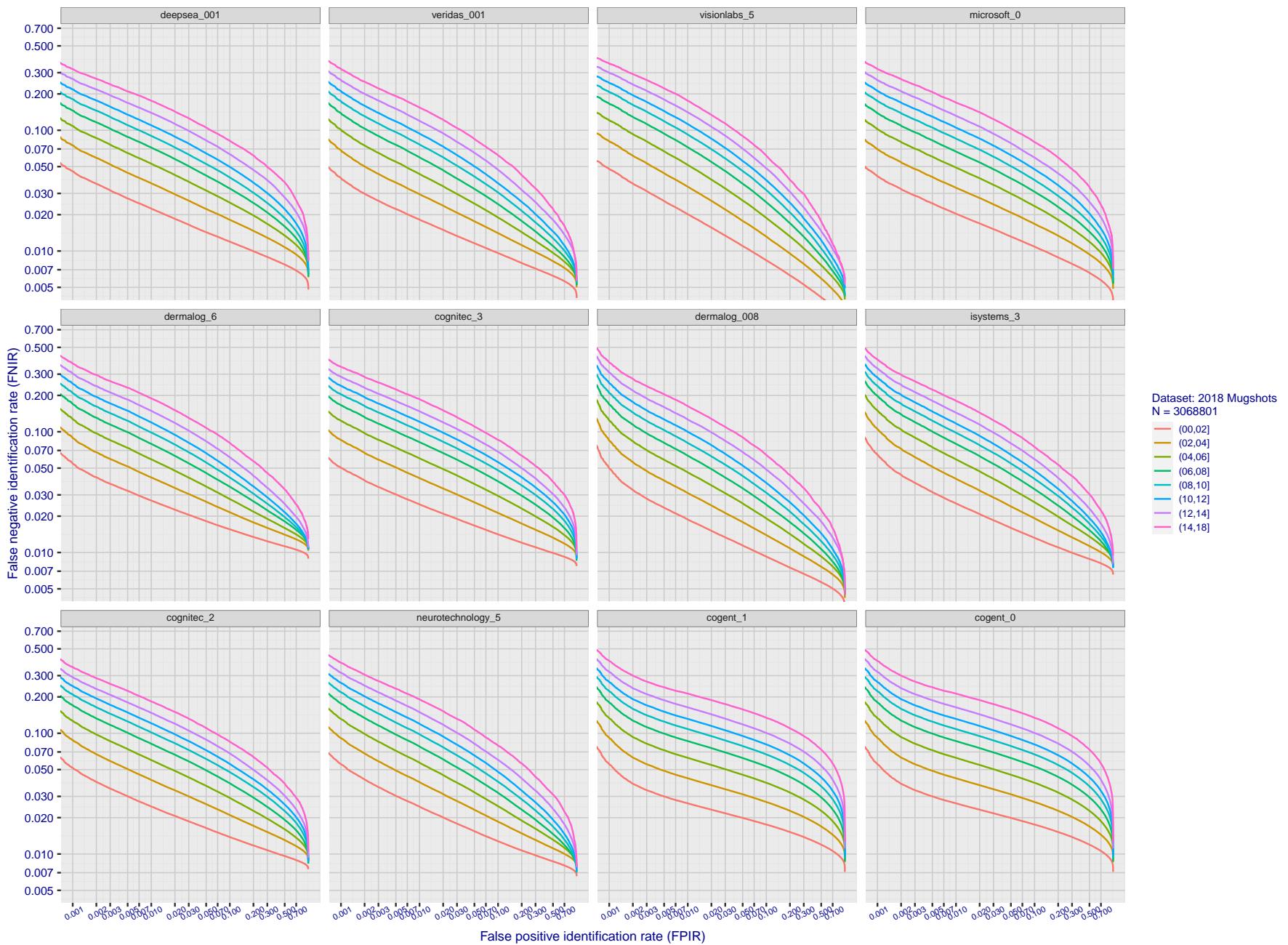


Figure 101: [FRVT-2018 Mugshot Ageing Dataset] Identification miss rates vs. FPIR by time-elapsed. The oldest image of each individual is enrolled. Thereafter, all more recent images are searched. Miss rates are computed over all searches noted in row 17 of Table 1 and binned by number of years between search and initial enrollment. FPIR is computed from the same FRVT 2018 non-mates noted in row 3 of Table 1 with $N = 3\,000\,000$.

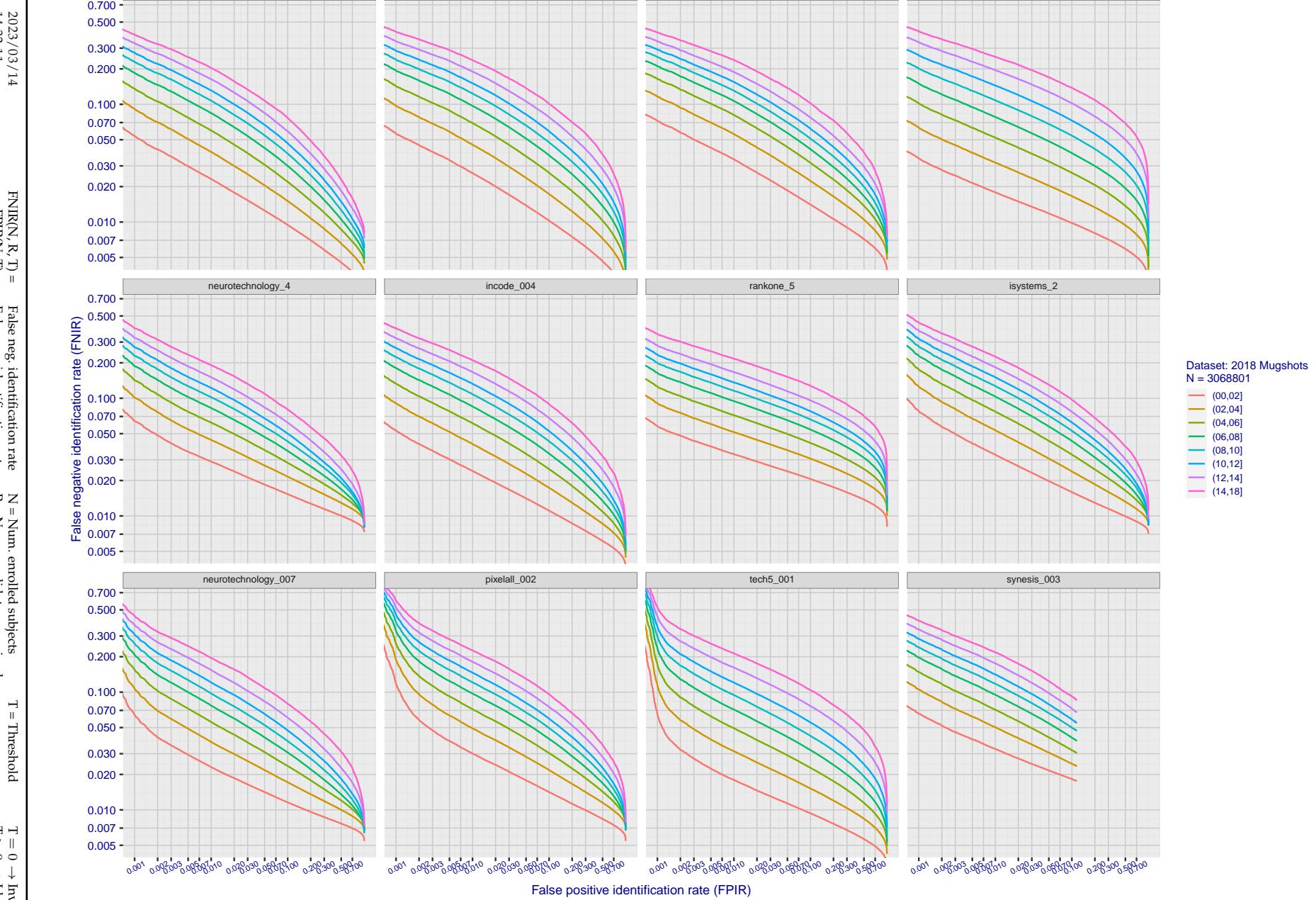


Figure 102: [FRVT-2018 Mugshot Ageing Dataset] Identification miss rates vs. FPIR by time-elapsed. The oldest image of each individual is enrolled. Thereafter, all more recent images are searched. Miss rates are computed over all searches noted in row 17 of Table 1 and binned by number of years between search and initial enrollment. FPIR is computed from the same FRVT 2018 non-mates noted in row 3 of Table 1 with $N = 3\,000\,000$.

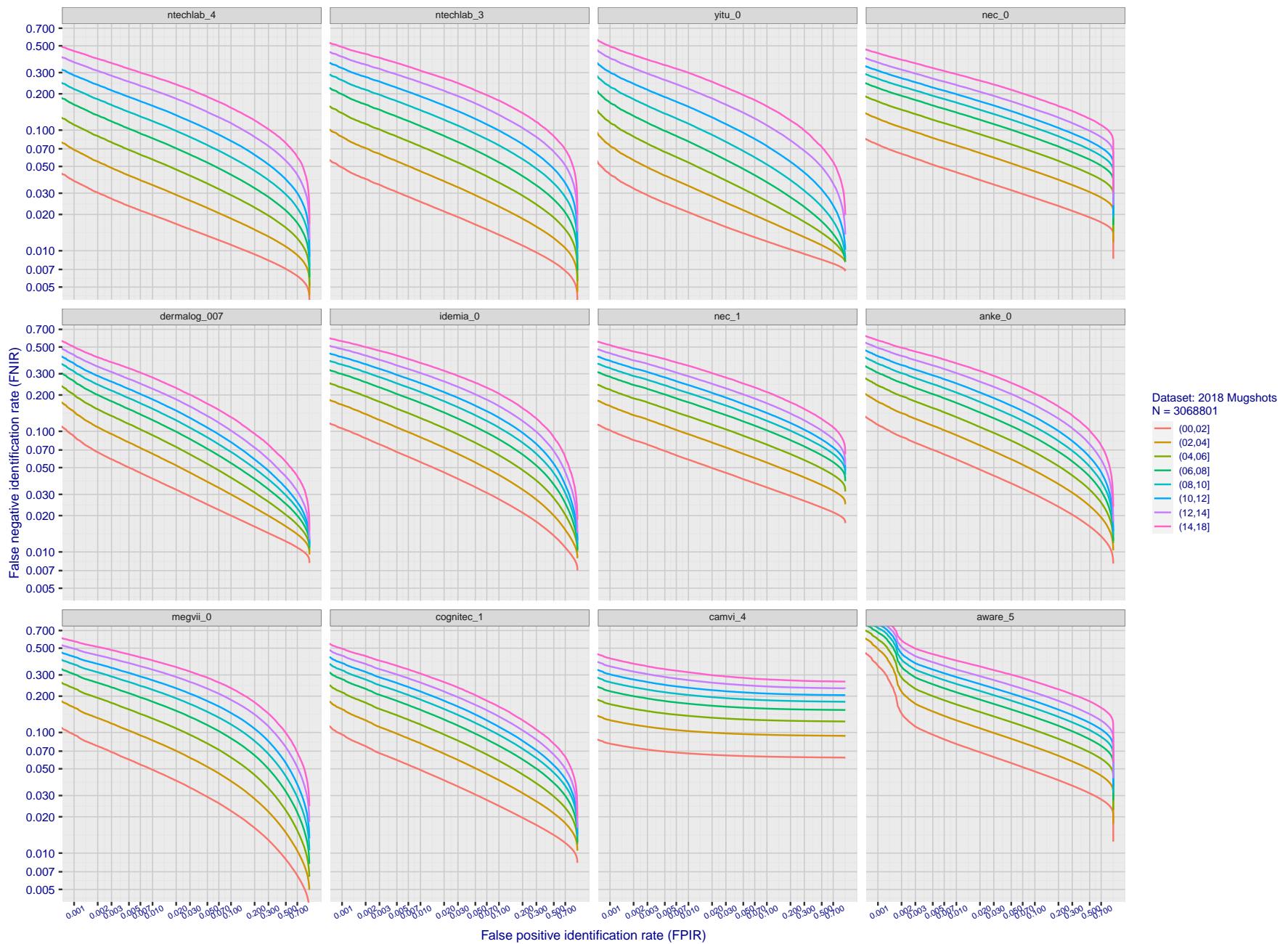


Figure 103: [FRVT-2018 Mugshot Ageing Dataset] Identification miss rates vs. FPIR by time-elapsed. The oldest image of each individual is enrolled. Thereafter, all more recent images are searched. Miss rates are computed over all searches noted in row 17 of Table 1 and binned by number of years between search and initial enrollment. FPIR is computed from the same FRVT 2018 non-mates noted in row 3 of Table 1 with $N = 3\,000\,000$.

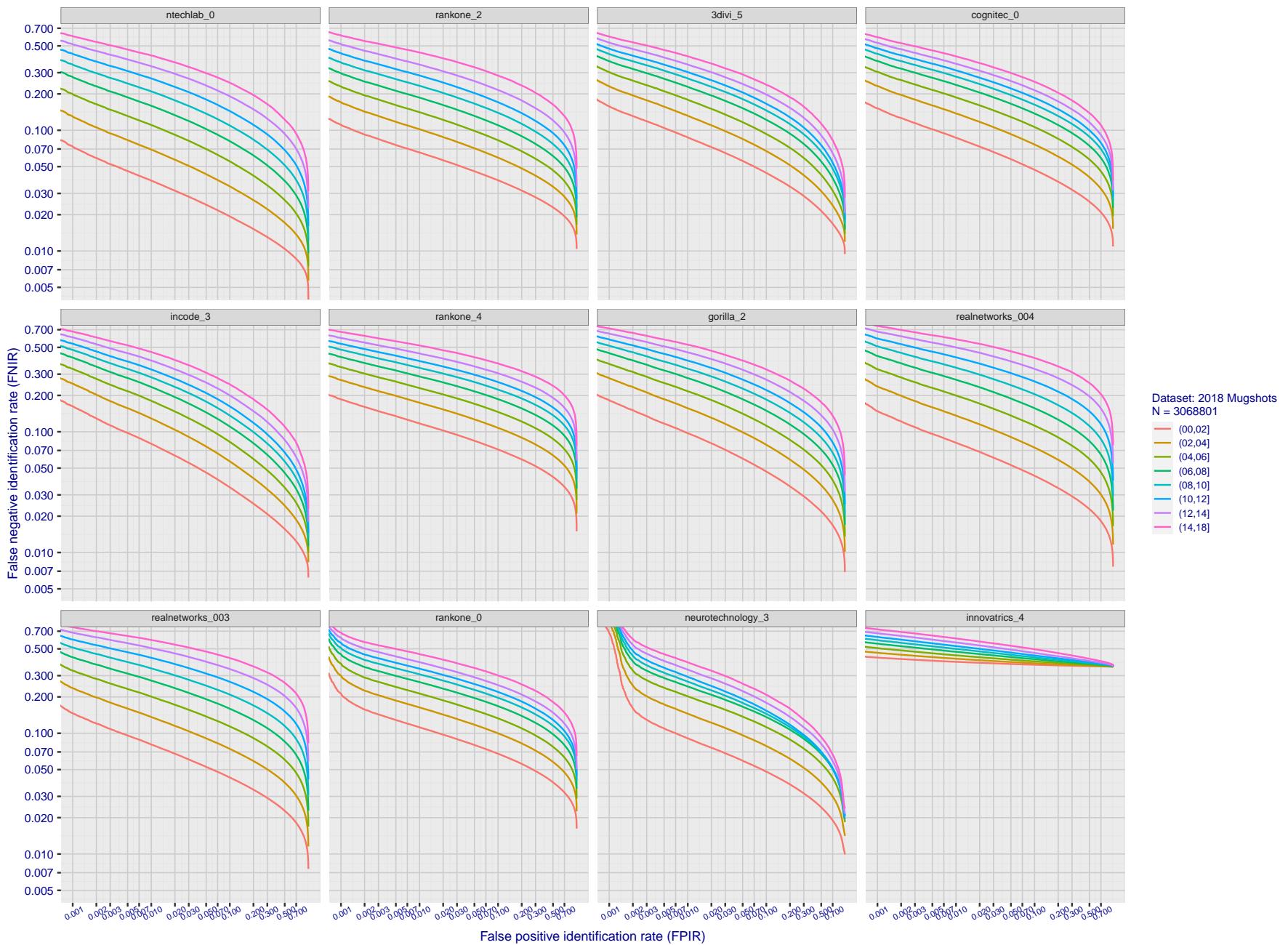


Figure 104: [FRVT-2018 Mugshot Ageing Dataset] Identification miss rates vs. FPIR by time-elapsed. The oldest image of each individual is enrolled. Thereafter, all more recent images are searched. Miss rates are computed over all searches noted in row 17 of Table 1 and binned by number of years between search and initial enrollment. FPIR is computed from the same FRVT 2018 non-mates noted in row 3 of Table 1 with $N = 3\,000\,000$.

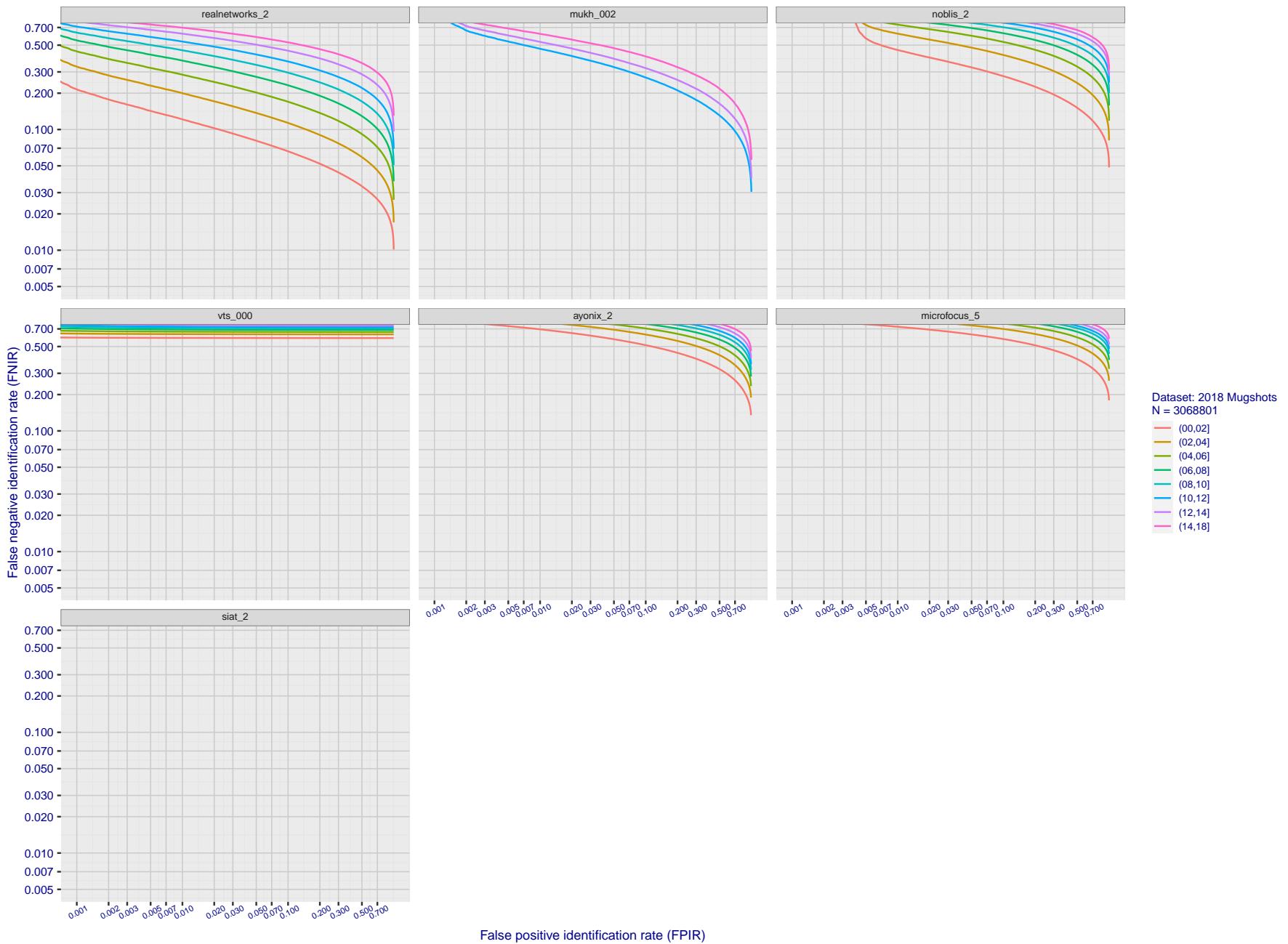


Figure 105: [FRVT-2018 Mugshot Ageing Dataset] Identification miss rates vs. FPIR by time-elapsed. The oldest image of each individual is enrolled. Thereafter, all more recent images are searched. Miss rates are computed over all searches noted in row 17 of Table 1 and binned by number of years between search and initial enrollment. FPIR is computed from the same FRVT 2018 non-mates noted in row 3 of Table 1 with $N = 3\,000\,000$.

2023/03/14 14:32:11	$\text{FNIR}(N, R, T) =$ $\text{FPTR}(N, T) =$	False neg. identification rate False pos. identification rate	$N =$ Num. enrolled subjects $R =$ Num. candidates examined	$T =$ Threshold $T > 0 \rightarrow$ Identification	$T = 0 \rightarrow$ Investigation
------------------------	---	--	--	---	-----------------------------------

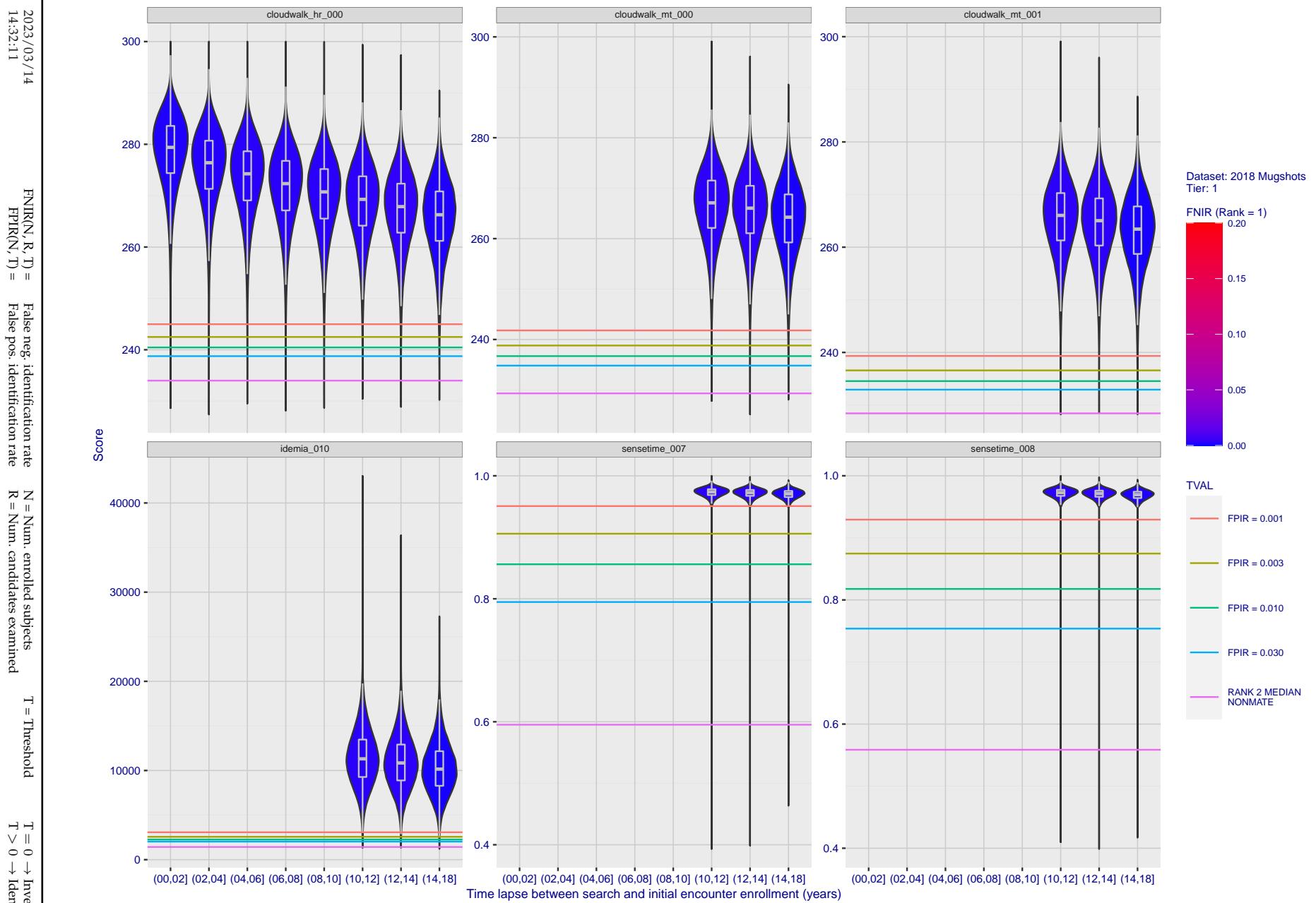


Figure 106: [FRVT-2018 Mugshot Ageing Dataset] Native mate scores vs. time-elapsed. The oldest image of each individual is enrolled. Thereafter, all more recent images are searched. Mated score distributions are computed over all searches noted in row 17 of Table 1 binned by number of years between search and initial enrollment.

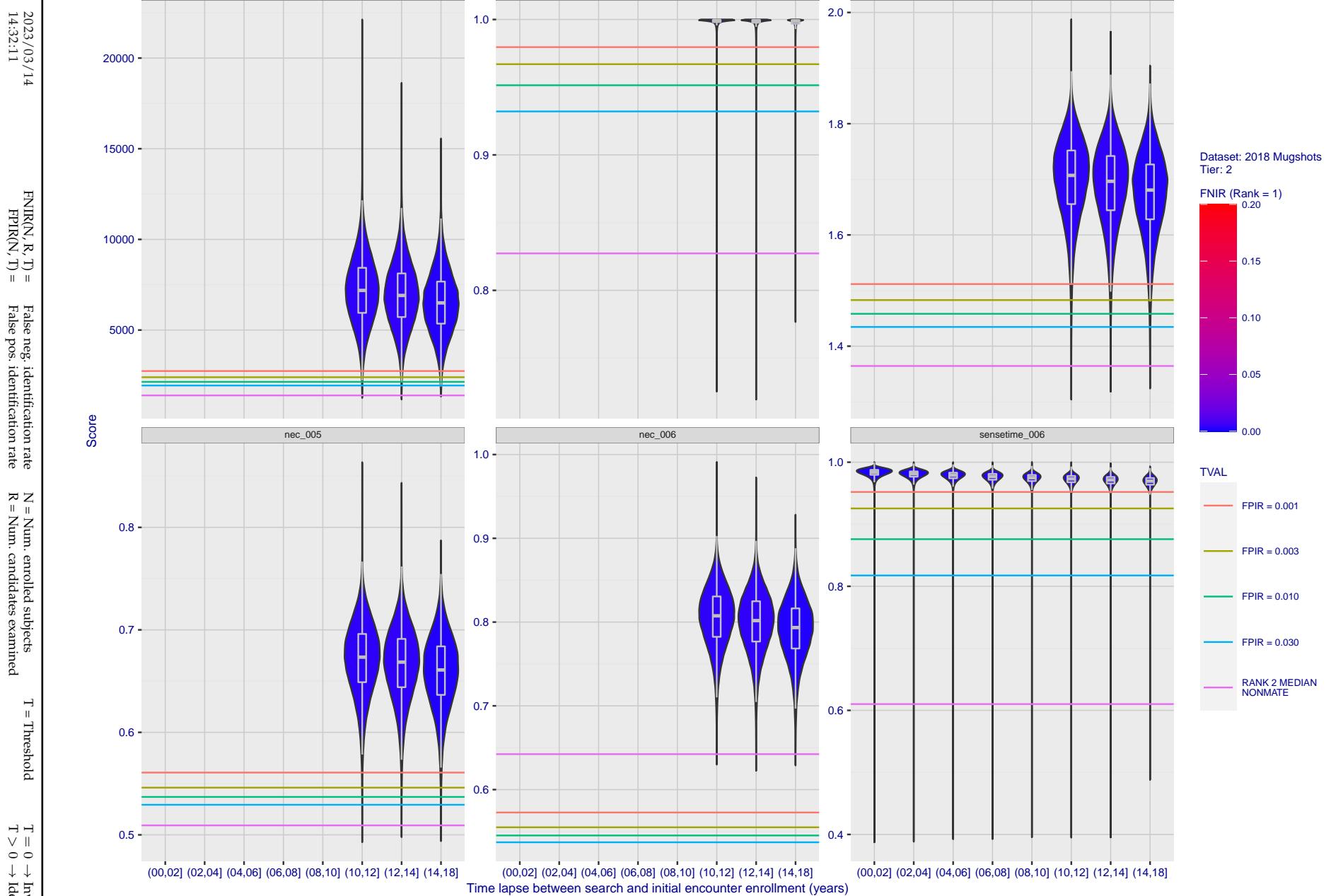


Figure 107: [FRVT-2018 Mugshot Ageing Dataset] Native mate scores vs. time-elapsed. The oldest image of each individual is enrolled. Thereafter, all more recent images are searched. Mated score distributions are computed over all searches noted in row 17 of Table 1 binned by number of years between search and initial enrollment.

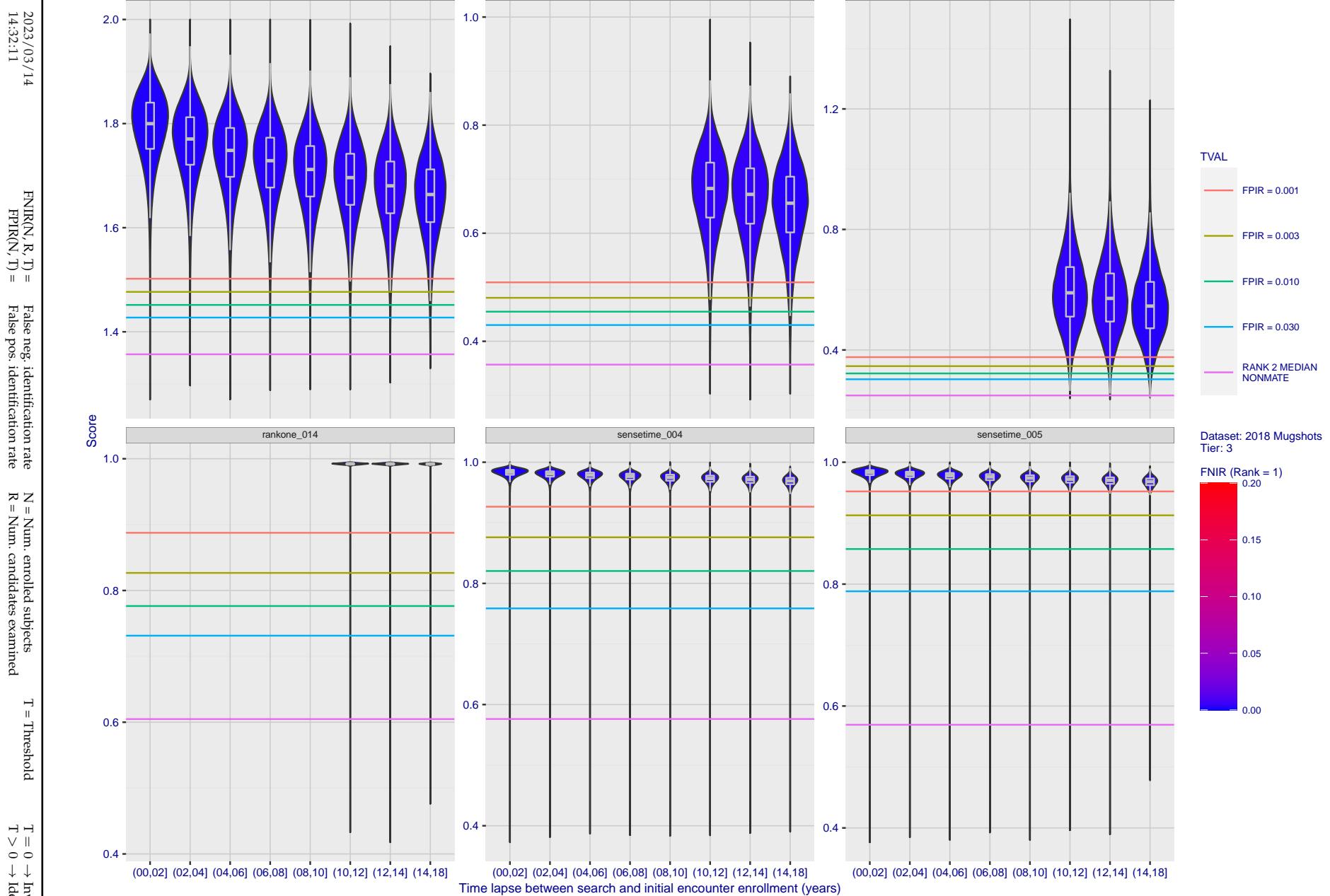


Figure 108: [FRVT-2018 Mugshot Ageing Dataset] Native mate scores vs. time-elapsed. The oldest image of each individual is enrolled. Thereafter, all more recent images are searched. Mated score distributions are computed over all searches noted in row 17 of Table 1 binned by number of years between search and initial enrollment.

2023/03/14
14:32:11FNIR(N, R, T) = False neg. identification rate
FPIR(N, T) = False pos. identification rateN = Num. enrolled subjects
R = Num. candidates examined

T = Threshold

T = 0 → Investigation
T > 0 → Identification

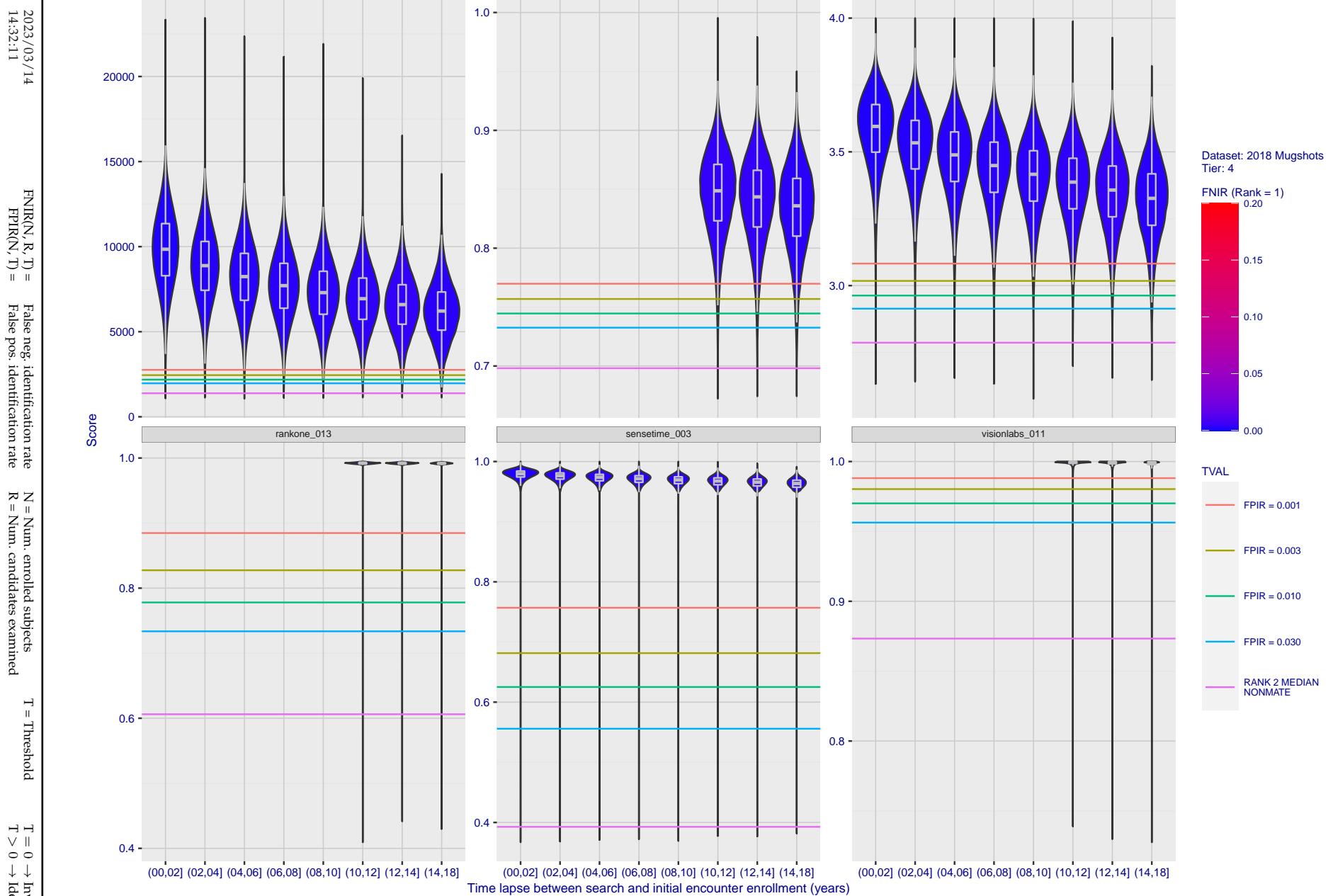


Figure 109: [FRVT-2018 Mugshot Ageing Dataset] Native mate scores vs. time-elapsed. The oldest image of each individual is enrolled. Thereafter, all more recent images are searched. Mated score distributions are computed over all searches noted in row 17 of Table 1 binned by number of years between search and initial enrollment.

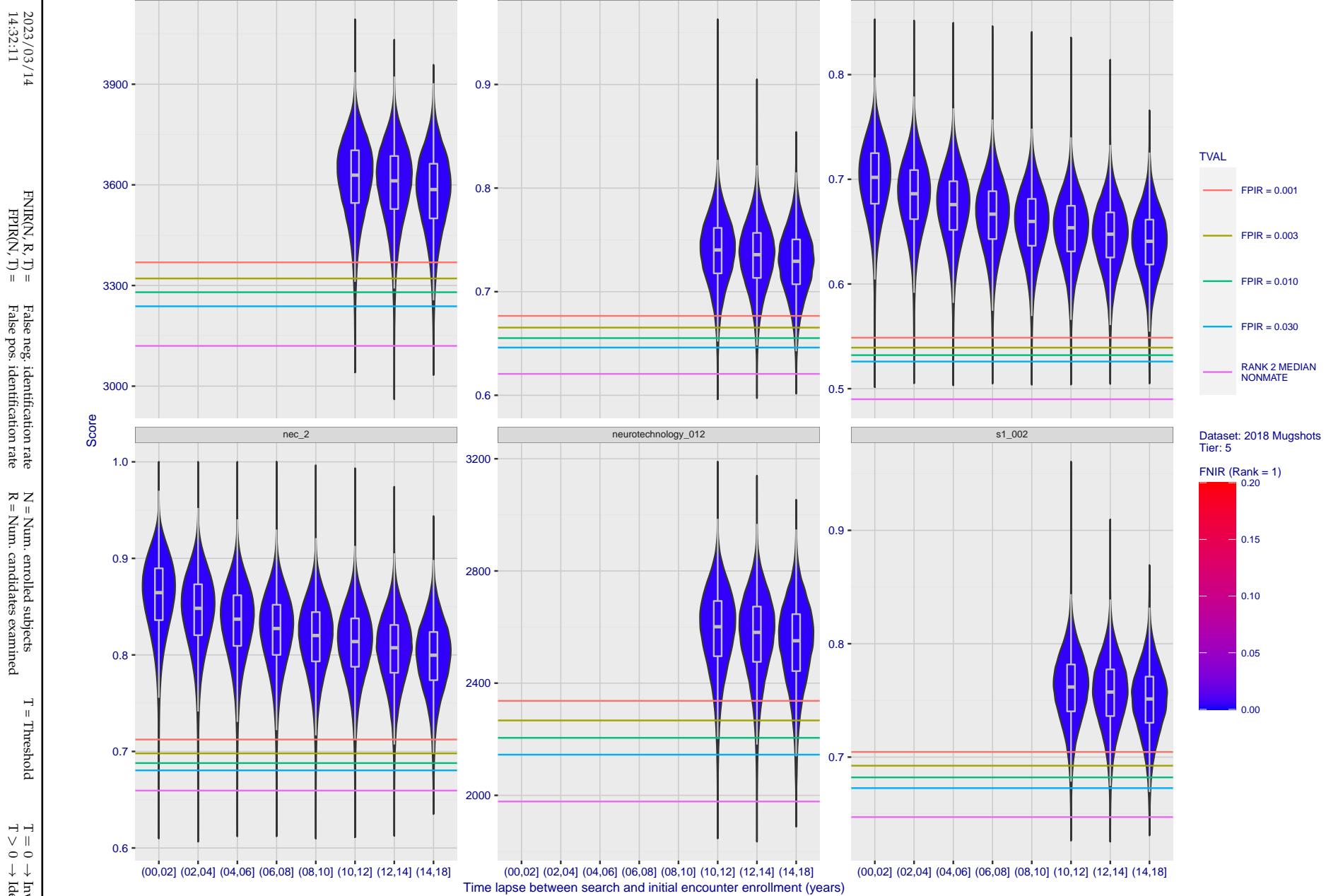


Figure 110: [FRVT-2018 Mugshot Ageing Dataset] Native mate scores vs. time-elapsed. The oldest image of each individual is enrolled. Thereafter, all more recent images are searched. Mated score distributions are computed over all searches noted in row 17 of Table 1 binned by number of years between search and initial enrollment.

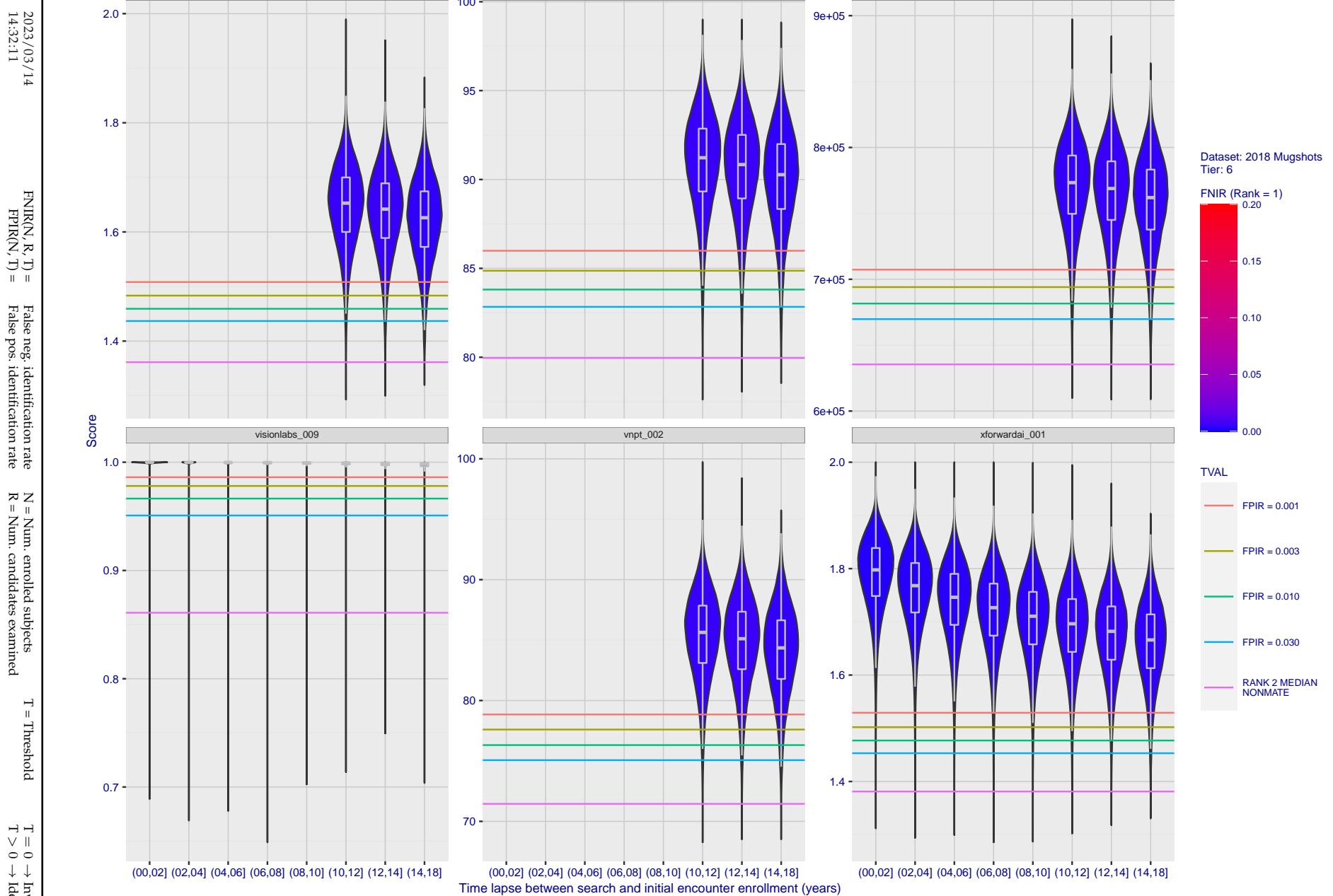


Figure 111: [FRVT-2018 Mugshot Ageing Dataset] Native mate scores vs. time-elapsed. The oldest image of each individual is enrolled. Thereafter, all more recent images are searched. Mated score distributions are computed over all searches noted in row 17 of Table 1 binned by number of years between search and initial enrollment.

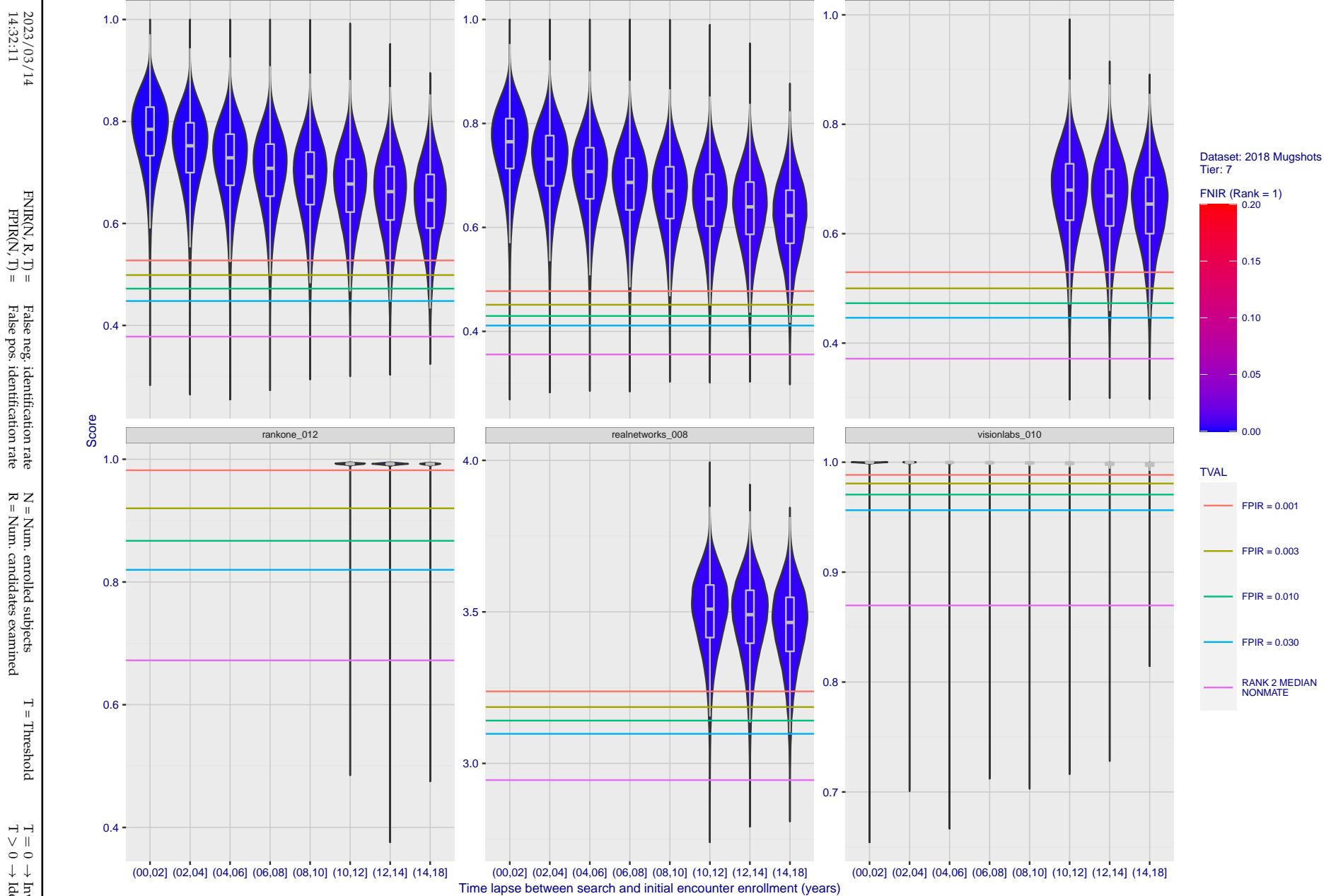


Figure 112: [FRVT-2018 Mugshot Ageing Dataset] Native mate scores vs. time-elapsed. The oldest image of each individual is enrolled. Thereafter, all more recent images are searched. Mated score distributions are computed over all searches noted in row 17 of Table 1 binned by number of years between search and initial enrollment.

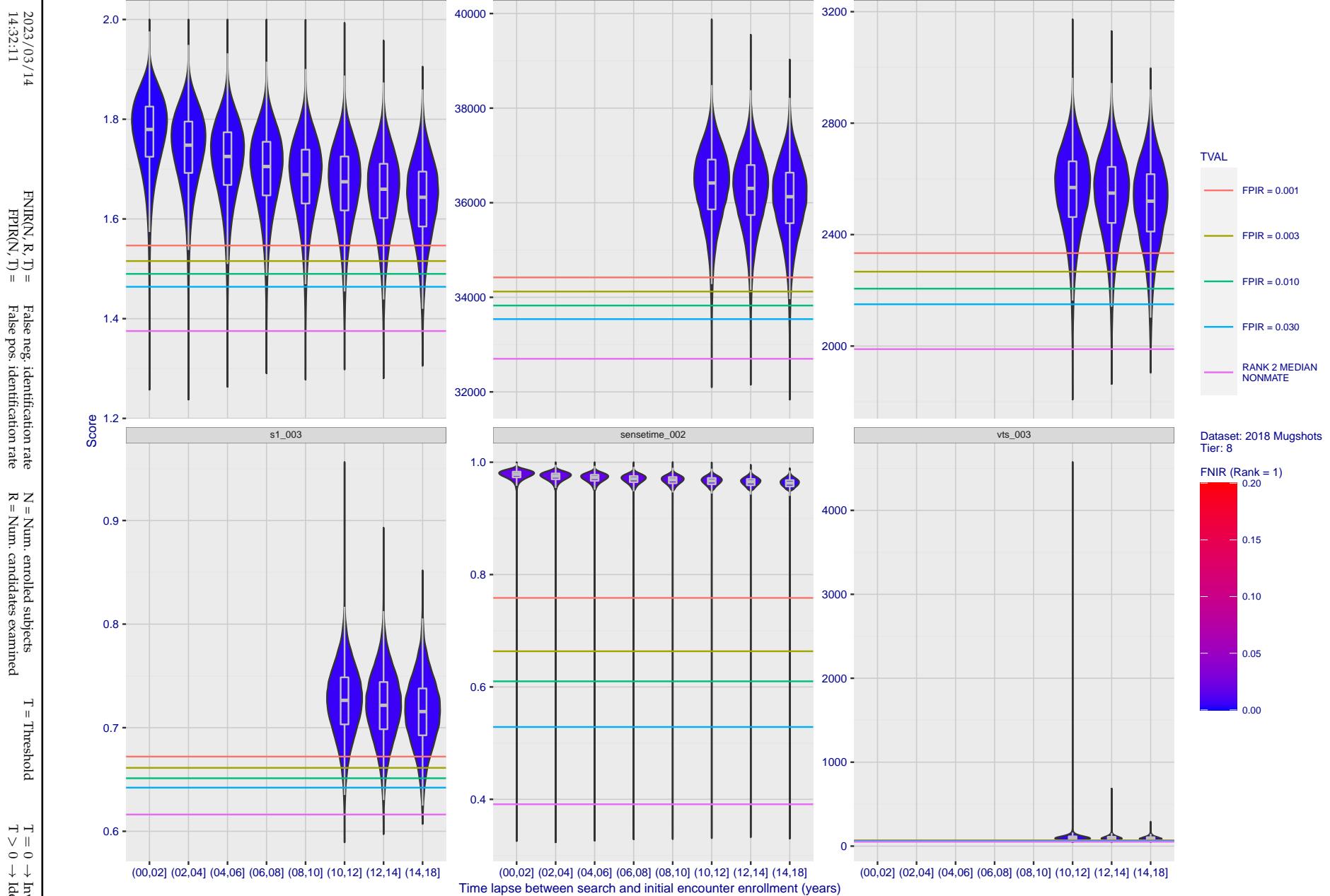


Figure 113: [FRVT-2018 Mugshot Ageing Dataset] Native mate scores vs. time-elapsed. The oldest image of each individual is enrolled. Thereafter, all more recent images are searched. Mated score distributions are computed over all searches noted in row 17 of Table 1 binned by number of years between search and initial enrollment.

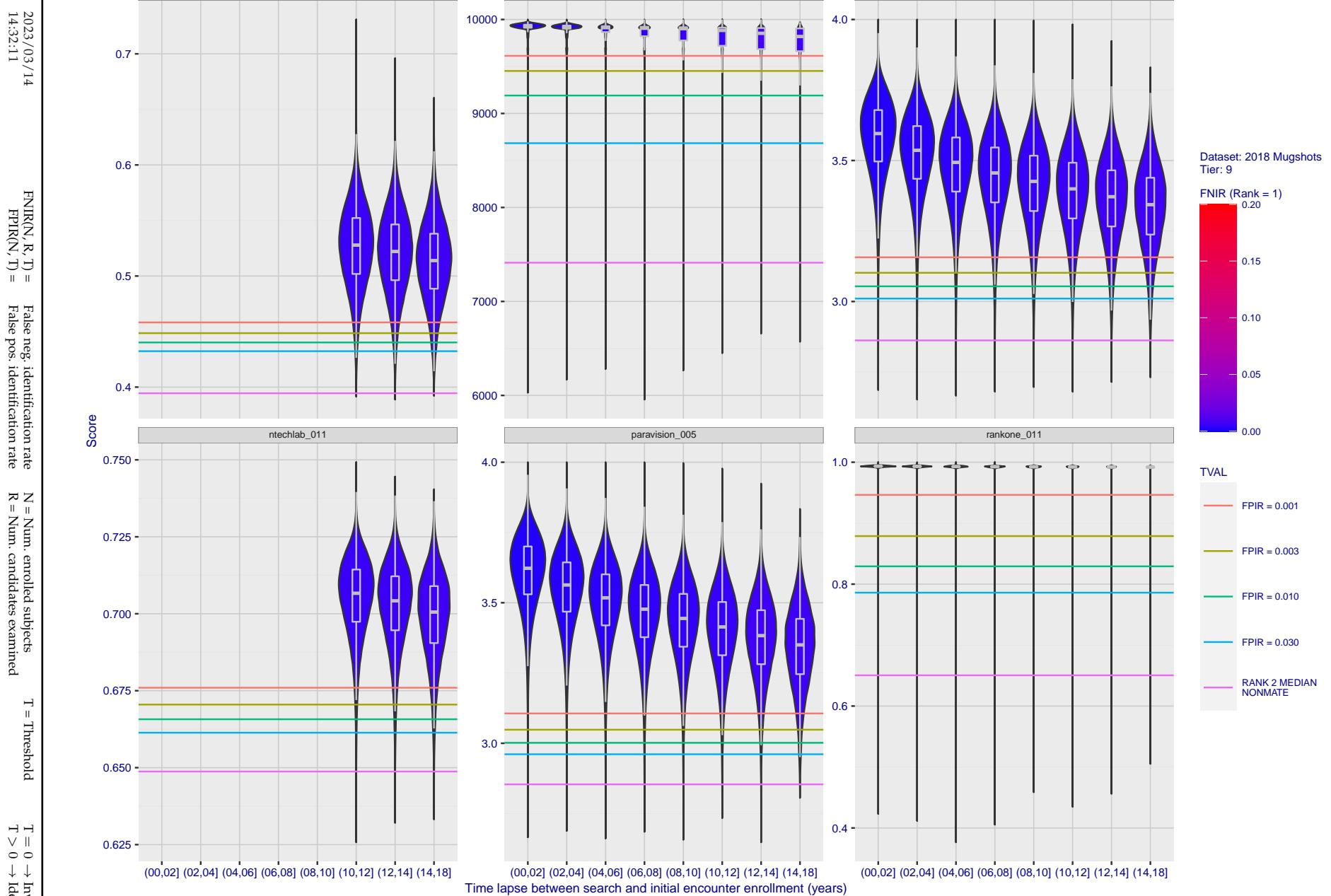


Figure 114: [FRVT-2018 Mugshot Ageing Dataset] Native mate scores vs. time-elapsed. The oldest image of each individual is enrolled. Thereafter, all more recent images are searched. Mated score distributions are computed over all searches noted in row 17 of Table 1 binned by number of years between search and initial enrollment.

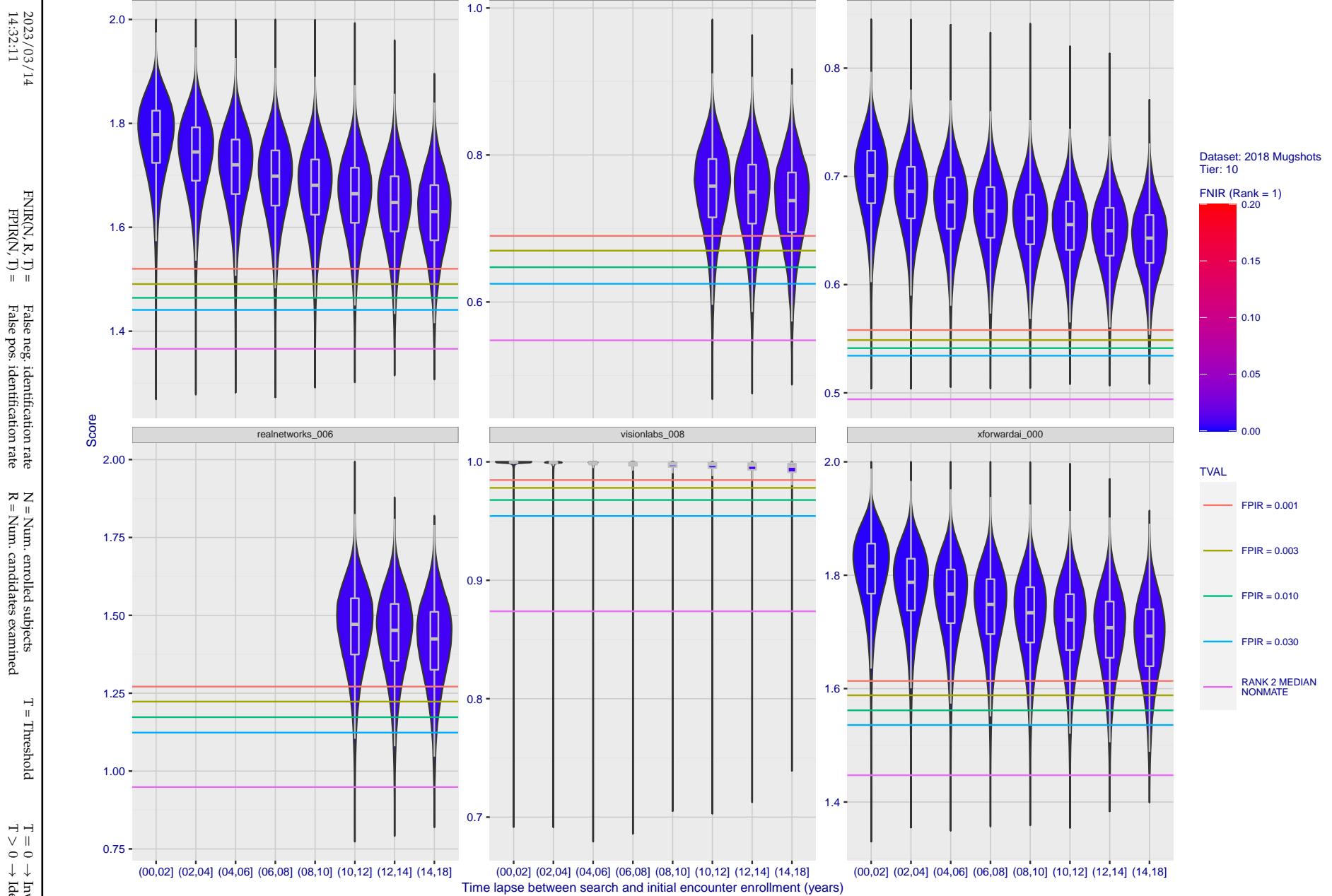


Figure 115: [FRVT-2018 Mugshot Ageing Dataset] Native mate scores vs. time-elapsed. The oldest image of each individual is enrolled. Thereafter, all more recent images are searched. Mated score distributions are computed over all searches noted in row 17 of Table 1 binned by number of years between search and initial enrollment.

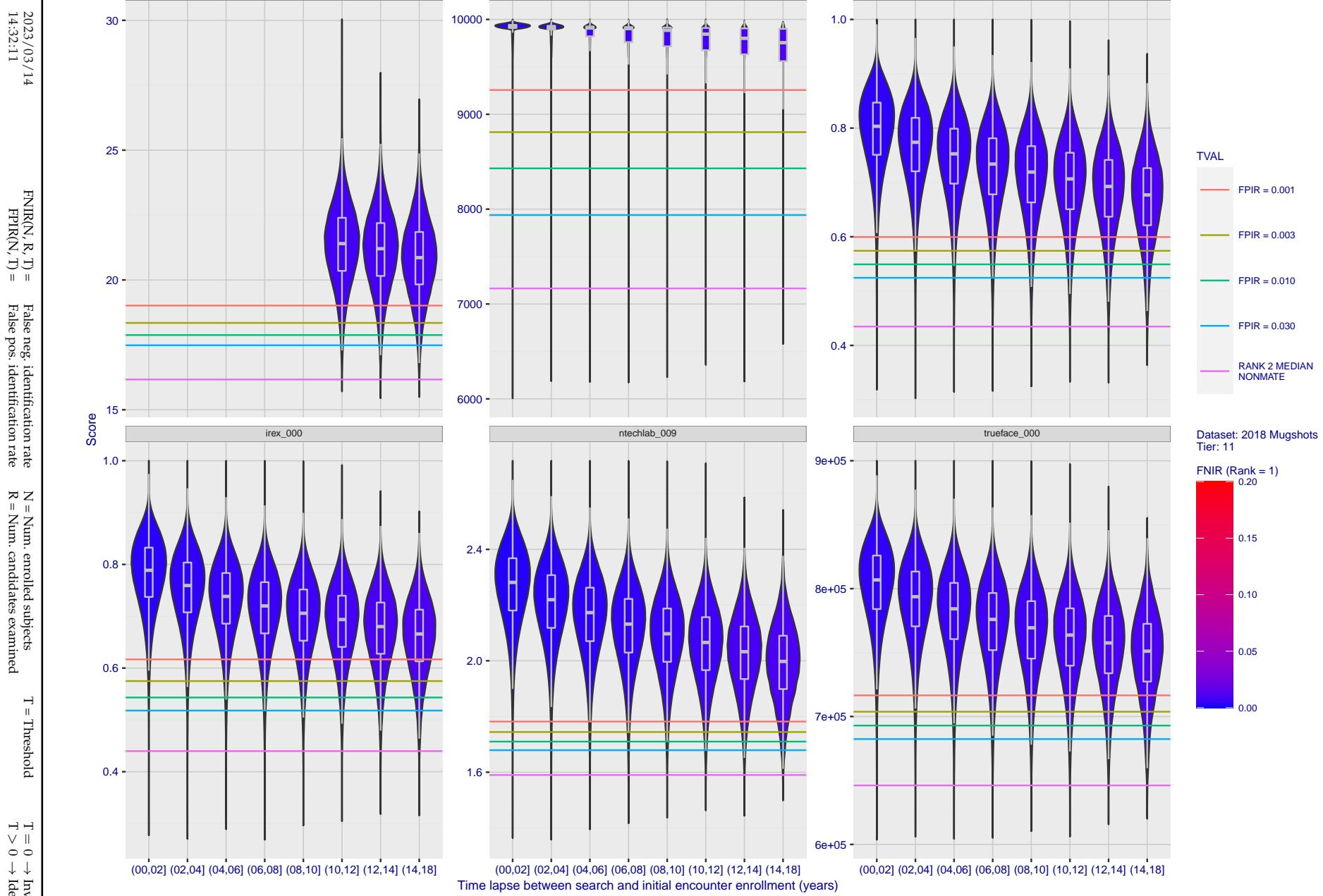


Figure 116: [FRVT-2018 Mugshot Ageing Dataset] Native mate scores vs. time-elapsed. The oldest image of each individual is enrolled. Thereafter, all more recent images are searched. Mated score distributions are computed over all searches noted in row 17 of Table 1 binned by number of years between search and initial enrollment.

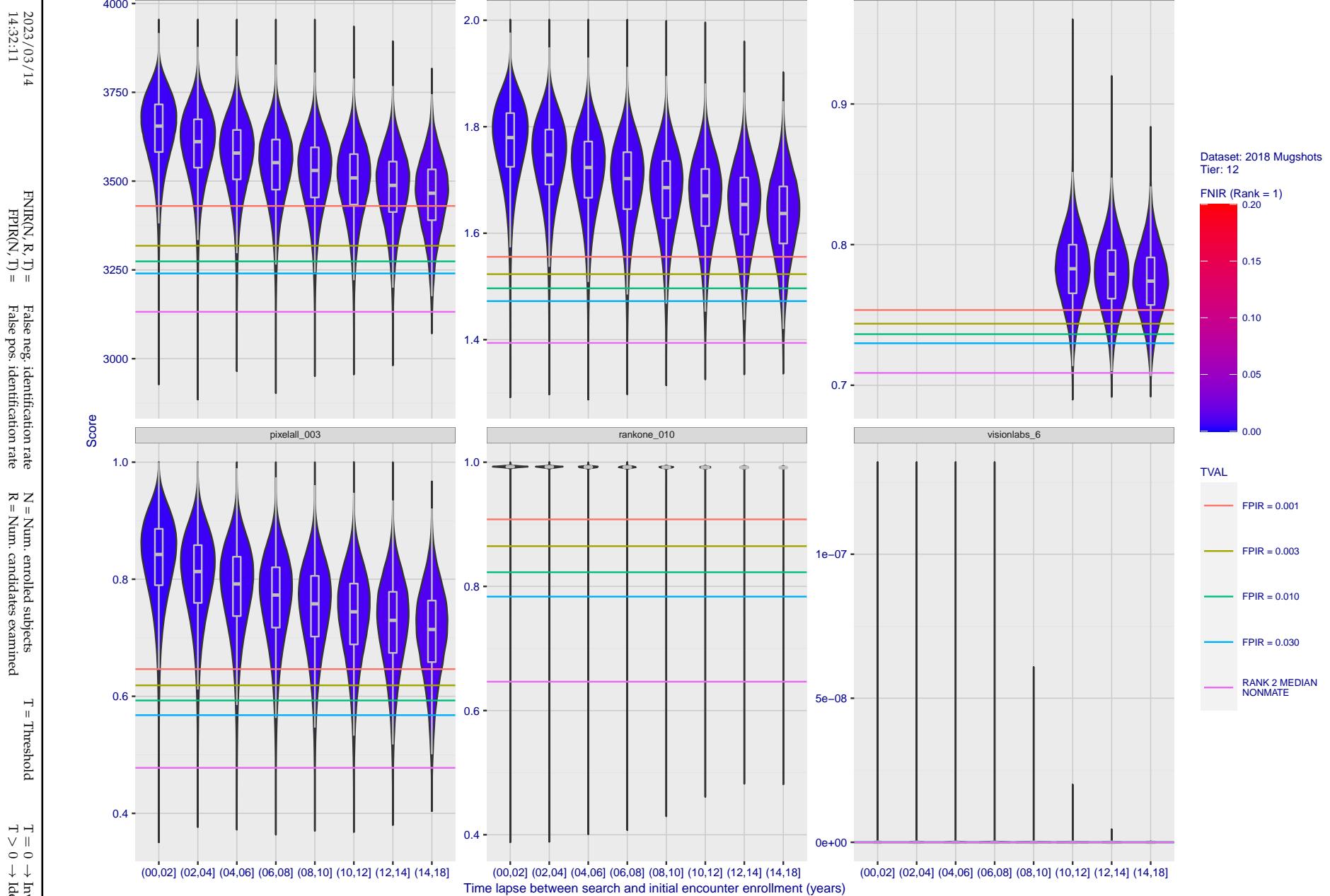


Figure 117: [FRVT-2018 Mugshot Ageing Dataset] Native mate scores vs. time-elapsed. The oldest image of each individual is enrolled. Thereafter, all more recent images are searched. Mated score distributions are computed over all searches noted in row 17 of Table 1 binned by number of years between search and initial enrollment.

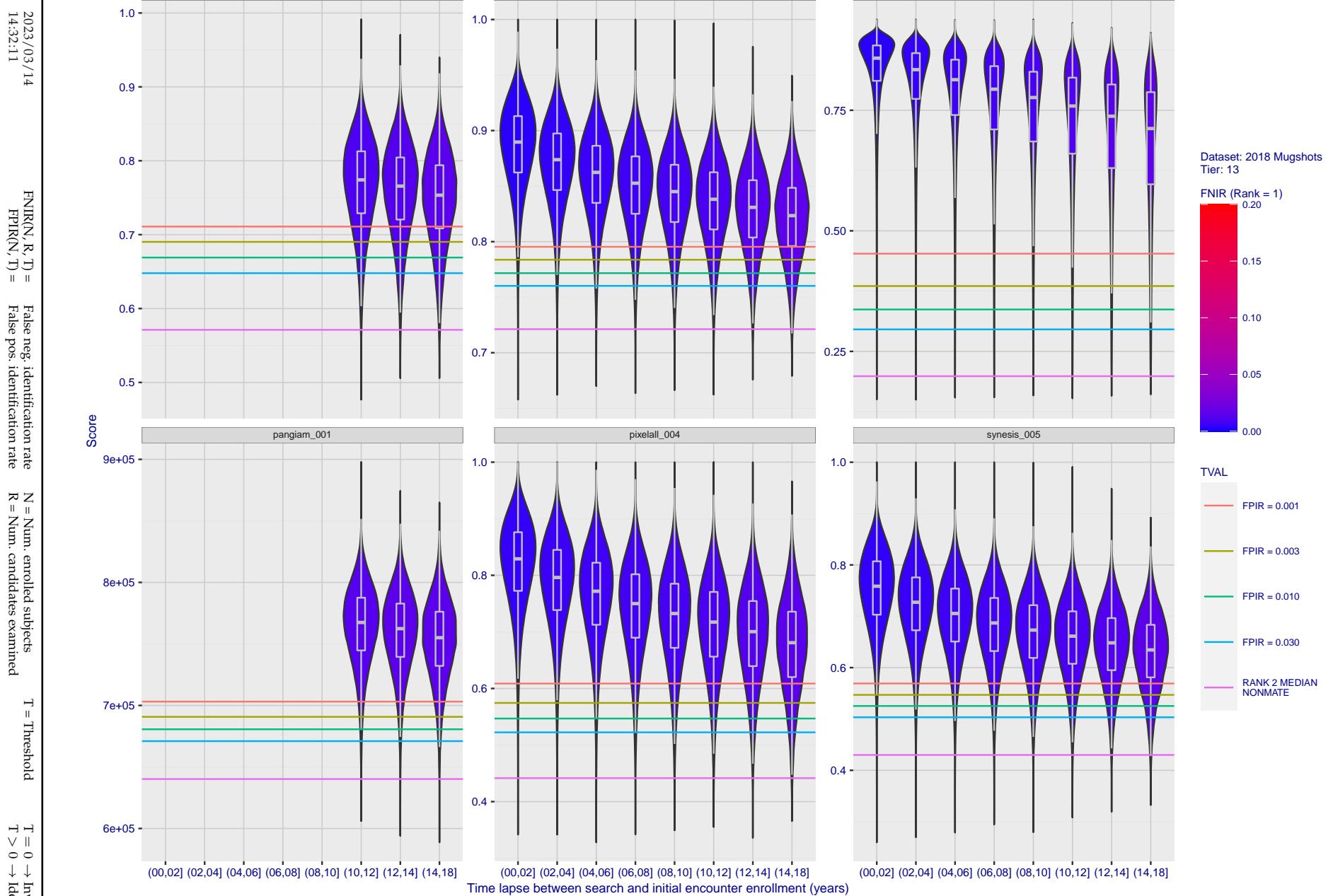


Figure 118: [FRVT-2018 Mugshot Ageing Dataset] Native mate scores vs. time-elapsed. The oldest image of each individual is enrolled. Thereafter, all more recent images are searched. Mated score distributions are computed over all searches noted in row 17 of Table 1 binned by number of years between search and initial enrollment.

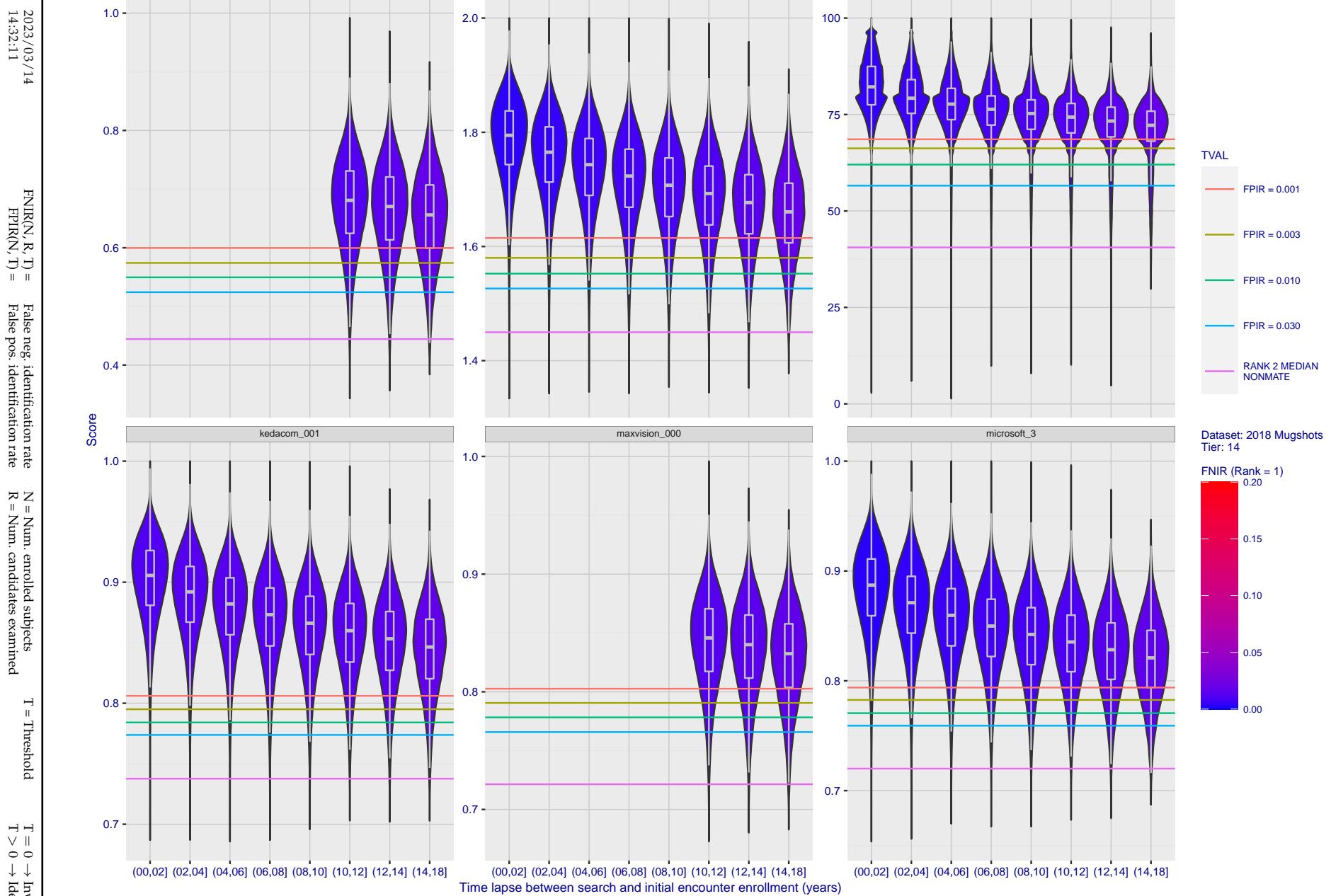


Figure 119: [FRVT-2018 Mugshot Ageing Dataset] Native mate scores vs. time-elapsed. The oldest image of each individual is enrolled. Thereafter, all more recent images are searched. Mated score distributions are computed over all searches noted in row 17 of Table 1 binned by number of years between search and initial enrollment.

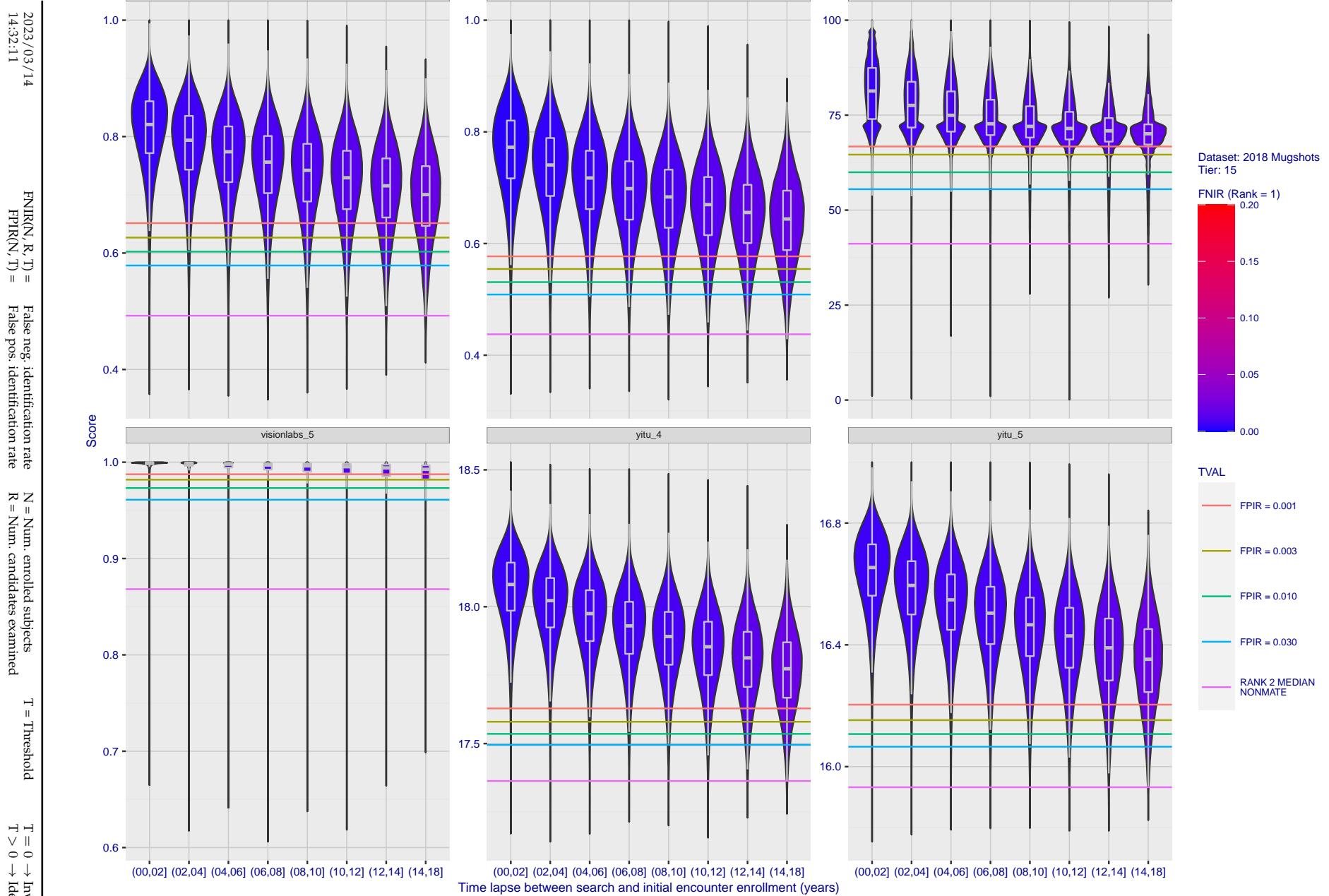


Figure 120: [FRVT-2018 Mugshot Ageing Dataset] Native mate scores vs. time-elapsed. The oldest image of each individual is enrolled. Thereafter, all more recent images are searched. Mated score distributions are computed over all searches noted in row 17 of Table 1 binned by number of years between search and initial enrollment.

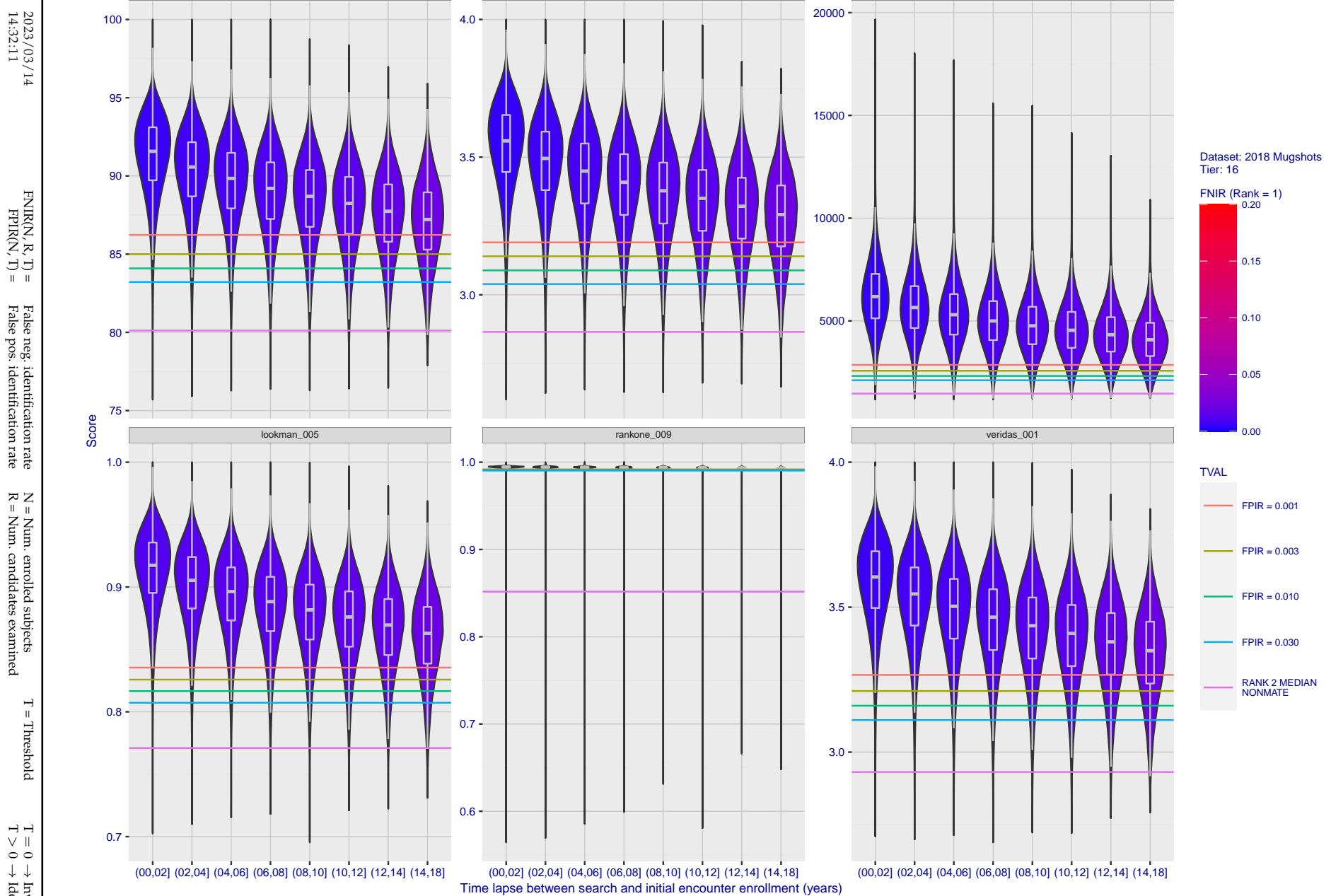


Figure 121: [FRVT-2018 Mugshot Ageing Dataset] Native mate scores vs. time-elapsed. The oldest image of each individual is enrolled. Thereafter, all more recent images are searched. Mated score distributions are computed over all searches noted in row 17 of Table 1 binned by number of years between search and initial enrollment.

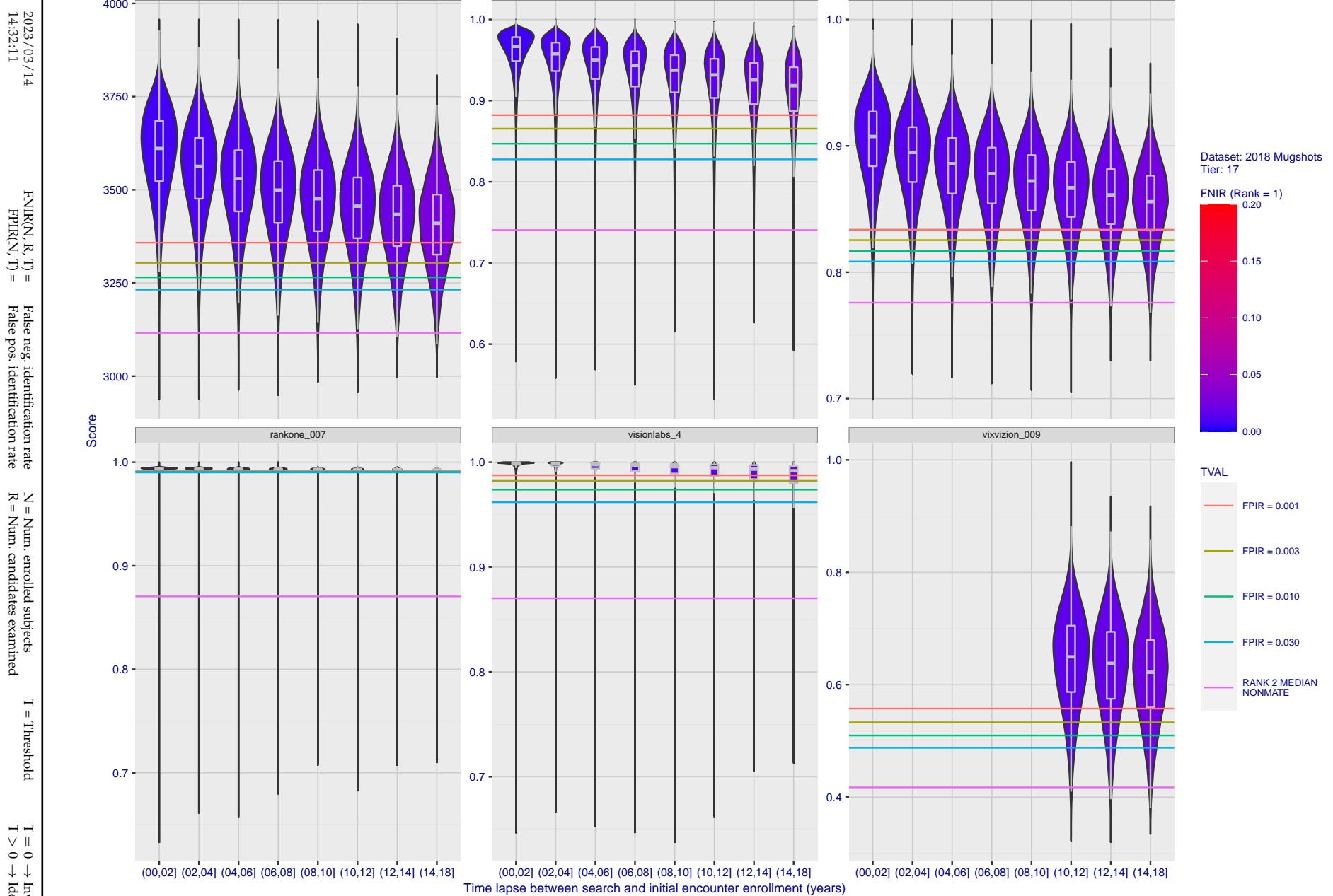


Figure 122: [FRVT-2018 Mugshot Ageing Dataset] Native mate scores vs. time-elapsed. The oldest image of each individual is enrolled. Thereafter, all more recent images are searched. Mated score distributions are computed over all searches noted in row 17 of Table 1 binned by number of years between search and initial enrollment.

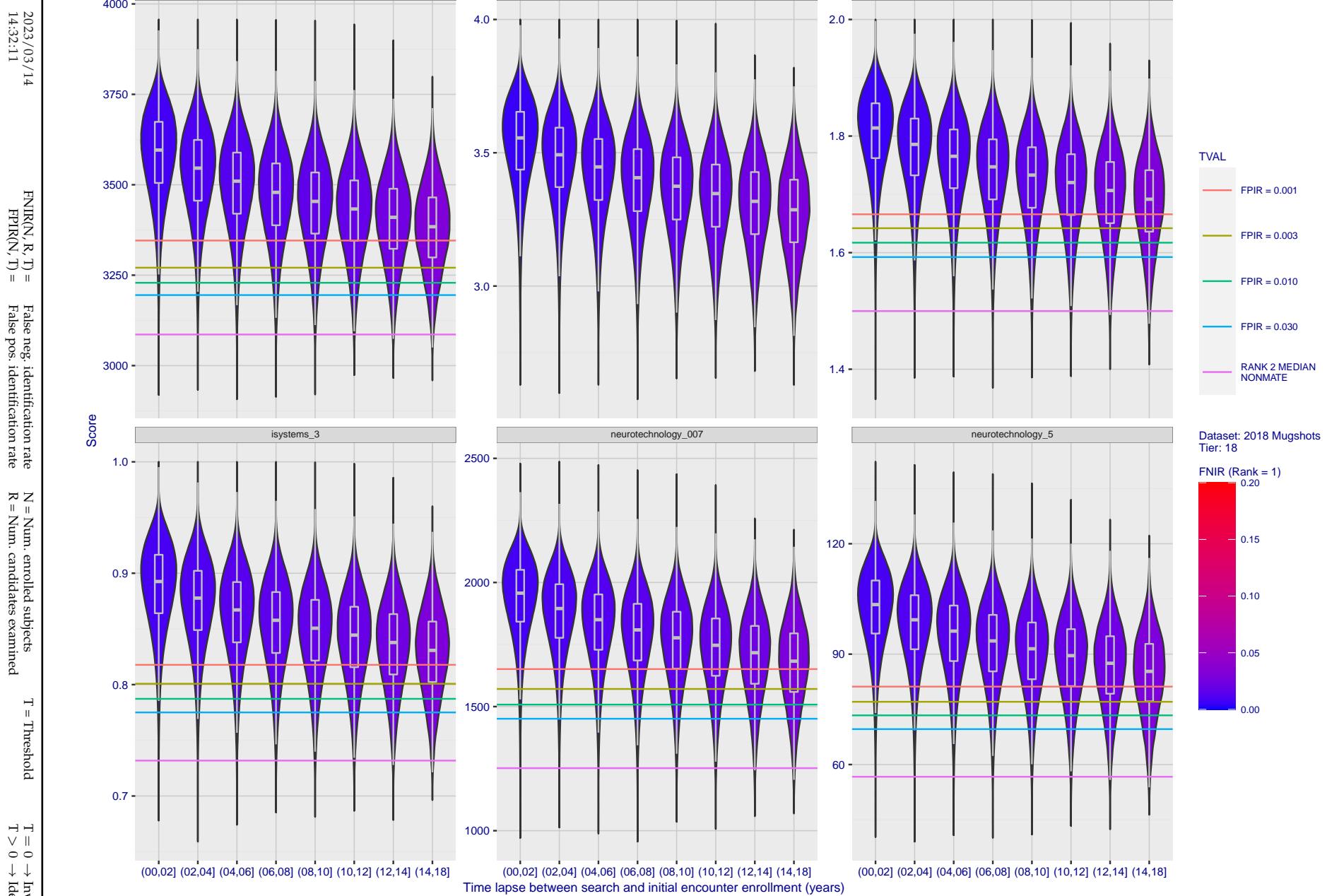


Figure 123: [FRVT-2018 Mugshot Ageing Dataset] Native mate scores vs. time-elapsed. The oldest image of each individual is enrolled. Thereafter, all more recent images are searched. Mated score distributions are computed over all searches noted in row 17 of Table 1 binned by number of years between search and initial enrollment.

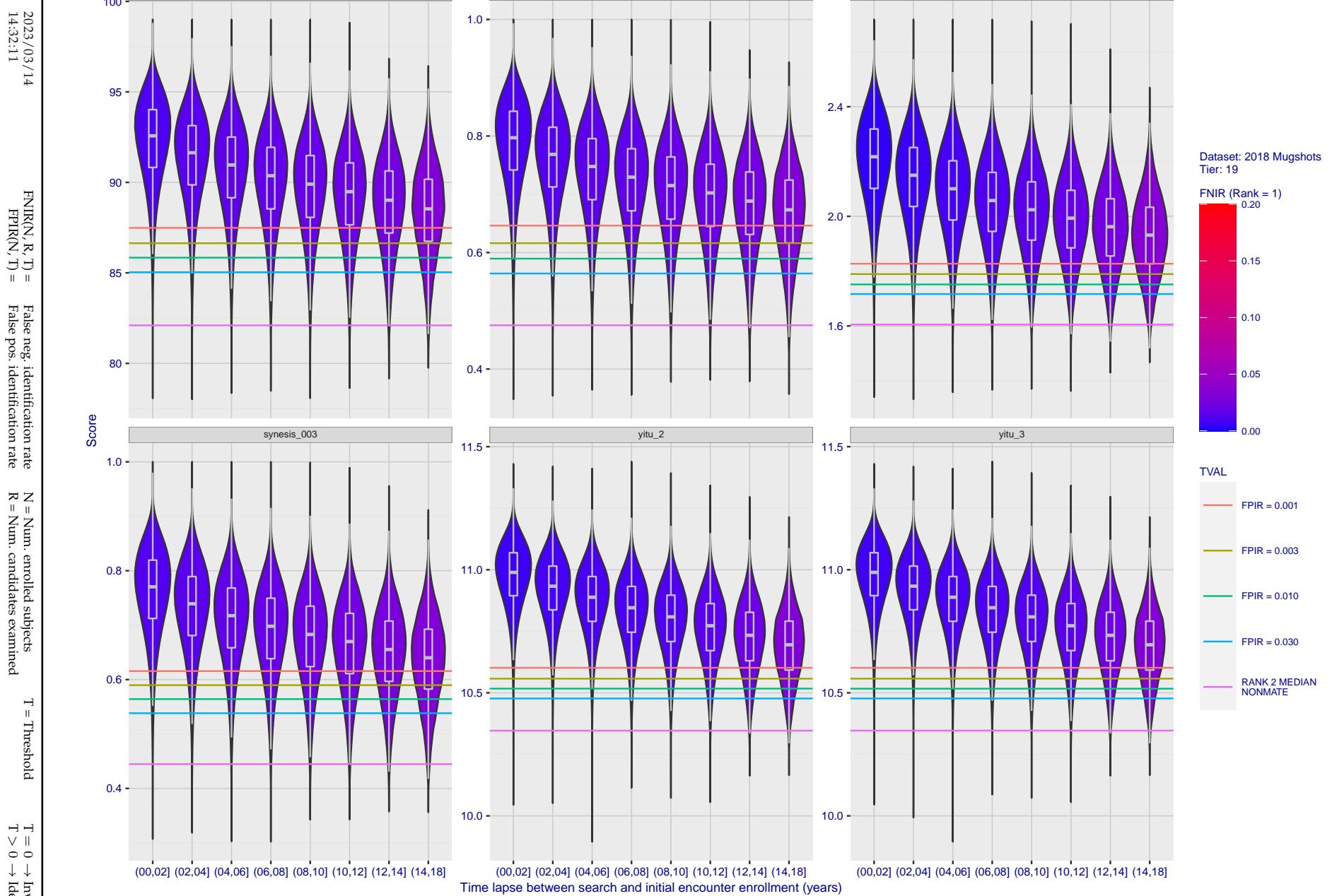


Figure 124: [FRVT-2018 Mugshot Ageing Dataset] Native mate scores vs. time-elapsed. The oldest image of each individual is enrolled. Thereafter, all more recent images are searched. Mated score distributions are computed over all searches noted in row 17 of Table 1 binned by number of years between search and initial enrollment.

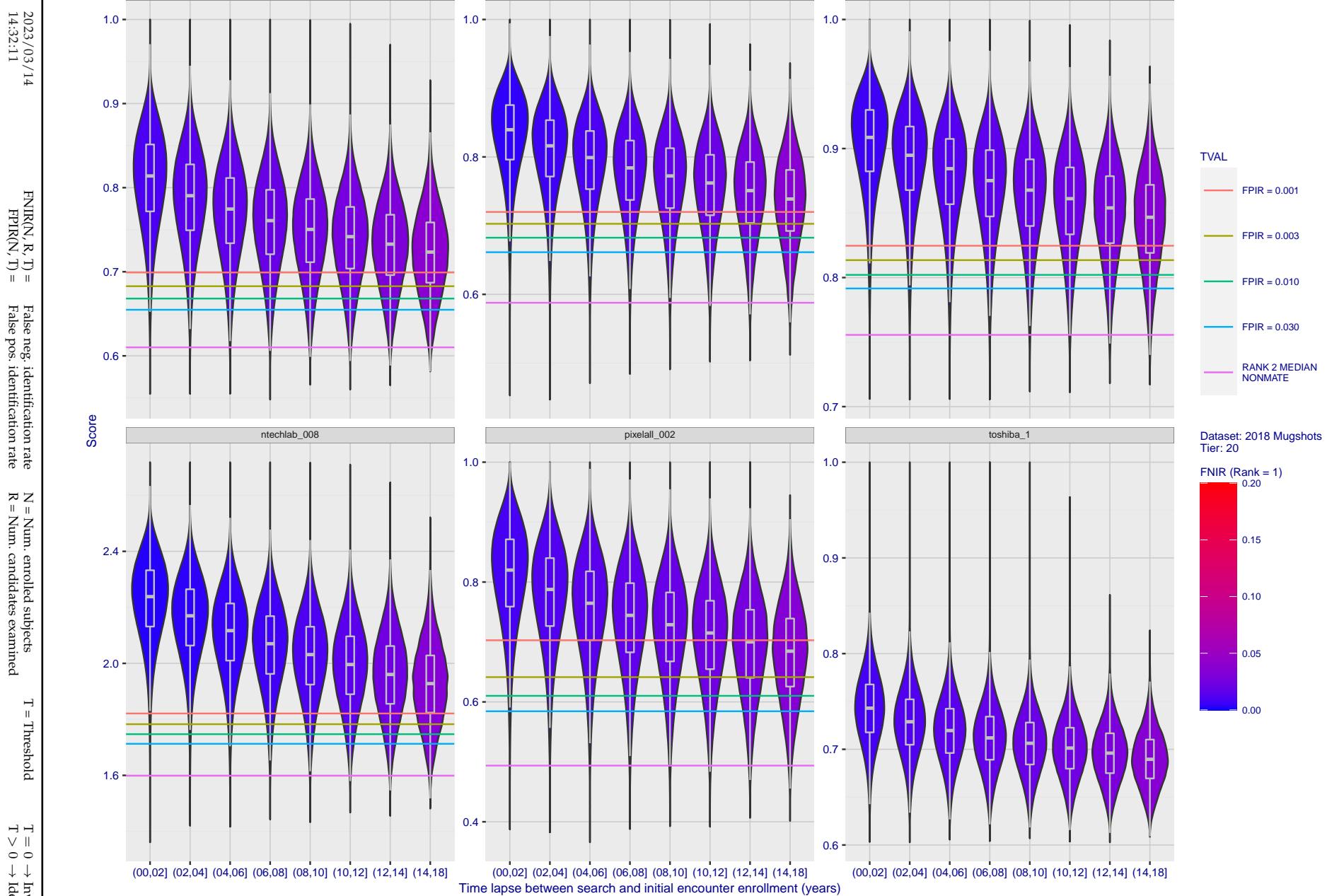


Figure 125: [FRVT-2018 Mugshot Ageing Dataset] Native mate scores vs. time-elapsed. The oldest image of each individual is enrolled. Thereafter, all more recent images are searched. Mated score distributions are computed over all searches noted in row 17 of Table 1 binned by number of years between search and initial enrollment.

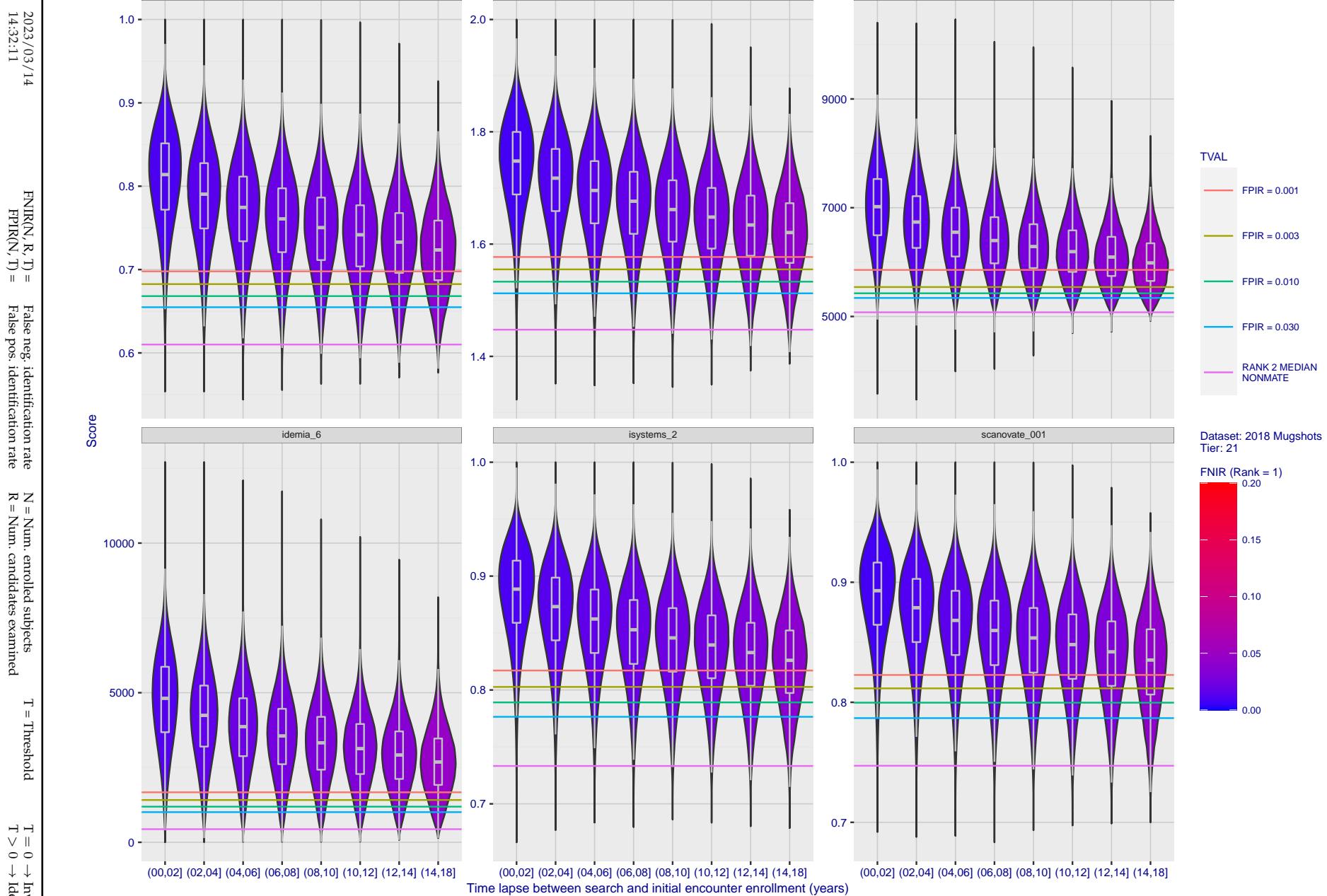


Figure 126: [FRVT-2018 Mugshot Ageing Dataset] Native mate scores vs. time-elapsed. The oldest image of each individual is enrolled. Thereafter, all more recent images are searched. Mated score distributions are computed over all searches noted in row 17 of Table 1 binned by number of years between search and initial enrollment.

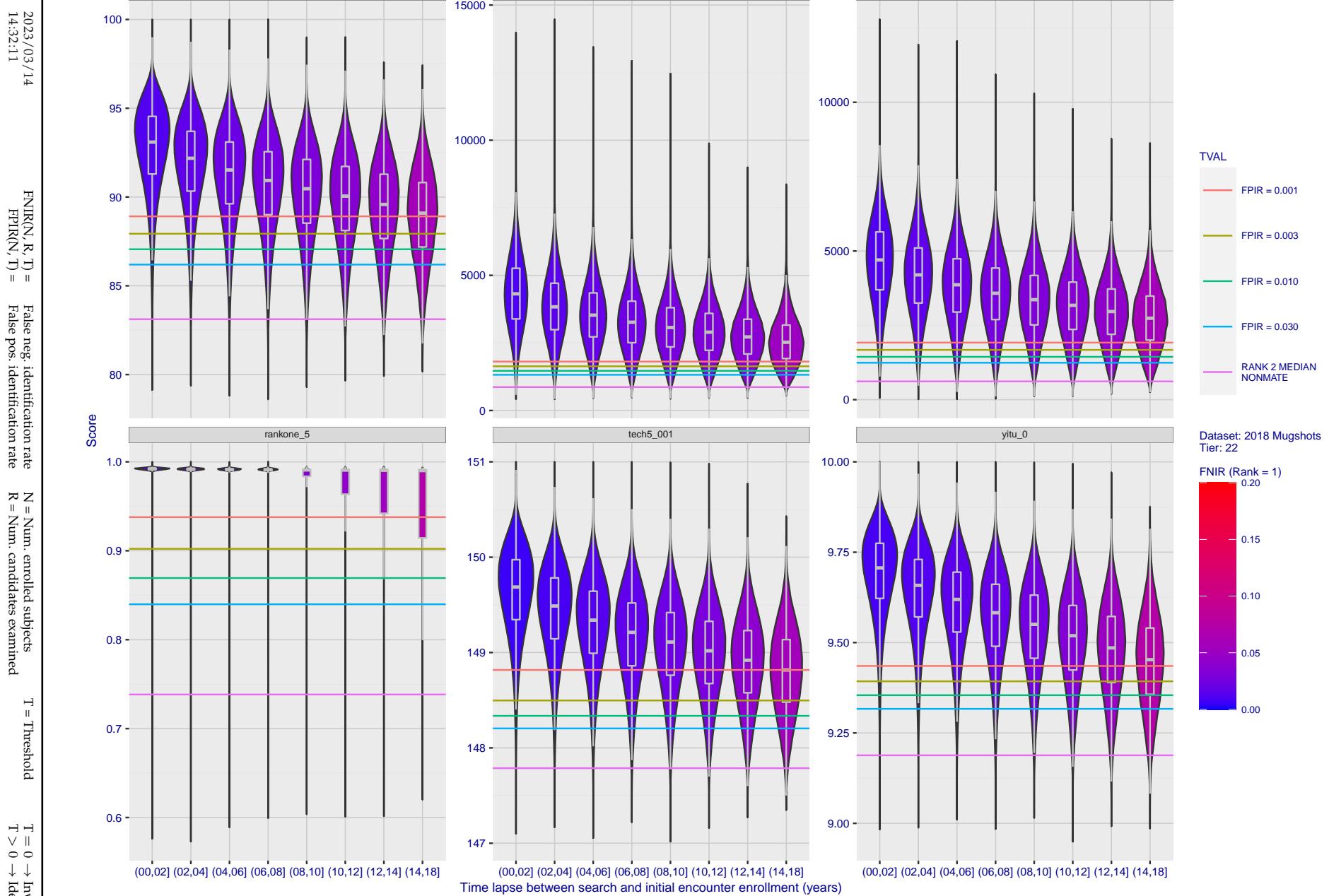


Figure 127: [FRVT-2018 Mugshot Ageing Dataset] Native mate scores vs. time-elapsed. The oldest image of each individual is enrolled. Thereafter, all more recent images are searched. Mated score distributions are computed over all searches noted in row 17 of Table 1 binned by number of years between search and initial enrollment.

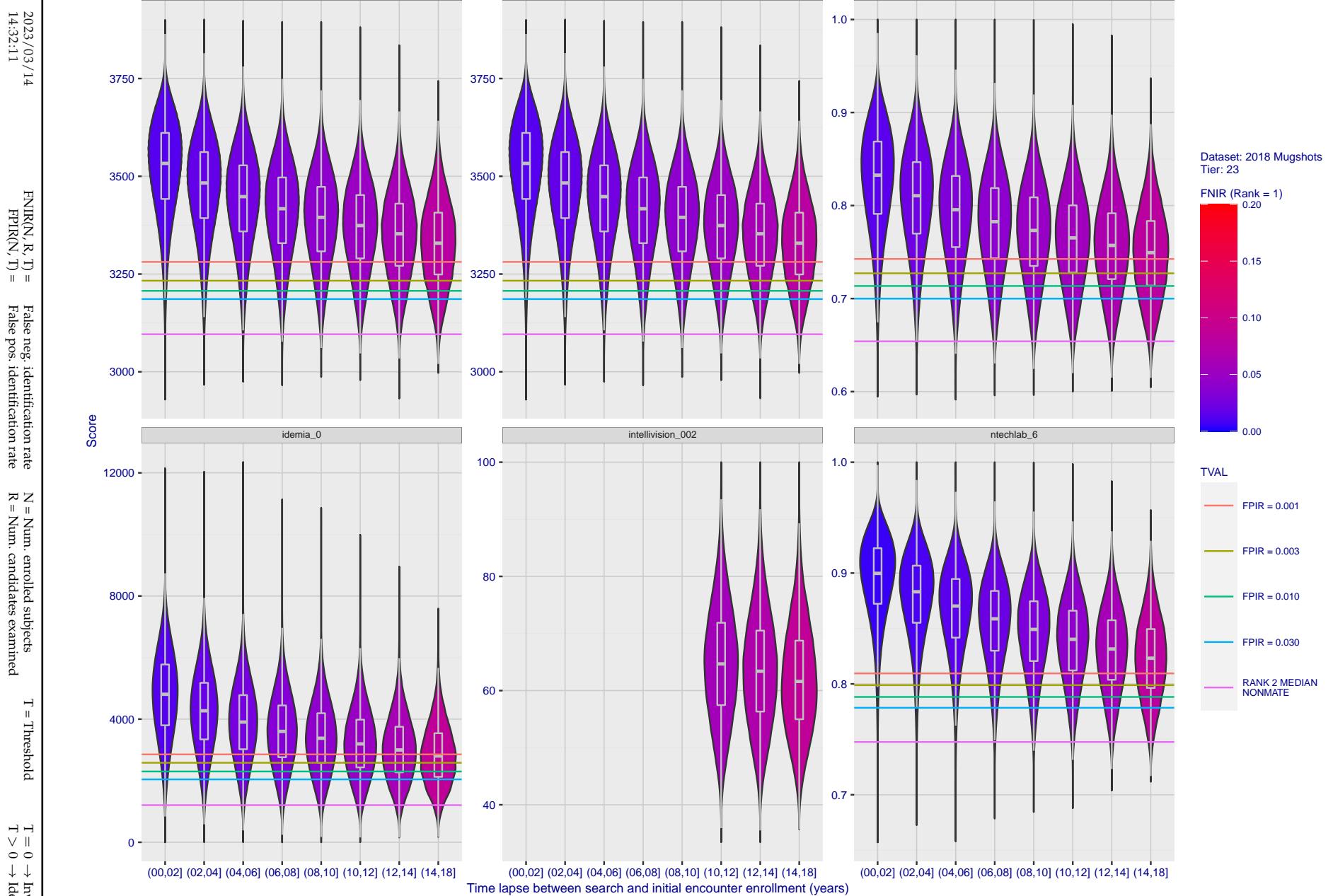


Figure 128: [FRVT-2018 Mugshot Ageing Dataset] Native mate scores vs. time-elapsed. The oldest image of each individual is enrolled. Thereafter, all more recent images are searched. Mated score distributions are computed over all searches noted in row 17 of Table 1 binned by number of years between search and initial enrollment.

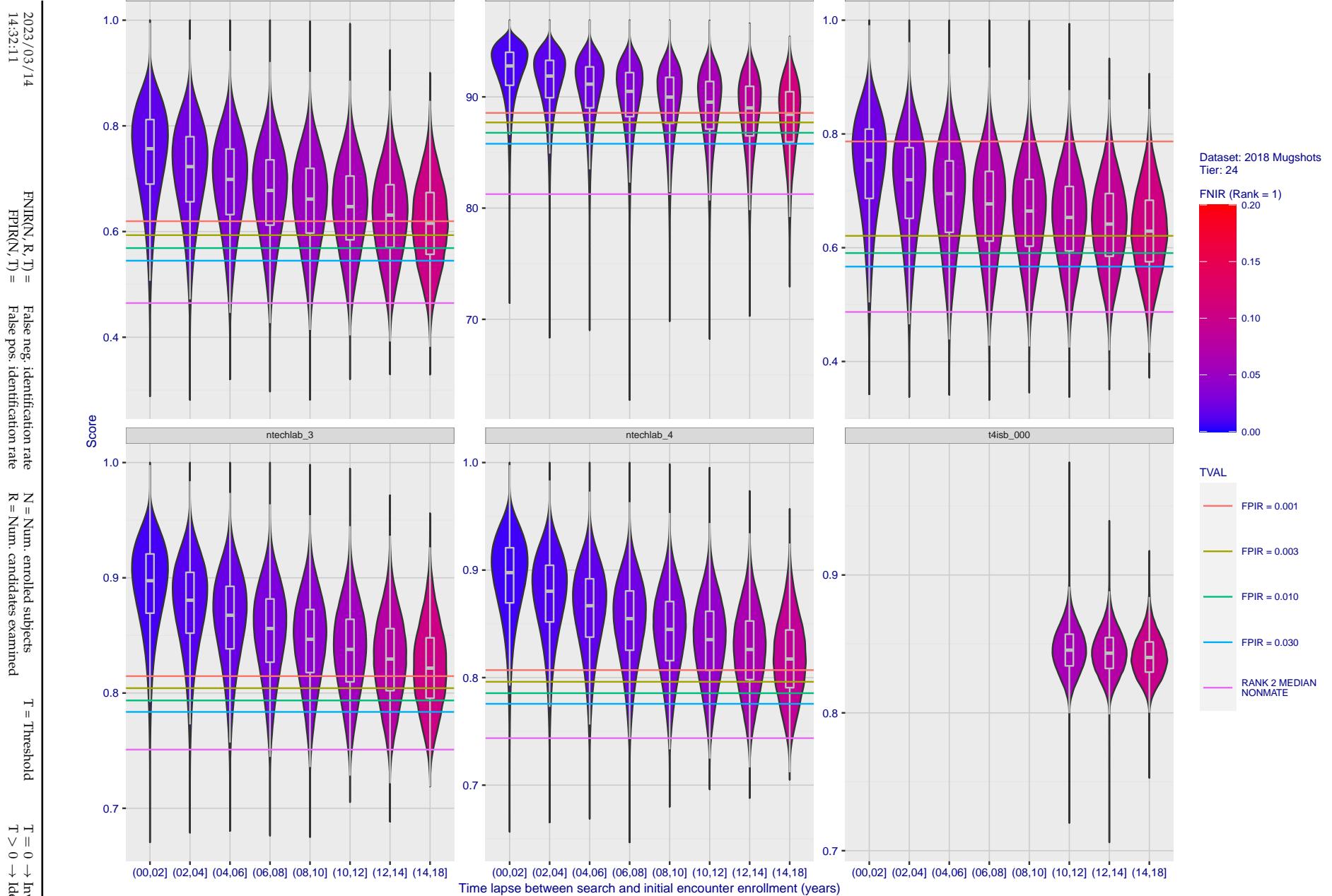


Figure 129: [FRVT-2018 Mugshot Ageing Dataset] Native mate scores vs. time-elapsed. The oldest image of each individual is enrolled. Thereafter, all more recent images are searched. Mated score distributions are computed over all searches noted in row 17 of Table 1 binned by number of years between search and initial enrollment.

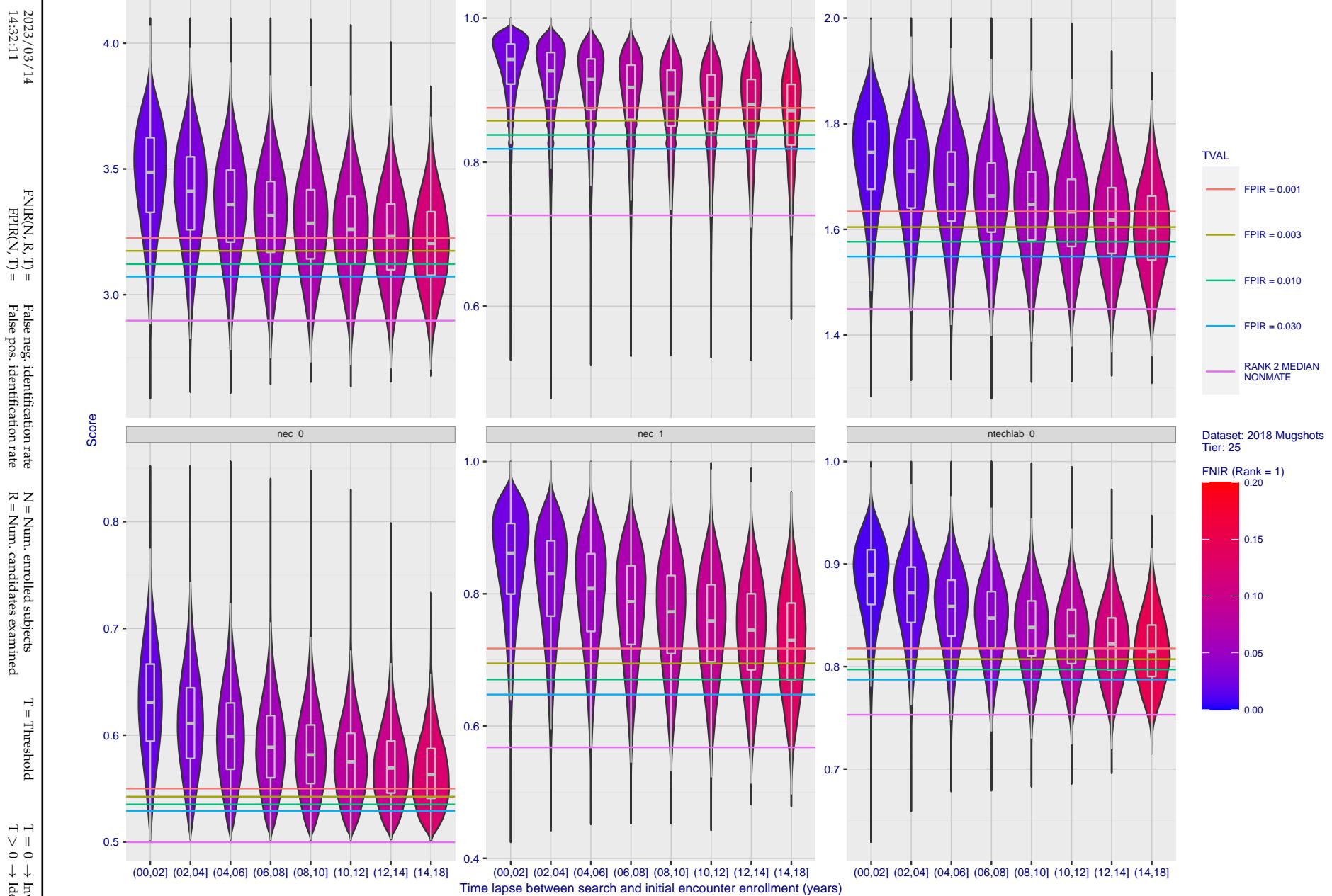


Figure 130: [FRVT-2018 Mugshot Ageing Dataset] Native mate scores vs. time-elapsed. The oldest image of each individual is enrolled. Thereafter, all more recent images are searched. Mated score distributions are computed over all searches noted in row 17 of Table 1 binned by number of years between search and initial enrollment.

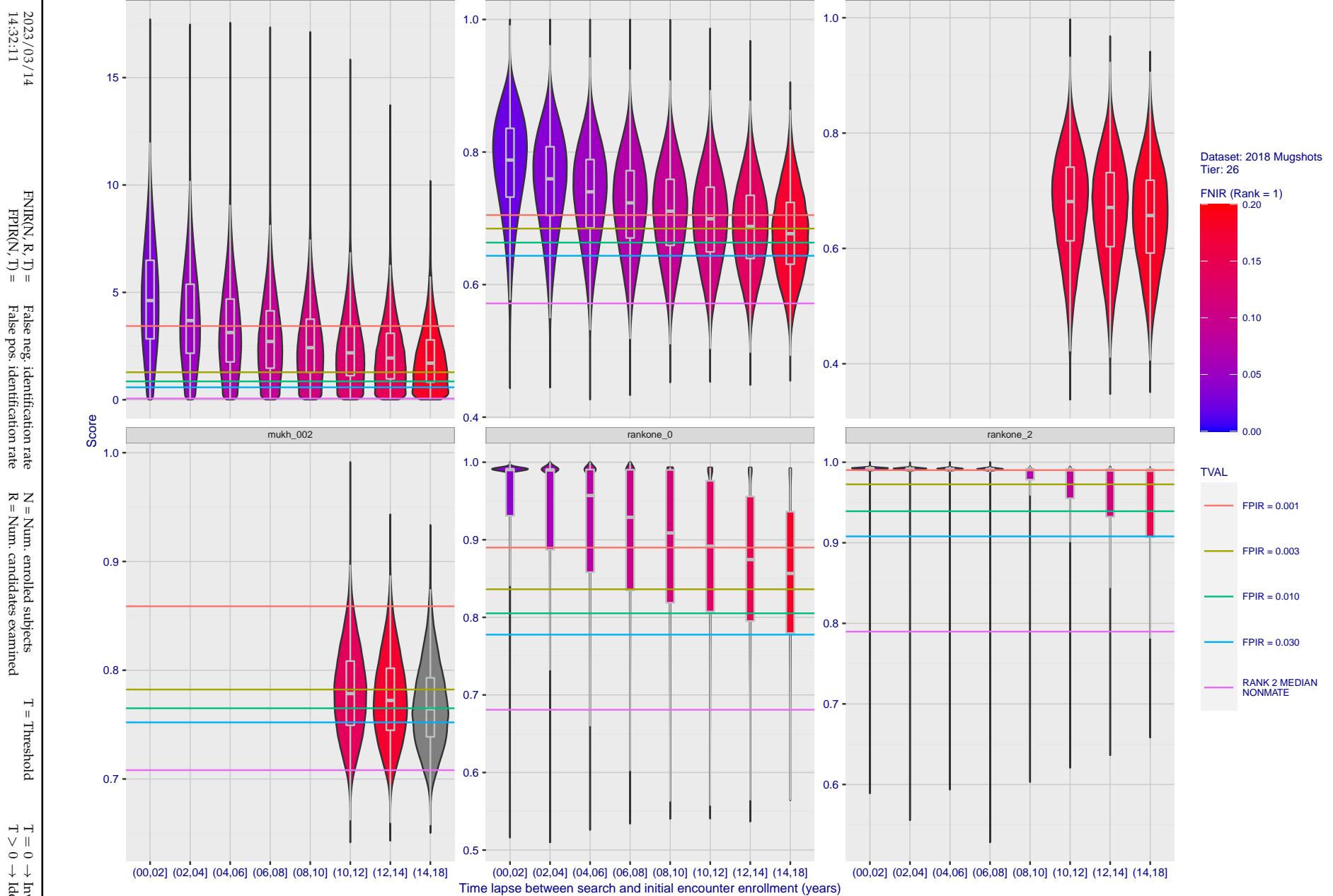


Figure 131: [FRVT-2018 Mugshot Ageing Dataset] Native mate scores vs. time-elapsed. The oldest image of each individual is enrolled. Thereafter, all more recent images are searched. Mated score distributions are computed over all searches noted in row 17 of Table 1 binned by number of years between search and initial enrollment.

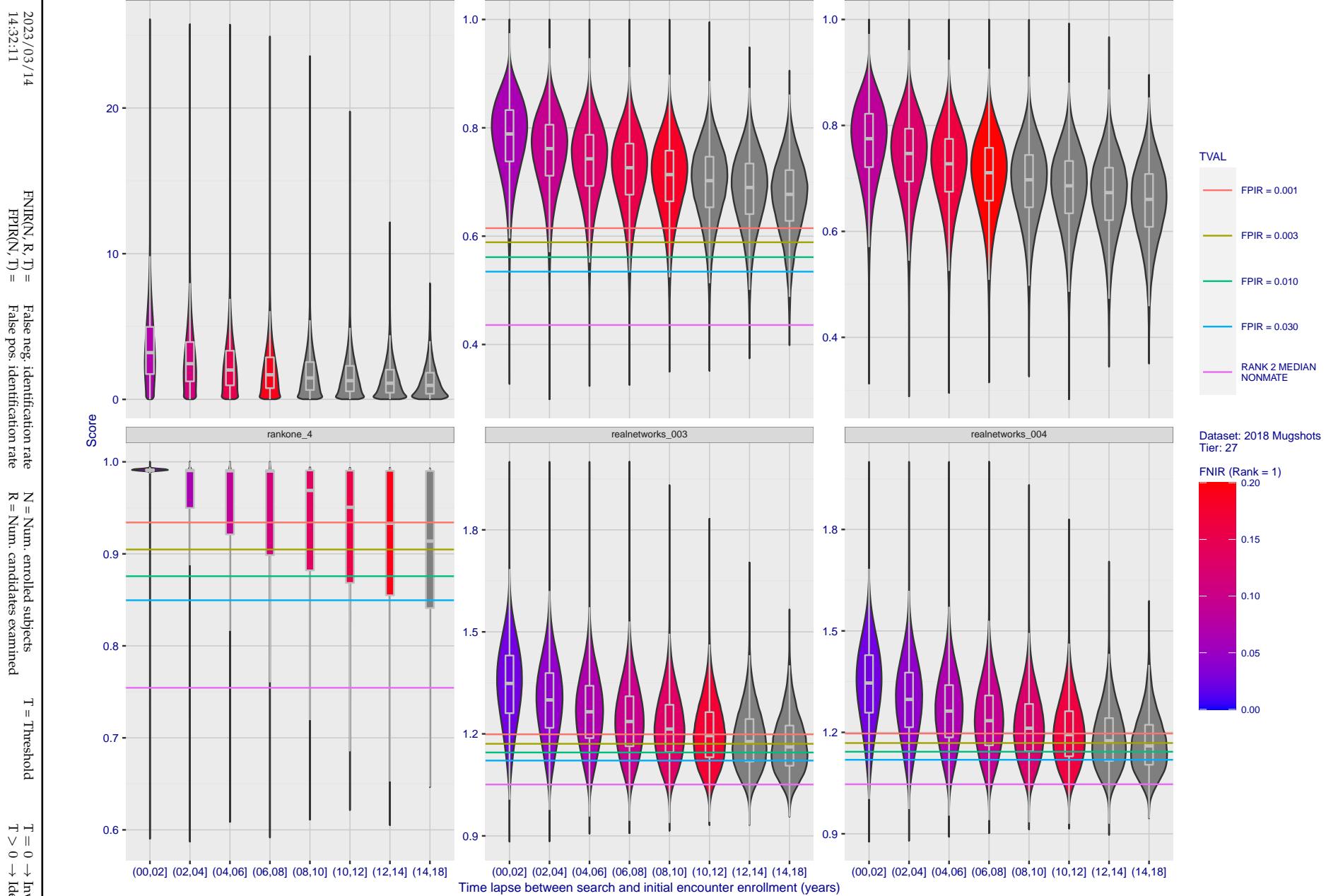


Figure 132: [FRVT-2018 Mugshot Ageing Dataset] Native mate scores vs. time-elapsed. The oldest image of each individual is enrolled. Thereafter, all more recent images are searched. Mated score distributions are computed over all searches noted in row 17 of Table 1 binned by number of years between search and initial enrollment.

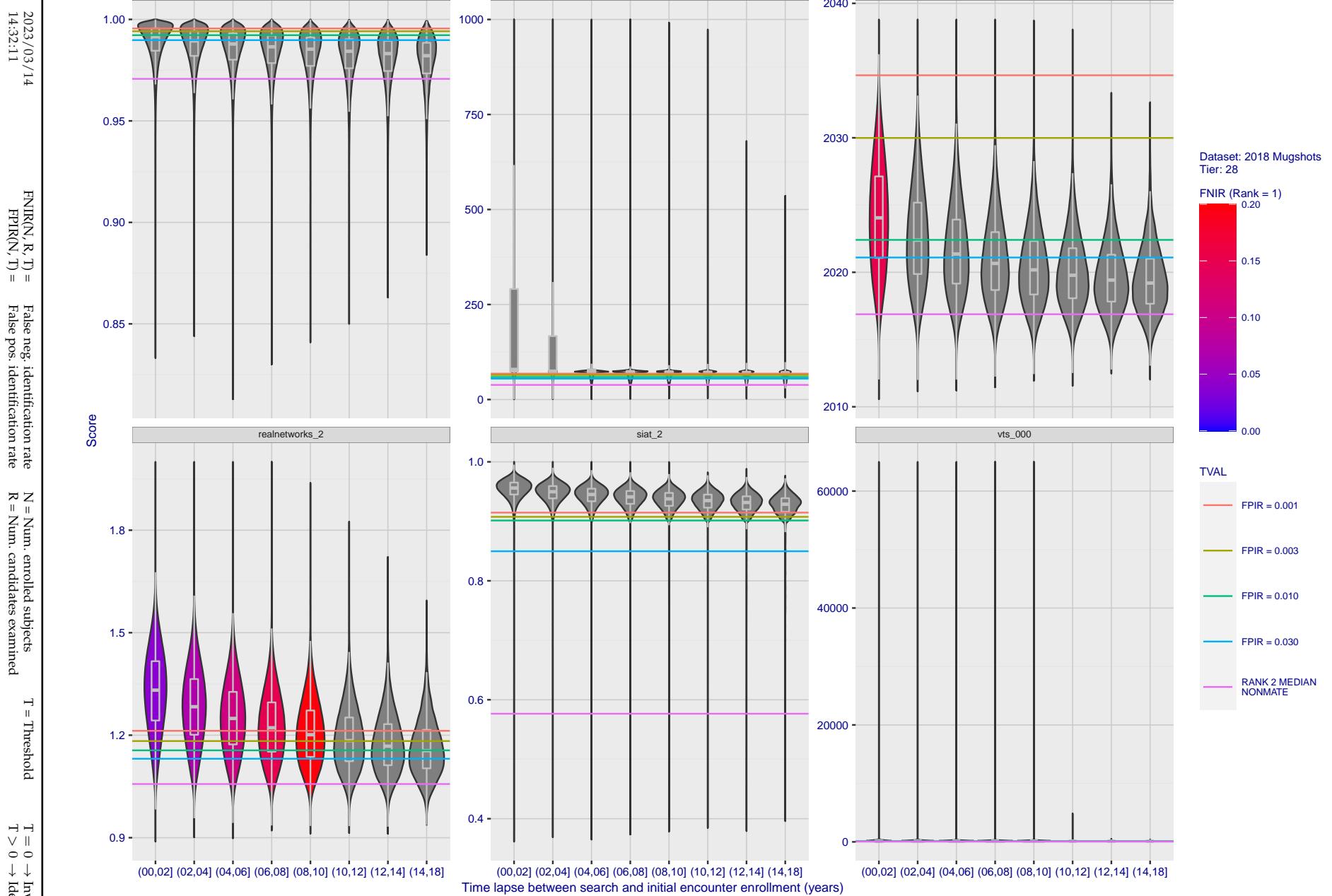


Figure 133: [FRVT-2018 Mugshot Ageing Dataset] Native mate scores vs. time-elapsed. The oldest image of each individual is enrolled. Thereafter, all more recent images are searched. Mated score distributions are computed over all searches noted in row 17 of Table 1 binned by number of years between search and initial enrollment.

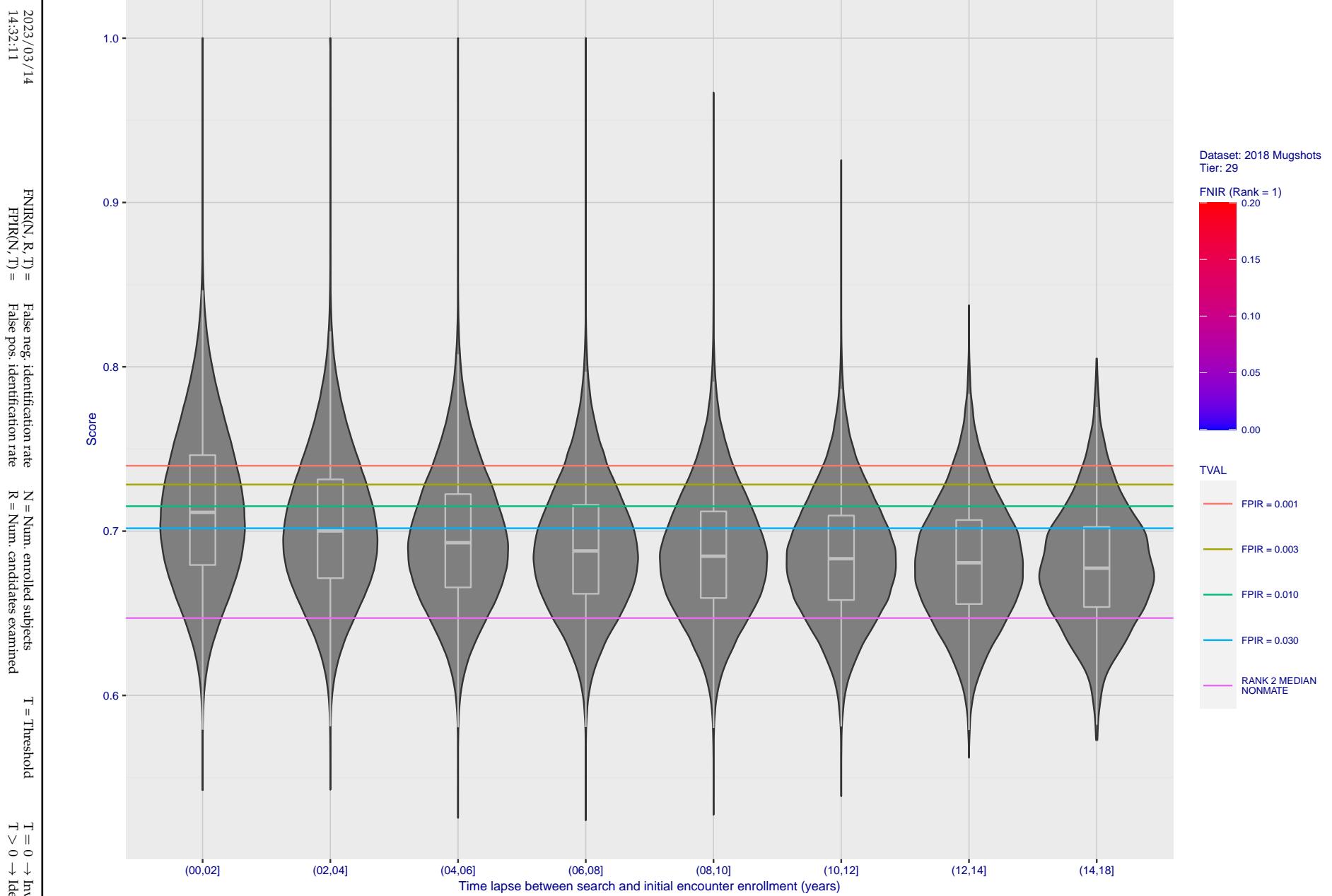


Figure 134: [FRVT-2018 Mugshot Ageing Dataset] Native mate scores vs. time-elapsed. The oldest image of each individual is enrolled. Thereafter, all more recent images are searched. Mated score distributions are computed over all searches noted in row 17 of Table 1 binned by number of years between search and initial enrollment.

Appendix C Effect of enrolling multiple images

2023/03/14
14:32:11FNIR(N, R, T) = False neg. identification rate
FPIR(N, T) = False pos. identification rateN = Num. enrolled subjects
R = Num. candidates examined

T = Threshold

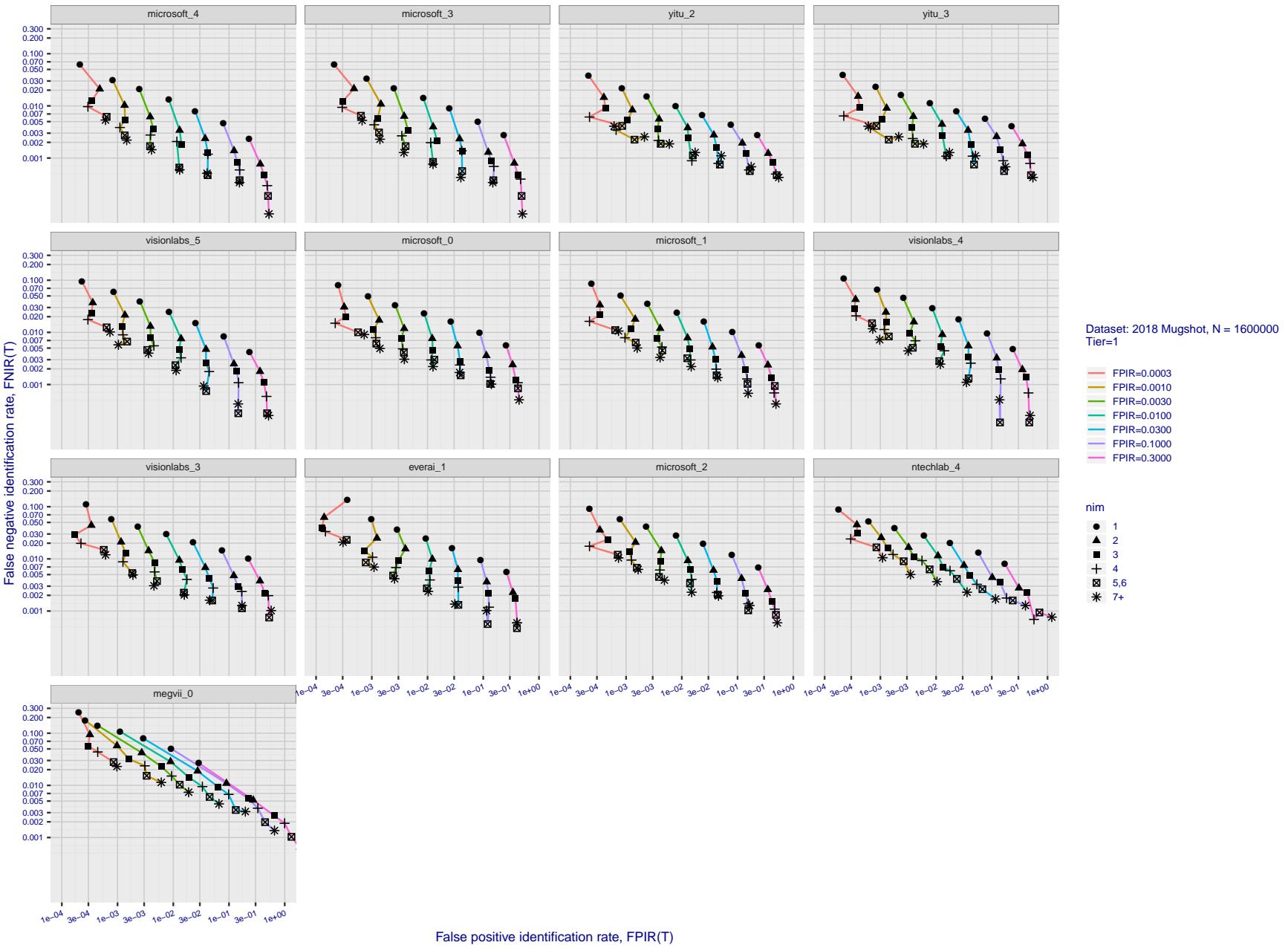
T = 0 → Investigation
T > 0 → Identification

Figure 135: [FRVT-2018 Mugshot Dataset] Effect of enrolling multiple images for each identity. The plot shows an identification miss rates vs. false positive rates, at seven operating thresholds. The enrolled population size is fixed. The images are enrolled with lifetime-consolidation - see section 2.3.

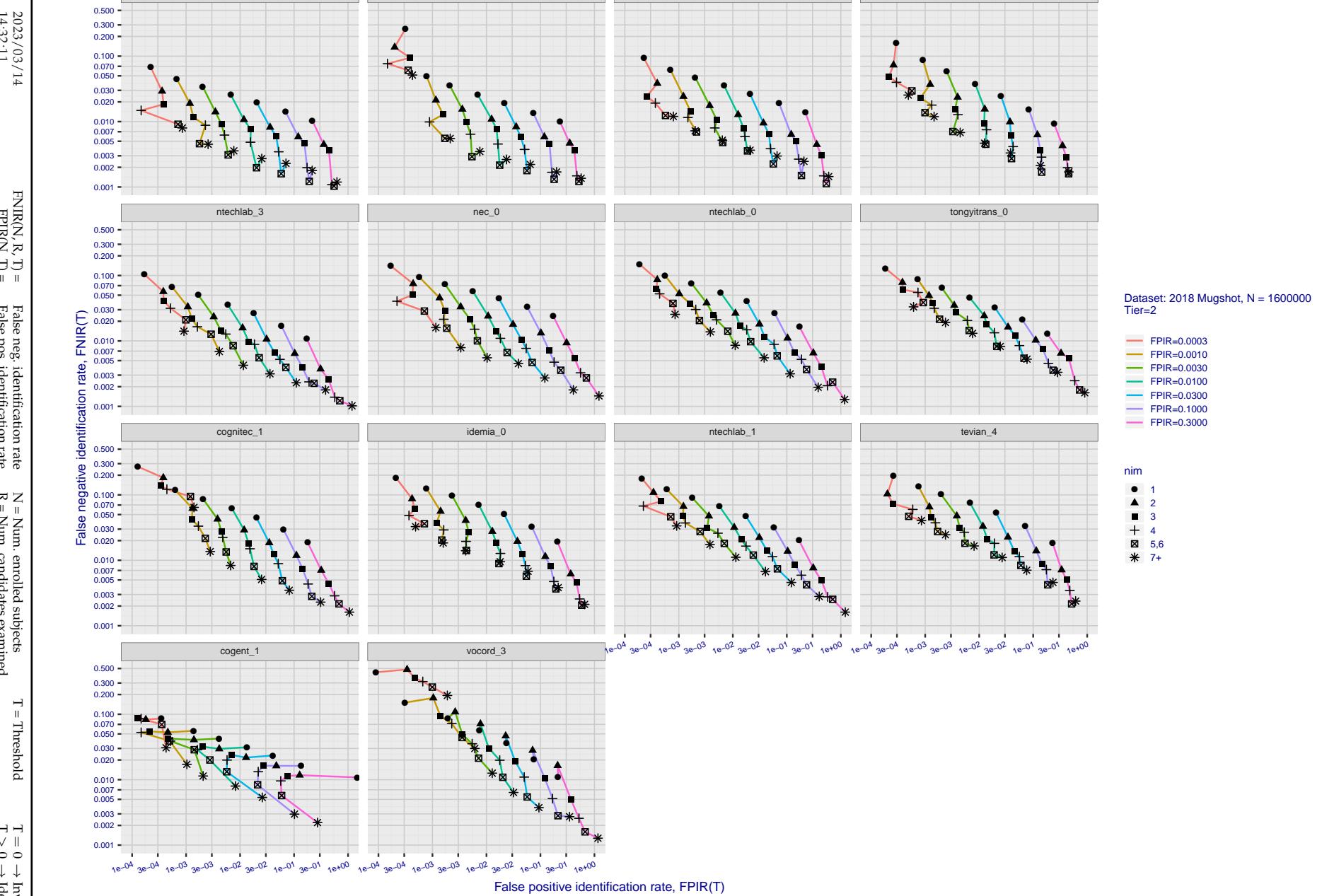


Figure 136: [FRVT-2018 Mugshot Dataset] Effect of enrolling multiple images for each identity. The plot shows an identification miss rates vs. false positive rates, at seven operating thresholds. The enrolled population size is fixed. The images are enrolled with lifetime-consolidation - see section 2.3.

2023/03/14
14:32:11FNIR(N, R, T) = False neg. identification rate
FPIR(N, T) = False pos. identification rateN = Num. enrolled subjects
R = Num. candidates examined

T = Threshold

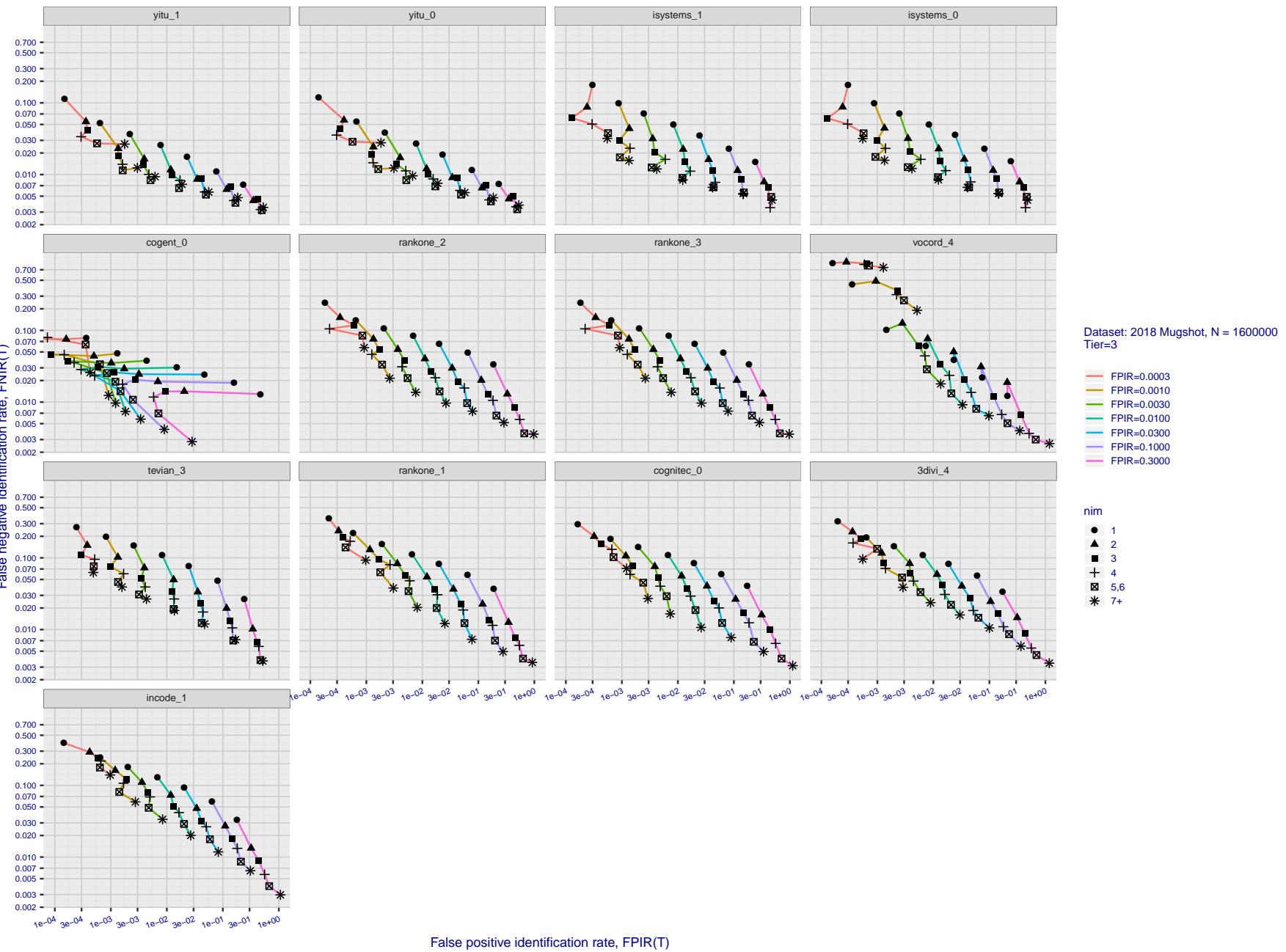
T = 0 → Investigation
T > 0 → Identification

Figure 137: [FRVT-2018 Mugshot Dataset] Effect of enrolling multiple images for each identity. The plot shows an identification miss rates vs. false positive rates, at seven operating thresholds. The enrolled population size is fixed. The images are enrolled with lifetime-consolidation - see section 2.3.

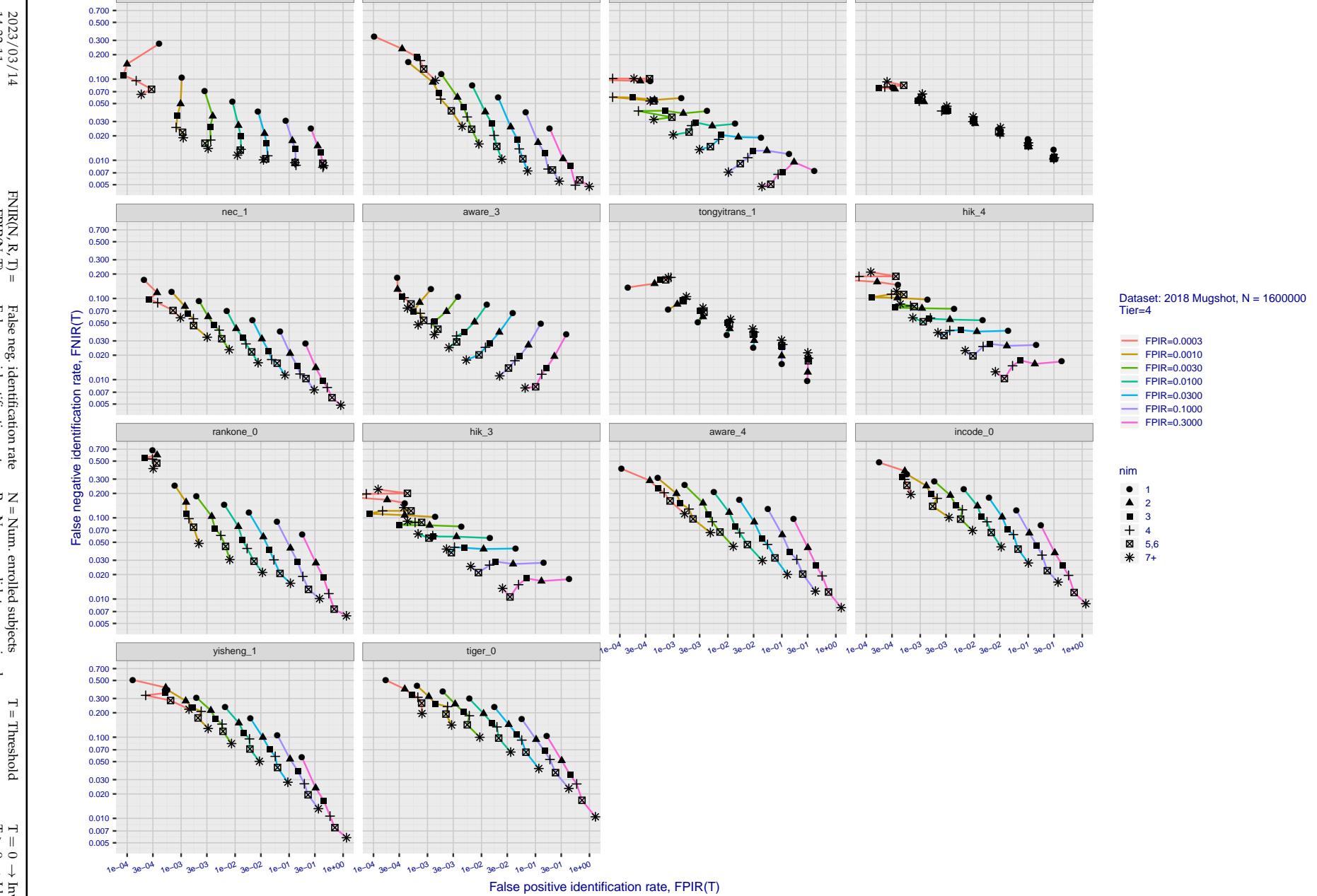


Figure 138: [FRVT-2018 Mugshot Dataset] Effect of enrolling multiple images for each identity. The plot shows an identification miss rates vs. false positive rates, at seven operating thresholds. The enrolled population size is fixed. The images are enrolled with lifetime-consolidation - see section 2.3.

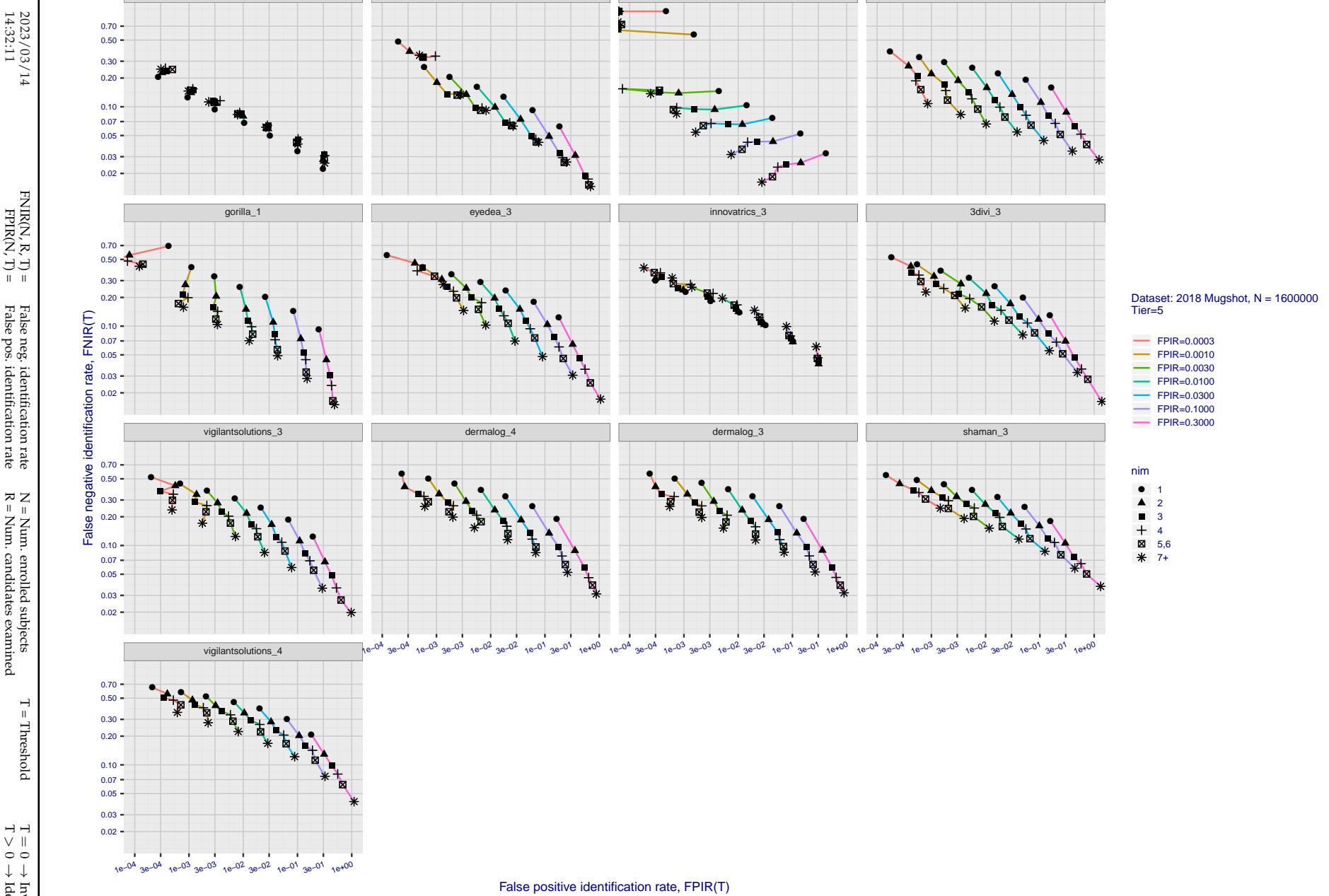


Figure 139: [FRVT-2018 Mugshot Dataset] Effect of enrolling multiple images for each identity. The plot shows an identification miss rates vs. false positive rates, at seven operating thresholds. The enrolled population size is fixed. The images are enrolled with lifetime-consolidation - see section 2.3.

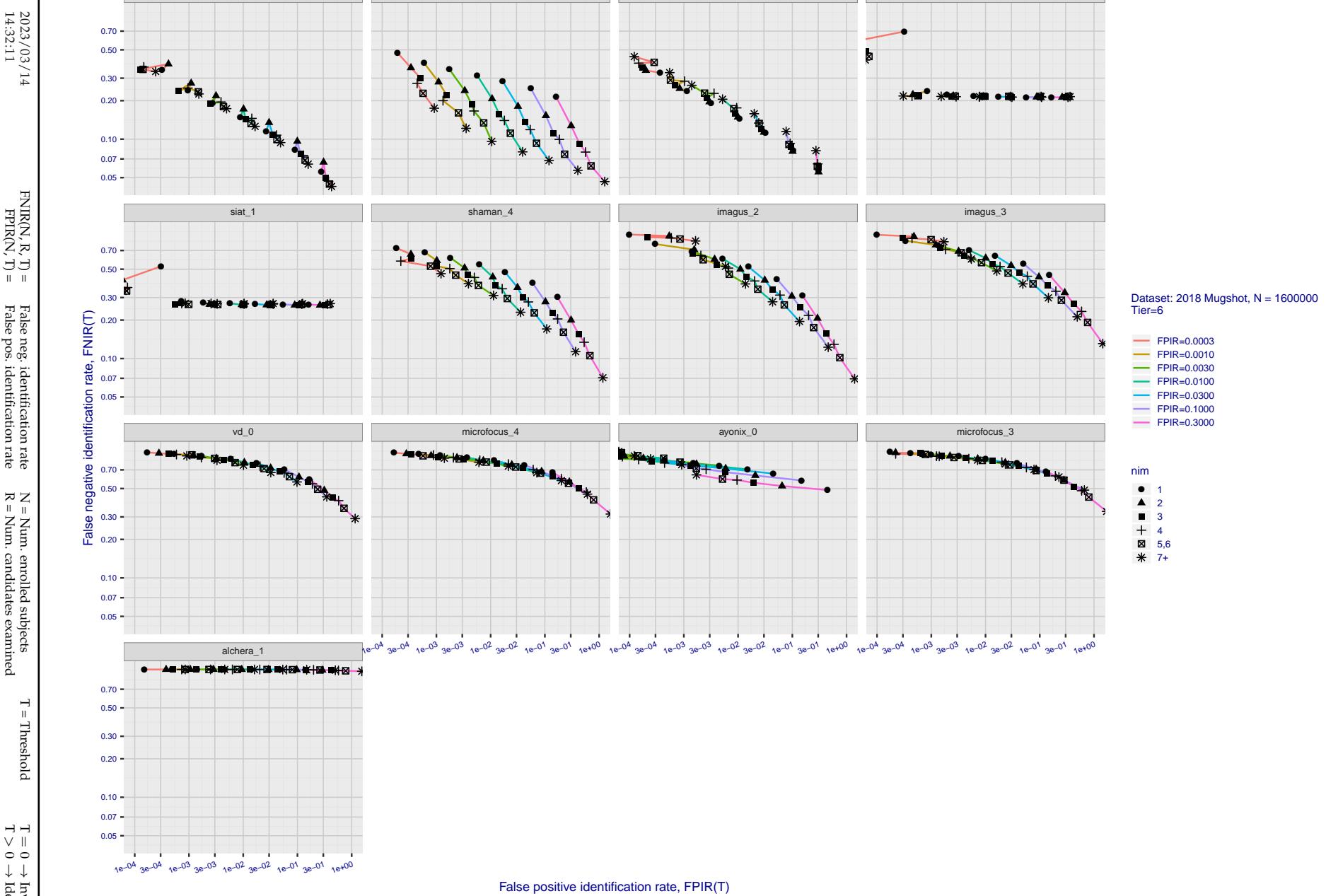


Figure 140: [FRVT-2018 Mugshot Dataset] Effect of enrolling multiple images for each identity. The plot shows an identification miss rates vs. false positive rates, at seven operating thresholds. The enrolled population size is fixed. The images are enrolled with lifetime-consolidation - see section 2.3.

Appendix D Accuracy with poor quality webcam images

2023/03/14 14:32:11	$\text{FNIR}(N, R, T) =$ $\text{FPTR}(N, T) =$	False neg. identification rate False pos. identification rate	$N =$ Num. enrolled subjects $R =$ Num. candidates examined	$T =$ Threshold $T > 0 \rightarrow$ Identification	$T = 0 \rightarrow$ Investigation
------------------------	---	--	--	---	-----------------------------------

2023/03/14
14:32:11
 $\text{FNIR}(N, R, T) =$ False neg. identification rate
 $\text{FPFR}(N, T) =$ False pos. identification rate
 $N =$ Num. enrolled subjects
 $R =$ Num. candidates examined
 $T =$ Threshold
 $T = 0 \rightarrow$ Investigation
 $T > 0 \rightarrow$ Identification

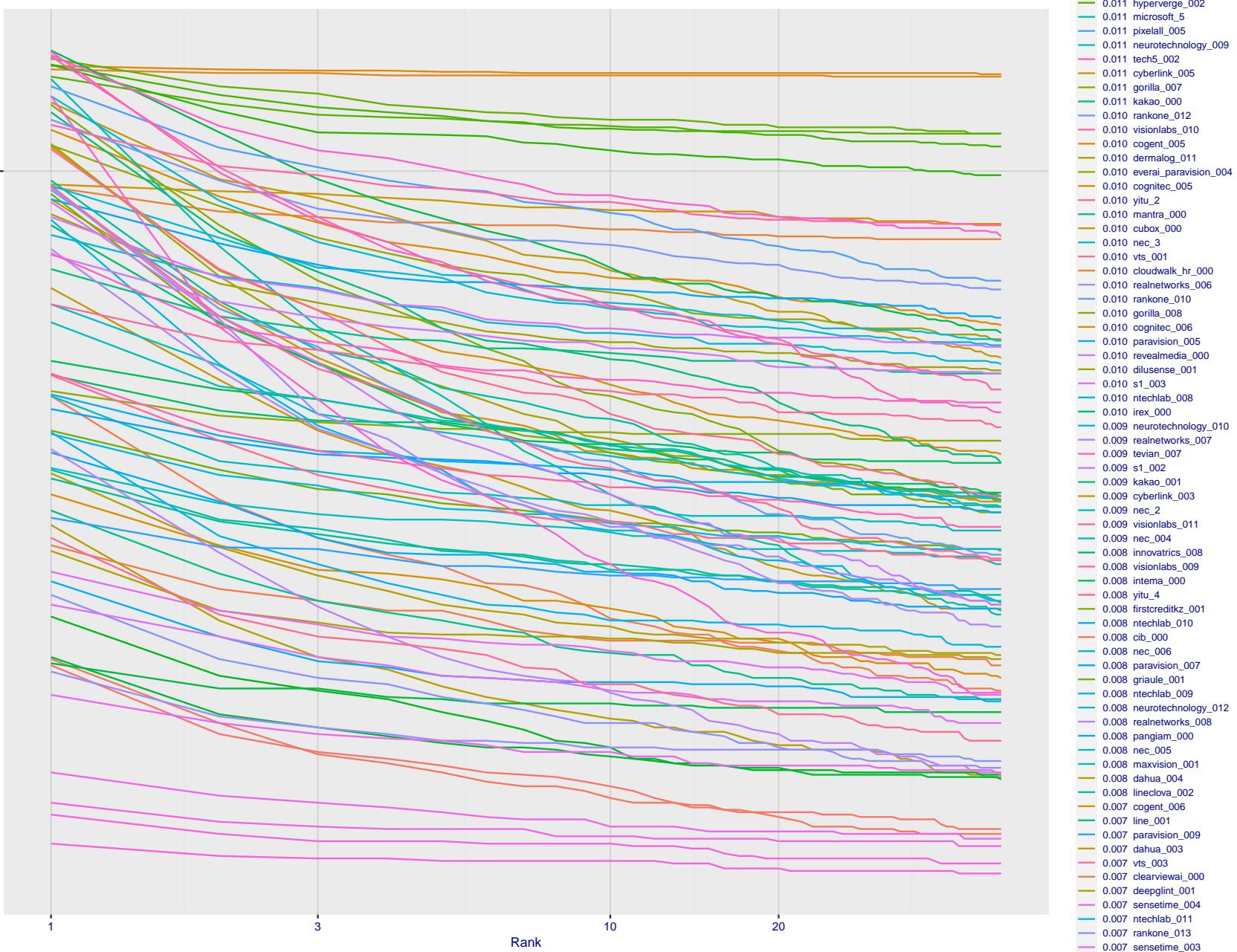


Figure 141: [Webcam Dataset] Identification miss rates vs. rank. The results apply to cross-domain recognition in which webcams are searched against enrolled mugshots. The FNIR values are higher than those for mugshot-mugshot identification due to low image resolution, lighting and less constrained subject pose in webcam images - see Figure 6.

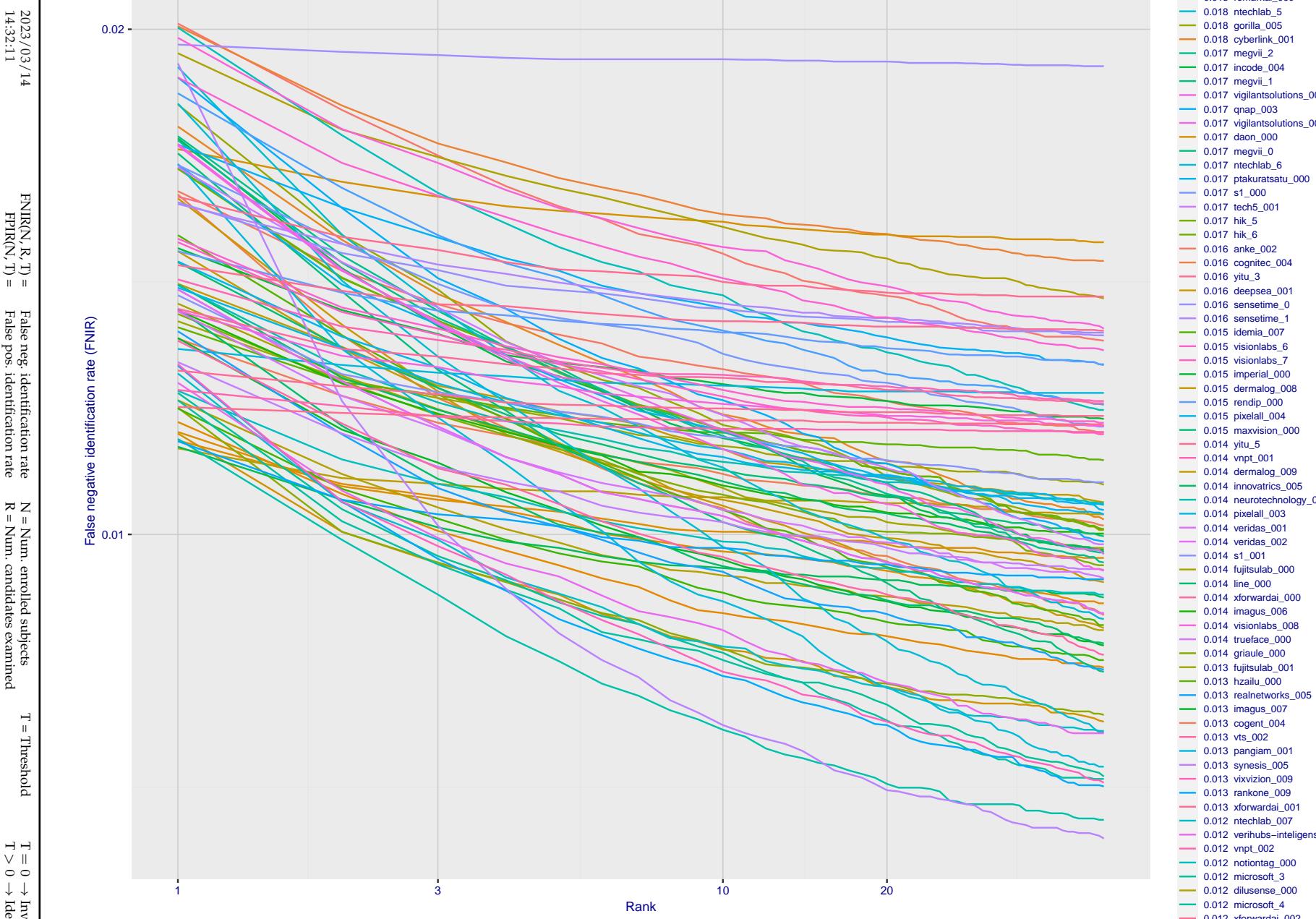


Figure 142: [Webcam Dataset] Identification miss rates vs. rank. The results apply to cross-domain recognition in which webcams are searched against enrolled mugshots. The FNIR values are higher than those for mugshot-mugshot identification due to low image resolution, lighting and less constrained subject pose in webcam images - see Figure 6.

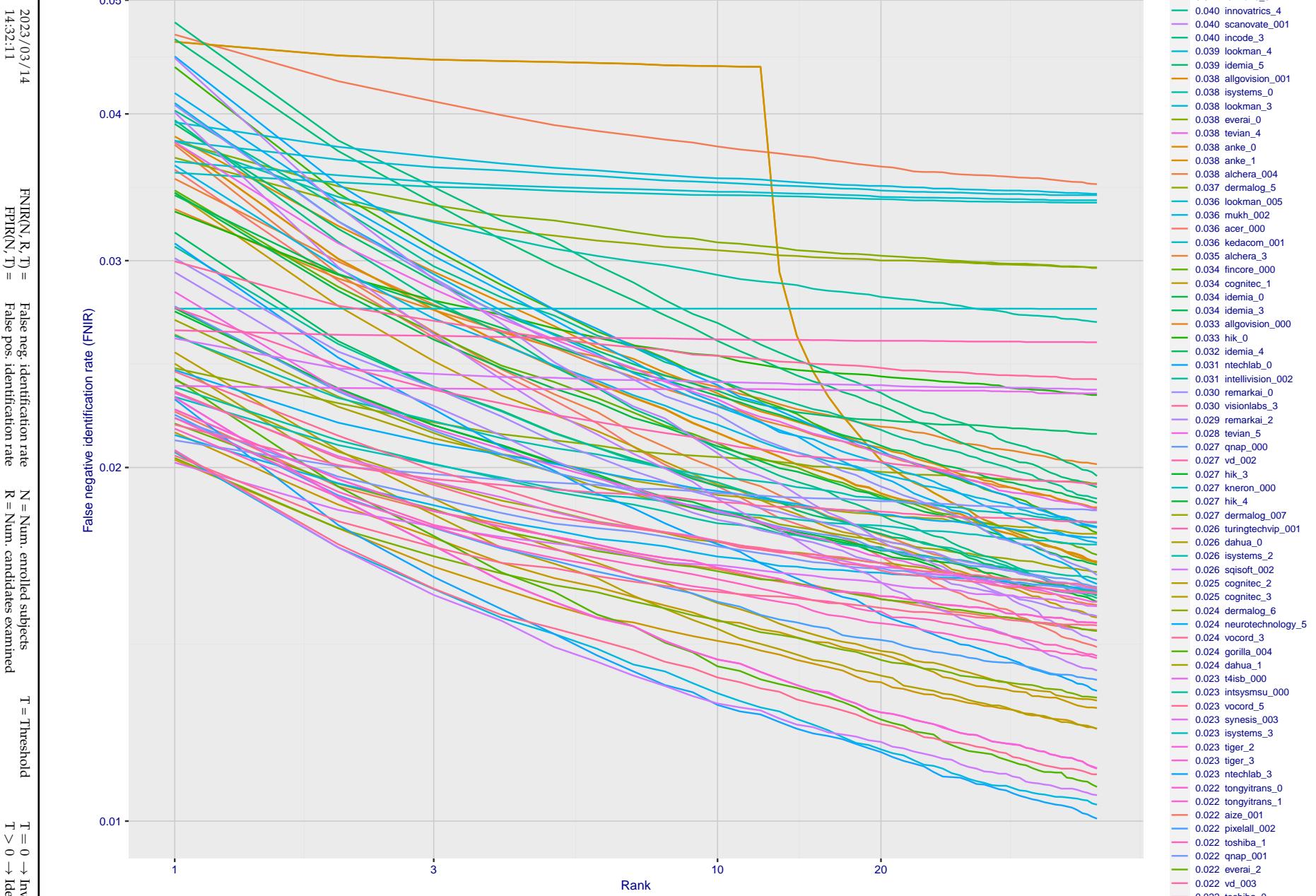


Figure 143: [Webcam Dataset] Identification miss rates vs. rank. The results apply to cross-domain recognition in which webcams are searched against enrolled mugshots. The FNIR values are higher than those for mugshot-mugshot identification due to low image resolution, lighting and less constrained subject pose in webcam images - see Figure 6.

2023/03/14
14:32:11
FNIR(N, R, T) = False neg. identification rate
FPIR(N, T) = False pos. identification rate
N = Num. enrolled subjects
R = Num. candidates examined
T = Threshold
T = 0 → Investigation
T > 0 → Identification

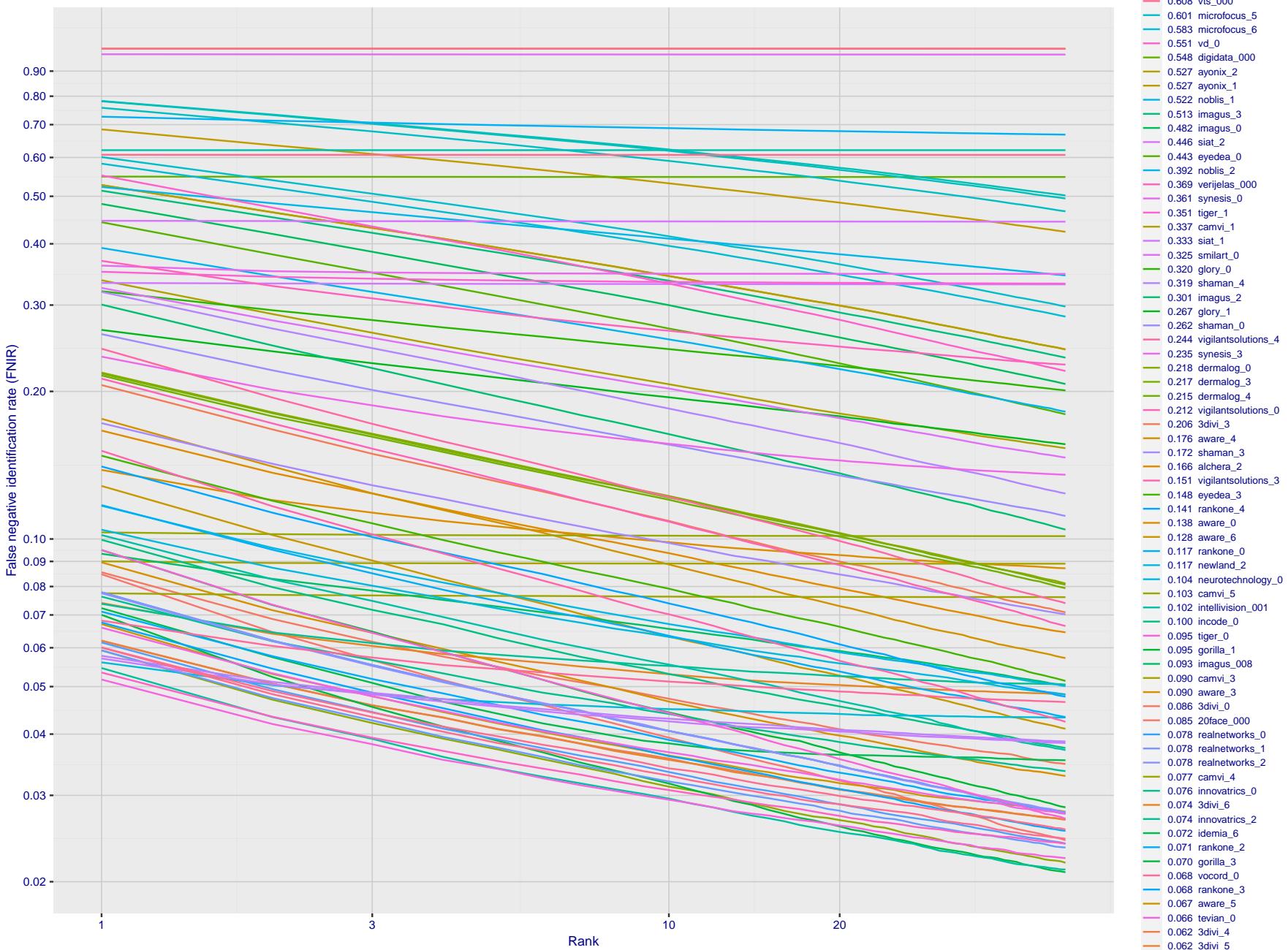


Figure 144: [Webcam Dataset] Identification miss rates vs. rank. The results apply to cross-domain recognition in which webcams are searched against enrolled mugshots. The FNIR values are higher than those for mugshot-mugshot identification due to low image resolution, lighting and less constrained subject pose in webcam images - see Figure 6.

2023/03/14 14:32:11	$\text{FNIR}(N, R, T) =$ $\text{FPTR}(N, T) =$	False neg. identification rate False pos. identification rate	$N =$ Num. enrolled subjects $R =$ Num. candidates examined	$T =$ Threshold $T > 0 \rightarrow$ Identification	$T = 0 \rightarrow$ Investigation
------------------------	---	--	--	---	-----------------------------------

2023/03/14

14:32:11

FNIR(N, R, T) = False neg. identification rate
FPIR(N, T) = False pos. identification rateN = Num. enrolled subjects
R = Num. candidates examined

T = Threshold

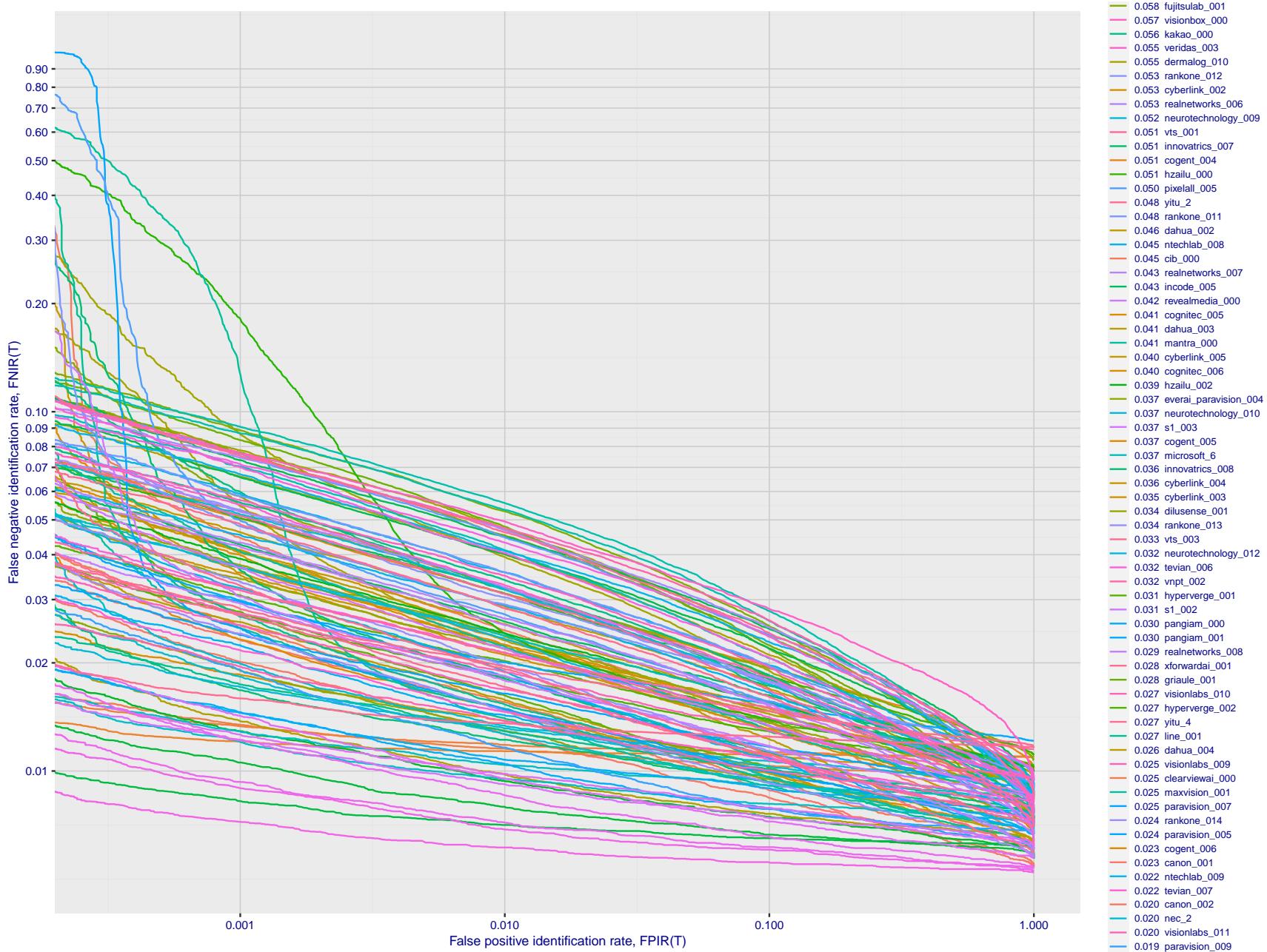
T = 0 → Investigation
T > 0 → Identification

Figure 145: [Webcam Dataset] Identification miss rates vs. false positive rates. The results apply to cross-domain recognition in which webcams are searched against enrolled mugshots. The FNIR values are higher than those for mugshot-mugshot identification due to low image resolution, lighting and less constrained subject pose in webcam images - see Figure 6.

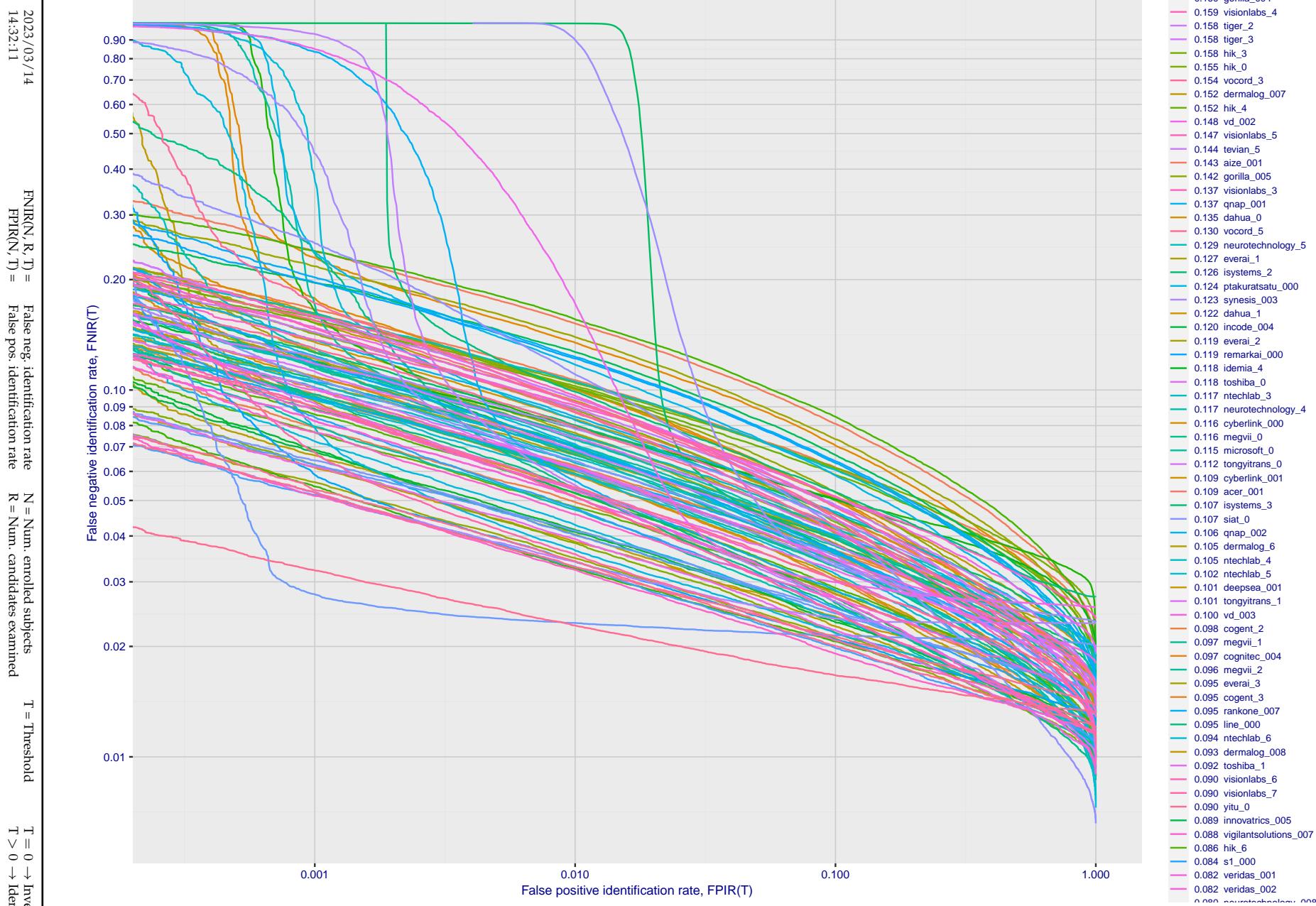


Figure 146: [Webcam Dataset] Identification miss rates vs. false positive rates. The results apply to cross-domain recognition in which webcams are searched against enrolled mugshots. The FNIR values are higher than those for mugshot-mugshot identification due to low image resolution, lighting and less constrained subject pose in webcam images - see Figure 6.

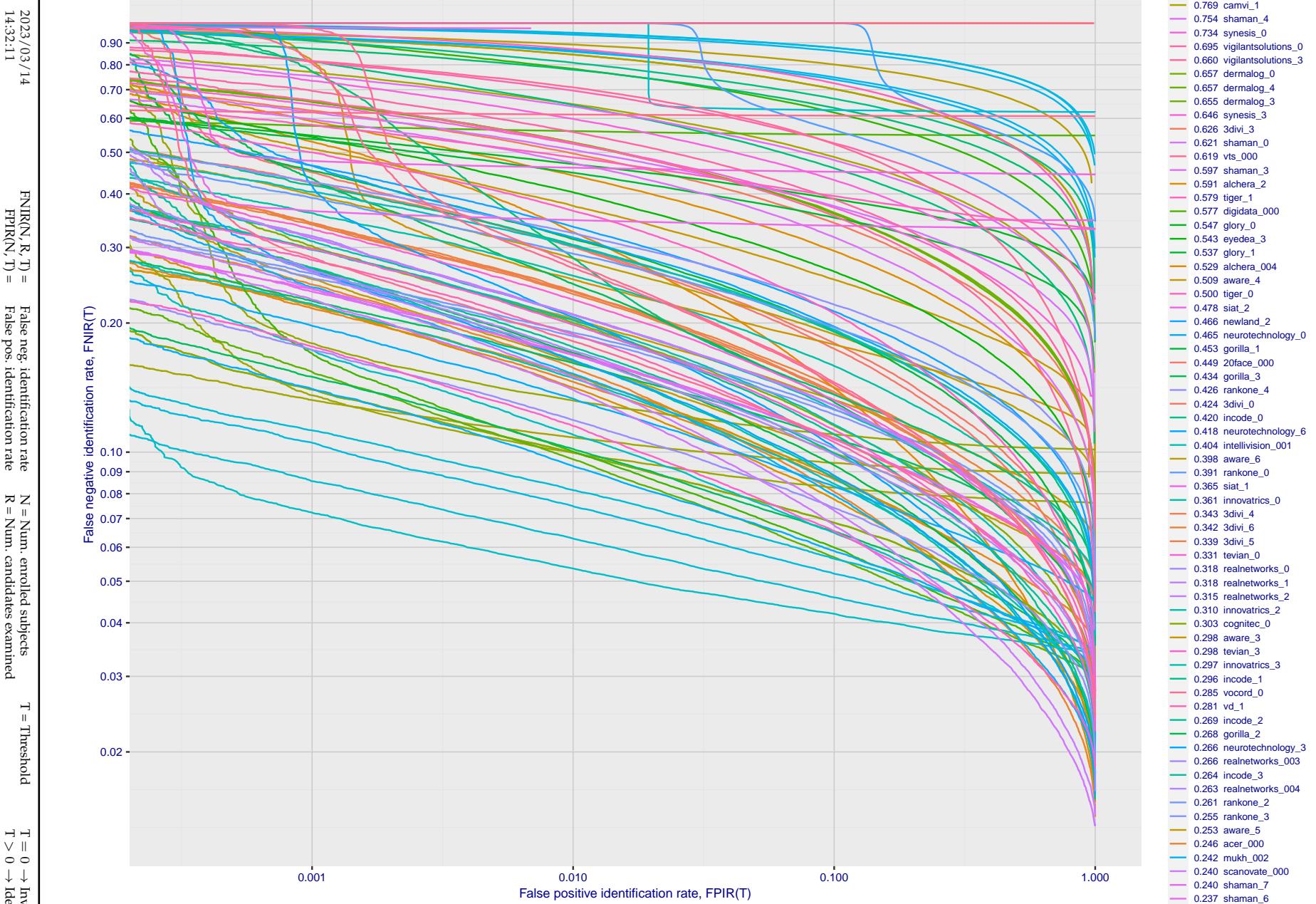


Figure 147: [Webcam Dataset] Identification miss rates vs. false positive rates. The results apply to cross-domain recognition in which webcams are searched against enrolled mugshots. The FNIR values are higher than those for mugshot-mugshot identification due to low image resolution, lighting and less constrained subject pose in webcam images - see Figure 6.

Appendix E Accuracy for profile-view to frontal recognition

Figures 148 - 150 gives accuracy results for searching 100 000 mated and 100 000 non-mated profile-view images against the same FRVT 2018 frontal enrollment dataset, $N = 1\,600\,000$, used in the main mugshot trials. This experiment corresponds to row-13 of Table 1. An example of profile-view image is given in Figure 7.

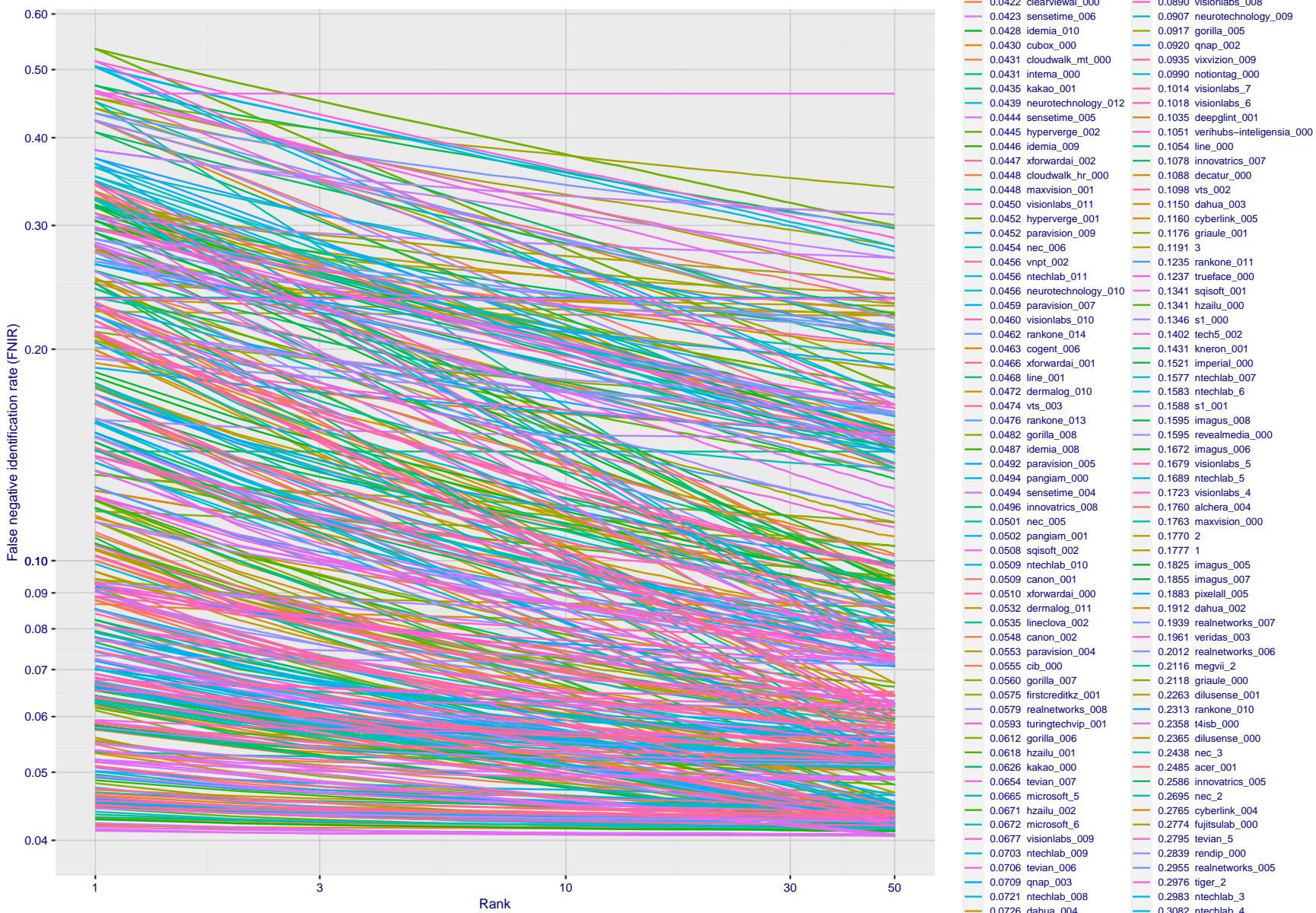


Figure 148: [Mugshot and profile-view dataset] Rank-based accuracy. For some of the more accurate Phase 3 algorithms the figure plots error tradeoff characteristics for frontal and profile-view searches into an enrolled set of $N = 1\,600\,000$ frontal images. Note that some algorithms fail on profile-view images with $\text{FNIR} \rightarrow 1$ - this evaluation did not ask developers to provide profile-view capability. Some algorithms, on the other hand, give FNIR approaching that for frontal-view searches using c. 2010 algorithms. The best result is that 91% of profile-view searches yield the correct mate at rank 1, and better than 94% in the top-50 candidates.

2023/03/14

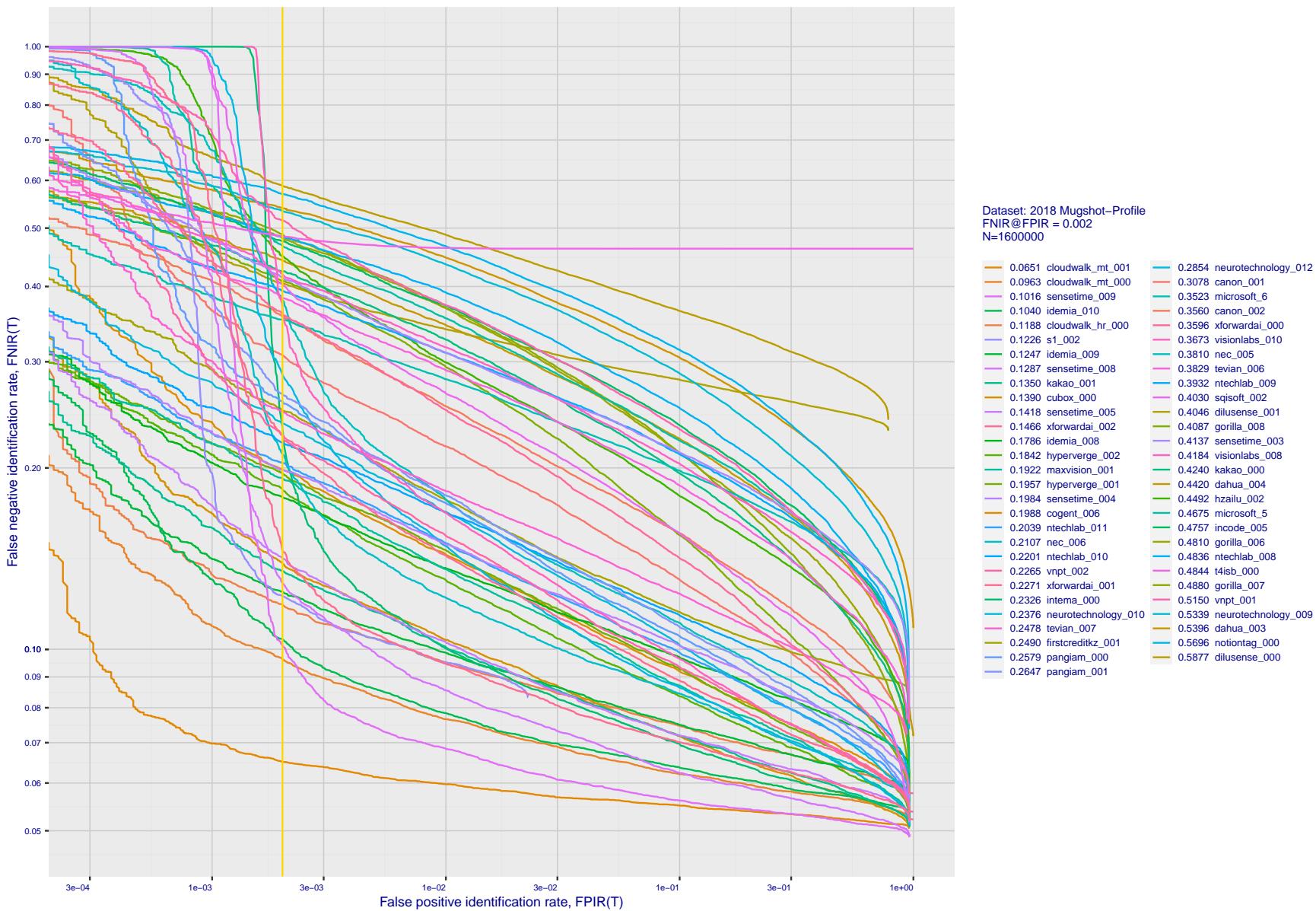
FNIR(N, R, T) = False neg. identification rate
FPIR(N, T) = False pos. identification rateN = Num. enrolled subjects
R = Num. candidates examinedT = Threshold
 $T = 0 \rightarrow$ Investigation
 $T > 0 \rightarrow$ Identification

Figure 149: [Mugshot and profile-view dataset] Threshold-based accuracy. For some of the more accurate Phase 3 algorithms the figure plots error tradeoff characteristics for frontal and profile-view searches into an enrolled set of $N = 1\,600\,000$ frontal images. Note that some algorithms fail on profile-view images with $\text{FNIR} \rightarrow 1$ - this evaluation did not ask developers to provide profile-view capability. Some algorithms, on the other hand, give FNIR approaching that for frontal-view searches using c. 2010 algorithms.

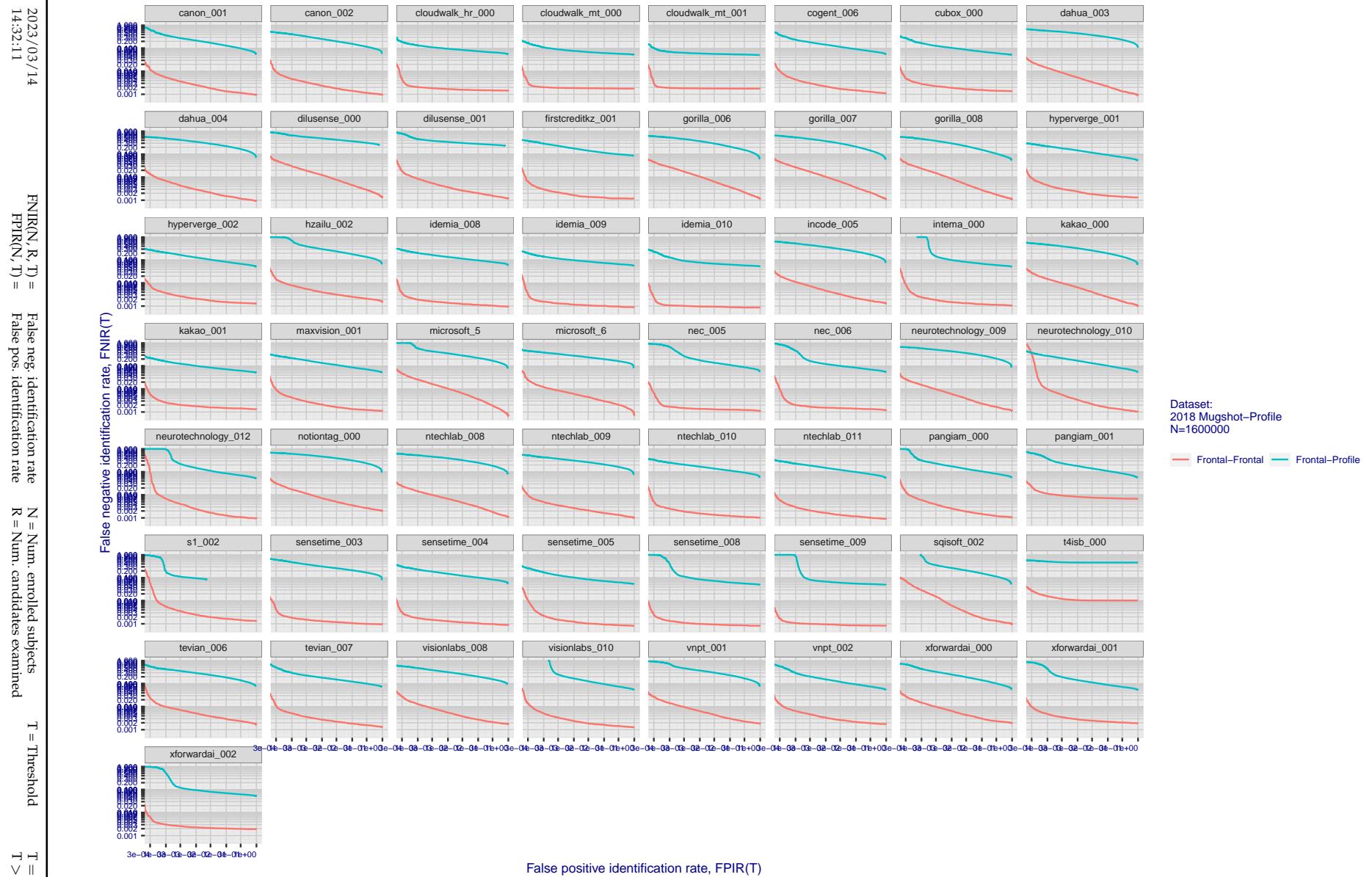


Figure 150: [Mugshot and profile-view dataset] Speed-accuracy tradeoff. For some of the more accurate Phase 3 algorithms the figure plots error tradeoff characteristics for frontal and profile-view searches into an enrolled set of $N = 1\,600\,000$ frontal images. Some algorithms fail on profile-view images with $\text{FNIR} \rightarrow 1$ - this evaluation did not ask developers to provide profile-view capability. Some algorithms, on the other hand, give FNIR approaching that for frontal-view searches using c. 2010 algorithms. Blue lines connect points of equal threshold from which it is evident that some algorithms would give markedly higher false positive outcomes if profile-view images were searched in a system configured for frontal searches. This would be a vulnerability in an access control system.

Appendix F Search duration

As in and prior tests, this section documents search speeds spanning three orders of magnitude. In applications where search volumes are high enough, this will have implications for hardware requirements especially for large N or when search duration is appreciably larger than the time it takes to prepare a template from the search image(s). Further, given very large (and growing) operational databases, the scalability of algorithms is important. It has been reported previously [8] that search duration can scale sublinearly with enrolled population size N. Further there has been considerable recent research on indexing, exact [13] and approximate nearest neighbor search [1,13] and fast-search [14,16].

Figure 151 charts the search duration measurements presented earlier in Tables 2 - 4.

- ▷ Most algorithms scale linearly. For those in that category, there is a wide range in speed with search durations ranging from 82 milliseconds for a 12 million gallery (for NEC-3) to more than 40 seconds (for Yitu-3, Toshiba-2) and even higher for less accurate algorithms.
- ▷ Some developers (Camvi, Dermalog, EverAI, Innovatrics, and Visionlabs) provide algorithms whose template search durations grow approximately logarithmically i.e. $T(N) \sim \log N$ with the constant a varying between implementations. In the figure this model is fit using the point $T(1) = 0$, and $T(640\,000)$. This very sublinear behaviour affords extremely fast search times in very large galleries. One caveat for the sublinear algorithms is that their fast-search data structures can require considerable computation time - on the order of hours - for N in the millions, and this scales mildly super-linearly, i.e. $O(N^b), b > 1$. There are exceptions: the Camvi algorithms take minutes; and Innovatrics' scale sublinearly.

2023/03/14 14:32:11	$\text{FNIR}(N, R, T) =$ $\text{FPTR}(N, T) =$	False neg. identification rate False pos. identification rate	$N =$ Num. enrolled subjects $R =$ Num. candidates examined	$T =$ Threshold $T > 0 \rightarrow$ Identification	$T = 0 \rightarrow$ Investigation
------------------------	---	--	--	---	-----------------------------------

2023/03/14
14:32:11FNIR(N, R, T) = False neg. identification rate
FPFR(N, T) = False pos. identification rateN = Num. enrolled subjects
R = Num. candidates examined

T = Threshold

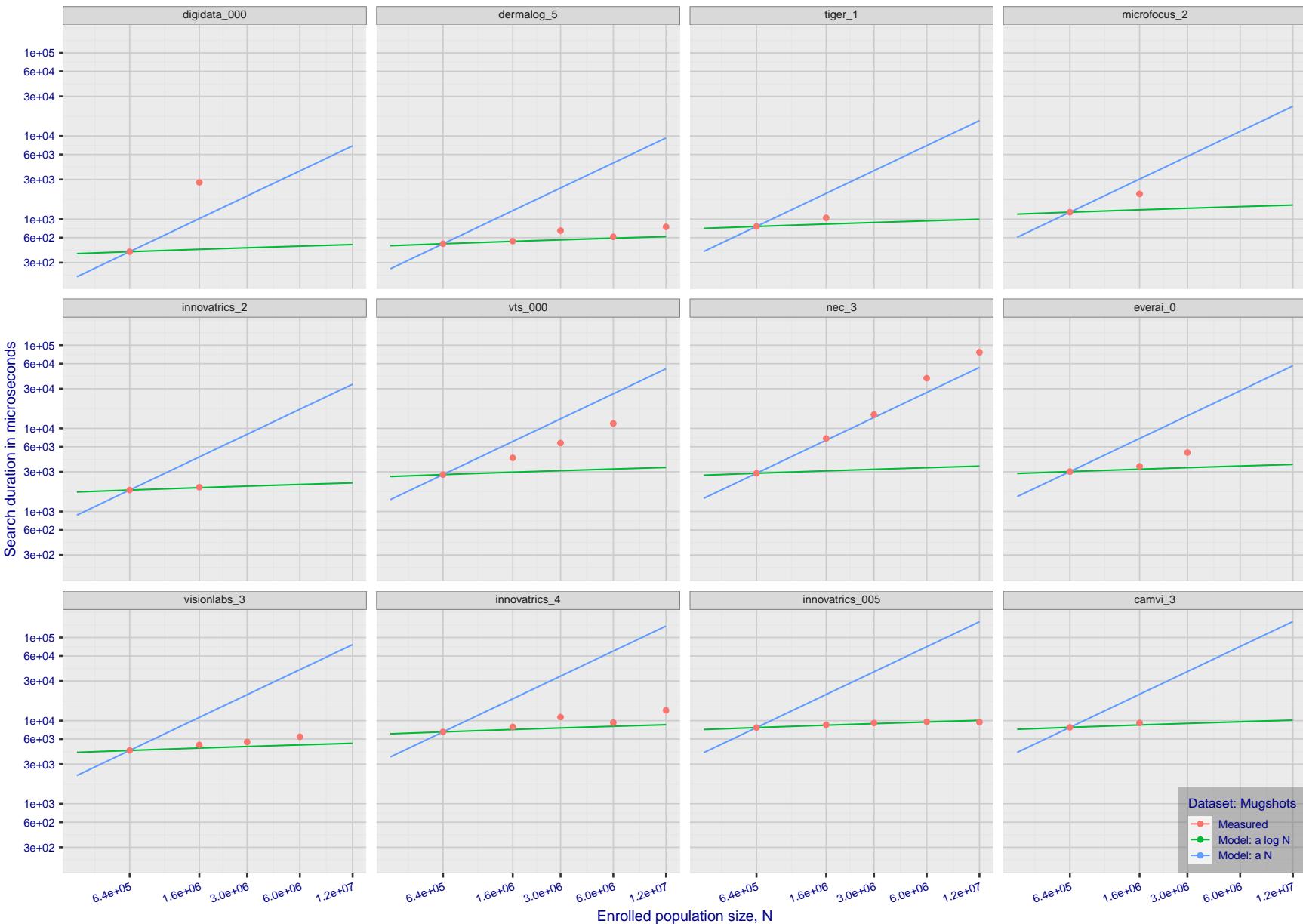
T = 0 → Investigation
 $T > 0 \rightarrow$ Identification

Figure 151: [Mugshot Dataset] Search duration vs. enrolled population size. In red are the actual point durations measured on a single c. 2016 core. The blue shows linear growth from $N = 640\,000$. The green line shows logarithmic growth from that point to $N = 1\,600\,000$. Note the sublinear growth from algorithms from Camvi, Dermalog, EverAI, Innovatrics, and Visionlabs. The tiger_1 algorithm is also sublinear, but inaccurate and inoperable at $N \geq 3000000$. This capability sometimes comes at the additional expense of converting a linear gallery data structure into whatever fast-search data structure is used. Note that search times are sometimes dominated by the template generation times shown in Table 28.

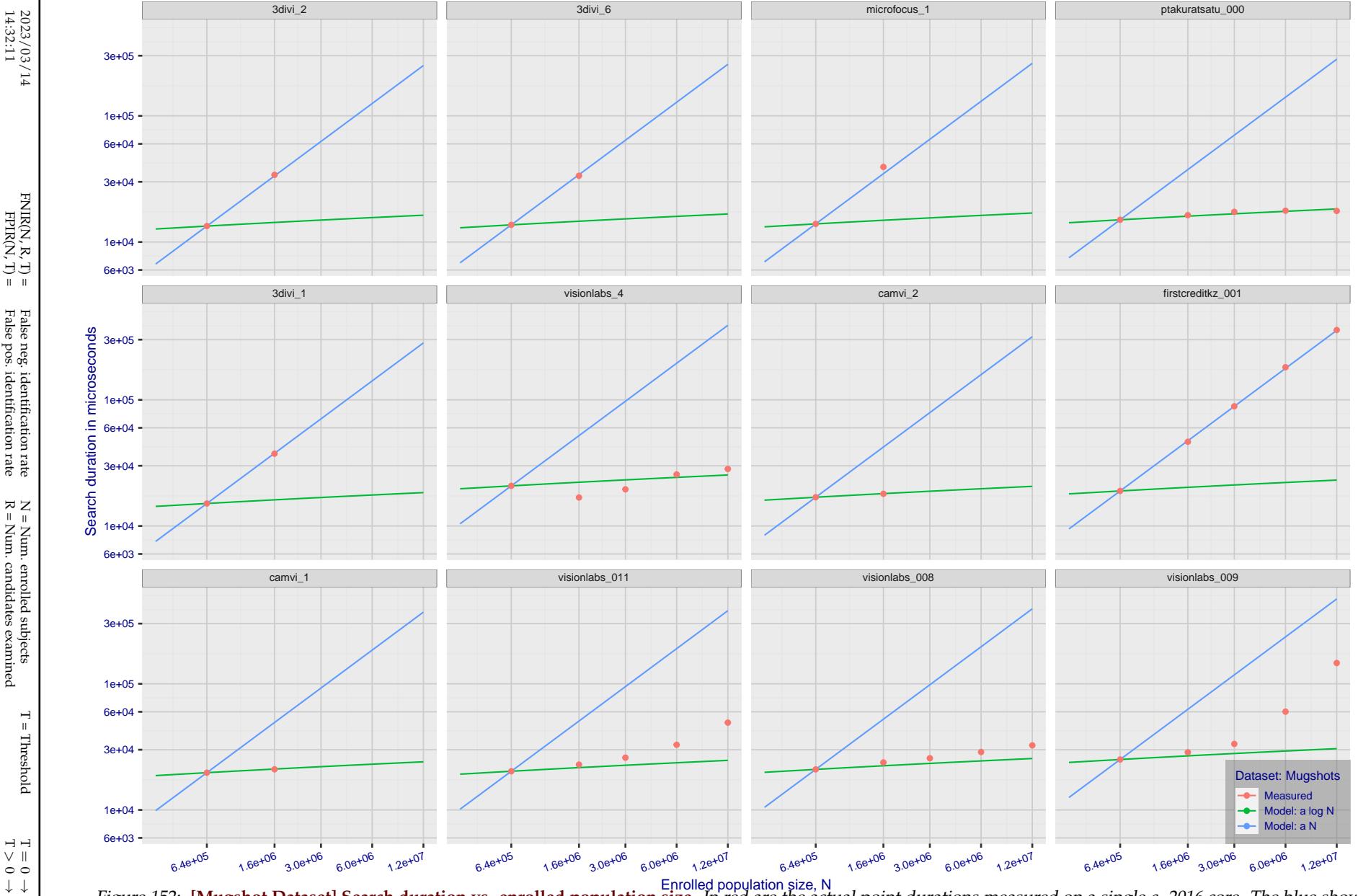


Figure 152: [Mugshot Dataset] Search duration vs. enrolled population size. In red are the actual point durations measured on a single c. 2016 core. The blue shows linear growth from $N = 640\,000$. The green line shows logarithmic growth from that point to $N = 1\,600\,000$. Note the sublinear growth from algorithms from Camvi, Dermalog, EverAI, Innovatrics, and Visionlabs. The tiger_1 algorithm is also sublinear, but inaccurate and inoperable at $N \geq 3000000$. This capability sometimes comes at the additional expense of converting a linear gallery data structure into whatever fast-search data structure is used. Note that search times are sometimes dominated by the template generation times shown in Table 28.

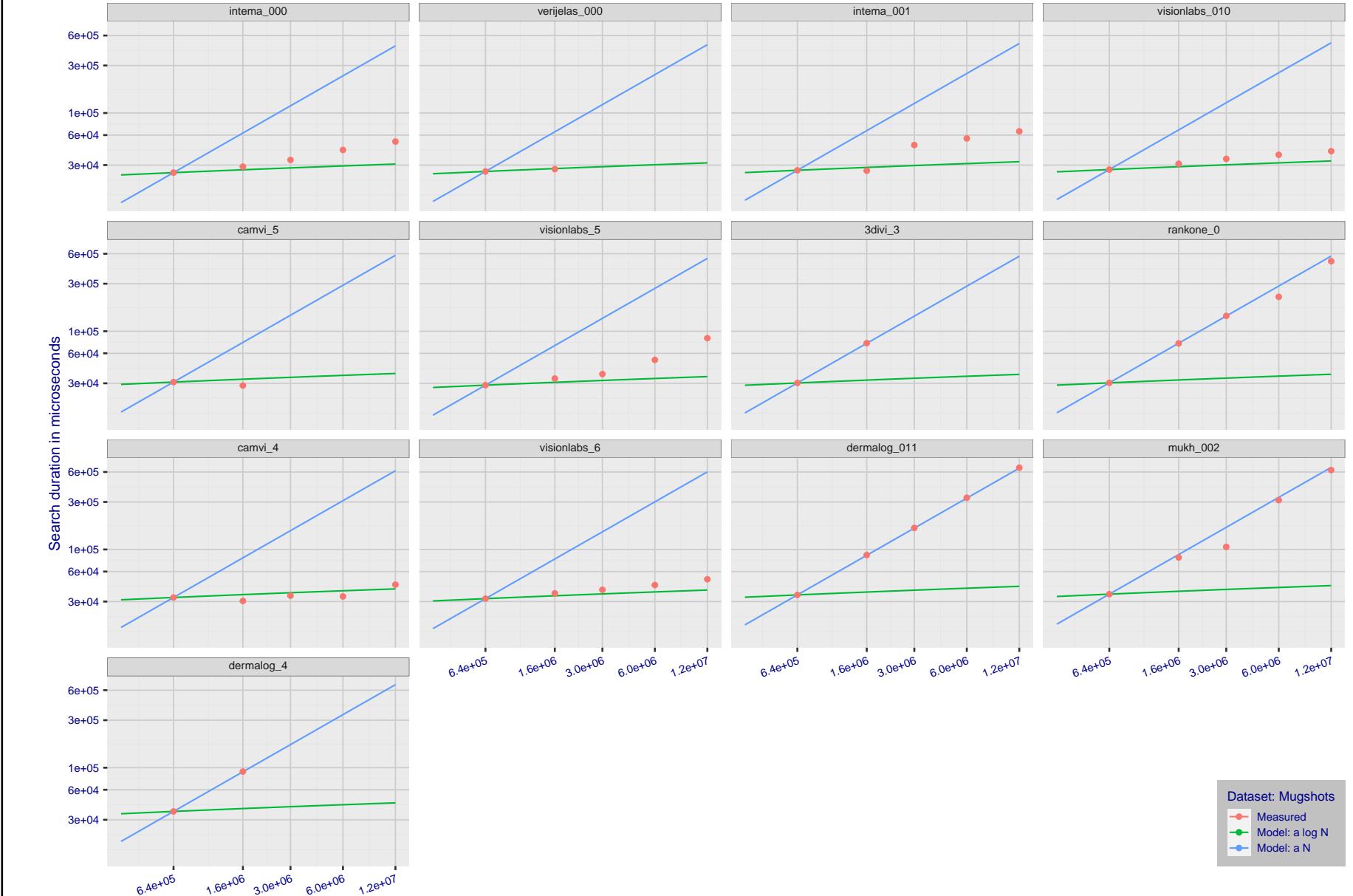


Figure 153: [Mugshot Dataset] Search duration vs. enrolled population size. In red are the actual point durations measured on a single c. 2016 core. The blue shows linear growth from $N = 640\,000$. The green line shows logarithmic growth from that point to $N = 1\,600\,000$. Note the sublinear growth from algorithms from Camvi, Dermalog, EverAI, Innovatrics, and Visionlabs. The tiger_1 algorithm is also sublinear, but inaccurate and inoperable at $N \geq 3000000$. This capability sometimes comes at the additional expense of converting a linear gallery data structure into whatever fast-search data structure is used. Note that search times are sometimes dominated by the template generation times shown in Table 28.

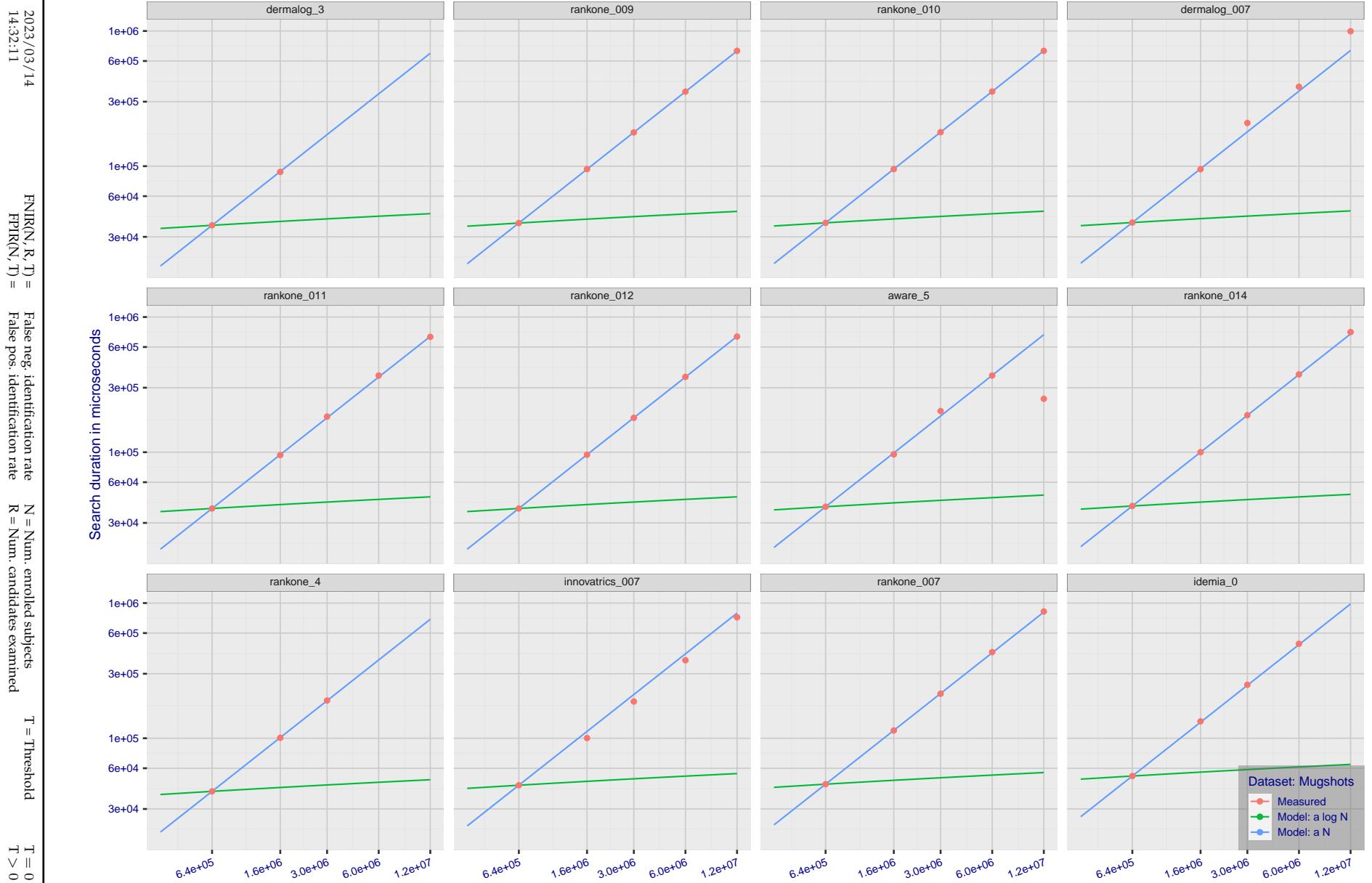
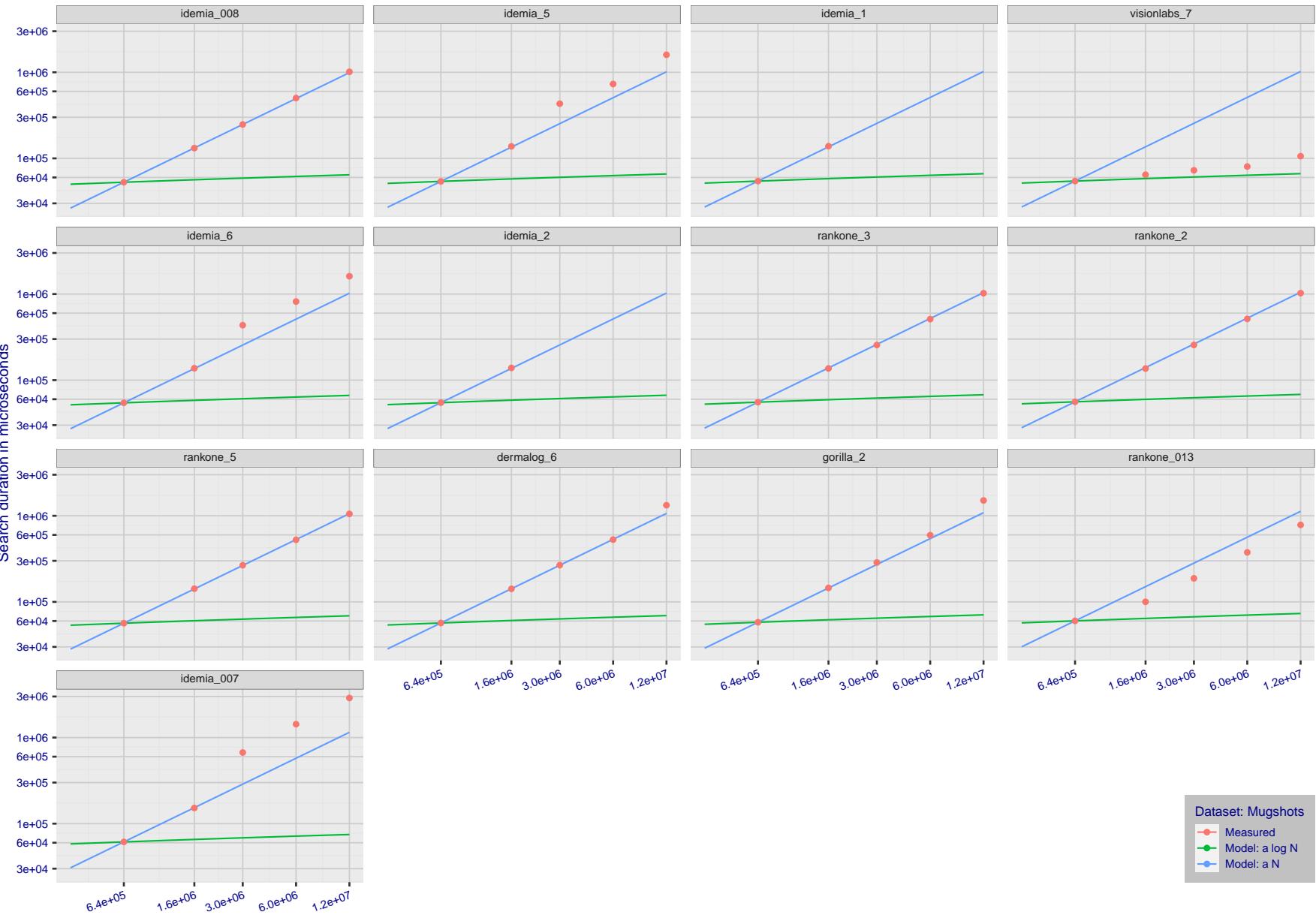


Figure 154: [Mugshot Dataset] Search duration vs. enrolled population size. In red are the actual point durations measured on a single c. 2016 core. The blue shows linear growth from $N = 640\,000$. The green line shows logarithmic growth from that point to $N = 1\,600\,000$. Note the sublinear growth from algorithms from Camvi, Dermalog, EverAI, Innovatrics, and Visionlabs. The tiger_1 algorithm is also sublinear, but inaccurate and inoperable at $N \geq 3000000$. This capability sometimes comes at the additional expense of converting a linear gallery data structure into whatever fast-search data structure is used. Note that search times are sometimes dominated by the template generation times shown in Table 28.

2023/03/14
14:32:11FNIR(N, R, T) = False neg. identification rate
FPIR(N, T) = False pos. identification rateN = Num. enrolled subjects
R = Num. candidates examined

T = Threshold

T = 0 → Investigation
 $T > 0 \rightarrow$ Identification

Enrolled population size, N

Dataset: Mugshots
● Measured
● Model: a log N
● Model: a N

Figure 155: [Mugshot Dataset] Search duration vs. enrolled population size. In red are the actual point durations measured on a single c. 2016 core. The blue shows linear growth from $N = 640\,000$. The green line shows logarithmic growth from that point to $N = 1\,600\,000$. Note the sublinear growth from algorithms from Camvi, Dermalog, EverAI, Innovatrics, and Visionlabs. The tiger_1 algorithm is also sublinear, but inaccurate and inoperable at $N \geq 3000000$. This capability sometimes comes at the additional expense of converting a linear gallery data structure into whatever fast-search data structure is used. Note that search times are sometimes dominated by the template generation times shown in Table 28.

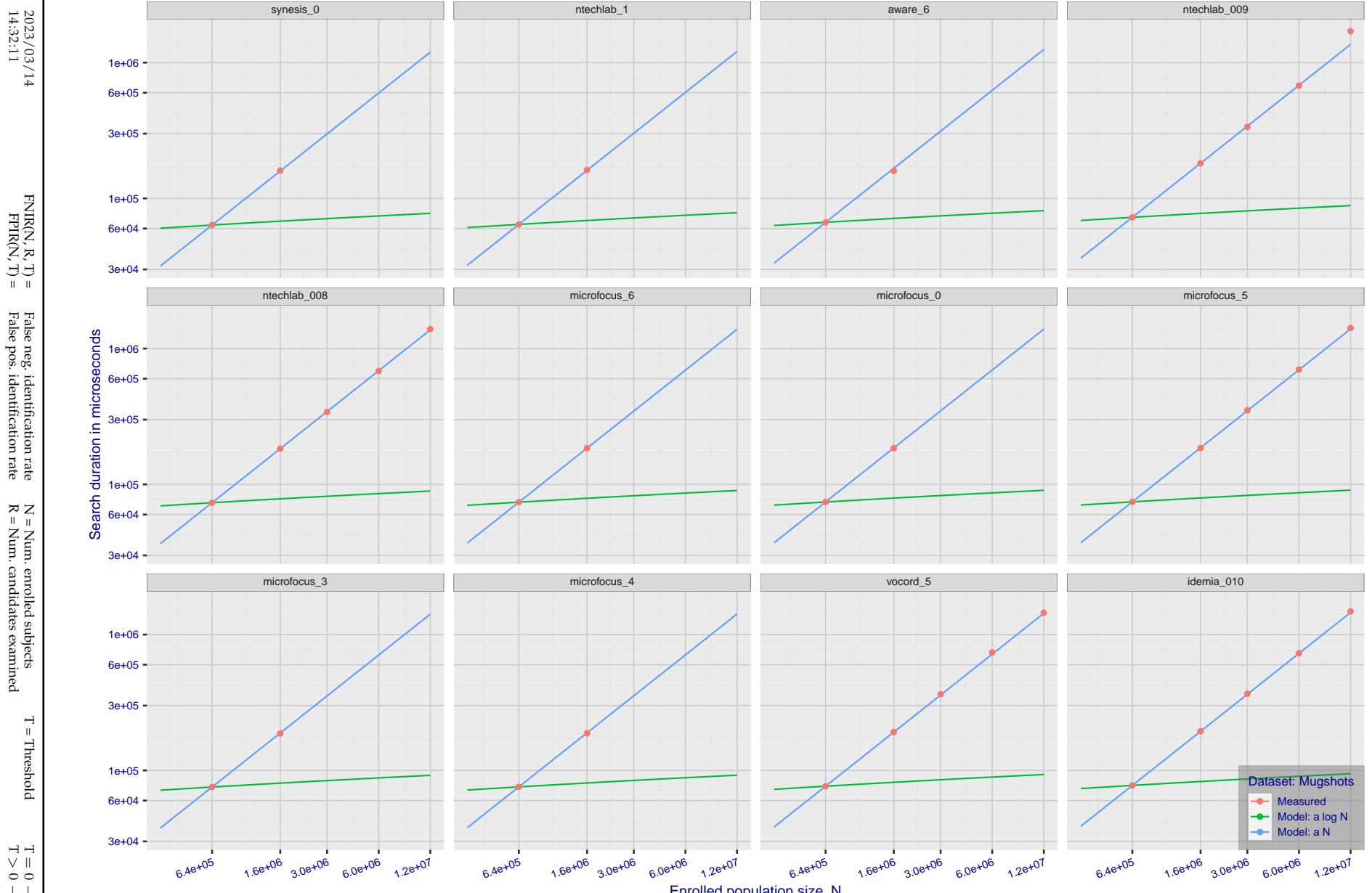


Figure 156: [Mugshot Dataset] Search duration vs. enrolled population size. In red are the actual point durations measured on a single c. 2016 core. The blue shows linear growth from $N = 640\,000$. The green line shows logarithmic growth from that point to $N = 1\,600\,000$. Note the sublinear growth from algorithms from Camvi, Dermalog, EverAI, Innovatrics, and Visionlabs. The tiger_1 algorithm is also sublinear, but inaccurate and inoperable at $N \geq 3000000$. This capability sometimes comes at the additional expense of converting a linear gallery data structure into whatever fast-search data structure is used. Note that search times are sometimes dominated by the template generation times shown in Table 28.

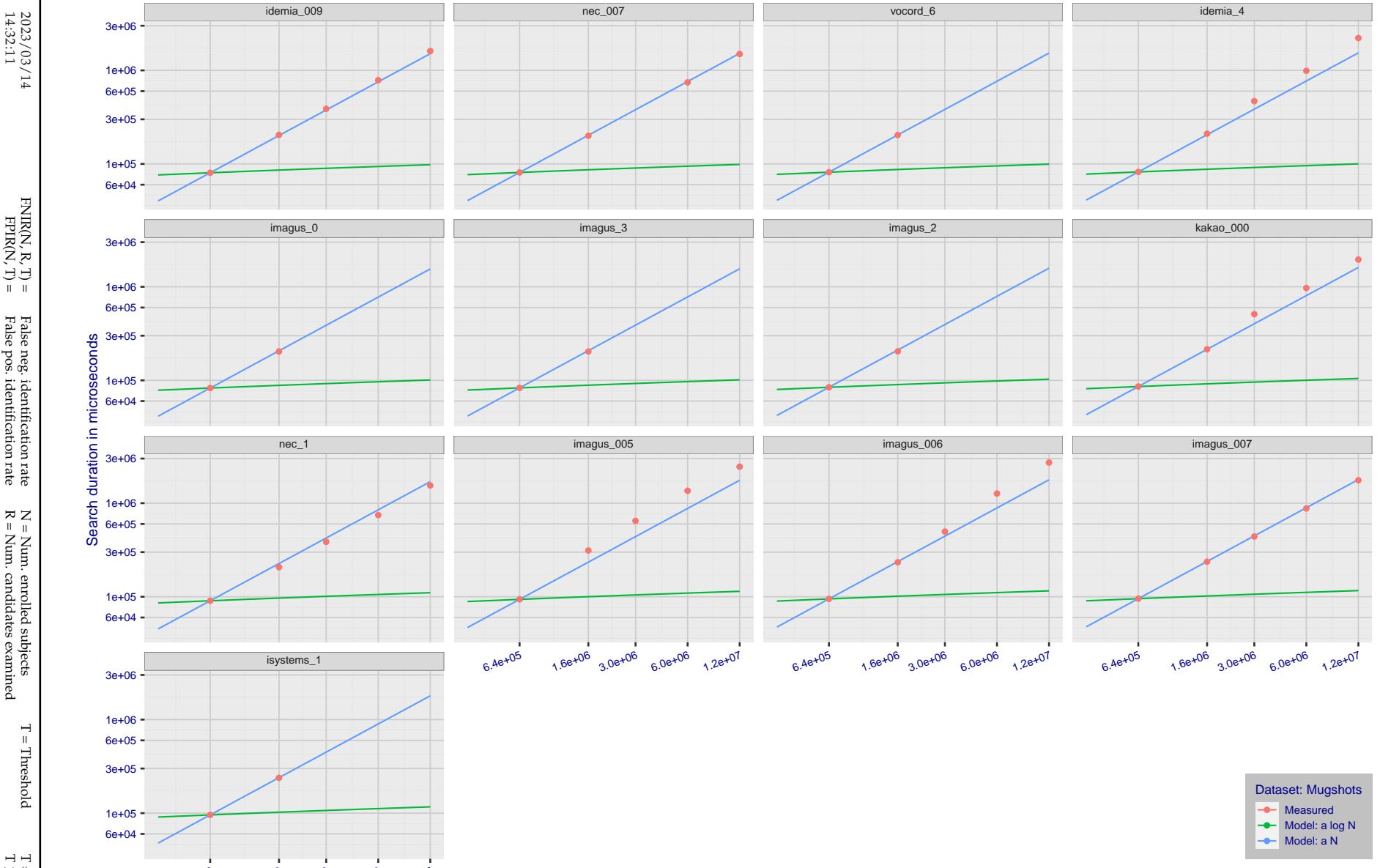


Figure 157: [Mugshot Dataset] Search duration vs. enrolled population size. In red are the actual point durations measured on a single c. 2016 core. The blue shows linear growth from $N = 640\,000$. The green line shows logarithmic growth from that point to $N = 1\,600\,000$. Note the sublinear growth from algorithms from Camvi, Dermalog, EverAI, Innovatrics, and Visionlabs. The tiger_1 algorithm is also sublinear, but inaccurate and inoperable at $N \geq 3000000$. This capability sometimes comes at the additional expense of converting a linear gallery data structure into whatever fast-search data structure is used. Note that search times are sometimes dominated by the template generation times shown in Table 28.

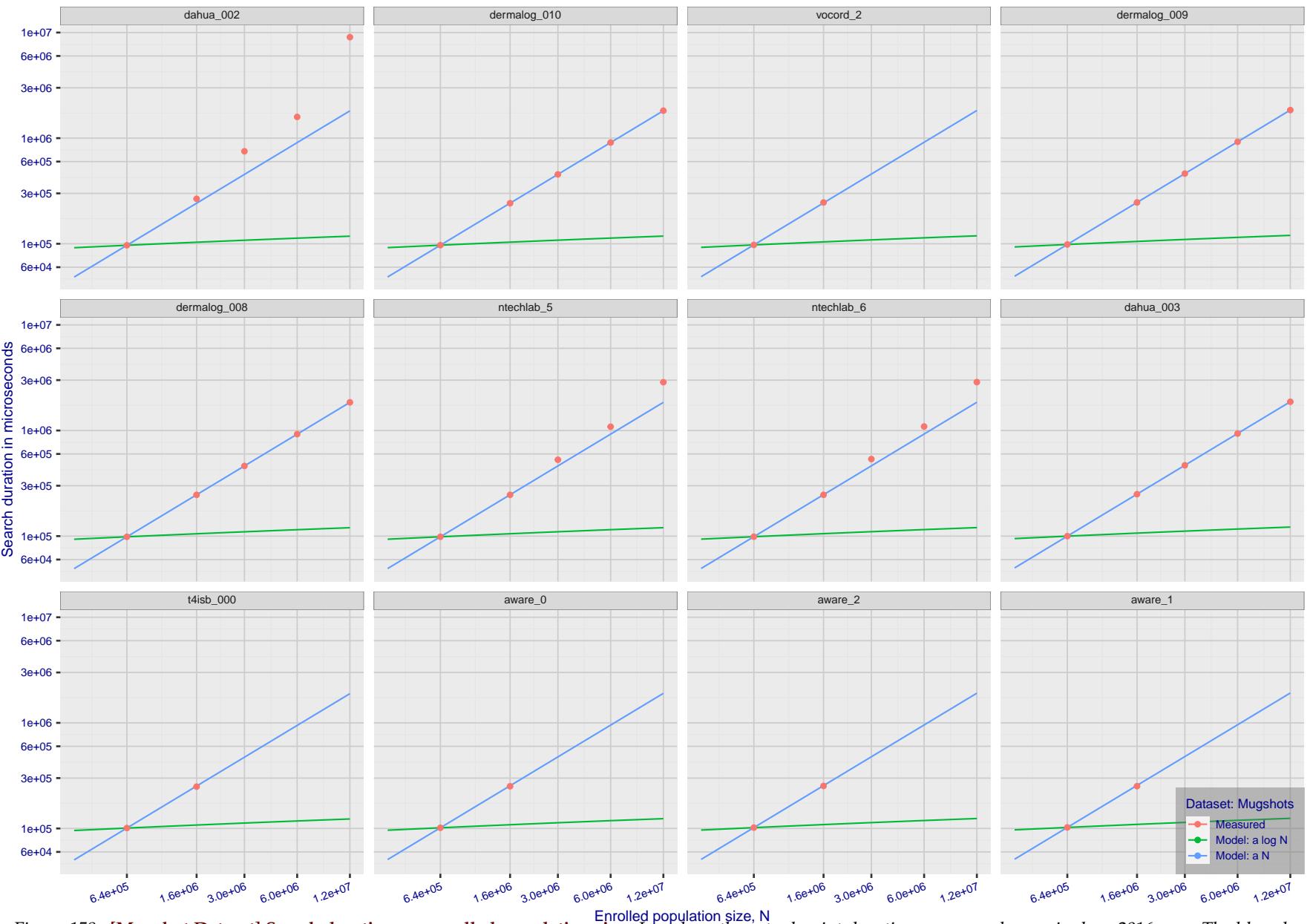


Figure 158: [Mugshot Dataset] Search duration vs. enrolled population size. In red are the actual point durations measured on a single c. 2016 core. The blue shows linear growth from $N = 640\,000$. The green line shows logarithmic growth from that point to $N = 1\,600\,000$. Note the sublinear growth from algorithms from Camvi, Dermalog, EverAI, Innovatrics, and Visionlabs. The tiger_1 algorithm is also sublinear, but inaccurate and inoperable at $N \geq 3000000$. This capability sometimes comes at the additional expense of converting a linear gallery data structure into whatever fast-search data structure is used. Note that search times are sometimes dominated by the template generation times shown in Table 28.

2023/03/14
14:32:11FNIR(N, R, T) = False neg. identification rate
FPIR(N, T) = False pos. identification rateN = Num. enrolled subjects
R = Num. candidates examined

T = Threshold

T = 0 → Investigation
 $T > 0 \rightarrow$ Identification

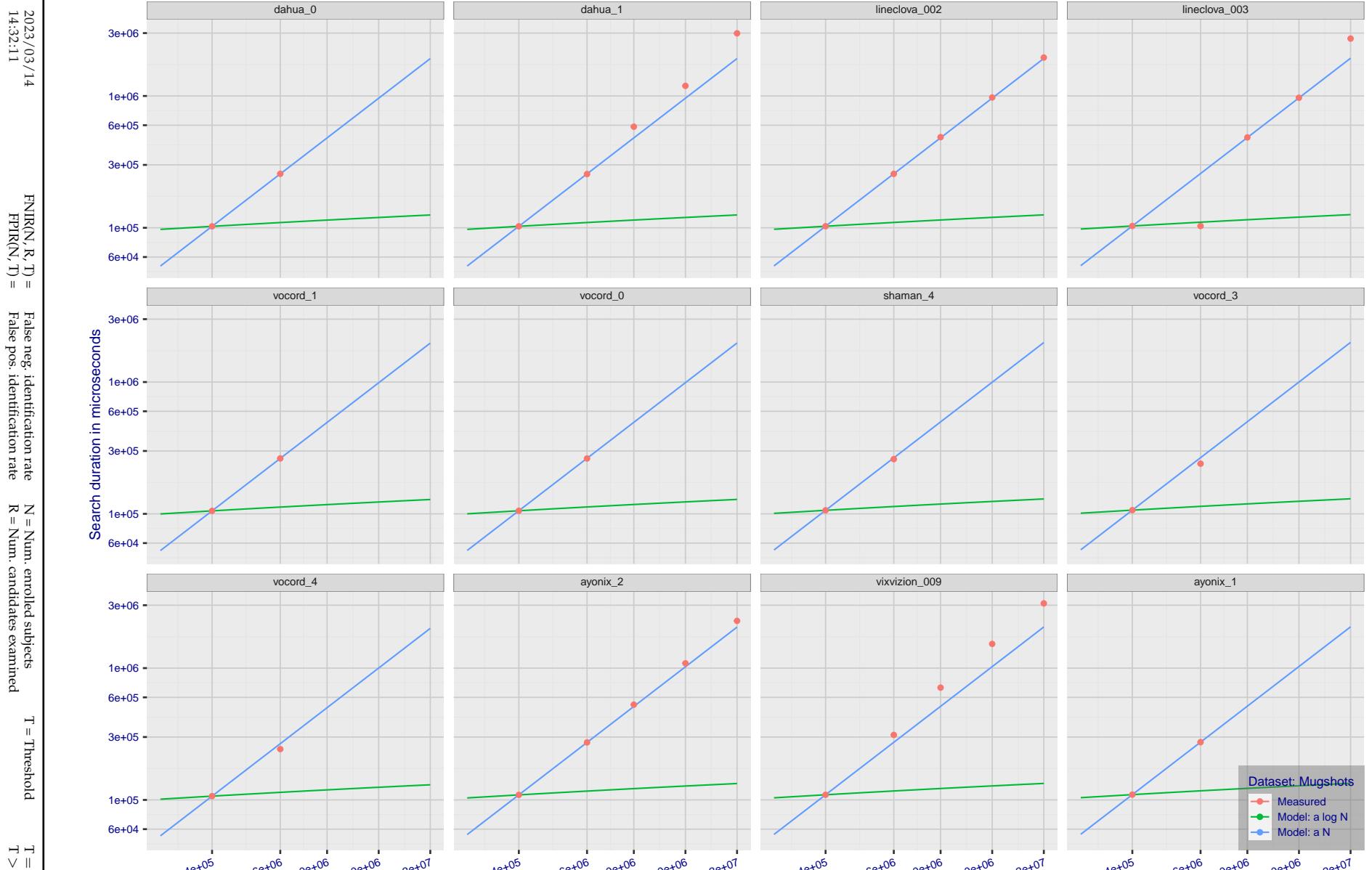


Figure 159: [Mugshot Dataset] Search duration vs. enrolled population size. In red are the actual point durations measured on a single c. 2016 core. The blue shows linear growth from $N = 640\,000$. The green line shows logarithmic growth from that point to $N = 1\,600\,000$. Note the sublinear growth from algorithms from Camvi, Dermalog, EverAI, Innovatrics, and Visionlabs. The tiger_1 algorithm is also sublinear, but inaccurate and inoperable at $N \geq 3000000$. This capability sometimes comes at the additional expense of converting a linear gallery data structure into whatever fast-search data structure is used. Note that search times are sometimes dominated by the template generation times shown in Table 28.

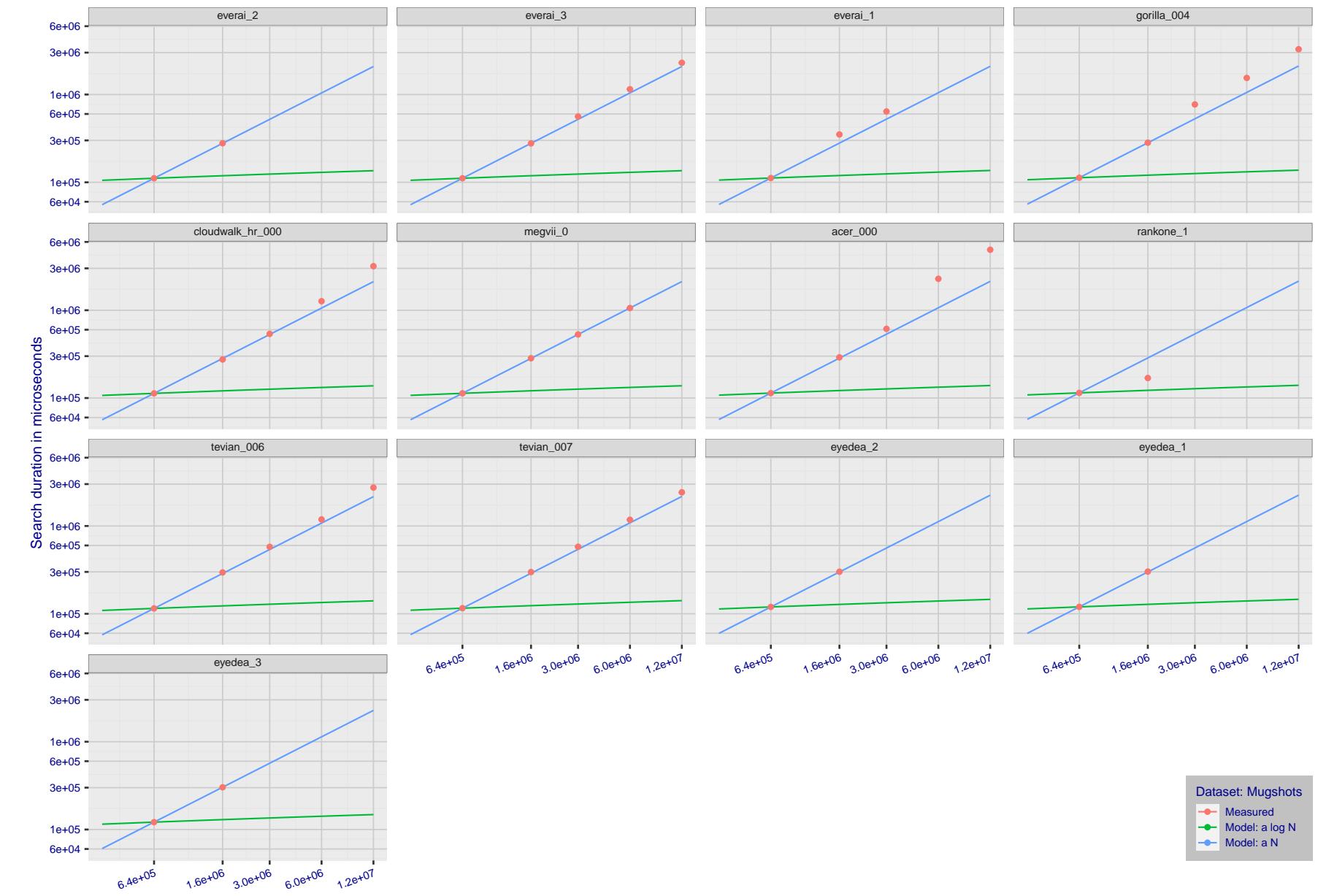


Figure 160: [Mugshot Dataset] Search duration vs. enrolled population size. In red are the actual point durations measured on a single c. 2016 core. The blue shows linear growth from $N = 640\,000$. The green line shows logarithmic growth from that point to $N = 1\,600\,000$. Note the sublinear growth from algorithms from Camvi, Dermalog, EverAI, Innovatrics, and Visionlabs. The tiger_1 algorithm is also sublinear, but inaccurate and inoperable at $N \geq 3000000$. This capability sometimes comes at the additional expense of converting a linear gallery data structure into whatever fast-search data structure is used. Note that search times are sometimes dominated by the template generation times shown in Table 28.

2023/03/14
14:32:11FNIR(N, R, T) = False neg. identification rate
FPIR(N, T) = False pos. identification rateN = Num. enrolled subjects
R = Num. candidates examined

T = Threshold

T = 0 → Investigation
 $T > 0 \rightarrow$ Identification

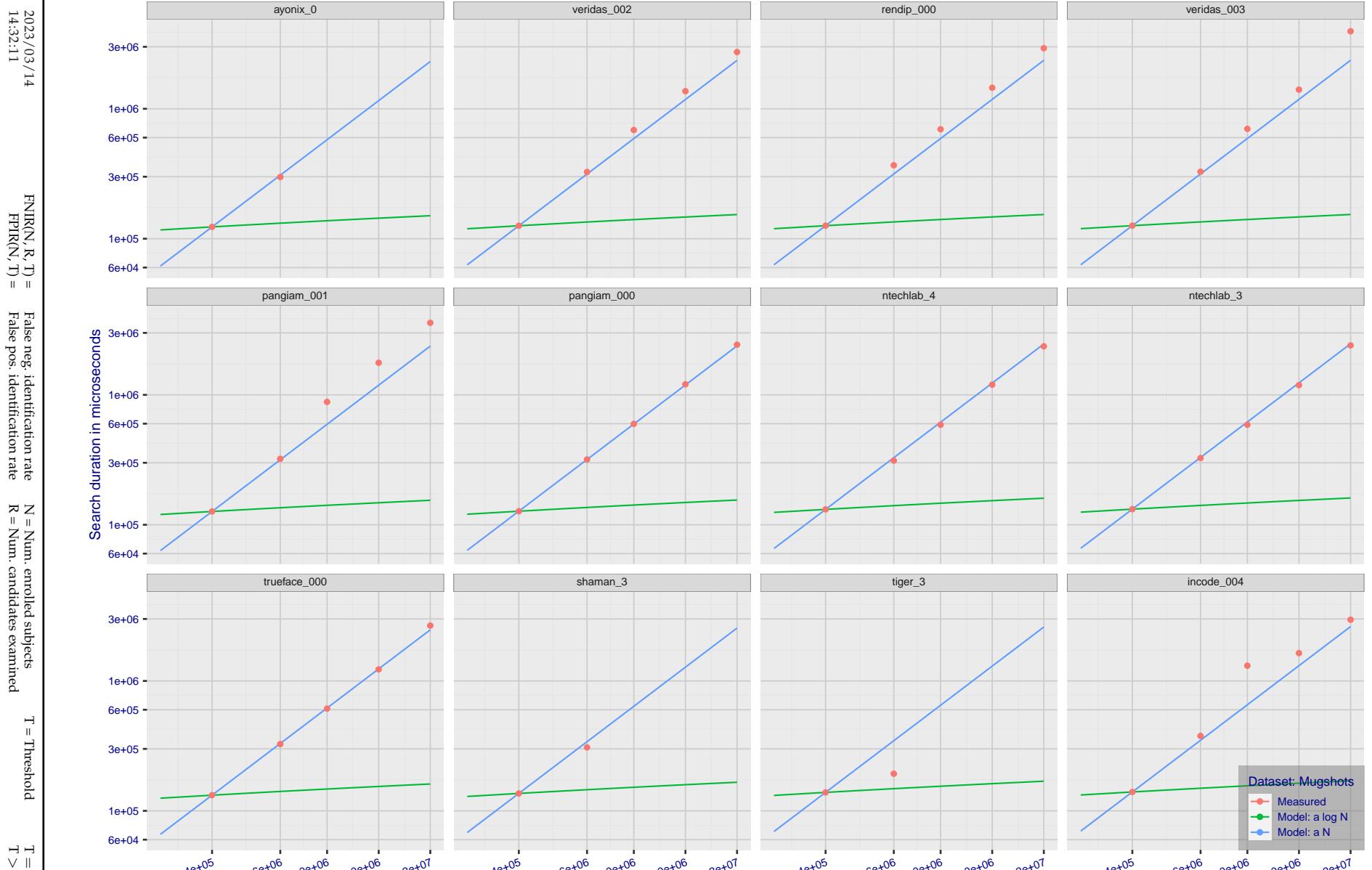


Figure 161: [Mugshot Dataset] Search duration vs. enrolled population size. In red are the actual point durations measured on a single c. 2016 core. The blue shows linear growth from $N = 640\,000$. The green line shows logarithmic growth from that point to $N = 1\,600\,000$. Note the sublinear growth from algorithms from Camvi, Dermalog, EverAI, Innovatrics, and Visionlabs. The tiger_1 algorithm is also sublinear, but inaccurate and inoperable at $N \geq 3000000$. This capability sometimes comes at the additional expense of converting a linear gallery data structure into whatever fast-search data structure is used. Note that search times are sometimes dominated by the template generation times shown in Table 28.

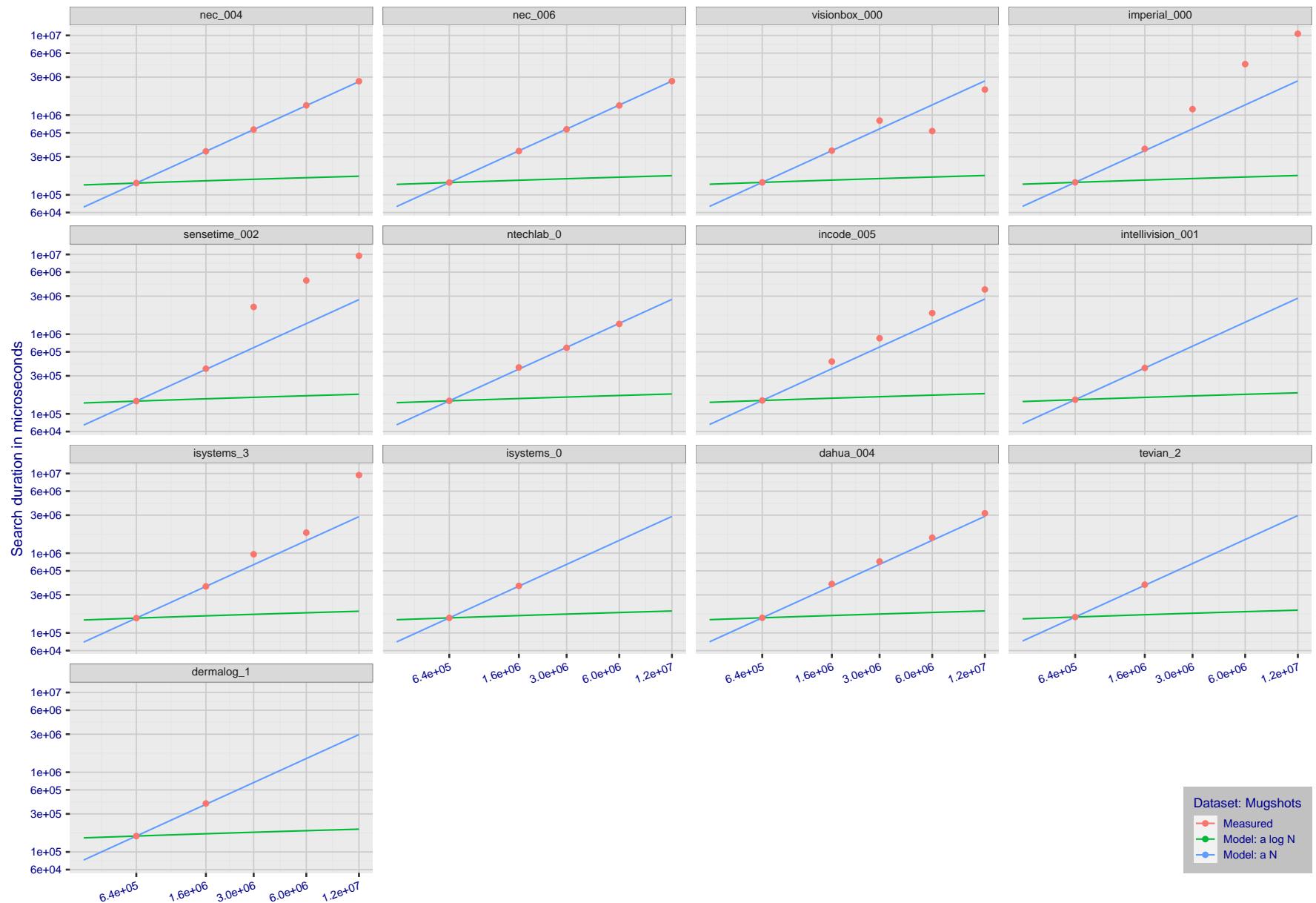


Figure 162: [Mugshot Dataset] Search duration vs. enrolled population size. In red are the actual point durations measured on a single c. 2016 core. The blue shows linear growth from $N = 640\,000$. The green line shows logarithmic growth from that point to $N = 1\,600\,000$. Note the sublinear growth from algorithms from Camvi, Dermalog, EverAI, Innovatrics, and Visionlabs. The tiger_1 algorithm is also sublinear, but inaccurate and inoperable at $N \geq 3000000$. This capability sometimes comes at the additional expense of converting a linear gallery data structure into whatever fast-search data structure is used. Note that search times are sometimes dominated by the template generation times shown in Table 28.

2023/03/14

FNIR(N, R, T) = False neg. identification rate
FPTR(N, T) = False pos. identification rateN = Num. enrolled subjects
R = Num. candidates examined

T = Threshold

T = 0 → Investigation
 $T > 0 \rightarrow$ Identification

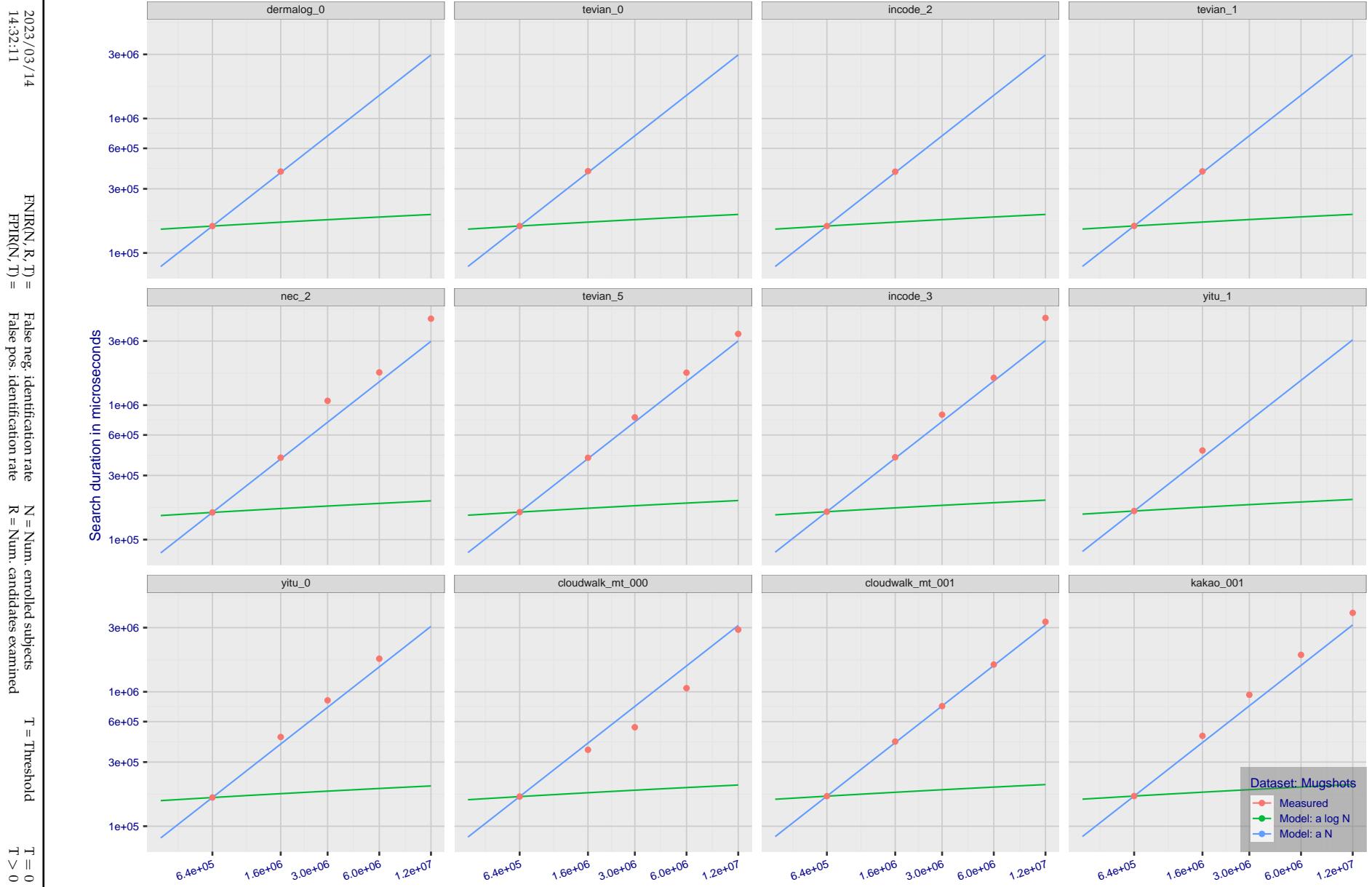


Figure 163: [Mugshot Dataset] Search duration vs. enrolled population size. In red are the actual point durations measured on a single c. 2016 core. The blue shows linear growth from $N = 640\,000$. The green line shows logarithmic growth from that point to $N = 1\,600\,000$. Note the sublinear growth from algorithms from Camvi, Dermalog, EverAI, Innovatrics, and Visionlabs. The tiger_1 algorithm is also sublinear, but inaccurate and inoperable at $N \geq 3000000$. This capability sometimes comes at the additional expense of converting a linear gallery data structure into whatever fast-search data structure is used. Note that search times are sometimes dominated by the template generation times shown in Table 28.

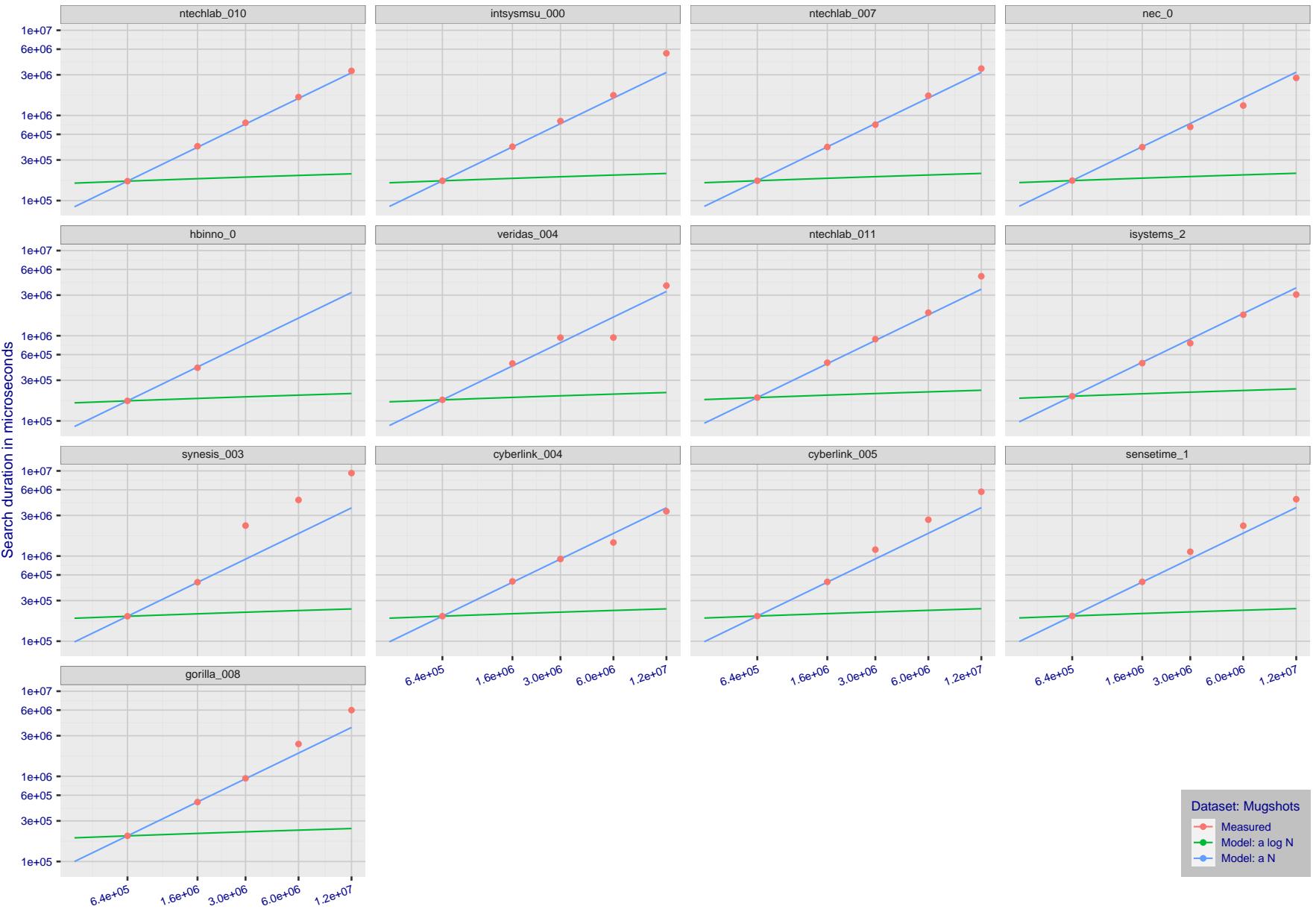


Figure 164: [Mugshot Dataset] Search duration vs. enrolled population size. In red are the actual point durations measured on a single c. 2016 core. The blue shows linear growth from $N = 640\,000$. The green line shows logarithmic growth from that point to $N = 1\,600\,000$. Note the sublinear growth from algorithms from Camvi, Dermalog, EverAI, Innovatrics, and Visionlabs. The tiger_1 algorithm is also sublinear, but inaccurate and inoperable at $N \geq 3000000$. This capability sometimes comes at the additional expense of converting a linear gallery data structure into whatever fast-search data structure is used. Note that search times are sometimes dominated by the template generation times shown in Table 28.

2023/03/14
14:32:11FNIR(N, R, T) = False neg. identification rate
FPIR(N, T) = False pos. identification rateN = Num. enrolled subjects
R = Num. candidates examined

T = Threshold

T = 0 → Investigation
 $T > 0 \rightarrow$ Identification

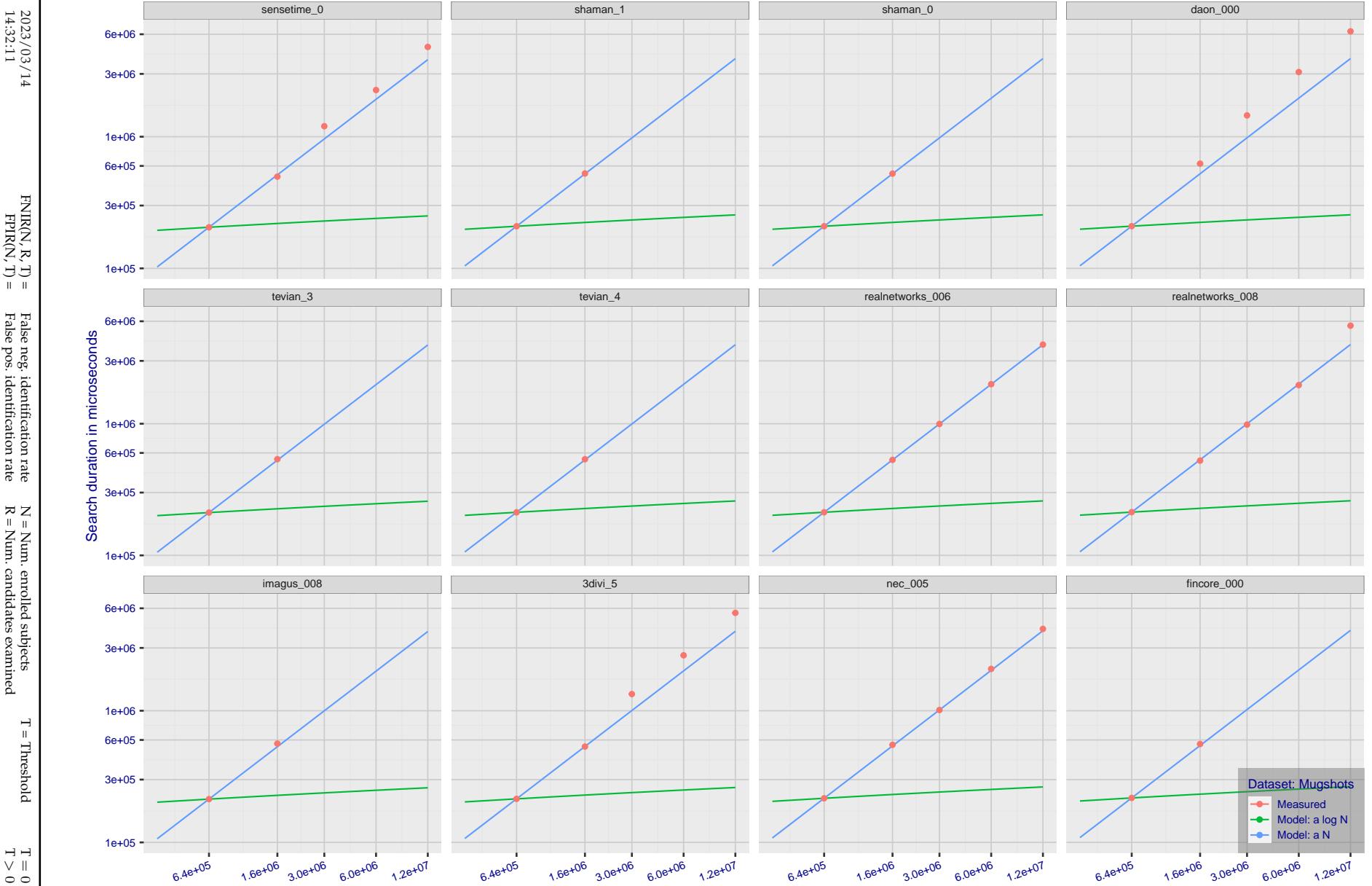


Figure 165: [Mugshot Dataset] Search duration vs. enrolled population size. In red are the actual point durations measured on a single c. 2016 core. The blue shows linear growth from $N = 640\,000$. The green line shows logarithmic growth from that point to $N = 1\,600\,000$. Note the sublinear growth from algorithms from Camvi, Dermalog, EverAI, Innovatrics, and Visionlabs. The tiger_1 algorithm is also sublinear, but inaccurate and inoperable at $N \geq 3000000$. This capability sometimes comes at the additional expense of converting a linear gallery data structure into whatever fast-search data structure is used. Note that search times are sometimes dominated by the template generation times shown in Table 28.

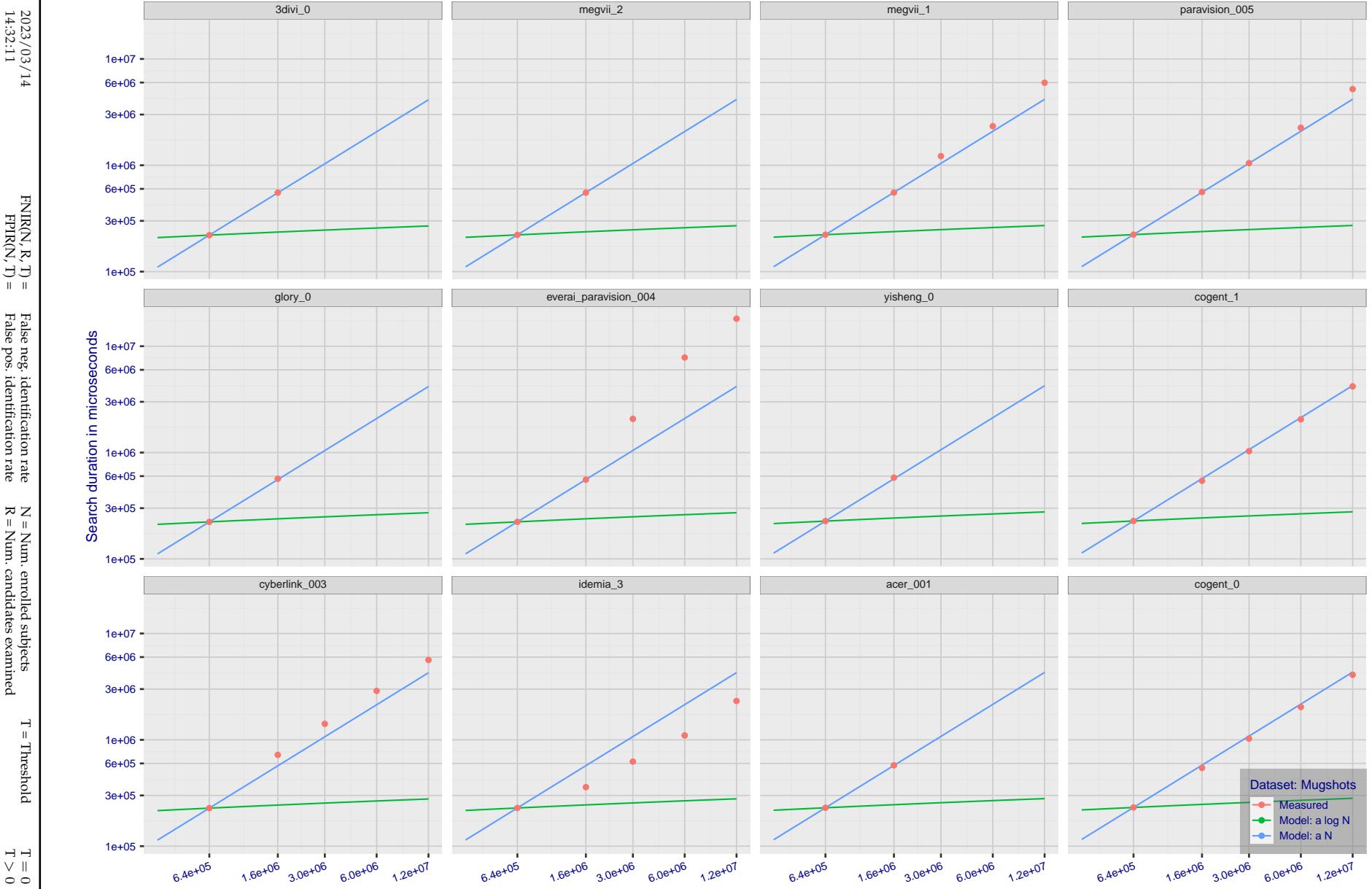


Figure 166: [Mugshot Dataset] Search duration vs. enrolled population size. In red are the actual point durations measured on a single c. 2016 core. The blue shows linear growth from $N = 640\,000$. The green line shows logarithmic growth from that point to $N = 1\,600\,000$. Note the sublinear growth from algorithms from Camvi, Dermalog, EverAI, Innovatrics, and Visionlabs. The tiger_1 algorithm is also sublinear, but inaccurate and inoperable at $N \geq 3000000$. This capability sometimes comes at the additional expense of converting a linear gallery data structure into whatever fast-search data structure is used. Note that search times are sometimes dominated by the template generation times shown in Table 28.

2023/03/14
14:32:11FNIR(N, R, T) = False neg. identification rate
FPTR(N, T) = False pos. identification rateN = Num. enrolled subjects
R = Num. candidates examinedT = Threshold
 $T = 0 \rightarrow$ Investigation $T > 0 \rightarrow$ Identification

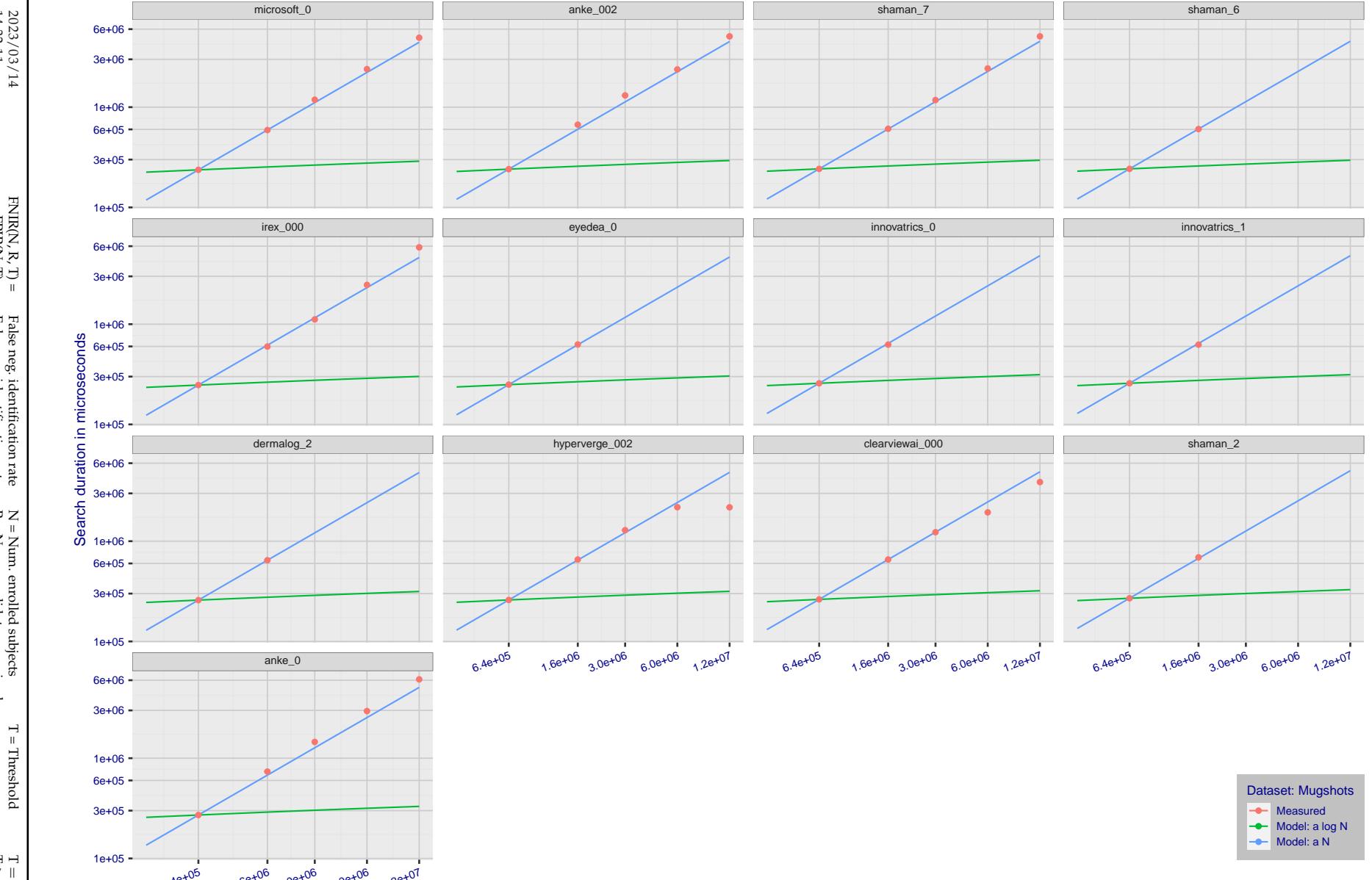


Figure 167: [Mugshot Dataset] Search duration vs. enrolled population size. In red are the actual point durations measured on a single c. 2016 core. The blue shows linear growth from $N = 640\,000$. The green line shows logarithmic growth from that point to $N = 1\,600\,000$. Note the sublinear growth from algorithms from Camvi, Dermalog, EverAI, Innovatrics, and Visionlabs. The tiger_1 algorithm is also sublinear, but inaccurate and inoperable at $N \geq 3000000$. This capability sometimes comes at the additional expense of converting a linear gallery data structure into whatever fast-search data structure is used. Note that search times are sometimes dominated by the template generation times shown in Table 28.

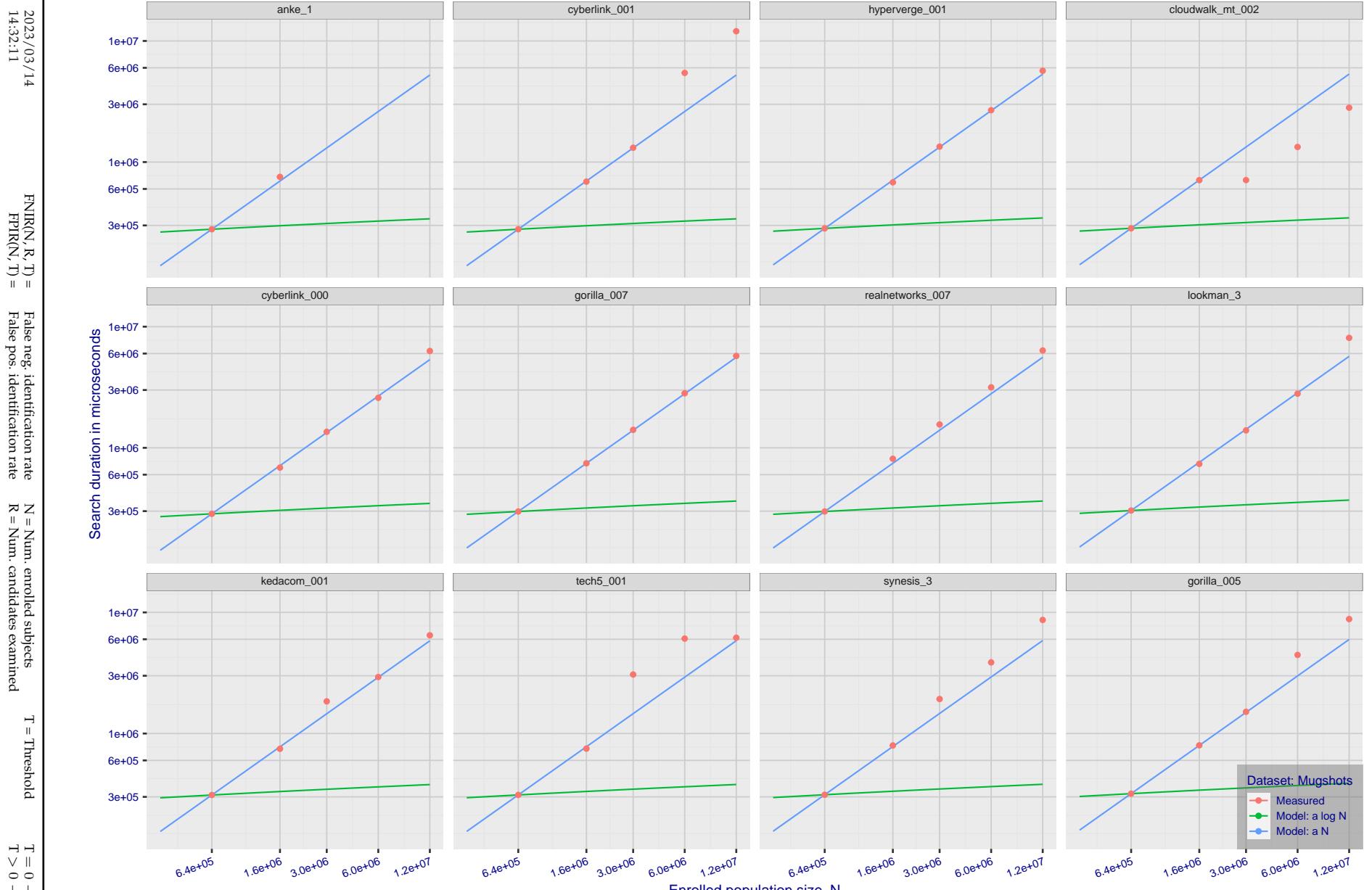


Figure 168: [Mugshot Dataset] Search duration vs. enrolled population size. In red are the actual point durations measured on a single c. 2016 core. The blue shows linear growth from $N = 640\,000$. The green line shows logarithmic growth from that point to $N = 1\,600\,000$. Note the sublinear growth from algorithms from Camvi, Dermalog, EverAI, Innovatrics, and Visionlabs. The tiger_1 algorithm is also sublinear, but inaccurate and inoperable at $N \geq 3000000$. This capability sometimes comes at the additional expense of converting a linear gallery data structure into whatever fast-search data structure is used. Note that search times are sometimes dominated by the template generation times shown in Table 28.

2023/03/14
14:32:11FNIR(N, R, T) = False neg. identification rate
FPIR(N, T) = False pos. identification rateN = Num. enrolled subjects
R = Num. candidates examined

T = Threshold

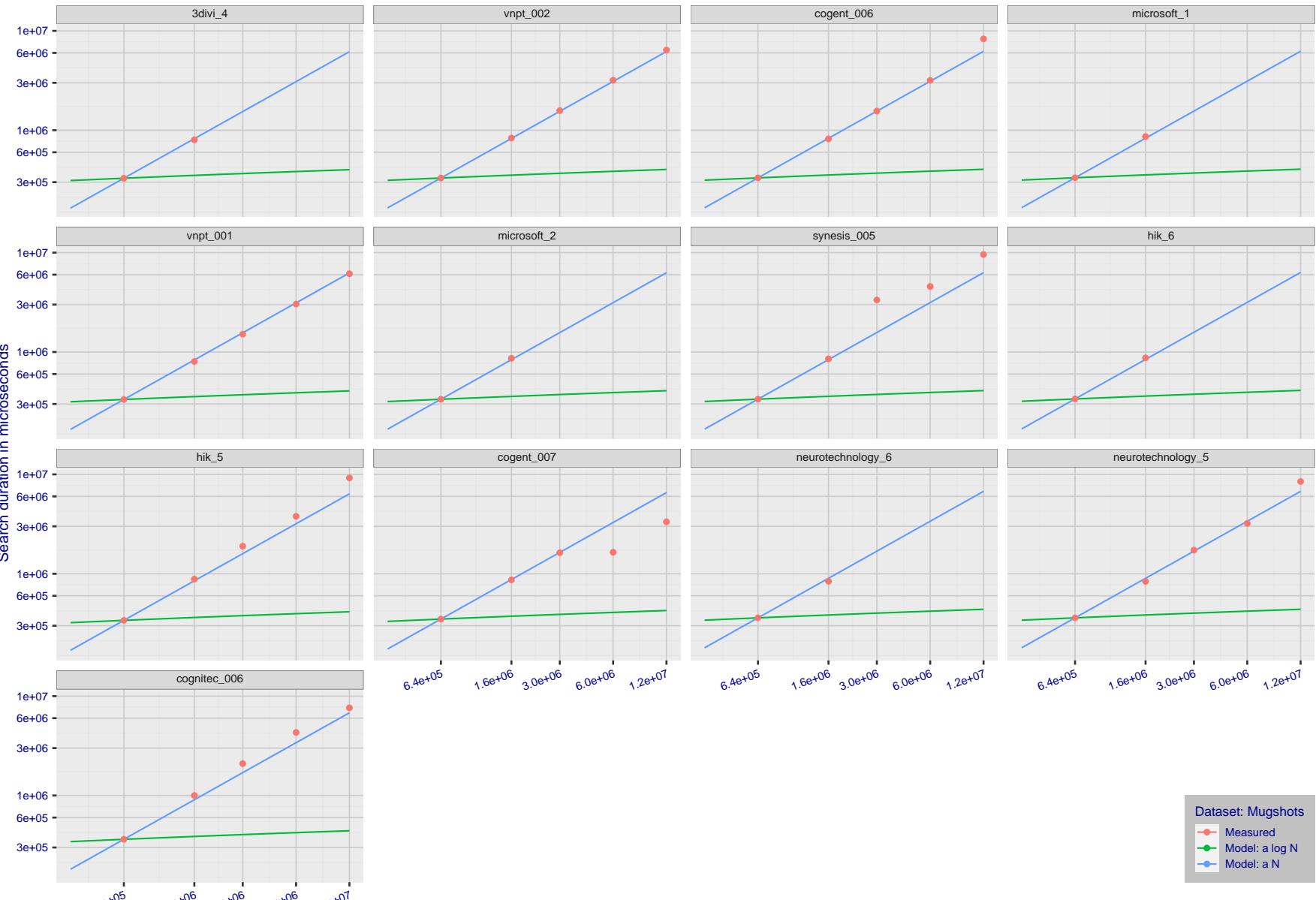
T = 0 → Investigation
T > 0 → Identification

Figure 169: [Mugshot Dataset] Search duration vs. enrolled population size. In red are the actual point durations measured on a single c. 2016 core. The blue shows linear growth from $N = 640\,000$. The green line shows logarithmic growth from that point to $N = 1\,600\,000$. Note the sublinear growth from algorithms from Camvi, Dermalog, EverAI, Innovatrics, and Visionlabs. The tiger_1 algorithm is also sublinear, but inaccurate and inoperable at $N \geq 3000000$. This capability sometimes comes at the additional expense of converting a linear gallery data structure into whatever fast-search data structure is used. Note that search times are sometimes dominated by the template generation times shown in Table 28.

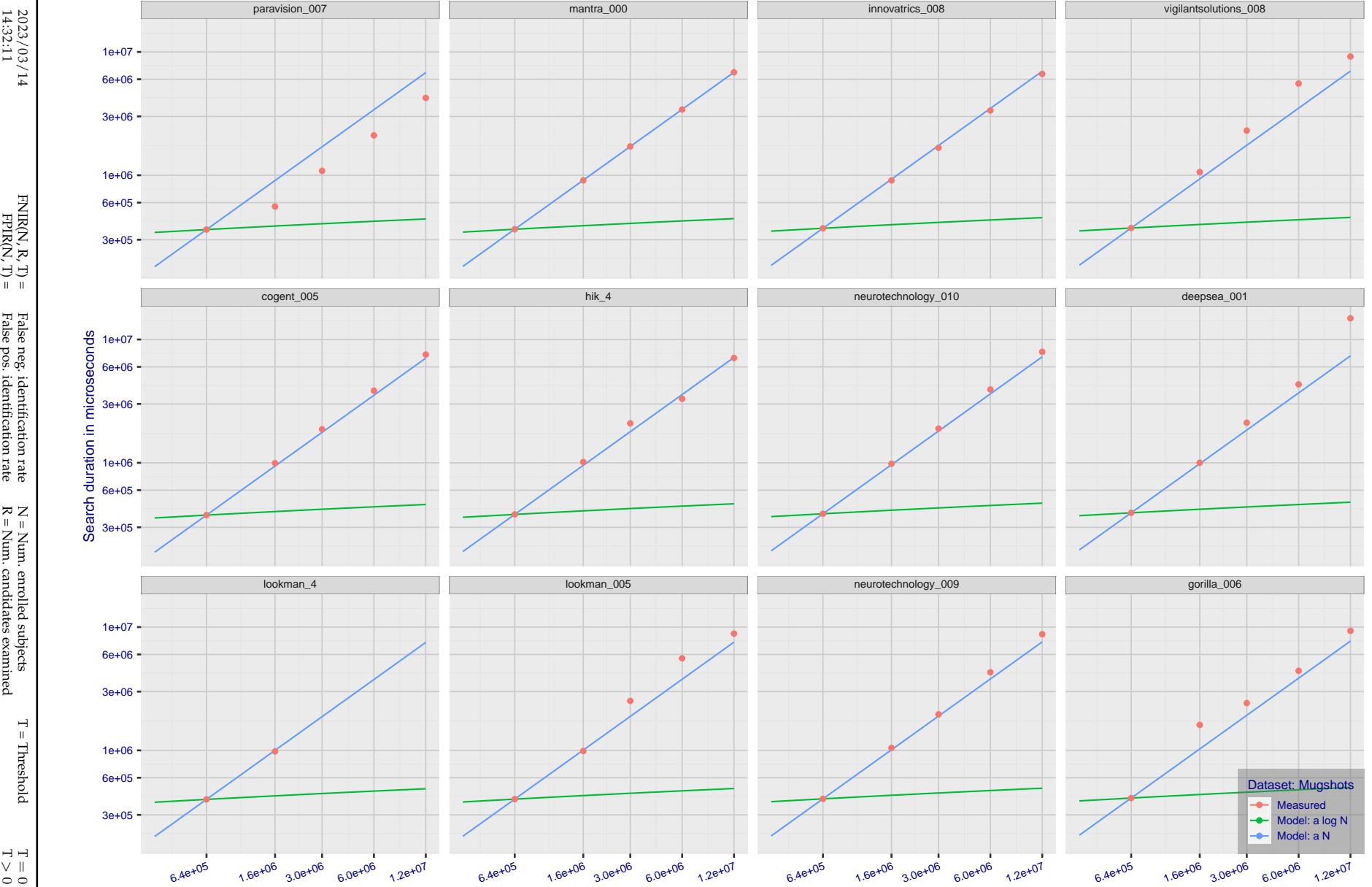


Figure 170: [Mugshot Dataset] Search duration vs. enrolled population size. In red are the actual point durations measured on a single c. 2016 core. The blue shows linear growth from $N = 640\,000$. The green line shows logarithmic growth from that point to $N = 1\,600\,000$. Note the sublinear growth from algorithms from Camvi, Dermalog, EverAI, Innovatrics, and Visionlabs. The tiger_1 algorithm is also sublinear, but inaccurate and inoperable at $N \geq 3000000$. This capability sometimes comes at the additional expense of converting a linear gallery data structure into whatever fast-search data structure is used. Note that search times are sometimes dominated by the template generation times shown in Table 28.

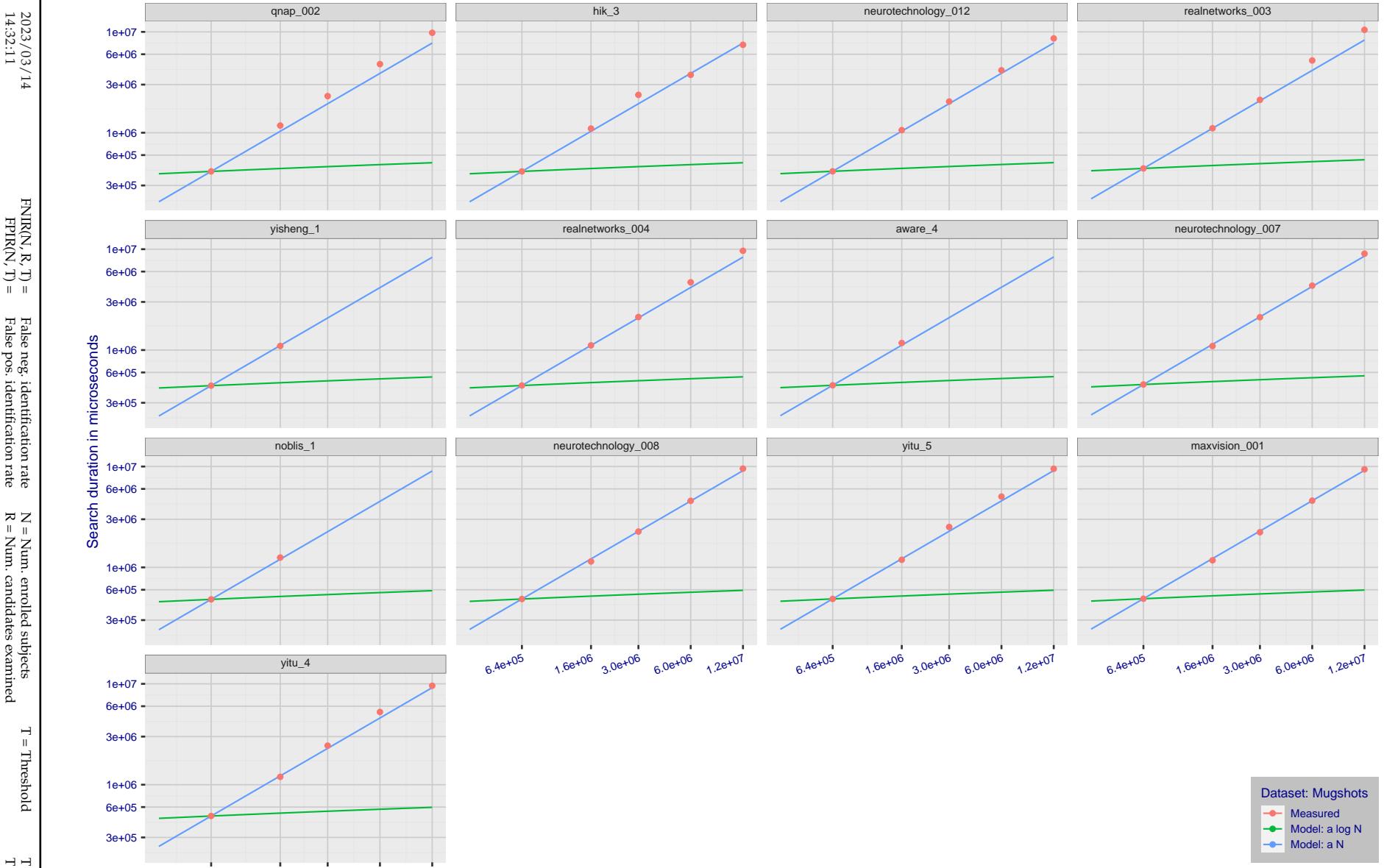


Figure 171: [Mugshot Dataset] Search duration vs. enrolled population size. In red are the actual point durations measured on a single c. 2016 core. The blue shows linear growth from $N = 640\,000$. The green line shows logarithmic growth from that point to $N = 1\,600\,000$. Note the sublinear growth from algorithms from Camvi, Dermalog, EverAI, Innovatrics, and Visionlabs. The tiger_1 algorithm is also sublinear, but inaccurate and inoperable at $N \geq 3000000$. This capability sometimes comes at the additional expense of converting a linear gallery data structure into whatever fast-search data structure is used. Note that search times are sometimes dominated by the template generation times shown in Table 28.

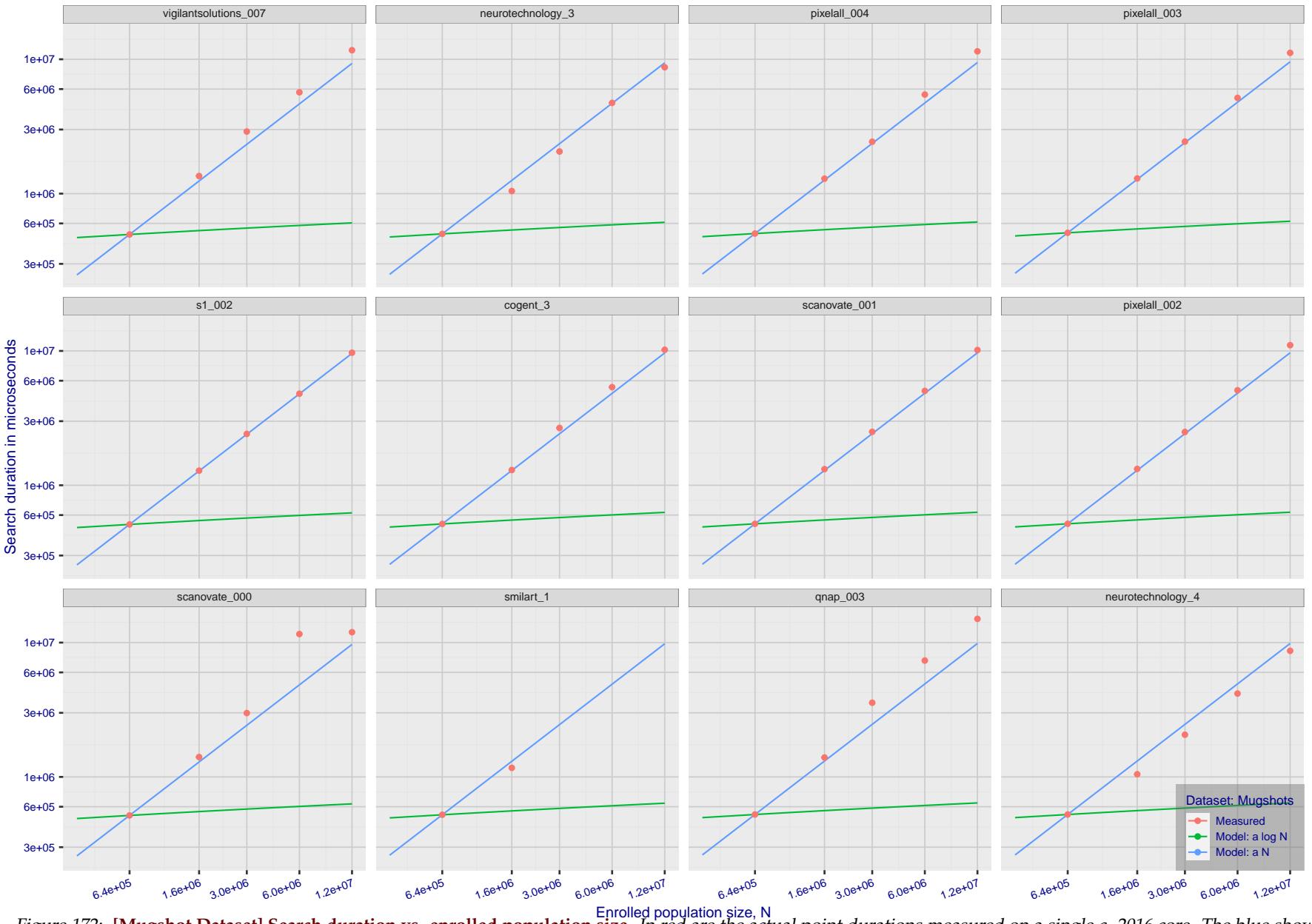


Figure 172: [Mugshot Dataset] Search duration vs. enrolled population size. In red are the actual point durations measured on a single c. 2016 core. The blue shows linear growth from $N = 640\,000$. The green line shows logarithmic growth from that point to $N = 1\,600\,000$. Note the sublinear growth from algorithms from Camvi, Dermalog, EverAI, Innovatrics, and Visionlabs. The tiger_1 algorithm is also sublinear, but inaccurate and inoperable at $N \geq 3000000$. This capability sometimes comes at the additional expense of converting a linear gallery data structure into whatever fast-search data structure is used. Note that search times are sometimes dominated by the template generation times shown in Table 28.

2023/03/14

FNIR(N, R, T) = False neg. identification rate

FPTR(N, T) = False pos. identification rate

N = Num. enrolled subjects

R = Num. candidates examined

T = Threshold

T = 0 → Investigation
T > 0 → Identification

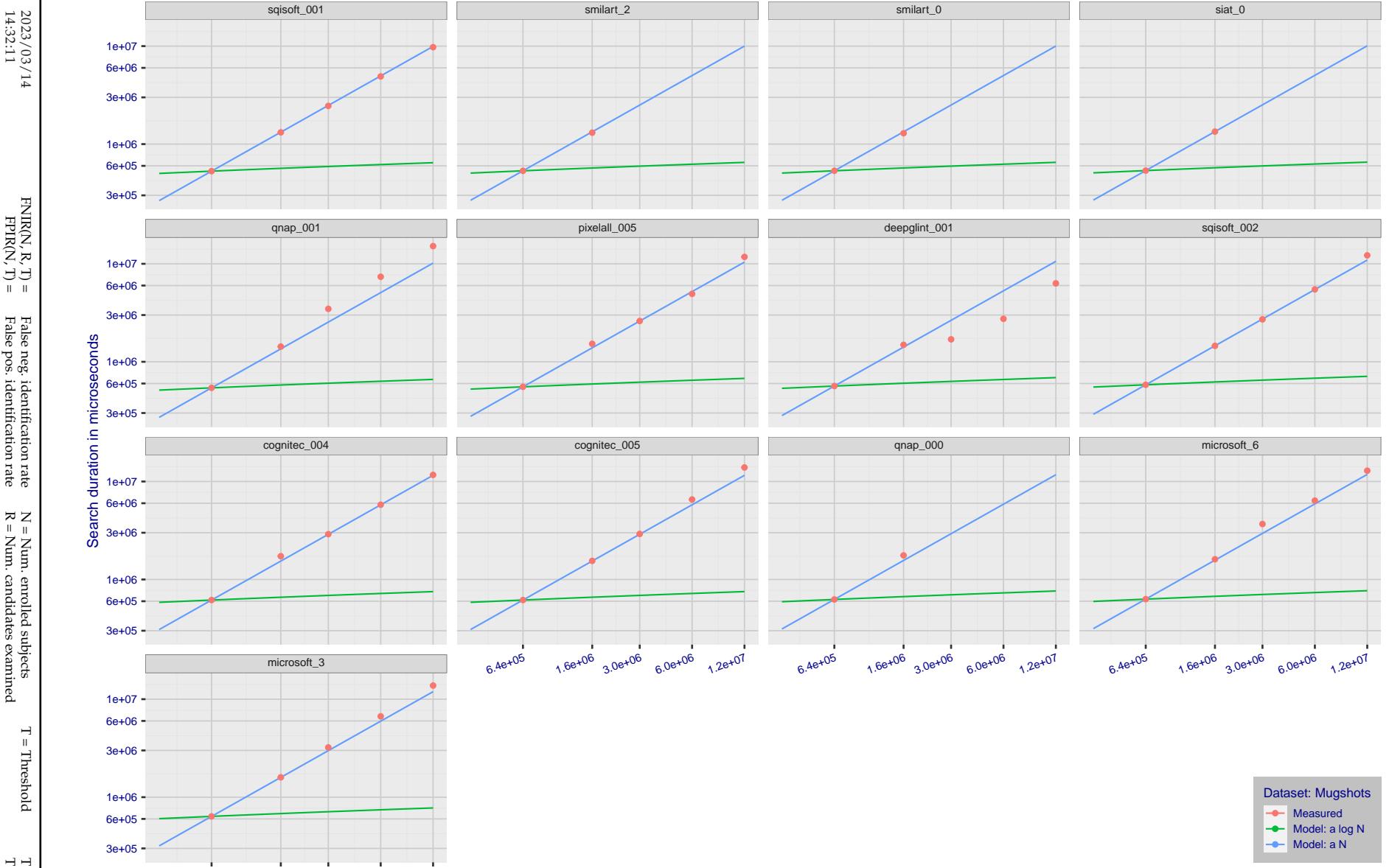


Figure 173: [Mugshot Dataset] Search duration vs. enrolled population size. In red are the actual point durations measured on a single c. 2016 core. The blue shows linear growth from $N = 640\,000$. The green line shows logarithmic growth from that point to $N = 1\,600\,000$. Note the sublinear growth from algorithms from Camvi, Dermalog, EverAI, Innovatrics, and Visionlabs. The tiger_1 algorithm is also sublinear, but inaccurate and inoperable at $N \geq 3000000$. This capability sometimes comes at the additional expense of converting a linear gallery data structure into whatever fast-search data structure is used. Note that search times are sometimes dominated by the template generation times shown in Table 28.

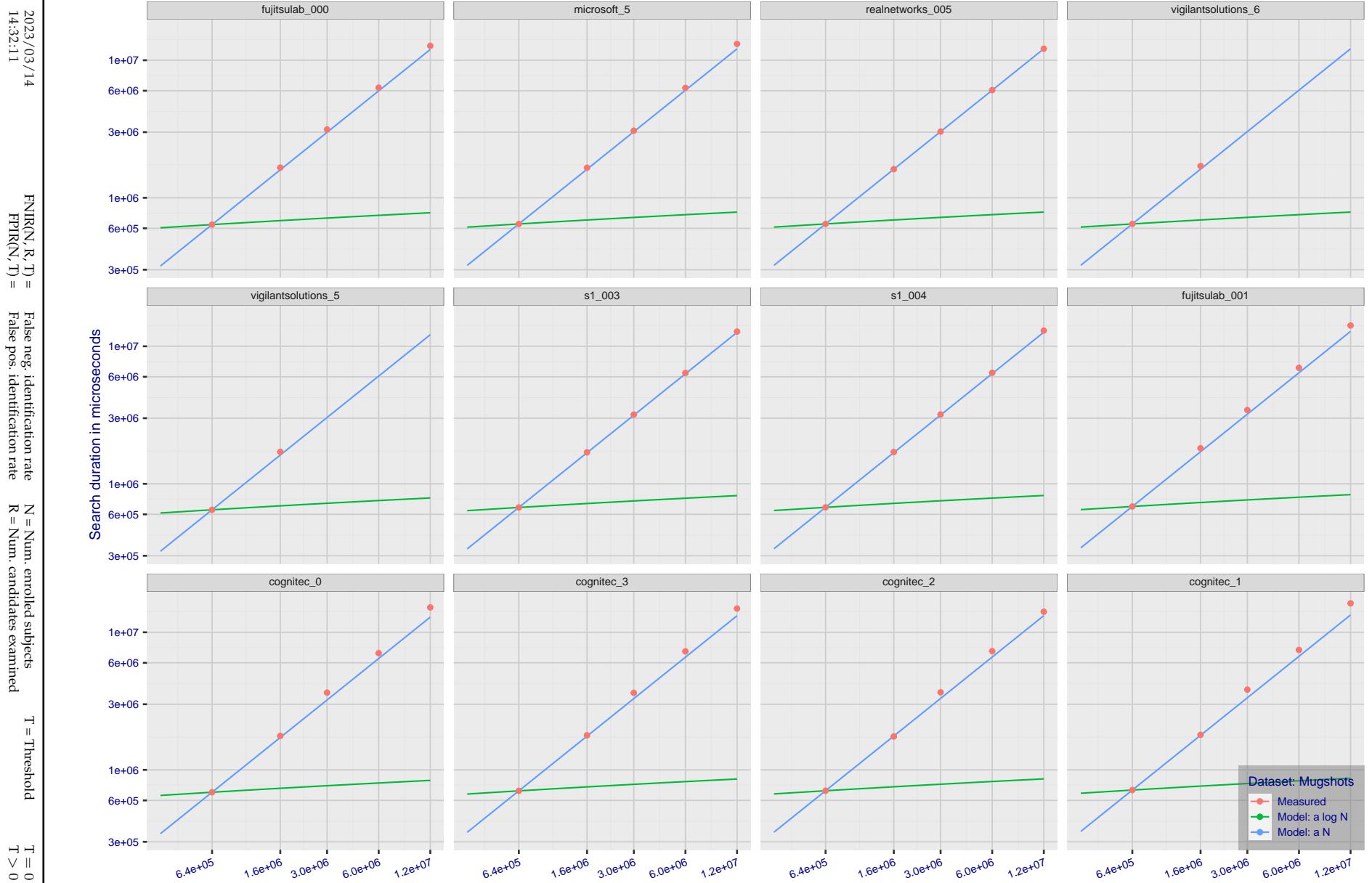


Figure 174: [Mugshot Dataset] Search duration vs. enrolled population size. In red are the actual point durations measured on a single c. 2016 core. The blue shows linear growth from $N = 640\,000$. The green line shows logarithmic growth from that point to $N = 1\,600\,000$. Note the sublinear growth from algorithms from Camvi, Dermalog, EverAI, Innovatrics, and Visionlabs. The tiger_1 algorithm is also sublinear, but inaccurate and inoperable at $N \geq 3000000$. This capability sometimes comes at the additional expense of converting a linear gallery data structure into whatever fast-search data structure is used. Note that search times are sometimes dominated by the template generation times shown in Table 28.

2023/03/14
14:32:11FNIR(N, R, T) = False neg. identification rate
FPIR(N, T) = False pos. identification rateN = Num. enrolled subjects
R = Num. candidates examined

T = Threshold

T = 0 → Investigation
 $T > 0 \rightarrow$ Identification

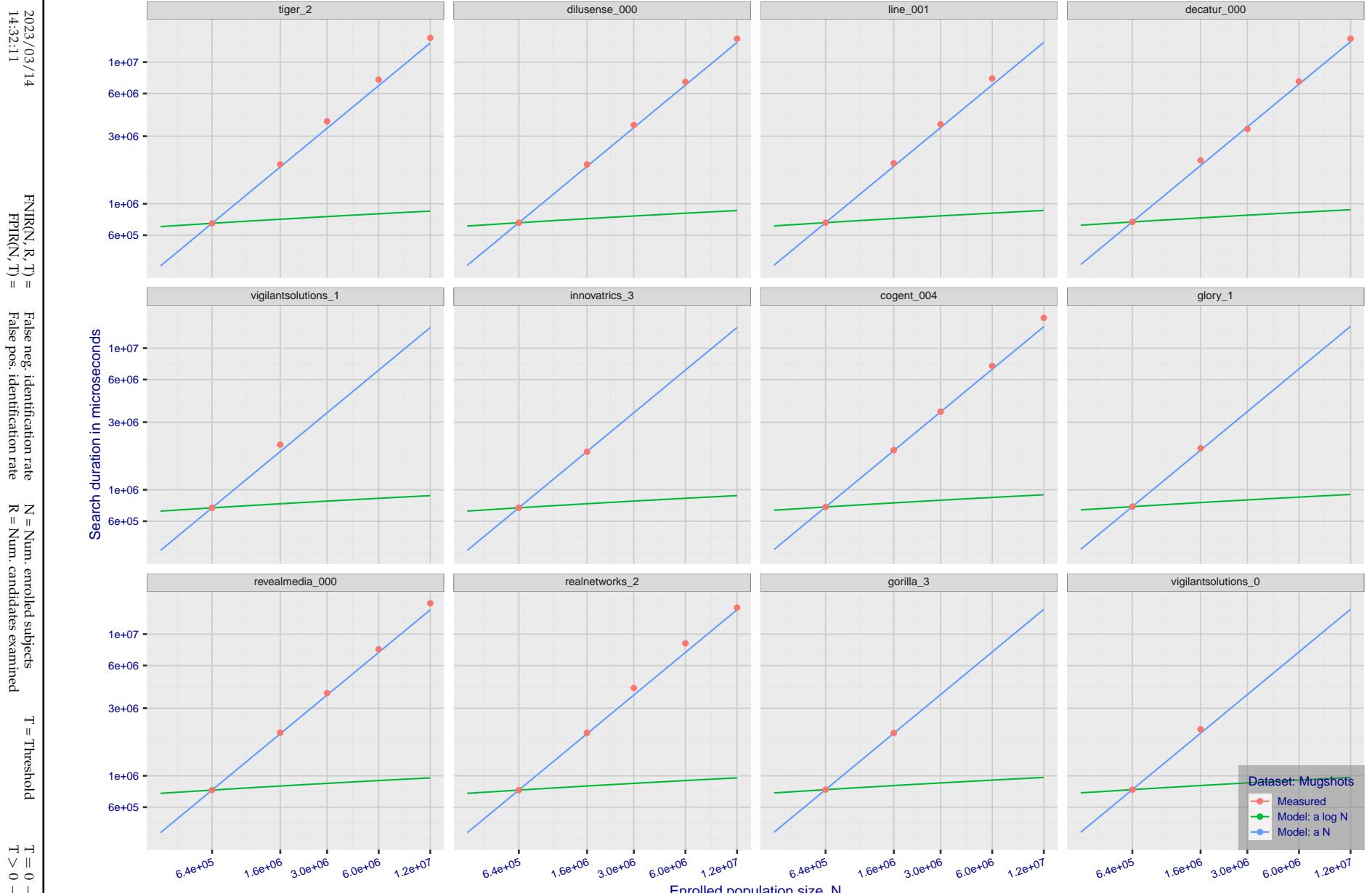


Figure 175: [Mugshot Dataset] Search duration vs. enrolled population size. In red are the actual point durations measured on a single c. 2016 core. The blue shows linear growth from $N = 640\,000$. The green line shows logarithmic growth from that point to $N = 1\,600\,000$. Note the sublinear growth from algorithms from Camvi, Dermalog, EverAI, Innovatrics, and Visionlabs. The tiger_1 algorithm is also sublinear, but inaccurate and inoperable at $N \geq 3000000$. This capability sometimes comes at the additional expense of converting a linear gallery data structure into whatever fast-search data structure is used. Note that search times are sometimes dominated by the template generation times shown in Table 28.

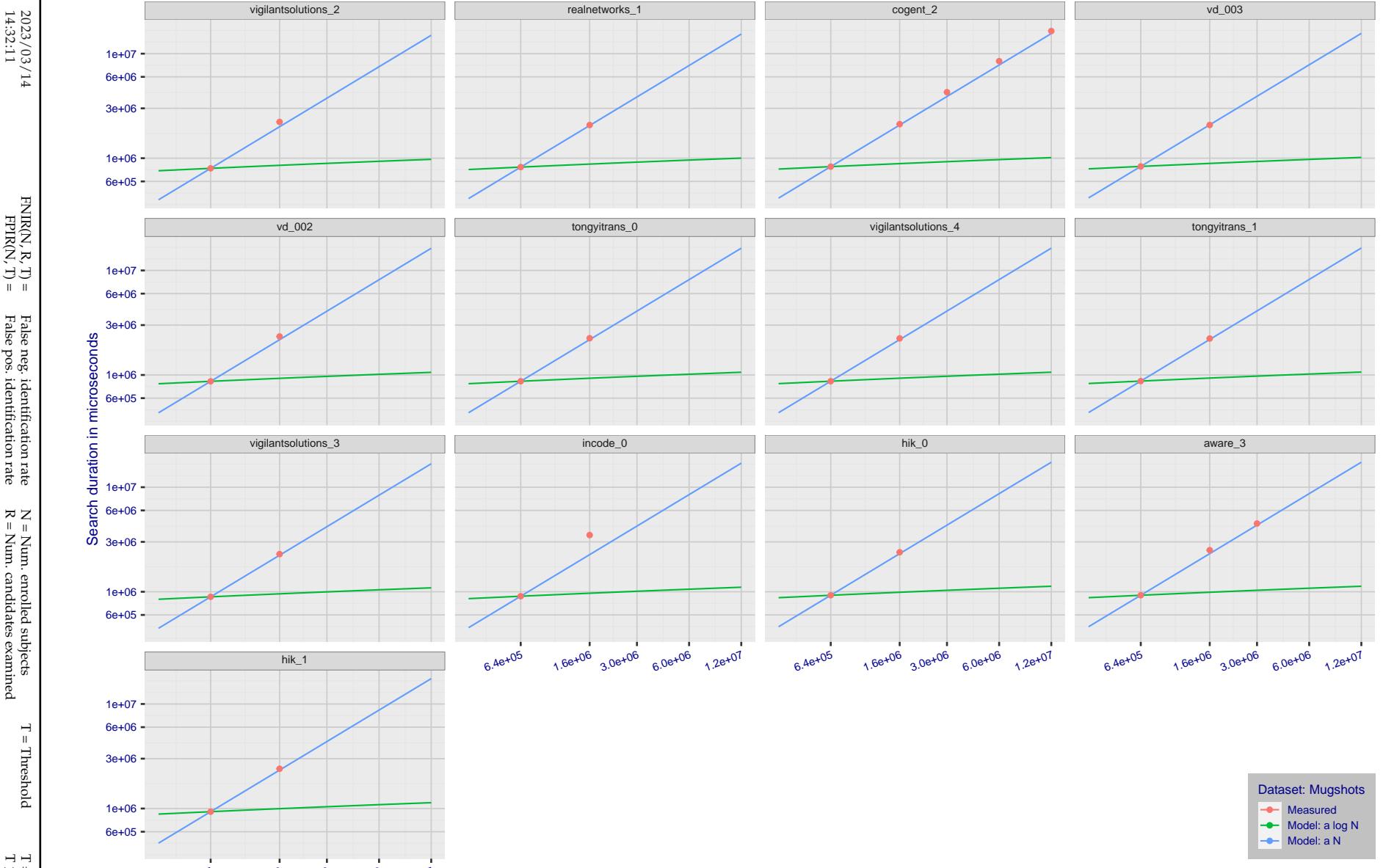


Figure 176: [Mugshot Dataset] Search duration vs. enrolled population size. In red are the actual point durations measured on a single c. 2016 core. The blue shows linear growth from $N = 640\,000$. The green line shows logarithmic growth from that point to $N = 1\,600\,000$. Note the sublinear growth from algorithms from Camvi, Dermalog, EverAI, Innovatrics, and Visionlabs. The tiger_1 algorithm is also sublinear, but inaccurate and inoperable at $N \geq 3000000$. This capability sometimes comes at the additional expense of converting a linear gallery data structure into whatever fast-search data structure is used. Note that search times are sometimes dominated by the template generation times shown in Table 28.

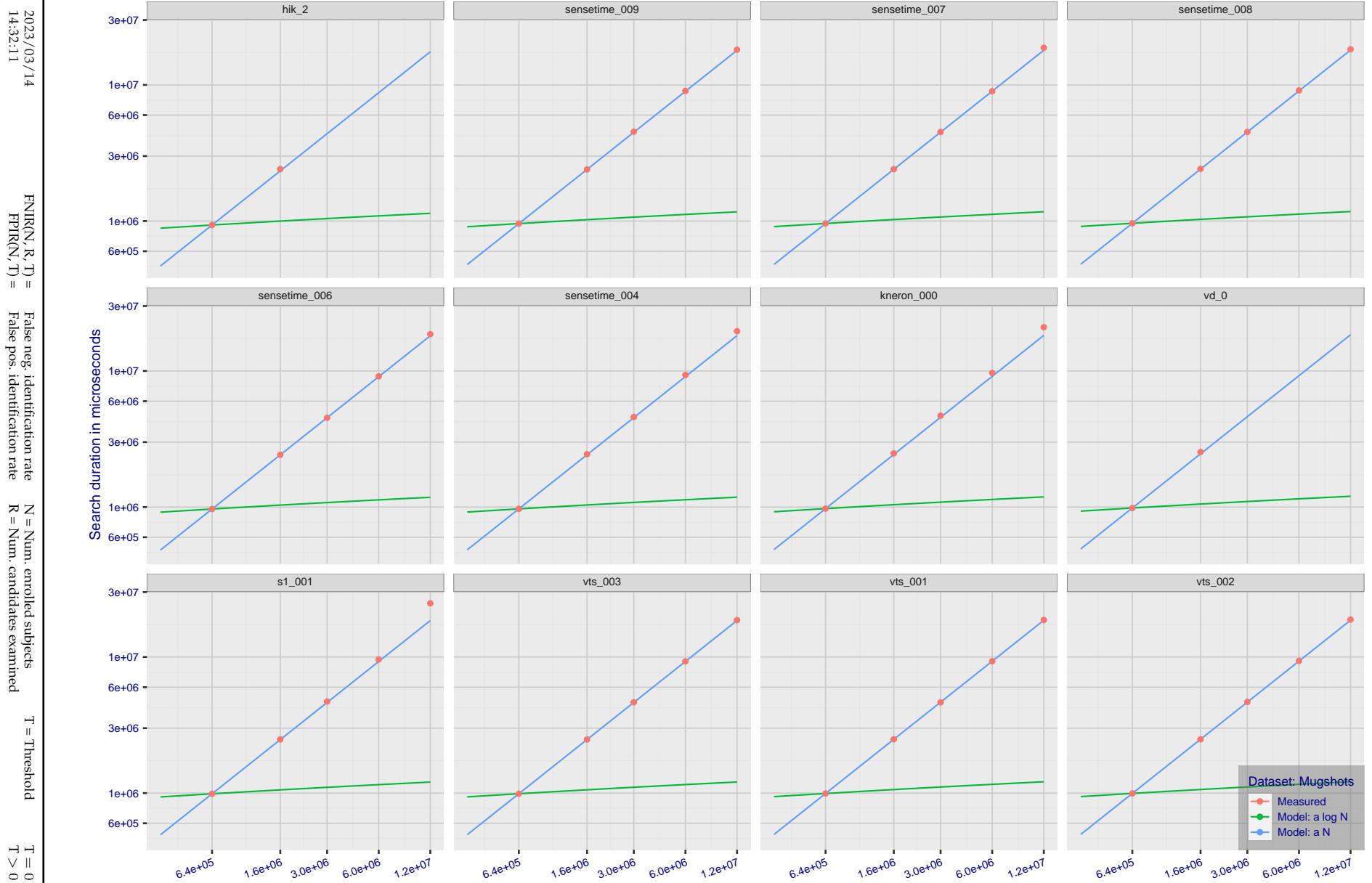


Figure 177: [Mugshot Dataset] Search duration vs. enrolled population size. In red are the actual point durations measured on a single c. 2016 core. The blue shows linear growth from $N = 640\,000$. The green line shows logarithmic growth from that point to $N = 1\,600\,000$. Note the sublinear growth from algorithms from Camvi, Dermalog, EverAI, Innovatrics, and Visionlabs. The tiger_1 algorithm is also sublinear, but inaccurate and inoperable at $N \geq 3000000$. This capability sometimes comes at the additional expense of converting a linear gallery data structure into whatever fast-search data structure is used. Note that search times are sometimes dominated by the template generation times shown in Table 28.

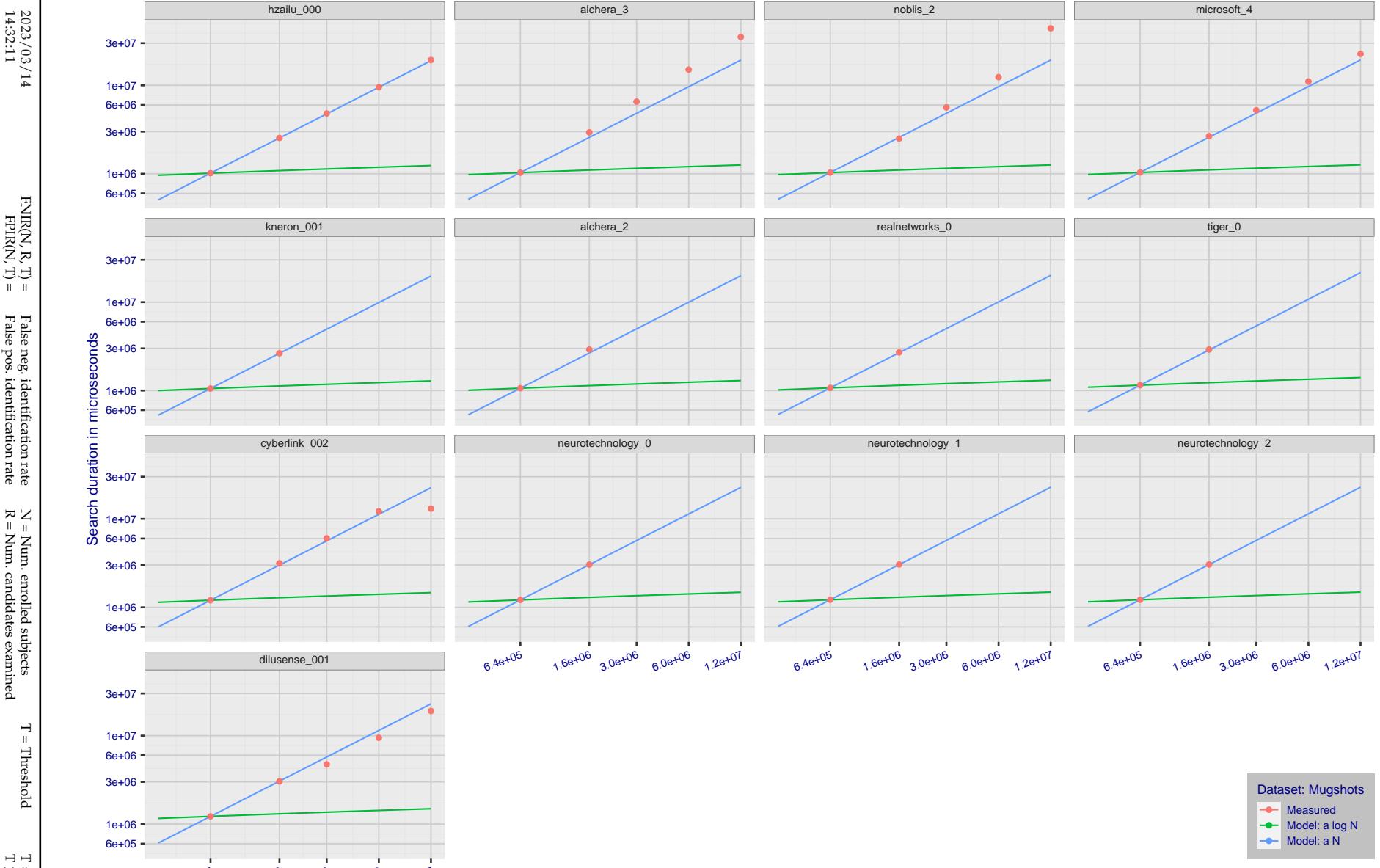


Figure 178: [Mugshot Dataset] Search duration vs. enrolled population size. In red are the actual point durations measured on a single c. 2016 core. The blue shows linear growth from $N = 640\,000$. The green line shows logarithmic growth from that point to $N = 1\,600\,000$. Note the sublinear growth from algorithms from Camvi, Dermalog, EverAI, Innovatrics, and Visionlabs. The tiger_1 algorithm is also sublinear, but inaccurate and inoperable at $N \geq 3000000$. This capability sometimes comes at the additional expense of converting a linear gallery data structure into whatever fast-search data structure is used. Note that search times are sometimes dominated by the template generation times shown in Table 28.

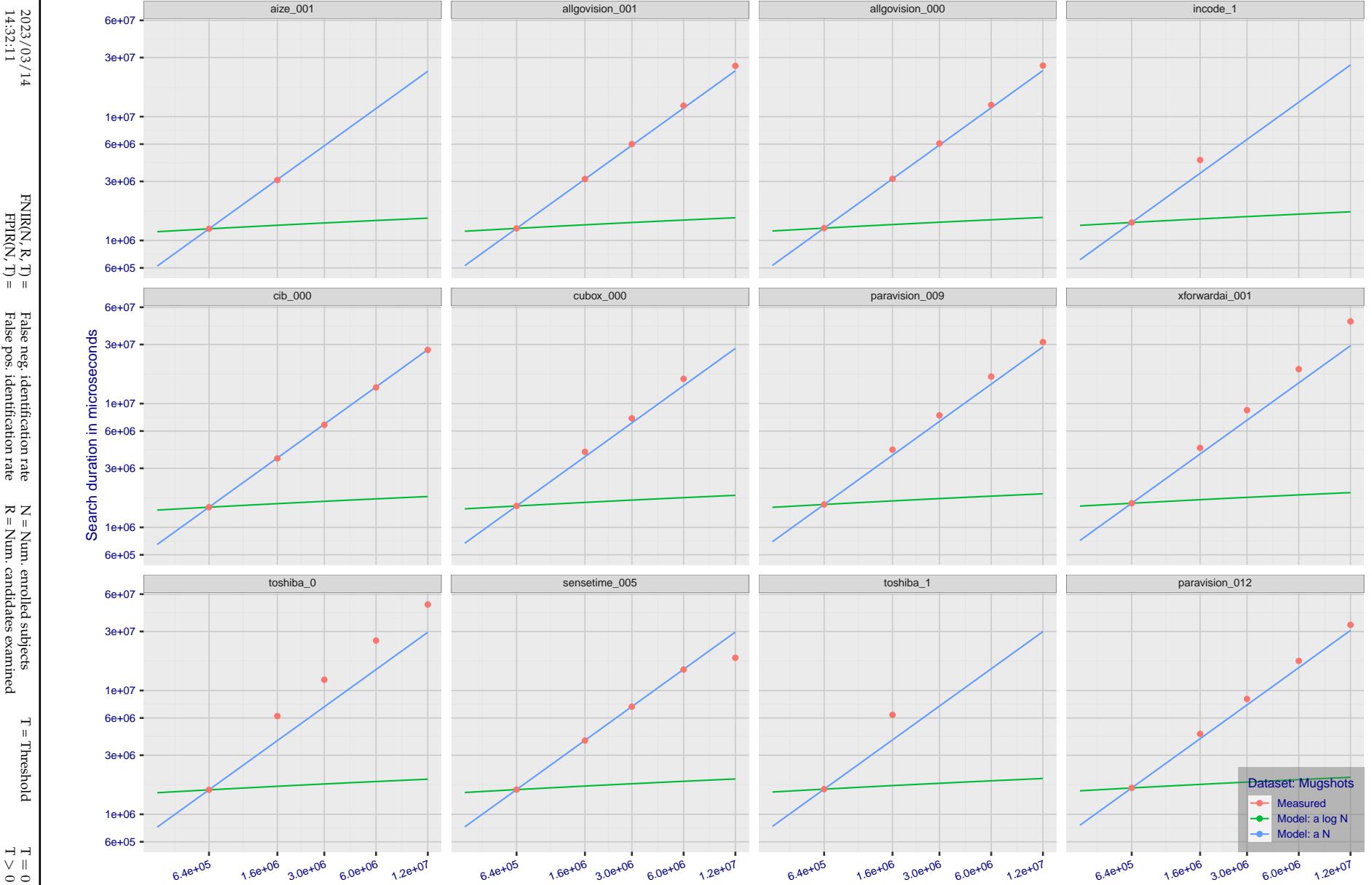


Figure 179: [Mugshot Dataset] Search duration vs. enrolled population size. In red are the actual point durations measured on a single c. 2016 core. The blue shows linear growth from $N = 640\,000$. The green line shows logarithmic growth from that point to $N = 1\,600\,000$. Note the sublinear growth from algorithms from Camvi, Dermalog, EverAI, Innovatrics, and Visionlabs. The tiger_1 algorithm is also sublinear, but inaccurate and inoperable at $N \geq 3000000$. This capability sometimes comes at the additional expense of converting a linear gallery data structure into whatever fast-search data structure is used. Note that search times are sometimes dominated by the template generation times shown in Table 28.

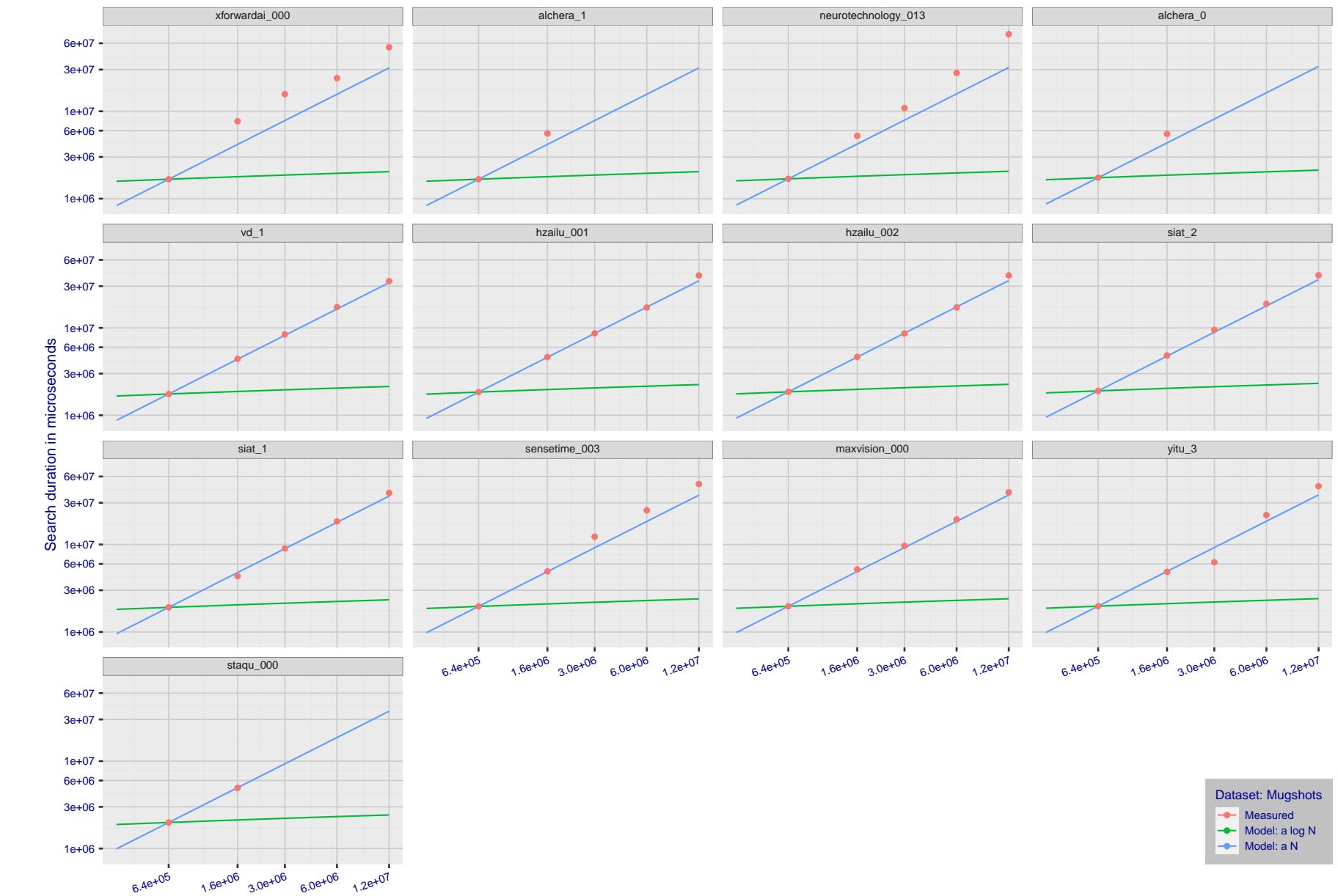


Figure 180: [Mugshot Dataset] Search duration vs. enrolled population size. In red are the actual point durations measured on a single c. 2016 core. The blue shows linear growth from $N = 640\,000$. The green line shows logarithmic growth from that point to $N = 1\,600\,000$. Note the sublinear growth from algorithms from Camvi, Dermalog, EverAI, Innovatrics, and Visionlabs. The tiger_1 algorithm is also sublinear, but inaccurate and inoperable at $N \geq 3000000$. This capability sometimes comes at the additional expense of converting a linear gallery data structure into whatever fast-search data structure is used. Note that search times are sometimes dominated by the template generation times shown in Table 28.

2023/03/14

14:32:11

FNIR(N, R, T) = False neg. identification rate
FPFR(N, T) = False pos. identification rateN = Num. enrolled subjects
R = Num. candidates examined

T = Threshold

T = 0 → Investigation
 $T > 0 \rightarrow$ Identification

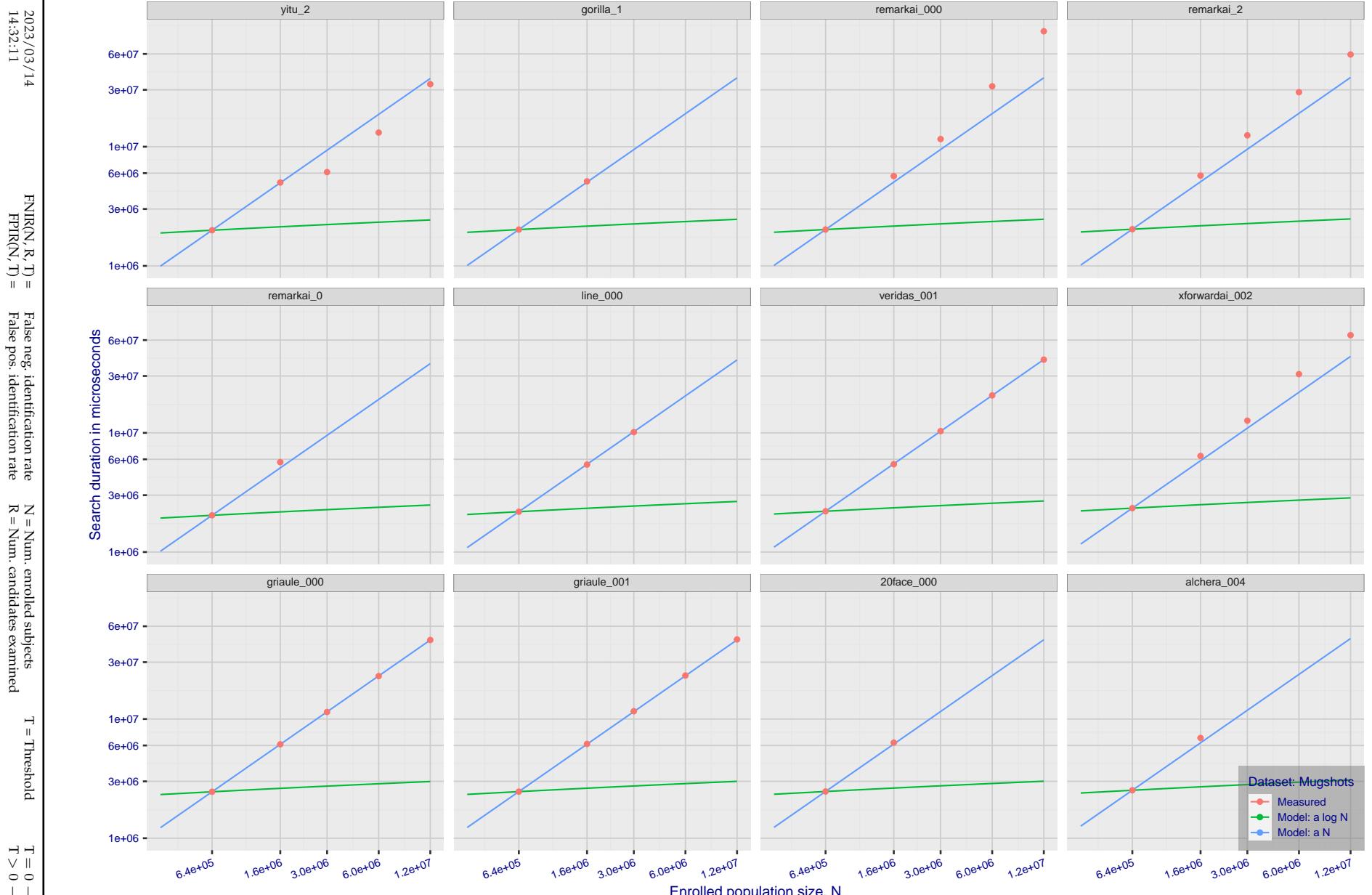


Figure 181: [Mugshot Dataset] Search duration vs. enrolled population size. In red are the actual point durations measured on a single c. 2016 core. The blue shows linear growth from $N = 640\,000$. The green line shows logarithmic growth from that point to $N = 1\,600\,000$. Note the sublinear growth from algorithms from Camvi, Dermalog, EverAI, Innovatrics, and Visionlabs. The tiger_1 algorithm is also sublinear, but inaccurate and inoperable at $N \geq 3000000$. This capability sometimes comes at the additional expense of converting a linear gallery data structure into whatever fast-search data structure is used. Note that search times are sometimes dominated by the template generation times shown in Table 28.

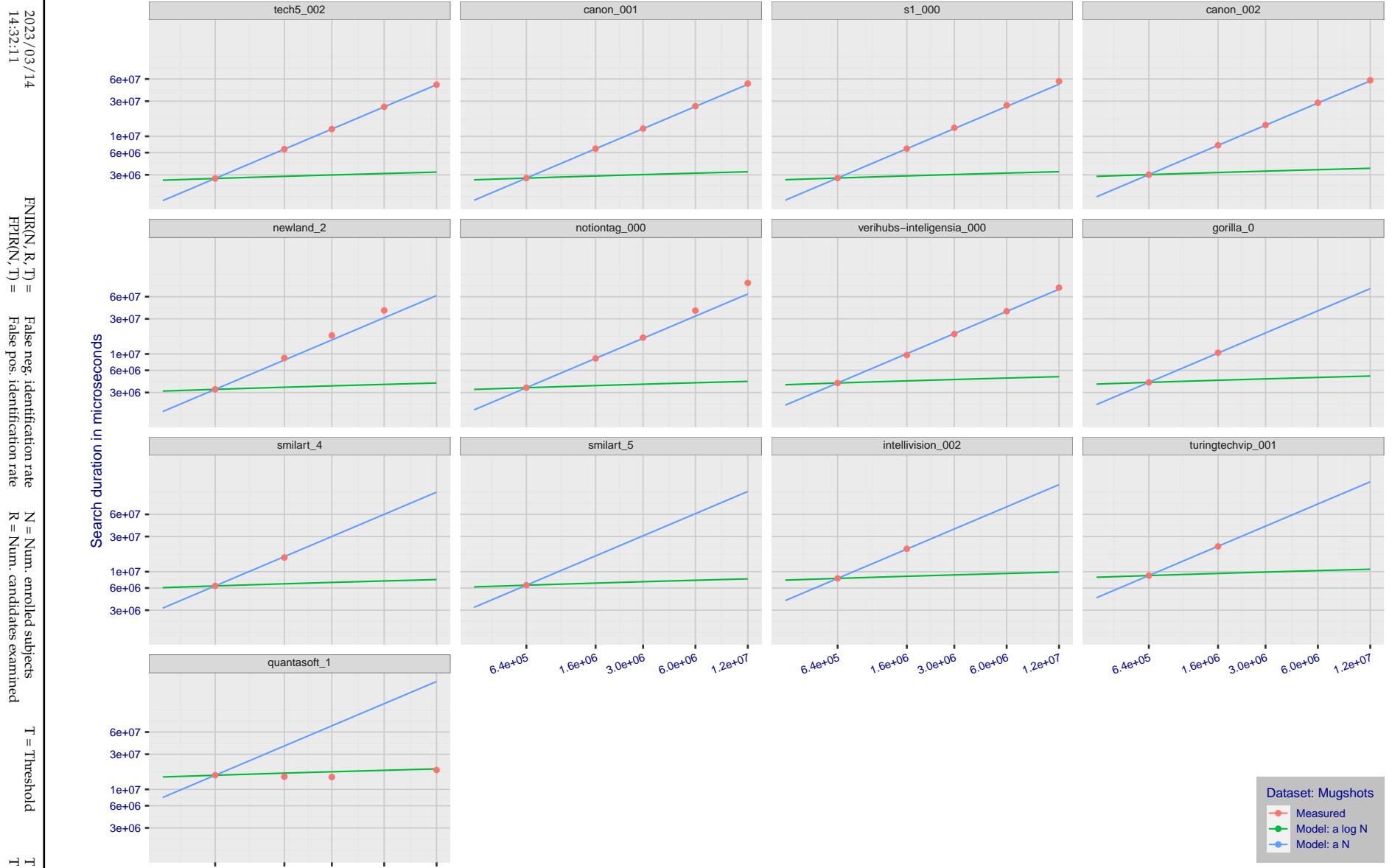


Figure 182: [Mugshot Dataset] Search duration vs. enrolled population size. In red are the actual point durations measured on a single c. 2016 core. The blue shows linear growth from $N = 640\,000$. The green line shows logarithmic growth from that point to $N = 1\,600\,000$. Note the sublinear growth from algorithms from Camvi, Dermalog, EverAI, Innovatrics, and Visionlabs. The tiger_1 algorithm is also sublinear, but inaccurate and inoperable at $N \geq 3000000$. This capability sometimes comes at the additional expense of converting a linear gallery data structure into whatever fast-search data structure is used. Note that search times are sometimes dominated by the template generation times shown in Table 28.

2023/03/14
14:32:11FNIR(N, R, T) = False neg. identification rate
FPIR(N, T) = False pos. identification rateN = Num. enrolled subjects
R = Num. candidates examined

T = Threshold

T = 0 → Investigation
 $T > 0 \rightarrow$ Identification

Appendix G Gallery Insertion Timing

2023/03/14
14:32:11FNIR(N, R, T) = False neg. identification rate
FPIR(N, T) = False pos. identification rateN = Num. enrolled subjects
R = Num. candidates examined

T = Threshold

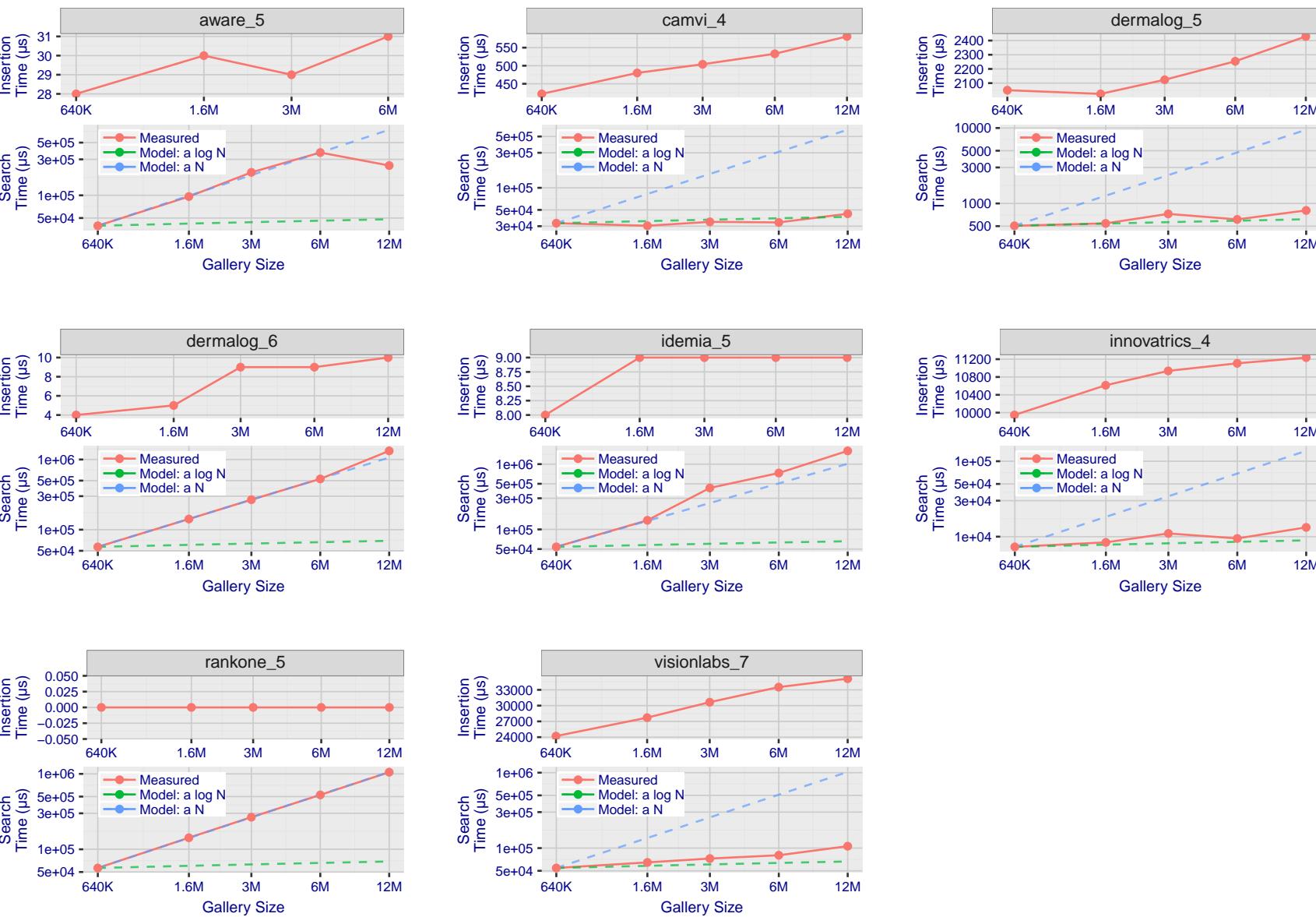
T = 0 → Investigation
T > 0 → Identification

Figure 183: [Mugshot Dataset] Gallery insertion duration vs. enrolled population size. This chart plots the time it takes to insert a single template into a finalized gallery, illustrated over increasing gallery sizes. For reference, search times on finalized galleries of corresponding sizes are plotted right underneath. Gallery insertion time plots were generated on algorithms that 1) successfully implemented gallery insertion with no errors and 2) that were run on galleries with N up to 12 000 000. Generally, only the more accurate algorithms were run on galleries with N up to 12 000 000.

2023/03/14
14:32:11FNIR(N, R, T) = False neg. identification rate
FPTR(N, T) = False pos. identification rateN = Num. enrolled subjects
R = Num. candidates examinedT = Threshold
T = 0 → Investigation

T > 0 → Identification

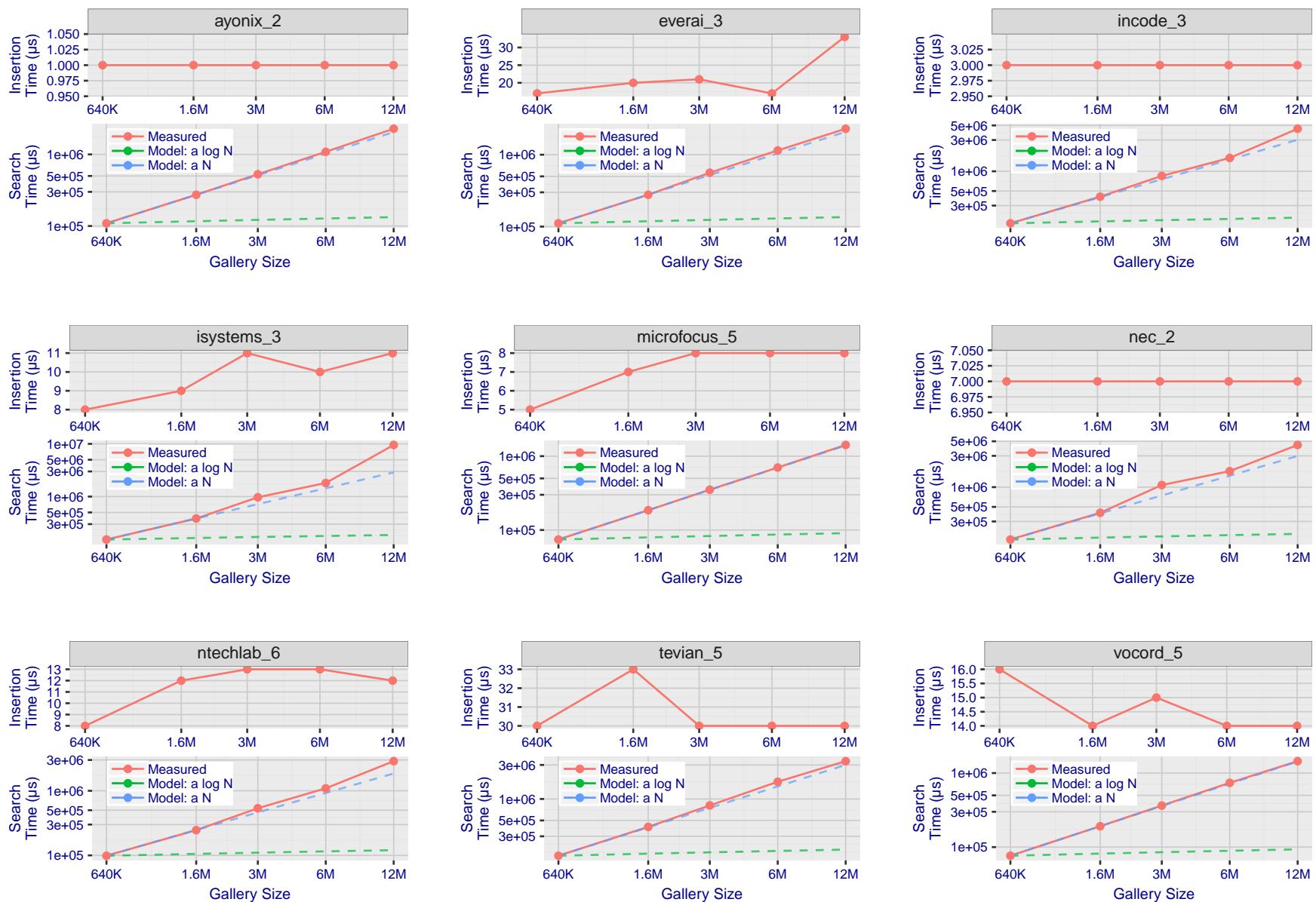


Figure 184: [Mugshot Dataset] Gallery insertion duration vs. enrolled population size. This chart plots the time it takes to insert a single template into a finalized gallery, illustrated over increasing gallery sizes. For reference, search times on finalized galleries of corresponding sizes are plotted right underneath. Gallery insertion time plots were generated on algorithms that 1) successfully implemented gallery insertion with no errors and 2) that were run on galleries with N up to 12 000 000. Generally, only the more accurate algorithms were run on galleries with N up to 12 000 000.

2023/03/14
14:32:11FNIR(N, R, T) = False neg. identification rate
FPTR(N, T) = False pos. identification rateN = Num. enrolled subjects
R = Num. candidates examined

T = Threshold

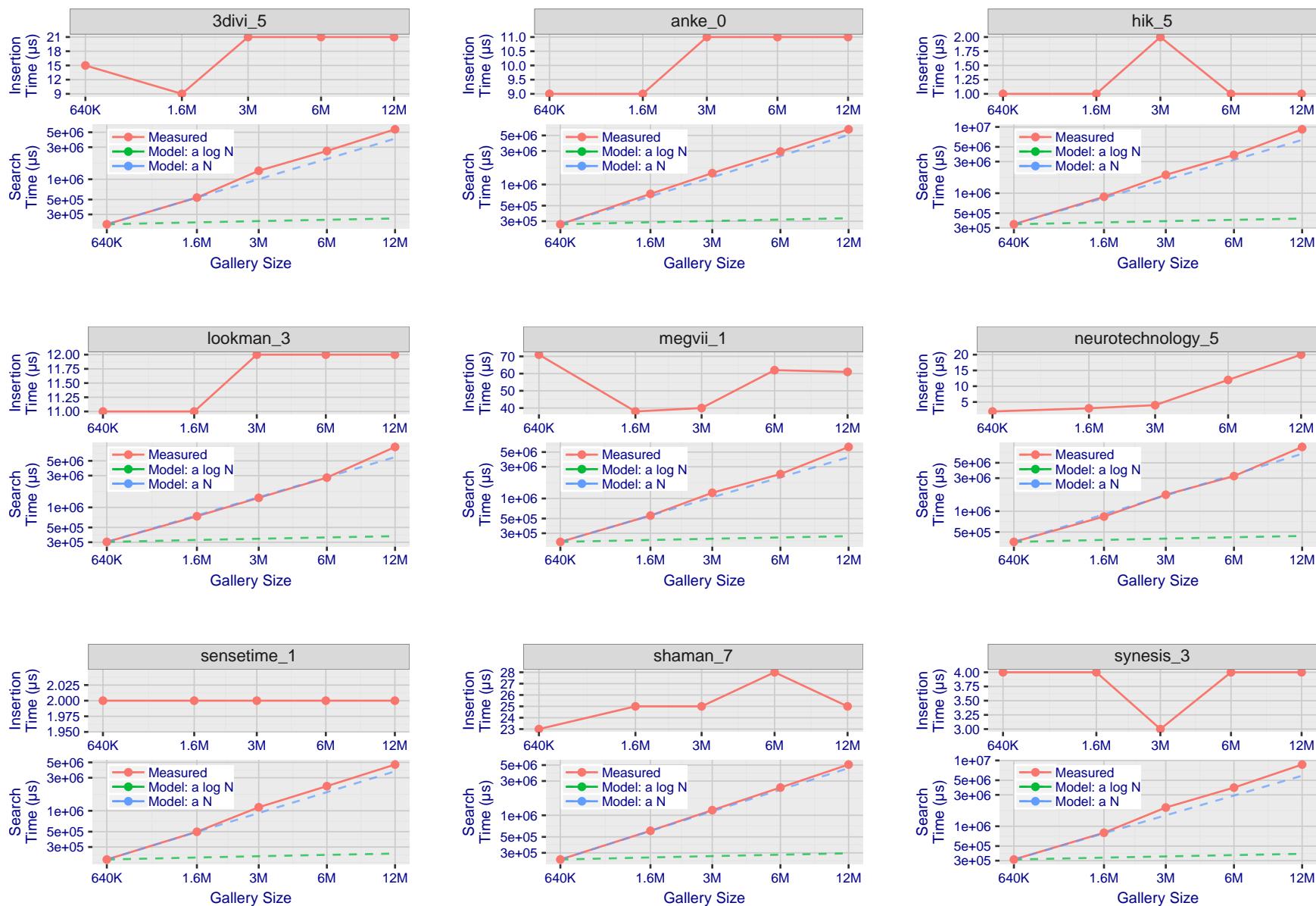
T = 0 → Investigation
 $T > 0 \rightarrow$ Identification

Figure 185: [Mugshot Dataset] Gallery insertion duration vs. enrolled population size. This chart plots the time it takes to insert a single template into a finalized gallery, illustrated over increasing gallery sizes. For reference, search times on finalized galleries of corresponding sizes are plotted right underneath. Gallery insertion time plots were generated on algorithms that 1) successfully implemented gallery insertion with no errors and 2) that were run on galleries with N up to 12 000 000. Generally, only the more accurate algorithms were run on galleries with N up to 12 000 000.

2023/03/14
14:32:11FNIR(N, R, T) = False neg. identification rate
FPTR(N, T) = False pos. identification rateN = Num. enrolled subjects
R = Num. candidates examinedT = Threshold
T = 0 → Investigation

T > 0 → Identification

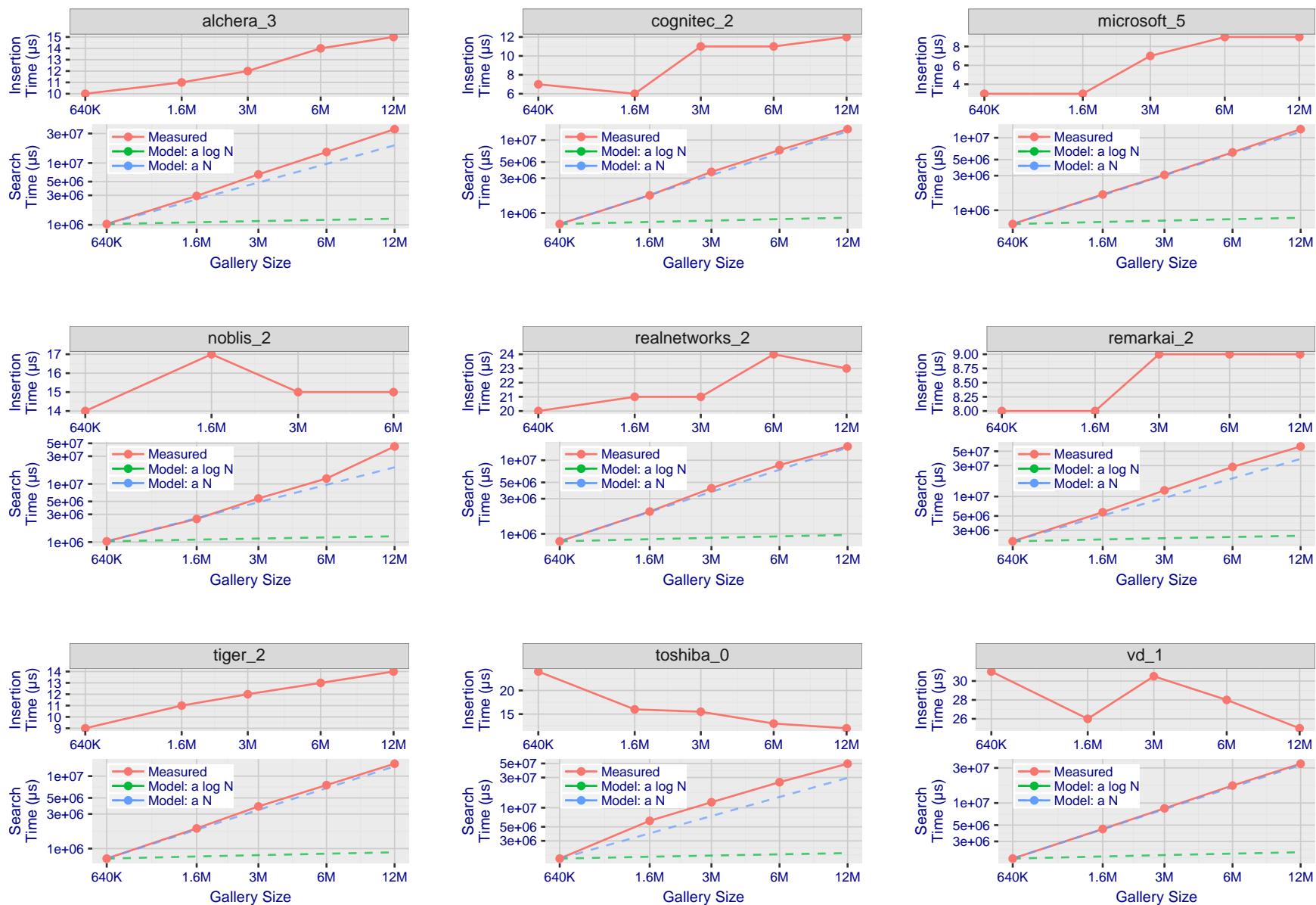


Figure 186: [Mugshot Dataset] Gallery insertion duration vs. enrolled population size. This chart plots the time it takes to insert a single template into a finalized gallery, illustrated over increasing gallery sizes. For reference, search times on finalized galleries of corresponding sizes are plotted right underneath. Gallery insertion time plots were generated on algorithms that 1) successfully implemented gallery insertion with no errors and 2) that were run on galleries with N up to 12 000 000. Generally, only the more accurate algorithms were run on galleries with N up to 12 000 000.

References

- [1] Artem Babenko and Victor Lempitsky. Efficient indexing of billion-scale datasets of deep descriptors. In *The IEEE Conference on Computer Vision and Pattern Recognition (CVPR)*, June 2016.
- [2] L. Best-Rowden and A. K. Jain. Longitudinal study of automatic face recognition. *IEEE Transactions on Pattern Analysis and Machine Intelligence*, 40(1):148–162, Jan 2018.
- [3] Blumstein, Cohen, Roth, and Visher, editors. *Random parameter stochastic models of criminal careers*. National Academy of Sciences Press, 1986.
- [4] Thomas P. Bonczar and Lauren E. Glaze. Probation and parole in the united statesm 2007, statistical tables. Technical report, Bureau of Justice Statistics, December 2008.
- [5] White D., Kemp R. I., Jenkins R., Matheson M, and Burton A. M. Passport officers' errors in face matching. *PLoS ONE*, 9(8), 2014. e103510. doi:10.1371/journal.pone.0103510.
- [6] P. Grother, G. W. Quinn, and P. J. Phillips. Evaluation of 2d still-image face recognition algorithms. NIST Interagency Report 7709, National Institute of Standards and Technology, 8 2010. <http://face.nist.gov/mbe> as MBE2010 FRVT2010.
- [7] P. J. Grother, R. J. Micheals, and P. J. Phillips. Performance metrics for the frvt 2002 evaluation. In *Proceedings of Audio and Video Based Person Authentication Conference (AVBPA)*, June 2003.
- [8] Patrick Grother and Mei Ngan. Interagency report 8009, performance of face identification algorithms. *Face Recognition Vendor Test (FRVT)*, May 2014.
- [9] Patrick Grother, George Quinn, and Mei Ngan. Face in video evaluation (five) face recognition of non-cooperative subjects. Interagency Report 8173, National Institute of Standards and Technology, March 2017. <https://doi.org/10.6028/NIST.IR.8173>.
- [10] Patrick Grother, George W. Quinn, and Mei Ngan. Face recognition vendor test - still face image and video concept, evaluation plan and api. Technical report, National Institute of Standards and Technology, 7 2013. http://biometrics.nist.gov/cs.links/face/frvt/frvt2012/NIST_FRVT2012.api_Aug15.pdf.
- [11] K. He, X. Zhang, S. Ren, and J. Sun. Deep residual learning for image recognition. In *2016 IEEE Conference on Computer Vision and Pattern Recognition (CVPR)*, pages 770–778, June 2016.
- [12] Gary B. Huang, Manu Ramesh, Tamara Berg, and Erik Learned-Miller. Labeled faces in the wild: A database for studying face recognition in unconstrained environments. Technical Report 07-49, University of Massachusetts, Amherst, October 2007.
- [13] Masato Ishii, Hitoshi Imaoka, and Atsushi Sato. Fast k-nearest neighbor search for face identification using bounds of residual score. In *2017 12th IEEE International Conference on Automatic Face & Gesture Recognition (FG 2017)*, pages 194–199, Los Alamitos, CA, USA, May 2017. IEEE Computer Society.
- [14] Jeff Johnson, Matthijs Douze, and Hervé Jégou. Billion-scale similarity search with gpus. *CoRR*, abs/1702.08734, 2017.

- [15] Ira Kemelmacher-Shlizerman, Steven M. Seitz, Daniel Miller, and Evan Brossard. The megaface benchmark: 1 million faces for recognition at scale. *CoRR*, abs/1512.00596, 2015.
- [16] Yury A. Malkov and D. A. Yashunin. Efficient and robust approximate nearest neighbor search using hierarchical navigable small world graphs. *CoRR*, abs/1603.09320, 2016.
- [17] Joyce A. Martin, Brady E. Hamilton, Michelle J.K. Osterman, Anne K. Driscoll, , and Patrick Drake. National vital statistics reports. Technical Report 8, Centers for Disease Control and Prevention, National Center for Health Statistics, National Vital Statistics System, Division of Vital Statistics, November 2018.
- [18] O. M. Parkhi, A. Vedaldi, and A. Zisserman. Deep face recognition. In *British Machine Vision Conference*, 2015.
- [19] P. Jonathon Phillips, Amy N. Yates, Ying Hu, Carina A. Hahn, Eilidh Noyes, Kelsey Jackson, Jacqueline G. Cava-zos, Géraldine Jeckeln, Rajeev Ranjan, Swami Sankaranarayanan, Jun-Cheng Chen, Carlos D. Castillo, Rama Chellappa, David White, and Alice J. O'Toole. Face recognition accuracy of forensic examiners, superrecognitioners, and face recognition algorithms. *Proceedings of the National Academy of Sciences*, 115(24):6171–6176, 2018.
- [20] Florian Schroff, Dmitry Kalenichenko, and James Philbin. Facenet: A unified embedding for face recognition and clustering. *CoRR*, abs/1503.03832, 2015.
- [21] Jeroen Smits and Christiaan Monden. Twinning across the developing world. *PLOS ONE*, 6(9):1–5, 09 2011.
- [22] Yaniv Taigman, Ming Yang, Marc'Aurelio Ranzato, and Lior Wolf. Deepface: Closing the gap to human-level performance in face verification. In *Proceedings of the 2014 IEEE Conference on Computer Vision and Pattern Recognition, CVPR '14*, pages 1701–1708, Washington, DC, USA, 2014. IEEE Computer Society.
- [23] A. Towler, R. I. Kemp, and D White. *Unfamiliar face matching systems in applied settings*. Nova Science, 2017.
- [24] Working Group 3. Ed. M. Werner. *ISO/IEC 19794-5 Information Technology - Biometric Data Interchange Formats - Part 5: Face image data*. JTC1 :: SC37, 2 edition, 2011. <http://webstore.ansi.org>.
- [25] David White, James D. Dunn, Alexandra C. Schmid, and Richard I. Kemp. Error rates in users of automatic face recognition software. *PLoS ONE*, 10:1–14, October 2015.
- [26] Bradford Wing and R. Michael McCabe. Special publication 500-271: American national standard for information systems data format for the interchange of fingerprint, facial, and other biometric information part 1. Technical report, NIST, September 2015. ANSI/NIST ITL 1-2015.
- [27] Andreas Wolf. Portrait quality - (reference facial images for mrtd). Technical report, ICAO, April 2018.
- [28] D. Yadav, N. Kohli, P. Pandey, R. Singh, M. Vatsa, and A. Noore. Effect of illicit drug abuse on face recognition. In *2016 IEEE Winter Conference on Applications of Computer Vision (WACV)*, pages 1–7, Los Alamitos, CA, USA, mar 2016. IEEE Computer Society.